High-resolution sequence stratigraphy in a Mesoproterozoic intracratonic sag basin, the Tombador Formation, Chapada Diamantina Basin, Brazil

by

Antonio Jorge Campos Magalhães

A thesis submitted in partial fulfillment of the requirements for the degree of

Doctor of Philosophy

Department of Earth and Atmospheric Sciences
University of Alberta

ABSTRACT

Studies applying sequence stratigraphy to the Precambrian sedimentary record have been limited and have focused on low-resolution applications due to problems in preservation, deformation/metamorphism, and diagenesis. However, higher-resolution studies are possible where geometry, facies definition, and facies relationships are well-definable, such as that presented by the Mesoproterozoic Tombador Formation in the Chapada Diamantina (diamond-bearing plateau) Basin. Despite its very old age, this unit underwent localized very low-grade metamorphism, and the exposure and preservation are exceptional, affording a unique opportunity to observe changes at the sub-seismic scale (high-resolution sequence stratigraphy). Furthermore, this unit enables researchers to unravel the processes that dominated the deposition and understand their stratigraphic evolution, as few such pristine data sets are available anywhere in the world for that time interval.

The data for this study were collected from several sources, including detailed and regional seismic-scale photo-mosaics; 1869.8 m of vertical section with a detailed facies description at a 1:40 scale; 697 paleocurrent readings; 1870 m of gamma ray (GR) logs with a 20-cm space sample; a 6.2-km ground penetrating radar (GPR) survey; and the description of 106 thin sections. The vertical description of the facies and stratigraphic sections, calibrated with the GR logs, the photo-mosaics, the GPR survey, and the petrography of sandstones allowed for the interpretation of the depositional systems, the identification of key stratigraphic surfaces, and the external geometry of the sequences.

Higher-rank depositional sequence boundaries are placed at the base of the extensive amalgamated fluvial sand sheets or at the base of the alluvial fan conglomeratic successions that indicate basinward shifts of facies. The hierarchy system that applies to the Tombador Formation includes sequences of different orders, which are defined as follows: sequences

associated with a particular tectonic setting are designated as 'first order' and are separated by first-order sequence boundaries where changes in the tectonic setting are recorded; second-order sequences represent the major subdivisions of a first-order sequence and reflect change cycles in the stratal stacking pattern observed at 10^2 m scale (i.e., 200-300 m); changes in the stratal stacking pattern at 10^1 m scale indicate third-order sequences (i.e., 40-70 m); and changes in the stratal stacking pattern at 10^0 m scale are assigned to the fourth order (i.e., 8-12 m). Changes in paleogeography due to relative sea level changes are recorded at all hierarchical levels with a magnitude that increases with the hierarchical rank. Thus, the Tombador Formation corresponds to one first-order sequence, representing a distinct sag basin fill in the polycyclic history of the Espinhaço Supergroup in Chapada Diamantina. An angular unconformity separates the fluvial-estuarine to the alluvial fan deposits and marks the second-order boundary. Below the angular unconformity, third-order sequences register deposition of unincised fluvial and tide-dominated estuarine systems and exhibit a lowstand fluvial sand sheet, an undifferentiated transgressive-highstand sand-rich floodplain, a transgressive estuarine, and highstand shoreface strata. In contrast, the third-order sequences above the angular unconformity are characterized by fining-upward continental alluvial successions composed of conglomerates overlain by fluvial and eolian strata; however, the data are inconclusive regarding whether these successions were downstream or upstream controlled. Hence, no systems tract nomenclature was used. Fourth-order sequences are clearly recognized at the third-order transgressive systems tract, and they exhibit distinct facies associations depending on their occurrence at the estuarine or fluvial domains. At the estuarine domain, they are composed of tidal channel, tidal bar and overlying shoreface heterolithic strata. At the fluvial domain, there are two types of fourth-order sequences: a) those preserved at the sand-rich floodplain, which are composed of cyclic successions of sand-bed braided or distal ephemeral sheetflood deposits capped by eolian sand sheet or mudstone layers, and b) those preserved at the tide-influenced braided fluvial sand sheet, which consist of cyclic successions of fluvial strata bounded by tide-influenced intervals. Fine grained intervals from shoreface heterolithic and sand-rich floodplain deposits constitute fourth-order sequence boundaries that at the reservoir approach, constitute the most important horizontal heterogeneity and hence the preferable boundaries of production zones. The criteria applied to assign sequence hierarchies in the Tombador Formation are based on rock attributes, are easy to apply, and can be used as a baseline for the study of sequence stratigraphy in Precambrian and Phanerozoic basins placed in similar tectonic settings.

Preface

This thesis is an original work as part of the doctoral project fully sponsored by the Brazilian oil company, Petrobras. Some of the research conducted for this thesis forms part of two research collaboration projects celebrated between Petrobras and two Brazilian Universities (Universidade de Brasilia, led by Professor Farid Chemale Jr., and the Universidade Federal do Rio Grande do Sul led by Professor Claiton M. S. Scherer). This research has led to four papers, which compose the body of the following chapters and Appendix 1. For those related to chapters 2, 3, 5, I was responsible for data collection, analysis as well as the manuscript composition. The co-authors contributed with manuscript edits for the papers. O. Catuneanu was the supervisory author and was involved with concept formation and manuscript composition. The facies description and interpretation of the paper in Appendix 1 are my original work, as well as the definition of basinal cycles in the Chapada Diamantina Basin.

Chapter 2 of this thesis has been published as A.J.C. Magalhães, C.M.C. Scherer, G.P Raja Gabaglia, and O. Catuneanu, "Mesoproterozoic delta systems of the Açuruá Formation, Chapada Diamantina, Brazil," *Precambrian Research*, vol. 257 (2015), 1-21.

Chapter 3 has been published as A.J.C. Magalhães, C.M.S. Scherer, G.P. Raja Gabaglia, M.B. Bállico, and O. Catuneanu, "Unincised fluvial and tide-dominated estuarine systems from the Mesoproterozoic Lower Tombador Formation, Chapada Diamantina basin, Brazil, *Journal of South American Earth Sciences*, vol. 56 (2014), 68-90.

Chapter 4 reports the findings of the Ground Penetrating Radar (GPR) survey carried out on the studied successions.

Chapter 5 has been published as A.J.C. Magalhães, G.P. Raja Gabaglia, C.M.S. Scherer, M.B. Bállico, F. Guadagnin, E. Bento Freire, L.R. Silva Born, and O. Catuneanu, "Sequence hierarchy in a Mesoproterozoic interior sag basin: from basin fill to reservoir scale, the Tombador Formation, Chapada Diamantina Basin, Brazil, *Basin Research*, (2015), 1-40, doi: 10.1111/bre.12117.

Chapter 6 presents the connection between chapters 2 through 5 and support from the petrographic analysis, as well as the conclusions and further inverstigations.

Chapter 7 lists the references used throughout the thesis.

The Appendices section exhibits complementary data. The Appendix 1 has been published as F. Guadagnin, F. Chemale Jr, A.J.C. Magalhães, A. Santana, I. Dussin, and L. Takehara, "Age

constraints on crystal-tuff from the Espinhaço Supergroup - Insight into the Paleoproterozoic to Mesoproterozoic intracratonic basin cycles of the Congo-São Francisco Craton," *Gondwana Research*, vol. 27 (2015), 363-376.

Acknowledgments

First and foremost my deepest gratitude goes to my advisor Octavian Catuneanu and my friend Guilherme Pederneiras Raja Gabaglia. Both have been a continuous source of inspiration and support, and their help and encouragement played an important role in the final completion of this study. Carlos Bruhn approved, supported and offered me the best conditions to run the project. Claiton Scherer provided valuable suggestions and guidance throughout the entire project. Francisco Pinheiro is acknowledged for GPR data acquisition and processing. Marcela M. Vieira brought an important contribution on petrographic analysis.

Funding for field work was available through Petrobras and Brazilian Universities. A great number of undergraduate students from the Universidade Federal da Bahia and the Universidade Federal do Rio Grande do Sul made my life easier during field work. Stimulating discussions with Carlos Arregui, Cícero Paixão Pereira, Daniel Galvão Fragoso, Ednilson Bento Freire, Eduardo Rodrigues, Faride Chemale Jr, Felipe Guadagnin, Francisco Pinheiro Filho, Lilian Siva Born, Manoela Bállico, and Ricardo Savini helped me to fine tune some ideas expressed in this document. Thanks to all of them.

The completion of this project would not have been possible without the encouragement and support of my wife Lidia and my kids, Paula and Pedro. Their understanding, love and support made it all possible.

Table of Contents

List of Tables

Chapter2

Chapter 3

Chapter 4

Chapter 5

List of Figures

Chapter 2

Chapter 3

Chapter 4

Chapter 5

Chapter 1 - Introduction

The Precambrian provides the opportunity to observe Earth's processes at a broader scale, allowing a better understanding of geological themes such as the mechanisms controlling accommodation and stratigraphic cyclicity. An approach based on sequence hierarchy is considered the best way to interpret the stratigraphic framework because Precambrian basins are often characterized by poor stratal preservation and by a general lack of age control (Martins-Neto, 2009; Catuneanu et al., 2005). In this approach, the relative significance of sequence stratigraphic units that develop at different scales of observation is resolved via the concept of hierarchy (Catuneanu et al., 2011).

Almost all researchers agree that by c. 2 Ga, plate tectonism was well stablished on Earth. However, by the Mesoproterozoic, when operation of Phanerozoic-style plate tectonics is accepted almost universally, a strong inter-relationship between such processes and those of mantle plumes remains as the most probable first-order control on crustal evolution (Eriksson & Catuneanu, 2004). So far, there is a few studies applying sequence stratigraphy to the Precambrian sedimentary record, which are focused on low-resolution applications due to problems in preservation, deformation/metamorphism, and diagenesis, which tend to define lower-order sequences related to major stages of basinal reorganisation (Catuneanu & Eriksson, 1999; Eriksson et al., 2005c; Catuneanu et al., 2005). Lower-order sequences have also been recognized in the Espinhaço Supergroup (Danderfer & Dardene, 2002; Guimarães et al., 2008; Danderfer et al., 2009; Martins-Neto, 2009; Chemale Jr. et al., 2010; Alkmim & Martins-Neto, 2012). However, higher-resolution studies are possible where facies, facies relationships, and geometry can be well defined (e.g., Ramaekers & Catuneanu, 2004; Eriksson & Catuneanu, 2004; Eriksson et al., 2005b,c), as can be seen in the Chapada Diamantina Basin.

This study aims to demonstrate that a high-resolution stratigraphic approach in a Mesoproterozoic intracratonic sag basin is possible, even given the differences of tectonic and sedimentary controls when compared Precambrian and Phanerozoic sedimentary successions. Therefore, it presents a sequence stratigraphic analysis carried out from the regional (basin fill) to the reservoir (high-resolution) scale in the Chapada Diamantina Basin (Northeast Brazil); this basin contains the most complete non-metamorphosed geological record of the

Espinhaço Supergroup in the São Francisco craton. The studied units present thick successions recording high-resolution information about the evolution of fluvial, deltaic, estuarine, shallow marine, and alluvial fan systems at the time of deposition. Despite the very old age of the deposits, their exposure and preservation are exceptional, allowing a unique opportunity to observe changes at the sub-seismic scale (high-resolution sequence stratigraphy), to unravel processes that dominated deposition and to understand their stratigraphic evolution during the Mesoproterozoic, as few other data sets are available anywhere in the world for this time interval. Moreover, these units underwent localized, very low-grade metamorphism, and the sedimentary rocks still exhibit many primary structures.

The integration of different data acquired from distinct methods is the key for a comprehensive high-resolution stratigraphic study. Thus, this study integrates different data acquired from distinct methods, such as detailed to the regional seismic-scale photo-mosaics; a 1,869.8 m of vertical section with detailed facies description at a 1:40 scale; 697 paleocurrent measuraments from cross-strata in sandstone; a 1,870 m of gamma ray (GR) log with a 20-cm space sample; a 6.2-km ground penetrating radar (GPR) survey; and a petrographic analysis from 106 thin sections. The sequence stratigraphic nomenclature follows the terminology of Catuneanu et al. (2011). Outcrops and gamm-ray logs data supported high-resolution sequence stratigraphic analyses, whereas seismic scale photomosaics, regional unconformities, and change of the zircon age signatures allowed lower resolution interpretation.

This study establishes a sequence stratigrahic framework from low- to high-resolution stratigraphy in a Mesoproterozoic intracratonic sag basin that can be used as a baseline for the study of sequence stratigraphy in Precambrian and Phanerozoic basins placed in similar tectonic settings. Additionally, a methodological application to petroleum reservoir stratigraphic compartmentalization is also proposed.

Chapter 2 - "Mesoproterozoic delta systems of the Açuruá Formation, Chapada Diamantina, Brazil," ***Precambrian Research*****, vol. 257 (2015), 1-21.**

ABSTRACT

Facies analysis, distinct depositional paleoflow directions and grain size ranges suggest that different fluvial systems fed coeval distinct, independent river-dominated and tide-dominated braid delta systems in the Mesoproterozoic Açuruá Formation. The river-dominated delta system is characterized by: a) vertical stacking of parasequences up to 30 m which are characterized by coarsening- and thickening-upward trends; b) gradationally based vertical succession of prodelta, delta front, distributary channels, and floodplain; c) grain size of sandstone from delta front and distributary channels varies respectively from very fine to medium and medium to coarse; d) lacking of wave or tide reworking suggests delta development in a relatively low energy marine basin; e) paleocurrent readings indicate delta front sandstone bodies shifting laterally towards NE to SE directions. The tide-dominated delta system is characterized by: a) vertical stacking of parasequences up to 25 m which are characterized by coarsening- and thickening-upward trends; b) gradationally based vertical succession of prodelta, delta front and tide-influenced distributary channels; c) grain size of sandstone from delta front and tide-influenced distributary channels varies respectively from very fine to coarse and fine to granular; d) abundance of tide-influenced sedimentary structures suggest tidal dominated delta development; e) consistent bidirectional paleocurrents with northwards ebb-tide direction and no lobe shifting. The studied braid delta systems belong to a highstand system tract and as such, they exhibit classic parasequence sets with progradational stacking pattern. The facies association variability and overall characteristics of these Mesoproteozoic delta systems are compatible with delta systems of all ages. However, contrary to typically Phanerozoic deltas – which are characterized by progradational clinoforms – the coalescence of the studied braid delta facies associations promoted fairly sheet-like geometry limited by marine flooding surface that more likely resulted from the response of deposition on shallow and wide epeiric sea.

Keywords: Mesoproterozoic; Chapada Diamantina; Açuruá Formation; river-dominated delta, tide-dominated delta

2.1. Introduction

Several papers have addressed the facies characterization and depositional environment interpretation of Precambrian deltaic systems (Chakraborty et al., 2009; Chakraborty and Paul, 2008; Eriksson et al., 2004, 1998, 1995; Heubeck and Lowe, 1994; Nocita & Lowe, 1990; Eriksson, 1973). However, those studies are mainly based on vertical facies analysis that typifies one specific kind of delta system such as fan delta on tectonically controlled setting (e.g. Corcoran et al., 1998) or braid delta on cratonic setting (e.g. Eriksson et al., 1995). Review of the literature reveals a virtual absence of documented lateral coexistence of distinct deltaic systems with different dynamics (e.g. river- and tide-dominated) at the same age, especially for the Precambrian.

The Lower Mesoproteorozoic deltaic successions from the Açuruá Formation are exposed in the Chapada Diamantina, northeastern Brazil. In spite of the very old age, the exposure and the preservation are exceptional, affording a unique opportunity to unravel processes that dominated deltaic deposition and overall geometry during the Mesoproterozoic, as few such pristine data sets are available anywhere in the world for that time interval. Besides, the area underwent localized very low grade of metamorphism and the sedimentary rocks still exhibit many primary structures. Thus, the Açuruá Formation possesses thick successions that contain high resolution information about the evolution of delta systems at the time of deposition. Previous studies based on vertical facies distribution on the Açuruá Formation have recognized deltaic facies - and tidal influence at some specific locations along the Sincorá range - and proposed depositional system sketches to explain the stratigraphic succession of this unit (Montes, 1977; Pedreira et al., 1989; Pedreira & Margalho, 1990; Bonfim & Pedreira, 1990; Guimarães & Pedreira, 1990; Dominguez, 1993; Pedreira, 1994, 1997; Santana, 2007; Aragão, 2009; Santos, 2009; Santos, 2011; Souza Jr., 2011, Rebouças, 2011).

In this paper we present the findings of an integrated study that was carried out to identify the characteristics and to propose a paleogeographic reconstruction for the delta systems from the Açuruá Formation in the Chapada Diamantina basin. Thus, the aims of this paper are threefold. First, we document the lateral coexistence of river- and tide-dominated delta systems. Second, we discuss the characteristics and the facies associations of those coeval deltaic successions. Third, we establish a sequence stratigraphy framework in which the studied succession of the Açuruá Formation is composed of a highstand system tract. Our data demonstrate the characteristic overall coarsening-upward vertical stacking pattern what agree with the statement of similarity of processes between these Mesoproterozoic and Phanerozic delta depositional processes, which suggests the same dynamic balance between sediment supply and accommodation controlled the development of deltaic sequences of any age (Eriksson et al., 2004, 1998). To reach these objectives 6 vertical sections oriented along the depositional strike direction, each 10 to 350 m thick, were measured and analysed in detail. Facies analyses were supported by paleocurrent readings and gamma ray (GR) logs helped on the definition of stacking patterns and stratigraphic surfaces.

2.2. Geological setting

The Paleo-Neoproterozoic Espinhaço Supergroup crops out in two regions in the north part of São Francisco Craton, Bahia state, Brazil: the setentrional Espinhaço and the Chapada Diamantina (figure 1). Between Statherian and Tonian, a series of intracratonic basins were formed into which volcanic and sedimentary rocks were deposited, collectively called the Espinhaço Supergroup (Pedreira & De Waele, 2008). Its basement consists of Paleoproterozoic, older than 1.8 Ga, to Archean metamorphic and igneous rocks (Silva et al., 1997; Leite, 2002; Barbosa & Sabaté, 2004). According to Danderfer and Dardene (2002), the Espinhaço basin is defined as (a) polycyclic, characterized by several stratigraphic cycles related to the stages of basin formation; (b) multi-temporal, each cycle developed during a defined time-slice; and (c) polyhistoric, each cycle translated in a response to a certain geodynamic process.

In the Chapada Diamantina region, the Espinhaço Supergroup can be subdivided into two main tectonic domains limited by João Correia - Barra do Mendes lineament: the western Chapada Diamantina (WC) and the eastern Chapada Diamantina (EC, Fig. 2.1) (Jardim de Sá et al., 1976). In the western domain there are tight folds, volcanism, and metamorphism reaching the green schist facies. In the eastern domain the folds are opened, the igneous activity is restricted to mafic intrusions, the metamorphism is very low, and the rocks still show primary structures. Those important structural features are related to the Brasiliano collisions (from 950-520 Ma) that led to the assembly of Gondwanaland and the formation of the orogenic belts that defined the boundaries of the São Francisco Craton (Alkmim, 2004). The Espinhaço Supergroup in the Chapada Diamantina region records the deposition on

Statherian rift, Calymmian sag and Stenian-Tonian rift-sag basins; the Calymmian sag phase is represented by the Paraguaçu Group and the Tombador Formation (Fig. 2.2, Guadagnin et al., 2015).

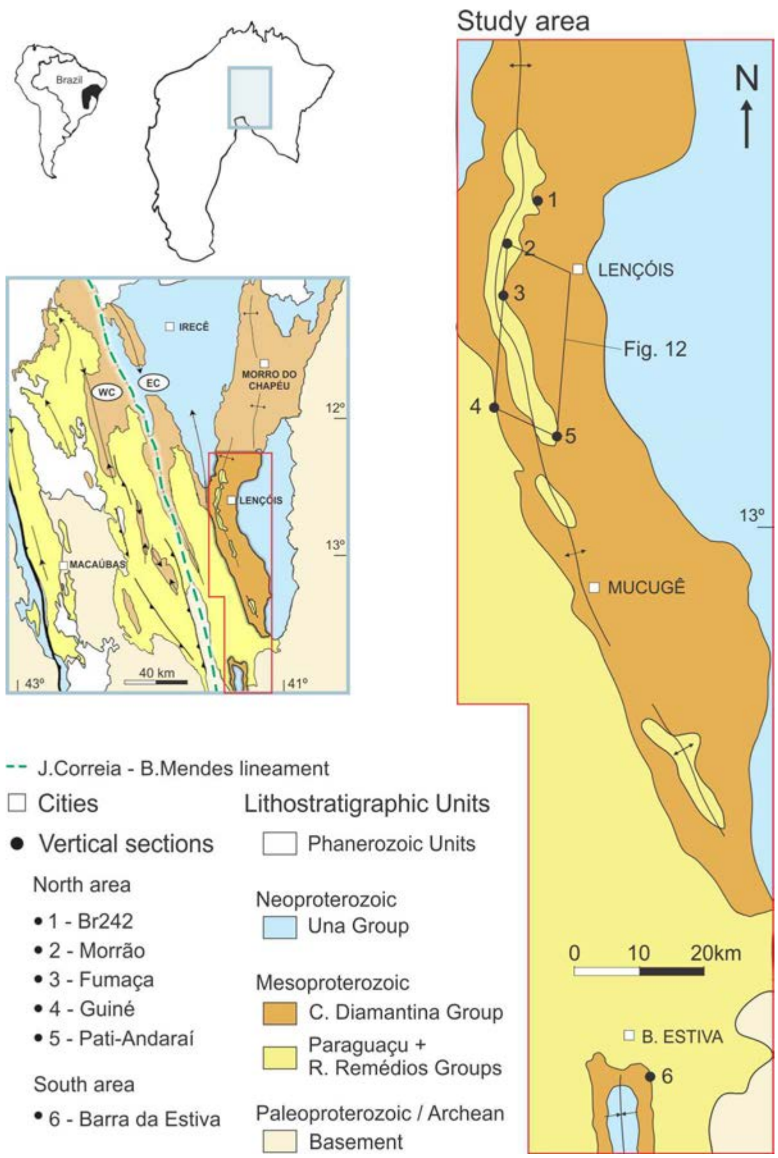

Fig. 2.1. Simplified geological map of the Chapada Diamantina. The study area is mainly located at the eastern domain along the Sincorá range, the geomorphologic expression of the Pai Inacio anticline (modified from Pedreira, 1994; Delgado et al., 2003; and Cruz, 2004). EC - Eastern Chapada Diamantina; WC – Western Chapada Diamantina.

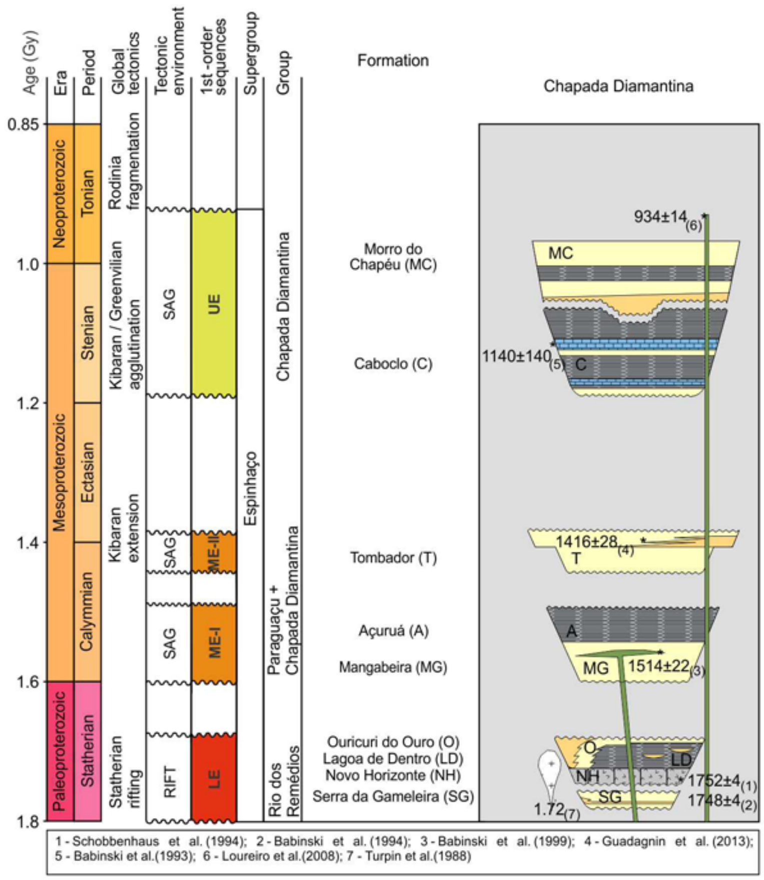

Fig. 2.2. Stratigraphic chart for the Chapada Diamantina basin as well as the relationship of the Açuruá Formation and adjacent lithostratigraphic units (modified from Guadagnin et al., 2015). Abbreviations: LE – Lower Espinhaço; ME – Middle Espinhaço; UE – Upper Espinhaço

Deltaic successions from the Açuruá Formation overlie eolian deposits from the Mangabeira Formation and both units compose the Paraguaçu Group (Guimarães et al., 2008). The contact between those units is gradual, characterizing a marine flooding on previous continental packages. Based on a study on the western Chapada Diamantina, Guimarães et al. (2008) interpreted a lowstand system tract represented by eolian deposits of the Mangabeira Formation, a transgressive system tract consisting of intertidal and subtidal sediments of the Lower Açuruá Formation and a highstand system tract composed of shallow marine, coastal, tidal, and delta-front deposits of the Upper Açuruá Formation. The upper contact of this unit with the overlying Tombador Formation is marked by a regional unconformity (Pedreira, 1994; Pedreira and De Waele, 2008; Guadagnin et al, 2015).

The study area is located in the Sincorá range (Fig. 2.1) in the eastern Chapada Diamantina, a 200 km long and 20 km wide mountain range with many cliffs approximately 400 m in height, along which the upper portion of the Açuruá Formation can be mapped with good precision due to the excellent vertical and lateral continuity of the outcrops. The range is the geomorphologic expression of Pai Inacio anticline.

2.3. Methodology

Siliciclastic strata belonging to the Açuruá Formation are exposed in the valleys and cliffs along the Sincorá range. In the north area, five vertical sections 8 to 18 km apart from each other were measured mainly on the eastern limb of the Pai Inacio anticline where the structural dip rarely exceeds 15o. In the south area one vertical section was measured. In the central area, data from Pedreira (1994) were integrated to this study. A total of 495 metres of rock succession was described. Facies description was done at the scale 1:40 to assure high-resolution data such as lithology, grain size, sedimentary structure, paleocurrent directions, and structural strike and dip measures. Despite the low grade metamorphism, facies description follows the nomenclature used for sedimentary rocks. Facies and facies association analysis preceded the interpretation of the depositional environment. These analyses combined with paleocurrent data, stratigraphic thicknesses, stacking patterns, and photomosaics provided a paleogeographic reconstitution of the delta systems and a qualitative idea about the external geometry and distribution of the facies associations. In this paper, the definition of river- or tide-dominated delta follows the approach proposed by Bhattacharya (2006), which takes into account the measurement on vertical sections of physical proportion of facies that were formed by tide, wave, or fluvial processes to classify the delta type. Spectral gamma ray logging was done with a portable radiation detector RS-230 directly on outcrops, in all vertical sections, with 20 cm or 1 m spacing, depending on the thickness and variability of facies. The detector was placed orthogonally to the bedding plane on non-weathered rock surfaces to assure good readings of concentrations of K, U and Th, with one minute sampling time. Vertical gamma ray profile was plotted and compared with the facies description for each vertical section. In this study, the total count of gamma ray log was used qualitatively to differentiate sandstone from mudstone.

2.4. Facies analysis

Ten facies are recognized in the Açuruá Formation based on lithology, grain size, and sedimentary structures (Table 2.1), and are herein discussed according to the classification scheme of Miall (1996).

2.4.1. Massive sandstone (Sm)

2.4.1.1. Description

This is the most abundant facies type and represents 38.4% of the total succession. Facies Sm is light cream to gray in colour and consists of fine- to coarse-grained sandstone, massive or with faint planar cross-bedding or horizontally laminated sets. It composes sets and cosets moderately sorted, and relatively uniform to coarsening-upward vertical grain size profile (Fig. 2.3A). Geometrically, this facies is arranged into up to 1 m thick tabular bodies that extend laterally for several tens to hundreds of metres. The lower contact is usually transitional with facies Sr and sharp with facies St, Sh and Fl. The upper boundary is flat with facies Sh and Fl.

2.4.1.2. Interpretation

This facies is interpreted as resulting from transport and deposition of sediments by short-lived high-density flows which are responsible for dumping of sediments at a rate too fast for hydraulic sorting processes to work effectively. The high-density flow is probably maintained in suspension by the combined effect of turbulence, buoyant support and dispersive pressure (Lowe, 1988; Smith, 1986).

2.4.2. Trough cross-bedded sandstone (St)

2.4.2.1. Description

Facies St represents 26.6% of the total succession and most commonly occurs associated with others sandstone facies. This facies is light cream to gray in colour and consists of fine- to very coarse-grained, locally granular sandstone. It occurs arranged into trough cross-bedded sets and cosets moderately sorted with uniform to fining-upward grain size profile (Fig. 2.3B). Subrounded granules lag and tangential to the base cross-bedding are common at the bottom of this facies intervals. Geometrically, facies St occurs as lenticular to tabular bodies from 0.2

to 2 m thick that extend laterally for ten to hundreds of metres. Some of them are wedge-shaped with lateral pinch-out into massive sandstone. The lower boundary is erosional or sharp with facies Fl, Fm, Sm, Sp, and Sh. The upper contact is sharp and flat with overlying facies Sp, Sm, Sh, and locally with Sr.

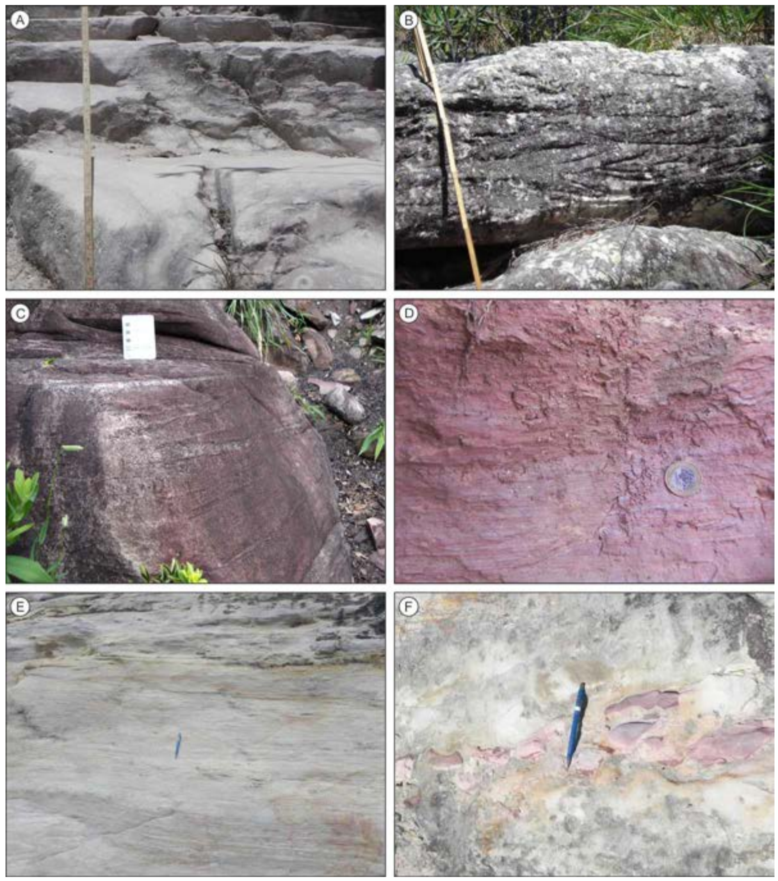

Fig. 2.3. Characteristic examples of facies recognized in the Açuruá Formation in the Sincorá range. A) Massive sandstone facies Sm. Stick is 0.6 m long. B) Trough cross-bedded sandstone facies St. Stick is 1 m long. C) Horizontally laminated sandstone facies Sh. D, E) Laminated mudstone facies Fl. F) Mud-clast rich sandstone facies Si.

2.4.2.2. Interpretation

Facies St is interpreted to form by migration of sinuous-crested (3-D) dunes in lower flow regime conditions (Reineck and Singh, 1973). In similar context of the grain-size and depth water, sinous-crested dunes are developed at higher flow speeds rather than straight-crested dunes (facies Sp). This diferentiation relates to the growth of three-dimensional separation vortices in the lee of the dunes as shear stress increases within the turbulent outer layer (Miall, 1996)

2.4.3. Horizontally to low-angle laminated sandstone (Sh)

2.4.3.1. Description

This facies represents 15.3% of the total succession and consists of very fine- to coarse-grained sandstone that is light cream to gray and reddish to violet in colour. The first occurs as flat bedded, horizontally laminated or with low angle cross-bedding (less than 15^{o}) arranged into sets and cosets moderately sorted with uniform grain size profile (Fig. 2.3C). No parting lineation was observed. Low angle sets are always less than 20 cm thick. Horizontal laminated sets are up to 30 cm thick. Both horizontally laminated and low angle sets exhibits moderately sorted sandstone units which grain size are always equal or finer than those from St and Sp facies. Geometrically, the facies Sh occurs as tabular to lenticular bodies up to 1 m thick that extend laterally for a few metres, generally intercalated and with sharp lower and upper contacts with facies St and Sp. The reddish to violet facies Sh consists of fine-grained sandstone that compose hard, well cemented layers up to 0.8 m that overlies coarsening-upward and thickening-upward trends of facies Sm. The upper contact of reddish to violent facies Sh is sharp with overlying facies Fl or abrupt with facies Sm.

2.4.3.2. Interpretation

Horizontal to low-angle lamination is particularly diagnostic of sandy, high-energy shallow flows that can readily approach and exceed Froude numbers of unity (Langford and Bracken, 1987), or rapid variations in discharge such that transcritical and supercritical bedforms cannot equilibrate during rapid drops in flow stage, preventing reworking into subcritical bedforms (Alexander and Fielding, 1997). Plane-bed are the result of upper flow regime flat-bed conditions, which are the stable-bed configuration in flows that exert a comparatively high shear stress on the stream bed, and thus produce parallel lamination in the sands (Turner, 1981, Best and Bridge, 1992). Low-angle cross-bedding are the product of the migration of bedforms with low-relief that have a high wavelength/amplitude ratio that are formed in conditions transitional between lower and upper flow regime (Todd, 1996).

2.4.4. Massive mudstone (Fm)

2.4.4.1. Description

Facies Fm represents 7.3% of the total succession and consists of light cream light green, reddish or purple siltstone and claystone with interbeds of fine-grained sandstone with mud clasts and ripple cross-lamination. The facies Fm is generally massive to weakly laminated (Fig. 2.3D). Units of this facies appear to possess either lenticular or sheet-like geometries. The sheet-like units are generally up to 2 m thick that extends laterally for hundreds of metres. Lenticular units are generally up to 1 m thick. In both cases the lower contact is abrupt with facies St, Sp and Sm. The upper contact is erosive, truncated by facies St, Sp, or Sm bodies.

2.4.4.2. Interpretation

Facies Fm is interpreted as low energy deposits formed by suspension fallout accompanied by periodic input of current transported sands (Bridge, 2006).

2.4.5. Laminated mudstone (Fl)

2.4.5.1. Description

This facies represents 4.2% of the total succession and consists of laminated claystone and siltstone units interbedded with millimetre- to centimetre-thick massive siltstone layers (Fig. 2.3E). Interlaminated siltstone horizons exhibit interbedding with thin, less than 0.2 m thick layers of very fine-grained sandstones from facies Sm and Sr composing heterolithic intervals up to 40 m thick. Heterolithic intervals commonly exhibit lenticular bedding, wavy bedding, and rod-shaped cracks. Facies Fl occurs in a variety of colours such as light green, reddish, purple, and cream. Geometrically, this facies is arranged into up to 80 m thick, laterally extensive sheet-like bodies. The lower contact is abrupt with facies Sm, St, Sh, Fm, and transitional with facies Sr. The upper boundary is gradational to sharp with facies Sr, St, Stt, and Sm.

2.4.5.2. Interpretation

Facies Fl is interpreted to represent low-energy suspension sedimentation and lower flow regime planar bedding (Simons et al., 1965). Rod-shaped cracks are interpreted as diastasis cracks (Cowan & James, 1992).

2.4.6. Mud clast-rich sandstone (Si)

2.4.6.1. Description

This facies represents 3.1% of the total succession and is always present as discrete levels interbedded with facies Sm, Sh, or St. It consists of reddish, massive, fine- to very coarse-grained sandstone rich in mud clasts. The clast population is poorly sorted, which size varies from 1 to 20 cm. The shape of clasts is always elliptical to tabular but most are angular to sub-angular. They occur scattered in the bed or locally concentrated, mostly parallel to the base (Fig. 2.4A). Geometrically, facies Si consists of lens or tabular intervals 20 – 40 cm thick within sandy deposits. The lower and upper contacts are abrupt with facies Sm, St, Sh, and Fm.

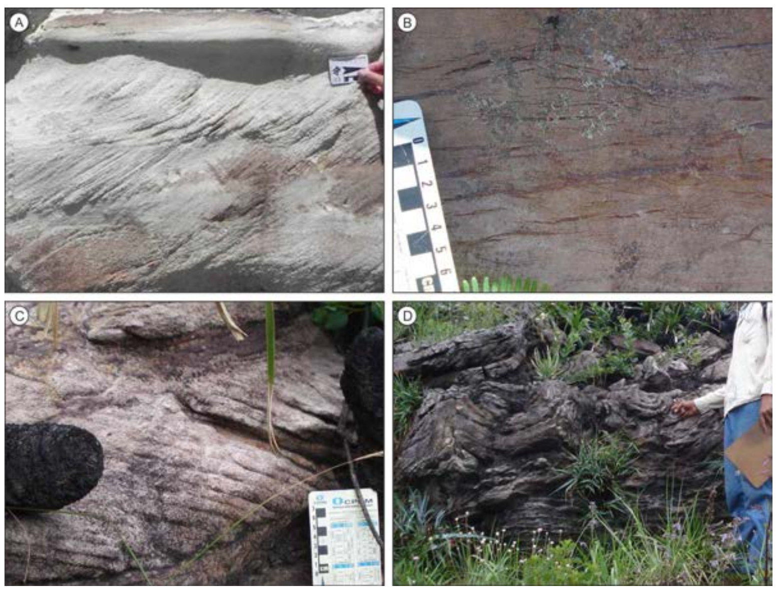

Fig. 2.4. Characteristic examples of facies recognized in the Açuruá Formation in the Sincorá range (continuation). A) Tidal bundled sandstone facies Stt. B) Ripple cross-laminated sandstone facies Sr. C) Planar cross-bedded sandstone facies Sp. D) Contorted sandstone facies Sc.

2.4.6.2. Interpretation

The general massive form of the beds, the predominance and disorganized pattern of angular to sub-angular poorly sorted mud clasts, all suggest relatively rapid sedimentation from a high energy flow. The characteristics of facies Si are consistent with deposition from storm events (Suter, 2006) or in the deepest part of streams (Miall, 1988, Collinson, 1996). Lack of evidence of storm events (e.g. expressive erosional surface at the bottom and hummocky cross-bedded strata associated with it) doesn´t support the first hypothesis. The common association of facies Si as discrete layers within trough cross-bedded and massive sandstones or in abrupt contact with mudstones suggests this facies was deposited as a channel lag in lower flow regime conditions.

2.4.7. Tidal bundled sandstone (Stt)

2.4.7.1. Description

This facies represents 2.4% of the total succession and consists of fine- to coarse-grained light cream to light gray sandstone. Individual sandstone bed exhibits stratification sets from 1 to 4 cm thick that are separated by mud drapes (tidal bundles) and that are locally truncated by slightly concave up to flat reactivation surfaces. Facies Stt occurs arranged into trough cross-bedded sets and cosets, moderately to poorly sorted, with granules scattered or along stratification surfaces (Fig. 2.4B). Its thicknesses range between 0.4 to 2.5 m with coarsening-upward grain size pattern. Cross-strata orientation is bidirectional N-S with predominant direction to the north. Geometrically, this facies occurs as lenticular to tabular bodies 0.2 to 1 m thick - enveloped by thin (less than 10 cm thick) mudstone layers - that extend laterally for ten to hundreds of metres. The lower and upper contacts are sharp, locally erosional, with facies Sr, Sh and Fl.

2.4.7.2. Interpretation

The presence of tidal bundles, mud drapes between stratification sets, reactivation surfaces, and the predominance of bidirectional orientation of trough cross strata indicates facies Stt was deposited under tide influence in the lower flow regime (Dalrymple, 2010; Visser, 1980). Lack of wavy influenced structures suggests deposition below the fairweather wave base level. Reactivation surfaces on cross strata indicate changing in the frontal face of subaqueous sand dune in response to variation in the direction of tidal currents and hence, erosion on top of bars (Shanley et al., 1992). Thickness variations of foresets in vertical section parallel to the flow may be related to neap-spring-neap moon cycles tide fluctuations; mud drapes in the foresets indicate mud deposition during low energy stages of tidal cycles (Visser, 1980). The predominance of paleocurrents with the same direction (northwards) from cross-bedded strata from facies St indicates ebb tide was dominant at the south area.

2.4.8. Ripple cross-laminated sandstone (Sr)

2.4.8.1. Description

This facies, which represents 1.4% of the total succession, usually occurs underlying thickening- and coarsening-upward cycles of facies Sm and St, or overlying facies St and Sm. In both cases facies Sr consists of light cream to light gray, very fine- to fine-grained sandstone that is generally well sorted and that is interlaminated with mudstone horizons. This facies is fine- to medium-bedded that rests on flat, non-erosional base and that contains abundant asymmetrical ripple marks. The medium-bedded sets occur as up to 0.5 m thick lenticular elongated bodies that underlie coarsening- and thickening-upward facies Sm trends. Sets exhibits uniform or coarsening-upward vertical grain size profile (Fig. 2.4C). The fine-bedded sets overlies thin beds of facies St and Si and occurs as up to 0.2 m thick wedge-shaped bodies that pinch out laterally within a few metres, exhibit fining-upward vertical grain size profile, and that contain flat bedding and load casts. The mudstone interbeds, which drape the sandstone units, are 0.1 to 20 cm thick. The cross strata in both facies St and Sr dip consistently in the same direction. This facies generally grades laterally into mudstones of facies Fm and Fl.

2.4.8.2. Interpretation

The presence of asymmetrical current ripples and cross lamination draped by clay lamination indicates deposition via alternating subaqueous traction and suspension processes (Miall, 1996). This facies is interpreted as migration of ripple microforms in lower-flow-regime conditions (Allen, 1963). Interlamination with mudstone layers reflects pulsatory periodic flow (Todd, 1996).

2.4.9. Planar cross-bedded sandstone (Sp)

2.4.9. 1. Description

This facies, which represents 0.7% of the total succession, consists of fine- to coarse-grained, locally pebbly, sandstone that usually overlies facies St, Sm, and Sh. It is light cream to light gray in colour. Sets of facies Sp are generally 20 cm thick that form lenticular to tabular bodies up to 1.3 m thick. These sets extend laterally over tens of metres and exhibit relatively uniform vertical grain size profile (Fig. 2.4D). Some of them are wedge shaped and pinch-out into facies Sm. The thickness of planar cross-bedded strata typically decreases with decreasing grain size. The lower boundary is sharp with facies St, Sm, Sh. The upper contact is flat with facies Sm and Sh.

2.4.9.2. Interpretation

Facies Sp is interpreted to form by migration of straight-crested bedforms. The decimetrical planar cross-bedded sets are related to dune size bedforms, while metric cross-bedded sets are generated by avalanching on the slipfaces of simple bars (Reineck and Singh, 1973; Collinson and Thompson, 1989).

2.4.10. Contorted sandstone (Sc)

2.4.10.1. Description

This facies represents 0.5% of the total succession and consists of very fine- to coarse-grained sandstone that exhibits highly distorted stratification forming chaotic patterns. The disturbed lamination consists of bundles of laminae that display irregular thinning and thickening while losing their lateral geometric continuity. Thickness of disturbed lamination ranges from 0.1 to 0.3 m (facies St) and from 0.05 to 0.2 m (facies Stt). The original non deformed bed is observed laterally to the contorted strata and can be of two types: sets of facies St up to 1.5 m thick or sets of facies Stt up to 3 m thick. Layers with disturbed laminations are generally fairly parallel to the bedding of overlying and underlying layers (Fig. 2.4E). No faults were observed associated with this facies. Geometrically, facies Sc occurs as lenticular to tabular bodies with sharp lower and upper boundaries with facies Fl, Fm, Sm, Sp, St, and Stt.

2.4.10.2. Interpretation

The presence of irregular convolute or highly distorted stratification suggest liquefaction and/or fluidization processes probably triggered by overloading or slumps (Berra and Felleti, 2011).

Table 2.1. Summary of the characteristic features of the facies types recognized in the Açuruá Formation.

Facies	Lithology	Sedimentary structures	Geometry	Thickness (m)	Extent and lateral relationships	Contacts	% succes-sion	Interpretation
Sm	Fine- to coarse-grained sandstone. Light cream to light gray in colour	Massive or faint lamination	Lenticular to tabular	0.2 – 1	Sand bodies extend over tens of metres, truncated by facies St, Sp	Lower boundary is transitional with facies Sr and sharp with facies St, Sh, Fl; upper boundary is sharp with facies Sh and Fl	38.4	Deposition from hyperconcentrated flows
St	Fine- to very coarse-grained sandstone; may be granular. Light cream to gray in colour	Trough cross-stratification with granules lags at the base. Tangential cross-stratification at the bottom	Lenticular to tabular	Up to 2	Sand bodies extend over tens to hundreds of metres; wedge shaped lateral pinch-out	Lower boundary is erosional or sharp with facies Fl, Fm, Sm, Sp, Sh; upper boundary is sharp with facies Sp, Sm, Sh, and Sr	26.6	Migration of sinuous-crested subaqueous bedforms (3D), lower flow regime
Sh	Very fine- to coarse-grained sandstone. Light cream to gray, and reddish to violet in colour	Horizontal and low angle (<15^{o}) lamination	Tabular to lenticular	0.2 – 1	Sand bodies extend over a few metres, interbedded with facies St, Sp. Purple sandstone generally overlies facies Sm	Lower and upper boundaries are sharp with facies Sp, Sm. Reddish to violet sandstone upper contact is sharp with facies Fl	15.3	Plane-bed flow under upper flow regime, or migration of bedforms with a high wavelength / amplitude ratio in conditions transitional between lower and upper flow regime

Table 2.1 (continued)

Facies	Lithology	Sedimentary structures	Geometry	Thickness (m)	Extent and lateral relationships	Contacts	% succes-sion	Interpretation
Fm	Massive or weakly laminated siltstone interbedded with thin sandstone. Light green, reddish or purple in colour	Massive or faint horizontal lamination; lenticular bedding, wavy bedding, dessication cracks	Thin, sheet-like units	Up to 40	Generally extends over hundreds of metres, commonly truncated by facies St, Stt, Sm	Lower boundary is gradational with facies Sr and sharp with facies St, Sp; upper boundary is erosional with facies St, Sp, Sm	7.3	Deposition from suspension and weak tractive flows; periodic exposure at dry conditions
Fl	Laminated claystone interbedded with siltstone and thin sandstone. Light green, red, purple, and cream in colour	Horizontal lamination, lenticular bedding, wavy bedding, rod-shaped cracks	Medium to thick, sheet-like units	Up to 80	Generally extends over hundreds of metres	Lower boundary is sharp with facies Sm, St, Sh, Fm and transitional with facies Sr; upper boundary is gradational to sharp with facies Sr, St, Stt, and Sm	4.2	Deposition from suspension and weak bottom currents below storm wave base level
Si	Mud clast rich fine- to medium-grained sandstone. Reddish in colour	Massive, mud clasts	Lenticular	0.2 – 0.4	Discontinuous bodies that pinch-out after about a few metres	Lower and upper boundary are sharp with facies Sm, St, Sh, and Fm	3.1	Channel lag deposit, lower flow regime
Stt	Fine- to coarse-grained sandstone. Light cream to light gray in colour	Trough cross-stratification, granules scattered or along stratification surfaces, tidal bundles, mud couples	Lenticular to tabular	0.2 – 1	Sand bodies extend over tens of metres; wedge shaped lateral pinch-out; common intercalation of facies Fl	Lower and upper boundaries are sharp with facies Sr, Sh, and Fl	2.4	Migration of sinuous-crested subaqueous bedforms (3D) under tidal indluence; lower flow regime

Table 2.1 (continued)

Facies	Lithology	Sedimentary structures	Geometry	Thickness (m)	Extent and lateral relationships	Contacts	% succession	Interpretation
Sr	Very fine- to fine-grained sandstone. Light cream to light gray in colour	Ripple cross-lamination	Lenticular to tabular	0.2 – 0.5	Discontinuous lenticular sand bodies which pinch-out laterally after some tens of metres	Lower contact is sharp with facies St and Fl; upper boundary is gradational with facies Sm, St or sharp with Fm facies	1.4	Ripples migration under unidirectional flow; lower flow regime
Sp	Fine- to coarse-grained sandstone, may be pebbly. Light cream to light gray in colour	Planar cross-stratification	Lenticular to tabular	0.2 – 1	Sand bodies extend over tens of metres; wedge shaped lateral pinch-out; common intercalation of facies Fl and Fm	Lower boundary is sharp with facies St, Sm, Sh; upper boundary is sharp with facies Sm, Sh and Fm	0.7	Migration of straight-crested subaqueous bedforms (2D); lower flow regime
Sc	Very fine- to coarse-grained sandstone. Light cream to light gray in colour	Convolution	Lenticular	0.5 – 3	Usually extends for a few tens of metres	Lower and upper boundaries are sharp with facies Fl, Fm, Sm, Sp, St, Stt	0.5	Convolution triggered by overloading and/or localized slump

Table 2.2. Summary of facies associations recognized in the Açuruá Formation in the Sincorá range.

Facies Association	Code	Facies components	Description	Other features	Gamma ray pattern	Paleocurrent	Interpretation
Prodelta to distal delta-front	PD	Fl Sm Sr	Sheet-like mudstone bodies up to 20 m thick that extend more than 8 kilometres; upper contact is gradational due to interbedding of very fine- to fine-grained sandstone beds from RDF and TDF		Serrate, progradational	Mainly to the NE and subordinately to the SW (South area)	Deposition and accumulation from suspension and or traction at prodelta do distal delta-front, below storm wave base level
River-dominated delta-front	RDF	Sm Sh Si St Sp Sr	Thickening- and coarsening-upward sheet-like sandstone bodies up to 60 m thick that extend over hundreds of metres; gradational basal contact, abrupt upper contact. Overlies PD	Firmgrounds (?)	Block and serrate, progradational	Variable to NE/SE (North area)	Progradation of delta-front lobes with lobes shifting
Tide-dominated delta-front	TDF	Sm Sh St Stt Sp Sr	Thickening- and coarsening-upward sheet-like sandstone bodies thicker than 10 m that extend over hundreds of metres; gradational basal contact, abrupt upper contact. Overlies PD	Soft-sediment deformation	Block and serrate, progradational	Mainly to the N and subordinately to the S (South area)	Progradation of delta-front lobes with tidal influence and no lobes shifting. Localized convolution triggered by overloading
Distributary fluvial channel	FCH	St Sp Sc Si	Poorly channelized to sheet-like sandstone bodies up to 10 m thick that extend over hundreds of metres; basal surface concave up, erosional, or irregular, tops sharp, erosional, or abrupt; composed of stacked trough and planar cross-stratified sets arranged into fining-upward cycles. Overlies RDF	Soft-sediment deformation	Fining-upward	Variable to E/SE (North area)	Poorly channelized braided fluvial channels and distributary channels. Localized convolution due to overloading

Table 2.2 (continued)

Facies Association	Code	Facies components	Description	Other features	Gamma ray pattern	Paleocurrent	Interpretation
Tide-influenced distributary fluvial channel	TCH	St Sp Sm Sh	Sheet-like to poorly channelized sandstone bodies up to 25 m thick that extend over and tens of metres; basal surfaces concave up, erosional, or flat, tops sharp; composed of stacked trough and planar cross-stratified sets arranged into fining-upward cycles. Overlies TDF. Upper contact covered by vegetation	Granules scattered or along stratification sets	Fining-upward	Mainly to the N, subordinately to the S (South area)	Poorly channelized tide-influenced braided fluvial channels and distributary channels
Floodplain	FP	Fm Sm Sr	Sheet-like mudstone bodies up to 2 metres thick that extend over hundreds of metres. Lower boundary abrupt with RDF, TDF, TCH, and FCH; upper contact is sharp with or truncated by RDF and FCH	Lenticular and wavy bedding	Serrate with lower values compared with PD		Delta floodplain

2.5. Facies Associations

Six types of facies associations are identified in the Açuruá Formation based on their sediment textures, sedimentary structures, paleocurrent indicators, lateral and vertical arrangement of facies, and gamma ray log response (Table 2.2, Fig. 2.5). Together, all of these facies association combine to form the entire exposed sections of the Açuruá Formation, which vary from at least 250 - 350 m in the studied area.

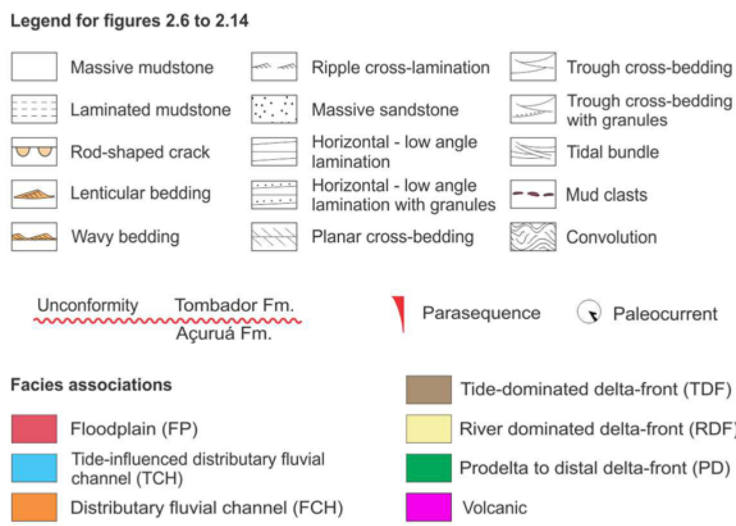

Fig. 2.5. Legend for Figs. 2.6 to 2.14.

2.5.1. Prodelta to distal delta-front facies association (PD)

2.5.1.1. Description

This facies association composes up to 20 m thick sheet-like successions that can be traced laterally for distances in excess of 8 km in strike direction. Its bottom is composed of claystone and siltstone that grade upwards to up to 2 m thick heterolithic intervals. The heterolith is formed of interbeds of claystone, siltstone, and fine-grained massive or ripple cross-laminated sandstones (facies Fl, Sm and Sr). The vertical stacking of mudstone and heterolith promotes serrate, coarsening- and thickening-upward pattern as much as 8 m thick that is reflected in the GR logs. The lower contact was not observed, whereas the upper boundary is gradational through interbedding of very fine- to fine-grained sandstones from river- and tide-dominated delta front facies associations (RDF and TDF), respectively (Fig. 2.6).

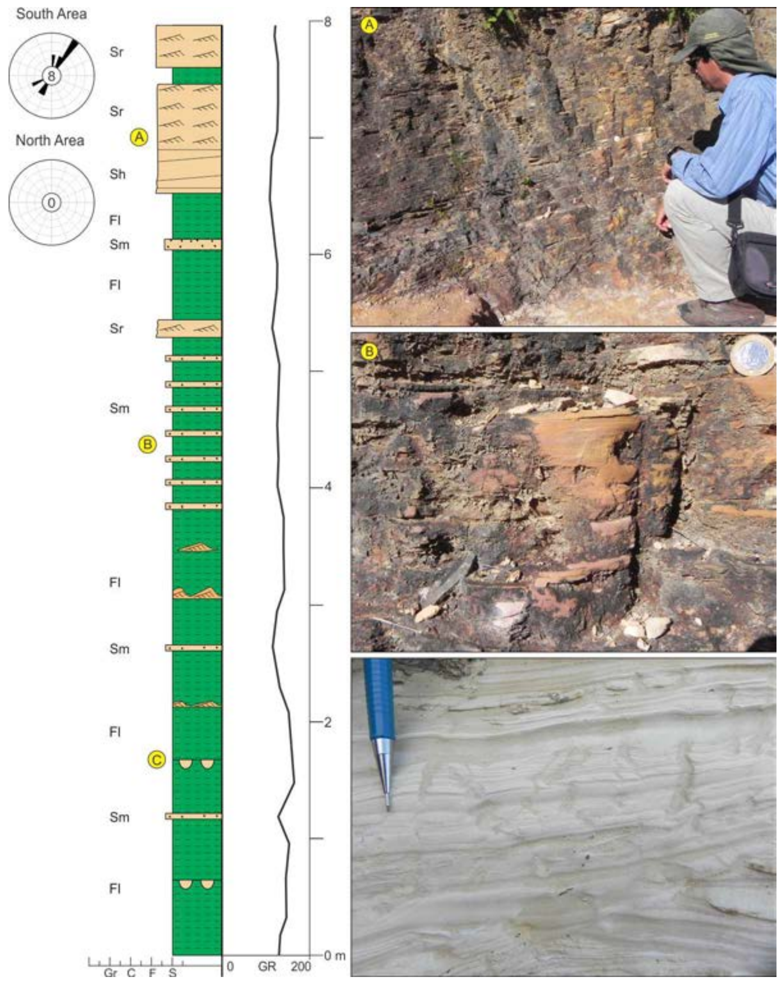

Fig 2.6. Measured vertical section and GR log of the prodelta to distal delta-front facies association (PD) exhibits classical progradational, coarsening-up succession. From bottom to top: C) laminated mudstone (facies Fl) with diastasis crack; B) very fine-grained laminated sandstone (facies Sh); A) fine-grained sandstone with low angle and ripple cross-lamination (facies Sh/Sr).

2.5.1.2. Interpretation

Lack of evidence of tractive processes suggests laminated mudstones were deposited from suspension on calm water setting, without action of bottom currents, below the storm wave base level where hemipelagic "background" silt and mud sedimentation from hypopycnal plumes dominated (Bhattacharya, 2006; Orton and Reading, 1993). Thin massive to ripple cross-laminated sandstone beds likely represent the transition from prodelta to the distal toes of delta-front deposits (Bhattacharya, 2006). The coarsening- and thickening-upward pattern is interpreted as parasequence (Van Wagoner, 1995).

2.5.2. River-dominated delta-front facies association (RDF)

2.5.2.1. Description

This facies association consists of up to 80 m thick coarsening- and thickening-upward sandstone successions that coalesce laterally and forms sheet-like sandstone bodies. Such bodies can be traced for several kilometres along strike direction. Internally it is composed of 8 to 20 m thick cycles that combine the sandstone facies Sm, Sr, Sh, Sp, St, and Si in different proportions. The lower boundary of the cycles is gradational to sharp with facies Fl, Sm, and Sr forming a tangential surface that goes steeper updip. The top of such cycles is marked by a) well cemented, reddish to violet, fine-grained, horizontally laminated sandstone bed, or b) sharp to erosive contact with facies St. The cycles exhibit coarsening- and thickening-upward trends that are also seen on GR logs. Paleoflow direction is consistently unidirectional eastwards but with variations towards NE, SE, and SSE directions. The RDF has transitional basal contact with the underlying PD. The upper contact is flat with distributary fluvial channel (FCH) or floodplain facies associations (FP; Fig. 2.7).

2.5.2.2. Interpretation

The predominance of facies generated by unidirectional currents associated with coarsening- and thickening-upward cycles associated with mud clast-rich sandstones and trough cross-bedded sandstones at the top of these cycles suggests progradation of parasequences on river-dominated delta-front environment (Bhattacharya, 1991; 2006, 2010; Van Wagoner, 1995). The association with facies St marks fluvial influence. This combination of facies is typical of distributary mouth-bar environments (Pulham, 1989; Bhattacharya & Walker, 1992). The occurrence of underlying PD facies association corroborates this hypothesis. Variations in paleocurrents indicate delta-front sand bodies shifting to fill available topographic lows between constructed sand bodies (Plink-Björklund, 2011). The reddish to violet cemented sandstones that occur at the top of coarsening- and thickening-upward cycles likely represent firmgrounds - formed when delta front sand bars were temporarily abandoned - or minor marine flooding surfaces on top of parasequences (Van Wagoner, 1995). In Phanerozoic deltaic successions, surfaces with these characteristics at the top of delta mouth bar lobes are generally bioturbated (Gilbert and Robles, 2005; MacEachern and Bann, 2008).

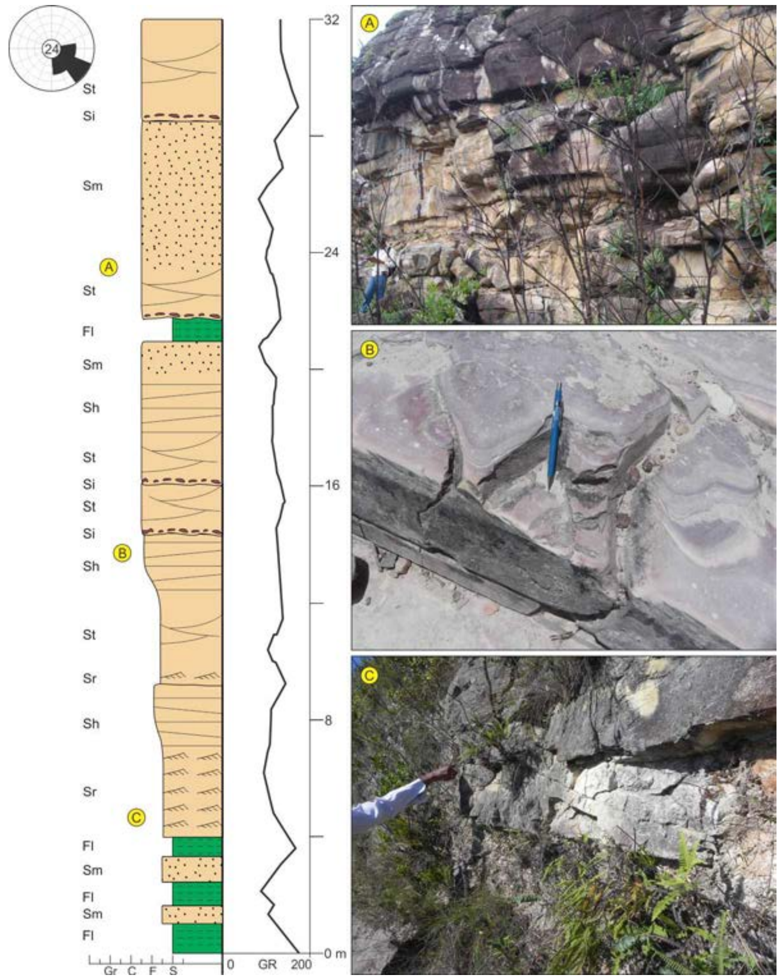

Fig. 2.7. Measured vertical section and GR log of the river-dominated delta-front facies association (RDF) exhibits classical progradational, coarsening-up succession. From bottom to top: C) toe of a delta-lobe with low-angle lamination (facies Sh); B) cemented, massive to weakly laminated mudstone (facies Fm) related to firmground; A) massive to low-angle laminated sandstone (facies Sm/Sh).

2.5.3. Tide-dominated delta-front facies association (TDF)

2.5.3.1. Description

This facies association consists of 10 to 40 m thick coarsening- and thickening-upward sandstone successions. Internally it is composed of cycles which thicknesses range from 0.5 to 2.5 m that exhibit coarsening- and thickening-upward trends and that is composed in ascending order of combination of sandstones from facies Sr, Sh, Sp and St. Such trends are also observed on GR log. The cycles contain sandstone with tidal bundles, mud drapes, reactivation surfaces (facies Stt), and localized contorted sandstone (facies Sc). The cycle lower boundary is gradational to sharp with facies Fl, Sm, and Sr, forming low angle surface (dipping less than 8^{o}), whereas the upper boundary is abrupt to erosive with trough cross-bedded sandstone (facies St). Trough cross-bedded strata from facies St and Stt are mainly oriented to the north and less frequently to the south. The TDF facies association was only described at the south area and has transitional basal contact with the underlying PD facies association. The upper contact is flat with tide-influenced distributary fluvial channel facies association (TCH; Fig. 2.8).

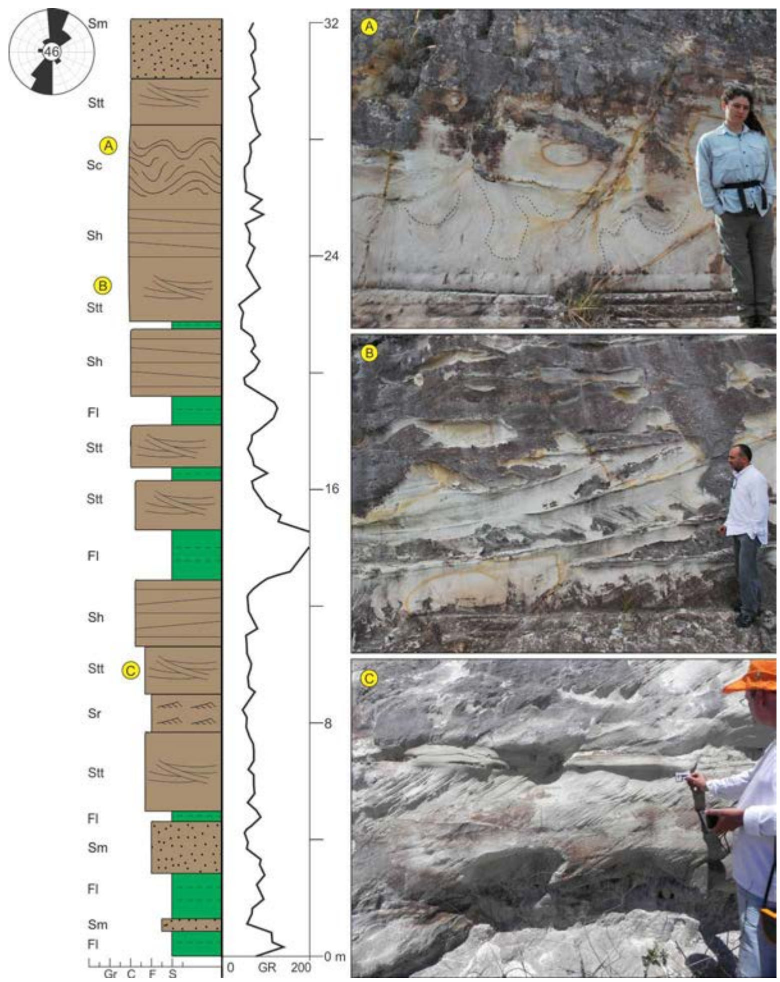

Fig. 2.8. Measured vertical section and GR log of the tide-dominated delta-front facies association (TDF) exhibits classical progradational, coarsening-up succession. From bottom to top: C, B) tidal-bundled sandstone (facies Stt), A) contorted sandstone (facies Sc).

2.5.3.2. Interpretation

The vertical coarsening- and thickening-upward succession of facies associated with tide reworking suggests progradational pattern of parasequences on tide-dominated delta-front environment (Willis et al., 1999, Van Wagoner, 1995). The occurrence of prodelta deposits just below this succession corroborates this hypothesis. Tide reworking with change of flow direction is evidenced by reactivation surfaces, bidirectional tidal bundles, cross-strata, and mud drapes in cross-sets. Gentle dipping bounding surface between sandstone beds suggest that aggradation took place during progradation (Willis et al., 1999). Consistent northwards paleocurrents are indicative of development of elongated no-shifting delta-front sandstone bodies. The dominant northwards direction of paleocurrents in the tide-influenced fluvial channel facies association (TCH) suggests tidal bar development was triggered by ebb-tide paleoflow. Convolution is localized and likely formed due to high sedimentation rate and/or slumps on the delta front (Bhattacharya, 2006) rather than be triggered by seismic events (Berra & Felletti, 2011).

2.5.4. Distributary fluvial channel facies association (FCH)

2.5.4.1. Description

This facies association consists of 10 to 30 m thick sheet-like sandstones succession that is formed by fining-upward grain size packages and that can be traced laterally for tens to hundreds of metres. Individual bed thicknesses vary from 0.5 to 2 m thick and also exhibit fining-upward trends. Flat, irregular, or concave up scour surface is developed at the base of such beds and are usually overlain by angular to subangular mud clasts (facies Si). This erosive basal surface generally truncates sandstone facies Sp and St or massive mudstone (facies Fm). Internally, the bed is composed of sandstone facies St, Sp, and Sh. Lenticular to wedge-shaped contorted beds (facies Sc) up to 1.5 m thick and that extend laterally for tens of meters occur interbedded with St and Sp facies. Vertical stacking of sandstone and mudstone promotes block to serrate pattern in the GR log. Paleoflow direction is variable, with a tendency to the E/SE. The lower and upper boundaries are sharp with RDF (Fig. 2.9).

2.5.4.2. Interpretation

The presence of sandstone bodies limited at the base by erosive concave-up erosive surfaces (5^a order surface of Miall, 1996) that are internally dominated by unidirectional oriented planar and trough cross-strata and with a well-developed fining-upward grain-size trend suggests this facies association represents fluvial channel deposits (Collinson, 1996). The occurrence of these sandstones associated with the RDF indicates they represent fluvial-dominated distributary channels. The lateral and vertical association between cross-bedded sandstones and massive mudstones likely represents preserved remnants of distributary channels cutting into the muddy delta plain. Based on thickness of sandstone bed sets (less than 2 m thick), channels were probably shallow and wide. The limited lateral occurrence of contorted sandstone beds suggests soft-sediment deformation as a result from high sedimentation rates, which is a common feature in river-dominated deltas (Bhattacharya, 2006).

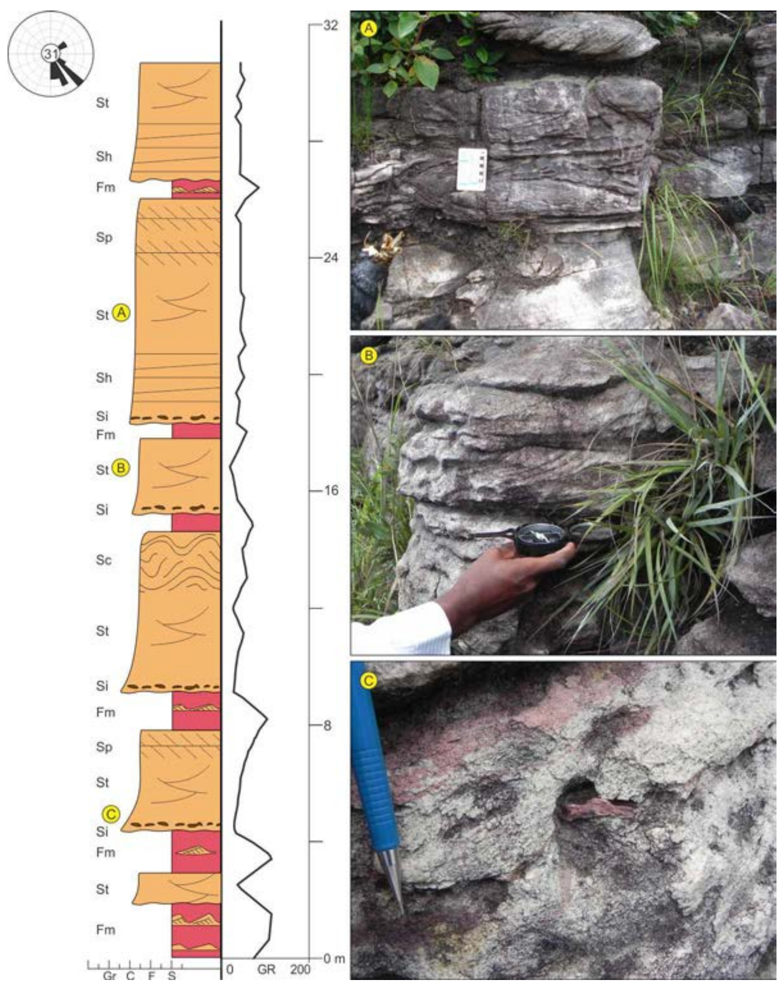

Fig. 2.9. Measured vertical section and GR log of the distributary fluvial channel facies association (FCH). A, B) trough cross-bedded sandstone; C) massive sandstone with mudclast (facies Si).

2.5.5. Tide-influenced distributary fluvial channel facies association (TCH)

2.5.5.1. Description

The TCH consists of 20 m thick fining-upward sandstone succession. It forms a sheet-like sandstones body that extends laterally for tens to hundreds of metres. Internally, TCH is composed of sandstone beds up to 2 m thick with internal fining-upward trends and flat to concave-up basal erosional surface. The beds are composed of coarse-grained sandstone from facies St, Sp, Sm, and Sh. Granules are common, either along the stratification or scattered within the beds. Massive mudstones layers (facies Fm) up to 1.5 m thick are truncated by sandstone bodies. Vertical stacking of sandstone and mudstone exhibits block to serrate pattern in GR log. The orientation of cross-strata is predominantly northwards (N5) with subordinate evidence of flow reversal (N185). The TCH facies association was only identified at the south area. Its lower contact is sharp with TDF. The upper boundary was not observed at the field because of vegetation cover (Fig. 2.10).

2.5.5.2. Interpretation

The presence of sandstone bodies limited by abrupt to concave-up erosive surfaces (5^a order surfaces of Miall, 1996), formed by coarse grain size, with internal fining-upward trends and trough-cross bedding, suggest that this facies association represents fluvial channel deposits (Collinson, 1996). Besides, the occurrence of cross-strata oriented in the opposite direction of the main paleoflow indicates tidal influence (Visser, 1980). The fact that TCH overlies TDF is strong evidence it represents tide-influenced fluvial dominated distributary channels. Interbedded siltstone deposits were probably deposited in the delta plain; however, the lack of marine influence (e.g., wavy lamination, ravinement surfaces) indicates that tide reworking was restricted to the channels. Based on thickness of sandstone bed sets (less than 2 m thick), channels were probably shallow and wide. The relatively coarse to granular grain size suggests a high-energy fluvial system fed the distributary delta channels.

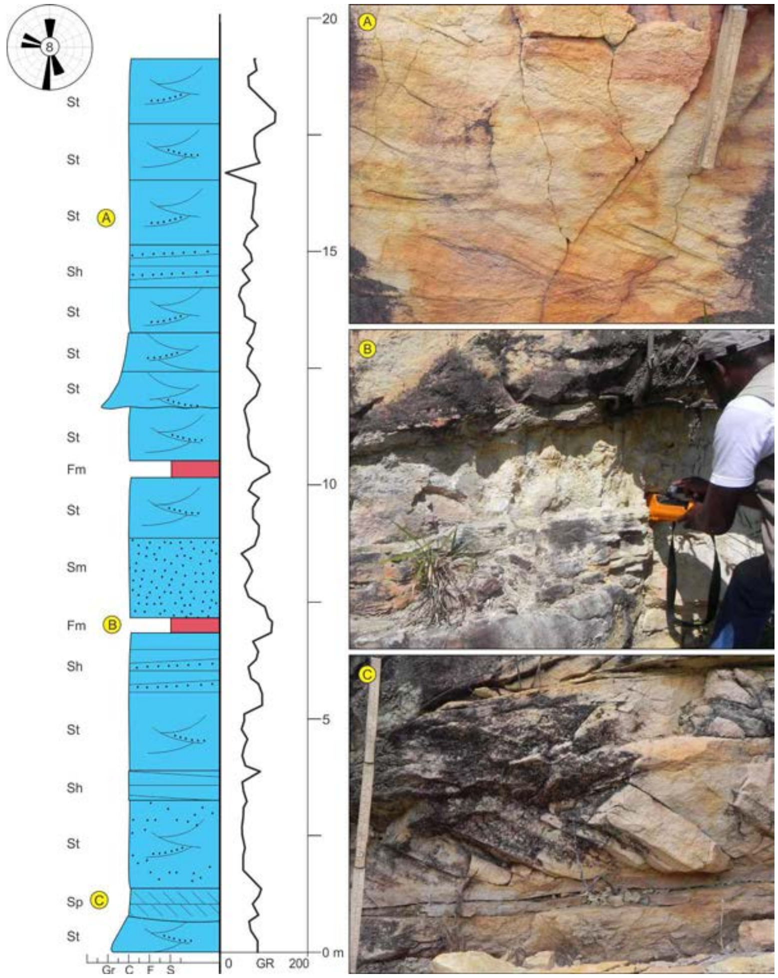

Fig. 2.10. Measured vertical section and GR log of the tide-influenced distributary fluvial channel facies association (TCH). Stick is 0.2 m long in A and 0.6 m long in C. Note tidal-bundles in photos A and C, and mudstone layer in photo B.

2.5.6. Floodplain facies association (FP)

2.5.6.1. Description

Description:

This facies association consists of up to 2 m thick massive mudstone and interbeds of centimetric sandstone layers locally truncated by the FCH or TCH facies associations. The overall geometry of this facies association is sheet-like, and it can be traced laterally for hundreds of metres along strike direction. The FP facies association is claystone and siltstone dominated and composed of light cream, reddish, purple and light green levels with thin interbeds of laminated mudstone. Neither paleosol nor pedogenic alteration (e.g. carbonate or siliceous nodules) were observed. FP typically exhibits serrate pattern with lower GR values than those from PD. It has abrupt lower boundary with the RDF, TDF, and FCH. The upper contact is sharp with or truncated by RDF and FCH (Fig. 2.11).

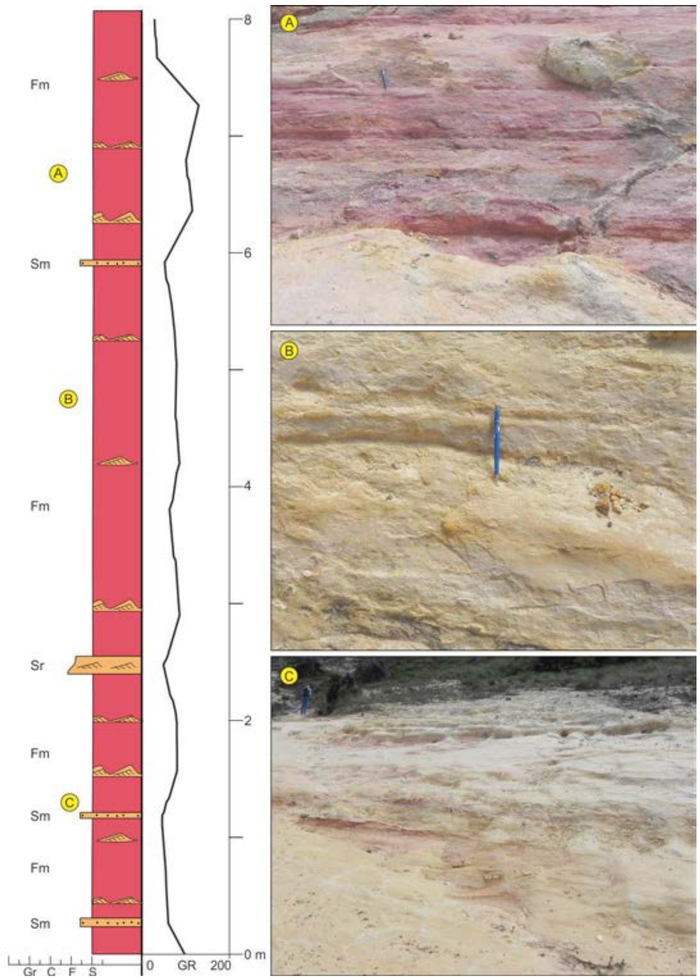

Fig. 2.11. Measured vertical section and GR log of the floodplain facies association (FP), with laminated (A) to massive mudstone (B,C). Note a pen for scale in A and a man in C.

2.5.6.2. Interpretation

The fine grain size and extensive sheet-like geometry of this facies association indicates deposition over a wide area that can represent two distinct depositional settings: (a) lateral overflows of channels during fluvial floods (overflow lobes) or (b) distal portions of ephemeral, high energy sheetfloods deposits (Spalletti and Piñol, 2005; Hampton and Horton, 2007). The occurrence of floodplain closely associated and with truncated by FCH and TCH reinforces the interpretation of deceleration of ephemeral unconfined or poorly-confined sheetfloods (Turnbridge, 1981; Hampton and Horton, 2007) that rapidly decreased their energy before finally dissipating to enable deposition of fine-grain sediments (Williams, 1971). This facies association is characteristic of distal braid plains, particularly in arid regions where ephemeral runoff forms a network of shallow, interlacing, possible poorly defined channels (Miall, 1996).

2.6. Discussion

The literature is rich in case studies based on delta typification in the Phanerozoic (e.g., Plink-Björklund, 2011; Bhattacharya, 2010, 2006; Tänavsuu-Milkeviciene and Plink-Björklund, 2009; Willis et al., 1999; Dalrymple, 1999; Coleman, 1981; Coleman and Wright, 1975) and in the Precambrian (e.g., Chakraborty et al., 2009; Chakraborty and Paul, 2008; Eriksson et al., 2004; Heubeck and Lowe, 1994; Nocita & Lowe, 1990; Eriksson, 1973; Eriksson et al., 1995). In this study, facies associations point towards river-dominated delta systems in the north to central area and tide-dominated delta system in the south area. Their characteristics agree with the overall depositional parameters envisaged for the Precambrian such as lack of vegetation, minor mud content, and wide braided fluvial systems feeding braid-delta systems (Corcoran et al., 1998; Eriksson et al., 2004; Bose et al., 2013) which could be subject to tidal reworking. Moreover, some additional characteristic features of the braid delta systems of the Açuruá Formation are herein assigned: a) vertical stacking of parasequences; b) gradationally based vertical succession of facies associations; c) grain size of distributary channel sandstone; d) wave or tide reworking; e) paleocurrent patterns.

2.6.1. River-dominated deltas

River-dominated deltas developed in the north and central area of the Sincorá range and their main characteristics include:

a) Vertical stacking of parasequences up to 30 m which are characterized by coarsening- and thickening-upward trends (Figs. 2.6, 2.7, and 2.9). Parasequences are bounded by flooding surfaces which can be traced laterally for distances in excess of 40 km (Fig. 2.12);

b) Gradationally based vertical succession of PD, RDF, FCH, and FP is exposed on the cliffs. No evidence of erosion or fluvial scour both on vertical section and on photomosaics reinforces the sheet-like geometry of facies associations (Figs. 2.13, 2.14);

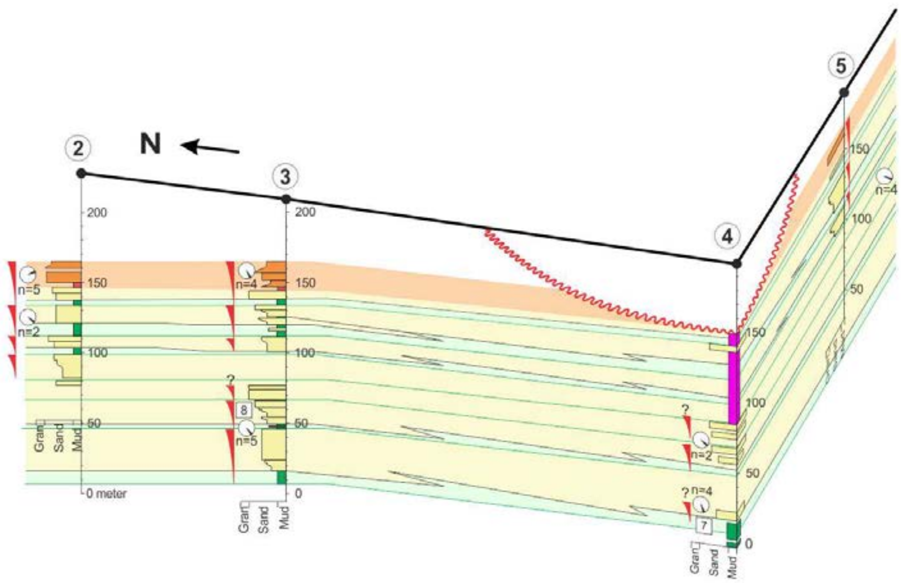

Fig 2.12. Fence diagram exhibits sheet-like geometry of parasequences. The unidirectional paleocurrent pattern and vertical stacking of prograding parasequences support the river-dominated delta depositional model at the north area. See Fig. 2.1 for vertical sections location.

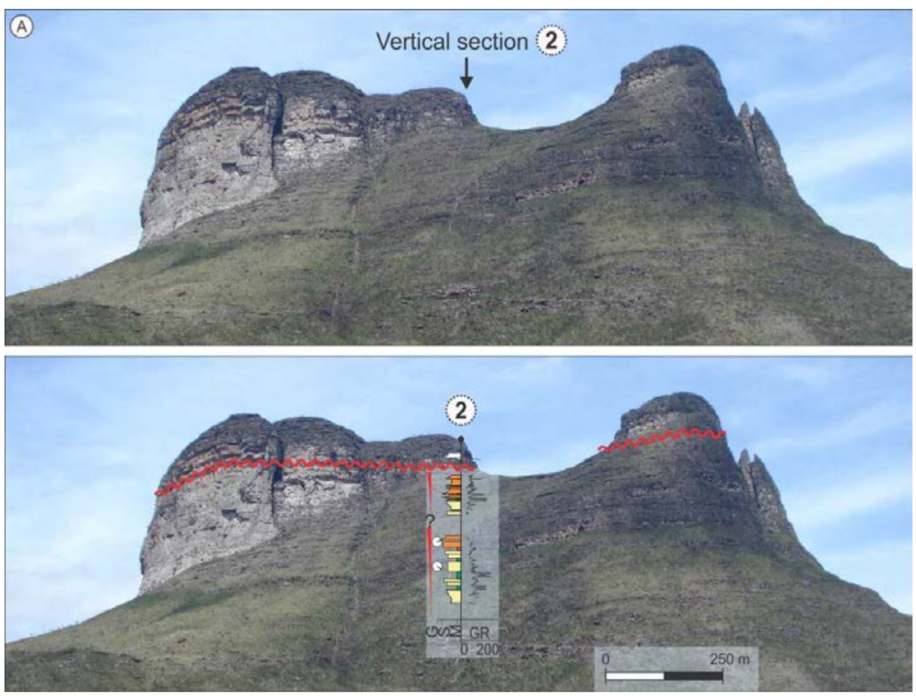

Fig. 2.13. Normal regressive highstand river-dominated deltaic succession exhibits gradational conformably transition from prodelta to delta front and delta plain. Note the sheet like geometry of the strata. The red line marks the angular unconformity between the Açuruá and the overlying Tombador Formation. See Fig. 2.1 for vertical sections location.

c) Grain size of sandstone from RDF and FCH varies respectively from very fine to medium and medium to coarse. In average, fine-grained sandstone characterizes RDF compared to medium-coarse-grained sandstone from FCH (Fig. 2.15);

d) Lacking of wave or tide reworking suggests delta development in a relatively low energy marine basin (Figs. 2.7, 2.9);

e) Paleocurrent readings of RDF and FCH indicate sandstone bodies shifting laterally towards NE to SE directions (Figs. 2.16, 2.17).

The fence diagram exhibits facies association variability compatible with river dominated delta system (Fig. 2.12). Furthermore, photo-mosaics don't exhibit progradational clinoforms but strata with fairly sheet-like geometry (Fig. 2.13). Such tabular geometry is represented at the along-strike stratigraphic cross-section (Fig. 2.14) and more likely resulted from the coalescence of braid delta facies associations as the response of deposition on shallow and wide epeiric sea (Eriksson et al., 2004). Map view of paleocurrent pattern from delta front sandstone suggests some degree of compensational shifting of active delta front bodies (Fig. 2.17; Plink-Björklund, 2011). Shifting of delta front sandstone bodies during progradation reinforces the development of a prominent paleogeomorphology of the coastline into a relative low energy marine basin, typical of river-dominated delta system (Coleman & Wright, 1975; Coleman, 1981). Shallow, wide, and relatively poorly defined distributary channels also exhibit sheet-like geometry probably due to their active shifting (Figs. 2.9, 2.12, 2.13, 2.14; Tirsgaard, 1993). No evidence of tide or wavy reworking was recognized in any vertical sections at the north area. Moreover, our paleocurrent data indicate NE to SE trend, which do not match with previous work (Pedreira, 1994) because the NW/SW trend described by that author is currently interpreted as tide-dominated estuarine deposits from the overlying Tombador Formation. The paleocurrent patterns and vertical stacking of parasequences suggest river-dominated delta system from the Açuruá Formation prograded eastwards in the north and central area (Fig. 2.17).

2.6.2. Tide-dominated delta

Tide-dominated delta system developed in the south area of the Sincorá range and was identified only at the vertical section 6 (Fig. 2.1). Its main characteristics include:

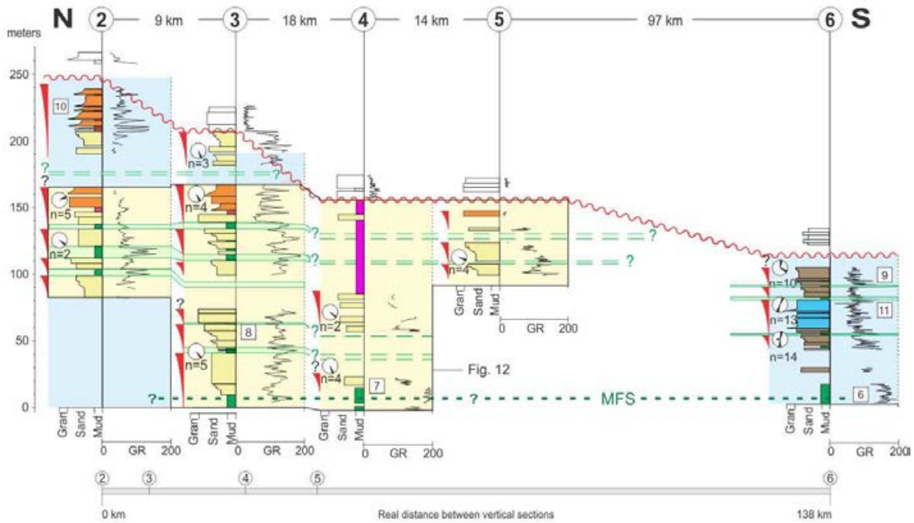

Fig. 2.14. Stratigraphic section of the Açuruá Formation. A condensed section is interpreted at the bottom of the regressive stacking pattern in vertical sections 4 and 6, and thus it contains a MFS. The highstand system tract is composed of parasequences limited by flooding surfaces. Note the sheet-like external geometry of the deltaic deposits. See Fig. 2.1 for vertical sections location. Figure numbers are indicated inside white squares. Abbreviations: MFS – maximum flooding surface; GR – gamma ray.

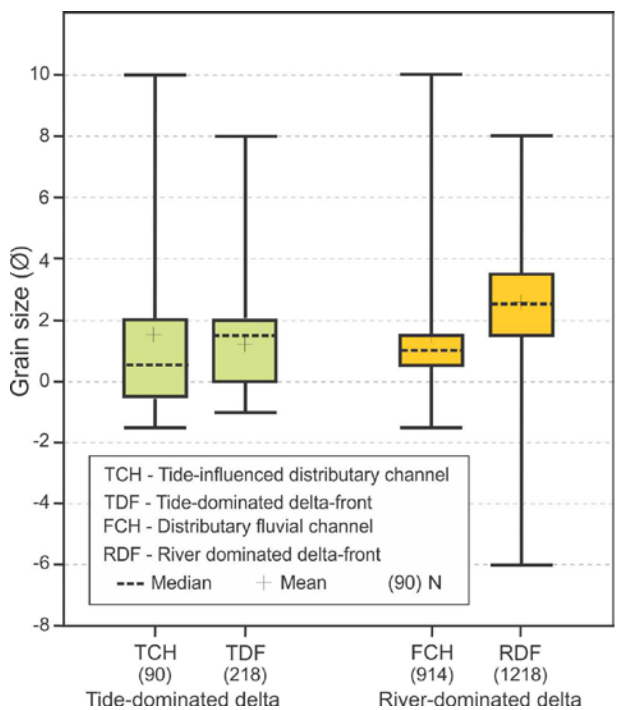

Fig. 2.15. Grain size distribution for river- and tide-dominated delta systems of the Açuruá Formation. Coarser grain size for distributary channel and delta-front sandstones suggests higher energy fluvial system feed the tide-dominated delta compared to the river-dominated delta.

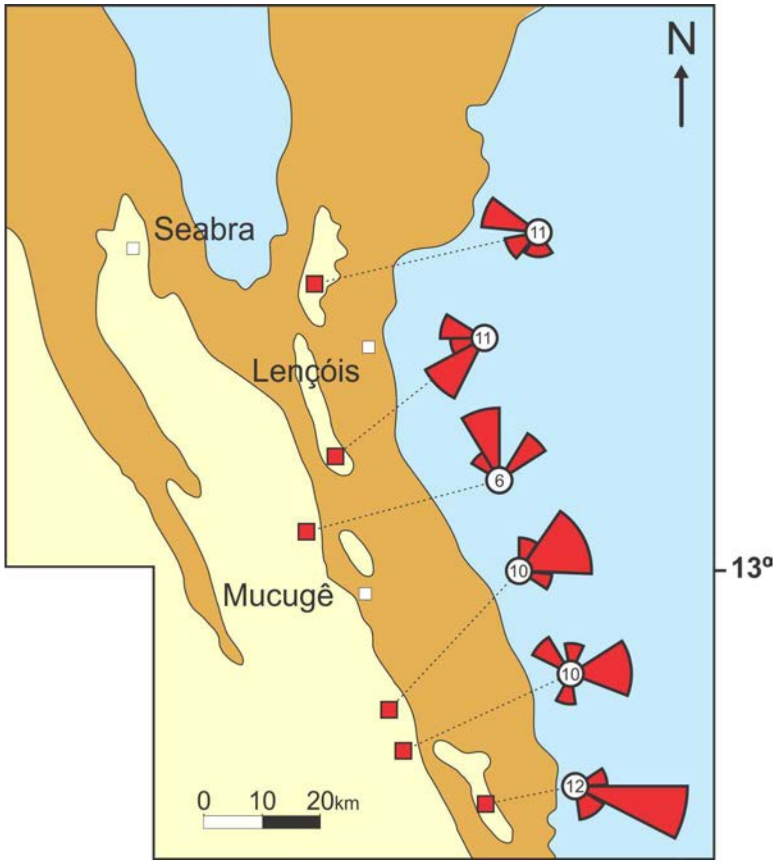

Fig. 2.16. Paleocurrents of fluvial sandstones from the Mangabeira and the Açuruá Formations (Pedreira, 1994). Paleocurrents to the west quadrant are currently interpreted as belonging to estuarine sandstones from the Tombador Formation.

a) Vertical stacking of parasequences up to 25 m which are characterized by coarsening- and thickening-upward trends bounded by flooding surfaces (Figs. 2.6, 2.8, 2.10, 2.14);

b) Gradationally based vertical succession of PD, TDF, and TCH (Fig. 2.14);

c) Grain size of sandstone from TDF and TCH varies respectively from very fine to coarse and fine to granular. In average, fine-grained sandstone characterizes TDF compared to coarse-grained sandstone from TCH (Fig. 2.15);

d) Abundance of tide-influenced sedimentary structures suggests tidal dominated delta development (Figs. 2.4A and 2.10);

e) Consistent bidirectional paleocurrents with northwards ebb-tide direction and no delta front sandstone bodies shifting (Figs. 2.8, 2.10, and 2.17).

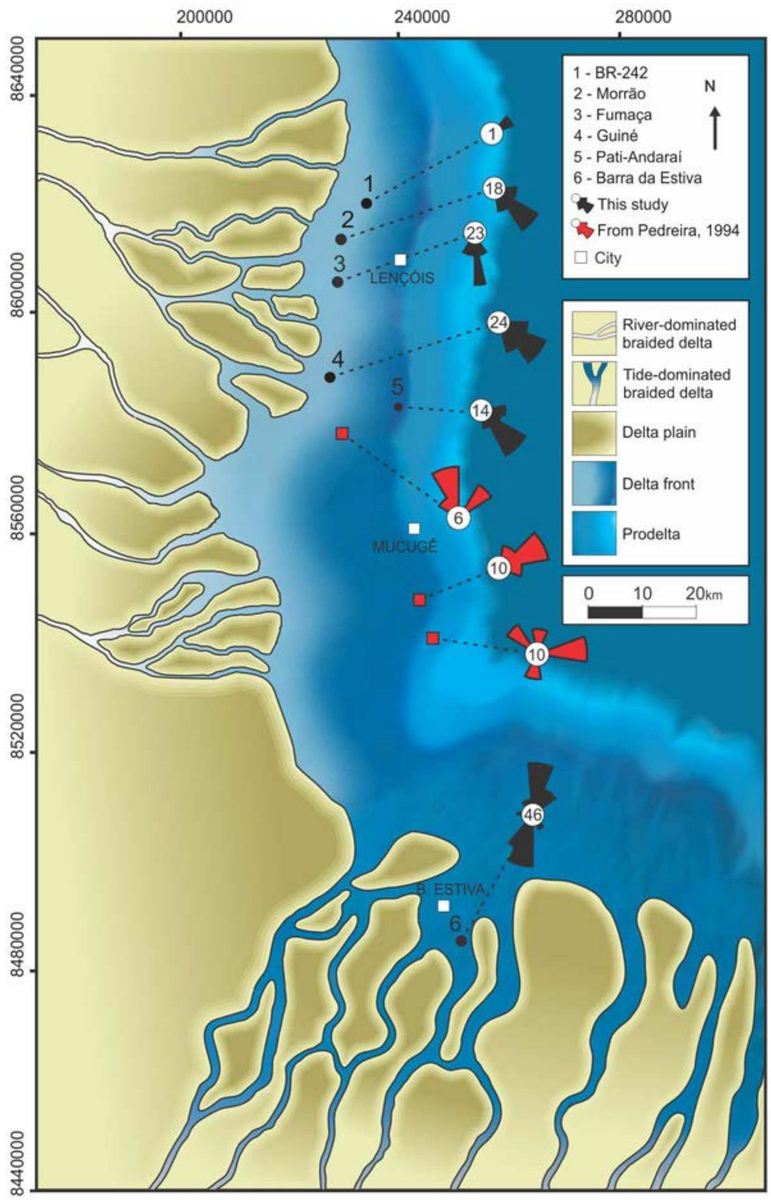

Fig. 2.17. Paleogeographic reconstruction of the Açuruá Formation in the Sincorá range. Two coeval braid delta systems seem to have existed during the Mesoproterozoic in the Chapada Diamantina: a river-dominated in the north and central area, and a tide-dominated in the south area.

Tidal deposits are quite common in the Precambrian (Eriksson et al., 2004), and are commonly found in tide-influenced delta or tide-dominated estuarine systems. The distinction between them in the geological record is based on facies successions. Delta systems exhibit progradational stacking pattern, thus related to regressive coastlines (Bhattacharya, 2010). The vertical section 6 exhibits progradational pattern of parasequences that is typically associated with delta systems (Figs. 2.8, 2.14). Consistent bimodal paleocurrent pattern reinforces tidal influence, and thus, the development of elongated delta front sandstone bodies rather than bodies shifting (Willis et al., 1999). Therefore, the proposed paleogeographic reconstruction for the tide-dominated delta system of the Açuruá Formation exhibits elongated N-S aligned bodies roughly perpendicular to the shoreline as well as several tide-influenced distributary shallow and wide channels on the delta plain (Fig. 2.17). The coarsening- and thickening-upward trend and paleocurrent patterns indicate that the tide-dominated delta system prograded northwards.

The lack of marine reworking in the north area suggests tides were not active all over the basin but some local conditions should have incremented tidal energy in the south area such as embayment, delta funnel-shape morphology, or other topographic restrictions that could have increased the tidal regime (Plink-Björklund, 2011). Moreover, the relatively coarser grain size of sandstone from TDF and TCH (Fig. 15) more likely resulted from a combination of processes to develop the tide-dominated delta: a) higher energy fluvial system feeding the delta in the south area to bring coarser-grained sediments, and b) local conditions in the south area to enhance tidal effect in such a way tides could rework the fluvial input and imprint theirs effect on the sediments.

2.6.3. Stratigraphic framework

The delta systems of the Açuruá Formation are composed of parasequences (Van Wagoner, 1995) which are recognized by coarsening-upward trends in grain size vertical profile and GR logs. The parasequences include deposits from prodelta to delta plain settings (Figs. 2.12, 2.14). The maximum preserved 30 m thickness of the parasequences probably represents the minimum water depth into which delta front deposits prograded. Parasequence sets as much as 100 m thick are characterized by gradationally based progradational stacking pattern with no fluvial or wave scouring, two main characteristics of normal regression (Catuneanu, 2006). The top of delta succession is bounded at the unconformity with the overlying estuarine and fluvial deposits from the Tombador Formation.

In addition to the unconformity with the Tombador Formation this study identifies another stratigraphic key surface: the maximum flooding surface (MFS). The MFS is assigned within the mudstone interval that underlies the progradational parasequence sets in the vertical sections 4 and 6 (Figs. 2.12, 2.14). This mudstone interval is interpreted here as a condensed section based on the identification of a convergence of mudstone interval with the highest GR values at the bottom of the regressive stacking pattern (Galloway, 1989; Posamentier and Allen, 1999), and thus it contains the MFS (Carter et al., 1998; Zecchin and Catuneanu, 2013). GR logs show a good correlation between gamma values and lithology. Generally, sandstone has average GR values smaller than 120 counts per second (cps) whereas mudstone has average GR values higher than 120 cps. An ongoing petrographic study reveals illite as the most frequent clay mineral in thin sections (Gomes, personal communication). Coarsening- and fining-upward trends are interpreted in a similar way it is used in the petroleum industry: the higher the total GR value, the muddier the interval. This premise, once supported by facies analysis, allows the interpretation of stacking patterns, and hence the assignment of stratigraphic surfaces (e.g. the MFS). Therefore, the studied braid delta systems belong to a highstand system tract and as such, they exhibit classic parasequence sets with progradational stacking pattern. The facies association variability and overall characteristics of these Mesoproteozoic delta systems are compatible with delta systems of all ages. However, contrary to typically Phanerozoic deltas – which are characterized by progradational clinoforms – the coalescence of the studied braid delta facies associations promoted fairly sheet-like geometry limited by marine flooding surface that more likely resulted from the response of deposition on shallow and wide epeiric sea.

2.7. Conclusions

The range of facies and their arrangement into cyclic regressive coarsening- and thickening-upward trends favours the interpretation that the upper portion of the Açuruá Formation records the deposition of braid delta successions. The characteristics of facies, grain size, and paleocurrent patterns indicate coeval but distinct river- and tide-dominated deltas at the north and the south area, respectively. In the north area the delta front sandstone packages exhibit paleocurrent pattern that suggests compensational shifting of sand bodies. In the south area, coarser grain size of delta-front and distributary channel sandstone indicates a relatively higher energy fluvial system fed the tide-dominated delta. The studied succession of the Açuruá Formation registers part of a highstand system tract, in which the progradation of parasequence sets promoted fairly tabular, continuous along the paleo-coastline, sand-rich sheet like packages limited by marine flooding surfaces. The top of delta succession is bounded at the unconformity with the overlying estuarine and fluvial deposits from the Tombador Formation.

2.8. Acknowledgments

This research was completed as part of the doctoral project carried out by the first author and fully sponsored by Petrobras. Cicero Pereira and Edison Sato (Federal University of Bahia) partly provided the funds for field trips. Acácio Araújo, Cleison Santos, Jaime Souza Jr., Mateus Aragão, Paulo Santos, and Valter Rebouças assisted in the field and helped to process the data. Gustavo Barros is acknowledged for his drafting skills. We also thank Chris Fedo, Vaijanthi Sethuraman, and the anonymous journal reviewers for their helpful and constructive comments that greatly improved the manuscript.

2.9. References

Alexander, J. and Fielding, C.R. 1997, Gravel antidunes in the tropical Burdekin River, Queensland, Australia: Sedimentology 44, 327–337.

Alkmim, F.F., 2004. O que faz de um cráton um cráton? O cráton de São Francisco e as revelações Almeidianas ao delimitá-lo. In: Manteso-Neto, V.; Bartorelli, A.; Carneiro, C.D.R., Brito Neves, B.B. (Eds.), Geologia do continente Sul-Americano: evolução da obra de Fernando Flávio Marques de Almeida, pp. 17-35.

Allen, J.R.L., 1963. The classification of cross-stratified units, with notes on their origin. Sedimentology 2, 93–114.

Aragão, M.O., 2009. Ambientes Sedimentares em Torno da Discordância Entre as Formações Tombador e Guiné, Chapada Diamantina, Bahia. Unpublished undergraduate monography, Universidade Federal da Bahia, 91 pp.

Babinski,M., Van Schmus,W.R., Chemale Jr., F., Brito Neves, B.B., Rocha, A.J.D., 1993. Idade isocrônica Pb/Pb emrochas carbonáticas da Formação Caboclo, emMorro do Chapéu. 2º Simpósio do Craton do São Francisco. Brazilian Geological Society, Salvador, pp. 160–163.

Babinski, M., Brito Neves, B.B., Machado, N., Noce, C.M., Uhlein, A., van Schmus, W.R., 1994. Problemas da metodologia U/Pb em zircões de vulcânicas continentais: caso do Grupo Rio dos Remédios, Supergrupo Espinhaço, no Estado da Bahia. In: Anais 42# Congresso Brasileiro de Geologia, Sociedade Brasileira de Geologia, Balneário Camboriú, vol. 2, pp. 409e410.

Babinski, M., Pedreira, A.J., Brito Neves, B.B., Van Schmus, W.R., 1999. Contribuição à geocronologia da Chapada Diamantina. 7° Simpósio Nacional de Estudos Tectônicos. Brazilian Geological Society, Lençóis, pp. 118–120.

Barbosa, J.S.F., Sabaté, P., 2004. Archean and Paleoproterozoic crust of the São Francisco Craton, Bahia, Brazil: geodynamic features. Precambrian Research 133, 1–27.

Berra, F., Felletti, F., 2011. Syndepositional tectonics recorded by soft-sediment deformation and liquefation structures (continental Lower Permian sediments, Southern Alps, Northern Italy): Stratigraphic significance. Sedimentary Geology 235, 249-263.

Best, J., Bridge, J., 1992. The morphology and dynamics of low amplitude bedwaves upon upper stage plane beds and preservation of planar laminae. Sedimentology 39, 737-752.

Bhattacharya, J.P., 1991. Regional to subregional facies architecture of river-dominated deltas in the Alberta subsurface, Upper Cretaceous Dunvegan Formation. In: Miall, A.D. and Tyler, N. (Eds.), The Three-Dimensional Facies Architecture of Terrigenous Clastic Sediments, and Its Implications for Hydrocarbon Discovery and Recovery, Concepts and Models in Sedimentology and Paleontology, SEPM (Society for Sedimentaty Geology) Special Publication 3, 289-206.

Bhattacharya, J.P., 2006. Deltas. In: Posamentier, H.W. and Walker, R.G. (Eds.), Facies Models Revisted, SEPM (Society for Sedimentaty Geology) Special Publication 84, 237-292.

Bhattacharya, J.P., 2010. Deltas. In: James, N.P. and Dalrymple, R.W. (Eds.), Facies Models 4, Geologial Association of Canada IV, Series Geotext 6, 233-264.

Bhattacharya, J.P., Walker, R.G., 1992. Deltas. In: Walker, R.G. and James, N.P. (Eds.), Facies Models: Response to Sea Level Change. Geologial Association of Canada, pp. 157-177.

Bomfim, L.F., Pedreira, A.J., 1990. Geologia da Chapada Diamantina Oriental, Bahia (Folha Lençóis). In: Bomfim, L.F., Pedreira, A.J., (Orgs.), Programa de Levantamentos Geológicos Básicos do Brasil. Lençóis (Folha SD.24-V-A-V) Estado da Bahia, Texto Explicativo, DNPM/CPRM, Brasília, pp. 25-73.

Bose, P.K., Eriksson, P.G., Sarkar, S., Wright, D.T., Samanta, P., Mukhopadhyay, S., Mandal, S., Banerjee, S., Altermann, W., 2013. Sedimentation patterns during the Precambrian: a unique record? Marine and Petroleum Geology 33, 34-68.

Bridge, J.S., 2006. Fluvial facies models: recent developments. In: Posamentier, H.,Walker, R.G. (Eds.), Facies Models Revisited, SEPM (Society for Sedimentaty Geology) Special Publication 84, 85–170.

Carter, R.M., Fulthorpe, C.S., Naish, T.R., 1998. Sequence concepts at seismic and outcrop scale: the distinction between physical and conceptual stratigraphic surfaces. Sedimentary Geology 122, 165-179.

Catuneanu, O., 2006. Principle of sequence stratigraphy. Elsevier, Amsterdam, 375 pp.

Chakraborty, P.P., Paul, S., 2008. Force regressive wedges on a Neoproterozoic siliciclastic shelf: Chandarpur Group, Central India. Precambrian Research 162, 227-247.

Chakraborty, P.P., Sarkar, A., Das, K., Das, P., 2009. Alluvial fan to storm-dominated shelf transition in the Mesoproterozoic Singhora Group, Chattisgarh Supergroup, Central India. Precambrian Research 170, 88-106.

Coleman, J.M., 1981. Deltas process of deposition and models for exploration. 2nd Ed. Burgress Publishing Company, 194 pp.

Coleman, J.M., Wright, L.D., 1975. Modern river deltas: variability of processes and sand bodies. In: Broussard, M.L., (Ed.), Deltas, Models for Exploration. Houston Geological Society, pp. 99-149.

Collinson, J.D., 1996. Alluvial sediments In: Reading, H.G., (Ed.), Sedimentary environments and facies, 3rd Ed. Blackwell Publishing, Oxford, pp. 37-82.

Collinson, J.D., Thompson, D.B., 1989. Sedimentay structures (2nd Edition). Unwin, London, 207 pp.

Corcoran, P.L., Mueller, W.U., Chown, E.H., 1998. Climatic and tectonic influences on fan deltas and wave- to tide-controlled shoreface deposits: evidence from the Archaean Keskarrah Formation, Slave Province, Canada. Sedimentary Geology 120, 125-152.

Cowan, C.C. & James, N.P. 1992. Diastasis cracks: mechanically generated synaeresis-lyke cracks in Upper Cambrian shallow water oolite and ribbon carbonates. Sedimentology 39, 1101-1118.

Cruz, S.C.P., 2004. A interação entre o Aulacógeno do Paramirim e o Orógeno Araçuaí-Oeste Congo. Unpublished PhD thesis, Universidade Federal de Ouro Preto, 503 pp.

Dalrymple, R.W., 1999. Tide-dominated deltas, do they exist or are they all estuaries? American Association of Petroleum Geologists Annual Convention, San Antonio, Texas, Official Program with Abstracts, p. A29.

Dalrymple, R.W., 2010. Tidal depositional systems. In: James, N.P. and Dalrymple, R.W. (Eds.), Facies Models 4. Geologial Association of Canada IV, Series GEOtext 6, 201-231.

Danderfer, A., Dardenne, M.A., 2002. Tectonoestratigrafia da bacia Espinhaço na porção centro-norte do cráton do São Francisco: registro de uma evolução polihistórica descontínua. Revista Brasileira de Geociências 32 (4), 449–460.

Delgado, I.M., Souza, J.D., Silva, L.C., Filho, N.C.S., Santos, R.A., Pedreira, A.J., Guimarães, J.T., Angelim, L.A.A., Vasconcelos, A.M., Gomes, I.P., Filho, J.V.L., Valente, C.R., Perrota, M.M., Heineck, C.A., 2003. In: Bizzi, L.A. Schobbenhaus, C. Vidotti, R.M. Gonçalves, J.H., (Eds.), Geotectônica do Escudo Atlântico. Geologia, Tectônica e Recursos Minerais do Brasil, CPRM, Brasília. 334 pp.

Dominguez, J.M.L., 1993. As coberturas do Craton do São Francisco: Uma abordagem do ponto de vista da análise de bacias. In: Dominguez, J.M.L. and Misi A. (Eds.), O Cráton do São Francisco, SBG/SGM/CNPQ, Salvador, pp. 137-159.

Eriksson, K.A., 1973. The Timeball Hill Formation – a fossil delta. Journal of Sedimentary Petrol. 43(4), 1046-1053.

Eriksson, P.G., Reczko, B.F.F., Boshoff, A.J., Schreiber, U.T., Neut, M.V., Snyman, C.P., 1995. Architectural elements from Lower Proterozoic braid-delta and high-energy tidal flat deposits in the Magaliesberg Formation, Transvaal Supergroup, South Africa. Sedimentary Geology 97, 99-117.

Eriksson, P.G., Condie, K.C., Trisgaard, H., Muller, W., Altermann, W.; Catuneanu, O., Chiarenzali, J., 1998. Precambrian clastic sedimentation systems. Sedimentary Geology 120, 5-53.

Eriksson, P.G., Bumby, A.J., Popa, M., 2004. Sedimentation through time. In: Eriksson, P.G.; Altermann, W., Nelson, D.R., Mueller, W.U., Catuneanu O., (Eds.), The Precambrian Earth: Tempos and Events. Elsevier, Amsterdam. pp. 593-680.

Galloway, W.E., 1989. Genetic straigraphic sequences in basin analysis, I. Architecture and genesis of flooding-surface bounded depositional units. American Association of Petroleum Geologists Bulletin 73, 125-142.

Gilbert, J.M., Robles, J.M., 2005. Firmground ichnofacies recording high-frequency marine flooding events (Langhian transgression, Vallès-Penedès Basin, Spain). Geologica Acta 3 (3), 295-305.

Guadagnin, F., Chemale Jr, F., Magalhães, A.J.C., Santana, A., Dussin, I., Takehara, L., 2015. Age constraints on crystal-tuff from the Espinhaço Supergroup — Insight into the Paleoproterozoic to Mesoproterozoic intracratonic basin cycles of the Congo-São Francisco Craton. Gondwana Research, 27, 363-376.

Guimarães, J.T., Santos, R.A., Melo. R.C., 2008. Geologia da Chapada Diamantina Ocidental (Projeto Ibitiara–Rio de Contas). Salvador, Companhia Baiana de Pesquisa Mineral – CBPM/ Companhia Pesquisa de Recursos Minerais – CPRM. Série Arquivos Abertos 31, 64p.

Guimarães, J.T., Pedreira, A.J., 1990. Geologia da Chapada Diamantina Oriental, Bahia. Folha Utinga. In: Guimarães J.T., Pedreira, A.J., (Orgs.), Programa de Levantamentos Geológicos Básicos do Brasil. Utinga (Folha SD 24-V-A-II) Estado da Bahia, Texto Explicativo, DNPM/CPRM, Brasília, pp. l19-92.

Hampton, B.A., Horton, B.K., 2007. Sheetflow fluvial processes in a rapidly subsiding basin, Altiplano plateau, Bolivia. Sedimentology 54, 1121-1147.

Heubeck, C., Lowe, D.R., 1994. Depositional and tectonic setting of the Archean Moodies Group, Barbeton Greenstone Belt, South Africa. Precambrian Research 68, 257-290.

Jardim de Sá, E.F., Bartels, R.L., Brito Neves, B.B., McReath, I., 1976. Geocronologia e o modelo tectono-magmático da Chapada Diamantina e Espinhaço Setentrional, Bahia. In: XXIX Congresso Brasileiro de Geologia, Ouro Preto, Sociedade Brasileira de Geologia, Anais 4, 205-257.

Langford, R., Bracken, B., 1987. Medano Creek, Colorado, a model for upper-flow-regime fluvial deposition: Journal of Sedimentary Petrology 57, 863–870.

Leite, C.M.M., 2002. A evolução geodinâmica da orogênese Paleoproterozoica nas regiões de Capim Grosso – Jacobina e Pintadas – Mundo Novo (Bahia, Brasil): metamorfismo, anatexia crustal e tectônica. Unpublished PhD thesis, Universidade Federal da Bahia, UFBA, 414 pp.

Loureiro, H.S.C., Lima, E.S., Macedo, E.R., Silveira, F.V., Bahiense, I.C., Arcanjo, J.B.A., Moraes Filho, J.C., Neves, J.P., Guimarães, J.T., Teixeira, L.R., Abram, M.B., Santos, R.A., Melo, R.C., 2008. Projeto Barra–Oliveira dos Brejinhos Geological map. Brazilian Geological Survey and Bahia Mineral Research Company, scale 1:200.000.

Lowe, D.R., 1988. Suspended-load fallout rate as an independent variable in the analysis of current structures. Sedimentology 35, 765-776.

MacEachern, J.A., Bann, K.L., 2008. The role of ichnology in refining shallow marine facies models. In: Hampson, G.J., Steel, R.J., Burgess, P.M., Dalrymple, R.M., (Eds.), Recent Advance in Models of Siliciclastic Shallow-Marine Environment, SEPM (Society for Sedimentaty Geology) Special Publication 90, 73-116.

Miall, A.D., 1996. The Geology of Fluvial Deposits: Sedimentary Facies, Basin Analysis, and Petroleum Geology. Springer-Verlag, Berlin, 582 pp.

Miall, A.D., 1988. Architectural-element and bounding surface in fluvial deposits: anatomy of the Kayenta Formation (Lower Jurassic), southwest Colorado. Sedimentary Geology 55, 233-262.

Montes, M.L., 1977. Os Conglomerados Diamantíferos da Chapada Diamantina - Bahia, Brasil. Brasília, Unpublished MsC dissertation, Universidade Federal de Brasilia, 102 pp.

Nocita, B.W., Lowe, D.R., 1990. Fan-delta sequence in the Archean Fig Tree Group, Barbeton Greenstone Belt, South Africa. Precambrian Research 48, 375-393.

Orton, G.J., Reading, H.G., 1993. Variability of deltaic processes in terms of sediment supply, with particular emphasis on grain size. Sedimentology 40, 475–512.

Pedreira, A.J., 1994. O supergrupo Espinhaço na Chapada Diamantina Centro–Oriental, Bahia: sedimentologia, estratigrafia e tectônica. Unpublished PhD thesis, Universidade de São Paulo, 125 pp.

Pedreira, A. J., 1997. Sistemas deposicionais da Chapada Diamantina Centro-oriental, Bahia. Revista Brasileira de Geociências 27, 229-240.

Pedreira, A.J., Dossin, I.A., Uhlein, A., Dossin, T.M., Garcia, A.J.V., 1989. Kibaran (Mid-Proterozoic) evolution and mineralizations in Eastern Brazil. IGCP 255 Newsletter 2, 57-63.

Pedreira, A.J., Margalho, R.S.F.X., 1990. Geologia da Chapada Diamantina Oriental, Bahia (Folha Mucugê). In: Pedreira, A.J., Margalho, R.S.F.X., (Orgs.), Programa de Levantamentos Geológicos Básicos do Brasil. Mucugê (Folha SD.24-V-C-II), Estado da Bahia, Texto Explicativo, DNPM/CPRM, Brasília, pp.19-68.

Pedreira, A.J., De Waele, B., 2008. Contemporaneous evolution of the Palaeoproterozoic-Mesoproterozoic sedimentary basins of the São Francisco-Congo Craton. In: Pankhurst, R.J., Trouw, R.A.J., Brito Neves, B.B., De Wit, M.J., (Eds.), West Gondwana: Pre-Cenozoic Correlations Across the South Atlantic Region, London, Geological Society Special Publication 294, 33-48.

Plink-Björklund, P., 2011. Effects of tides on deltaic deposition: Causes and responses, Sedimentary Geology 279, 107-133.

Posamentier, H.W., Allen, G.P., 1999. Siliciclastic sequence stratigraphy: concepts and applications. SEPM (Society for Sedimentaty Geology) Special Publication, Concepts in Sedimentology and Paleontology 7, 210 pp.

Pulham, A.J., 1989. Controls on internal structure and architecture of sandstone bodies within Upper Carboniferous fluvial-dominated deltas, County Clare, western Ireland. In: Whately M.K.G., Pickering, K.T., (Eds.), Deltas: Sites and Traps for Fossil Fuels, Geological Society Special Publication 41, 179-203.

Rebouças, V.O., 2011. Estratigrafia de sequências da Formação Açuruá nas proximidades de Guiné, Chapada Diamantina – Bahia. Undergraduate monography, Universidade Federal da Bahia, 84 pp.

Reineck, H.E., Singh, I.B., 1973. Depositional Sedimentary Environment with reference to Terrigenous Clastics. Springer-Verlag, 439 pp.

Santana, A., 2007. Ciclicidade no registro sedimentar do intervalo superior do Grupo Paraguaçu, Mesoproterozoico, Chapada Diamantina. Undergraduate monography, Universidade Federal da Bahia, 76 pp.

Santos, C.M., 2009. Análise Estratigráfica das Formações Guiné – Tombador, Chapada Diamantina, Bahia. Undergraduate monography, Universidade Federal da Bahia, 136 pp.

Santos, P.R.S., 2011. Sistema deposicional da Formação Açuruá nos arredores de Guiné, Chapada Diamantina-Ba. Undergraduate monography, Universidade Federal da Bahia, 90 pp.

Schobbenhaus, C., Hoppe, A., Baummann, A., Lork, A., 1994. Idade U/Pb do vulcanismo Rio dos Remédios Chapada Diamantina, Bahia. In: Scheibe, L.F. (Org.), 38° Congresso Brasileiro de Geologia. Brazilian Geological Society, 397–398.

Shanley, K.W., McCabe, P.J., Hettinger, R.D., 1992, Tidal influences in Cretaceous fluvial strata from Utah, USA: a key to sequence stratigraphic interpretation. Sedimentology 39, 905–930.

Silva, L.C., McNaughton, N.J., Melo, R.C., Fletcher, I.R., 1997. U-Pb Shrimp ages in the Itabuna-Caraíba TTG high-grade complex: the first window beyond the Paleoproterozoic overprint of the eastern Jequié Craton, NE Brazil. In: II ISGAM – International Symposium on Granites and Associated Mineralisations, Sociedade Brasileira de Geologia, Salvador, Brazil, pp.282-283.

Simons, D.B., Richardson, E.V., Nordin, C.F.Jr., 1965. Sedimentary structures generated by flow in alluvial channels. In: Middleton, G.V., (Ed.), Primary Sedimentary Structures and Their Hydrodynamic Interpretation. SEPM (Society for Sedimentaty Geology) Special Publication 12, 34-52.

Smith, G.A., 1986. Coarse-grained nonmarine volcaniclastic sediment: Terminology and depositional process. Geological Society of America Bulletin 97, 1-10.

Souza Junior, J.P., 2011. Sistema deposicional das Formações Tombador e Açuruá na cidade de Barra da Estiva, Bahia. Uundergraduate monography, Universidade Federal da Bahia, 104 pp.

Spalletti, L.A., Piñol, F.C., 2005. From Alluvial Fan to Playa: An Upper Jurassic 1167 Ephemeral Fluvial System, Neuquén Basin, Argentina. Gondwana Research 8, 363-383.

Suter, J.R., 2006. Facies models revisited: clastic shelves. In: Posamentier, H.W. and Walker, R. (Eds.), Facies Models Revisited, SEPM (Society for Sedimentaty Geology) Special Publication 84, 339-398.

Tänavsuu-Milkeviciene, K., Plink-Björklund, P., 2009. Recognizing tide-dominated versus tide-influenced deltas: Middle Devonian Strata of the Baltic Sea. Journal of Sedimentary Research 79, 887-905.

Tirsgaard, H., 1993. The architecture of Precambrian high energy tidal channel deposits: an example from the Lyell Land Group (Eleonore Bay Supergroup), northeast Greenland. Sedimentary Geology 88, 137-152.

Todd, S.P., 1996. Process deduction from flucial sedimentary structures. In: Carling, P.A., Dawson, M.R., (Eds.), Advances in fluvial dynamics and stratigraphy. John Wiley & Sons, pp 299-350.

Turnbridge, I.P., 1981. Sandy high-energy flood sedimentation – some criteria for recognition, with an example form the Devonian of southwest England. Sedimentary Geology 28, 79-95.

Turner, B.R., 1981. Possible origin of low angle cross-strata and horizontal lamination in Beaufort Group sandstones of the southern Karoo Basion. Transactions of the Geological Society of South Africa 84, 193-197.

Turpin, L., Maruejol, P., Cuney, M., 1988. U–Pb, Rb–Sr and Sm–Nd chronology of granitic basement hydrothermal albitites and uranium mineralizations (Lagoa Real, South Bahia, Brazil). Contributions to Mineralogy and Petrology 98, 139–147.

Van Wagoner, J.C., 1995. Overview of sequence stratigraphy of foreland basin deposits: terminology, summary of papers, and glossary of sequence stratigraphy. In: Van Wagoner, J.C., Bertram, G.T., (Eds.), Sequence Stratigraphy of Foreland Basin Deposits. American Association of Petroleum Geologists Memoir 64, pp.ix-xxi.

Visser, M.J., 1980. Neap-spring cycles reflected in Holocene subtidal large-scale bedforms deposits: a preliminary note. Geology 8, 543-546.

Williams, G.E., 1971. Flood deposits of the sand-bed ephemeral streams of central Australia. Sedimentology 17, 1-4.

Willis, B.J., Bhattachayra, J.P., Gabel, S.L., White, C.D., 1999. Architecture of a tide-influenced river delta in the Frontier Formation of central Wyoming, USA. Sedimentology 46, 677-688.

Zecchin, M., Catuneanu, O., 2013. High-resolution sequence stratigraphy of clastic shelves I: Units and bounding surfaces. Marine and Petroleum Geology 39, 1-25.

Chapter 3 - "Unincised fluvial and tide-dominated estuarine systems from the Mesoproterozoic Lower Tombador Formation, Chapada Diamantina basin, Brazil, *Journal of South American Earth Sciences*, vol. 56 (2014), 68-90.

ABSTRACT

The Mesoproterozoic Lower Tombador Formation Formation is formed of shallow braided fluvial, unconfined to poorly-channelized ephemeral sheetfloods, sand-rich floodplain, tide-dominated estuarine, and shallow marine sediments. Lowstand braided fluvial deposits are characterized by a high degree of channel amalgamation interbedded with ephemeral, intermediate sheetflood sandstones. Sand-rich floodplain sediments consist of intervals formed by distal sheetflood deposits interbedded with thin layers of eolian sandstones. Tide-dominated estuarine successions are formed of tide-influenced sand-bed braided fluvial, tidal channel, tidal sand flat and tidal bars. Shallow marine intervals are composed of heterolithic strata and tidal sand bars. Seismic scale cliffs photomosaics calibrated with vertical sections indicate high lateral continuity of sheet-like depositional geometry for fluvial-estuarine successions. These geometric characteristics associated with no evidence of incised-valley features nor significant fluvial scouring suggest that the Lower Tombador Formation registers deposition of unincised fluvial and tide-dominated systems. Such a scenario is a natural response of the interplay between sedimentation and fluctuations of relative sea level on the gentle margins of a sag basin. This case study indicates fluvial-estuarine successions exhibit the same facies distributions, irrespective of being related to unincised or incised-valley systems. Moreover, this case study can serve as a starting point to better understand the patterns of sedimentation for Precambrian basins formed in similar tectonic settings.

Keywords: unincised fluvial; unincised tide-dominated estuary; Precambrian; Tombador Formation; Chapada Diamantina.

3.1. Introduction

It is widely recognized that Precambrian channel systems were braided in all environments (deltaic, tidal, alluvial, and fluvial) as a consequence of lack of vegetation and poor soils development, and that the sheet-like geometry of many pre-vegetation deposits indicates that flood channels on unconfined braid-plain systems were significantly wider than younger counterparts (Cotter, 1978; Fuller, 1985; Els, 1990; Rainbird, 1992; Miall, 1996; Long, 2004; Bose et al., 2012). Moreover, unincised lowstand alluvial deposits should be more common on the rock record than what is documented in the literature (Posamentier, 2001). On the other hand, the facies models for estuary and incised-valley environment have proliferated in the literature (Boyd et al., 2006; Dalrymple, 2010; Maynard et al., 2010).

The Lower Mesoproterozoic Tombador Fm. is exposed in the Chapada Diamantina basin, Northeastern Brazil. This unit comprises thick successions that contain high resolution information about the evolution of fluvial and estuarine systems at the time of deposition. In spite of the very old age, the exposure and the preservation are exceptional, affording a unique opportunity to unravel processes that dominated fluvial and estuarine deposition and overall geometry during the Mesoproterozoic, as few such pristine data sets are available anywhere in the world for that time interval. Besides, that unit underwent localized very low grade metamorphism and the sedimentary rocks still exhibit many primary structures. Previous works have interpreted the deposits of the Tombador Fm. based on studies carried out on regional scale (Pedreira, 1994; Pedreira & De Waele, 2008; Guimarães et al., 2008; Loureiro et al., 2009) or detailed scale (Castro, 2003; Santana, 2009; Santos, 2009; Silva Filho, 2009; Araujo, 2012).

In this paper we present the findings of an integrated study based on facies analysis, supported by gamma ray logs and seismic scale photomosaic interpretation, that was carried out to identify the characteristics, understand the evolution, and to propose a paleogeographic reconstruction for the fluvial and tide-dominated estuarine systems from the Lower Tombador Fm. in the Chapada Diamantina basin. Thus, the aim of this paper is threefold. First, we identify facies associations and their overall geometry. Second, we integrate those facies associations in depositional systems and propose a stratigraphic framework. Third, we recognize the unincised character of the lowstand fluvial and transgressive tide-dominated estuarine deposits. The data presented here suggest unincised fluvial-estuarine systems exhibit the same facies distribution found in estuaries related to incised-valley systems and offer an example to better understand the patterns of sedimentation for Precambrian basins placed in similar tectonic settings.

3.2. Regional Setting

The Chapada Diamantina is located in the São Francisco craton (Fig. 3.1). The São Francisco and Congo cratons are stable Archean/Paleoproterozoic blocks (Almeida, 1977). Some authors argue the craton represents a fragment of the Rodinia supercontinent assembled at 1.0 Ga (Brito Neves et al., 1999; Campos Neto, 2000; Alkmim & Martins-Neto, 2001; Brito Neves, 2003) while others suggest it does not (Krönner & Cordani, 2003, Pisarevski et al.; 2003). This once coherent landmass broke up in Cretaceous during the opening of the Atlantic Ocean (Pedreira & De Waele, 2008). The evolution of Paleo to Mezoproterozoic sedimentary cover in the São Francisco craton started with the Statherian intracratonic extensive regime, between 1.8–1.6 Ga, that promoted continental rifting and ensuing bimodal volcanism suite followed by psamite continental sedimentation, which are well preserved in the Espinhaço rift system (Jardim de Sá et al., 1976; Inda & Barbosa, 1978; Brito Neves et al., 1999; Jardim de Sá, 1981, Costa & Inda, 1982, Delgado et al., 2003). The rift basins expanded in the Calymmian, between 1.6–1.4 Ga, with sedimentary deposits of transitional and marine environments comprising the rift-sag basins of the Espinhaço Supergroup (Delgado et al., 2003).

Guimarães et al. (2008) suggests that the Chapada Diamantina basin evolved in three distinct tectonic phases (pre-rift, rift and post-rift sag basin). Following the post-rift phase (Paraguaçu Group), another sag-basin was developed and filled by sediments of the Chapada Diamantina Group. The Chapada Diamantina basin can be subdivided into two main tectonic domains limited by João Correia - Barra do Mendes lineament: the Western Chapada Diamantina and the Eastern Chapada Diamantina (Jardim de Sá et al., 1976). In the Western domain there are tight folds, volcanism, and metamorphism reaching the green schist facies whereas in the Eastern domain the folds are open, igneous activity is restricted to mafic intrusions, the metamorphism is very low, and the rocks still exhibit primary structures. Those important structural features are related to the Brasiliano collisions (from 950-520 Ma) that led to the assembly of Gondwanaland and the formation of the orogenic belts that defined the boundaries of the São Francisco craton (Alkmim, 2004).

The Tombador Fm. was deposited in a sag basin (Fig. 3.2) and is composed of sedimentary rocks representative of shallow marine, transitional (estuarine) and continental (alluvial fan, fluvial, and eolian) depositional environments that lies unconformably over deltaic deposits of the Açuruá Fm. (Pedreira, 1994; Castro, 2003; Guimarães et al., 2008; Loureiro et al., 2009).

Petrographic studies revealed sandstones reached high diagenesis stage and low-grade metamorphism towards the South of the Sincorá Range (Varajão & Gomes, 1997; Battilani et al., 1999).

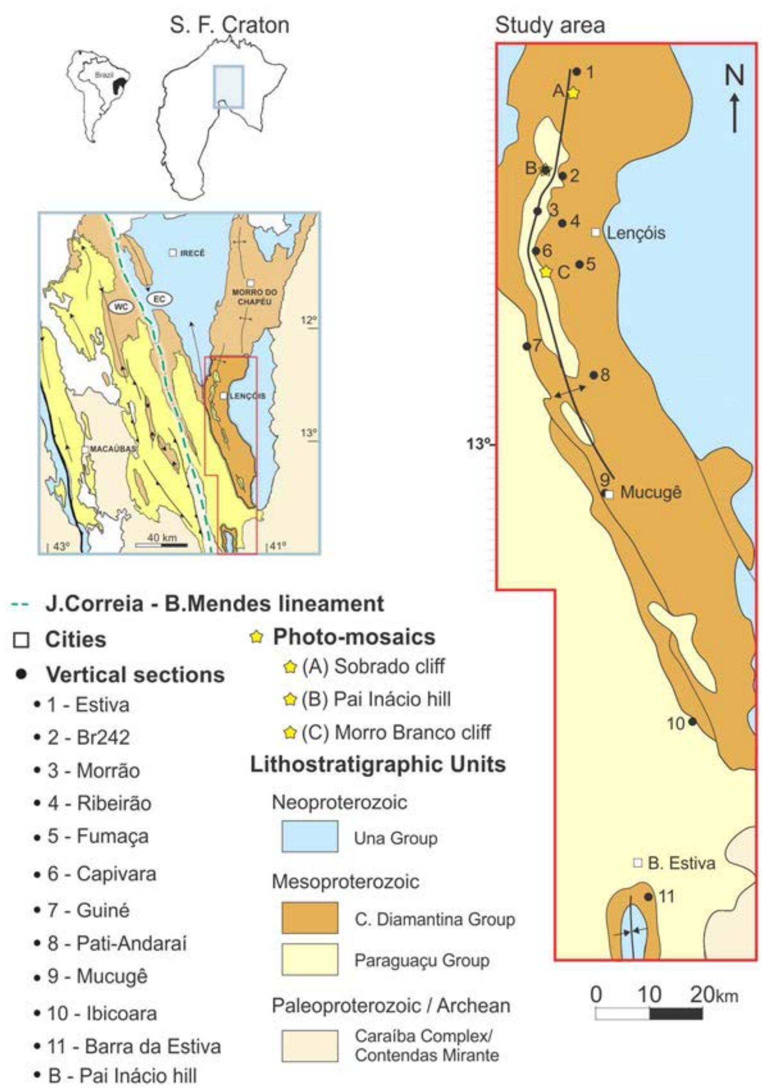

Fig. 3.1. Simplified geological map of the Chapada Diamantina. The study area is mainly located at the eastern domain along the Sincorá Range, the geomorphologic expression of the Pai Inacio anticline (modified from Pedreira, 1994 and Alkmin & Martins-Neto, 2011). Abbreviations: WC – Western Chapada Diamantina; EC – Eastern Chapada Diamantina.

The study area is located in the Sincorá Range (Fig. 3.1), in the Eastern Chapada Diamantina. The current topography reflects its geological structure and reveals the stratigraphy underneath. The Sincorá Range – a 200 km long and 20 km wide mountain range with many cliffs approximately 400 m high - is the geomorphologic feature of Pai Inácio anticline, along which the Tombador Fm. crops out and has excellent vertical (up to 400 m) and lateral (up to 20 km) continuity. Based on facies associations described along the Sincorá Range, the Tombador Fm. can be subdivided in two portions: the Lower and the Upper Tombador Fm. The Upper Tombador is characterized by the occurrence of diamond-bearing conglomerates, fluvial and eolian strata (Bállico, 2012) whereas the Lower Tombador is composed mainly of fluvial and tide-dominated deposits (this paper).

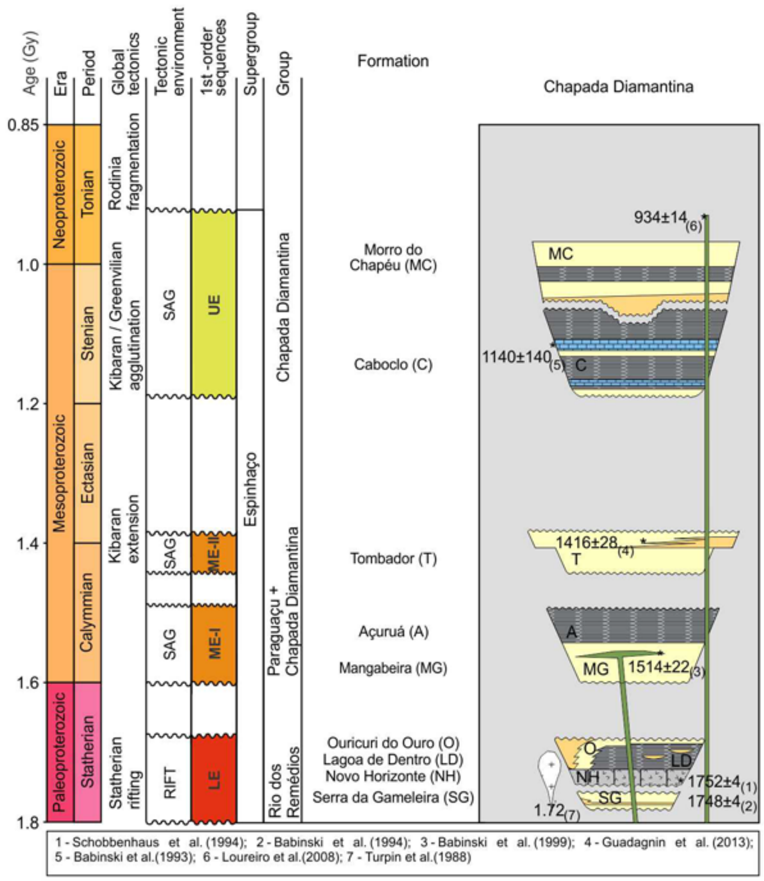

Fig. 3.2. Stratigraphic Chart for the Chapada Diamantina basin as well as the relationship of the Tombador Fm. and adjacent lithostratigraphic units (modified from Guadagnin et al., 2015).

3.3. Methods

This study was carried out mostly on the eastern flank of Pai Inácio anticline (Fig. 3.1) where the structural dip hardly exceeds 15°. A total of 1,138 metres of rock succession was described. Facies description was done at the scale 1:40 to assure high-resolution data such as lithology, grain size, sedimentary structures, paleocurrent direction, and structural strike and dip measures. Paleocurrent data were measured from cross-strata in sandstone bodies. Spectral gamma ray logging was done with a portable radiation detector RS-230 on all vertical sections with 20 cm space sampling. Vertical gamma ray profile was plotted and compared with the facies description for each vertical section. In this study, the total count of gamma ray log was used qualitatively to differentiate sandstone from mudstone. Facies association (based on Miall, 1996) preceded interpretation of depositional processes and systems. Vertical sections and GR logs calibrated the location of stratigraphic surfaces and the interpretation of depositional geometries on seismic-scale photomosaic and cross-section.

3.4. Facies associations

Facies description is based on lithology, grain size, and sedimentary structures. The description and interpretation of facies and facies associations are given in Table 1 and Figs. 3.3, 3.4, and 3.5. The various facies associations occur as roughly tabular sand-dominated strata, which can be interpreted in sequence stratigraphic terms. Depositional sequence boundaries are placed at the base of extensive amalgamated fluvial sand sheets while maximum regressive surfaces are marked at the contact between fluvial sand sheet and estuarine or between fluvial sand sheet and sand-rich floodplain intervals. Thus, five depositional sequences are identified at the studied interval, which are mainly composed of lowstand (fluvial) and transgressive (estuarine or sand-rich floodplain) systems tracts. However, the description and discussion of stratigraphic sequences in the Lower Tombador Fm. is beyond the scope of this paper. The following facies associations (Table 2) were identified in the Lower Tombador Fm.:

3.4.1. Sand-bed braided fluvial facies association (SBB)

3.4.1.1. Description

This facies association mainly consists of trough-cross stratified sandstone (facies St, Fig. 3.3A) and minor low angle cross-stratified (facies Sl), tabular cross-stratified (facies Sp), and massive (facies Sm) medium-grained to granular sandstone. Centimetric (up to 5 cm) subangular mud clasts are found in some strata. St facies exhibits uniform grain size or fining-upward trend, and is organized in cosets, each composed of 2 to 5 sets of decimeter-scale cross-strata. Bounding surfaces of cosets delineate meter-scale lenticular bodies, and are marked by changes in thicknesses and grain size. Such surfaces are slightly flat to concave-up rarely exceeding 1 m in relief, often erosional. Sometimes it is preceded by scours filled with cross-bedded granular sandstone. At the top, some sandstone bodies exhibit asymmetric, centimeter-scale ripple marks and horizontally laminated (facies Sh) laterally discontinuous, thin (up to 0.5 m thick) sandstone beds.

The SBB is characterized by the homogeneity of facies and the abundance of low-hierarchy erosional surfaces (Fig. 3.6). The large-scale geometry of the SBB suggest the architecture is dominated by several meters thick units that are fairly tabular and laterally continuous for more than 1000 m in directions both parallel to perpendicular to main dips of cross-beds. Paleocurrent directions obtained from cross-strata point to a main southwestward axial flow. The lower and upper contacts of SBB are, respectively, erosional and sharp with the adjacent units.

3.4.1.2. Interpretation

The occurrence of sandstones bodies with trough cross-stratification bounded by erosive surfaces with coarse grains lying above them suggests deposition of fluvial channels (Collinson, 1996). These erosive surfaces are interpreted as the thalweg of the main channels (5^o order surface of Miall, 1996). Lenticular to roughly tabular sandstone bodies composed of cross-stratified strata are interpreted as accreting bedforms deposited inside fluvial channels. The uniformity of this facies association indicates the preferential preservation of channel and fluvial bar deposits. Amalgamated sandstone beds bounded by low relief erosive irregular surfaces suggests such surfaces more likely represent accretion surfaces, which implies that succeeding flood events resulted in aggradation of macroforms rather than erosion of previous deposits. The intraformational mud clasts are related to erosion of the overbank area during lateral channel migration, and their subsequent redeposition to form channel lag. Finer-grained laminated sandstone is interpreted as bar-top deposits or bar-flank sand sheet that accumulated in the shallowest part of channels under upper flow regime (Smith, 1972; Cant & Walker, 1978; Miall, 1985). The predominant fairly tabular large-scale geometry resulted from amalgamation of broad and shallow braided channels deposits, which likely occupied the full width of the floodplain that are typical of shallow sand-bed braided river (Miall, 1996).

Table 3.1. Description and interpretation of the sedimentary facies comprising the Lower Tombador Fm.

Facies	Code	Description	Interpretation
Trough cross-stratified sandstone	St	Light cream to light red, fine- to very coarse-grained, locally granular sandstone; with medium- to small-scale trough cross-stratification and ripple marks. This facies occurs as lenticular to sheet-like beds up to 1.5 m thick	Migration of sinuous-crested subaqueous bedforms (3D), lower flow regime
Trough cross-stratified eolian sandstone	Ste	Light gray, fine- to coarse-grained, bimodal sandstone with medium- to large-scale trough cross-stratification. Common structures include grain flow and grain fall. Usually occurs as isolated bed up to 1.5 m thick.	Migration of sinuous-crested eolian bedforms (3D), lower flow regime
Tidal bundled sandstone	Stt	Light cream, gray and light red, fine to medium-grained sandstone with tidal bundle, reactivation surfaces and mud couplets. Tidal bundle commonly exhibit thickness variations of forests and sets bounded by mud layers. Usually occurs as lenticular to sheet-like beds up to 1. 5 m.	Migration of sinuous-crested subaqueous bedforms (3D) under tidal indluence; lower flow regime (Visser, 1980)
Planar cross-stratified sandstone	Sp	Light gray, fine- to coarse-grained sandstone with medium- to small-scale tabular cross-stratification in up to 0.5 m thick beds.	Migration of straight-crested subaqueous bedforms (2D); lower flow regime
Low angle laminated sandstone	Sl	Light gray, fine- to coarse-grained sandstone with low angle lamination (<15^{o}). Usually forms centimetric beds with supercritical ripples on top	Planar bedding generated under upper flow regime, or migration of bedforms with a high wavelength / amplitude ratio in conditions transitional between lower and upper flow regime.
Massive sandstone	Sm	Light cream to light gray, fine- to coarse-grained structureless sandstone. This facies occurs as decimetric layers sometimes with faint stratification.	Deposition from hyperconcentrated flows or obliteration of primary structures by diagenesis
Horizontally laminated sandstone	Sh	Light gray and reddish, very fine- to medium-grained sandstone with horizontal lamination that forms sheet-like bed up to 0.5 m	Planar bedding generated under upper flow regime
Inverse graded laminated sandstone	She	Light gray, very fine- to medium-grained sandstone with horizontal lamination, inverse grading and granular ripple, composing up to 70 cm thick beds.	Planar bedding generated under upper flow regime, or migration of eolian bedforms with a high wavelength / amplitude ratio
Ripple cross-laminated sandstone	Sr	Light cream to light gray, very fine- to fine-grained sandstone, with ripple cross-lamination and ripple marks. Usually occurs as discrete layers on top of fining upward succession of medium- to fine-grained sandstone (facies St, Sl or Sh)	Subcritical to supercritical ripples migration under uni- or bidirectional flow; lower flow regime

Table 3.1. (continued)

Facies	Code	Description	Interpretation
Heterolithic mudstone and sandstone	He	Intercalation between laminated sandstone and mudstone in millimetric to centimetric layers. Sandy strata are massive, planar laminated, or with ripple marks with deposition of mudstone in the ripple troughs. Mudstone exhibits wavy lamination. Centimetric layer of medium-grained sandstone with granules scattered occurs at the base. This facies forms sheet-like beds up to 3 m thick with broad lateral extent which can commonly be traced over 1000 m	Alternation between deposition from traction and from suspension followed by wave reworking. Medium-grained sandstone with granules scattered is interpreted as transgressive lag (Posamentier and Vail, 1988)
Laminated mudstone	Fl	Light green and reddish, laminated claystone interbedded with siltstone that occur as discrete centimetric layers between Stt facies beds. Common structures include lenticular and wavy bedding	Deposition from suspension and weak bottom currents
Massive siltstone	Fm	Light green, gray and reddish, massive or faint horizontally laminated siltstone. Usually occurs as discrete up to 0.4 m thick layers on top of fining upward succession of medium- to fine-grained sandstone	Deposition from suspension and weak tractive flows

Table 3.2. Description and synthesis of the facies associations found in the Lower Tombador Fm.

Facies Association	Code	Facies components	Description	Gamma ray pattern	Paleocurrent	Interpretation	Depositional setting
Sand-bed braided fluvial	SBB	St Sp Sh Sm Fm	Sheet-like to poorly channelized sandstone bodies up to 3 m thick that extend over and tens to hundreds of meters; basal surfaces concave up, erosional, or flat, top sharp; composed of stacked sets arranged into uniform grain size or fining-upward cycles	Blocky, low values	Unidirectional, mainly to the SW	Poorly channelized braided fluvial characterized by discharge fluctuations with deposition of lower-stage bedforms during peak flow and erosion of bottom surface and subsequent deposition in transitional to upper stage flow in poorly confined shallow currents	Fluvial braidplain
Intermediate sheet flood	ISF	St Sl Sm Sp Ste Sr	Sheet-like sandstone bodies up to 10 m thick that extend over tens to hundreds of meters; internally arranged into amalgamated uniform to fining-upward successions mostly formed by facies Sl	Blocky, low values	Unidirecional, predominantly to NW	Deposition from high-energy flash flood, unconfined sheets and poorly defined fluvial channels. Localized wind reworking forming isolated dunes	Fluvial braidplain
Sand-rich floodplain (intermediate/ distal sheet flood)	SFP	Sl Sh She Sm Sr Fm	Sheet-like sandstone bodies up to 14 m thick that extend over tens to hundreds of meters; internally composed of fining-upward successions of facies Sl, Sh, Sr to Fm and presence of discrete eolian layers and isolated eolian dunes	Serrate, with higher values in front of siltstone layers	Unidirectional, mainly to N-NW	Deposition of distal ephemeral flash floods. The fining-upward successions reveal the cyclical nature of the deposits, in which initial higher energy floods rapidly reach the waning stage. It represents a downstream equivalent to ISF	Fluvial braidplain

Table 3.2. (continued)

Facies Association	Code	Facies components	Description	Gamma ray pattern	Paleocurrent	Interpretation	Depositional setting
Tide-influenced sand-bed braided fluvial	TSB	St Sp Sh Sm Sr Fm	Sheet-like to poorly channelized sandstone bodies up to 3 m thick that extend over and tens to hundreds of meters; basal surfaces concave up, erosional, or flat, top sharp; composed of stacked sets arranged into uniform grain size or fining-upward cycles. Presence of small scale trough-cross bedding and asymmetric ripples oriented (to SE/NE), against the main paleoflow	Not logged	Mainly to SW/NW and subordinately to SE/NE	Poorly channelized braided fluvial characterized by tidal influence	Inner estuary
Tidal sand-flat	TSF	St Sh Sr Sm	Sheet-like sandstone bodies up to 2 m thick that extend over tens of meters; internally composed of centimetric sets with sharp, slightly undulating, erosive bases and frequently with alternation of facies Sh and Sr	Not logged	Predominantly to NW and subordinately to NE-SE	Deposition in high energy tidal sand flat. Facies St are interpreted as formed under upper flow regime associated to dominant (ebb) tide while facies Sr are interpreted as formed during lower flow regime associated both to dominant and subordinate tides	Tidal flat
Tidal channel	TCH	St Sp Sm Fl	Amalgamated lenticular to sigmoidal sandstone bodies bounded by mud drapes that form up to 5 m thick succession with channel-like shape; concave up erosive basal surface truncates TB or SHF; TCH is usually overlain by TB and occasionally by SHF	Blocky, low values	Mainly to the NW and subordinately to the SE	Deposition filling tidal channels which cut tidal bars and shoreface deposits	Inner estuary

Table 3.2. (continued)

Facies Association	Code	Facies components	Description	Gamma ray pattern	Paleocurrent	Interpretation	Depositional setting
Tidal bar	TB	Stt St Sm Fl	Lenticular bodies up to 2.5 m thick that extend laterally over tens of meters; internally composed of sets of facies Stt bounded by mud drapes; individual sets exhibit fairly symmetrical ripples on top. Also, elongated coarse-grained sandstone bodies interbedded with thin heterolithic strata that compose up to 7 m thick intervals truncated at the top by SBB	Serrate, higher peaks in front of mudstone layers	Mainly to NW and subordinately to NE/SE	Subtidal deposition of tidal bar deposits, which are characterized by recurrence of sandstone beds with tidal bundle, mud drapes and reactivation surfaces	Outer estuary
Shoreface	SHF	St Sm Sr He Fl	Sheet-like heterolithic bed up to 3 m thick and broad lateral extent that can be traced over 1000 m	Serrate, high values	--	Shoreface deposition and accumulation from suspension and or traction	Shallow marine

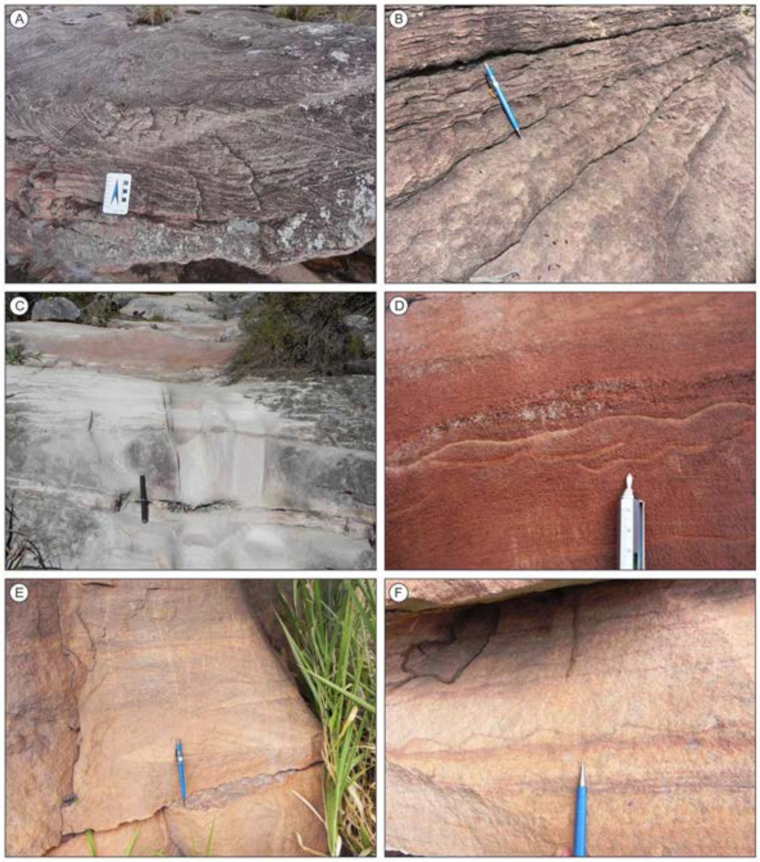

Fig. 3.3. Photos of selected examples of fluvial-related facies. A) trough cross-bedding in sand-bed braided fluvial strata; B) laminated sandstone with supercritical ripples on top; C) fining-up succession of medium- to fine-grained sandstone to siltstone; D) fine-grained sandstone with granular ripples and mud drapes; E) trough cross-bedded sandstone; F) at the top of sandstone from photo E, asymmetric ripples are oriented to the opposite direction of fluvial paleoflow.

3.4.2. Intermediate sheetflood facies association (ISF)

3.4.2.1. Description

This facies association is mainly composed of sandstone with low angle-cross stratification (facies Sl, Fig. 3.3B) and minor massive (facies Sm), trough cross-stratified (facies St), tabular cross-stratified (facies Sp) medium- to very coarse-grained sandstone with granules dispersed, and ripple cross-laminated (facies Sr) medium- to fine-grained sandstone. Sl sandstone is organized in cosets that delineate large-scale tabular bodies. Internally, 2 to 10 cm thick sets exhibit supercritical ripples on the top and flat, horizontal to low angle slightly erosive basal bounding surface. Sm, St, and Sp sandstones form isolated, up to 1 m thick beds composed of structureless and medium-scale planar and trough-cross bedded cosets. Sr sandstone occurs as thin (up to 0.3 m thick) strata on top of Sl or Sp intervals, usually with fining upward trend overlain by discrete (less than 0.4 m thick) massive mudstone beds. Isolated medium-scale trough cross-bedded medium-grained sandstone with grain flow and grain fall (facies Ste) is found in some vertical sections. Bounding surfaces are horizontal to low-angle, slightly erosive, and marked by changes of facies.

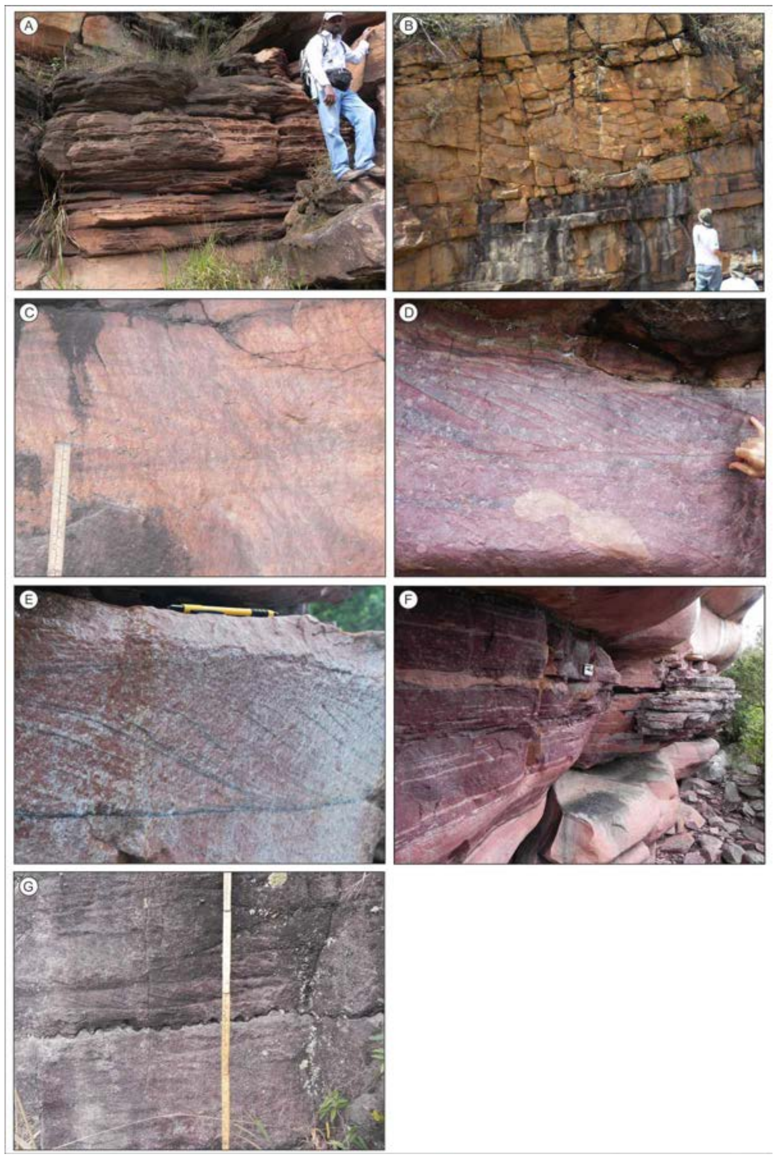

Fig. 3.4. Photos of selected tidal facies and shoreface. A) medium- to coarse-grained laminated sandstone; B) Lenses of sandstones filling tidal channel (lateral accretion?); C) those lenses are formed of tangential to trough cross-bedded sandstone; D, E) tidal bundles and reactivation surfaces in well cemented medium-grained sandstone; F) reddish heterolithic; G) facies very coarse-grained trough cross-bedded sandstone with stylolites.

The geometry of the larger-scale strata of ISF suggests the dominance of amalgamated tabular bodies less than 15 m thick (Fig. 3.7) that are laterally continuous for more than 100 m. Paleocurrent directions obtained from cross-strata show wide dispersion from southwest to northeast with main direction to northwest. The lower and upper contacts of ISF are, respectively, erosional and sharp with the adjacent units.

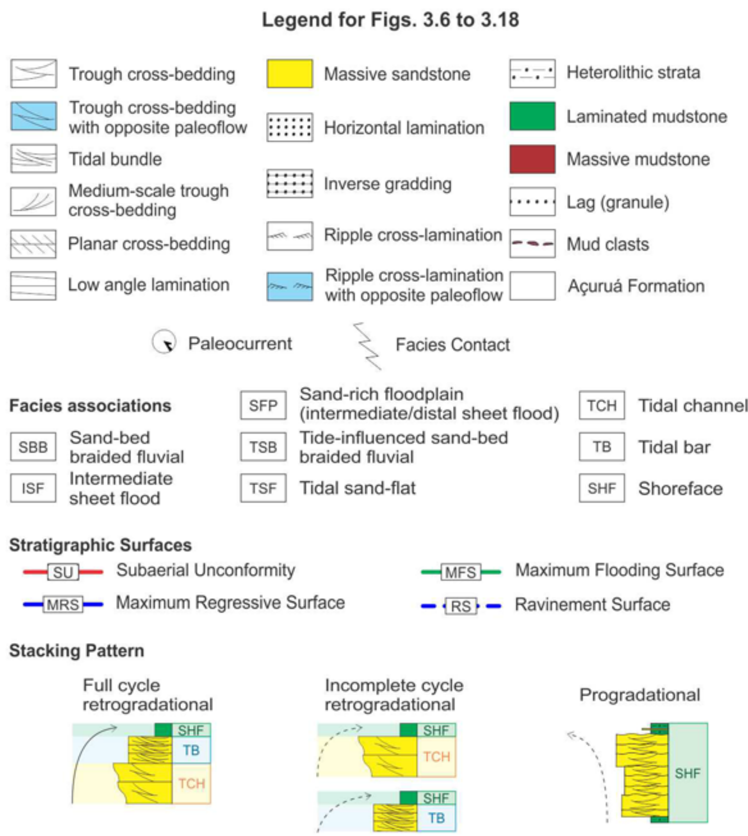

Fig. 3.5. Legend for Figs. 3.6 to 3.18.

3.4.2.2. Interpretation

The tabular sandbodies with a slightly undulating erosive base and the predominance of low-angle cross-bedded sandstones are interpreted as the result of high-energy flood deposition, unconfined sheets and poorly defined fluvial channels (Nemec and Postma, 1993; Blair, 2000). Thin, sheet-like bodies composed of laminated sandstones are interpreted as the result of a series of ephemeral unconfined sheetfloods, which quickly decelerate at the end of the flow and hence allow development of supercritical ripples (Turnbridge, 1981; Hampton & Horton, 2007). Tabular sandstone bodies with medium size trough cross stratification (St) represents the migration of sinuous-crested simple sand bars, indicating fluctuations on the flow regimen between the floods. Massive sandstones (facies Sm) are interpreted as resulting from transport and deposition of sediments by short-lived high-density flows, which are responsible for dumping sediments at a rate too fast for hydraulic sorting processes to work effectively. The high-density flow is probably maintained in suspension by the combined effect of turbulence, buoyant support and dispersive pressure (Lowe, 1988). Medium-scale trough cross-bedded sandstone with grain flow and grain fall is interpreted as isolated eolian dune.

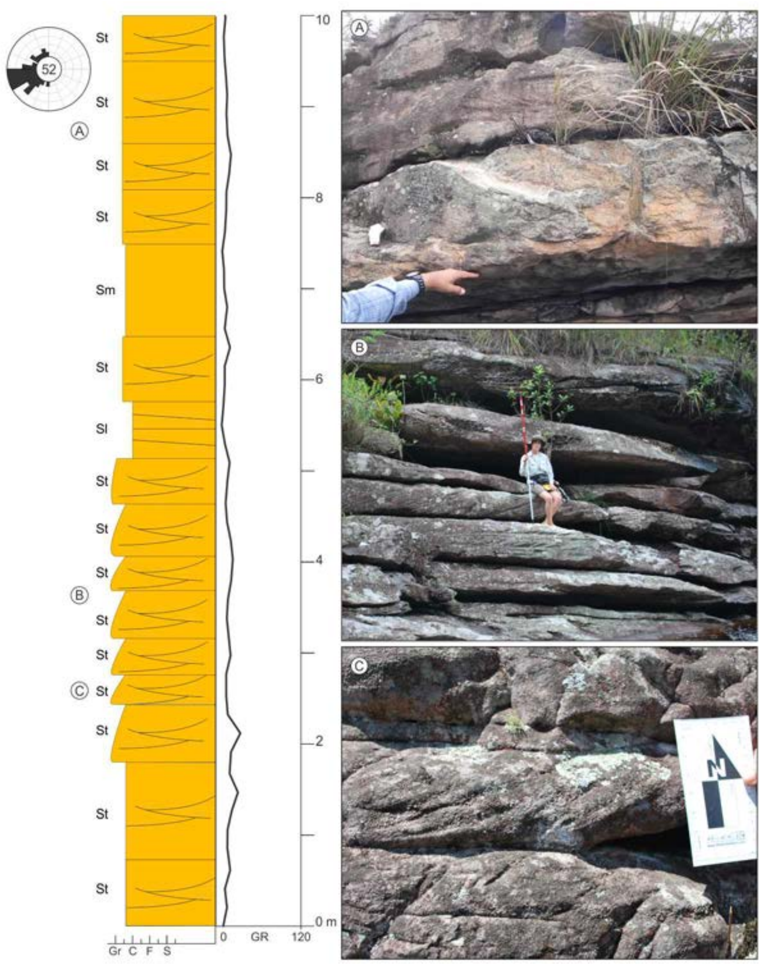

Fig. 3.6. Representative example of Sand-bed braided fluvial facies association (SBB). Facies code and location of diagnostic photos are given at the left of the column.

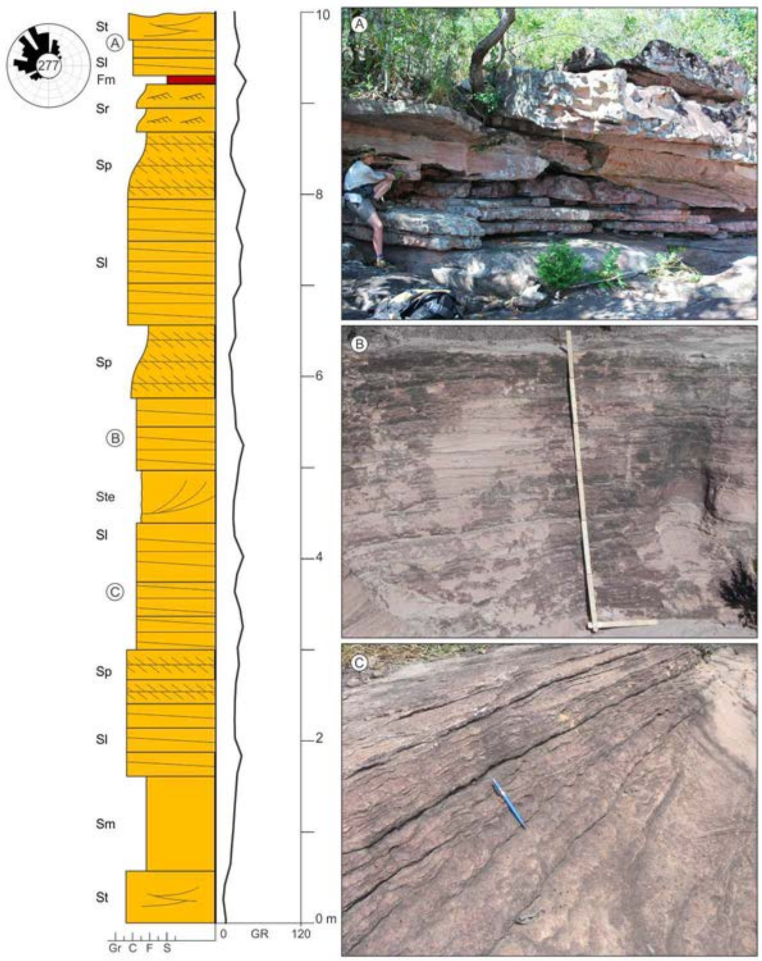

Fig. 3.7. Representative example of Intermediate sheetflood facies association (ISF). Facies code and location of diagnostic photos are given at the left of the column. Note the scarcity of mudstone.

3.4.3. Sand-rich floodplain: intermediate/distal sheetflood facies association (SFP)

3.4.3.1. Description

This facies association is characterized by uniform grain size or fining upward successions of medium- to fine-grained sandstone to siltstone. Individual fining upward succession is about 1.40 m thick, capped by mud drapes or siltstone layers up to 0.4 m thick (Fig. 3.3C). Sandstone is massive (facies Sm), laminated (facies Sh) or low angle cross-stratified (facies Sl), trough cross-bedded (facies St), and ripple cross-bedded (facies Sr) capped by mud drapes. Fine-grained laminated sandstone with inverse grading and granular ripples (facies She) up to 70 cm thick forms discrete layers interbedded with fine grained-sandstone and mudstone (Fig. 3.3D). Siltstone is massive, commonly interbedded with facies She, or on top of fining-upward successions. Bounding surfaces are planar and sharp, marked by changes in grain size or in sedimentary structures of adjacent facies.

The large-scale geometry of SFP indicates it constitutes tabular body up to 14 m thick, with flat and non-erosive basal surface, that is laterally continuous for hundreds of meters (Fig. 3.8). Paleocurrent readings exhibit wide dispersion, but the main vector points northward. The lower and upper contact of SBB are, respectively, sharp and erosional with the adjacent units.

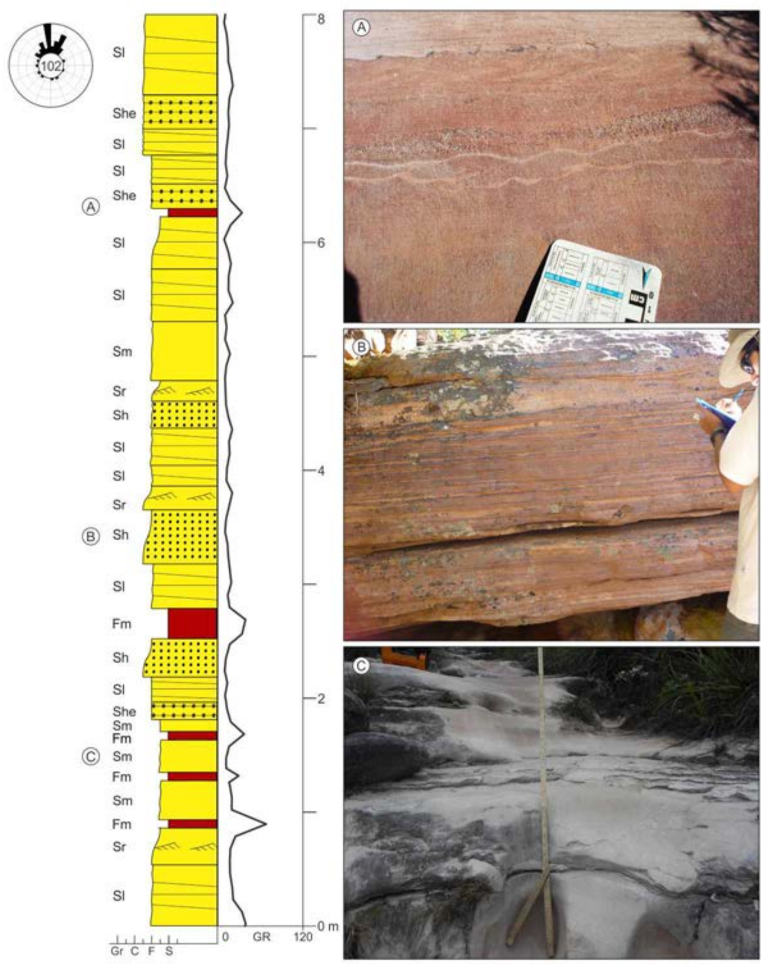

Fig. 3.8. Representative example of Sand-rich flood plain (distal sheetflood) facies association (SFP). Facies code and location of diagnostic photos are given at the left of the column. Note the granular ripples and mud drapes on photo A.

3.4.3.2. Interpretation

Laterally extensive tabular sandstone beds composed of fining up successions indicate deceleration of ephemeral unconfined or poorly-confined sheetfloods (Turnbridge, 1981;

Hampton & Norton, 2007) that rapidly decreased their energy before finally dissipating to enable deposition of fine-grained sediments (Williams, 1971). This facies association is characteristic of distal braid plains, particularly in arid regions where ephemeral runoff forms a network of shallow, interlacing, possible poorly defined channels (Miall, 1986). Interbedding of ephemeral sheetflood deposits and sandstones with inverse grading and granular ripples suggests eolian reworking and deposition. Eolian sand sheet sandstones, siltstones beds, and mud drapes are strong evidence of high water table level because the capillarity effect of the rising water table traps sand and favors mud and eolian sand sheet sandstones deposition (Tirsgaard & Øxnevad, 1998). The occurrence of distinct sand-rich floodplain intervals on top of the previous fluvial facies associations (SBB and IFF) reinforces changing on depositional conditions (Marconato et al., 2013).

3.4.4. Tide-influenced sand-bed braided fluvial facies association (TSB)

3.4.4.1. Description

This facies association consists of medium-grained to granular trough cross-stratified sandstone ripple marks, and minor low angle cross-stratified (facies Sl), massive (facies Sm), and ripple cross-laminated (facies Sr) sandstone (Fig. 3.3E, F). Centimetric (up to 5 cm) subangular mud clasts occur dispersed in the matrix. St sandstone exhibits uniform grain size or fining-upward trend, and form cosets, each composed of 2 to 5 sets of decimeter-scale cross beds whose bounding surface are slightly flat to concave-up rarely exceeding 1 m in relief, delineating large scale lenticular bodies. Bounding surfaces of cosets are marked by changes in thicknesses and grain size, and are often erosional. At the top, some cosets exhibit asymmetric centimeter-scale ripple marks.

The TSB is characterized by the homogeneity of facies and the abundance of low-hierarchy erosional surfaces (Fig. 3.9). The large-scale geometry of the SBB suggest the architecture is dominated by several meters thick units that are fairly tabular and laterally continuous for more than 1000 m in directions both parallel to perpendicular to main dips of cross-beds. Paleocurrent directions obtained from cross-strata point to a westward flow; less frequent small-scale trough cross-bedding and asymmetric ripples oriented to southeast are also found. The lower and upper contact of TSB is transitional; with the adjacent units.

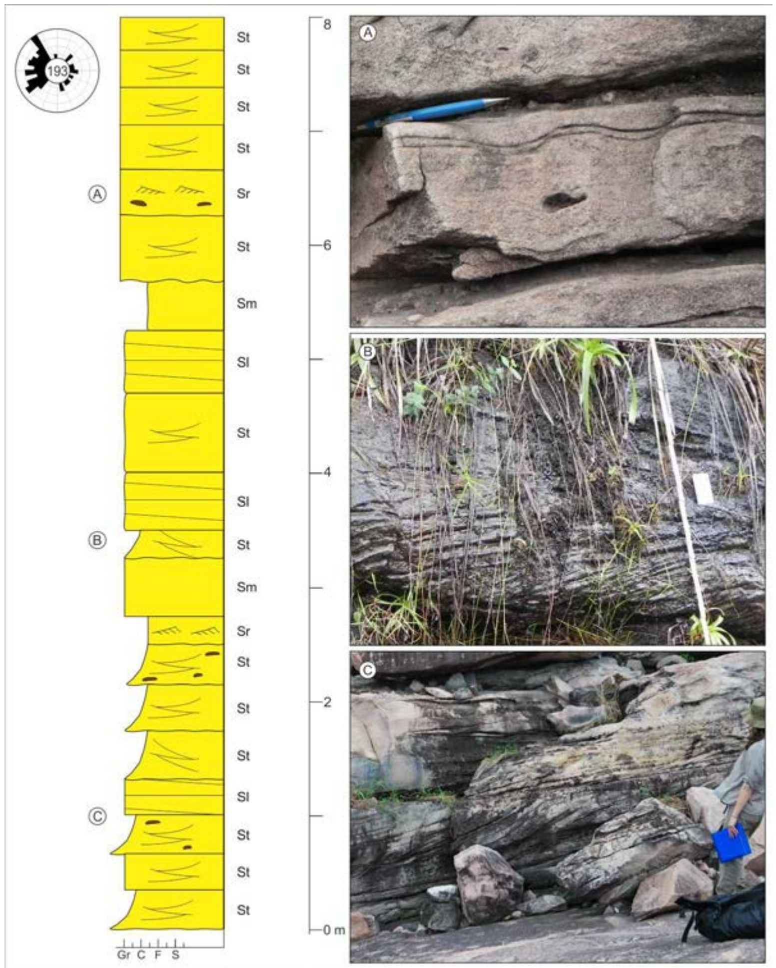

Fig. 3.9. Representative example of Tide-influenced sand-bed braided fluvial facies association (TSB). Facies code and location of diagnostic photos are given at the left of the column. Note the mud clast mould and the asymmetric ripple oriented to the opposite direction of the main fluvial paleoflow (in this case given by planar cross-bedding above the pencil, photo A).

3.4.4.2. Interpretation

The occurrence of cross-stratified sandstones bodies with mud clasts, fining-upward grain size trend, predominant paleocurrent direction, and frequent internal erosive surfaces suggest deposition in fluvial channels (Bristow, 1993; Collinson, 1996). The multiple erosion surfaces indicate repeated episodes of cut and fill. However, asymmetric ripples and trough cross-strata with opposite paleocurrent direction relative to the main fluvial paleoflow indicate reverse currents, strong evidence that shallow sand-bed braided channels were reworked by tides as the fluvial system debouched into the sea (Eriksson & Simpson, 2004).

3.4.5. *Tidal sand flat facies association (TSF)*

3.4.5.1. *Description*

This facies association is dominated by amalgamated sand sheet internally composed of horizontal laminated (facies Sh), ripple cross-laminated (facies Sr) sandstone, and trough cross-bedded sandstone (facies St). Sandstone is coarse- to medium-grained, arranged in individual beds with sharp, slightly undulating, erosive bases. Sets are centimetric (up to 0.2 m thick), characterized by successions of Sh overlain by Sr sandstone up to 1 m thick. St strata are 0.5 – 0.8 m thick, interbedded with Sh-Sr successions (Fig. 3.4A).

The TSF is characterized by up to 10 m thick tabular packages (Fig. 3.10), which are laterally continuous for hundreds of meters. Paleocurrent readings point westward and subordinately eastward. The lower and upper contacts are sharp to erosive with the adjacent units.

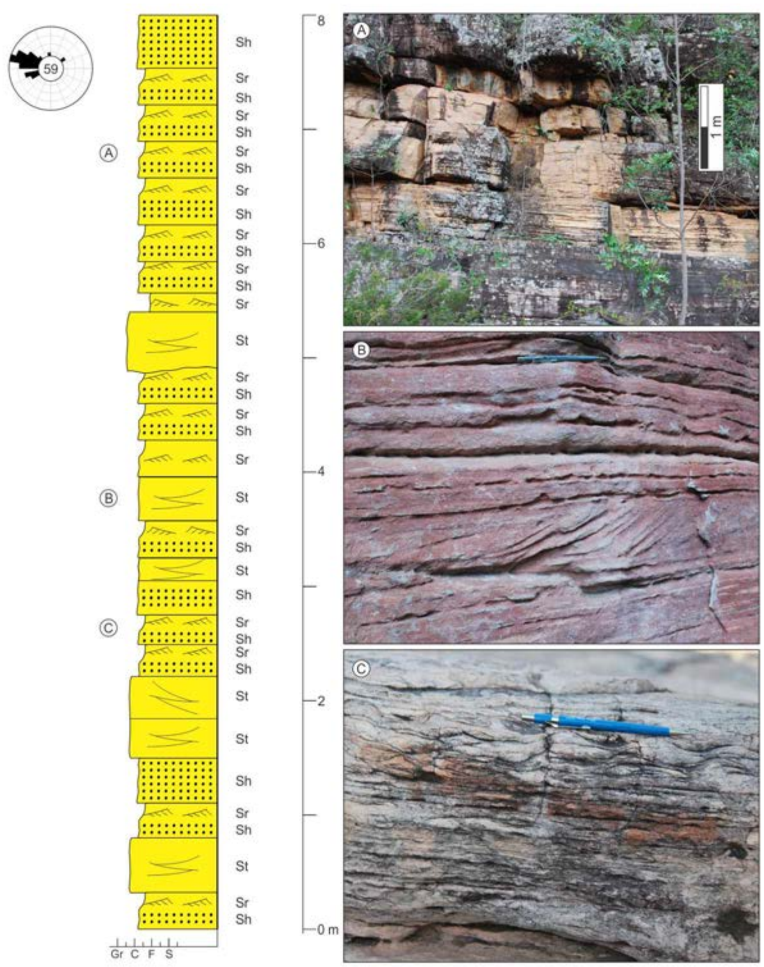

Fig. 3.10. Representative example of Tidal sand flat facies association (TSF). Facies code and location of diagnostic photos are given at the left of the column.

3.4.5.2. Interpretation

The occurrence of sandstones with bidirectional paleoflow direction suggests deposition under tidal influence (Eriksson & Simpson, 2004). Horizontal parallel laminated sandstones succeeded by ripple cross-laminated sandstones with bidirectional paleoflow are common in high-energy tidal sand flats (Dalrymple et al. 1985, 1990; Dalrymple, 1992; Plink-Björklund, 2005). The horizontal laminated sandstone are interpreted as deposits formed in upper flow regime associated with the main tides, and the ripple cross-laminated sandstones are interpreted as formed in lower flow regime derived from subordinate tide currents. Upper-flow-regime parallel lamination predominates in the shallower parts of the outer (tide-influenced) straight reach of the estuary (Boyd et al., 2006). Tidal sand flats are formed under upper-flow-regime because, on average, tidal-current speed increases into the estuary so that the area headward of the elongated bar is characterized by extensive sand flats with parallel lamination (Dalrymple, 2010). The trough cross-bedded sandstone more likely represents migration of sinuous crested dunes deposited during tide flows.

3.4.6. Tidal channel facies association (TCF)

3.4.6.1. Description

The TCH is characterized by the channel-like external geometry (Fig. 3.11), which is tens of meters wide and up to 5 m deep on direction approximately perpendicular to the main paleoflow. This facies association consists of amalgamated lenticular sandstone bodies that fill the channel scours (Fig. 3.4B). Internally, sandstone is medium- to coarse-grained, mostly with tangential and trough cross-bedding (Fig. 3.4C, facies St) and less frequently with planar cross-stratification (facies Sp), low angle cross-bedding (facies Sl) and structureless (facies Sm). Some sandstone strata exhibit contorted lamination, dish and pillar structure. Mud drapes are common between the foresets and sets of sandstone are bounded by laminated to massive mudstone, which forms lenticular layers up to 0.1 m thick that extend laterally for some meters. The channel shape fill is complex, with internal scours filled by sandstone lenses and mudstone drapes; in some cases lenticular sandstone bodies are organized in sigmoidal, laterally succeeding bodies whose toesets are tangential to the basal channel scour. In most cases sigmoidal bodies exhibit cross-bedded strata oriented perpendicularly to the sigmoidal bounding surfaces.

The channel bottom surface is clearly concave up and erosional while the upper contact is flat with the adjacent units. Paleocurrents are bidirectional mainly in the westward direction.

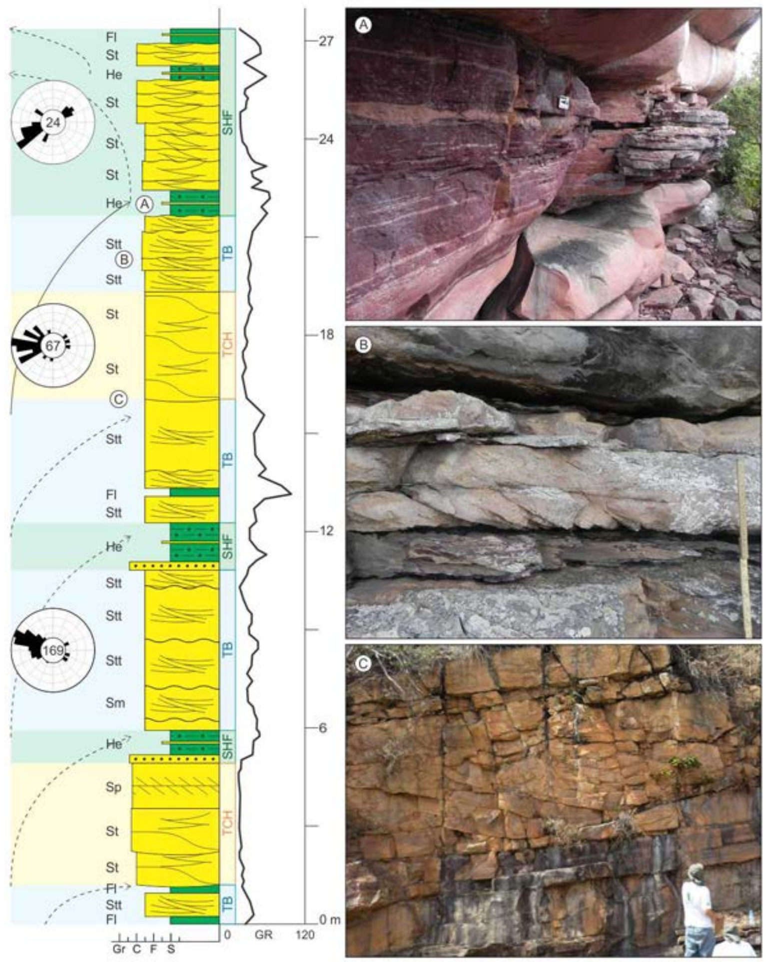

Fig. 3.11. Representative example of Tidal channel (TCH), Tidal (TB), and Shoreface (SHF) facies associations. Facies code and location of diagnostic photos are given at the left of the column. The vertical section is characterized by several incomplete retrograding stacking (dashed arrows) of TCH/TB/SHF. Note the lenticular shape of sandstone filling a channel (photo C), tidal bundles (photo B), and the sheet like geometry of shoreface heterolithic strata (photo A).

3.4.6.2. Interpretation

The channel-like geometry, filled with sandstones lenses enveloped by mud drapes and bidirectional paleocurrent, suggest deposition filling tidal channels (Boyd et al., 2006). The lenticular sandstone bodies are interpreted as macroforms that fill the channels. Cross-strata with paleoflow approximately perpendicular to the sigmoidal bounding surfaces suggest lateral accretion bedding associated to tidal channels with high sinuosity (Dalrymple, 2010). The vertical thickness of 3 - 5 m is interpreted to be the maximum depth of the channels. The predominance of paleocurrents oriented westwards, the same direction of fluvial cross-strata, indicates ebb-tide was paleoflow dominant direction.

3.4.7. Tidal bar facies association (TB)

3.4.7.1. Description

This facies association consists of tangential cross-stratified and tidal bundled (facies Stt) fine- to coarse-grained sandstones (Figs. 4D, E), minor planar cross-stratification (facies Sp), and massive (facies Sm). Stt strata generally show reactivation concave down surfaces regularly spaced, mud drapes in the foresets and locally ripples climbing up the bottom part of and in opposite direction to that of the larger scale cross-strata. Simple or composed 1 to 1.5 m thick cross strata are superbly exposed in many sections. Simple cross strata have steeper dip (25 to 30^{o}) and foresets show different thickness in vertical section parallel to the paleoflow. Cross strata exhibit fairly symmetrical ripples on top and are bounded by mud drapes deposited on flat dipping surfaces that in the same direction of the cross strata or laminated to massive mudstone beds up to 0.4 m thick. Commonly sandstone elongated lenses are amalgamated to each other, forming up to 2.5 m thick elongated bodies that extend laterally for some tens of meters. Some sets exhibit truncated wavy lamination. At the upper portion of TB intervals coarse- to very coarse-grained trough cross-bedded sandstone (facies St), rich in mud clasts and stylolites (Fig. 3.4G), is arranged in tabular to elongated beds less than 0.8 m thick. Mud clasts are up to 4 cm long, sub-angular to sub-rounded.

The main characteristic of this facies association is its elongated lenticular shape filled with facies Stt and enveloped by mud drapes (Fig. 3.11). It forms fairly tabular bodies that extend laterally for hundreds of meters. Bidirectional paleocurrent readings indicate westwards main direction (N280^{o}) and eastwards subordinated direction (N130^{o}). The lower contact is flat to slightly erosive while the upper contact is commonly abrupt with the adjacent units.

3.4.7.2. Interpretation

The occurrence of cross-stratified sandstones with bidirectional paleocurrents, tidal bundles, mud drapes in the foresets, reactivation surfaces, and ripples climbing up the foresets in opposite direction of the main paleoflow suggest development of subtidal sandstone bars (Dalrymple, 2010). The presence of relatively frequent fairly symmetrical ripples on top of cosets is evidence of wave reworking. Cosets bounded by low angle surfaces more likely indicate dunes migration on top of tidal bars. Reactivation surfaces on cross strata indicate changing in the frontal face of subaqueous sand dune in response to variation in the direction of tidal currents and hence, erosion on top of bars (Shanley et al., 1992). Thin mud drapes capping foresets are the product of suspended mud settling during the slack-water phase between the tides (Visser, 1980). Thickness variations of foresets in vertical section parallel to the flow may be related to neap-spring-neap moon cycles (Visser, 1980). Bidirectional paleocurrents reflect opposite direction of tidal currents, ebb-tide being the most frequent direction (westwards, based on SBB paleocurrents).

3.4.8. Shoreface facies association (SHF)

3.4.8.1. Description

This facies association consists of heterolithic strata (facies He) that are composed of interbedded mudstone and sandstone (Fig. 3.4F). Mudstone is mostly wavy-laminated claystone and siltstone (facies Fl). Sandstones are fine- to medium-grained, massive (facies Sm), or with ripple cross-lamination (facies Sr). The base of heterolithic strata is marked by thin (less than 0.3 m thick) granular to very coarse-grained sandstone layer, with irregular to flat basal erosive surface.

The SHF consists of very distinctive heterolithic tabular body up to 3 m thick that can be traced laterally for hundreds to thousands of meters. The bottom contact is sharp and erosive while the upper contact is abrupt to slightly erosive with the adjacent units (Fig. 3.11).

3.4.8.2. Interpretation

Heterolithic strata with tabular geometry and abrupt to gently erosive basal contact are interpreted as transgressive lower shoreface deposits overlying tidal bars or tidal channel. Laminated and massive mudstone was deposited from suspended mud settling (McCormick & Grotzinger, 1993). Sandstones and mudstones with wavy ripples are interpreted as deposited on lower shoreface above the normal wave base level (Simpson et al., 2002). Wavy truncated lamination corroborates the wave activity on shoreface during deposition of this facies association. The very coarse-grained to granular layers on the base represent transgressive lags formed by wave ravinement surface during transgressions (Bruun, 1962; Swift et al., 1972; Swift, 1975; Nummendal & Swift, 1987, Dominguez & Wanless, 1991).

3.5. Depositional settings and the unincised character of the Lower Tombador Formation – Discussion

The Lower Tombador is mainly composed of fluvial and tide-dominated successions (Table 2) that are herein discussed in terms of depositional systems.

3.5.1. Fluvial braidplain

It is widely recognized that Precambrian channel systems were braided in all environments (deltaic, tidal, alluvial, and fluvial) as a consequence of lack of vegetation and poor soils development, which in turn promoted rapid runoff of surface water and high rate of channel migration compared to vegetated systems from the Phanerozoic (Cotter, 1978; Miall, 1996; Bose et al., 2012). In the Lower Tombador Fm. fluvial braidplain comprises 47% of the total succession and it is formed of SBB, ISF and SFP, a group of facies associations that is commonly found in other Precambrian fluvial braidplains (Schumm, 1968, 1977; Long, 1978; Sønderholm & Tirsgaard, 1998; Eriksson et al., 2004).

Composed SBB and ISF intervals are characterized by up to 35 m thick successions overlain by up to 20 m thick SFP deposits (Figs. 3.12, 3.13). Intercalation of SBB and ISF indicates fluvial sandstone aggradation under high variation of fluvial discharge. Sand-bed braided fluvial deposits are indicative of perennial or semi-perennial fluvial systems with low energy variations. Preferential oriented westwards paleoflow implies a source area located to the east. Unidirectional paleoflow, blocky stacking pattern, coarser grain size and minor mudstone interbeds suggest high degree of channel amalgamation (low accommodation rate) typical of topsets of lowstand systems tract. Lack of significant fluvial scours implies fluvial channels were entrenched (those that are inset within an active floodplain) rather than incised channels (those that have downcut and have become detached from their former floodplain, sensu Woolfe et al., 1998). In contrast, ephemeral sheetfloods are associated with flash, ephemeral and high energy floods similar to Bijou Creek model (Miall, 1996).

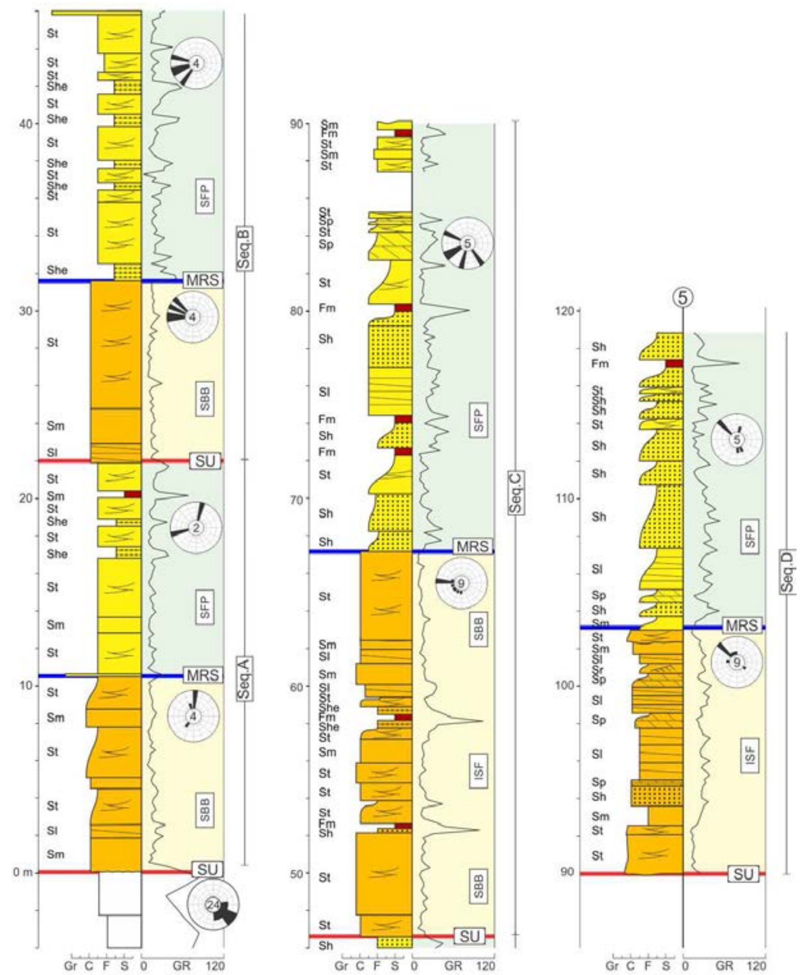

Fig. 3.12. Measured vertical section 5 exhibits sand-bed braided fluvial (SBB) and intermediate sheetflood (ISF) overlain by sand-rich floodplain (SFP). Erosive surfaces are sharp and flat, without evidence of fluvial scouring. Note SFP exhibits finer grain size, more frequent presence of mudstone, and serrate GR pattern compared with SBB/ISF. Sequences A-D are composed of lowstand SBB and transgressive SFP systems tracts. The subaerial unconformity at the base of Seq. A coincides with the angular unconformity between the Açuruá and the Tombador formations. Facies code is given at the left of the column. See location of vertical section on Fig. 3.1.

Sand rich floodplain intervals represent intermediate to distal, ephemeral sheetfloods that formed fine-grained subaqueous deposits and interbeds of eolian sand sheet**.** Mudstone intervals and localized thin eolian sand sheet intervals (Fig. 3.8) suggest low availability of dry sand, and thus indicates a depositional setting in which the water table was relatively high, and/or sheetfloods were frequent enough to hinder the capacity of transport and deposition by wind action (Kocurek et al., 1992). Such characteristics suggest sand-rich fluvial floodplain compose undifferentiated transgressive to highstand deposits.

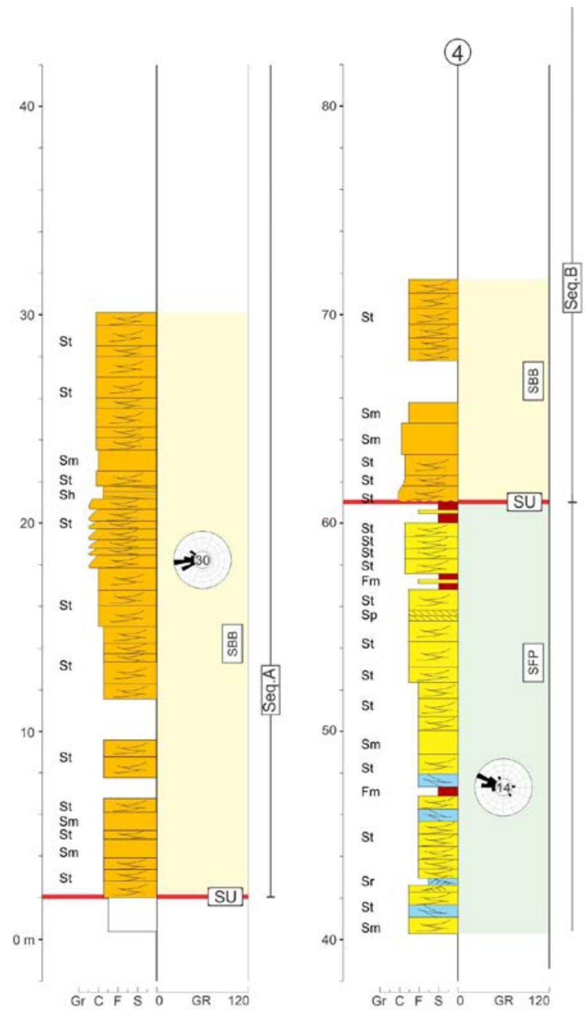

Fig. 3.13. Measured vertical section 4 exhibits sand-bed braided fluvial (SBB) and overlying sand-rich floodplain (SFP). Note trough cross-bedded sandstone from SFP with bimodal paleocurrent direction at 40 – 48 m interval. The subaerial unconformity at the base of Seq. A coincides with the angular unconformity between the Açuruá and the Tombador formations. Facies code is given at the left of the column. See location of vertical section on Fig. 3.1.

3.5.2. Tide-dominated estuary and shoreface

Tidal deposits are quite common in the Precambrian (Eriksson et al., 2004). In the Lower Tombador Fm. tidal deposits and shoreface comprise 33% of the total succession. The dominant presence of tidal deposits compared to deposits with oscillatory flows indicates a tide-dominated coast was connected to the fluvial braidplain. The facies associations indicate a paleogeography in which braided rivers reached the shoreline and provided sediments to be reworked by tides (TSF, TCH and TB). Such coastal configuration indicates two possibilities:

tide-dominated delta or tide-dominated estuarine systems. The distinction between them in the geological record is based on facies successions. Delta systems exhibit progradational stacking pattern, thus related to regressive coastlines (Dalrymple & Choi, 2007; Bhattacharya, 2010). In contrast, tide-dominated estuarine systems are characterized by retrogradational stacking pattern, and hence related to transgressive coastlines (Dalrymple, 2010). Vertical sections exhibit succession of tidal channel/tidal sand flat and tidal bar that are eventually overlain by shoreface heterolithic facies associations (Fig. 3.11). In the Tombador Fm., however, less than complete preservation is more likely. Such succession is clearly retrogradational and thus it is interpreted as transgressive tide-dominated estuarine system. Overlying some TSB successions, coarse-grained tidal sand bars and heterolithic strata exhibit conformable, thinning-upward pattern that is truncated on top by fluvial deposits (Fig. 3.14). This thinning-upward trend is interpreted as a response of reducing accommodation of the highstand systems tract, which is bounded at the top by a subaerial unconformity.

Overall, tidal and shoreface successions form tabular deposits. Such geometric characteristic suggests a coastal area connected to a wide and low gradient alluvial braidplan, whose distal deposits were reworked by strong tidal currents and formed tidal channels and tidal bars. Tidal sand flat were more likely deposited at portions of the coast without the fluvial influence (Fig. 3.15). During periods of transgression estuaries developed, tides extended their effects upstream on fluvial braidplain, and sand-rich floodplain aggraded.

Tidal reworking is a criterion that is unique to making a stratigraphic interpretation of the fluvial sequences at the Precambrian. Within the alluvial strata, the period of maximum flooding is not represented by a condensed section but is instead represented by the invasion of tidal processes into areas formerly dominated by purely fluvial processes (Shanley & McCabe, 1994). The action of tidal processes on the fluvial domain is represented by cross-strata and asymmetric ripples oriented to the opposite direction of the main fluvial paleoflow (Fig. 3.13). Thus, the tidal channel/tidal bar/shoreface successions deposited downdip in the estuary correlate to the sand-rich floodplain sediments deposited updip on the fluvial braidplain. The facies zonation on the Tombador Fm. estuarine systems is represented by shoreface, tidal bars, and tidal channels/tidal sand flat/tide-influenced fluvial, respectively.

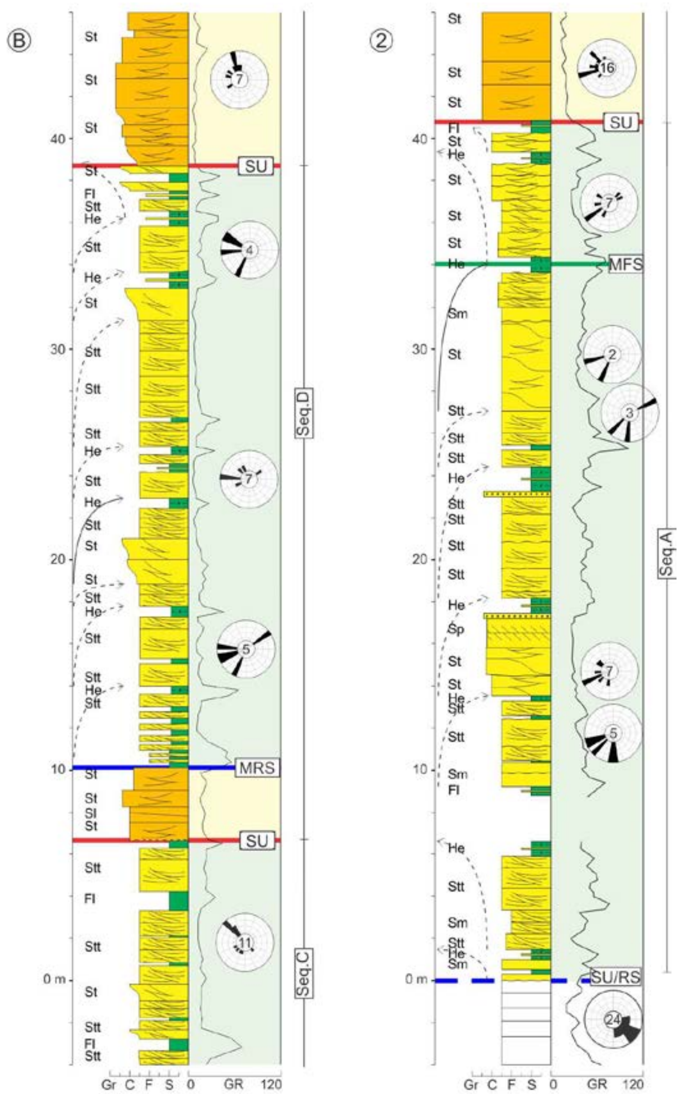

Fig. 3.14. Measured vertical sections B and 2 exhibit fluvial-estuarine successions. A complete estuarine succession (solid arrow) is formed by retrogradational stacking pattern defined by tidal channel - tidal bar - shoreface heterolithic strata. In the Lower Tombador Fm. less than complete preservation is more likely (dashed arrows). In this location, a ravinement surface at the base of Seq. A replaced the subaerial unconformity shown in Figs. 12 and 13 (the unconformity between the Açuruá and the Tombador formations). Facies code is given at the left of the column. See location of vertical sections on Fig. 3.1.

One aspect that differentiates the estuarine systems of the Lower Tombador compared to those from the Phanerozoic is related to lithological characteristics. Contrary to typically modern mud-rich tide-dominated coasts – in which feeding activity of benthonic organisms also contributes to the transformation of mud into pellets that are deposited on their original depositional locus - tide-dominated estuarine system from the Tombador Fm. exhibits low mud/sand ratio that is very similar to other Proterozoic successions (Tirsgaard, 1993; Eriksson et al., 1998). Nevertheless, the presence of tidal bundle with mud-draped foresets and heterolithic shoreface facies are direct evidence of mud deposition on tide-dominated estuarine system of the Lower Tombador Fm. Additional evidence of tidal processes were also observed, such as: (a) bipolar-bimodal pattern of paleocurrents in estuarine or fluvial succesions, (b) reactivation surfaces with sigmoidal geometry regularly spaced, and (c) systematic thicknesses variation of foresets that compose tidal bundles.

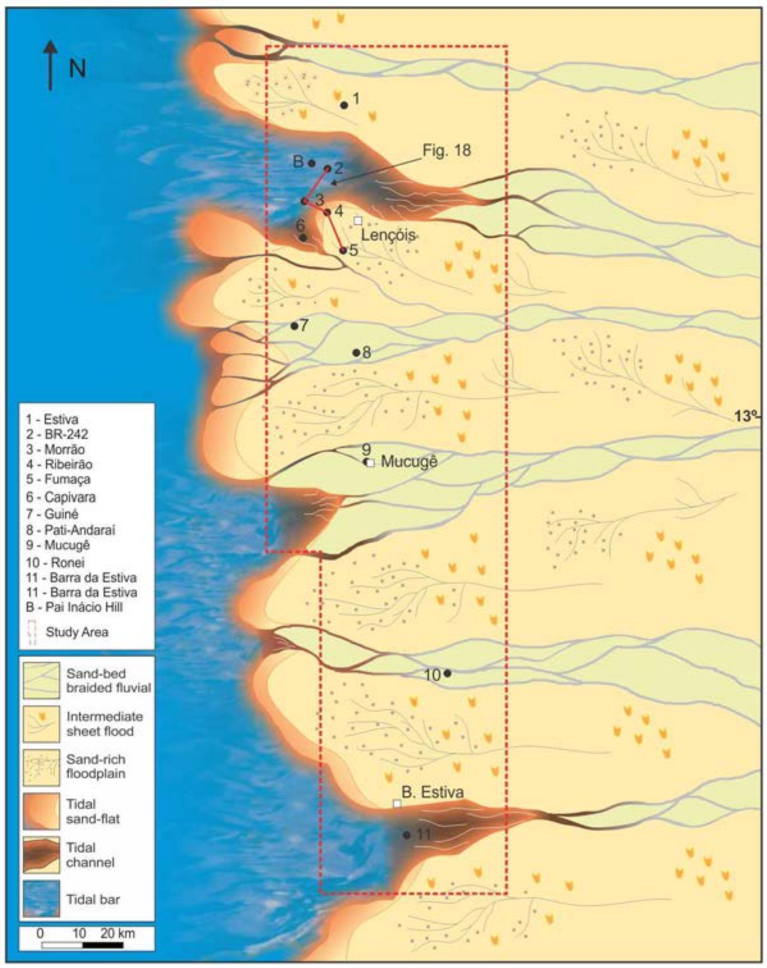

Fig. 3.15. Paleogeographic reconstruction for the Lower Tombador Fm. during transgression: a tide-dominated coast was linked to a wide and shallow fluvial braidplain.

3.5.3. Unincised character of the Lower Tombador Formation

The Mesoproterozoic fluvial and estuarine system from the Tombador Fm. exhibits a fundamental difference when compared to Phanerozoic and modern ones. Phanerozoic estuarine systems are generally associated with subsequent transgressions on fluvial incised-valleys that were formed during lowering of relative sea-level (e.g. Boyd et al., 2006; Dalrymple, 2010; Maynard et al., 2010). The studied fluvial-estuarine successions form tabular, sheet-like geometry with broad lateral continuity, without any evidence of fluvial incised-valley (Fig. 3.16). Exposures on N-S oriented seismic scale cliffs allowed the identification and correlation of fluvial-estuarine successions along approximately the depositional strike direction (Fig. 3.17). Such successions compose depositional sequences that are approximately 25-40 m thick and exhibit changing of facies from lowstand fluvial to transgressive estuarine systems; in some of them, highstand shallow marine strata are preserved (Fig. 3.18). A cross-section along depositional strike direction shows the distribution of facies resulting from transgression of the estuary, followed by estuary infilling and progradation of sand bars, tidal flats, and sand-rich floodplain (Fig 18). This facies distribution is similar to that found in estuaries related to incised-valley systems.

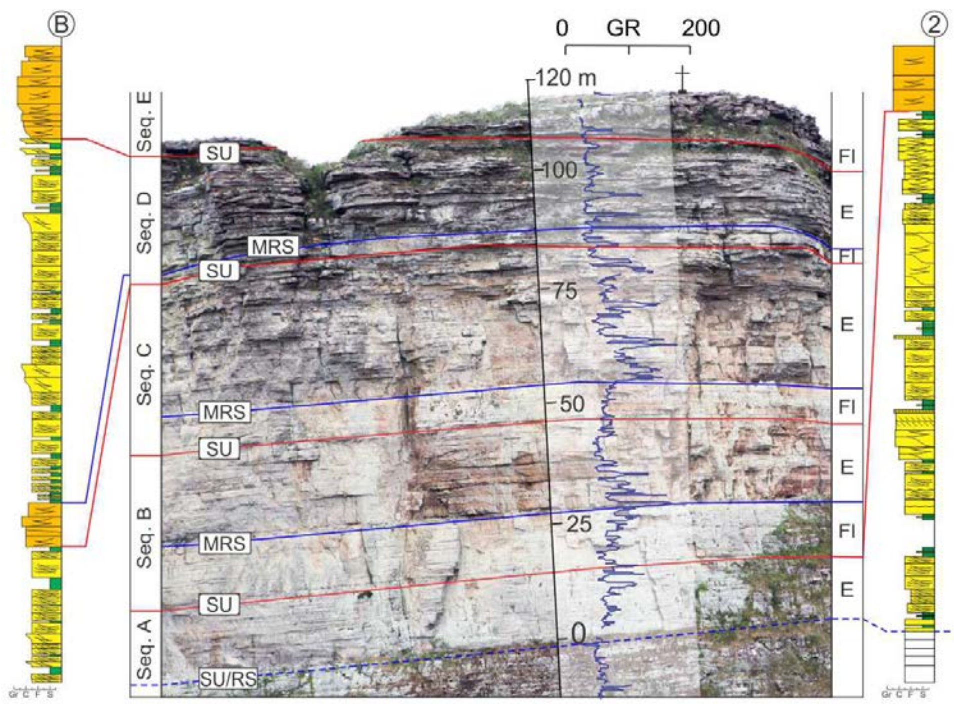

Fig. 3.16. Pai Inacio hill photomosaic showing sheet-like geometry of interpreted sequences A-E, which are formed of lowstand fluvial and transgressive estuarine successions. Vertical section B was measured at the Pai Inacio trail while vertical section 2 is located 3 km eastwards from the hill. See detailed view of vertical sections B and 2 on Fig. 3.14 and their locations on Fig. 3.1. Abbreviations: E – estuarine and shoreface intervals; Fl – fluvial strata.

Among the fourteen criteria used for the recognition of estuarine and incised-valley systems (Boyd et al., 2006), the valley feature is, off course, the most important. A system may be qualified as incised-valley if it fulfills a significant amount of those criteria. The Lower Tombador Fm. fluvial and tide-dominated estuarine successions do not fit in most of them (Table 3) because no incised-valley feature was identified. Nevertheless, the studied succession matches the criteria related to sequence boundary and transgression but those are not exclusive of incised-valley systems and may be applied to unincised fluvial-estuarine systems as well.

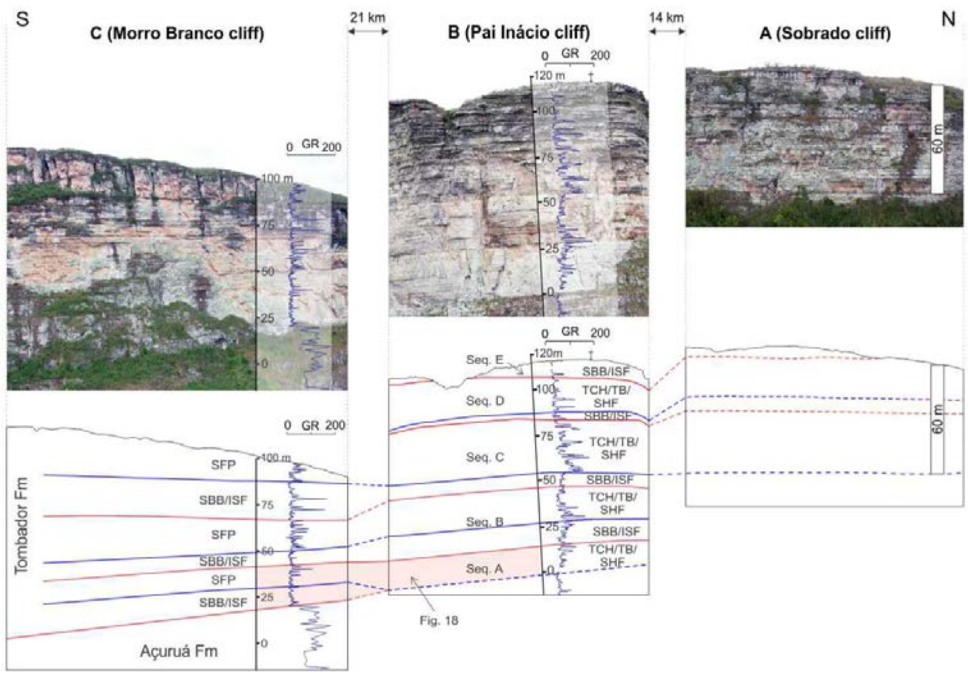

Fig. 3.17. Regional depositional strike-oriented cross-section exhibits sub-parallel geometry of unincised fluvial-estuarine sequences. Facies association codes area given for each sequence (Seq. A-E). Distortion on stratigraphic surfaces is partially due to parallax. Gamma Ray at Morro Branco cliff is projected from vertical section 5, which is located approx. 7 km to the west. The cross-section is oriented along the Pai Inacio anticline axis, which nose dips northwards. See Fig. 3.1 for location of photo-mosaics.

Lack of fluvial incision may be related to three interconnected factors: (i) nature of the fluvial system, (ii) basin morphology, and (iii) no climate-controlled significant increase in fluvial discharge. Fluvial systems from the Tombador Fm. are characterized by shallow braided channels and unconfined to poorly channelized sheetfloods. These systems have lower incision potential because the energy of the flows tends to dissipate laterally, and thus reducing the potential to erode and deepening of channels. Besides, the Tombador Fm. was deposited in a shallow and low gradient sag basin margin (Guimarães et al., 2008; Guadagnin et al., 2015), without significant variation on gradient to trigger incision, what configures a perfect scenario in which there are no significant changes on fluvial graded profile during lowering of relative base level. Hence, incision does not happen and sediment bypass is the dominant process (Woolfe et al., 1998; Posamentier, 2001; Wellner & Bartek, 2003). Climate has been proved as an important allogenic factor on fluvial incision in the Phanerozoic, (Schumm et al., 1987; Blum, 1992; Schumm & Ethridge, 1994; Blum & Price, 1998), and in the Precambrian, river systems would have been more susceptible to paleoclimate change (Bose et al., 2012). Variations in fluvial discharge in the Precambrian Lower Tombador Fm. are more likely related to intercalation of SBB and ISF; whether or not they are climate-controlled is a matter for debate. Thus, the evolution of unincised system in the Lower Tombador Fm. may be described as follows. During periods of lowered relative sea level, rivers flowed on a gentle dipping shelf surface and hence by-pass of sediments and unincised fluvial systems were formed. Lowstand fluvial sand sheet aggraded followed by periods of transgression in which estuaries developed, tides extended their effects upstream, and sand-rich floodplain aggraded. Therefore, the conspicuous tabular external geometry of fluvial-estuarine successions is a natural consequence of deposition on low gradient substrate. As sag basins are characterized by low subsidence rate, the interplay between sedimentation and fluctuations of relative sea level resulted in relatively thin, sheet-like unincised fluvial-estuarine successions.

3.6. Conclusion

The Lower Tombador Fm. records deposition of unincised fluvial and tide-dominated estuarine systems. Fluvial successions are composed of lowstand sand-bed braided and intermediate sheetflood fluvial and undifferentiated transgressive to highstand sand-rich fluvial floodplain. The tide-dominated estuarine succession is formed by retrogradational stacking of tide-influenced braided fluvial channels, tidal channels, tidal sand flats and tidal bars that are eventually overlain by heterolithic strata and highstand coarser-grained tidal sand bars. The observed facies distribution is similar to that found in estuaries related to incised-valley systems. Paleogeographic reconstruction suggests shallow braided and ephemeral sheetflood fluvial systems crossed a wide, gentle fluvial braidplain linked to a tide-dominated coast. During periods of lowered relative sea level, rivers flowed on a gentle dipping surface and hence by-pass of sediments and unincised fluvial systems were formed. Lowstand fluvial sand sheet aggraded followed by periods of transgression during which estuaries developed, tides extended their effects upstream, and sand-rich floodplain aggraded.

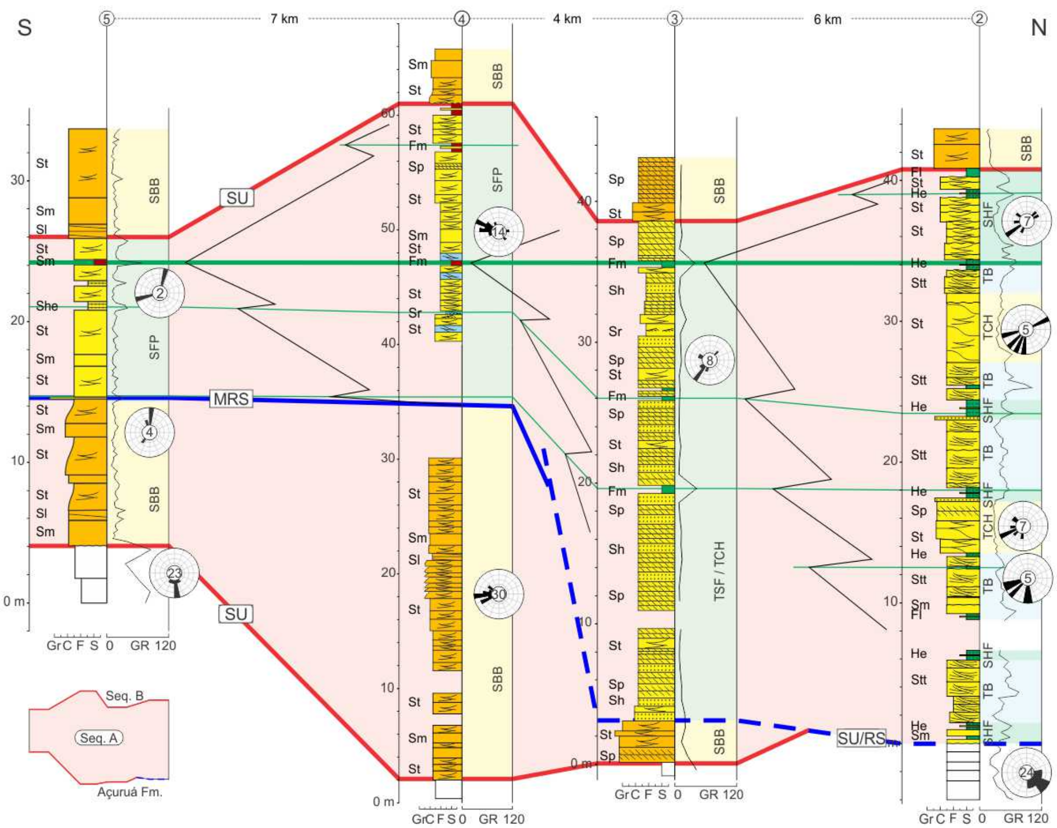

Fig. 3.18. Cross-section along depositional strike direction in Sequence A, showing the distribution of facies resulting from transgression of the estuary, followed by estuary infilling and progradation of tidal sand bars, tidal flats, and sand-rich floodplain. This facies distribution observed in the Lower Tombador Fm. is similar to that found in estuaries related to incised-valley systems. The maximum flooding surface was chosen as the datum. Note that heterolithic shoreface strata from estuarine succession (vertical sections 2 and 3) are correlated to tide-influenced fluvial and fine-grained intervals from fluvial succession (vertical sections 4 and 5). Tidal influence at fluvial domain is identified by cross-strata and asymmetric ripples oriented at the opposite main fluvial paleoflow, as observed at 40 – 48 m interval in vertical section 4. At vertical sections 2 and 3, lower sequence boundary is marked by a ravinement surface that replaced the subaerial unconformity. Vertical exaggeration illustrates the irregularity of the unconformity surfaces; gradient of the lower sequence boundary surface ranges from 0.16^{o} to 0.03^{o}.

The interplay between sedimentation on gentle substrate and fluctuations of relative sea level in the Mesoproterozoic Tombador sag basin resulted in sheet-like conspicuous geometry of unincised fluvial and tide-dominated estuarine successions. The described scenario contributes to a better understanding of fluvial and estuarine sedimentation in Precambrian basins placed in similar tectonic settings.

Table 3.3. Criteria for the recognition of estuarine and incised-valley systems (Boyd et al., 2006) applied to the Lower Tombador Fm.

Criteria for the recognition of Estuarine and Incised-Valley Systems (Boyd et al., 2006)	**Lower Tombador Formation**		
	Yes	**No**	**Observation**
Negative (i.e., erosional) paleotopography feature, the base of which truncates underlying strata		✓	Fluvial system is braided, unconfined and with broad lateral continuity.
Base and walls of the Incised-Valley (IV) represent a sequence boundary	✓	✓	Sequence boundary at the base of fluvial sand sheet. No valley walls were recognized
Trunk river and its tributaries are incised		✓	Fluvial system is braided, unconfined and with broad lateral continuity.
More downdip facies (marine, estuarine) deposited on top of more updip facies (terrestrial)	✓		It implies transgression but the criterion is not exclusive for IV systems.
Onlap on the valley base and walls		✓	Onlap was not identified
Sequence boundary at the base and a transgressive surface within the fill of a simple valley		✓	No valley feature recognized. SU at the base of fluvial sand sheet and MRS on its top. This criterion is not exclusive for IV systems
Channels contained within the valleys should be substantially smaller than the valley itself		✓	No valley feature recognized.
Estuaries are transgressive tidally influenced environments that constitute an important and distinctive components of IV in their seaward parts	✓	✓	No valley feature recognized
The mixing of fresh and salty water is a fundamental characteristics of estuary	--	--	No data available
Estuaries receive sedimentation input from both the marine and terrestrial ends of the system	✓		This criterion is not exclusive for IV systems
E&IVs contain a characteristic mix of sedimentary facies (include terrestrial, estuarine, marine facies and range from fluvial, to tidal-fluvial channel, bayhead delta, central basin, barrier, and tidal sand ridge)	✓	✓	No bayhead delta and central basin facies were recognized.
The central zone of incised-valleys estuaries is occupied by a low-energy region	--	--	No low energy deposits were recognized ant the central zone

Table 3 (continued)

Criteria for the recognition of Estuarine and Incised-Valley Systems (Boyd et al., 2006)	Lower Tombador Formation		
	Yes	No	Observation
In the case of valley incision during regression and relative sea-level fall due to steepening of the fluvial profile as a result of seaward extension of the river, the regional marine gradient is greater than the terrestrial gradient of the river valley	✓	✓	This criterion is not exclusive for IV systems
E&IV deposits occupy fluvial drainage corridors, with valleys occurring especially in areas of subtle downward flexure and / or parallel to fault traces		✓	Fluvial system is braided, unconfined and with broad lateral continuity. No data available on structural control of fluvial system

3.7. Acknowledgements

This research was completed as part of the doctoral project carried out by the first author and fully sponsored by Petrobras. Cicero Pereira and Edison Sato (Federal University of Bahia) partly provided the funds for field trips. We thank Acácio Araujo, Alexandre Zanata, Carlos Victor S. Filho, Cleison Santos, Jaime Souza Jr., Mateus Aragão, Paulo Santos, Rafael Santana, and Valter Rebouças for their assistance in the field and/or help to process data. Gustavo Barros is acknowledged for his drafting skills. We also thank Carlos Arregui, James Kellogg, Michael Holz and the anonymous journal reviewer for their helpful and constructive comments that greatly improved this paper.

3.8. References

Alkmim, F.F., 2004. O que faz de um cráton um cráton? O cráton de São Francisco e as revelações Almeidianas ao delimitá-lo. In: Manteso-Neto, V.; Bartorelli, A.; Carneiro, C.D.R.; Brito Neves, B.B.B. (Eds.), Geologia do continente Sul-Americano: evolução da obra de Fernando Flávio Marques de Almeida. São Paulo, pp. 17-35.

Alkmim, F.F., Martins-Neto, M., 2011. A bacia intracratônica do São Francisco: Arcabouço estrutural e cenários evolutivos. In: Pinto, C. P. $ Martins-Neto, M. A. (Eds.), Bacia do São Francisco: geologia e recursos naturais. SBG/MG, Belo Horizonte, pp. 9-30.

Almeida, F.F.M., 1977. O craton de São Francisco. Revista Brasileira de Geociências 7(4), 349-364.

Araujo, A.J.S., 2012. Análise estratigráfica das Formações Açuruá e Tombador nas proximidades de Barra da Estiva, Chapada Diamantina-Ba. Unpublished undergraduate monography, Universidade Federal da Bahia, 41 pp.

Bállico, M.B., 2012. Análise de facies e sequências deposicionais em sistemas continentais e estuarinos do topo da Formação Tombador, Mesoproterozóico, Chapada Diamantina, Brasil. Unpublished undergraduate monography, Universidade Federal do Rio Grande do Sul, 100 pp.

Battilani, G.A.; Varajão, A.D.; Gomes, N.S., 1999. Metamorphic degree variation in Proterozoic sandstones of the Tombador Formation, Bahia State, Brazil. Zbl. Geol. Paläont. Teil I, (7-8), 917-926.

Bhattacharya, J.P., 2010. Deltas. In: James, N.P. and Dalrymple, R.W. (Eds.), Facies Models 4, Geological Association of Canada IV, Series Geotext 6, 233-264.

Blair, T.C., 2000. Sedimentology and progressive tectonic unconformities of the sheetflood-dominated Hells Gate alluvial fan, Death Valley, California. Sedimentary Geology 132, 233-262.

Blum, M.D., 1992. Climatic and eustatic controls on Gulf Coastal Plain sedimentation: an example from the late Quaternary of the Colorado River. In: Armentrout, J.M. and Perkins, R.F. (Eds.), Sequence stratigraphy as an exploration tool: concepts and practices in the Gulf Coast. SEPM, Gulf Coast Section, Eleventh Annual Research Conference, Houston, pp. 71-84.

Blum, M.D.; Price, D.M., 1998. Quaternary alluvial plain construction in response to glacio-eustatic and climatic controls, Texas Gulf Coast Plain. In: Shanley, K., McCabe, P. (Eds.), Relative role of eustasy, climate, and tectonism in continental rocks. SEPM, Special Publication 59, 31-48.

Bose, P.K.; Eriksson, P.G.; Sarkar, S.; Wright, D.T.; Samanta, P.; Mukhopadhyay, S.; Mandal, S.; Banerjee, S.; Altermann, W., 2012. Sedimentation patterns during the Precambrian: A unique record? Marine and Petroleum Geology 33, 34-68.

Boyd, R.; Dalrymple, R.W.; Zaitlin, B.A., 2006. Estuarine and incised-valley facies models. In Posamentier, H.W.; Walker, R.G. (Eds.), Facies Models Revisited. SEPM Special Publication 84, 171-235.

Bristow, C.S., 1993. The interaction between channel geometry, water flow, sediment transport and deposition in braided rivers. In: Best, J.L.; Bristow, C.L. (Eds.), Braided rivers. Geological Society of London Special Publication 75, 13-72

Brito Neves, B.B.; Campos Neto, M.C.; Fuck, R.A., 1999. From Rodinia to Western Gondwana: an approach to the Brasiliano-Pan African Cycle and orogenic collage. Episodes 22(3), 155-166.

Brito Neves, B. B. 2003. A saga dos descendentes de Rodínia na construção do Gondwana. Revista Brasileira de Geociências 33(1), 77-88.

Bruun, P. 1962. Sea-level rise as a cause of shore erosion. American Society of Civil Engineers Proceedings, Journal of the Waterways and Harbors Division 88, 117-130.

Campos Neto, M.C., 2000. Orogenic systems from Southwestern Gondwana. An approach to Brasiliano-Pan African Cycle and orogenic collage in Southeastern Brazil. In: Cordani, U.G.; Milani, E.J.; Thomaz Filho, A.; Campos, D.A. (Eds.), Tectonic evolution of South America. 31st Int. Geol. Congress. Rio de Janeiro, pp. 335-365.

Cant. D.J.; Walker, R.G., 1978. Fluvial processes and facies sequences in sandy braided South Saskatchewan River, Canada. Sedimentology 25, 625-648.

Castro, M.R., 2003. Estratigrafia de Sequências na Formação Tombador, Grupo Chapada Diamantina, Bahia. PhD Thesis, Universidade São Paulo. 128p.

Catuneanu, O., 2006. Principle of sequence stratigraphy. Elsevier, 386 pp.

Collinson, J.D., 1996. Alluvial sediments. In: Reading, H.G. (Ed.), Sedimentary environments: processes, facies and stratigraphy, Blackwell Science, London, Third Edition, 37-82.

Costa, L.A.M.; Inda, H.A.V., 1982. O aulacógeno do Espinhaço. Revista Ciências da Terra 1, 13-18.

Cotter, E., 1978. The evolution of fluvial style, with special reference to the central Appalachian palaeozoic. In: Miall, A.D. (Ed.), Fluvial Sedimentology. Canadian Society of Petroleum Geologists, Memoir 5, 361-383.

Dalrymple, R.W., 2010. Tidal depositional systems. In: James, N.P.; Dalrymple, R.W. (Eds.), Facies Models 4. Geological Association of Canada IV. Series: GEOtext 6, 201-231.

Dalrymple, R.W., 1992. Tidal depositional systems. In: Walker, R.G.; James, N.P. (Eds.), Facies Models: response to sea level changes. Geology Association of Canada, pp. 195-218.

Dalrymple, R.W. and Choi, K. 2007. Morphologic and facies trends through the fluvial-marine transition in tide-dominated depositional systems: A schematic framework for environmental and sequence-stratigraphic interpretation. Earth-Science Reviews 81 (3-4), 135-174.

Dalrymple, R.W.; Knight, R.J.; Zaitlin, B.A.; Middleton, G.V., 1990. Dynamics and facies model of a macrotidal sand-bar complex. Cobequid Bay-Salmon River Estuary. Sedimentology 37, 577-612.

Dalrymple, R.W., Narbonne, G.M., Smith, L., 1985. Eolian action and the distribution of Cambrian shales in North America. Geology 13, 607-610.

Delgado, I.M., Souza, J.D., Silva, L.C., Filho, N.C.S., Santos, R.A., Pedreira, A.J., Guimarães, J.T., Angelim, L.A.A., Vasconcelos, A.M., Gomes, I.P., Filho, J.V.L., Valente, C.R., Perrota, M.M., Heineck, C.A., 2003. Geotectônica do Escudo Atlântico. In: Bizzi, L.A.; Schobbenhaus, C.; Vidotti, R.M.; Gonçalves, J.H. (Eds.), Geologia, Tectônica e Recursos Minerais do Brasil. CPRM, Brasília.

Dominguez, J. M. L., and Wanless, H. R. 1991. Facies architecture of a falling sea-level strandplain, Doce River coast, Brazil. In: Swift, D. J. P.; Oertel, G. F.; Tillman, R. W.; Thorne, J. A. (Eds.), Shelf sand and sandstone bodies: geometry, facies and sequence stratigraphy. International Association of Sedimentologists Special Publication 14, 259-281.

Els, B.G., 1990. Determination of some palaeohydraulic parameters for a fluvial Witwatersrand succession. South African Journal of Geology 93, 531-537.

Eriksson, E.G., Condie, K.C., Tirsgaard, H., Mueller, W.U., Altermann, W., Miall, A.D., Aspler, L.B., Catuneanu, O. and Chiarenzelli, J.R., 1998. Precambrian clastic sedimentation systems. Sedimentary Geology 120, 5-53.

Eriksson, K.A.; Simpson, E.L., 2004. Precambrian Tidalites: recognition and significance. In: Eriksson, P.G.; Altermann, W.; Nelson, D.R.; Mueller, W.U.; Catuneanu, O. (Eds.), The Precambrian Earth: Tempos and Events. Elsevier, Amsterdam, pp. 631-642.

Eriksson, P.G., Bumby, A.J., Popa., M., 2004. Sedimentation through time. In: Eriksson, P.G.; Altermann, W.; Nelson, D.R.; Mueller, W.U.; Catuneanu, O. (Eds.), The Precambrian Earth: Tempos and Events. Elsevier, Amsterdam, pp. 593-680.

Fuller, A.O., 1985. A contribution to the conceptual modelling of pre-Devonian fluvial systems. Transactions of the Geological Society of South Africa 88, 189-194.

Guadagnin, F.; Chemale Jr., F.; Magalhães, A.J.C.; Santana, A.; Dussin, I.; Takehara, L., 2015. Age constraints on crystal-tuff from the Espinhaço Supergroup – Insights into the

Paleoproterozoic to Mesoproterozoic intracratonic basin cycles of the Congo- São Francisco Craton. Gondwana Research, 27, 363-376.

Guimarães, J.T.; Santos, R.A.; Melo, R.C., 2008. Geologia da Chapada Diamantina Ocidental (Projeto Ibitiara–Rio de Contas). Salvador, Companhia Baiana de Pesquisa Mineral – CBPM/ Companhia Pesquisa de Recursos Minerais – CPRM. Série Arquivos Abertos 31, 64p.

Hampton, B.A.; Horton, B.K., 2007. Sheetflow fluvial processes in a rapidly subsiding basin, Altiplano plateau, Bolivia. Sedimentology 54, 1121-1147.

Inda, H.A.V.; Barbosa, J.F., 1978. Texto explicativo para o mapa geológico do Estado da Bahia escala 1:1.000.000. SME/COM. Salvador, 137p.

Jardim de Sá, E.F., 1981. A Chapada Diamantina e a Faixa Santo Onofre: um exemplo de tectônica intra-placa no Proterozóico Médio do Craton do São Francisco. In: Inda, H.A.V.; Marinho, M.M.; Duarte, F.B. (Eds.), Geologia e Recursos Minerais do Estado da Bahia. Secretaria de Minas e Energia do Estado da Bahia, Textos Básicos 4, 111-120.

Jardim de Sá, E.F.; Bartels, R.L.; Brito Neves, B.B.; McReath, I., 1976. Geocronologia e o modelo tectono-magmático da Chapada Diamantina e Espinhaço Setentrional, Bahia. In: XXIX Congresso Brasileiro de Geologia, Ouro Preto, SBG. Anais 4, 205-257.

Kocurek, G.; Townsley, E.Y.; Havholm, K.; Sweet, M.L., 1992. Dune and dune-field development on Padre Island, Texas, with implications for interdune deposition and water-table-control on accumulation. Journal of Sedimentary Petrology 62, 622-636.

Kröner, A. & Codani, U. 2003. African, southern India and South American cratons were not part of the Rodinia supercontinent: evidence from field relationships and geochronology. Tectonophysics 375, 325-352.

Long, D.G.F., 1978. Proterozoic stream deposits: some problems of recognition and interpretation of ancient sandy fluvial systems. In: Miall, A.D. (Ed.), Fluvial Sedimentology. Canadian Society of Petroleum Geologists Memoir V, pp. 313-342.

Long, D.G.F., 2004. Precambrian rivers. In: Eriksson, P.G.; Altermann, W.; Nelson, D.R.; Mueller, W.U.; Catuneanu, O. (Eds.), The Precambrian Earth: Tempos and Events. Elsevier, Amsterdam, pp. 660-663.

Loureiro, H.S.C.; Bahiense, I.C.; Neves, J.P., Guimarães, J.T.; Teixeira, L.R.; Santos, R.A.; Melo, R.C., 2009. Geologia e recursos minerais da parte norte do corredor de deformação do Paramirim (Projeto Barra-Oliveira dos Brejinhos): Estado da Bahia. Salvador: CPRM (Serviço Geológico do Brasil), Programa Recursos Minerais do Brasil. Convênio CBPM-CPRM. Série Arquivos Abertos 33, 122p.

Lowe, D.R., 1988. Suspended-load fallout rate as an independent variable in the analysis of current structures. Sedimentology 35, 765-776.

Marconato, A.; Almeida, R.P.; Turra, B.B.; Fragoso-Cesar, A.R.S., 2014. Pre-vegetation fluvial floodplains and channel-belts in the Late Neoproterozoic-Cambrian Santa Bárbara group (Southern Brazil). Sedimentary Geology 300, 49-61.

Maynard, J.R.; Feldman, H.R.; Alway, R., 2010. From bars to valleys: the sedimentology and seismic geomorphology of fluvial to estuarine incised-valley fills of the Grand Rapids Formation (Lower Cretaceous), Iron River Field, Alberta, Canada. Journal of Sedimentary Research 80, 611-638.

McCormick, D.S.; Grotzinger, J.P., 1993. Distinction of marine from alluvial facies in the Paleoproterozoic (1.9 Ga) Burnside Formation, Kilihigok Basin, N.W.T., Canada. Journal of Sedimentary Petrology 63, 398-419.

Miall, A.D., 1996. The Geology of Fluvial Deposits: Sedimentary Fácies, Basin Analysis, and Petroleum Geology. Springer-Verlag, Berlin, 582p.

Miall, A.D., 1985. Architectural element analysis: a new method of facies analysis applied to fluvial deposits: Earth-Science Reviews 22, 261–308.

Nemec, W.; Postma, G., 1993. Quaternary alluvial fans in southwestern Crete: sedimentation processes and geomorphic evolution. In: Marzo, M; Puigdefabregas, C. (Eds.), Alluvial Sedimentation. Internal Association of Sedimentologists Special Publication 17, 235-276.

Nummendal, D. and Swift, D. J. P. 1987. Transgressive stratigraphy at sequence-bounding unconformities: some principles derived from Holocene and Cretaceous examples. In: Nummendal, D.,; Pilkey, O. H.; Howard, J. D. (Eds.), Sea-level fluctuation and coastal evolution, Society of Economics Paleontologists and Mineralogists Special Publication 41, 241-260.

Pedreira, A.J., 1994. O supergrupo Espinhaço na Chapada Diamantina Centro–Oriental, Bahia: sedimentologia, estratigrafia e tectônica. PhD Thesis. Universidade de São Paulo, USP. 125 pp.

Pedreira, A.J.; De Waele, B., 2008. Contemporaneous evolution of the Palaeoproterozoic-Mesoproterozoic sedimentary basins of the São Francisco-Congo Craton. In: Pankhurst, R.J., Trouw, R.A.J., Brito Neves, B.B.; De Wit, M.J. (Eds.), West Gondwana: Pre-Cenozoic Correlations Across the South Atlantic Region. Geological Society, London, Special Publications 294, 33-48.

Pisarevsky, S. A.; Wingate, M. T. D.; Powell, C. M.; Johnson, S.; Evans, D. A. D. 2003. Models of Rodinia assembly and fragmentation. Geological Society Special Publication 206, 35-55.

Plink-Björklund, P., 2005. Stacked fluvial and tide-dominated estuarine deposits in high-frequency (fourth-order) sequences of the Eocene Central Basin, Spitsbergen. Sedimentology 52, 391-428.

Posamentier, H.W., 2001. Lowstand alluvial bypass systems: incised vs. unincised. American Association of Petroleum Geologists Bulletin 85, 1771-1793.

Rainbird, R.H., 1992. Anatomy of a large-scale braid-plain quartzarenite from the Neoproterozoic Shaler group, Victoria Island, Northwest Territories, Canada. Canadian Journal of Earth Sciences 29, 2537-2550.

Santana, R.O., 2009. Estratigrafia de Sequências de Alta Resolução da Base da Formação Tombador, nos Arredores de Lençóis, Chapada Diamantina-Ba. Unpublished undergraduate monography, Universidade Federal da Bahia, 124 p.

Santos, C.M., 2009. Análise Estratigráfica das Formações Guiné-Tombador, Chapada Diamantina, Bahia. Unpublished undergraduate monography, Universidade Federal da Bahia, 122p.

Schumm, S.A., 1968, Speculations concerning paleohydrologic controls of terrestrial sedimentation. Geological Society of America Bulletin 79, 1573-1588.

Schumm, S.A., 1977. The Fluvial System. John Wiley, London, 377 pp.

Schumm, S.A.; Ethridge, F.G., 1994. Origin, evolution, and morphology of fluvial systems. In: Dalrymple, R.W.; Boyd, R.; Zaitlin, B.A. (Eds.), Incised-valleys systems: origin and sedimentary sequences. SEPM, Special Publication 51, 11-27.

Schumm, S.A.; Mosley, M.P.; Weaver, W.E., 1987. Experimental fluvial geomorphology. New York, Willey, 413 pp.

Shanley, K.W., McCabe, P.J., Perspective on the sequence stratigraphy of continental strata. American Association of Petroleum Geologists Bulletin 78, 544-568.

Shanley, K.W., McCabe, P.J.; Hettinger, R.D., 1992. Tidal influence in Cretaceous fluvial strata from Utah, USA: a key to sequence stratigraphic interpretation. Sedimentology 39, 905–930.

Silva Filho, C.V.R., 2009. Sistemas deposicionais nas Formações Tombador e Guiné nos arredores do Morro do Pai Inácio, Chapada Diamantina–BA. Unpublished undergraduate monography, Universidade Federal da Bahia, 120p.

Simpson, E.L.; Dilliard, K.A.; Rowell, B.F.; Higgins, D., 2002. The fluvial-to-marine transition within the post-rift Lower Cambrian Hardyston Formation, Eastern Pennsylvania, USA. Sedimentary Geology 147, 127-142.

Smith, N.D., 1972. Some sedimentological aspects of planar cross-stratification in a sandy braided river. Journal of Sedimentary Petrology 42, 624-634.

Sønderholm, M.; Tirsgaard, H., 1998. Proterozoic flucial styles: response to changes in accommodation space (Rivieradal sandstones, eastern North Greenland). Sedimentary Geology 120, 257-274.

Swift, D.J.P. 1975. Barrier-island genesis: evidence from the central Atlantic shelf, eastern USA. Sedimentary Geology 14, 1-43.

Swift, D.J.P.; Kofoed, J.W.; Saulsbury, F.B.; Sears, P.C. 1972. Holocene evolution of the shelf surface, central and southern Atlantic shelf of North America. In: Swift, D.J.P.; Duane, D.B.; Pilkey, O.H. (Eds.), Shelf sediment transport: process and pattern, Stroudsburg, Pennsylvania, Dowden, pp-499-574.

Tirsgaard, H., 1993. The architecture of Precambrian high energy tidal channel deposits: an example from the Lyell Land Group (Eleonore Bay Supergroup), northeast Greenland. Sedimentary Geology 88, 137-152.

Tirsgaard, H.; Øxnevad, I.E.I., 1998. Preservation of pre-vegetational mixed fluvio–aeolian deposits in a humid climatic setting: an example from the Middle Proterozoic Eriksfjord Formation, Southwest Greenland. Sedimentary Geology 120, 295-317.

Turnbridge, I.P., 1981. Sandy high-energy flood sedimentation – some criteria for recognition, with an example from the Devonian of SW England. Sedimentary Geology 28, 79-95.

Varajão, A.D.; Gomes, N.S., 1997. Petrological significance of illitic clays in Proterozoic sandstones of the Tombador Formation, Chapada Diamantina, Brazil. Zbl. Geol. Paläont. Teil I, (3-6), 767-778.

Visser, M.J., 1980. Neap-spring cycles reflected in Holocene subtidal large-scale bedforms deposits: a preliminary note. Geology 8, 543-546.

Wellner, R.W.; Bartek, L.R., 2003. The effect of sea level, climate, and shelf physiography on the development of incised-valley complexes: A modern example from the East China Sea: Journal of Sedimentary Research 73, 926–940.

Williams, G.E., 1971. Flood deposits of the sand-bed ephemeral streams of central Australia. Sedimentology 17, 1-4.

Woolfe, K.J.; Larombe, P.; Naish, T.; Purdon, R.G., 1998. Lowstand rivers need not incise the shelf: an example from the Great Barrier Reef, Australia, with implications for sequence stratigraphic models: Geology 26, 75–78.

Chapter 4 - Ground penetrating radar for facies architecture and high-resolution stratigraphy: examples from the Mesoproterozoic, Chapada Diamantina Basin, Brazil.

4.1. Introduction

Ground Penetrating Radar (GPR) surveys on Phanerozoic sedimentary rocks and modern sediments have been used widely in the last decade. They include, for example, Ordovician and Carboniferous turbidite sequences and Tertiary fluvial sandstone (Thompson et al., 1995; Jol et al., 1996; Corbeanu et al., 2001; Bristow and Jol, 2003; Pringle et al., 2003; Ashworth et al., 2011; Eilertsen et al., 2011; Jorry & Biévre, 2011; Costas & FitzGerald, 2011). However, the application of GPR in the Precambrian is unusual in the literature (Tirén et al., 2001) and has hitherto been carried out in the Chapada Diamantina Basin.

GPR signals reflect prominently from the boundaries between materials with contrasting electrical impedance (Brewster & Annan, 1994). In cemented, non-porous rock, reflections are generated from the boundaries of facies with distinct electrical impedance. In contrast, in sediments, water content exerts a major control on electrical permittivity, a primary property affecting impedance (Annan, 2001).

This chapter documents the findings of GPR surveys on fluvial, deltaic, estuarine, and shallow marine Mesoproterozoic siliciclastic successions from the Espinhaço Supergroup in the Chapada Diamantina Basin. In this study, GPR was used to interpret primary sedimentary structures and architectural elements, as well as to confirm the mappability of stratigraphic surfaces from outcrops to the subsurface. The findings of this study shed new light on the application of GPR in other Precambrian sedimentary basins.

4.2. Methods

A total of 6.2 Km were examined using a GPR SIR 3000 radar system (Geophysical Survey Systems, Inc.) with 200 and 400 MHz antennae. The data were collected in a continuous mode comprising 200 m long GPR lines, each one with control points spaced at 50 m along the shoulder of a paved road in front of outcrops from the Açuruá and Tombador Formations (Figs. 4.1 and 4.2). Antennae polarization was orthogonal to the line direction (Table 4.1).

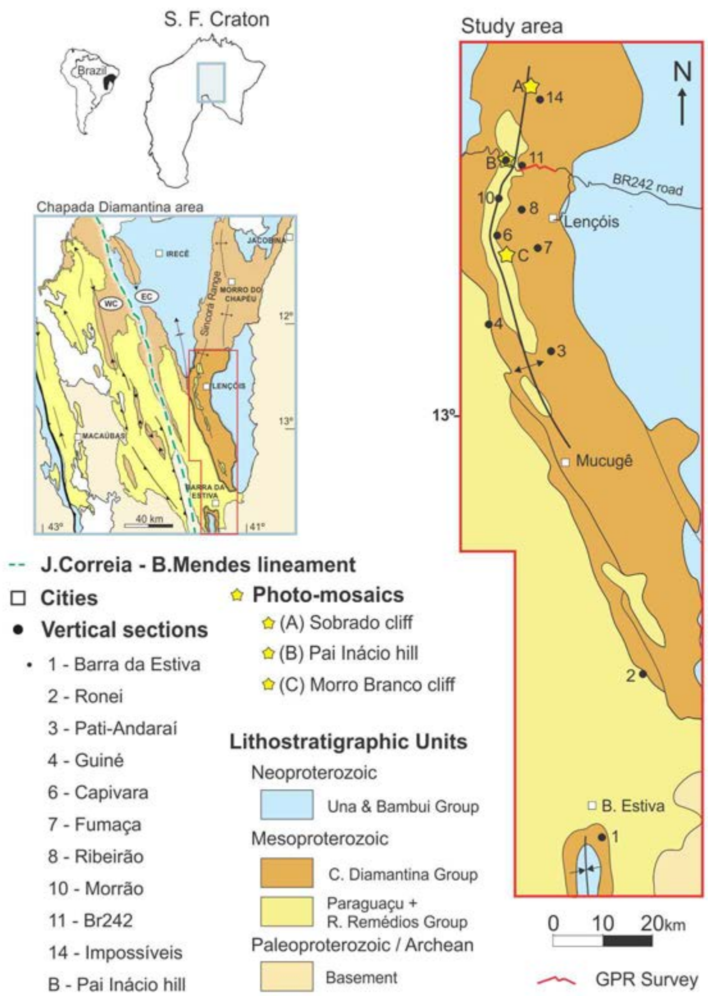

Fig. 4.1. Location of the GPR survey (i.e., the red line along the BR242 road). Geologic map modified from Alkmim & Martins Neto, 2012.

Tests were completed to assure high quality signals, such as surveys on the top of outcrops to reproduce the geometry of sand bodies, changing antennae to check the resolution, and adjusting the parameters, among others. The 400 MHz antenna was chosen to achieve penetration depth with high resolution. Transect images ran approximately along the dip strata direction. A total station theodolite was used to measure the vertical thickness of a sandstone bed used to calculate the velocity (0.13 m/ns). The velocity and dielectric properties measured from samples in laboratory confirmed the values used during field acquisition (Table 4.2). Radar images were processed using the REFLEX© software WIN 1.4 from Sandmeier Software (Karlsruhe, Germany). Raw data were filtered using background removal and averaging. A basic processing routine was applied and included topographic correction, time zero correction, header gain removal, band pass frequency adjustment, background removal, energy decay, spectral whitening, diffraction stacking, automatic gain control, signal saturation correction, trace stacking and migration.

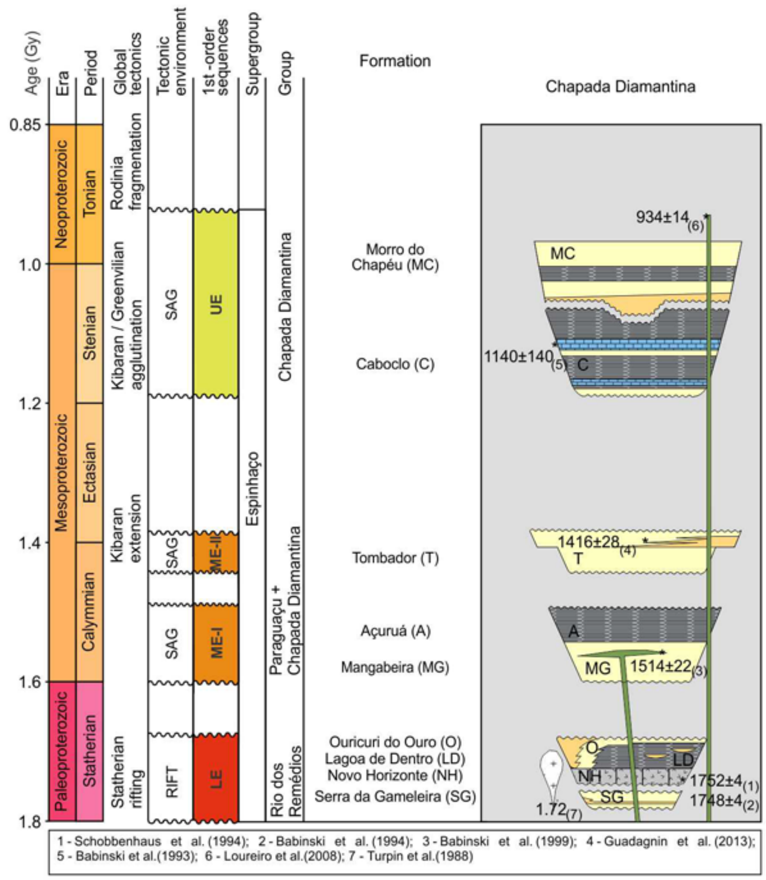

Fig. 4.2. Stratigraphic chart of the Chapada Diamantina Basin (modified from Guadagnin et al., 2015). Abbreviations used for first-order sequences: LE-Lower Espinhaço, ME-I-Middle Espinhaço I, ME-II- Middle Espinhaço II, UE-Upper Espinhaço.

The nomenclature used in this chapter follows the recommendation of Bristow & Jol (2003), such as: (1) the use of GPR profiles or GPR images instead of *radargrams*; (2) the term reflection(s) when describing GPR profiles (reflectors are the subsurface interfaces where the reflections are generated); and (3) objective stratigraphic terminology to describe the reflection patterns (i.e., oblique, continuous, etc.). Stratigraphic and facies interpretation from the GPR data were based on the identification of characteristic features of the reflections and their correlations to the sedimentary or structural features (Jol & Bristow, 2003). The sequence stratigraphic interpretation and nomenclature for the studied succession is based on Magalhães et al., 2015b, presented at chapter 5.

Table 4.1 - Acquisition parameters used on the GPR survey in the Chapada Diamantina Basin.

Acquisition (400 MHz)	Parameters
Step size (cm)	2
Lenght of time window (ns)	150
Time sampling interval (ns/unit)	0.1464844
Antennae separation (offset)	0
Line length (m)	200
Line control points	each 50 m
Antennae polarization	orthogonal
Mean velocity (m/ns)	0.13
Trace staking	16

Table 4.2 - Rock sample velocities and dielectric constants from the Tombador Formation, Chapada Diamantina Basin.

Facies association	Dieletric constant	Velocity (m/ns)
Tidal channel	4.5446	0.1407257
Shoreface heterolithic	5.2075	0.1314639

4.3. Results and Radar facies

GPR signals prominently reflect from boundaries between materials with contrasting electrical impedance (Brewster & Annan, 1994). In sediments, water content exerts a major control on electrical permittivity, a primary property affecting impedance; in contrast, reflections in cemented, non-porous rock are generated at the contact between sedimentary intervals with distinct electrical impedance (Annan, 2001).

In the Chapada Diamantina Basin, GPR signal emitted through a 400 MHZ antenna penetrated up to 8 m with excellent resolution, irrespective of the litostratigraphic unit under investigation. Radar facies are described in terms of reflection continuity, shape, amplitude, internal reflection configuration and external form. Thus, five main radar facies can be documented in the several radar images and correlated to sedimentary or structural features on the outcrops as follows (Fig. 4.3):

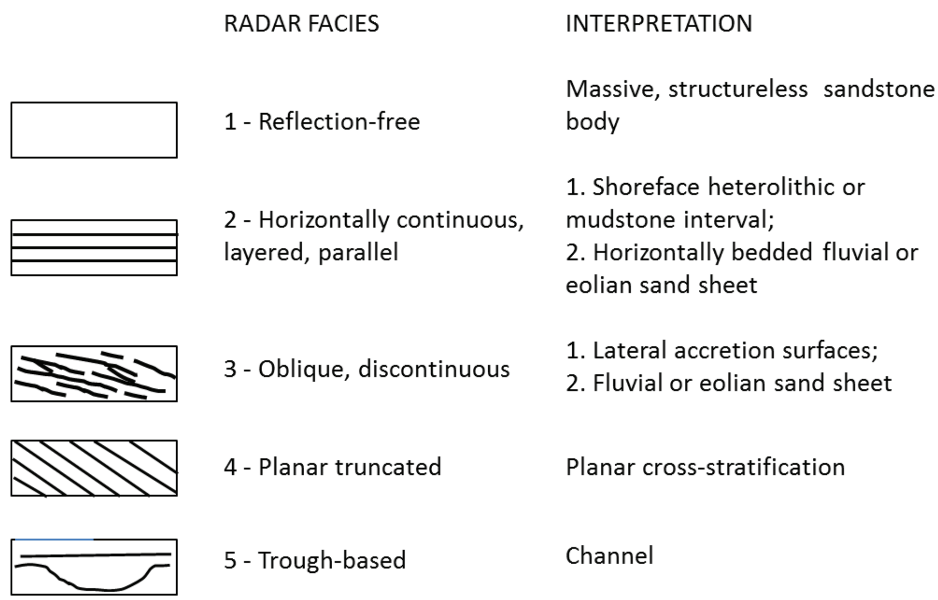

Fig. 4.3. Summary of radar facies and their interpretation for the Mesoprotezoic successions in the Chapada Diamantina Basin.

Petrographic studies in the Tombador Formation indicate sandstones are well cemented by early diagenetic quartz overgrowths and detrital or autigenic illite, sericite and muscovite are the most frequently found clay minerals (Varajão & Gomes, 1997; Battilani et al., 1999). A petrographic analysis (this study) indicates sandstones are mainly quartz arenites and detrital to autigenic illite, sericite, and muscovite are the most frequent clay minerals in the Tombador Formation (Fig. 4.4).

4.3.1. Delta plain succession

Distributary channel and delta plain deposits from the Açuruá Formation are exposed at a 182 m long road-cut. Distributary channels are composed of medium-grained, massive or with trough cross-stratification sandstones bounded by erosive concave up basal surfaces. A delta plain is formed of sub-horizontal to sigmoidal bodies of medium- to fine-grained massive sandstones and minor massive mudstones layers probably related to longitudinal accretion bars migration (Magalhães et al., 2015a).

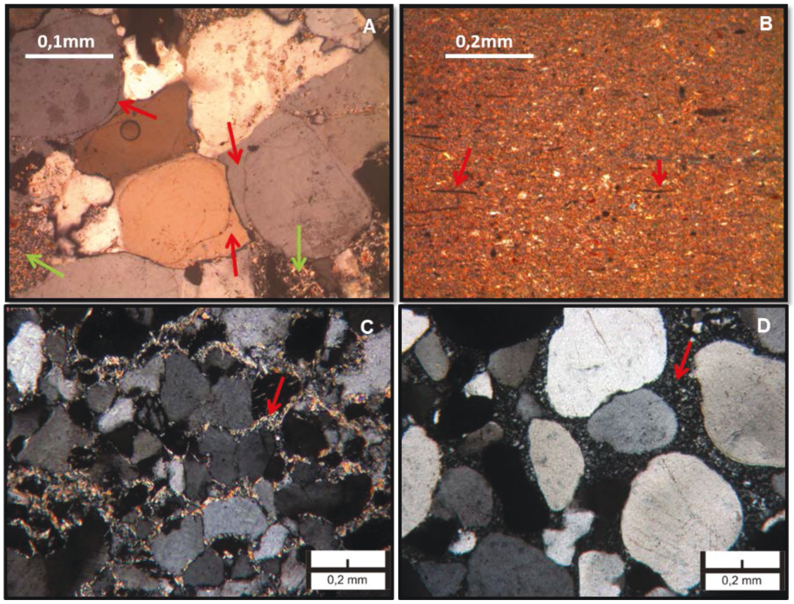

Fig. 4.4. Optical micrograph of the selected samples from the Tombador Formation. (A) Transgressive tidal bar sandstone from sequence A showing quartz grains surrounded by overgrowths (red arrows) and authigenic illite (green arrows, crossed polarizers). (B) Overall aspect of mudstone from the transgressive shoreface heterolithic interval from sequence A, in which detrital muscovite (red arrows) occurs oriented parallel to stratification (plane-polarized light). (C) Mechanically infiltrated clay coatings transformed into illite in lowstand fluvial sandstone from sequence C (red arrow, crossed polarizers). (D) Silex cementation in fluvial sandstone from sequence G (red arrow, crossed polarizers). Thin sections of photos A and B were made from the same samples of Table 4.2.

The GPR image closely resembles what is observed in the outcrop (Fig. 4.5). The image is composed of three radar facies: (a) facies 5 exhibits trough-based features bounded by basal concave up reflections that characterize distributary channels; (b) facies 3 shows oblique to sub-parallel, discontinuous reflections related to delta plain deposits; and (c) facies 1 illustrates reflection-free bodies enveloped by facies 3. According to Ékes & Friele (2003), a reflection-free facies may signify: (1) massive homogenous lithological units; (2) the presence of highly conductive dissolved minerals in the groundwater; or (3) the presence of sediments containing high clay content that attenuate the GPR signals. Thus, the reflection-free configuration is interpreted as massive sandstone bodies on the delta plain or the filling distributary channels.

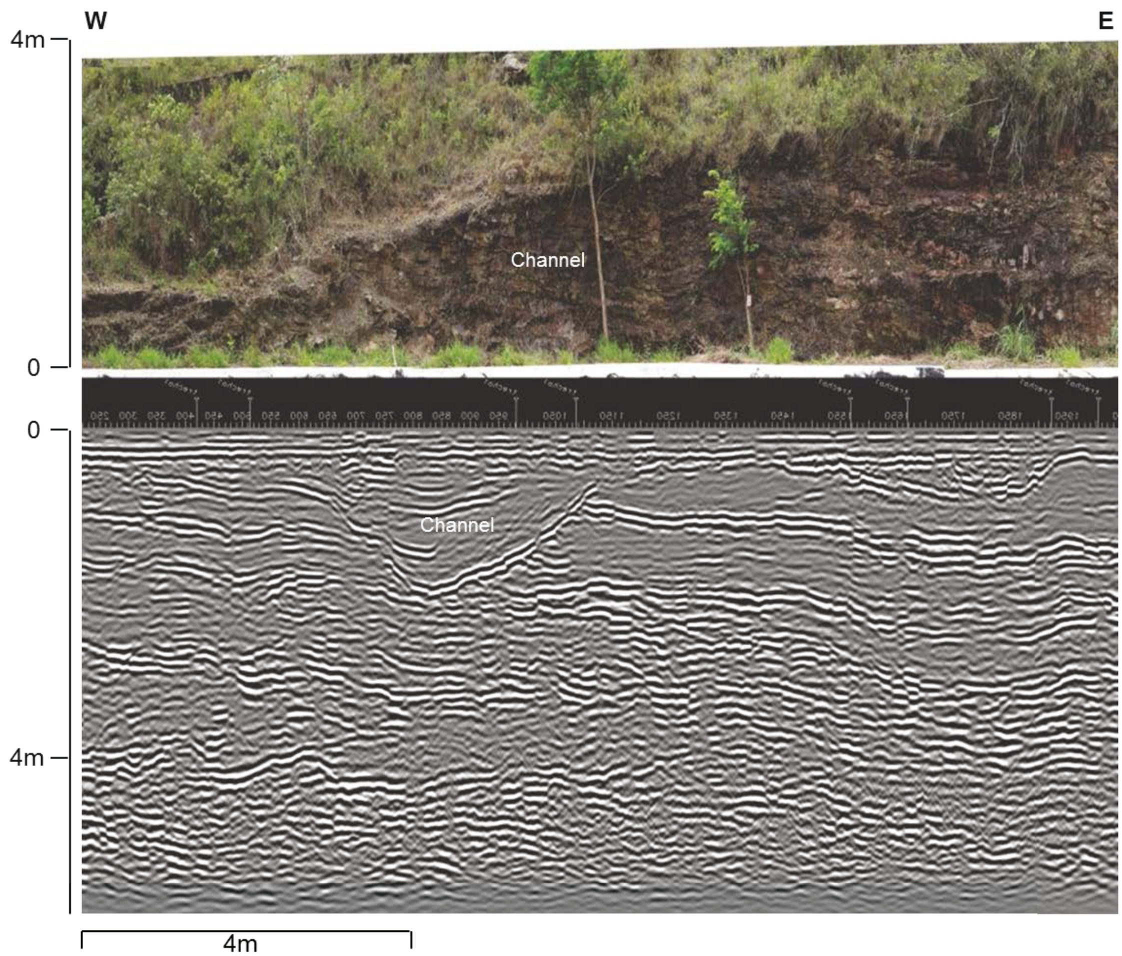

Fig. 4.5. Distributary channel on the delta plain (Açuruá Formation). The channel erosive concave up basal surface is observed both on the GPR line and on the photography of the outcrop. See the location of the GPR line on Fig. 4.1.

4.3.2. Estuarine succession

Detailed estuarine successions of the Tombador Formation are described by Magalhães et al., 2014 and Magalhães et al., 2015b (chapters 3 and 5, respectively). They are usually composed of retrogradational stacking pattern of tidal channel, tidal bar and shoreface heterolithic deposits. The GPR image mirrored a 276.5 m long road cut outcrop of transgressive estuarine succession from sequence A and presents three radar facies (Fig. 4.6): (a) facies 5 exhibits erosive concave up bottom surface truncating underlying reflections that characterize tidal channels; (b) facies 1 presents reflection-free bodies bounded by high-amplitude, continuous reflections, that are related to tidal bars or massive sandstone filling channels; (c) facies 2 shows horizontally continuous, layered, parallel reflection patterns forming tabular intervals associated with shoreface heterolithic deposits.

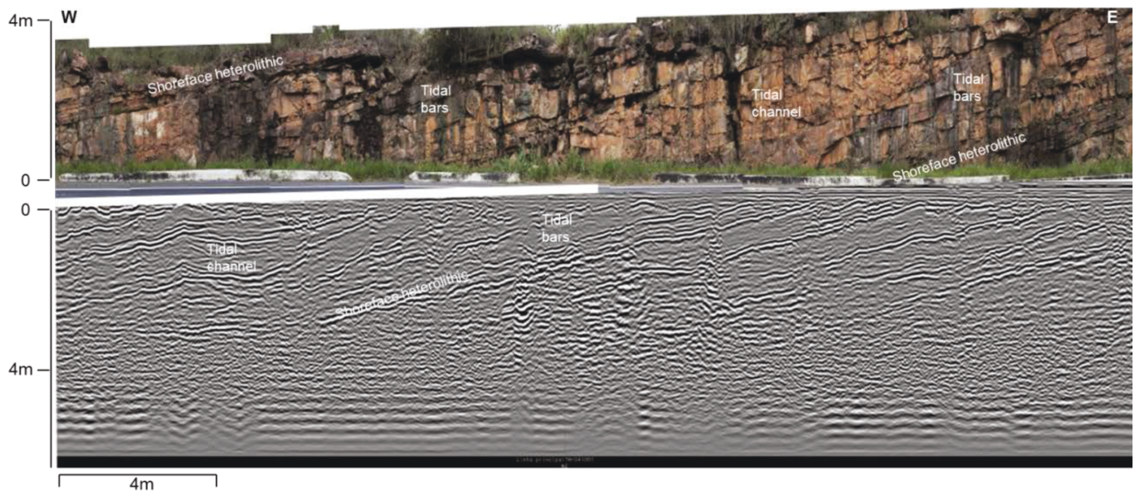

Fig. 4.6. Transgressive estuarine succession from sequence A showing concave up erosive basal surface of tidal channel truncating tidal bars sand bodies. Note that the horizontal laminated shoreface heterolithic interval extends to the subsurface and is clearly observed both on the photomosaic and on the GPR line. The velocities and dielectric constants reported in Table 4.2 were measured from samples collected in this outcrop. See the location of the GPR line on Fig. 4.1.

4.3.3. Fluvial succession

Fluvial succession from the Tombador Formation are characterized by the following: (a) a sand-bed braided fluvial sand sheet composed of medium- to coarse-grained sandstones with planar and trough cross-stratification or (b) a proximal or intermediate ephemeral sheet flood and medium- to coarse-grained sandstone with horizontal lamination, planar and trough cross-bedding (Magalhães et al., 2014; 2015a,b; chapters 2 and 5, respectively). Mechanically infiltrated clay coating is the most important diagenetic feature found in these sandstones.

The GPR image exhibits the same sedimentary structures observed in the outcrops from sequence F and presents three radar facies: (a) facies 2 consists of horizontally continuous, high- to medium-amplitude parallel reflections associated with braided sand sheets of ephemeral sheet floods; (b) facies 4 shows planar truncated medium to low-amplitude reflections that characterize planar cross-bedding in fluvial sandstones; and (c) facies 1 reflection-free configuration is interpreted as massive fluvial sandstone beds (Fig. 4.7).

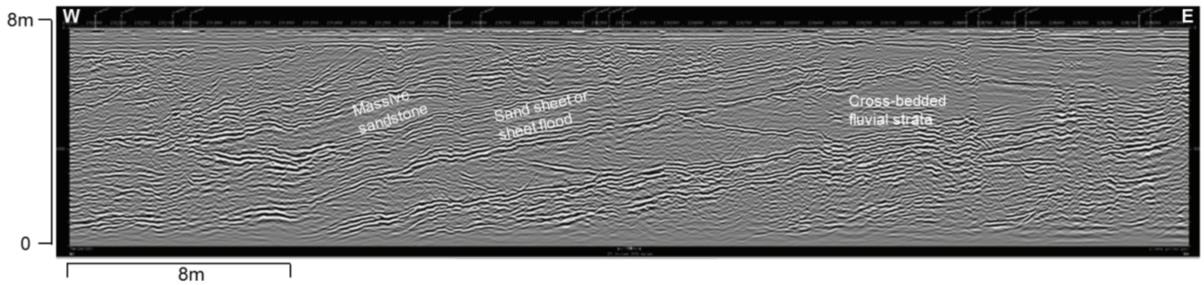

Fig. 4.7. Radar facies showing massive, sand sheet or sheet flood, and cross-bedding in fluvial sandstone from sequence F. See the location of the GPR line on Fig. 4.1.

4.4. Radar images and high-resolution stratigraphy

Radar images supported by facies analysis revealed that, in the subsurface, the unconformity between the Açuruá and Tombador Formations is placed at the contact between radar facies 3, related to delta plain deposits, and overlying radar facies 1, associated to tidal bars (Fig. 4.8).

Radar images supported by facies analysis from estuarine successions were used to interpret the high-resolution genetic sequences (Magalhães et al., 2015b). Radar stratigraphy from the estuarine successions in the Tombador Formation indicates that fourth-order sequences exhibit a retrogradational stacking pattern composed of tidal channels, tidal bars and overlying shoreface heterolithic strata. Truncations at the tidal channels basal erosive concave-up surfaces characterize the subaerial unconformities that are easily mapped, provided the channel bottom is imaged. In contrast, shoreface heterolithic strata exhibit horizontally continuous parallel reflections that are reliable to map throughout the outcrop to the subsurface (i.e., on the GPR image, Fig. 4.9).

4.5. Discussion

The GPR survey achieved an excellent resolution and penetration in the Mesoproterozoic studied successions. Facies analysis and petrographic data were critical for determining which factors most influenced dielectric permittivities. The data indicate that clay and sandstone mineralogy at the study site can account for the strong reflections that occur. Strong GPR reflections at the sandstone/mudstone bed contacts are interpreted to result from distinct dielectric values (Table 4.2). In contrast, clean sandstone with less mudstone interbeds exhibit reflection free a GPR response.

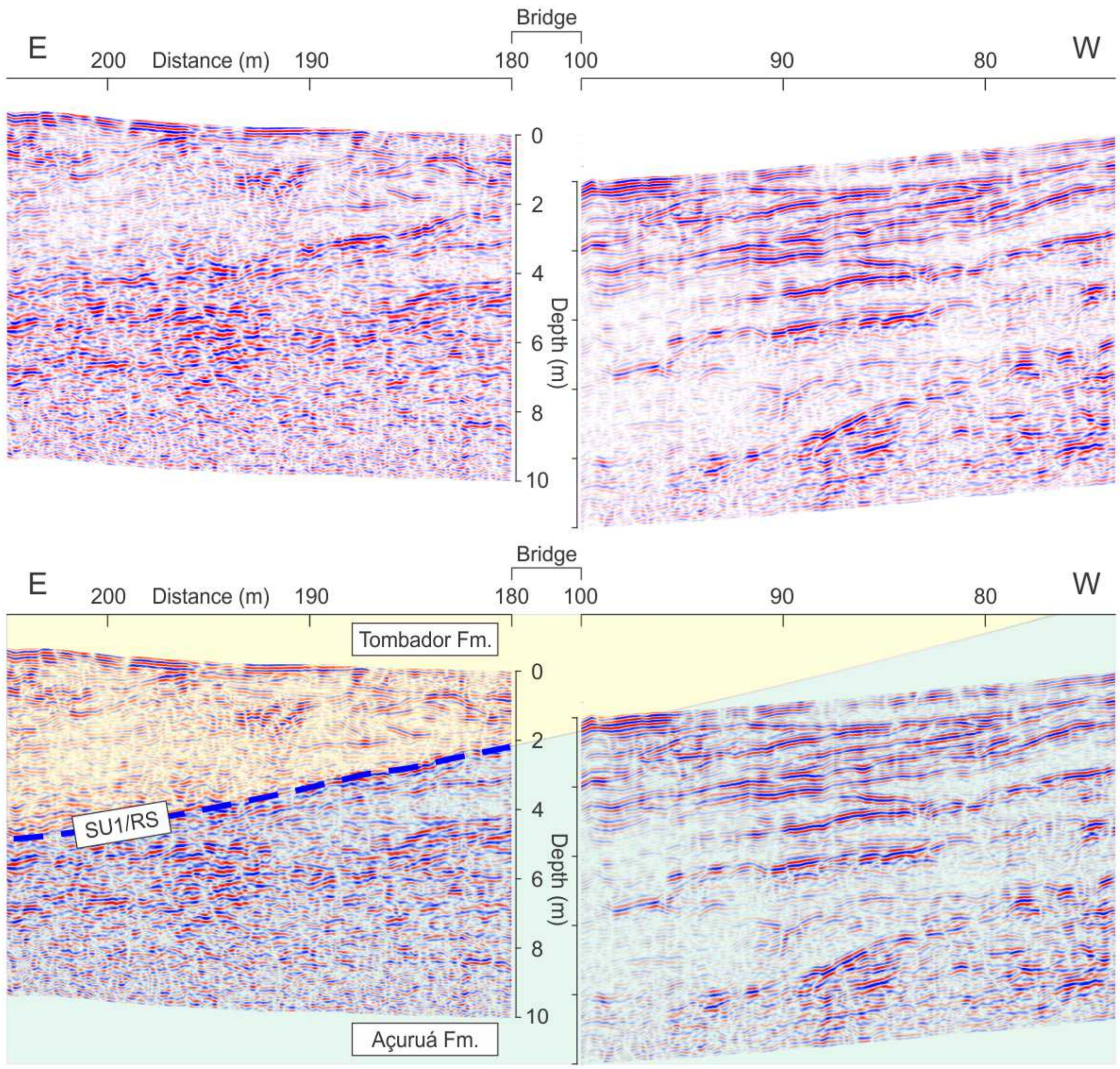

Fig. 4.8. GPR line showing sequence A lower boundary (lithostratigraphically, the contact between the Açuruá and the Tombador Formations). In this location, SU1 and a tide ravinement surface are superimposed. Below the contact, the Açuruá Formation is characterized by three radar facies related to a delta plain setting: a- trough-shaped features bounded by basal concave-up reflections (distributary channels), b- oblique to sub-parallel discontinuous reflections (delta plain), and c- reflection-free bodies enveloped by facies b (massive sandstone bodies filling distributary channels). Above the contact, the Tombador Formation is characterized by reflection-free bodies bounded by high-amplitude, continuous reflections that are related to tidal bars. See Fig. 1 for GPR line location. Abbreviations: SU1 – subaerial unconformity 1, RS – tidal ravinement surface.

Petrographic data indicate sandstones are completely cemented because of advanced diagenesis, and autigenic illite is the most common clay mineral in both the sandstones and the mudstones (Varajão and Gomes, 1997; Battilani et al., 1999). Moreover, the petrographic analysis (this study) indicates that sandstones are quartz arenites ($Q_{99.77}F_{0.20}RF_{0.03}$, Folk, 1974), and detrital to autigenic illite, sericite, and muscovite are the most frequent clay minerals in the Tombador Formation (Fig. 4.4). Such minerals exhibit high electrical resistivity and dielectric constant values (Table 4.3). Typical diagenetic features include: a) early diagenetic quartz overgrowths that prevented mechanical compaction and preserved no porosity; b) dissolution of feldspars, micas, and mud intraclasts and transformation into illite, sericite, and muscovite; c) quartz or silex cementation that is the most abundant. These characteristics favoured the penetration of GPR signals in sandstones and mudstones because they do not attenuate the GPR signals.

Table 4.3 - Dielectric constant and resistivity of quartz, muscovite, and sericite (Beblo et al., 1982).

Mineral	Dieletric constant	Resistivity (Ωm)
Quartz	4.3 - 4.6	3.8×10^{10} - 2×10^{14}
Muscovite	6.19 - 9.0	10^{12} - 10^{14}
Sericite	19.55 - 25.35	-

Distinct radar facies are closely correlated to the stratigraphic units on outcrops and hence, allowed the definition of sedimentary structures, sand-body geometries, facies associations, and stratigraphic surfaces. Radar stratigraphy applied on the estuarine succession confirmed the mappability of shoreface heterolithic intervals from the outcrop to the subsurface (Fig. 4.9). The cyclicity and lateral extent of these intervals can also be observed on photomosaics (Fig. 4.10). Thus, the shoreface heterolithic facies association is interpreted as representing the end of transgression for each fourth-order sequence, and hence, are potential candidates to include the maximum flooding surface (Magalhães et al., 2015b). The definition of fourth-order genetic sequences is crucial to identify high-resolution stratigraphic compartmentalization that, at the reservoir approach, implies on the definition of production zones.

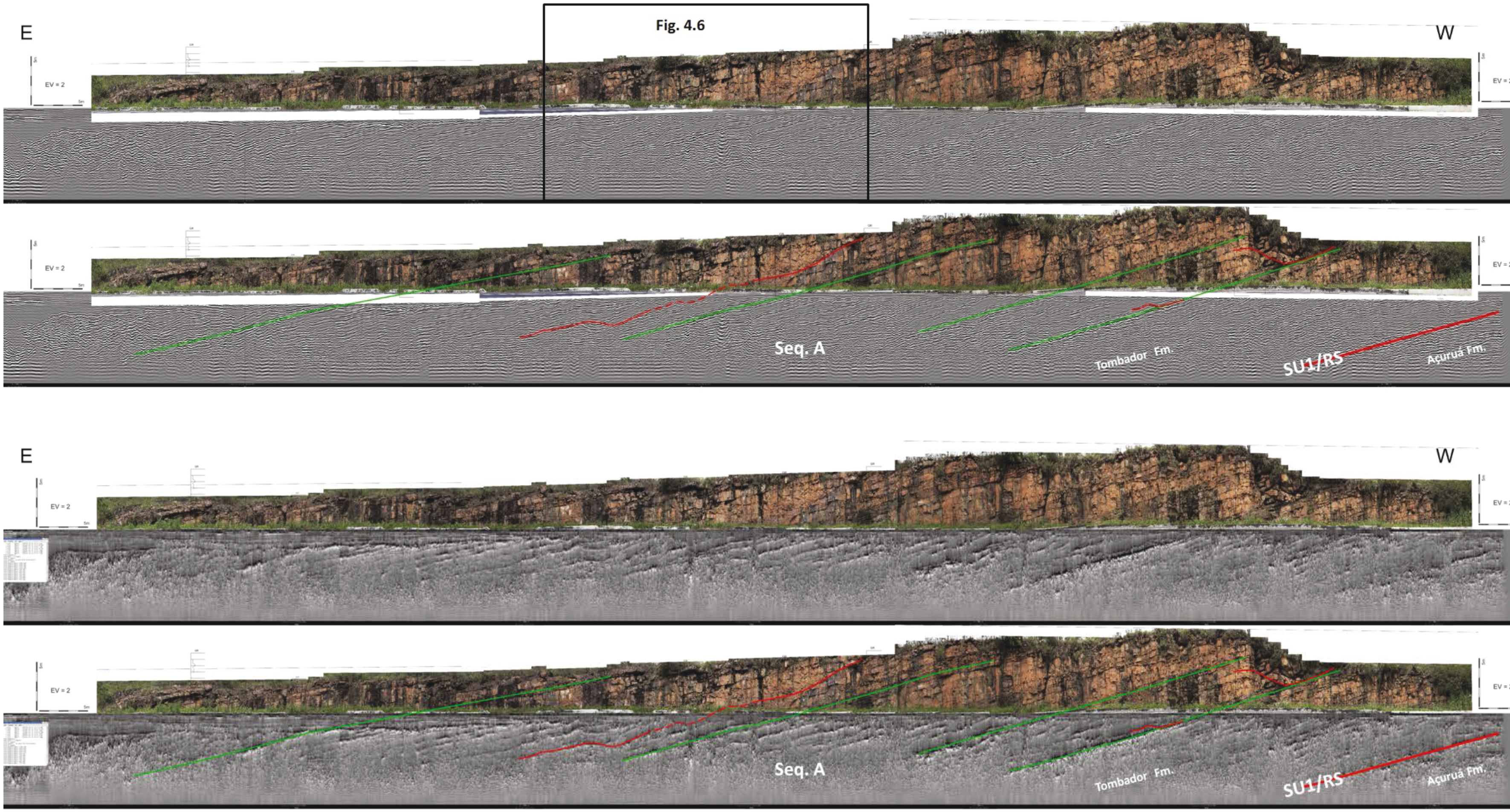

Fig. 4.9. Photomosaic and GPR line showing transgressive estuarine successions from sequence A. Note that heterolithic shoreface intervals are easily mapped (i.e., MFS, in green) whereas SU are not (i.e., bottom tidal channel erosive and concave up surfaces, in red), and hence, five fourth-order genetic sequences are identified (compare with Fig. 29 of chapter 5). GPR line with Tecva processing (below) emphasizes the high amplitude signals and the stratal geometry. Abbreviations (as defined in chapter 5): SU - subaerial unconformity in red, RS – tidal ravinement surface, maximum flooding surface in green, Seq. A – third-order sequence A. Location of Fig. 4.6 is indicated. See location of the GPR line on Fig. 4.1.

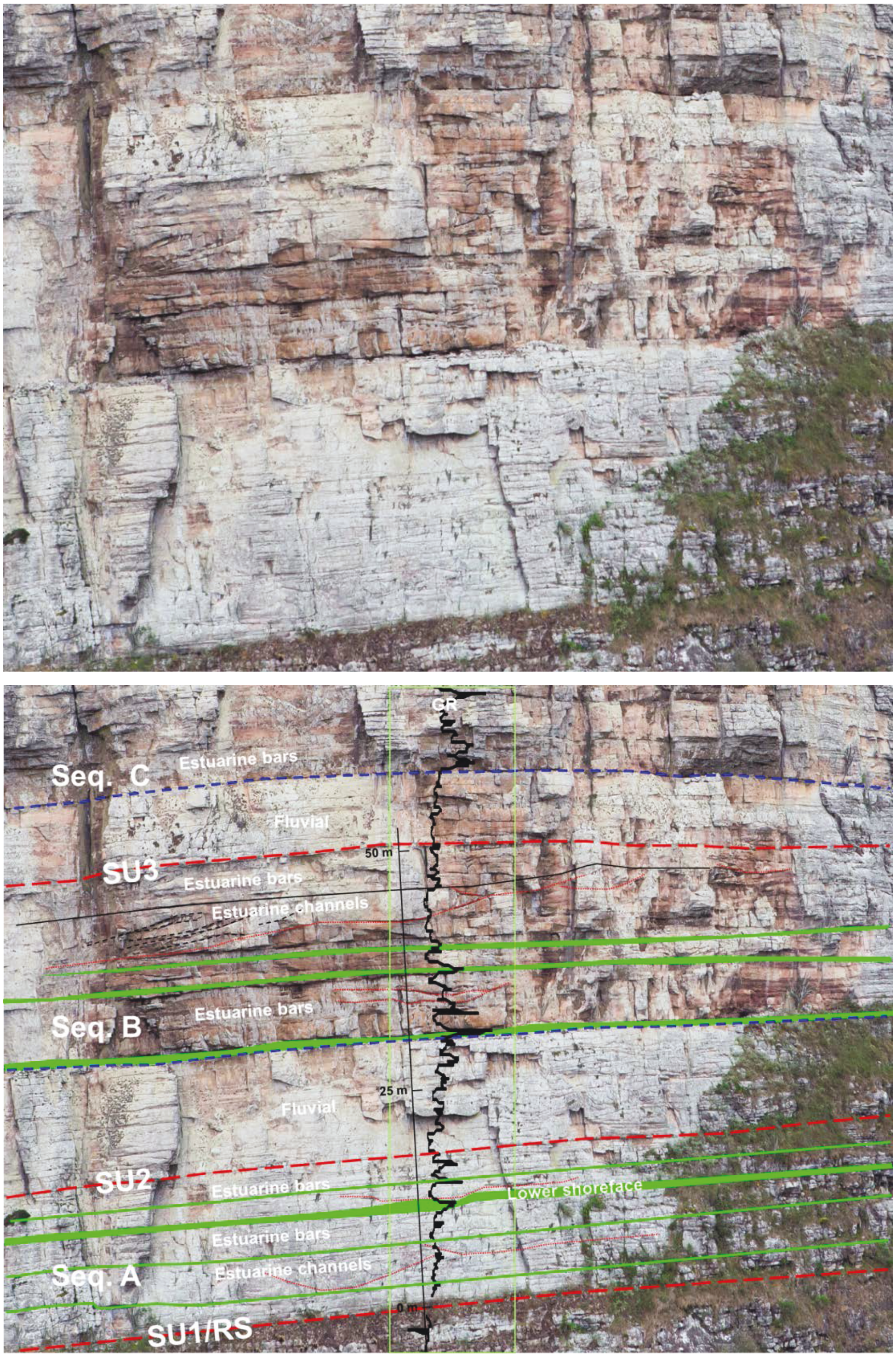

Fig. 4.10. Detailed photo of sequences A-B at Pai Inacio cliff. Note the high-frequence cyclicity and lateral continuity of heterolithic shoreface intervals (in green), as well as the localized scours at the base of the tidal channels. Sequence stratigraphic interpretation is presented at chapter 5. See location of Pai Inácio cliff in Fig. 4.1 (i.e., vertical section B). Abbreviations: GR - Gamma ray log in black; SU - subaerial unconformity in red; RS – tidal ravinement surface; Seq. – third-order sequence; Maximum regressive surface in blue.

4.6. Conclusions

GPR surveys in Precambrian sedimentary rocks were demonstrated to be of great importance to sedimentologic and stratigraphic studies. In the Chapada Diamantina Basin, GPR signals penetrated 8 m using a 400 MHz antenna with excellent resolution. Radar facies and architectural elements were interpreted according to their reflection pattern and external shape, but their interpretation on the GPR lines remains strongly dependent on facies analysis. Compared to photo-mosaics of the outcrops and supported by the vertical sections, the GPR images confirmed the reflection patterns that depict primary sedimentary structures, rock-body geometry, facies association, and stratigraphic surfaces interpretation. It is likely that such result is a response from well cemented non-porous quartz arenite and mudstone in which detrital and authigenic illite, sericite, and muscovite are the most common clay minerals. Radar images applied to estuarine successions not only confirmed the retrogradational stacking pattern composed of tidal channels, tidal bars and overlying shoreface heterolithic intervals but also the mappability of stratigraphic surfaces from the outcrops to the subsurface. Thus, the images played an important role on the interpretation of the high-resolution fourth-order stratigraphic sequences presented in chapter 5.

4.7. Acknowledgments

This chapter is part of this doctoral project, which was fully sponsored by Petrobras. The GPR survey was performance by Prof. Francisco Pinheiro Filho and his team from the University of Rio Grande do Norte, Brazil, to whom I am deeply grateful. Gustavo Barros is acknowledged for his drafting skills. Thorough revision provided by Francisco Pinheiro Filho and Octavian Catuneanu greatly improved this manuscript.

4.8. References

Annan, A.P. 2001. Ground Penetration Radar - Workshop notes. Sensors and Software Inc. Mississauga, Ontário, Canada, 192 pp.

Ashworth, P.J.; Smith, G.H. S.; Best, J.L.; Bridges, J.S.; Lane, S.N.; Lunt, I.A.; Reesink, A.J.H.; Simpson, C.J. & Thomas, R.E. 2011. Evolution and sedimentology of a channel fill in the sandy braided South Saskatchewan River and its comparison to the deposits of an adjacent compound bar. Sedimentology, 58, 1860-1883.

Battilani, G.A.; Varajão, A.F.D.C. & Gomes, N.S. 1999. Metamorphic degree variation in proterozoic sandstones of the Tombador Formation, Bahia State, Brazil. Zbl. Geol. Paläont. Teil I, (7-8), 917-926.

Beblo, M.; Berktold, A.; Bleil, U.; Gebrande, H.; Grauert, B.; Haack, U.; Haak, V.; Kern, H.; Miller, H.; Petersen, N.; Pohl, J.; Rummel, F. & Schopper, J.R. 1982. Physical properties of rocks. In: K.H. Hellwege (Ed.), Numerical Data and Functional Relationships in Science and Technology. Springer-Verlag Berlin, Heidelberg, NewYork.

Brewster, M.L. & Annan, A.P. 1994. Ground penetrating radar monitoring of a controlled DNAPL release: 200 MHz radar. Geophysics, 59, 1211-1221.

Bristow, C. S. & Jol, H. M. 2003. An introduction to ground penetrating radar (GPR) in sediments. In: Bristow, C. S. & Jol, H. M. (Eds.), Ground Penetrating Radar in Sediments. Geological Society, London, Special Publications, 211, 1-7.

Corbeanu, R. M., Soegaard, K., Szerbiak, R.B., Thurmond, J.B., McMechan, G.A., Wang, D., Snelgrove, S., Forster, C.B. & Menitove, A. 2001. Detailed internal architecture of a fluvial channel sandstone determined from outcrop cores, and 3-D ground-penetrating radar: Examples form the Middle Cretaceous Ferron Sandstone, east-central Utah. American Association of Petroleum Geologists Bulletin 85, 1583-1608.

Costas, S. & FitzGerald, D. 2011. Sedimentary architecture of a spit-end (Salisbury Beach, Massachusetts): The imprints of sea-level rise and inlet dynamics. Marine Geology, 284, 203-216.

Eilertsen, R. S., Corner, G. D., Aasehim, O. & Hansen, L. 2011. Facies characteristics and architecture related to palaeodepth of Holocene fjord-delta sediments. Sedimentology 58, 1784-1809.

Ékes, C. & Friele, P. 2003. Sedimentary architecture and post-glacial evolution of Cheekye fan, soutwertern British Columbia, Canada. In: Bristow, C. S. & Jol, H. M. (Eds.), Ground Penetrating Radar in Sediments. Geological Society, London, Special Publication 211, 87-98.

Folk, R.L. 1974. Petrology of sedimentary rocks. Hemphills, Austin, Texas.

Guadagnin, F.; Chemale Jr., F.; Magalhães, A.J.C.; Santana, A.; Dussin, I.; Takehara, L., 2015. Age constraints on crystal-tuff from the Espinhaço Supergroup – Insights into the Paleoproterozoic to Mesoproterozoic intracratonic basin cycles of the Congo- São Francisco Craton. Gondwana Research, 27, 363-376.

Jol, H. M., Smith, D. G. & Meyers, R. A., 1996. Digital ground penetrating radar (GPR): An improved and very effective geophysical tool for studying modem coastal barriers (examples for the Atlantic, Gulf and Pacific coasts, U.S.A.). Journal of Coastal Research 12, 960-968.

Jol, H.M. & Bristow, C.S., 2003. GPR in sediments: advice on data collection, basic processing and interpretation, a good practice guide. In: Bristow, C. S. & Jol, H. M. (Eds.), Ground Penetrating Radar in Sediments. Geological Society, London, Special Publication 211, 9-27.

Jorry, S. J. & Biévre G., 2011. Integration of sedimentology and ground-penetrating radar for high-resolution imaging of a carbonate platform. Sedimentology 58, 1370-1390.

Magalhães, A.J.C.; Scherer, C.M.S., Raja Gabaglia, G.P. Bállico, M.B. & Catuneanu, O. 2014. Unincised fluvial and tide-dominated estuarine systems from the Mesoproterozoic Lower Tombador Formation, Chapada Diamantina basin, Brazil. Journal of South American Earth Sciences 56, 68-90.

Magalhães, A.J.C.; Scherer, C.M.S.; Raja Gabaglia, G.P. & Catuneanu, O. 2015a. Mesoproterozoic delta systems of the Açuruá Formation, Chapada Diamantina, Brazil. Precambrian Research 257, 1-21.

Magalhães, A.J.C, Raja Gabaglia, G.P., Scherer, C.M.S., Bállico, M.B., Guadagnin, F., Bento Freire, E., Silva Born, L.R.. & Catuneanu, O. 2015b. Sequence hierarchy in a Mesoproterozoic interior sag basin: from basin fill to reservoir scale, the Tombador Formation, Chapada Diamantina Basin, Brazil. Basin Research, 1-40, doi: 10.1111/bre.12117.

Pringle, J.K., Westerman, A.R., Clark, J.D., Guest, J.A., Ferguson, R.J. & Gardiner, A.R. 2003. The use of vertical radar profiling (VRP) in GPR surveys of ancient sedimentary strata. In: Bristow, C. S. & Jol, H. M. (Eds.), Ground Penetrating Radar in Sediments. Geological Society, London, Special Publication 211, 225-246.

Thopson, C., McMechan, G., Szerbiak, P. & Gaynor, N. 1995. Three-dimensional GPR imaging of compex stratigraphy within the Ferron sandstone, Castle Valley, Utah. Symposium on the Application of Geophysics to Engineering and Environmental Problems. Preceedings, 435-543.

Tirén, S.A., Wänstedt, S. & Sträng, T. 2001. Moredalen - a canyon in the Fennoscandian Shield and its implication on site selection for radioactive waste disposal in south-eastern Sweden. Engineering Geology 61, 99-118.

Varajão, A.D.; Gomes, N.S., 1997. Petrological significance of illitic clays in Proterozoic sandstones of the Tombador Formation, Chapada Diamantina, Brazil. Zbl. Geol. Paläont. Teil I, (3-6), 767-778.

Chapter 5 - "Sequence hierarchy in a Mesoproterozoic interior sag basin: from basin fill to reservoir scale, the Tombador Formation, Chapada Diamantina Basin, Brazil, *Basin* Research (2015), 1-40, doi:10.1111/bre.12117.

ABSTRACT

The Tombador Formation exhibits depositional sequence boundaries placed at the base of extensive amalgamated fluvial sand sheets or at the base of alluvial fan conglomeratic successions that indicate basinward shifts of facies. The hierarchy system that applies to the Tombador Formation includes sequences of different orders, which are defined as follows: sequences associated with a particular tectonic setting are designated as 'first order' and are separated by first-order sequence boundaries where changes in the tectonic setting are recorded; second-order sequences represent the major subdivisions of a first-order sequence and reflect cycles of change in stratal stacking pattern observed at 10^2 m scales (i.e., 200-300 m); changes in stratal stacking pattern at 10^1 m scales indicate third-order sequences (i.e., 40-70 m); and changes in stratal stacking pattern at 10^0 m scales are assigned to the fourth order (i.e., 8-12 m). Changes in paleogeography due to relative sea level changes are recorded at all hierarchical levels, with a magnitude that increases with the hierarchical rank. Thus, the Tombador Formation corresponds to one first-order sequence, representing a distinct intracratonic sag basin fill in the polycyclic history of the Espinhaço Supergroup in the Chapada Diamantina Basin. An angular unconformity separates fluvial-estuarine to alluvial fan deposits and marks the second-order boundary. Below the angular unconformity the third-order sequences record fluvial to estuarine deposition. In contrast, above the angular unconformity these sequences exhibit continental alluvial successions composed of conglomerates overlain by fluvial and eolian strata. Fourth-order sequences are recognized within third-order transgressive systems tract, and they exhibit distinct facies associations depending on their occurrence at estuarine or fluvial domains. At the estuarine domain, they are composed of tidal channel, tidal bar and overlying shoreface heterolithic strata. At the fluvial domain the sequences are formed of fluvial deposits bounded by fine-grained or tidal influenced intervals. Fine grained intervals are the most reliable to map in fourth-order sequences because of their broad laterally extensive sheet-like external geometry. Therefore, they constitute fourth-order sequence boundaries that, at the reservoir approach, constitute the

most important horizontal heterogeneity and, hence, the preferable boundaries of production zones. The criteria applied to assign sequence hierarchies in the Tombador Formation are based on rock attributes, are easy to apply, and can be used as a baseline for the study of sequence stratigraphy in Precambrian and Phanerozoic basins placed in similar tectonic settings.

Keywords: Intracratonic sag basin, sequence hierarchy, basin fill, reservoir scale, Tombador Formation, Chapada Diamantina

5.1. Introduction

Studies applying sequence stratigraphy to the Precambrian sedimentary record have been limited and have focused on low-resolution applications due to problems in preservation, deformation/metamorphism, and diagenesis, which tend to define second-order sequences related to major stages of basinal reorganisation (Catuneanu & Eriksson, 1999; Eriksson et al., 2005c; Catuneanu et al., 2005). However, higher-resolution studies are possible, where geometry, facies definition, and facies relationships are well definable (e.g., Ramaekers & Catuneanu, 2004; Eriksson & Catuneanu, 2004; Eriksson et al., 2005b,c). The relative significance of sequence stratigraphic units that develop at different scales of observation is resolved via the concept of hierarchy (Catuneanu et al., 2011). Moreover, the Precambrian provides the opportunity to observe Earth's processes at a broader scale and thus gain an improved understanding of issues such as the mechanisms governing stratigraphic cyclicity and the variability thereof (Catuneanu et al., 2005).

Because Precambrian basins are often characterized by poor stratal preservation and by a general lack of age control, an approach based on sequence hierarchy is considered the best way to interpret the stratigraphic framework (Martins-Neto et al., 2001; Catuneanu et al., 2005; Alkmim & Martins-Neto, 2012). The approach and the concept of sequence hierarchy applied to the Espinhaço Supergroup led to the recognition of first- and second-order sequences (Danderfer & Dardene, 2002; Guimarães et al., 2008; Danderfer et al., 2009; Martins-Neto, 2009; Chemale Jr. et al., 2010; Alkmim & Martins-Neto, 2012). However, no high-resolution stratigraphic study has hitherto been carried out.

The Chapada Diamantina (diamond-bearing plateau) Basin holds the most complete non-metamorphosed geological record of the Espinhaço Supergroup in the São Francisco craton, which is a Proterozoic tectonic unit located in the central-eastern part of Brazil. The Lower Mesoproterozoic Tombador Formation possesses thick successions that contain high-resolution information about the evolution of fluvial, estuarine, and alluvial fan systems at the time of deposition. Despite the formation's the very old age, the exposure and preservation are exceptional, affording a unique opportunity to observe changes at sub-seismic scale (high-resolution sequence stratigraphy) and to unravel processes that dominated deposition and understand their stratigraphic evolution during the Mesoproterozoic, as few such pristine data sets are available anywhere in the world for that time interval. Moreover, this unit underwent localized very low-grade metamorphism, and the sedimentary rocks still exhibit many primary structures. Previous works have interpreted the deposits of the Tombador Formation based on studies carried out on a regional scale (Pedreira, 1994; Pedreira & De Waele, 2008; Guimarães et al., 2008; Loureiro et al., 2009) or a detailed scale (Castro, 2003; Santana, 2009; Santos, 2009; Silva Filho, 2009; Araujo, 2012).

This study presents a sequence stratigraphic analysis carried out from the regional to high-resolution scale on the Mesoproterozoic Tombador Formation. The study was based on data gathered from several sources, such as radiometric dating, seismic-scale photomosaics, facies analysis, gamma ray logs and ground-penetrating radar. Thus, the aims of this paper are twofold. First, we define clear and practical criteria to assign a sequence hierarchy. Second, we propose a stratigraphic framework with first- to fourth-order sequences. The criteria applied to assign sequence hierarchies in this paper are based on rock attributes, are easy to apply, and can be used as a baseline for the study of sequences in Precambrian and Phanerozoic basins placed in similar tectonic settings.

5.2. Geological Setting

The São Francisco and Congo cratons are stable Archean/Paleoproterozoic blocks (Almeida, 1977). The evolution of Proterozoic sedimentary cover in the São Francisco craton started with the Statherian intracratonic extensional regime between 1.8 and 1.6 Ga, which promoted continental rifting and an ensuing bimodal volcanism suite followed by psamite continental sedimentation that is well preserved in the Espinhaço rift system (Jardim de Sá et al., 1976;

Inda & Barbosa, 1978; Jardim de Sá, 1981; Costa & Inda, 1982; Delgado et al., 2003). The rift-sag basins expanded in the Calymmian, between 1.6 and 1.4 Ga, and preserved sedimentary deposits of transitional and marine environments (Delgado et al., 2003).

The Proterozoic cover units of the São Francisco craton occur in two distinct areas: the São Francisco Basin and the Paramirim aulacogen. Chapada Diamantina is a geomorphologic feature in the Paramirin aulacogen that gave its name to a Paleo-Mesoproterozoic sedimentary basin that evolved in three main basinal cycles: the Statherian rift, the Calymmian sag and the Stenian-Tonian sag (Guadagnin et al., 2015). This Basin can be subdivided into the Western and the Eastern Chapada Diamantina (Fig. 5.1, Jardim de Sá et al., 1976). The Western sector is characterized by tight folds, volcanic rocks, and green-schist facies metamorphic grade. In contrast, in the Eastern sector, the folds are opened, igneous activity is restricted to mafic intrusions, the metamorphism is very low, and the rocks still exhibit primary structures. These important structural features are related to Brasiliano collisions (from 950-520 Ma) that led to the assembly of Gondwanaland and the formation of the orogenic belts that defined the boundaries of the São Francisco craton (Alkmim, 2004).

The Tombador Formation was deposited in a sag basin (Guimarães et al., 2008; Guadagnin et al., 2015) and is composed of sedimentary rocks formed in continental (alluvial fan, fluvial, and eolian), estuarine, and shallow marine depositional environments (Pedreira, 1994; Savini & Raja Gabaglia, 1997; Castro, 2003; Guimarães et al., 2008; Loureiro et al., 2009; Silva Born, 2011; Bállico, 2012). Petrographic studies have revealed that sandstones reached a high diagenesis stage with an anchi-metamorphism grade towards the south of the Sincorá Range (Battilani et al., 1999; Varajão & Gomes, 1997). U-Pb radiometric data from detrital and volcanic zircons yield ages of 1394 ± 14 Ma (Gruber et al., 2011) and 1416 ± 28 Ma (Guadagnin et al., 2015) for the Tombador Formation (Fig. 5.2). This unit lies unconformably over deltaic deposits of the Açuruá Formation (Pedreira, 1994) and is overlain by shallow marine strata from the Caboclo Formation. The unconformity between the Tombador and Açuruá Formations has been recognized by several authors (Derby, 1906; Schobbenhaus & Kaul, 1971; Inda & Barbosa, 1978; Pedreira, 1994; Schobbenhaus, 1996; Guimarães et al., 2008). Based on paleocurrent directions and provenance studies in the Açuruá and Tombador Formations, Pedreira (1994) suggested that a tectonic tilt must have occurred prior to the deposition of the Tombador Formation. Such tectonics are related to a regional intraplate extensional regime established at 1350 Ma at the southeastern and western margins of the Congo craton (the Kibaran extension, which is represented by the Karagwe-Ankolian Belt and the Kunene Complex) and is interpreted as the sag basin-forming mechanism that allowed the Tombador Formation deposition (Guadagnin et al., 2015).

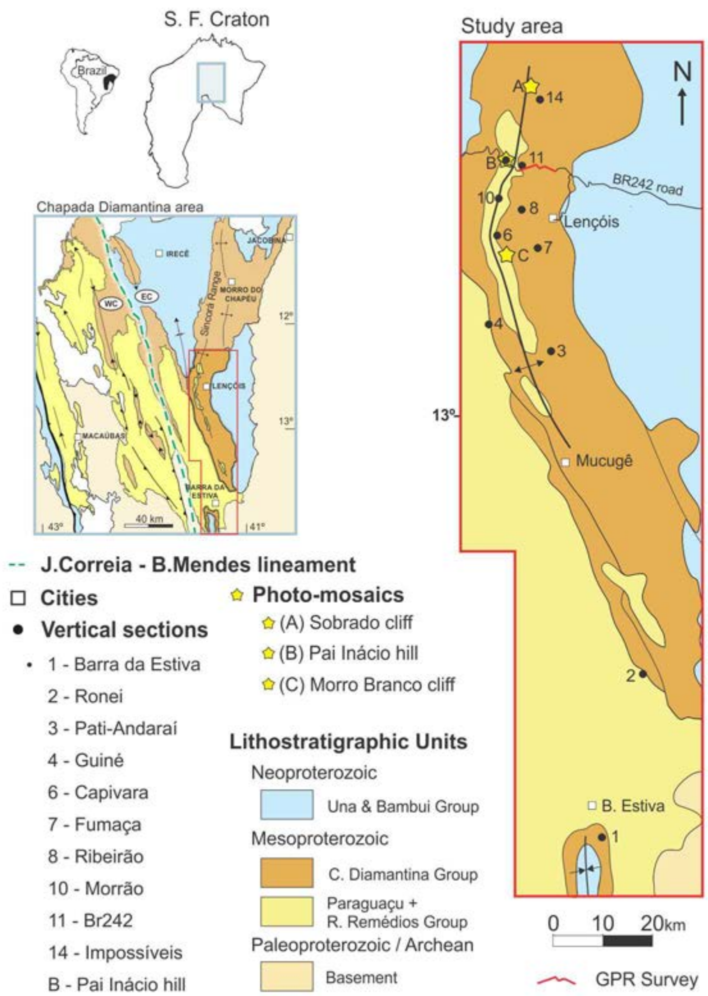

Fig. 5.1. Regional map showing the outline of the Chapada Diamantina area and the study area in the São Francisco craton. Abbreviations: WC-Western Chapada Diamantina, EC-Eastern Chapada Diamantina. Modified from Alkmim & Martins-Neto, 2012.

Studies on sequence stratigraphy applied to the Precambrian in the Chapada Diamantina were carried out either on a regional scale or on a very detailed scale within a small area. Regional studies recognized a tectonosequence related to rift and sag phases, such as the Supersequence Mangabeira-Açuruá and Supersequence Tombador-Caboclo (Dominguez, 1992; Pedreira, 1994; Guimarães et al., 2008; Pedreira & De Waele, 2008; Loureiro et al., 2009), whose boundaries agree with the sequence boundary concepts of Sloss et al. (1949). Detailed studies have focused on the local identification and correlation of sequences within the Açuruá and Tombador Formations (Castro, 2003; Santana, 2007; Santana, 2009; Santos, 2009; Rebouças, 2011, Araújo, 2012). More recently, some studies have proposed a regional correlation for the Espinhaço Supergroup between the Southern Espinhaço, the Northern Espinhaço, and the Chapada Diamantina (Danderfer et al., 2009; Chemale et al., 2010; Alkmim & Martins-Neto, 2012, Guadagnin et al., 2015).

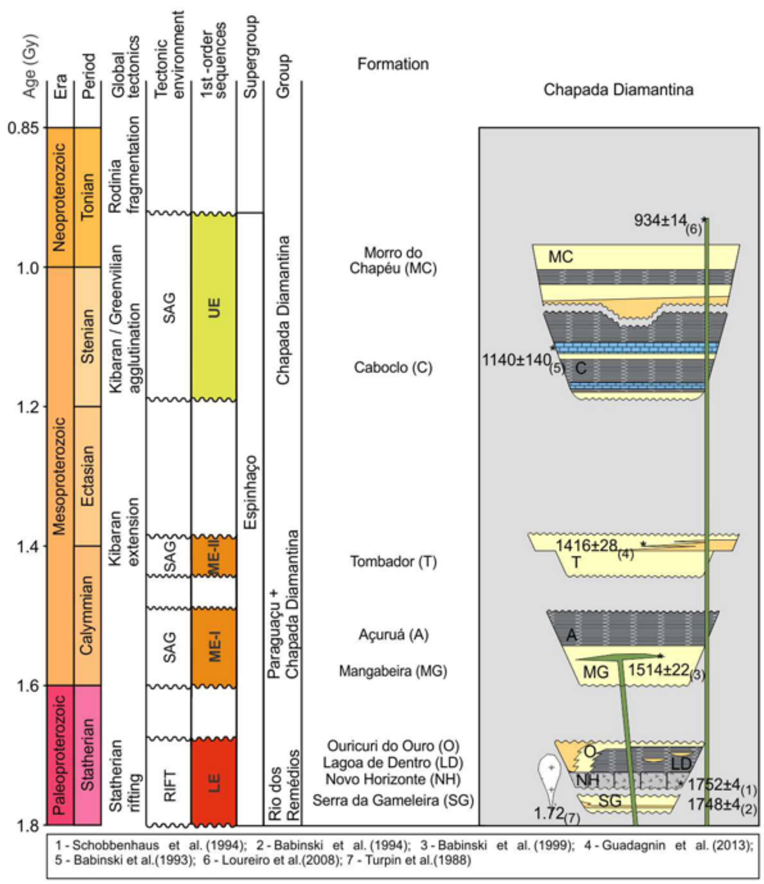

Fig. 5.2. Stratigraphic chart of the Chapada Diamantina Basin (modified from Guadagnin et al., 2015). Abbreviations used for first-order sequences: LE-Lower Espinhaço, ME-I-Middle Espinhaço I, ME-II- Middle Espinhaço II, UE-Upper Espinhaço.

5.2.1. Study area

The study area is located in the Eastern Chapada Diamantina, where the Tombador Formation crops out along the Sincorá Range, a 200-km-long and 25-km-wide mountain range with cliffs up to 400 m in height and a lateral continuity up to tens of kilometres both in the depositional strike and dip directions. The range is the geomorphological expression of the Pai Inácio anticline, a mega-fold oriented NNW-SSE (Danderfer, 1990) formed due to the tectonic inversion of the Chapada Diamantina Basin during the Brasiliano orogeny (Alkmim, 2004). The study area's current topography reflects its geological structure and reveals the stratigraphy underneath (Fig. 5.1).

5.3. Methods and data set

The integration of different data acquired from distinct methods is the key for a comprehensive high-resolution stratigraphic study. The data for this paper were collected from several sources, including detailed to regional seismic-scale photo-mosaics; 4000 m of vertical section with a detailed facies description at a 1:40 scale (2450 m) and a 1:100 scale (1550 m); 2037 paleocurrent readings from cross-strata in sandstone; 1875 m of gamma ray (GR) log with a 20-cm space sample; and a 6.2-km ground penetrating radar (GPR) survey. A description and interpretation of the facies and facies associations is given in Tables 1 and 2. Radiometric dating is provided in Guadagnin et al. (2015). The sequence stratigraphic nomenclature follows the terminology of Catuneanu et al. (2011). Low- and high-resolution sequence stratigraphic analyses are dependent on the scale of observation (Catuneanu et al., 2011). In this study outcrops and well-log data supported high-resolution sequence stratigraphic analyses whereas seismic scale photomosaics, regional unconformities, and changes of zircon age afforded lower resolution interpretation.

5.4. Facies associations

Facies description is based on lithology, grain size, and sedimentary structures (Fig. 5.3). The description and interpretation of facies and facies associations are given in Tables 5.1 and 5.2. The various facies associations occur as roughly tabular sand-dominated strata, which can be interpreted in sequence stratigraphic terms (Figs. 5.4 to 5.16). The following facies associations interpreted for the Tombador Formation are presented based on their depositional setting (Table 5.2).

Table 5.1. Description and interpretation of the sedimentary facies comprising the Tombador Formation.

Facies	Code	Description	Interpretation
Pebble- to bouder-supported chaotic conglomerate	Gci	Poorly sorted, clast-supported, and inverse graded conglomerate that forms lenticular beds up to 5 m thick.	Clast-rich debris flow (high strength) or pseudoplastic debris flow (low strength)
Pebble- to bouder-supported massive conglomerate	Gcm	Poorly sorted, clast-supported massive conglomerate that forms lenticular beds up to up to 5 m thick.	Pseudoplastic debris flow (inertial bedload, turbulent flow) or deposition by high-density hyperconcentrated flow
Pebble- to bouder-supported bedded conglomerate	Gh	Poorly sorted, clast-supported, horizontally bedded conglomerate that forms lenticular to elongate beds up to 2.5 m thick.	Longitudinal bedform, lag deposit, sieve deposit
Trough cross-stratified sandstone	St	Light cream to light red, fine- to very coarse-grained, locally granular sandstone; with medium- to small-scale trough cross-stratification and ripple marks. This facies occurs as lenticular to sheet-like beds up to 1.5 m thick	Migration of sinuous-crested subaqueous bedforms (3D), lower flow regime
Trough cross-stratified eolian sandstone	Ste	Light gray, fine- to coarse-grained, bimodal sandstone with medium- to large-scale trough cross-stratification. Common structures include grain flow and grain fall. Usually occurs as isolated bed up to 1.5 m thick.	Migration of sinuous-crested eolian bedforms (3D), lower flow regime
Tidal bundled sandstone	Stt	Light cream, gray and light red, fine to medium-grained sandstone with tidal bundle, reactivation surfaces and mud couplets. Tidal bundle commonly exhibit thickness variations of forests and sets bounded by mud layers. Usually occurs as lenticular to sheet-like beds up to 1. 5 m thick or as sigmoidal-cross-stratified beds up to 1 m thick bounded by reactivation surfaces.	Migration of sinuous-crested subaqueous bedforms (3D) under tidal indluence; lower flow regime (Visser, 1980)
Planar cross-stratified sandstone	Sp	Light gray, fine- to coarse-grained sandstone with medium- to small-scale tabular cross-stratification in up to 0.5 m thick beds.	Migration of straight-crested subaqueous bedforms (2D); lower flow regime
Low angle laminated sandstone	Sl	Light gray, fine- to coarse-grained sandstone with low angle lamination (<15^{o}). Usually forms centimetric beds with supercritical ripples on top	Plane-bed flow under upper flow regime, or migration of bedforms with a high wavelength / amplitude ratio in conditions transitional between lower and upper flow regime.

Table 5.1 (continued)

Facies	Code	Description	Interpretation
Massive sandstone	Sm	Light cream to light gray, fine- to coarse-grained structureless sandstone. This facies occurs as decimetric layers sometimes with faint stratification.	Deposition from hyperconcentrated flows or obliteration of primary structures by diagenesis
Horizontally laminated sandstone	Sh	Light gray and reddish, very fine- to medium-grained sandstone with horizontal lamination that forms sheet-like bed up to 0.5 m	Plane-bed flow under upper flow regime
Inverse graded laminated sandstone	She	Light gray, very fine- to medium-grained sandstone with horizontal lamination, inverse grading and granular ripple, composing up to 70 cm thick beds.	Plane-bed flow under upper flow regime, or migration of eolian bedforms with a high wavelength / amplitude ratio
Ripple cross-laminated sandstone	Sr	Light cream to light gray, very fine- to fine-grained sandstone, with ripple cross-lamination and ripple marks. Usually occurs as discrete layers on top of fining upward succession of medium- to fine-grained sandstone (facies St, Sl or Sh)	Subcritical to supercritical ripples migration under uni- or bidirectional flow; lower flow regime
Heterolithic mudstone and sandstone	He	Intercalation between laminated sandstone and mudstone in millimetric to centimetric layers. Sandy strata are massive, planar laminated, or with ripple marks with deposition of mudstone in the ripple troughs. Mudstone exhibits wavy lamination. Centimetric layer of medium-grained sandstone with granules scattered occurs at the base. This facies forms sheet-like beds up to 3 m thick with broad lateral extent which can commonly be traced over 1000 m	Alternation between deposition from traction and from suspension followed by wave reworking. Medium-grained sandstone with granules scattered is interpreted as transgressive lag (Posamentier and Vail, 1988)
Laminated mudstone	Fl	Light green and reddish, laminated claystone interbedded with siltstone that occur as discrete centimetric layers between Stt facies beds. Common structures include lenticular and wavy bedding	Deposition from suspension and weak bottom currents
Massive siltstone	Fm	Light green, gray and reddish, massive or faint horizontally laminated siltstone. Usually occurs as discrete up to 0.4 m thick layers on top of fining upward succession of medium- to fine-grained sandstone	Deposition from suspension and weak tractive flows

Table 5.2. Description and synthesis of the facies associations interpreted for the Tombador Formation.

Facies Association	Code	Facies components	Description	Gamma ray pattern	Paleocurrent	Interpretation	Depositional setting
Debris-flow deposit	DF	Gci, Gcm, Sh, St	Elongated to lenticular conglomerate bodies up to 40 m thick and erosive basal surface; it consists of amalgamated lenses of massive or inverse-graded conglomerate capped by or interbedded with horizontally laminated and trough-cross-bedded sandstone. Clasts are composed of sandstone and quartzite	Blocky, low values	--	Cohesionless debris flow characterized by multiple surges followed by short-lived aqueous sheetflood	Subaerial alluvial fan
Gravel-bed braided fluvial	GBF	Gcm, Gh, Sm, Sh, St	Sheet-like to poorly channelized conglomeratic bodies up to 5 m thick that extend laterally over hundreds of meters; basal surfaces sharp; composed of stacked sets arranged into fining-upward cycles. Clast are predominatly composed of subrounded granule to cobble of quartizite	Blocky, low values	Unidirectional, mainly to the S-SE	Poorly channelized shallow gravel-bed braided fluvial characterized by the presence of gravel and sand bedforms	Fluvial channel
Sand-bed braided fluvial	SBB	St, Sp, Sh, Sm, Fm	Sheet-like to poorly channelized sandstone bodies up to 3 m thick that extend laterally over tens to hundreds of meters; basal surfaces concave up, erosional, or flat, top sharp; composed of stacked sets arranged into uniform grain size or fining-upward cycles	Blocky, low values	Unidirectional, mainly to the SW	Poorly channelized braided fluvial characterized by discharge fluctuations with deposition of lower-stage bedforms during peak flow and erosion of bottom surface and subsequent deposition in transitional- to upper-stage flow in poorly confined shallow currents	Fluvial channel
Proximal / Intermediate sheetflood	ISF	St, Sl, Sm, Sp, Ste, Sr	Sheet-like sandstone bodies up to 10 m thick that extend laterally over tens to hundreds of meters; internally arranged into amalgamated uniform to fining-upward successions mostly formed by facies Sl	Blocky, low values	Unidirecional, predominantly to NW	Deposition from high-energy flash flood, unconfined sheets and poorly defined fluvial channels. Localized wind reworking forming isolated dunes	Fluvial braidplain
Eolian sand sheet and dune	ESD	Sl, She, Ste	Sheet-like sandstone bodies up to 3 m thick that extend laterally tens to hundreds of meters; internally composed of thin (up to 1.5 m thick) sets of facies Sl and She and localized Ste.	Blocky, low values	Unidirectional, mainly to NE	Deposition of eolian sand sheet and localized eolian dunes	Eolian

Table 5.2 (continued)

Facies Association	Code	Facies components	Description	Gamma ray pattern	Paleocurrent	Interpretation	Depositional setting
Distal sheetflood	DSF	Sl, Sh, She, Sm, Sr, Fm	Sheet-like sandstone bodies up to 14 m thick that extend laterally tens to hundreds of meters; internally composed of fining-upward successions of facies Sl, Sh, Sr to Fm and presence of discrete eolian layers and isolated eolian dunes	Serrate, with higher values in front of siltstone layers	Unidirectional, mainly to N-NW	Deposition of distal ephemeral flash floods. The fining-upward successions reveal the cyclical nature of the deposits, in which initial higher energy floods rapidly reach the waning stage. It is a downstream equivalent to ISF	Sand-rich floodplain (SFP)
Tide-influenced sand-bed braided fluvial	TSB	St, Sp Sh, Sm Sr, Fm	Sheet-like to poorly channelized sandstone bodies up to 3 m thick that extend laterally over tens to hundreds of meters; basal surfaces concave up, erosional, or flat, top sharp; composed of stacked sets arranged into uniform grain size or fining-upward cycles. Presence of small scale trough-cross bedding and asymmetric ripples oriented (to SE/NE), at the opposite direction of the main fluvial paleoflow	Not logged	Mainly to SW/NW and subordinately to SE/NE	Poorly channelized braided fluvial characterized by tidal influence.	Inner estuary / Fluvial braidplain
Tidal sand-flat	TSF	St, Sh, Sr, Sm	Sheet-like sandstone bodies up to 2 m thick that extend laterally over tens of meters; internally composed of centimetric sets with sharp, slightly undulating, erosive bases and frequently with alternation of facies Sh and Sr	Not logged	Predominantly to NW and subordinately to NE-SE	Deposition in high energy tidal sand flat. Facies St are interpreted as formed under upper flow regime associated to dominant (ebb) tide while facies Sr are interpreted as formed during lower flow regime associated both to dominant and subordinate tides	Tidal flat
Estuarine tidal channel	TCH	St, Sp, Sm, Fl	Amalgamated lenticular to sigmoidal sandstone bodies bounded by mud drapes that form up to 5 m thick succession with channel-like shape; concave up erosive basal surface truncates TB or SHF; TCH is usually overlain by TB and occasionally by SHF	Blocky, low values	Mainly to the SW and subordinately to the NE	Deposition filling tidal channels which cut tidal bars and shoreface deposits.	Inner estuary
Estuarine tidal bar	TB	Stt, St, Sm, Fl	Lenticular bodies up to 2.5 m thick that extend laterally over tens of meters; internally composed of sets of facies Stt bounded by mud drapes; individual sets exhibit fairly symmetrical ripples on top	Serrate, higher peaks in front of mudstone layers	Mainly to SW and subordinately to NE/SE	Subtidal deposition of tidal bar deposits, which are characterized by recurrence of sandstone beds with tidal bundle, mud drapes and reactivation surfaces.	Outer estuary

Table 5.2 (continued)

Facies Association	Code	Facies components	Description	Gamma ray pattern	Paleocurrent	Interpretation	Depositional setting
Offshore tidal bar	OTB	St, Sm, Sr, He, Fl	Elongated coarse-grained sandstone bodies (sand tidal bars) interbedded with thin heterolithic strata that compose up to 7 m thick intervals truncated at the top by SBB	Serrate, higher peaks in front of mudstone layers	Mainly to SW	Shoreface deposition and accumulation from suspension and traction.	Shallow marine
Shoreface heterolithic	SHF	He, Fl	Sheet-like heterolithic bed up to 3 m thick and broad lateral extent (> 1000 m), usually truncated at the top by TCH, TB or OTB.	High peak values	--	Shoreface deposition and accumulaton from suspension	Shallow marine

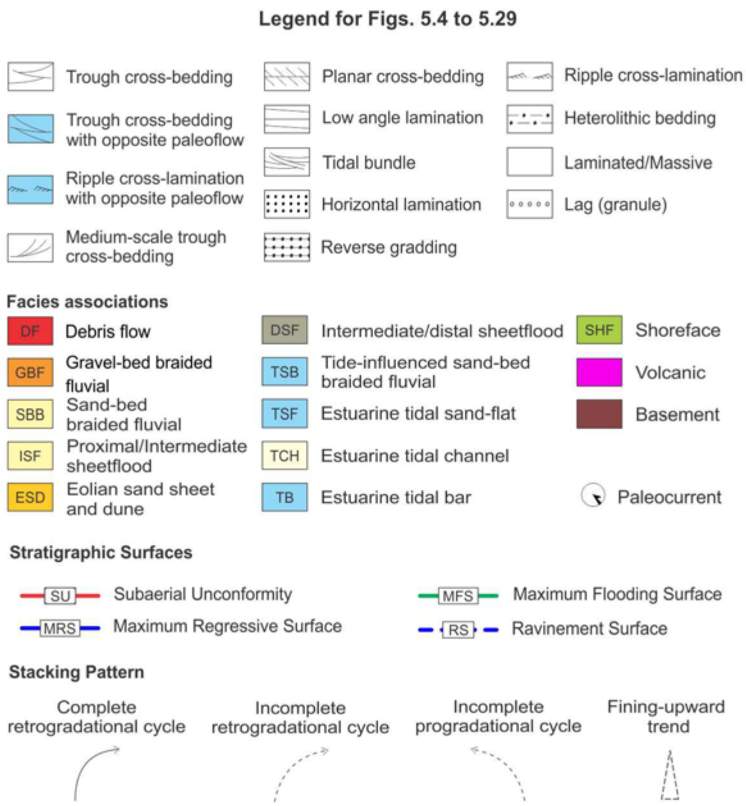

Fig. 5.3. Legend for Figs. 5.4 to 5.29.

5.4.1. Facies associations related to estuarine and shallow marine settings

5.4.1.1. Tidal channel (TCH) facies association

5.4.1.1.1. Description

The TCH is characterized by the channel-like external geometry that is tens of meters wide and up to 5 m deep on direction approximately perpendicular to the main paleoflow. This facies association consists of amalgamated lenticular sandstone bodies that fill the channel scours (Fig. 5.5). Internally, sandstone is medium- to coarse-grained, mostly with tangential and trough cross-bedding (facies St) and less frequently with planar cross-stratification (facies Sp), low angle cross-bedding (facies Sl) and structureless (facies Sm). Some sandstone strata exhibit contorted lamination, dish and pillar structure. Mud drapes are common between the foresets and sets of sandstone are bounded by laminated to massive mudstone, which forms lenticular layers up to 0.1 m thick that extend laterally for some meters. The channel shape fill is complex (Fig. 5.7B), with internal scours filled by sandstone lenses and mudstone drapes; in some cases lenticular sandstone bodies re organized in sigmoidal, laterally succeeding bodies whose toesets are tangential to the basal channel scour. In most cases sigmoidal bodies exhibit cross-bedded strata oriented perpendicularly to the sigmoidal bounding surfaces. The channel bottom surface is clearly concave up and erosional while the upper contact is flat with the adjacent units. Paleocurrents are bidirectional mainly in the westward direction.

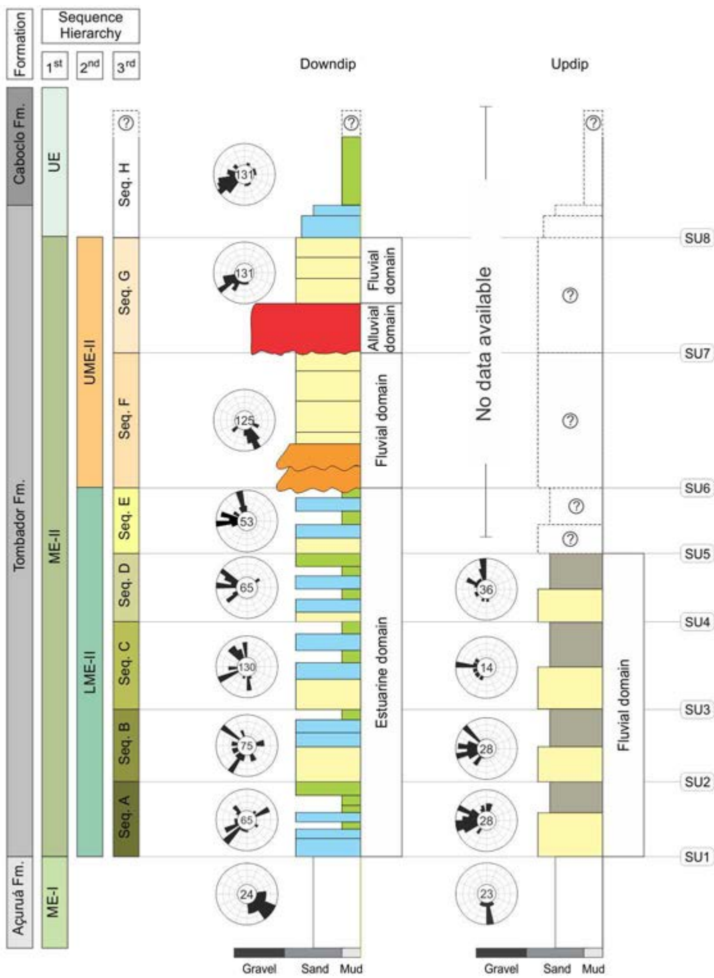

Fig. 5.4. Schematic vertical stacking of Sequences A-H and their facies associations. Lithostratigraphic units and first- to third-order sequences are given at the left. Subaerial unconformities are given at the right. Third-order sequences thicknesses are also indicated. Rose diagrams exhibit all paleocurrent readings from each third-order sequence at distinct paleoenvironment domains. Abbreviations: ME-I-Middle Espinhaço I, ME-II-Middle Espinhaço II, UE- Upper Espinhaço, LME-II- Lower Middle Espinhaço II, UME-II- Upper Middle Espinhaço II, Seq.- sequence, SU- subaerial unconformity.

5.4.1.1.2. Interpretation

The channel-like geometry, filled with sandstones lenses enveloped by mud drapes and bidirectional paleocurrent, suggests deposition filling tidal channels (Boyd et al., 2006). The lenticular sandstone bodies are interpreted as macroforms that fill the channels. Cross-strata with paleoflow approximately perpendicular to the sigmoidal bounding surfaces suggest lateral accretion bedding associated to tidal channels with high sinuosity (Dalrymple, 2010). The vertical thickness of 3-5 m is interpreted to be the maximum depth of the channels. The predominance of paleocurrents oriented westwards, the same direction of fluvial cross-strata, indicates that ebb-tide was paleoflow dominant direction.

5.4.1.2. Tidal sand flat (TSF) facies association

5.4.1.2.1.Description

This facies association is dominated by amalgamated sand sheet internally composed of horizontal laminated (facies Sh), ripple cross-laminated (facies Sr) sandstone, and trough cross-bedded sandstone (facies St). Sandstone is coarse-to medium-grained, arranged in individual beds with sharp, slightly undulating, erosive bases. Sets are centimetric (up to 0.2 m thick), characterized by successions of Sh overlain by Sr sandstone up to 1 m thick. St strata are 0.5-0.8 m thick, interbedded with Sh-Sr successions (Figs. 5.5, 5.10A). The TSF is characterized by up to 10 m thick tabular packages, which are laterally continuous for hundreds of meters. Paleocurrent readings point westward and subordinately eastward. The lower and upper contacts are sharp to erosive with the adjacent units.

5.4.1.2.2. Interpretation

The occurrence of sandstones with bidirectional paleoflow direction suggests deposition under tidal influence (Eriksson & Simpson, 2004). Horizontal parallel laminated sandstones succeeded by ripple cross-laminated sandstones with bidirectional paleoflow are common in high-energy tidal sand flats (Dalrymple et al., 1985, 1990; Dalrymple, 1992; Plink-Björklund, 2005). The horizontal laminated sandstone is interpreted as deposits formed in upper flow regime associated with the main tides, and the ripple cross-laminated sandstones are interpreted as formed in lower flow regime derived from subordinate tide currents. Upper-flow regime parallel lamination predominates in the shallower parts of the outer (tide-influenced) straight reach of the estuary (Boyd et al., 2006). Tidal sand flats are formed under upper-flow-regime because, on average, tidal-current speed increases into the estuary so that the area headward of the elongated bar is characterized by extensive sand flats with parallel lamination (Dalrymple, 2010). The trough cross-bedded sandstone more likely represents migration of sinuous crested dunes deposited during tide flows.

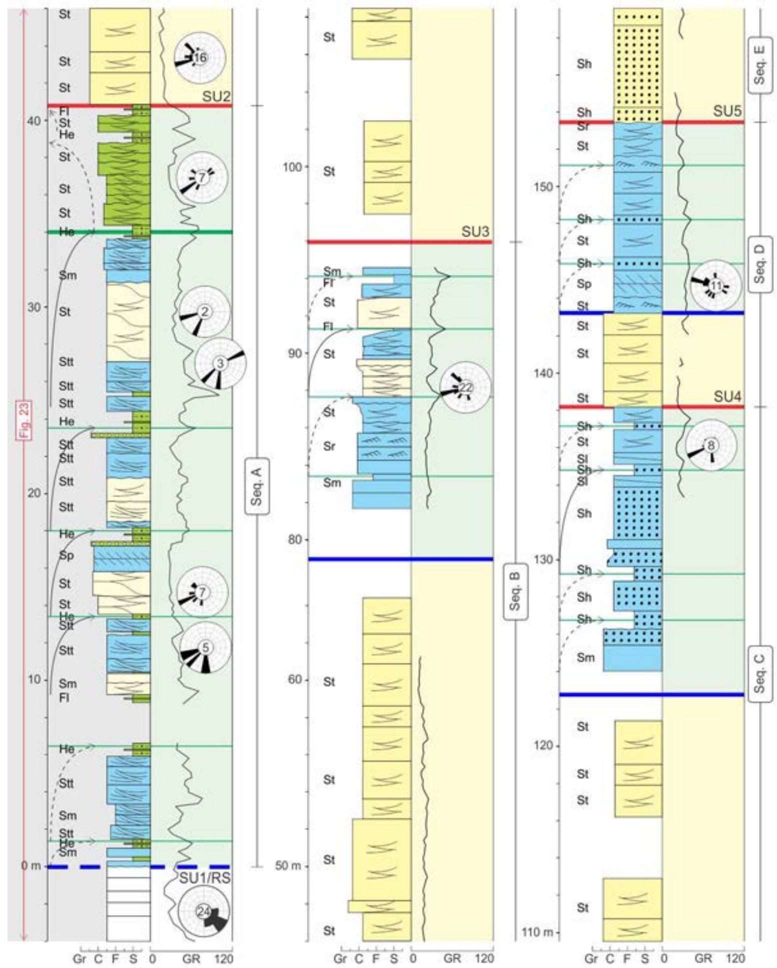

Fig. 5.5. Stratigraphic occurrence and thickness of Sequences A-E at the estuarine domain measured at vertical section 11. Note that estuarine successions exhibit a serrate pattern of the GR log that corresponds to a cyclic retrogradational stacking pattern of tidal channel, tidal bar, and shoreface strata. In contrast, fluvial successions are characterized by a monotony of facies resulting in a blocky pattern. Ripples and trough cross-stratification oriented at the opposite direction of the main fluvial paleoflow indicate tidal influence on fluvial strata (e.g., Seq. D. Compare the paleocurrent data from this vertical section with those from Fig. 5.4). The acronyms of facies are given at the left of the column, while stratigraphic surfaces, sequences identification, and related Figures are given at the right.

5.4.1.3. Tidal bar (TB) facies association

5.4.1.3.1. Description

This facies association consists of tangential cross-stratified and tidal bundled (facies Stt) fine- to coarse-grained sandstones, minor planar cross-stratification (facies Sp), and massive (facies Sm, Fig. 5.5). Stt strata (Fig. 5.11D) generally show reactivation concave down surfaces regularly spaced, mud drapes in the foresets and locally ripples climbing up the bottom part of and in opposite direction to that of the larger scale cross-strata. Simple or composed 1-1.5 m thick cross strata are superbly exposed in many sections. Simple cross strata have steeper dip (25-30^{o}) and foresets show different thickness in vertical section parallel to the paleoflow. Cross strata exhibit fairly symmetrical ripples on top and are bounded by mud drapes deposited on flat dipping surfaces in the same direction of the cross strata or laminated to massive mudstone beds up to 0.4 m thick. Commonly sandstone elongated lenses are amalgamated to each other, forming up to 2.5 m thick elongated bodies that extend laterally for some tens of meters. Some sets exhibit truncated wavy lamination. Bidirectional paleocurrent readings indicate westwards main direction (N280) and eastwards subordinated direction (N130). The lower contact is flat to slightly erosive while the upper contact is commonly abrupt with the adjacent units. At GPR line, TB is characterized by reflection-free bodies bounded by high-amplitude reflections (Fig. 5.6).

5.4.1.3.2. Interpretation

The occurrence of cross-stratified sandstones with bidirectional paleocurrents, tidal bundles, mud drapes in the foresets, reactivation surfaces, and ripples climbing up the foresets in opposite direction of the main paleoflow suggests development of subtidal sandstone bars (Dalrymple, 2010). The presence of relatively frequent fairly symmetrical ripples on top of cosets is evidence of wave reworking. Cosets bounded by low angle surfaces more likely indicate dunes migration on top of tidal bars. Reactivation surfaces on cross strata indicate changing in the frontal face of subaqueous sand dune in response to variation in the direction of tidal currents and hence, erosion on top of bars (Shanley & McCabe, 1994). Thin mud drapes capping foresets are the product of suspended mud settling during the slack-water phase between the tides (Visser, 1980). Thickness variations of foresets in vertical section parallel to the flow may be related to neap-spring-neap moon cycles (Visser, 1980).

Bidirectional paleocurrents reflect opposite direction of tidal currents, ebb-tide being the most frequent direction (westwards, based on SBB paleocurrents). The slightly erosive bottom surface results from tide scouring and hence, represents tide ravinement surface formed during transgressions (Allen & Posamentier, 1993).

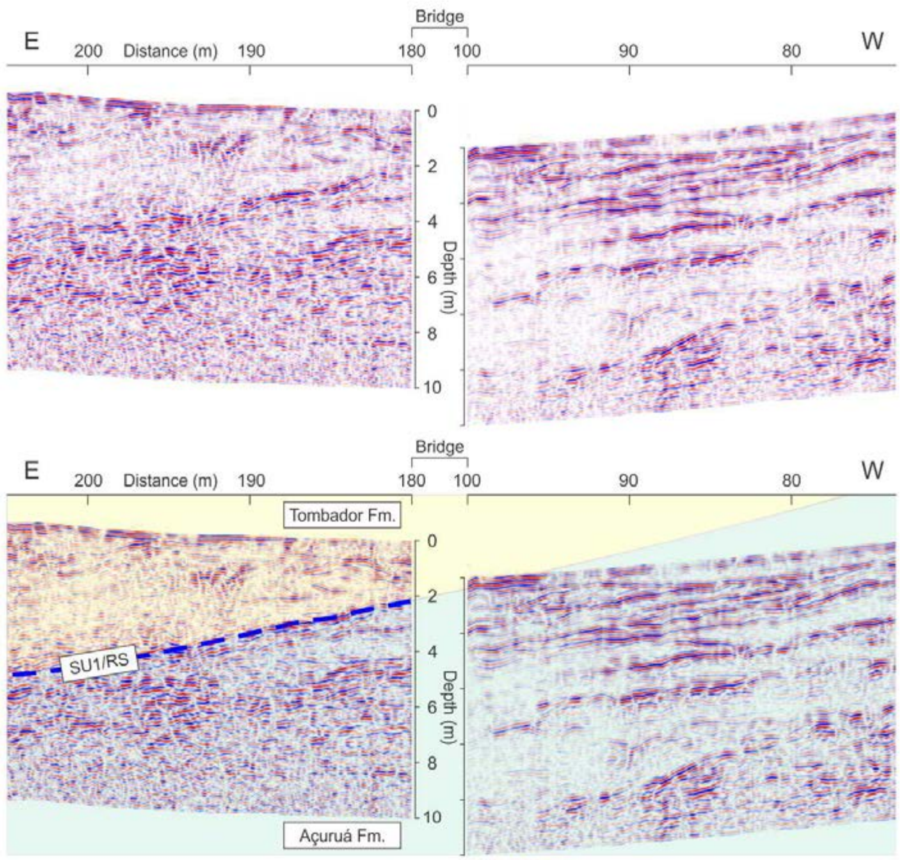

Fig. 5.6. GPR line showing Seq. A lower boundary (lithostratigraphically, the contact between the Açuruá and the Tombador Formations). In this location, SU1 and a tide ravinement surface are superimposed. Below the contact, the Açuruá Formation is characterized by three radar facies related to a delta plain setting: a- trough-shaped features bounded by basal concave-up reflections (distributary channels), b- oblique to sub-parallel discontinuous reflections (delta plain), and c- reflection-free bodies enveloped by facies b (massive sandstone bodies filling distributary channels). Above the contact, the Tombador Formation is characterized by reflection-free bodies bounded by high-amplitude, continuous reflections that are related to tidal bars. See Fig. 5.1 for GPR line location.

Fig. 5.7. Representative facies associations of Sequence A. (A) At the estuarine domain, a tide ravinement surface and SU1 are superimposed at the base of tidal bars overlying delta plain deposits; (B) tidal channel truncating tidal bar; (middle of photo C) lower shoreface heterolithic facies overlying tidal bar; (D) zoom on laminated mudstone from shoreface heterolithic interval; (E) trough cross-bedded sandstone with stylolite from offshore tidal bar. SU2 is placed at the erosive bottom of a sand-bed braided fluvial overlying tidal bar strata (F). At the fluvial domain, Sequence A exhibits, in ascending order, a sand-bed braided fluvial (G) and a sand-rich floodplain represented by the intercalation of fine-grained sandstone and siltstone beds (H). The stick in photos G and H is 0.6 m high. See photos location at Fig. 5.5 (photos A-F) and Fig. 5.8 (photos G-H). Abbreviations: SU-subaerial unconformity; RS-ravinement surface; SBB-sand-bed braided fluvial; SHF-shoreface; SFP-sand-rich floodplain; TB-tidal channel; TCH-tidal channel.

5.4.1.4. Offshore tidal bar (OTB) facies association

5.4.1.4.1. Description

This facies association consists of coarse-to very coarse-grained trough cross-bedded sandstone (facies St), rich in mud clasts and stylolites (Figs. 5.5, 5.7E). Mud clasts are up to 4 cm long, sub-angular to sub-rounded. Its elongated shape filled with facies St interbeds with thin (less than 0.5 m thick) wavy-laminated heterolithic strata. The main characteristic of this facies association is that sandstone bodies are arranged in tabular to elongated beds less than 0.8 m thick that exhibit coarsening- and thinning-upward trends. It forms tabular bodies with fairly symmetrical ripples on top that extend laterally for hundreds of meters. Unidirectional paleocurrent readings indicate westwards main direction (N280). The lower contact is flat to slightly erosive while the upper contact is commonly abrupt with shoreface heterolithic strata.

5.4.1.4.2. Interpretation

The occurrence of cross-stratified sandstones with fairly simetrical ripples on top, interbedded with heterolithic strata suggests development of subtidal sandstone bars (Dalrymple, 2010). Reactivation surfaces on cross strata indicate changing in the frontal face of subaqueous sand dune in response to variation in the direction of tidal currents and hence, erosion on top of bars (Shanley et al., 1994). Predominant unidrectional paleocurrents reflect westwards ebb-tide tidal currents, based on SBB paleocurrents. Sandstones and mudstones with wavy ripples are interpreted as deposited on lower shoreface above the normal wave base level (Simpson et al., 2002). The presence of relatively frequent fairly symmetrical ripples on top of sandstone cosets and wavy truncated lamination in heterolithic strata corroborates the wave activity on shoreface during deposition of this facies association.

5.4.1.5. Shoreface heterolithic (SHF) facies association

5.4.1.5.1. Description

This facies association consists of heterolithic strata (facies He) that are composed of interbedded mudstone and sandstone (Fig. 5.5). Mudstone is mostly wavy-laminated claystone and siltstone (facies Fl, Figs. 5.7C, D). Sandstones are fine- to medium-grained, massive (facies Sm), or with ripple cross-lamination (facies Sr). The base of heterolithic strata is marked by thin (less than 0.3 m thick) granular to very coarse-grained sandstone layer, with irregular to flat basal erosive surface (Figs. 5.11E, F). The SHF consists of very distinctive heterolithic tabular body up to 3 m thick that can be traced laterally for hundreds to thousands of meters. The bottom contact is sharp and erosive while the upper contact is abrupt to slightly erosive with the adjacent units.

5.4.1.5.2. Interpretation

Heterolithic strata with tabular geometry and abrupt to gently erosive basal contact are interpreted as transgressive lower shoreface deposits overlying tidal bars or tidal channel. Laminated and massive mudstone was deposited from suspended mud settling (McCormick & Grotzinger, 1993). Sandstones and mudstones with wavy ripples are interpreted as deposited on lower shoreface above the normal wave base level (Simpson et al., 2002). Wavy truncated lamination corroborates the wave activity on shoreface during deposition of this facies association. The very coarse-grained to granular layers on the base represent transgressive lags formed by wave ravinement surface during transgressions (Bruun, 1962; Swift et al., 1972; Swift, 1975; Nummendal & Swift, 1987; Dominguez & Wanless, 1991).

5.4.1.6. Tide-influenced sand-bed braided fluvial (TSB) facies association

5.4.1.6.1. Description

This facies association consists of medium-grained to granular trough cross-stratified sandstone ripple marks, and minor low angle cross-stratified (facies Sl), massive (facies Sm), and ripple cross-laminated (facies Sr) sandstone (Figs. 5.5, 5.13). Centimetric (up to 5 cm) subangular mud clasts occur dispersed in the matrix. St sandstone exhibits uniform grain size or fining-upward trend, and forms cosets, each composed of 2-5 sets of decimeter-scale crossbeds whose bounding surface is slightly flat to concave-up rarely exceeding 1 m in relief, delineating large scale lenticular bodies (Figs. 5.16A, B). Bounding surfaces of cosets are marked by changes in thicknesses and grain size, and are often erosional. At the top, some cosets exhibit asymmetric centimeter-scale ripple marks. The TSB is characterized by the homogeneity of facies and the abundance of low-hierarchy erosional surfaces. The large scale geometry of the SBB suggests that the architecture is dominated by several meters thick units that are fairly tabular and laterally continuous for more than 1000 m in directions both parallel to perpendicular to main dips of cross-beds. Paleocurrent directions obtained from cross-strata point to a westward flow; less frequent small-scale trough cross-bedding and asymmetric ripples oriented to southeast are also found. The lower and upper contact of TSB is transitional; with the adjacent units.

5.4.1.6.2. Interpretation

The occurrence of cross-stratified sandstones bodies with mud clasts, fining-upward grain size trend, predominant paleocurrent direction, and frequent internal erosive surfaces suggests deposition in fluvial channels (Bristow, 1993; Collinson, 1996). The multiple erosion surfaces indicate repeated episodes of cut and fill. However, asymmetric ripples and trough cross-strata with opposite paleocurrent direction relative to the main fluvial paleoflow indicate reverse currents, strong evidence that shallow sand-bed braided channels were reworked by tides as the fluvial system debouched into the sea (Eriksson & Simpson, 2004).

5.4.2. Facies associations related to continental settings

5.4.2.1. Sand-bed braided fluvial (SBB) facies association

5.4.2.1.1. Description

This facies association mainly consists of trough-cross stratified sandstone (facies St) and minor low angle cross-stratified (facies Sl), tabular cross-stratified (facies Sp), and massive (facies Sm) medium-grained to granular sandstone (Fig. 5.8). Centimetric (up to 5 cm) subangular mud clasts are found in some strata. St facies exhibits uniform grain size or fining-upward trend, and is organized in cosets, each composed of 2-5 sets of decimeter-scale cross-strata (Fig. 5.7G). Bounding surfaces of cosets delineate meter-scale lenticular bodies, and are marked by changes in thicknesses and grain size. Such surfaces are slightly flat to concave-up rarely exceeding 1min relief, often erosional. Sometimes it is preceded by scours filled with cross-bedded granular sandstone. At the top, some sandstone bodies exhibit asymmetric, centimeter-scale ripple marks and horizontally laminated (facies Sh) laterally discontinuous, thin (up to 0.5 m thick) sandstone beds. The SBB is characterized by the homogeneity of facies and the abundance of low-hierarchy erosional surfaces. The large scale geometry of the SBB suggests that the architecture is dominated by several meters thick units that are fairly tabular and laterally continuous for more than 1000 m in directions both parallel to perpendicular to main dips of cross-beds. Paleocurrent directions obtained from cross-strata point to a main southwestward axial flow. The lower and upper contacts of SBB are, respectively, erosional and sharp with the adjacent units.

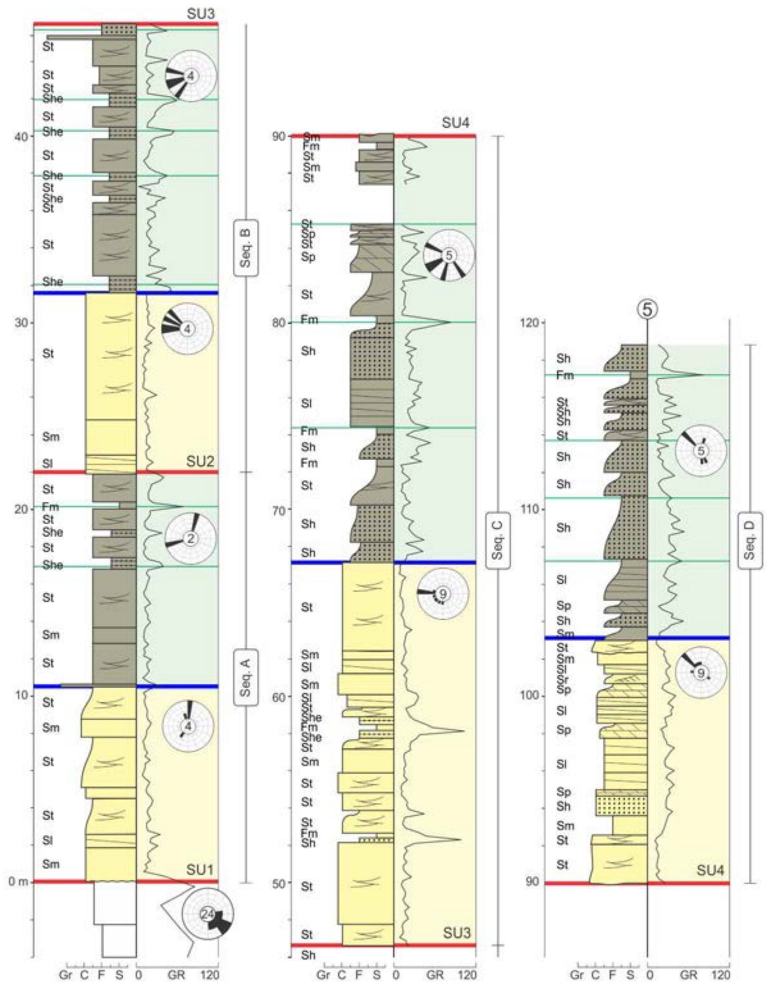

Fig. 5.8. Stratigraphic occurrence and thickness of Sequences A-D at the fluvial domain measured at vertical section 7. Subaerial unconformities (SU1-4) occur at the base of fluvial sand sheets (in yellow). Note the serrate pattern of the GR log associated with the sand-rich floodplain (in gray) in contrast to the blocky pattern in front of sand-bed braided or intermediate sheetflood sandstone (in yellow). Cyclic fine-grained intervals are candidates for lower-order hierarchy sequence boundaries. The acronyms of facies are given at the left of the column, while stratigraphic surfaces, sequences identification, and related Figures are given at the right. Compare the paleocurrent data from this vertical section with those from Fig. 5.4.

5.4.2.1.2. Interpretation

The occurrence of sandstones bodies with trough cross stratification bounded by erosive surfaces with coarse grains lying above them suggests deposition of fluvial channels

(Collinson, 1996). These erosive surfaces are interpreted as the thalweg of the main channels (5^a order surface of Miall, 1996). Lenticular to roughly tabular sandstone bodies composed of cross-stratified strata are interpreted as accreting bedforms deposited inside fluvial channels. The uniformity of this facies association indicates the preferential preservation of channel and fluvial bar deposits. Amalgamated sandstone beds bounded by low relief erosive irregular surfaces suggest that such surfaces more likely represent accretion surfaces, which implies that succeeding flood events resulted in aggradation of macroforms rather than erosion of previous deposits. The intraformational mud clasts are related to erosion of the overbank area during lateral channel migration, and their subsequent redeposition to form channel lag. Finer-grained laminated sandstone is interpreted as bar-top deposits or barflank sand sheet that accumulated in the shallowest part of channels under upper flow regime (Cant & Walker, 1978; Miall, 1985). The predominant fairly tabular large-scale geometry is resulted from amalgamation of broad and shallow braided channels deposits, which likely occupied the full width of the floodplain that are typical of shallow sand-bed braided river (Miall, 1996).

5.4.2.2. Intermediate sheetflood (ISF) facies association

5.4.2.2.1. Description

This facies association is mainly composed of sandstone with low angle-cross stratification (facies Sl) and minor massive (facies Sm), trough cross-stratified (facies St), tabular cross-stratified (facies Sp) medium- to very coarse-grained sandstone with granules dispersed, and ripple cross-laminated (facies Sr) medium- to fine-grained sandstone (Figs. 5.8, 5.13). Sl sandstone is organized in cosets that delineate large-scale tabular bodies. Internally, 2-10 cm thick sets exhibit supercritical ripples on the top and flat, horizontal to low angle slightly erosive basal bounding surface (Figs. 5.12D, 5.14C). Sm, St, and Sp sandstones form isolated, up to 1 m thick beds composed of structureless and medium-scale planar and trough-cross bedded cosets. Sr sandstone occurs as thin (up to 0.3 m thick) strata on top of Sl or Sp intervals, usually with fining upward trend overlain by discrete (less than 0.4 m thick) massive mudstone beds. Isolated medium-scale trough cross-bedded medium-grained sandstone with grain flow and grain fall (facies Ste) is found in some vertical sections. Bounding surfaces are horizontal to low-angle, slightly erosive, and marked by changes of facies. The geometry of the larger-scale strata of ISF suggests the dominance of amalgamated tabular bodies less than

15 m thick (Fig. 5.7G) that are laterally continuous for more than 100 m. Paleocurrent directions obtained from cross-strata show wide dispersion from southwest to northeast with main direction to northwest. The lower and upper contacts of ISF are, respectively, erosional and sharp with the adjacent units.

5.4.2.2.2. Interpretation

The tabular sandbodies with a slightly undulating erosive base and the predominance of low-angle cross-bedded sandstones are interpreted as the result of high-energy flood deposition, unconfined sheets and poorly defined fluvial channels (Nemec & Postma, 1993; Blair, 2000). Thin, sheet-like bodies composed of laminated sandstones are interpreted as the result of a series of ephemeral unconfined sheetfloods, which quickly decelerate at the end of the flow and hence allow development of supercritical ripples (Turnbridge, 1981; Hampton & Horton, 2007). Tabular sandstone bodies with medium size trough cross stratification (St) represent the migration of sinuous-crested simple sand bars, indicating fluctuations on the flow regimen between the floods. Massive sandstones (facies Sm) are interpreted as resulting from transport and deposition of sediments by short-lived high-density flows, which are responsible for dumping sediments at a rate too fast for hydraulic sorting processes to work effectively. The high density flow is probably maintained in suspension by the combined effect of turbulence, buoyant support and dispersive pressure (Lowe, 1988). Medium-scale trough cross-bedded sandstone with grain flow and grain fall is interpreted as isolated eolian dune.

5.4.2.3. Distal sheetflood (DSF) facies association (sand-rich floodplain SFP)

5.4.2.3.1. Description

This facies association is characterized by uniform grain size or fining upward successions of medium- to fine-grained sandstone to siltstone (Fig. 5.8). Individual fining upward succession is about 1.40 m thick, capped by mud drapes or siltstone layers up to 0.4 m thick. Sandstone is massive (facies Sm), laminated (facies Sh) or low angle cross-stratified (facies Sl), trough cross-bedded (facies St), and ripple cross-bedded (facies Sr) capped by mud drapes. Fine-grained laminated sandstone with inverse grading and granular ripples (facies She) up to 70 cm thick forms discrete layers interbedded with fine grained-sandstone and mudstone (Fig. 5.9). Siltstone is massive, commonly interbedded with facies She, or on top of fining-upward successions. Bounding surfaces are planar and sharp, marked by changes in grain size or in sedimentary structures of adjacent facies. The large-scale geometry of SFP indicates that it constitutes tabular body up to 14 m thick, with flat and non-erosive basal surface, that is laterally continuous for hundreds of meters. Paleocurrent readings exhibit wide dispersion, but the main vector points northward. The lower and upper contact of SBB are, respectively, sharp and erosional with the adjacent units.

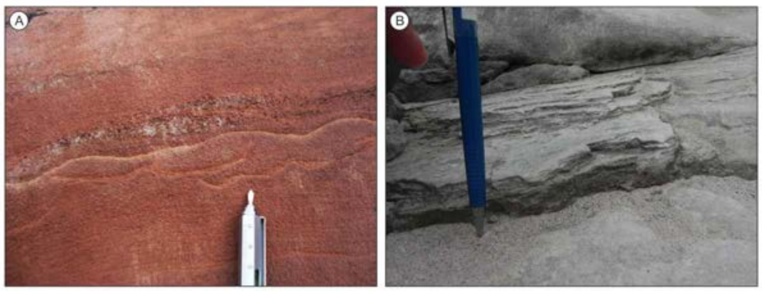

Fig. 5.9. Representative facies associations of Sequence B. (A) At the fluvial domain, the Seq. B. sand-rich floodplain exhibits granular ripples and mud drapes (B) and thin siltstone bed. At the estuarine domain, Seq. B is characterized by tidal channel, tidal bar and shoreface strata similar to those shown in Fig. 7. See photos location at Fig. 8.

Fig. 5.10. Representative facies associations of Sequence C. (A) At the estuarine domain, Seq. C exhibits upper flow regime sandstone from tidal sand-flat, while (B) at the fluvial domain, the sequence is characterized by the fining-upward grain size trend of sand-rich floodplain. See photos location at Fig. 5.5 (photo A) and Fig. 5.8 (photo 10B).

5.4.2.3.2. Interpretation

Laterally extensive tabular sandstone beds composed of fining up successions indicate deceleration of ephemeral unconfined or poorly-confined sheetfloods (Turnbridge, 1981; Hampton & Horton, 2007) that rapidly decreased their energy before finally dissipating to enable deposition of fine-grained sediments (Williams, 1971). This facies association is characteristic of distal braid plains, particularly in arid regions where ephemeral runoff forms a network of shallow, interlacing, possible poorly defined channels (Miall, 1996). Interbedding of ephemeral sheetflood deposits and sandstones with inverse grading and granular ripples suggests eolian reworking and deposition. Eolian sand sheet sandstones, siltstones beds, and mud drapes are strong evidence of high water table level (Kocurek & Havholm, 1993; Tirsgaard and Øxnevad, 1998). The occurrence of distinct intermediate/distal sheetflood intervals on top of the fluvial facies associations (SBB and IFF) reinforces changing on depositional conditions (Marconato et al., 2014). As such, DSF represents the sand-rich floodplain in the Chapada Diamantina.

5.4.2.4. Debris-flow deposit (DF) facies association

5.4.2.4.1. Description

This facies association consists of poorly-sorted, massive, clast-supported (facies Gcm) and inverse-graded (facies Gci) conglomerates (Fig. 5.13). Clasts are formed of boulder to granules of sandstone, white and green quartzite (Fig. 5.14E). Boulders are sub-angular (sandstone) to sub-rounded (quartzite); matrix is composed of coarse-grained sandstone. Conglomerate usually forms disorganized, sometimes normal or inverse-graded, amalgamated beds 5-10 m thick, locally capped by up to 0.5 m thick lenses of coarse-grained horizontally laminated and trough cross-stratified sandstone. The large scale geometry of the DF suggests that it forms elongated bodies 40-100 m thick. The basal surface is erosive and the upper surface is abrupt with adjacent units.

5.4.2.4.2. Interpretation

This facies association is interpreted to represent sediment-gravity-flow deposits. The clast-supported nature, poor sorting, absence of internal organisation and sandstone matrix, suggest deposition from no cohesive debris flows, in which sediments were transported by frictional grain interactions (Nemec & Steel, 1984; Blair & McPherson, 1994a, b). The occurrence of amalgamated beds suggests that the debris flows deposits consist of multiple surges (Davies, 1986, 1990; Major, 1997; Sohn, 1999). The coarse-grained laminated and trough cross-bedded sandstones are interpreted as sheetflood deposits, formed from aqueous flows that succeeded debris flows (Ballance, 1984; Wells, 1984).

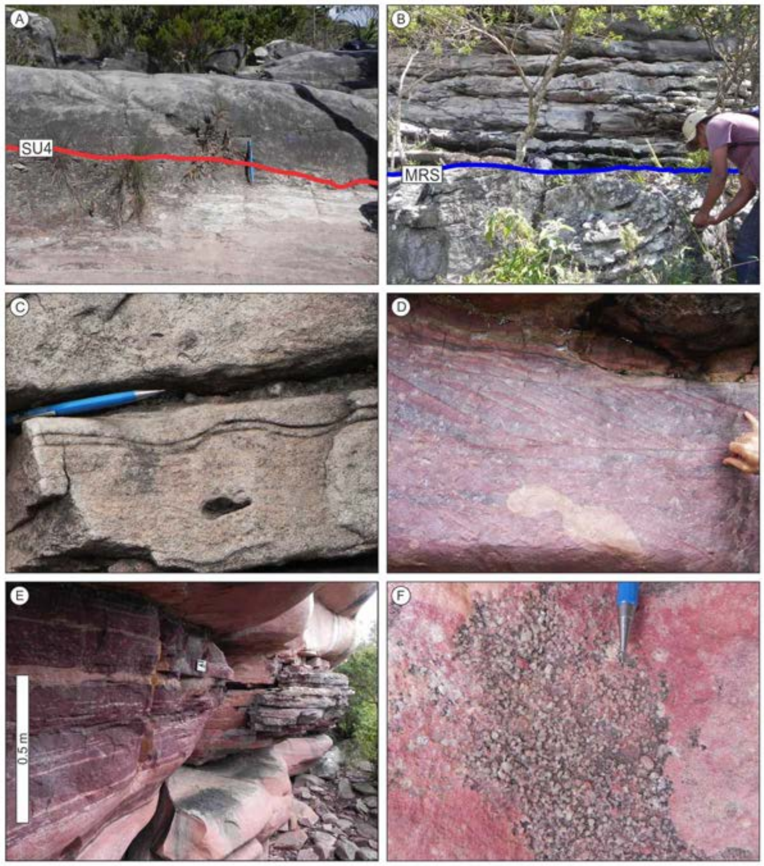

Fig. 5.11. Representative facies associations of Sequence D. At the fluvial domain, SU4 is placed at the bottom of a medium- to coarse-grained sand-bed braided fluvial deposit truncating sand-rich floodplain interval (A). At the estuarine domain, SRM is placed at the top of a fluvial sand-bed braided interval, which is overlain by an estuarine succession (B). The asymmetric ripple oriented to the opposite direction of the planar cross-bedding is indicative of a tidal influence on sand-bed braided fluvial sandstone (C). Tidal bundles and reactivation surface in tidal bar sandstone (D). Shoreface heterolithic facies (E); the transgressive lag is composed of granules and pebbles at the base of a shoreface heterolithic interval (F). See photos location at Fig. 5.5 (photo C), Fig 5.8 (photo A) and Fig. 5.23 (photos B, D-F).

5.4.2.5. Gravel-bed braided fluvial (GBF) facies association

5.4.2.5.1. Description

This facies association is composed of poorly-sorted, clast-supported conglomerate with sandy matrix and sandstone interbeds (Fig. 13). Clast size ranges from cobble to granule, composed of sub-rounded white and green quartzite and minor amount of other metamorphic rocks.

Conglomerate usually forms fining-upward cycles with erosive basal surface, from massive (facies Gcm) to horizontally stratified and incipient clast imbrications (facies Gh). It comprises 0.5-2.5 m thick beds with erosive basal surface that extend laterally for tens of meters (Fig. 5.14A). Sandstone is medium- to coarse-grained, with dispersed pebbles and cobbles, massive (facies Sm), horizontally-stratified (facies Sh), or trough cross-stratified (facies St). Sandstone beds consist of 0.3-0.6 m thick elongated bodies usually truncated at the top by overlying conglomerates. Paleocurrent readings from sandstone cross-strata point to a main southward flow. The large scale GBF geometry is characterized by 2-5 m thick sheet-like bodies that laterally extend for more than 500 m.

Fig. 5.12. Representative facies associations of Sequence E. At this location, SU 5 occurs at the base of an eolian sand sheet that overlies tide-influenced sand-bed braided fluvial sandstone (A, B). Zoom view of an eolian dune (C) and an intermediate sheetflood sandstone (D). These fluvial and eolian intervals are overlain by estuarine succession similar to those shown in Fig. 5.7. The acronyms of the facies associations are given at the Fig. 5.3. See photo A location at Fig. 5.5.

5.4.2.5.2. Interpretation

This facies association is interpreted as fluvial channel deposits (Miall, 1978, 1985). The occurrence of massive clast-supported conglomerates (facies Gcm) with a sandy matrix suggests deposition by high-density, hyperconcentrated flows (Wells and Harvey, 1987). Clast-supported conglomerates with horizontal stratification are interpreted as longitudinal gravel bar deposits (facies Gh). The stratified sandstones are interpreted as products of flat-bed, upper-flow regime (facies Sh) and of migration of sinuous crested dunes, deposited under lower-flow regime (facies St). The presence of facies Gcm with erosive base on the base of cycles suggests a high-energy flow, in which transported gravels are moved by high density dispersive forces along channels during high magnitude flooding periods. The massive sandstones that succeeded the conglomerates represent the deceleration periods of these floods (Todd, 1989). The occurrence of sheet-like conglomerate bodies with numerous minor internal erosion surfaces indicate predominance of gravel bedforms, characteristic of shallow, gravel-bed braided channels (Miall, 1996).

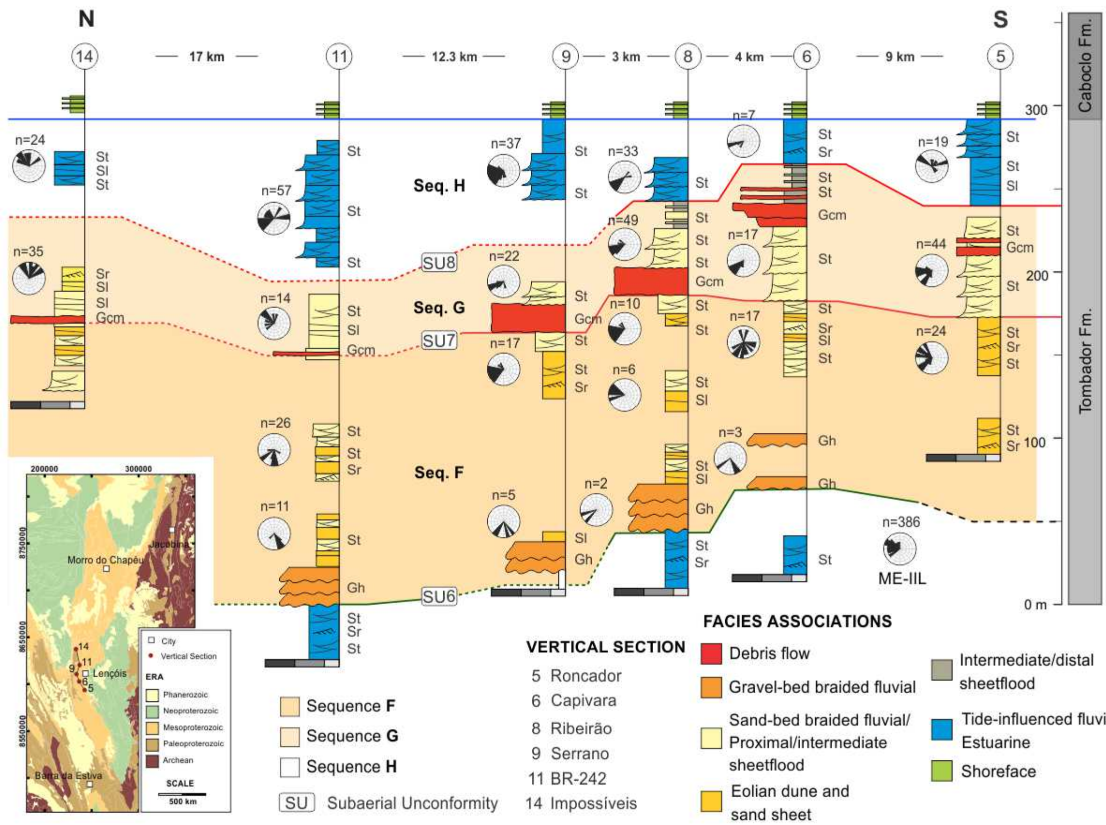

Fig. 5.13. Stratigraphic occurrence and thickness of Sequences F-H measured at vertical sections 14, 11, 9, 8, 6 and 5. Sequence boundaries (SU6-8) are marked based on the shift of facies and paleocurrents (compare the paleocurrent data from these vertical sections with those from Fig. 5.4). Note the continuity of eolian intervals in Seq. F and the facies variations within the alluvial fan in Seq. G (modified from Bállico, 2012). See location of this cross-section at Fig. 5.26. Facies acronyms are given at the right of the column.

5.4.2.6. Eolian sand sheet and dune (ESD) facies association

5.4.2.6.1. Description

This facies association consists of bimodal, moderately to well-sorted, fine- to coarse-grained sandstone (Fig. 5.13). ESD is composed of 0.3-1.5 m thick sets of horizontal (facies She) to low-angle cross-stratification (facies Sl, Figs. 5.12A, B) that locally is inversely graded and exhibits millimetric wind-ripple laminae. Occasionally, well-sorted, trough cross-bedded fine- to medium-grained sandstones are organized into isolated sets or cosets of facies Ste (Fig 5.14D) composed of grainfall and inversely-graded grainflow strata. From a view parallel to palaeoflow, cross-strata are tangential to their basal bounding surfaces. Paleocurrent reading from cross-strata show a mean paleoflow towards northeast. ESD composes tabular bodies up to 3 m thick and tens of meters wide with fairly tabular bounding surfaces.

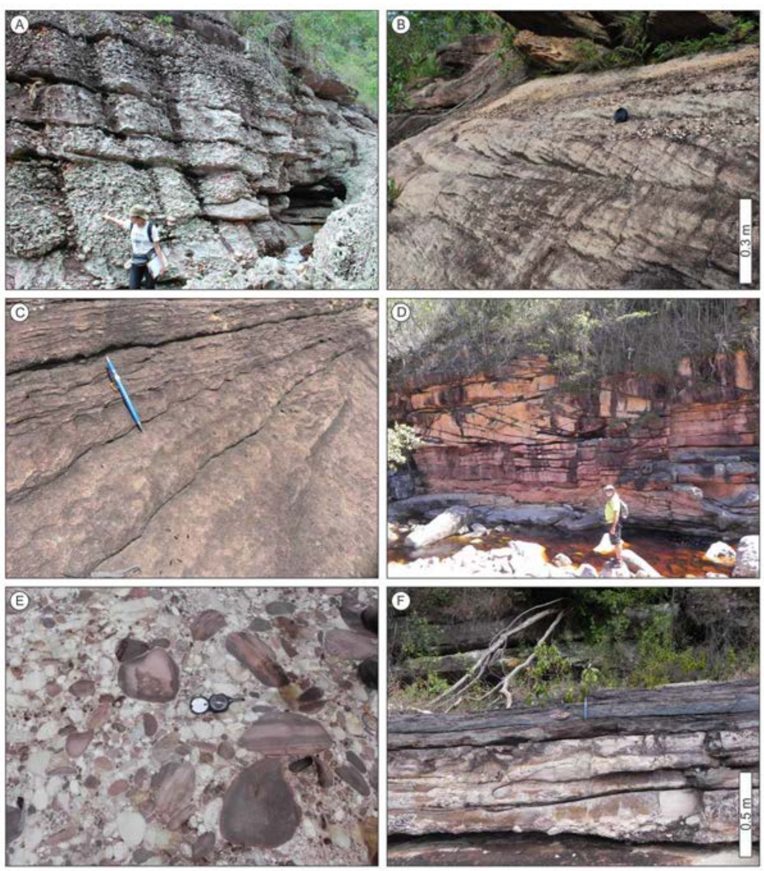

Fig. 5.14. Representative facies associations of Sequence F: (A) gravel-bed fluvial sandstones and conglomerates; (B) sand-bed braided fluvial; (C) intermediate sheetflood; and (D) eolian sandstones. Sequence G also contains (E) debris-flow conglomerates and (F) sand-rich floodplain deposits. See photos location at Fig. 5.13.

5.4.2.6.2. Interpretation

The bimodal sandstone with horizontal or low-angle cross-stratification and wind-ripple lamination is interpreted as eolian sandsheet deposit (Hunter, 1977; Kocurek & Nielson, 1986; Scherer, 2002; Scherer et al., 2007). The interbedded well-sorted, fine- to medium-grained sandstone organized into isolated sets or co-sets of trough cross-bedding with grainflow and grainfall strata is interpreted as eolian dune. The occurrence of grain flow strata indicates aeolian dunes with well-developed slipfaces. The presence of isolated cross-strata suggests dune migration over wide eolian sand sheet areas.

5.5. SUBAERIAL UNCONFORMITIES AND DEPOSITIONAL SEQUENCES IN THE TOMBADOR FORMATION

This study documents eight regional subaerial unconformities (SU1-8) in the Tombador Formation that register regional gaps in the stratigraphic record and are considered herein as depositional sequence boundaries. SU1-8 are placed at the base of extensive amalgamated fluvial sand sheets or at the base of alluvial fan conglomeratic successions, always indicating a basinward shift of facies and/or a change in depositional systems (Schum, 1993; Shanley & McCabe, 1994; Catuneanu, 2006; Fanti & Catuneanu, 2010). Maximum regressive surfaces are marked at the contact between fluvial sand sheet and estuarine or between fluvial sand sheet and sand-rich floodplain intervals. Based on the recognition of SU1-8, this study interprets eight depositional sequences, here named Seq. A-H in ascending order. Depending on their paleogeographic locations, Seq. A-H exhibit estuarine, fluvial, or alluvial fan successions, characterizing what is herein named estuarine, fluvial, or alluvial fan domains (Fig. 5.4).

5.5.1. SU1 and Seq. A description

SU1 is placed at the contact between fluvial-estuarine strata from the Tombador Formation and underlying deltaic deposits from the Açuruá Formation. The best exposure of this unconformity is at vertical section 11, at the bridge over the Mucugezinho River (Fig. 7A). This unconformity has been recognized by many authors (Derby, 1906; Schobbenhaus & Kaul, 1971; Inda & Barbosa, 1978; Pedreira, 1994; Schobbenhaus, 1996; Guimarães et al., 2008). Paleocurrent readings indicate a shift in the flow pattern across the unconformity:

sandstone cross-strata from the Açuruá Formation exhibit a SE trend (N132, n=24), while those from the lower Tombador Formation present a predominant SW/NW trend (Fig. 5.5). The unconformity is also visible at the GPR line (Fig. 5.6). The definition of SU1 is also supported by radiometric dating: volcanic dikes cutting the Paraguaçu Group (which includes the Açuruá Formation) yield the age 1514 ± 22 Ma (Babinski et al., 1999), while detrital and crystal tuff zircons in the upper Tombador Formation yield the ages 1394 ± 14 Ma (Gruber et al., 2011) and 1416 ± 28 Ma (Guadagnin et al., 2015), respectively. Thus, SU1 is a sequence boundary associated with a major hiatus (approximately 100 Ma).

5.5.1.1. Seq. A at the estuarine domain

Seq. A is composed of cyclic successions with a retrogradational stacking pattern of tidal channels, tidal bars, and shoreface heterolithic facies (Figs. 5.5, 5.7). Locally, a tide ravinement surface and SU1 are superimposed. The best exposure is at vertical section 11 (BR242 road close to the bridge over the Mucugezinho River). Tidal channels exhibit a concave-up erosive bottom surface; channels are tens of metres wide and up to 5 m thick and are filled with lens-shaped to sigmoidal sandstone bodies enveloped by mud drapes. Sandstone is medium- to coarse-grained, trough cross-bedded, and with mud drapes inside and between the foresets. Some sandstone lenses have contorted lamination and a dish and pillar structure. Tidal bars consist of amalgamated elongated lens-shaped bodies of sandstones up to 5 m thick with lateral continuity of hundreds of metres. Sandstone is fine- to coarse-grained with frequent tidal bundles; common sedimentary structures include tangential cross-stratification, herring-bone, planar cross-stratification, and fairly symmetrical ripple marks. Cosets are commonly enveloped by mudstone veneers. Shoreface heterolithic strata are composed of interbedded mudstone and sandstone. Mudstone is massive, parallel or wavy laminated. Sandstone is fine to medium grained, with wavy-ripple lamination. Shoreface heterolithic beds are tabular in shape, up to 3 m thick and laterally continuous for hundreds of metres to kilometres. The bottom contact is sharp and gently erosive over tidal channel and tidal bar sandstones, with transgressive lags composed of granules or very coarse sand grains. At the upper portion, Seq. A exhibits composed sets of offshore tidal bars and heterolithic strata. Cosets of sand tidal bars are less than 0.8 m thick, in which the grain size increases to coarse/very coarse and where mud clasts, trough cross-bedded sets, and stylolites are more abundant. Heterolithic strata are thin, less than 0.4 m. Offshore tidal bars and heterolithic strata exhibit a conformable thinning-up pattern. Seq. A is up to 45 m thick, and paleocurrent measurements (n=65) indicate a bidirectional flow predominantly to the SW (N225), with less frequent values to the NE (N57) (Fig. 5.4).

5.5.1.2. Seq. A at the fluvial domain

Seq. A consists of fluvial shallow braided sand sheet and intermediate sheetflood strata overlain by sand-rich floodplain deposits (Figs. 5.5, 5.7, 5.8). Braided sand sheets show erosive bottom surfaces and form poorly channelized bodies up to 4 m thick with broad lateral continuity. Sandstone is medium to coarse grained locally with granules to pebbles and is trough-cross stratified. Intermediate sheetflood sandstone is organized in cosets up to 1.5 m thick, each composed of several thin sets (0.02 to 0.1 m thick) with supercritical-climbing ripples on the top. Bounding surfaces are flat to low angle, slightly erosive, delineating large-scale tabular bodies. Sandstone is medium- to very coarse-grained with dispersed granules and low-angle cross stratification. The sand-rich floodplain is characterized by an interval up to 14 m thick that is composed of tabular cyclic successions of distal ephemeral sheetflood capped by eolian sand sheet or mudstone layers. Such successions exhibit uniform grain size and/or a fining-upward trend up to 3 m thick, capped by mud drapes or siltstone layers up to 0.4 m thick interbedded with eolian sandstone (Fig. 5.9). Distal sheetflood sandstone is medium- to fine-grained, laminated, low angle cross-bedded, ripple cross-bedded on top, and locally trough cross-stratified. Eolian sandstone is fine-grained, with reverse grading and granular ripples, and forms horizontally laminated beds up to 0.5 m thick. Locally, tide-influenced sand-bed braided fluvial intervals interbed with sand-rich floodplain deposits. The tide-influenced braided fluvial strata are formed by fine- to medium-grained trough cross-bedded sandstone in which some cross-strata and asymmetric ripples are oriented to the opposite direction of the main fluvial paleoflow. Overall, the whole fluvial interval is up to 25 m thick; paleocurrent directions (n=28) indicate predominant flow towards the west (N282) (Fig. 5.4).

5.5.2. SU2 and Seq. B description

5.5.2.1. Estuarine domain

SU2 is an erosional contact between the underlying offshore tidal bars and heterolithic strata of Seq. A and braided fluvial sand sheet of Seq. B. The best exposure of this unconformity is at vertical section 11, next to the bridge over the Mucugezinho River (Fig. 5.7F). Sequence B is formed of fluvial sand sheet and overlying cyclic estuarine successions that are quite similar to those from Seq. A (Fig. 5.5). Overall, the braided fluvial sand sheet consists of an interval up to 22 m thick composed of medium- to coarse-grained sandstones in which trough cross-stratification is marked by granules of white and green quartzites on the stratification surfaces. The estuarine succession is up to 25 m thick and is formed of cyclic successions with a retrogradational stacking pattern of tidal channel, tidal bar and heterolithic strata. Paleocurrent directions in the estuarine succession (n=75) indicate two predominant paleoflows: one southwestern oriented (N230) with a less frequent flow towards NE (N75), and other northwestern oriented (N315) with a less frequent flow towards SE (N165) (Fig. 5.4).

5.5.2.2. Fluvial domain

SU2 is marked at the contact between the braided fluvial sand sheet from Seq. B and the sand-rich floodplain from Seq. A (Fig. 5.8). Seq. B is formed of a braided fluvial sand sheet and intermediate sheetflood overlain by a sand-rich floodplain (Fig. 5.9) similar to what was previously described. Overall, the whole interval is up to 24 m thick, in which paleocurrent directions from fluvial cross-strata (n=28) point to NW-SW flow (N267) (Fig. 5.4).

5.5.3. SU3 and Seq. C description

5.5.3.1. Estuarine domain

SU3 is marked at the erosive basal surface of braided fluvial sandstones from Seq. C on top of the Seq. B estuarine successions. The best exposure of this unconformity is at vertical section 7 (Fig. 5.8). Seq. C consists of a braided fluvial sand sheet overlain by cyclic successions of tidal bars, tidal sand-flat and heterolithic shoreface strata. The shoreface and tidal bar are similar to what was previously described. The tidal sand-flat consists of up to 2-m-thick tabular beds composed of upper flow regime sandstone. UFR sandstone is medium- to coarse-grained, with horizontal and ripple-cross lamination (Figs. 5.5, 5.10). Seq. C is 40 m thick, composed of 5-m-thick fluvial and 35-m-thick estuarine and shoreface strata. Paleocurrent readings (n=130) indicate predominant flow to the NW and less frequent flow to the S-SE (Fig. 5.4).

5.5.3.2. Fluvial domain

SU3 is marked at the contact between the Seq. C braided fluvial sand sheet and the Seq. B sand-rich floodplain interval. Seq. C is formed of a braided fluvial sand sheet and intermediate sheetflood overlain by a sand-rich floodplain (Fig. 5.8). The sand-rich floodplain from Seq. C forms a 24-m-thick tabular sandstone body that comprises eleven cyclic fining-upward distal sheetflood successions up to 1.4 m thick each (Fig. 5.10B). The fining-upward trend is characterized by medium- to fine-grained sandstone to siltstone capped by mud layers up to 0.4 m thick. Sandstone is laminated or with low angle, trough and planar cross-bedded, and with asymmetrical ripple marks on top. The fluvial interval of Seq. C is up to 45 m thick, in which paleocurrent directions (n=14) indicate a predominant SW flow (N256) (Fig.5.4).

5.5.4. SU4 and Seq. D description

5.5.4.1. Estuarine domain

SU4 is marked at the erosive basal surface of braided fluvial sandstones from Seq. D over estuarine successions from Seq. C. The best exposure of this unconformity is at vertical section 11 (Fig. 5.5) and vertical section B (Fig. 5.1). There, Seq. D is composed of braided fluvial sand sheet and cyclic estuarine successions. The braided fluvial sand sheet is formed of coarse- to medium-grained sandstone with dispersed granules and exhibits medium-scale trough-cross stratification (approximately 1 m high). The estuarine cyclic successions comprise medium-grained to granular sandstone filling tidal channels, tidal bundles in tidal bars and shoreface heterolithic intervals up to 1.5 m thick with transgressive lags on its base (Figs. 5.5, 5.11). At the top, Seq. D exhibits thin (up to 0.5 m thick) offshore tidal bars interbedded with shoreface heterolithic facies. Sandstone is very-coarse-grained to granular and trough cross-stratified. Seq. D is 35 m thick, composed of a 5-m-thick braided fluvial sand sheet and a 30-m-thick estuarine succession. At the BR242 road (vertical section 11), 6 km east of Pai Inácio hill (vertical section B), Seq. D consists of a 15-m-thick braided fluvial interval. At the base, this interval is composed of 5-m-thick stacked poorly channelized bodies that are filled with medium-grained to granular, trough cross-bedded sandstones with mud clasts and ripple marks. Towards the top this interval is composed of 10-m-thick tide-influenced sand-bed braided fluvial sandstones, in which some ripples are oriented to the opposite direction of the main fluvial paleoflow. Paleocurrent readings from offshore tidal bar and tide-influenced fluvial sandstone cross-strata (n=65) indicate a bidirectional flow to the NW-SW (N270) and NE (N65) (Fig. 5.4).

5.5.4.2. Fluvial domain

SU4 is marked at the erosive basal surface of the braided fluvial sand sheet from Seq. D over the sand-rich floodplain interval from Seq. C (Fig. 5.8, 5.11). Seq. D is 37 m thick, composed of braided fluvial and sand-rich floodplain deposits. The braided fluvial sand sheet strata are approximately 12 m thick and composed of medium-grained to granular, trough cross-stratified sandstone. The sand-rich floodplain is at least 25 m thick and composed of several fining-upward successions of distal ephemeral sheetflood sandstone. This sandstone is medium- to fine-grained and horizontally laminated, with ripple cross lamination and centimetric mud drapes on top. Paleocurrent readings (n=36) indicate a predominantly N-NW oriented flow (Fig. 5.4).

5.5.5. SU5 and Seq. E description

5.5.5.1. Estuarine domain

SU5 is characterized by two types of overlying continental facies: sand-bed braided fluvial sand sheets and eolian facies. This unconformity is well exposed at vertical section 11 (Figs. 5.5, 5.12). Fluvial sandstone is coarse-grained to granular, with medium-scale trough cross-bedding. The ephemeral intermediate sheetflood is composed of poorly to moderately sorted, medium- to coarse-grained sandstone with dispersed granules and critical ripples on top. The eolian sand sheet consists of well-sorted, medium-grained, low angle cross-stratified sandstone. The eolian dune is characterized by grain fall and grain flow layers that compose medium- to large-scale cross-stratification (preserved thickness is approximately 1 m). These continental successions are overlain by cyclic successions of tidal channels, bars and shoreface heterolithic intervals that are similar to what was previously described. The thickness of Seq. E ranges from 50 to 100 m and is composed of estuarine successions up to 65 m thick that overlie up to 35 m thick fluvial deposits with localized interbeds of eolian strata. Overall, fluvial paleocurrent directions (n=53) indicate a dominant flow to the NW and W (Fig. 5.4), whereas scarce readings from eolian cross-bedded strata indicate an average paleo transport vector to NE (not indicated at Fig. 5.4). No vertical stacking of braided fluvial sand sheet and sand-rich floodplain deposits was observed related to Seq. E at all vertical sequences. Therefore, it is assumed that Seq. E was not characterized at the fluvial domain.

5.5.6. SU6 and Seq. F description

The top of Seq. E marks the most important change in the depositional style of the Tombador Formation. SU6 is an angular unconformity revealed by: (a) shift from estuarine facies (below) to fluvial conglomeratic sandstone above the unconformity (Figs. 5.4, 5.13, 5.14); (b) change in the flow pattern from a northwestern trend below the unconformity to a predominant southeast flow (n=125, N150) above the contact (Figs. 5.4, 5.13); (c) stratal truncation, as seen on a GPR line (Fig. 5.15). Seq. F is composed of fining-upward successions of clast-supported polimitic conglomerates and coarse-grained sandstones overlain by ephemeral intermediate sheetflood, eolian dune, and sand sheet sandstones (Bállico, 2012). Conglomerate, which is composed of well-rounded pebbles to granules of quartzite and coarse-grained sandstone, exhibits erosive irregular basal surface and trough cross-stratification and is interpreted as gravel-bed braided fluvial deposits. Intermediate sheetflood and eolian sandstone (similar to the aforementioned) comprise 75% of Seq. F's total succession. Overall, paleocurrent readings (n=125) from fluvial cross-strata indicate a predominant SE flow (N150), whereas eolian paleowind data indicate an average transport vector to NE with dispersion from NW to E (not indicated at Fig. 5.4). Seq. F comprises a fluvial-eolian succession 100 to 120 m thick that was characterized only at the fluvial domain.

5.5.7. SU7 and Seq. G description

The SU7 unconformity is marked by a shift in grain size from sandstones (intermediate sheetflood and eolian from Seq. F) below the unconformity to debris flow conglomerates from Seq. G above the contact (Figs. 5.13, 5.14). The debris flow deposit consists of clast-supported conglomerate that is composed of subrounded gravels of quartzite and subangular to subrounded granules to boulders of sandstone. Boulder is the dominant clast size. The conglomerate bed is 2 to 18 m thick. The aqueous sheetflood deposits interbedded with the conglomerates are composed of medium-grained to granular, massive, laminated, low-angle to trough cross-stratified sandstone (Bállico, 2012). This succession is overlain by proximal and intermediate ephemeral sheetflood sandstone interbedded with eolian dune and sand sheet sandstone. The top of the whole succession is marked by the occurrence of mud-rich floodplain intervals that include crystal tuff layers. Radiometric dating on volcanic zircons from the crystal tuff layer constrains the age of Seq. G to 1416 ± 28 Ma (Guadagnin et al., 2015), which agrees with the age of 1394 ± 14 Ma obtained by Gruber et al. (2011) on detrital zircons from fluvial floodplain mudstones at the upper portion of the Tombador Formation. The thickness of Seq. G ranges from 40 to 70 m. Paleocurrent data (n=131) from fluvial cross-strata indicate a semi-radial pattern with flow variation from South to West (Fig. 5.4). The variability of the facies association and the dispersion of fluvial paleoflow are typical of alluvial fan systems (Bállico, 2012). Seq. G was characterized only at the alluvial fan and fluvial domain.

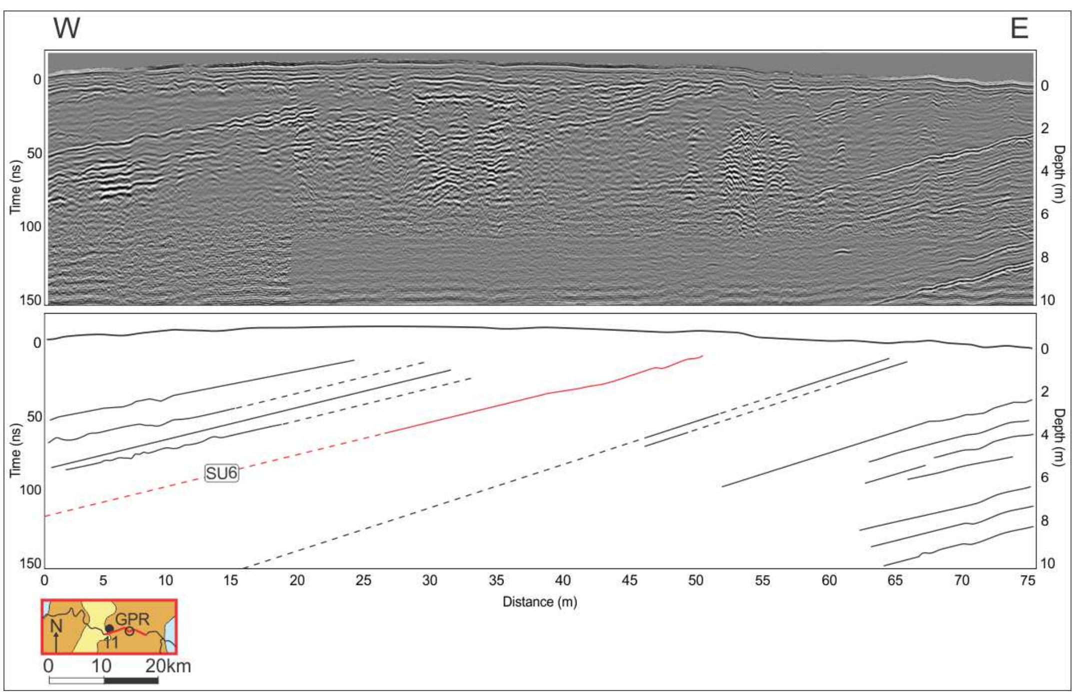

Fig. 5.15. GPR line showing reflectors that have distinct dip angles, which indicates the presence of an angular unconformity (SU6). Location of this GPR line (black circle) is given at the map at the left corner.

Beyond the study area, at nearby Jacobina city at the Northern Sincorá Range (Fig. 5.1), Silva Born (2011) described 150 m of braided fluvial, ephemeral sheetflood, and eolian sandstones associated with proximal alluvial fans overlying the unconformity with the Archean basement. Approximately 150 km from the study area, at the northwestern ending of the Western Chapada Diamantina, Loureiro et al. (2009) described approximately 330-m-thick successions of diamond-bearing metaconglomerates and braided fluvial metasandstones with paleocurrent directions to the SW overlying the unconformity with the Açuruá Formation. This succession is covered by approximately 120-m-thick eolian dunes and sand sheets deposits. The similarity of facies characteristics and paleocurrent patterns in the intervals described by Silva Born (2011) and Loureiro et al. (2009) suggest they are equivalent to Seq. G.

5.5.8. SU8 and Seq. H description

The uppermost unconformity observed in the Tombador Formation is SU8. It is marked at the contact of Seq. H marine-influenced deposits overlying the continental Seq. G (Figs. 5.4, 5.13, 16). In ascending order, Seq. H is formed of tide-influenced braided fluvial sandstone, tidal sand-flat, shoreface sandstone and mudstone. Tide-influenced braided fluvial deposits exhibit medium- to coarse-grained through-cross bedded sandstone. The tidal sand-flat is characterized by fine- to medium-grained, laminated, wavy ripple and ripple cross-laminated sandstone with flaser bedding. Shoreface deposits are composed of fine- to medium-grained sandstone with hummocky cross-stratification, wavy ripple and ripple cross-lamination and laminated to massive mudstone with wavy ripple-lamination and lenticular bedding. Seq. H consists of a succession at least 70 m thick in which paleocurrent readings from tide-influenced fluvial cross-bedded sandstones (n=131) indicate a bimodal direction, with a predominant flow to the SW (N233) and a secondary flow to the NE (N24) (Fig. 5.4). Paleocurrent directions from the tidal flat sandstones (n=83) indicate a bimodal flow, with a predominant direction towards NW-SW (N268) and a subordinate flow towards E-SE (N116). The sandstone from Seq. H exhibits gradual contact with overlying shallow marine mudstone from the Caboclo Formation, which has a published age of c. 1140 ± 140 Ma (Babinski et al., 1993). The comparison between the ages of Seq. G and Seq. H indicates SU8 is an unconformity associated with a major hiatus (100 to 400 Ma). The upper boundary of Seq. H was not investigated in this study.

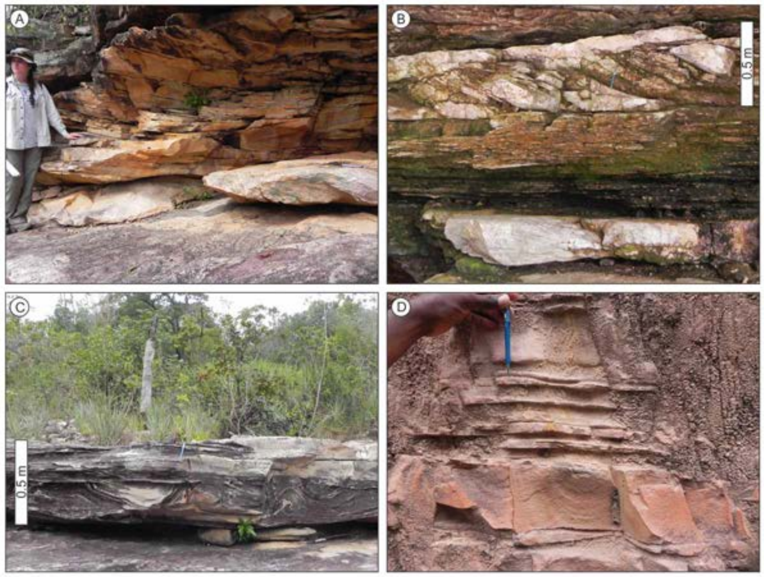

Fig. 5.16. Representative facies associations of Sequence H. Tide-influenced sand-bed braided fluvial sandstone (A,B); shallow marine sandstone with hummocky cross-stratification on top of a contorted bed (C); siltstone to mudstone strata (D).

5.6. Sequence Hierarchy - Discussion

In this paper, the approach used to classify and assign hierarchy to depositional sequences follows Catuneanu (2006): “the most important sequence boundaries in the stratigraphic record, designated as ‘first-order’, are genetically related to shifts in the tectonic setting that led to changes in the type of sedimentary basins ... because the formation and classification of all types of sedimentary basins is tied to tectonic criteria”. This author argued that “first-order sequences correspond to entire sedimentary basin fills, regardless of the origin and life span of each particular basin” and that “the classification of sequences and bounding surfaces should be approached on a case-by-case basis, starting from the premise that each sedimentary basin fill (i.e., the product of sedimentation within a particular tectonic setting/type of basin) corresponds to a first-order stratigraphic sequence. In turn, first-order basin fill successions are subdivided into second- and lower-order sequences as a function of the shifts in the balance between accommodation and sedimentation at various scales of observation, irrespective of time spans and the nature of the allogenic mechanisms that controlled the internal architecture of the basin fills” (see discussion on sequence hierarchy in Catuneanu, 2006).

Sequence hierarchy applied to Precambrian successions reported in the literature dealt with regional third-order scale at maximum resolution (Catunenau & Eriksson, 1999; Alkmim & Matins Neto, 2012; Eriksson & Catunenau, 2004; Eriksson et al., 2005b,c). In the Chapada Diamantina Basin, changes in paleogeography are recorded at all hierarchical levels, with a magnitude that increases with the hierarchical rank. Such changes – as a response of relative sea level fluctuations – should be supported by distinct physical attributes and facies shifts associated with sequence boundaries observed at different hierarchical orders (Embry, 2005; Catuneanu, 2006; Catuneanu et al., 2011). The following physical attributes were observed in the study area: regional unconformities, changes of zircon age signature, changes of paleoflow direction and shift of facies of different magnitudes. Therefore, the hierarchy system that applies to the Tombador Formation is based on changes of depositional trends that were observed in the rock record and includes sequences of different orders (Figs. 5.17, 5.18), which are defined as follows: sequences associated with a particular tectonic setting are designated as of 'first order' and are separated by first-order sequence boundaries where changes in the tectonic setting are recorded; second-order sequences represent the major subdivisions of a first-order sequence and reflect cycles of change in stratal stacking pattern observed at 10^2-m scales (i.e., 200-300 m); changes in stratal stacking pattern at 10^1-m scales indicate third-order sequences (i.e., 40-70 m); and changes in stratal stacking pattern at 10^0-m scales are assigned to the fourth order (i.e., 8-12 m).

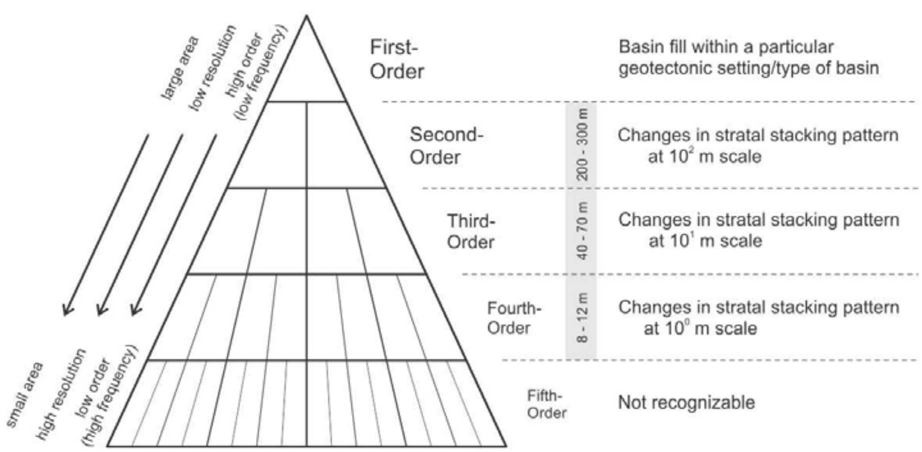

Fig. 5.17. Criteria for assigning sequence hierarchy in the Precambrian of the Chapada Diamantina (modified from Raja Gabaglia et al., 2006; triangle from Catuneanu, 2006).

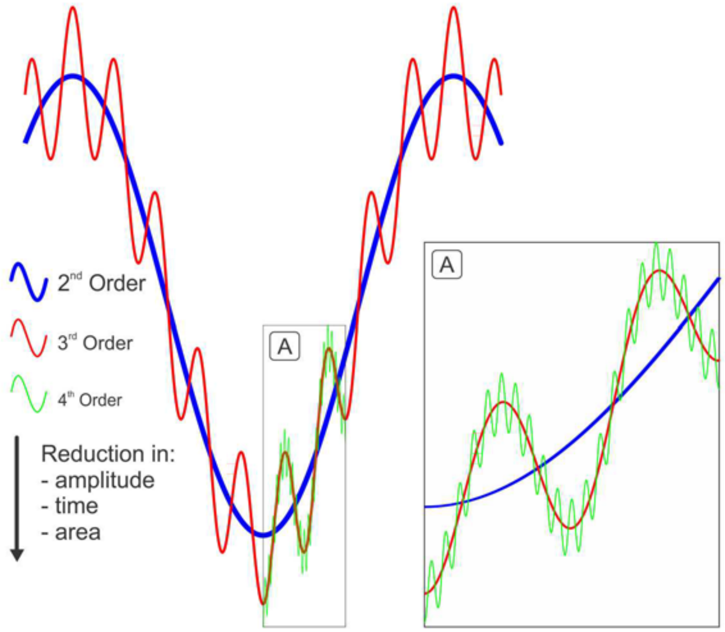

Fig. 5.18. Hypothetical relative sea level curves for second- to fourth-order hierarchies. The lower the hierarchy, the smaller the amplitude, the time span and the affected geographic area. Note that higher-order hierarchy superimposes its tendency on lower-order hierarchy.

5.6.1. First-order sequences

SU1 is a regional unconformity (sensu Sloss et al., 1949) that marks the onset of an intracratonic sag basin cycle of the geotectonic evolution of the Espinhaço Supergroup (Pedreira, 1994; Guimarães et al., 2008; Alkmim & Martins-Neto, 2012; Guadagnin et al., 2015). In the Chapada Diamantina Basin, the shift in the flow pattern across SU1 confirms the findings of Pedreira (1994), who argued that a tectonic tilt must have occurred to promote such a change of source areas (Fig. 5.5). Thus, SU1 separates two distinct first-order sequences herein named Middle Espinhaço I (ME-I) below the unconformity and Middle Espinhaço II (ME-II) above the contact (Fig. 5.4). The radiometric dating in Seq. G yields ages of 1394 ± 14 Ma (Gruber et al., 2011) and 1416 ± 28 Ma (Guadagnin et al., 2015). These ages register, at the Chapada Diamantina area, the intra-cratonic regional-scale extensional stress regime that took place at the southeastern and western margins of the Congo craton at c. 1375 Ma, i.e., the Kibaran extension (Guadagnin et al., 2015). This event is interpreted as the sag basin-forming mechanism that allowed ME-II deposition. Thus, it explains not only the tectonic tilt and the ensuing SU-1 emplacement but also the presence of volcanic and detrital zircons from which Seq. G age was obtained.

SU-8 is a sequence boundary associated with a major hiatus (100 to 400 Ma) between MEII and the Upper Espinhaço (UE) sequence. This hiatus is suggestive of a continental unconformity that separates two sag basin fill successions, and hence, Seq. H belongs to the UE first-order sequence (Fig. 5.4). Thus, Seq. H comprises the lower portion of a stratigraphic unit composed of transgressive sandstones (from the Tombador Formation) and overlying shallow marine mudstones (from the Caboclo Formation). The basin-forming mechanism related to Seq. H is hypothesized to result from the late Kibaran or Greenvilian events during the assembly of the Rodinia Supercontinent (Guadagnin et al., 2015). Previous interpretation assumed that these two formations were part of the same sedimentary succession (Dominguez, 1992, Pedreira, 1994; Guimarães et al., 2008; Lagoeiro et al., 2009, Alkmim & Martins Neto, 2012).

SU-1 and SU-8 are, respectively, the lower and the upper boundaries of ME-II, i.e., a first-order stratigraphic unit entirely included in the Tombador Formation that comprises Seq. A-G. The regional strike stratigraphic cross-section (Fig. 5.19) indicates ME-II extends further northwards from the study area, where it lies over an unconformity with the basement. Therefore, the Espinhaço Supergroup in the Chapada Diamantina includes four first-order sequences: Lower Espinhaço (LE), ME-I, ME-II, and UE, each related to a distinct and individualized basin fill cycle (Fig. 5.2). The time span related to basin-forming mechanisms and sedimentation for each of these first-order sequences is more likely smaller than the hiatuses associated with their sequence boundaries. In the Chapada Diamantina area, tectonics at the intra-plate and plate margins triggered extensions that led to the formation of rift (e.g., the Statherian rift event) and sag (e.g., the Kibaran event) basins, while compressions led to uplift and erosion (Guimarães et al., 2008; Lagoeiro et al., 2009; Guadagnin et al., 2015) and, hence, promoted first-order cyclicity.

5.6.2. Second-order sequences

The first-order ME-II Sequence is divided into two second-order units separated by SU-6 (the intra-Tombador angular unconformity) herein named Lower ME-II (LME-II, composed of Seq. A-E) and Upper ME-II (UME-II, composed of Seq. F-G). The shift of facies from fluvial-estuarine (Seq. A-E) to fluvial-alluvial fan (Seq. F-G) and the shift in the flow pattern recorded across SU6 are convincing evidence of basin reorganization (Bállico, 2012).

Moreover, the zircon age distribution in Seq. A-E indicates sources from the basement, which is older than 1.7 Ga. In contrast, the zircon age distribution and the composition of conglomerates in Seq. F-G suggest a contribution from the Espinhaço Supergroup, with ages between 1.4 and 1.7 Ga (Fig. 5.20). The same zircon age distribution recorded in samples from vertical sections 1 and 11 in Seq. LME-II (Fig. 5.21) indicates the strata from these sequences dip toward the north, and hence, it suggests SU8 is an angular unconformity. The occurrence of Seq. LME-II is restricted to the study area, while Seq. UME-II extends farther north and northwest beyond the Sincorá Range, where conglomerates overlie the unconformity with the basement or with the Açuruá Formation. Previous interpretations proposed a conglomerate occurrence at the base of the Tombador Formation (Inda & Barbosa, 1978; Loureiro et al., 2009). All data indicate Seq. UME-II records a major regression that was triggered by a tectonic tilt that increased the depositional area compared to that of ME-IIL. Therefore, SU6 marks the major subdivision of the MEII first-order sequence and, hence, subdivides that unit into two second-order sequences: LME-II and UME-II (Figs. 5.4, 5.21).

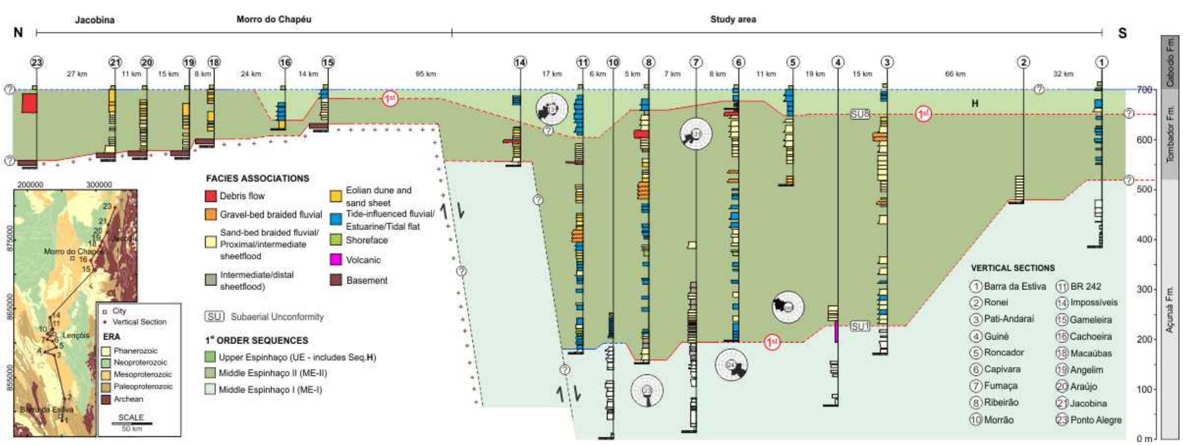

Fig. 5.19. Regional strike stratigraphic cross-section of first-order sequences ME-I, ME-II, and UE.

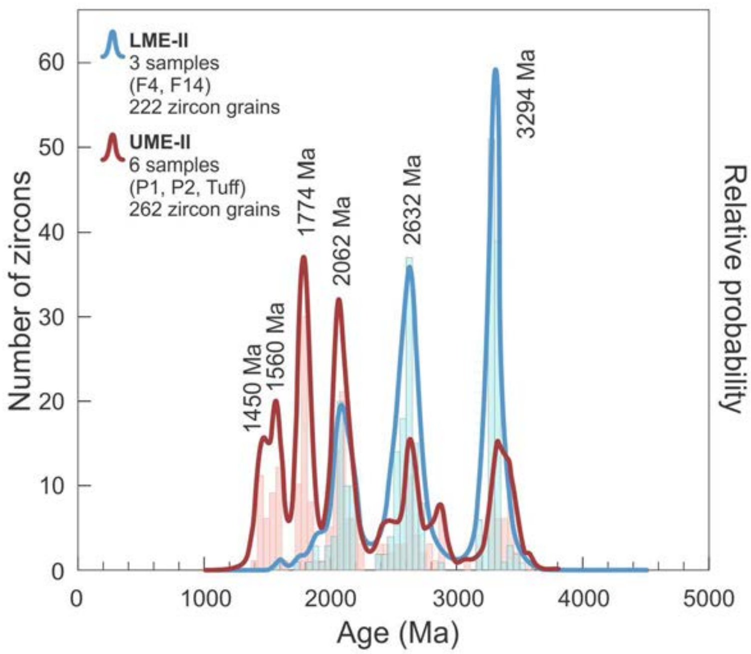

Fig. 5.20. Zircon ages signatures for Seq. LME-II indicate zircon grains are derived from the basement, which is older than 1.7 Ga. In contrast, the zircons ages for Seq. UME-II suggest a contribution from the Espinhaço Supergroup, with ages between 1.4 and 1.7 Ga (Guadagnin et al., 2015). See location of samples F4, F14, P1, P2 and Tuff in Fig. 5.21. Abbreviations: LME-II- Lower Middle Espinhaço II Sequence, UME-II- Upper Middle Espinhaço II Sequence.

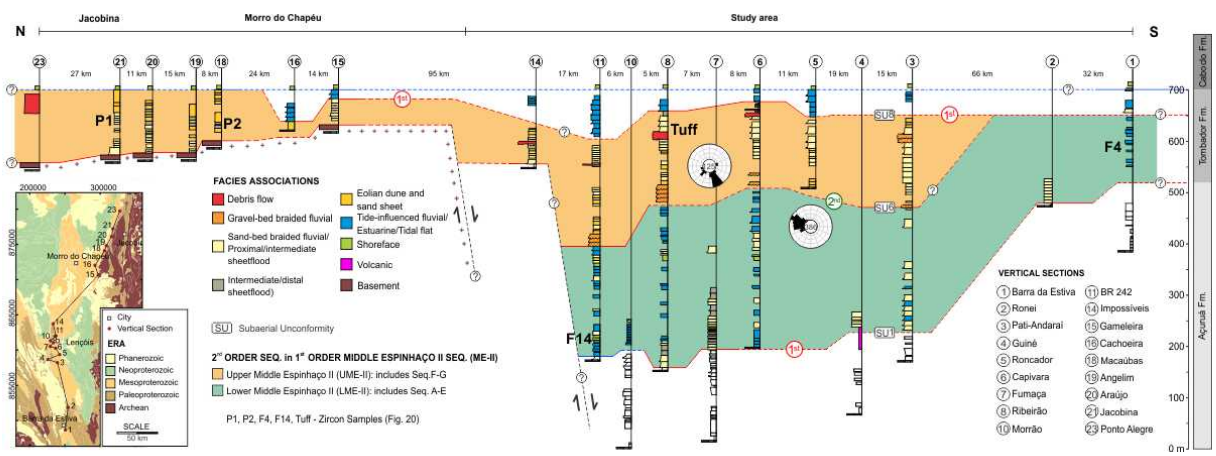

Fig. 21. Regional strike stratigraphic cross-section of second-order sequences LME-II and UME-II. The stratigraphic correlation is supported by the zircon age distribution, paleocurrent directions, and shift of depositional systems recorded across SU6. LME-II dips toward the north and has restricted occurrence to the study area; in contrast, UME-II extends toward the north/northwestern beyond the Sincorá Range. The dip of strata from sequence LME-II suggests SU8 is an angular unconformity.

5.6.3. Third-order sequences

Seq. A-G are included in the second-order LME-II and UME-II sequences and, hence, are considered of third-order hierarchy (Fig. 5.22). Seq. A-E consist of strata deposited in fluvial and estuarine domains. At the estuarine domain, their lower sequence boundaries are marked at subaerial unconformities generated by basinward shift of fluvial over estuarine facies (SU2-5). Locally, a tide ravinement surface and SU1 are superimposed. At the fluvial domain, the SU1-5 characterization is based on a shift of facies associations and paleocurrent trends. Seq. F-G are restricted to fluvial and alluvial domains without evidence of marine influence, their boundaries (SU6-7) being marked at the erosive basal surface of fluvial or alluvial fan successions (Fig. 5.4).

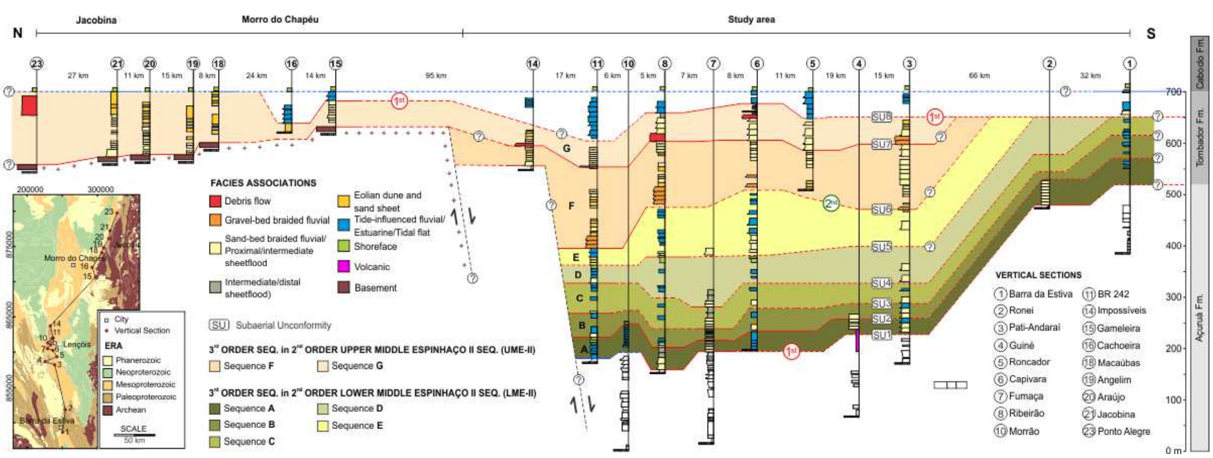

Fig. 5.22. Regional strike stratigraphic cross-section of third-order sequences A-G. Sequences are bounded by subaerial unconformities (SU 1-8) and exhibit fairly sheet-like geometry.

5.6.3.1. Third-order Seq. A-E

At the estuarine domain, Seq. A-E exhibit a thinning-upward trend of fluvial deposits and a thickening-upward trend of estuarine successions, which suggests progressively coastal encroachment (Fig. 5.23). The top of the fluvial sandstones is systematically marked by an abrupt contact with estuarine deposits. Weathering on these surfaces promotes grooves easily mappable along the cliffs. The concave-up geometry of the tidal channels, the amalgamation of tidal bars, and the tabular geometry of shoreface heterolithic deposits give the estuarine successions a laminated aspect in photos. In contrast, a blockier tabular pattern is observed in fluvial successions. Offshore tidal bars and heterolithic strata overlie estuarine successions in

Seq. A and D and compose a conformable thinning-up pattern that is bounded at the top by subaerial unconformities (Figs. 5.5, 5.23).

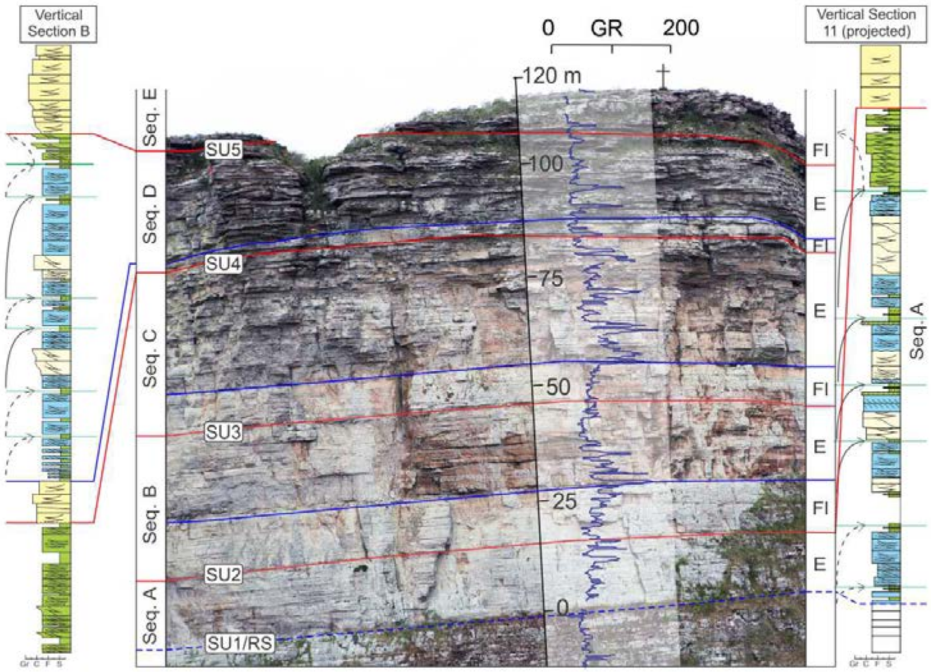

Fig. 5.23. Vertical stacking of third-order sequences A-E on photo-mosaic B (Pai Inacio hill) showing a thinning-upward trend of fluvial deposits and a thickening-upward trend of estuarine successions, which suggest progressive coastal encroachment. At this location, a tide ravinement surface and SU1 are superimposed. Subaerial unconformities SU2-5 are placed at the erosive bottom of fluvial sand sheets (massive, blocky aspect) overlying estuarine successions (laminated pattern). Maximum regressive surfaces (located at the top of fluvial successions) exhibit prominent surfaces due to the weathering of mud-rich estuarine layers that, in turn, promote high peaks in the GR log (in blue). Maximum flooding surfaces are placed within fine-grained shoreface strata. Note the similarity of facies successions in Seq. A and D presented at vertical sections B (measured at the hill) and 11 (measured on an outcrop located 3 km northwards from the hill). Abbreviations: E-estuarine, Fl-fluvial.

A complete third-order sequence at the estuary domain is composed of lowstand, transgressive, and highstand systems tracts. Fluvial deposits without evidence of tidal reworking are interpreted as belonging to a lowstand systems tract. These deposits are limited at their tops by maximum regressive surfaces or a tide ravinement surface. Tide-influenced fluvial sandstones and estuarine successions compose the transgressive systems tract. On top of it, the interval composed of offshore tidal bars and shoreface heterolithic facies associations exhibits coarsening- and thinning-upward trends, which suggests reducing in accommodation, and therefore represents the highstand systems tract. The differentiation from transgressive to highstand is based on the change of the stratal stacking pattern due to increased grain size, the presence of mud clasts, a relatively higher abundance of trough cross-bedding, and conformable thinning-up strata of tidal bars and shoreface heterolithic (reducing in accommodation) prior to subaerial unconformities (Figs. 5.5, 5.7, 5.23). These features suggest progradation during highstand (progressive reduction of accommodation).

A complete third-order sequence at the fluvial domain is formed of lowstand and transgressive/highstand systems tracts: the former is made up of amalgamated fluvial sand sheets/intermediate sheetfloods, and the latter is formed of tide-influenced braided fluvial and a sand-rich floodplain. The distinct characteristics of these facies associations promote a blocky and serrate pattern in the GR logs, respectively, which supports the assignment of SU1-5 (Fig. 5.8). Tidal reworking is a criterion that can be applied to sedimentary succession of any age but it is unique to making a stratigraphic interpretation of the fluvial sequences in the Precambrian. Within the alluvial strata, the period of maximum flooding is not represented by a condensed section but is instead represented by the invasion of tidal processes into areas formerly dominated by purely fluvial processes (Shanley & McCabe, 1994). The action of tidal processes on the fluvial domain is represented by cross-strata and asymmetric ripples oriented to the opposite direction of the main fluvial paleoflow (Figs. 5.5, 5.11). Landward, another effect of transgression on the fluvial system is the increase in accommodation that favours the deposition of a sand-rich floodplain. Relatively increase in the phreatic level is suggested by the presence of siltstone beds and mud drapes in the study area. Therefore, sand-rich floodplain represents undifferentiated transgressive/highstand deposits in the Chapada Diamantina.

At the seismic scale, the photo-mosaics of Seq. A-E (Fig. 5.24) exhibit a sheet-like geometry, fairly homogeneous thicknesses, no evidence of fluvial scouring, and cyclicity that can be traced for more than 35 km on the regional strike correlation along the cliffs of the Northern Sincorá Range. These characteristics suggest unincised fluvial and tide-dominated estuaries developed during the Seq. A-E deposition. Paleogeographic reconstruction indicates the deposition occurred on a coastal area connected to a wide and gently dipping alluvial braidplain whose distal deposits were reworked by tidal currents and formed tide-dominated successions (Fig. 5.25). Tidal sand flats were more likely deposited at portions of the coast without the fluvial influence. During periods of transgression, estuaries developed, tides extended their effects upstream on fluvial braidplains, and sand-rich floodplain aggraded. Thus, the tidal channel/tidal bar/shoreface successions deposited downdip in the estuary correlate to the sand-rich floodplain intervals updip on the fluvial braidplain. The conspicuous tabular stratal geometry of Seq. A-E is the response of the interplay between sedimentation on low gradient substrate and fluctuations of relative sea level in the Mesoproterozoic sag basin setting.

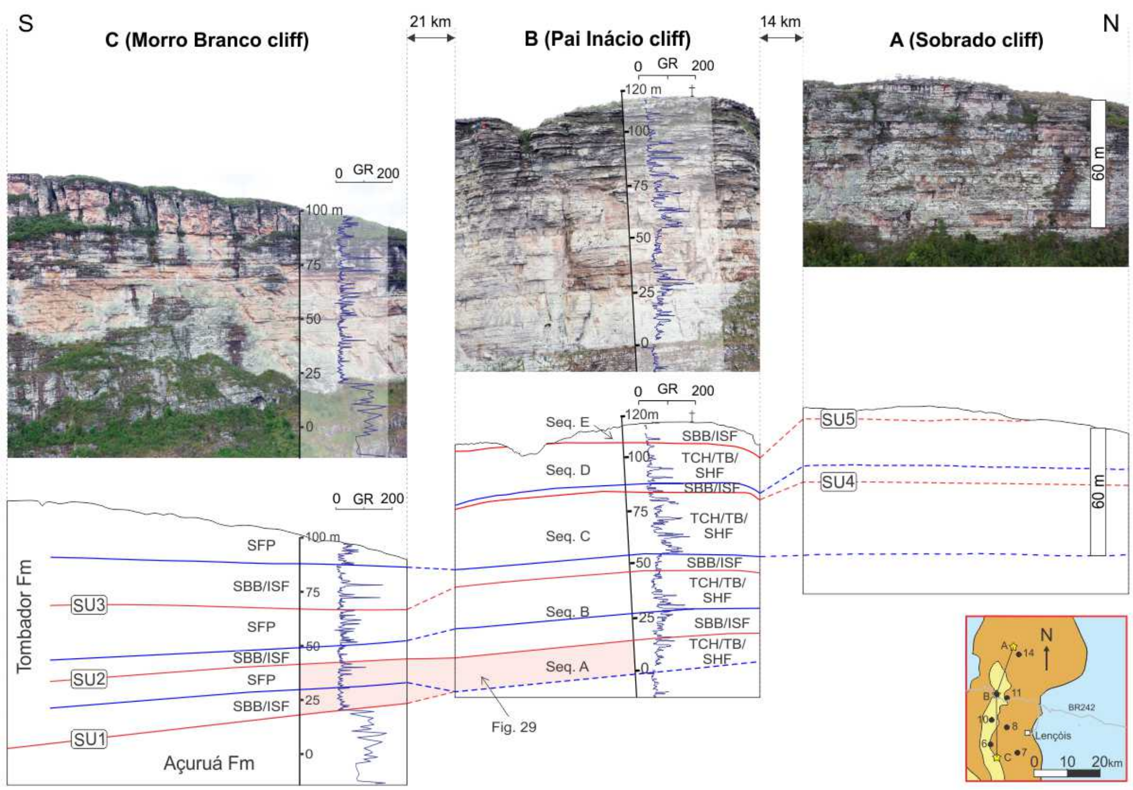

Fig. 5.24. N-S oriented cross-section showing sub horizontal, sheet-like geometry of third-order Seq. A-E along an approximately depositional strike direction. The stratigraphic interpretation is supported by seismic scale photo-mosaics, GR logs (in blue), and vertical sections. The GR log at -10-23 m interval (lithostratigraphically, the Açuruá Formation) at photo-mosaic C was acquired using 1-m space sampling. Acronyms of facies associations, stratigraphic surfaces and sequences are given at the overlay.

5.6.3.2. Third-order Seq. F-G

Seq. F-G are typical continental sequences that include the diamond-bearing conglomerates and exhibit abrupt contact between conglomeratic successions and overlying fluvial and eolian sandstone (Figs. 5.13, 5.14). This abrupt contact suggests the fluvial graded profile changed dramatically from a steeper condition (alluvial fan conglomeratic deposition) to a lower gradient condition (braided fluvial, ephemeral sheetfloods and eolian deposition).

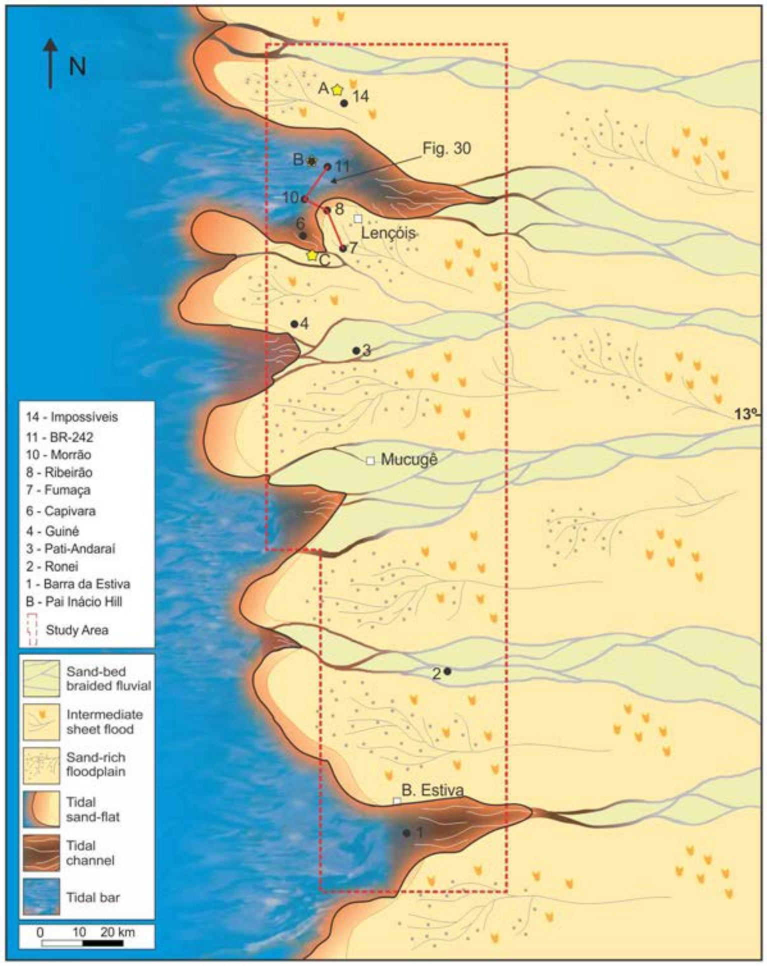

Fig. 5.25. The paleogeographic reconstruction of a transgressive systems tract from Seq. A-E suggests deposition occurred on a tide-dominated coast linked to a gentle and wide fluvial braidplain crossed by shallow, sand-bed braided rivers and ephemeral sheetfloods with minor eolian deposits.

The high-frequency intercalation between ephemeral fluvial and eolian deposits observed in Seq. F-G is extremely common in Proterozoic successions and such intercalation may be due to autocyclic or allocyclic factors (Eriksson et al., 1998, 2006; Alkmim & Martins Neto, 2012). The absence of well-defined drying or wetting cycles and the low lateral continuity of the eolian packages suggest coexistence between fluvial sheetfloods and eolian deposits and, hence, favour the interpretation of an autocyclic fluvio-eolian interaction (Silva Born, 2011; Bállico, 2012). On the other hand, the eolian deposits from Seq. F are much thicker (up to 20

m) than those from Seq. E (less than 2 m thick), thus reflecting suitable conditions for deposition and preservation (Kocurek & Lancaster, 1999; Mountney, 2012).

The abrupt and erosive contact at the base of Seq. G marks the establishment of alluvial fan overlying fluvial-eolian deposits from Seq. F, as suggested by the facies lateral variability and radial fluvial paleocurrent pattern (Blissenbach, 1954; Denny, 1967; Sohn et al., 1999; Went, 2005; Hadlari et al., 2006). The dominant fluvial paleoflow to the southwest and variations to the northwest and southeast suggest a source area located to the east/northeast (Bállico, 2012). The integration of data from this study with those from Silva Born (2012) and Bállico (2012) indicates the existence of three alluvial fans that had at least a 40-km coverage radius.

Although Seq. F-G do not exhibit a marine or tidal influence, it is inconclusive whether they were downstream or upstream controlled, and hence, no systems tract nomenclature was used (Fig. 5.26). An investigation along the depositional down-dip direction would provide such evidence, but the erosion extends southwards and precludes the study of those sequences.

5.6.4. Fourth-order sequences

The internal cyclicity in the third-order sequences is interpreted as a fourth-order hierarchy. Fourth-order sequences were recognized in Seq. A-E transgressive-highstand systems tracts, and they exhibit distinct facies successions depending on their occurrence at estuarine or fluvial domains (Fig. 5.27). Fourth-order sequences were not recognized in the Seq. A-E lowstand systems tract or in Seq. F-G because fluvial sandstones are amalgamated without significant changes of facies.

In ascending order, fourth-order sequences at the estuarine domain consist of tidal channel/tidal bar/shoreface heterolithic successions that are 8-10 m thick. Less frequently, such sequences are composed of offshore tidal bars and interbeds of shoreface heterolithic strata. The best exposures are at vertical section 11 (Fig. 5.5, Seq. A) and at vertical section B (Fig. 5.23, Seq. D). Gamma ray logs exhibit low values in front of sandstones from tidal channels and bars and higher peaks in front of shoreface heterolithic facies. On the GPR line (Fig. 5.28), tidal channels exhibit internal truncation and an erosive concave-up bottom surface that truncates underlying reflections; tidal bars consist of well-defined reflection-free bodies; and shoreface heterolithic deposits are characterized by a tabular parallel reflection pattern.

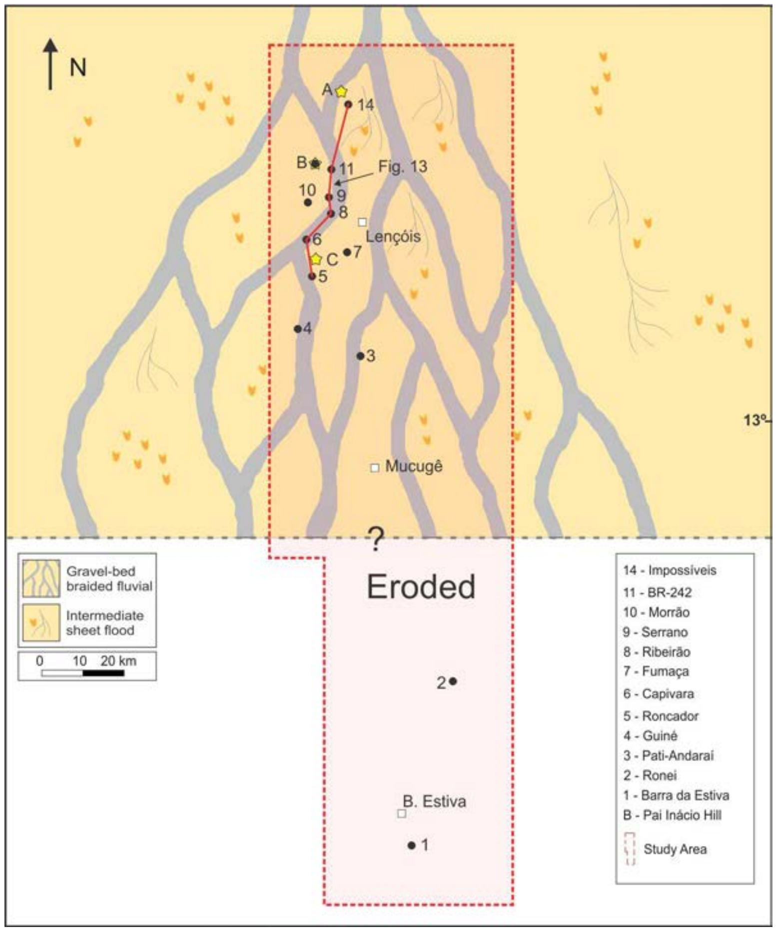

Fig. 5.26. Paleogeographic reconstruction of Seq. F showing the development of braided fluvial and proximal to intermediate sheet flood systems. The change of paleoccurrent directions from the Seq. A-E to the Seq. F is an evidence of basin reorganization (compare with Fig. 5.25).

Tidal deposits are quite common in the Precambrian (Eriksson & Simpson, 2004), and are commonly found in tide-influenced delta or tide-dominated estuarine systems. The distinction between them in the geological record is based on facies successions. Estuarine systems exhibit retrogradational stacking pattern, thus related to transgressive coastlines (Boyd et al., 2006). The retrogradational stacking pattern of the tidal channel, tidal bar and shoreface strata recorded at the vertical succession indicates subaerial unconformity and tide ravinement surfaces are superimposed and hence, no fourth-order lowstand deposit was preserved. The progradational stacking pattern of offshore tidal bars and shoreface heterolithic strata overlies the transgressive interval and indicates these successions belong to a highstand system tract (Fig. 5.23). In any case, the shoreface heterolithic intervals are truncated at the top by two superimposed surfaces (subaerial unconformity and tide ravinement surface). Thus, the shoreface heterolithic facies association is interpreted as representing the end of transgression for each fourth-order sequence, and hence, potentially candidate to include the maximum flooding surface.

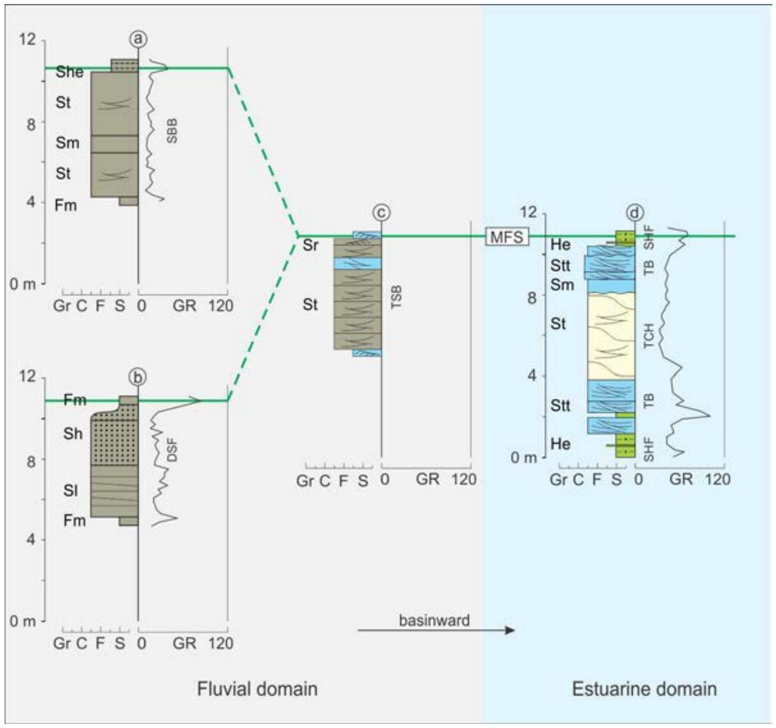

Fig. 5.27. Two possibilities of fourth-order sequences correlation showing successions of facies and facies associations observed on fluvial and estuarine domains. At the fluvial domain a fourth-order sequence is formed of the following facies associations: (a) sand-bed braided, (b) distal ephemeral sheetflood and (c) tide-influenced sand-bed braided fluvial deposits. At the estuarine domain a fourth-order sequence consists of (d) tidal channel, tidal bar and overlying shoreface heterolithic facies associations. The fourth-order sequences are bounded by maximum flooding surfaces that are included in fine-grained or tide-influenced intervals mappable along at least 17 km . The correlation a-c-d is observed at the transgressive systems tract of Seq. A (Fig. 5.30). The correlation b-c-d is observed at the transgressive systems tract of Seq. D (Figs. 5.8 and 5.23). The acronyms of facies and facies associations are given at the left and at the right of the columns, respectively. Abbreviation: MFS-maximum flooding surface.

The frequent occurrence of relatively narrow and shallow tidal channels associated with tidal bars may indicate that the vertical sections are most likely located in a middle estuary setting (Fig. 5.25) because at this location: a) they exhibit more frequent tidal sedimentary structures compared to inner estuary deposits, which are characterized by stronger fluvial influence and less frequent tidal sedimentary structures; b) tidal channels are increasingly wider and deeper towards the outer estuary (Fig. 5.29; Schoengut, 2011). The presence of shoreface heterolithic successions overlying tidal channels and tidal bars implies transgression took place, even though the vertical stacking of such deposits may be explained as a response of autocyclic variation within the estuarine system (i.e. fluvial discharge). Furthermore, the same retrogradational cyclic pattern of tidal channel, tidal bar, and shoreface deposits observed in the third-order Seq. A-E reinforces the allocyclic control on fourth-order sequences.

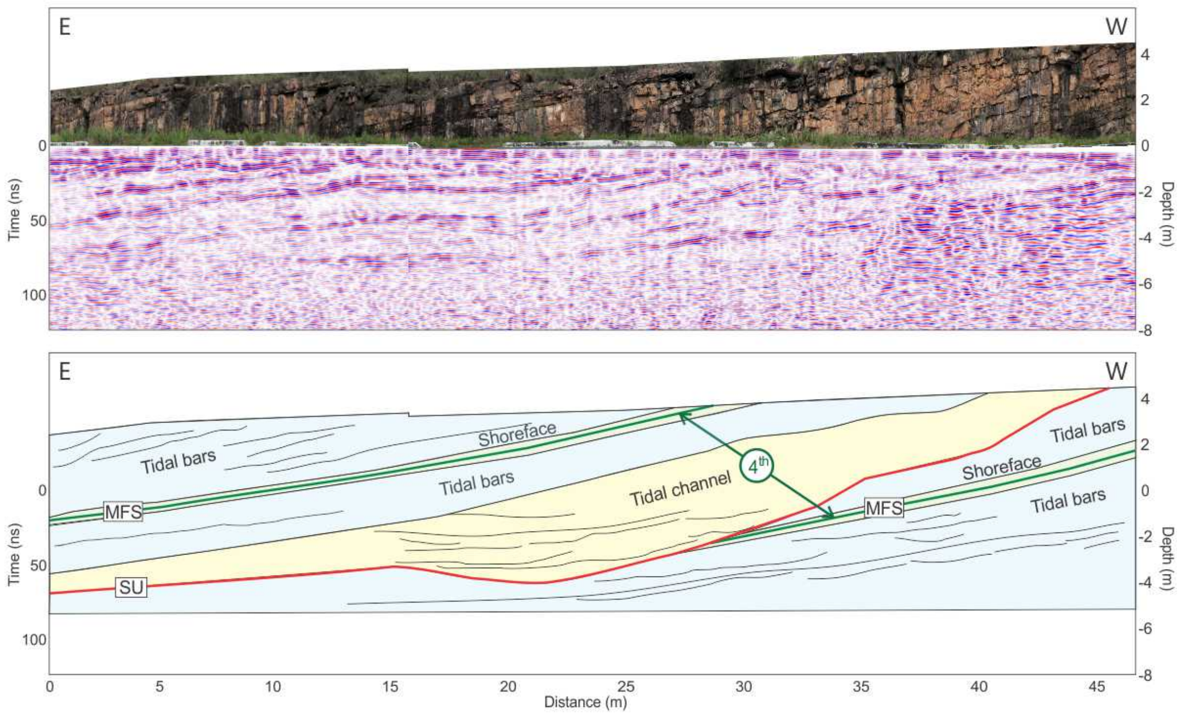

Fig. 5.28. Fourth-order sequences at the estuarine domain are well exposed on the outcrop and are clearly seen on the GPR line (400 MHz antenna).

In the Chapada Diamantina Basin, considering that deposition took place on a low gradient ramp in an intracratonic sag basin (Guimarães et al., 2008; Guadagnin et al., 2015) the preservation of fourth-order sequences at the estuarine domain implies a steep increase in accommodation; if the shoreline migrates landward with a nearly flat trajectory, because of a slow rate of accommodation, most of the estuarine succession is removed by ravinement scouring (Dalrymple, 2010). Transgressions not only triggered tide and wave ravinement but also extended the tidal influence on the distal portion of fluvial systems.

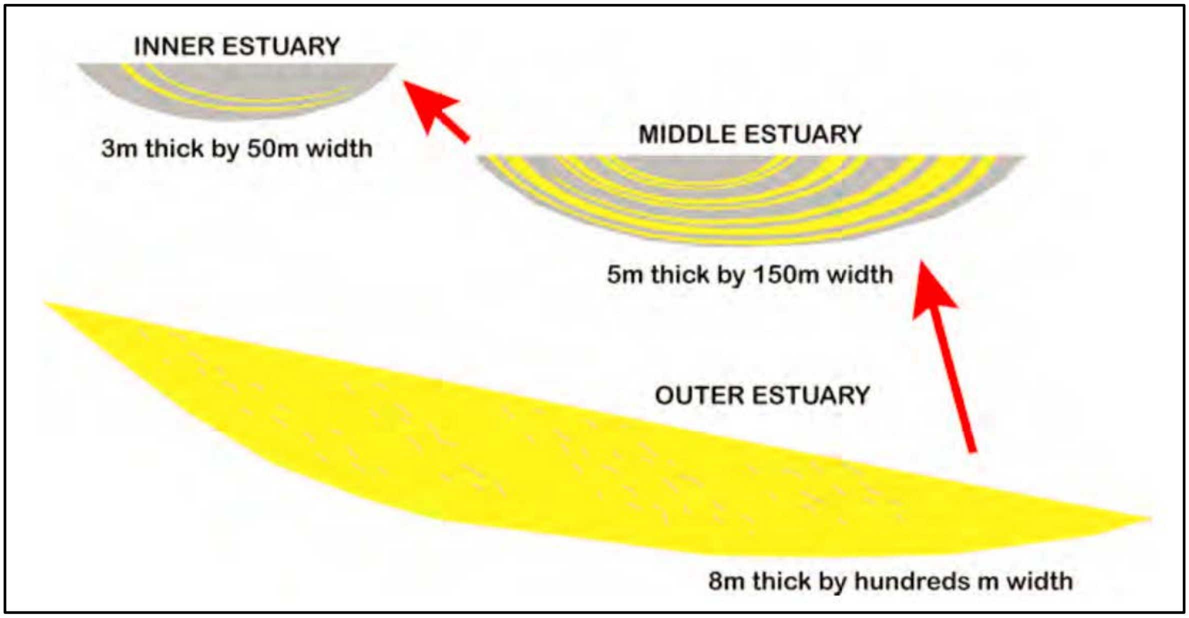

Fig. 5.29. Schematic drawing showing the expected size and shape of channel fill geobodies from different depositional locations at the Willapa Bay (Schoengut, 2011). Collors represent grain size: yellow = sand, gray = mud).

At the fluvial domain there are two types of fourth-order sequences (Fig. 5.27): a) those preserved at the sand-rich floodplain and, b) those preserved at the tide-influenced braided fluvial sand sheet. At the sand-rich floodplain, the sequences are composed of cyclic successions of distal ephemeral sheetflood capped by eolian sand sheet or mudstone layers up to 40 cm thick .The best exposures are at vertical section 7 (Fig. 5.8, Seq. A and C). At the fluvial sand sheet, the sequences consist of cyclic successions of fluvial strata bounded by centimeter-scale tide-influenced intervals, which are recognized by the presence of cross-strata or asymmetric ripples oriented at the opposite direction of the main fluvial paleoflow (Fig. 5.30).

Mappability is indeed one important criterion for assigning fourth-order stratigraphic surfaces because candidate surfaces that cannot be followed laterally over some kilometres are interpreted as autocyclic in origin and, hence, not useful for stratigraphic analysis. In this study, shoreface heterolithic and eolian and mudstone layers from the sand-rich floodplain intervals are the most reliable intervals to map because of their planar external geometry, higher mud content, gamma ray log and GPR responses. Furthermore, the eolian and mudstone layers and shoreface heterolithic intervals are chrono-equivalent intervals that more likely formed as a response of marine floodings. The stratigraphic section indicates these intervals are correlated at least for 17 km along the depositional strike direction (Fig. 5.30). Because the fourth-order sequences are bounded by MFS, they are more properly classified as genetic stratigraphic sequences (Galloway, 1989).

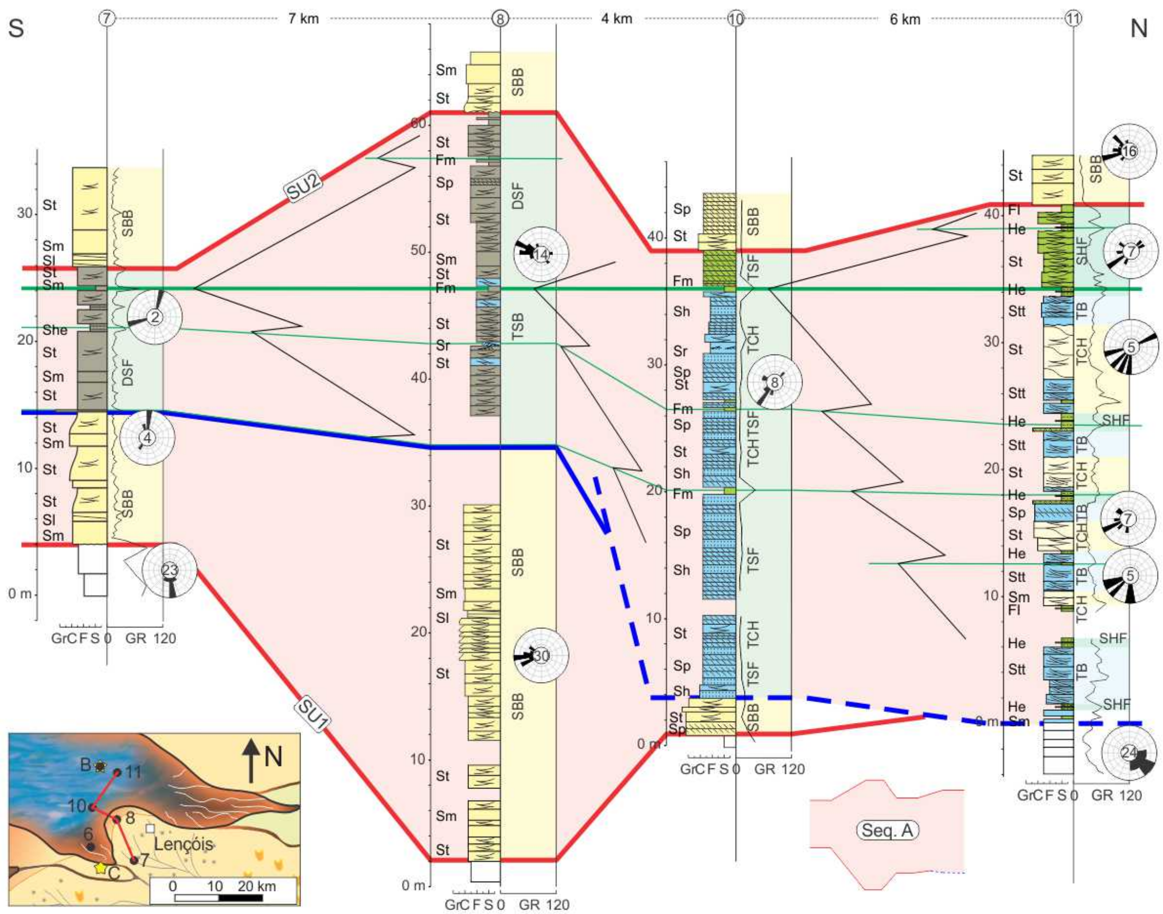

Fig. 5.30. S-N stratigraphic correlation of fourth-order genetic sequences in the third-order transgressive systems tract of Seq. A. The lowstand fluvial interval is characterized by vertical and lateral fluvial homogeneity, without effective vertical and horizontal flow barriers. However, chrono-equivalent fine-grained intervals from shoreface (SHF) and sand-rich floodplain (DSF) deposits include maximum flooding surfaces that promote the stratigraphic compartmentalization, and hence, allow the identification of four production zones (i.e. fourth-order sequences). Note that SU1 and a tide ravinement surface are superimposed at the vertical section 11. The acronyms of facies and facies associations are given at the left and at the right of the columns, respectively.

5.7. Sequence hierarchy applied to reservoir stratigraphic compartmentalization

At the petroleum industry, third-order hierarchy relates to exploration scale whereas fourth-order relates to reservoir scale (Catuneanu et al., 2011). In the production stage, sequence stratigraphic surfaces are used to assign production zones boundaries within petroleum reservoirs (Ainsworth, 2005, 2006; Pyrcz, 2005; McKie et al., 2010; Wonham et al., 2010).

This approach is used to propose the reservoir compartmentalization in Seq. A as presented at Fig. 5.30. As such, the maximum regressive surface may initially subdivide Seq. A into two main production zones: one equivalent to the lowstand and other represented by the transgressive-highstand systems tract. The vertical and lateral homogeneity of the lowstand sand-bed braided fluvial facies association (SBB) suggests this zone would have the best porosity, permeability, and lateral distribution. On the other hand, the presence of fine-grained facies (facies He, Fm, Sm, and She) strata promotes a series of horizontal heterogeneities within the transgressive and highstand interval. Such lower-order compartmentalization is better assigned based on fourth-order sequence boundaries. In fact, those intervals constitute the most important horizontal heterogeneities and effective barriers to vertical flow and, hence, are the preferable boundaries of production zones. Therefore, the stratigraphic compartmentalization indicates the third-order transgressive-highstand interval is composed of four production zones (i.e. fourth-order sequences). Nevertheless, despite their overall tabular (layer-cake) geometry, the dip and strike correlation of the fourth-order sequences exhibit facies variations between fluvial and estuarine domains that may constitute less effective barriers to horizontal flow.

5.8. Final remarks

The studies of the Tombador Formation performed by several authors in the last few years have integrated several methodologies and allow the synthesis of the stratigraphic record presented in this paper. Sequence identification in a Meso-Proterozoic siliciclastic sag setting is a task that, due to a lack of paleontological data, requires one to emphasise those criteria that have significant and reliable lateral and vertical expression among all of those proposed by the sequence stratigraphy methodology. Thus, fluvial and estuarine successions bounded by third- and fourth-order stratigraphic surfaces (e.g., SU/SRM and MFS, respectively) are clearly discriminated and correlated along tens of kilometres. The result is an unequivocal mappability and tracking of the lateral variability of such successions. In this framework, the moderate and gradual change of facies per interval along tens of kilometres support the unincised fluvial and tide-dominated estuarine depositional model for the Lower Tombador Formation. Moreover, clear and practical criteria were defined to assign sequence hierarchies based on stacking patterns observed at different scales, and hence, the hierarchy system that applies to the Tombador Formation includes sequences of different orders, which are defined as follows: sequences associated with a particular tectonic setting are designated as of 'first order' and are separated by first-order sequence boundaries where changes in the tectonic setting are recorded; second-order sequences represent the major subdivisions of a first-order sequence and reflect cycles of change in stratal stacking pattern observed at 10^2-m scales (i.e., 200-300 m); changes in stratal stacking pattern at 10^1-m scales indicate third-order sequences (i.e., 40-70 m); and changes in stratal stacking pattern at 10^0-m scales are assigned to the fourth order (i.e., 8-12 m). Changes in paleogeography due to relative sea level fluctuations are recorded at all hierarchical levels, with a magnitude that increases with the hierarchical rank. Key factors controlling deposition are tectonics (first and second orders) and the interplay between sedimentation and the relative sea-level changes (third and fourth orders). Therefore, the findings of this study encourage the application of those criteria to assign sequence hierarchies in Precambrian and Phanerozoic basins placed in similar tectonic settings.

However, some issues related to the Tombador Formation remain open, demanding further investigations, such as the following: (i) a search for evidence of downstream control on Seq. F-G westwards from the Sincorá Range; (ii) an attempt to define fourth-order sequences in fluvial and eolian intervals of Seq. F-G; (iii) an attempt to acquire data from the south of the Sincorá Range to extend the stratigraphic correlation of Seq. A-G; (iv) a paleogeographic reconstruction of the Tombador Formation encompassing the Western and the Eastern Chapada Diamantina; and (v) understanding the climate control on deposition.

5.9. Acknowledgements

This research was completed as part of the doctoral project carried out by the first author fully sponsored by Petrobras. Cicero Pereira and Edison Sato (Universidade Federal da Bahia) partly provided the funds for field trips. We thank all undergraduate and graduate students from Brazilian Universities (UFBA, UFRGS and UFRN) for their assistance in the field and/or help to process data. This study has the benefit of 15 years of field courses on high-resolution stratigraphy in the Chapada Diamantina sponsored by Petrobras, and great contributions from Eduardo Rodrigues, Carlos Arregui, José Daudt, Jose T. Guimarães, Farid Chemale Jr. and Daniel G. C. Fragoso. Gustavo Barros is acknowledged for his drafting skills. Thorough revision provided by Andreas Mulch, Michael Holz and an anonymous reviewer greatly improved this manuscript.

5.10. References

Ainsworth, R. B. (2005) Sequence stratigraphic-based analysis of reservoir connectivity: influence of depositional architecture – a case study form a marginal marine depositional setting. *Petroleum Geoscience* 11, 257-276.

Ainsworth, R. B. (2006) Sequence stratigraphic-based analysis of reservoir connectivity: influence of sealing faults – a case study from a marginal marine depositional setting. *Petroleum Geoscience* 12, 127–141.

Alkmim, F.F. (2004) O que faz de um cráton um cráton? O cráton de São Francisco e as revelações Almeidianas ao delimitá-lo. In: *Geologia do continente Sul-Americano: evolução da obra de Fernando Flávio Marques de Almeida* (Ed. By V. Manteso-Neto, A. Bartorelli, C.D.R. Carneiro, B.B.B. Brito Neves). São Paulo. pp. 17-35.

Alkmim, F.F. & Martins-Neto, M. (2012) Proterozoic first-order sequence sedimentary sequences of the São Francisco craton, eastern Brazil. *Mar. Pet. Geol*., 33, 127-139.

Allen, G. P., Posamentier, H. W. (1993) Sequence stratigraphy and facies model of an incised valley fill: the Gironde estuary, France. *J. Sed. Pet.* 63 (3), 378-391.

Almeida, F.F.M (1977) O craton de São Francisco. *Rev. Bras. Geoc*., 7(4), 349-364.

Araújo, A.J.S (2012) Análise estratigráfica das Formações Açuruá e Tombador nas proximidades de Barra da Estiva, Chapada Diamantina – Bahia. *Unpublished Monography*, Universidade Federal da Bahia, 40 pp.

Babinski, M., Van Schmus, W.R., Chemale Jr., F., Brito Neves, B.B. & Rocha, A.J.D. (1993) Idade isocrônica Pb/Pb em rochas carbonáticas da Formação Caboclo, em Morro do Chapéu. In: *Anais do 2º Simpósio do Craton do São Francisco*, Salvador, pp. 160-163.

Babinski, M., Brito Neves, B.B., Machado, N., Noce, C.M., Uhlein, A. & van Schmus, W.R. (1994) Problemas da metodologia U/Pb em zircões de vulcânicas continentais: caso do Grupo Rio dos Remédios, Supergrupo Espinhaço, no Estado da Bahia. In: Anais 42# Congresso Brasileiro de Geologia, Sociedade Brasileira de Geologia, Balneário Camboriú, vol. 2, pp. 409-410.

Babinski, M., Pedreira, A.J., Brito Neves, B.B. & Van Schmus, W.R. (1999) Contribuição à geocronologia da Chapada Diamantina. 7° Simpósio Nacional de Estudos Tectônicos. Brazilian Geological Society, Lençóis, pp. 118–120.

Ballance, P.F. (1984) Sheet-flow dominated gravel fans on the non-marine middle Cenozoic Simmler Formation, central California. *Sed. Geol.* 38, 337-359.

Bállico, M.B (2012) Análise de facies e sequências deposicionais em sistemas continentais e estuarinos do topo da Formação Tombador, Mesoproterozóico, Chapada Diamantina, Brasil. *Unpublished MsC Thesis*, Universidade Federal do Rio Grande do Sul. Porto Alegre. 100p.

Battilani, G.A., Varajão, A.D. & Gomes, N.S. (1999) Metamorphic degree variation in proterozoic sandstones of the Tombador Formation, Bahia State, Brazil. *Zbl. Geol. Paläont. Teil* I (7-8), 917-926.

Blair, T.C. (2000) Sedimentology and progressive tectonic unconformities of the sheetflood-dominated Hells Gate alluvial fan, Death Valley, California. *Sed. Geol.* 132, 233-262

Blair, T.C. & McPherson, J.G. (1994a) Alluvial fan processes and forms. In: *Geomorphology of deserts environments* (Ed. by A.D. Abrahams and A. Parsons), pp. 354-402 Chapman & Hall, London.

Blair, T.C. & McPherson, J.G. (1994b) Alluvial fans and their natural distinction from rivers based on morphology, hydraulic processes, sedimentary processes, and facies assemblages. *J. Sed. Res.* 64, 451-490.

Blissenbach, E. (1954) Geology of alluvial fans in semi-arid regions. *Geol. Soc. Am. Bull.* 65, 139-148.

Boyd, R., Dalrymple, R. W. & Zaitlin, B. A. (2006) Estuarine and incised-valley facies models. In: *Facies Models Revisited* (Ed. by H. Posamentier & R. Walker), *SEPM Spec. Public.* 84, 171-235.

Bristow, C.S. (1993) The interaction between channel geometry, water flow, sediment transport and deposition in braided rivers. In: *Braided rivers* (Ed. by J.L. Best and C.L. Bristow), *Spec. Publ. Geol. Soc.London* 75, 13-72

Bruun, P. (1962) Sea-level rise as a cause of shore erosion. American Society of Civil Engineers Proceedings, *Journal of the Waterways and Harbors Division* 88, 117-130.

Cant, D.J. & Walker, R.G. (1978) Fluvial process and facies sequences in the sandy braided South Saskatchewan River, Canada. *Sedimentology* 25, 625-648.

Castro, M.R. (2003) Estratigrafia de Sequências na Formação Tombador, Grupo Chapada Diamantina, Bahia. *Unpublished PhD Thesis*, Universidade São Paulo. 128p.

Catuneanu, O. (2006) *Principles of Sequence Stratigraphy*, Amsterdam, Elsevier, 375 p.

Catuneanu, O. & Eriksson, P.G. (1999) The sequence stratigraphic concept and the Precambrian rock record: an example from the 2.7–2.1 Ga Transvaal Supergroup, Kaapvaal craton. *Prec. Res*., 97, 215-251.

Catunenau, O., Martins-Neto, M.A. & Eriksson, P.G. (2005) Precambrian sequence stratigraphy. *Sed. Geol*., 176 (1-2), 67-95.

Catuneanu, O., Galloway, W.E., Kendall, C.G.St.C., Miall, A.D., Posamentier, H.W., Strasser, A. & Tucker, M.E. (2011) Sequence Stratigraphy: Methodology and Nomenclature. *Newsletter on Stratigraphy, Special Issue* 44(3), 173-245.

Chemale Jr, F., Dussin, I.A., Martins, M.S., Alkmim, F.F. & Queiroga, G. (2010) The Espinhaço Supergroup in Minas Gerais: a Stenian Basin? *VII South American Symposium on Isotope Geology*. Universidade de Brasília, pp. 552-555.

Collinson, J.D. (1996) Alluvial sediments. In: *Sedimentary Environments: Processes, Facies and Stratigraphy* (Ed.by H.G. Reading), pp. 37-82, Blackwell Science, London.

Costa, L.A.M. & Inda, H.A.V. (1982) O aulacógeno do Espinhaço. *Rev. Ciências da Terra,* 1, 13-18.

Dalrymple, R.W. (2010) Tidal depositional systems. In: *Facies Models 4* (Ed. by N.P James & R.W Dalrymple), *Geol. Ass. Can.* 6, 201-231.

Dalrymple, R.W., Narbonne, G.M. & Smith, L. (1985) Eolian action and the distribution of Cambrian shales in North America. *Geology* 13, 607-610.

Dalrymple, R.W., Knight, R.J. & Zaitlin, B.A.; Middleton, G.V. (1990) Dynamics and facies model of a macrotidal sand-bar complex. Cobequid Bay-Salmon River Estuary. *Sedimentology* 37, 577-612.

Danderfer, A. (1990) Análise descritiva e cinemática do Supergrupo Espinhaço na região da Chapada Diamantina, BA. *Unpublished MsC Thesis*, Universidade Federal de Ouro Preto, UFOP. 99p.

Danderfer, A. & Dardenne, M.A. (2002) Tectonoestratigrafia da bacia Espinhaço na porção centro-norte do cráton do São Francisco: registro de uma evolução polihistórica descontínua. *Rev. Brasil. Geocienc*., 32 (4), 449–460.

Danderfer, A., De Waele, B., Pedreira, A.J. & Nalini, H.A. (2009) New geochronological constraints on the geological evolution of Espinhaço basin within the São Francisco Craton – Brazil. *Prec. Res*., 170, 116-128.

Davies, T.R.H. (1986) Large debris flows: a macro-viscous phenomenon. *Acta Mech.* 63, 161-178.

Davies, T.R.H., (1990) Debris-flow surges—experimental simulation. *J. Hydrol*. 29, 18-46.

Denny, C.S. (1967) Fans and pediments. *Am. J. Sci*. 265, 81-105.

Delgado, I.M., Souza, J.D., Silva, L.C., Filho, N.C.S., Santos, R.A., Pedreira, A.J., Guimarães, J.T., Angelim, L.A.A., Vasconcelos, A.M., Gomes, I.P., Filho, J.V.L., Valente, C.R., Perrota, M.M. & Heineck, C.A. (2003) Geotectônica do Escudo Atlântico. In: *Geologia, Tectônica e Recursos Minerais do Brasil* (Ed. by L.A. Bizzi, C. Schobbenhaus, R.M. Vidotti and J.H. Gonçalves), CPRM, Brasília.

Derby, O.A. (1906) The Serra of Espinhaço, Brazil. *J. Geol*., 14, 314-401

Dominguez, J.M.L. (1992) Estratigrafia de sequências aplicada a terrenos pré-Cambrianos: exemplos para o Estado da Bahia. *Rev. Bras. Geocien*. 22(4), 422-436.

Dominguez, J. M. L. & Wanless, H. R. (1991) Facies architecture of a falling sea-level strandplain, Doce River coast, Brazil. In: *Shelf sand and sandstone bodies: geometry, facies and sequence stratigraphy* (Ed. by D. J. P. Swift, G. F. Oertel, R. W. Tillman, and J. A. Thorne), *Spec. Publ. Int. Ass. Sediment.* 14, 259-281.

Eriksson, P.G., Condie, K.C., Tisgaard, H., Mueller, W.U., Altermann, W., Miall, A.D., Aspler, L.B, Catuneanu, O. & Chiarenzelli, J.R. (1998) Precambrian clastic sedimentation systems. *Sed. Geol*. 120, 5-53.

Eriksson, K.A. & Simpson, E.L. (2004) Precambrian Tidalites: recognition and significance. In: *The Precambrian Earth: Tempos and Events* (Ed. by P.G. Eriksson, W. Altermann, D.R.Nelson, W.U. Mueller & O. Catuneanu), pp. 631-642. Elsevier, Amsterdam.

Eriksson, P.G. & Catuneanu, O. (2004) Third-order sequence stratigraphy in the Palaeoproterozoic Daspoort Formation (Pretoria Group, Transvaal Supergroup), Kaapvaal craton. In: *The Precambrian Earth: tempos and events* (Ed. by P.G. Eriksson, W. Altermann, D.R. Nelson, W.U. Mueller, & O. Catuneanu), p. 724– 35.

Eriksson, P. G., Catunenau, O., Sarkaf, S. & Tirsgaard, H. (2005a) Patterns of sedimentation in the Precambrian. *Sed. Geol*., 176, 17-42.

Eriksson, P.G., Catuneanu, O., Nelson, D.R. & Popa, M (2005b) Controls on Precambrian sea level change and sedimentary cyclicity. *Sed. Geol*. 176, 43-65.

Eriksson, P.G., Catuneanu, O., Els, B.G., Bumpy, A.J., Van Rooy, J.L. & Popa, M. (2005c) Kaapval craton: changing first- and second-order controls on sea level from c. 3.0 Ga to 2.0 Ga. *Sed. Geol*. 176, 121-148.

Eriksson, K.A., Simpson, E.L. & Mueller, W. (2006) An unusual fluvial to tidal transition in the mesoarchean Moodis Group, South Africa: A response to high tidal range and active tectonics. *Sed. Geol*. 190, 13-24.

Fanti, F. & Catuneanu, O. (2010) Fluvial sequence stratigraphy: the Waipiti Formation, West-Central Alberta, Canada. *J. Sed. Res*., 80, 320-338.

Galloway, W.E. (1989) Genetic stratigraphic sequences in basin analysis, I. Architecture and genesis of flooding-surface bounded depositional units. *AAPG Bull*., 73, 125-142.

Gruber, L., Pimentel, M.M., Brito Neves, B.B., Armstrong, R. & Fuck. R.A. (2011) Proveniência U-Pb em zircão (SHRIMP) da Formação Tombador, Grupo Chapada Diamantina, BA. *Anais do XIII Congr. Bras. Geoquímica*, pp. 1155-1158.

Guadagnin, F., Chemale Jr., F., Magalhães, A.J.C., Santana, A., Dussin, I. & Takehara, L. (2015) Age constraints on crystal-tuff from the Espinhaço Supergroup – Insights into the Paleoproterozoic to Mesoproterozoic intracratonic basin cycles of the Congo- São Francisco Craton. *Gond. Res*. 27, 363-376.

Guimarães, J.T., Santos, R.A. & Melo, R.C. (2008) Geologia da Chapada Diamantina Ocidental (Projeto Ibitiara–Rio de Contas). Salvador, Companhia Baiana de Pesquisa Mineral – CBPM/ Companhia Pesquisa de Recursos Minerais – CPRM. *Série Arquivos Abertos*, 31, 64p.

Hadlari, T., Rainbird, R.H., J. Donaldson, J.A. (2006) Alluvial, eolian and lacustrine sedimentology of a Paleoproterozoic half-graben, Baker Lake Basin, Nunavut, Canada. *Sed. Geol.* 190, 47-70.

Hampton, B.A. & Horton, B.K. (2007) Sheetflow fluvial processes in a rapidly subsiding basin, Altiplano plateau, Bolivia. *Sedimentology* 54, 1121-1147.

Hunter, R.E. (1977) Terminology of cross-stratified sedimentary layers and climbing-ripple structures. *J. Sed. Petrol*. 47, 697-706.

Inda, H.A.V. & Barbosa, J.F. (1978) Texto explicativo para o mapa geológico do Estado da Bahia escala 1:1.000.000. SME/COM. Salvador, 137p.

Jardim de Sá; E.F., Bartels, R.L., Brito Neves, B.B. & McReath, I. (1976) Geocronologia e o modelo tectono-magmático da Chapada Diamantina e Espinhaço Setentrional, Bahia. *XXIX Congr. Bras.Geol. Anais,* 4, 205-257.

Jardim de Sá, E.F. (1981) A Chapada Diamantina e a Faixa Santo Onofre: um exemplo de tectônica intra-placa no Proterozóico Médio do Craton do São Francisco. In: *Geologia e Recursos Minerais do Estado da Bahia* (Ed. by H.A.V. Inda, M.M Marinho & F.B. Duarte) Secretaria de Minas e Energia do Estado da Bahia, *Textos Básicos* 4, 111-120.

Kocurek, G. & Havholm, K. G. (1993) Eolian sequence stratigraphy – a conceptual framework. In: *Siliciclastic Sequence Stratigraphy . Recent Developments and Applications* (Ed. by P.W. Weimer and H.W. Posamentier), *AAPG Memoir* 58, 393-409.

Kocurek, G. & Lancaster, N. (1999) Aeolian system sediment state: theory and Mojave Desert Kelso dune field example. *Sedimentology,* 46, 505-515

Kokureck, G. & Nielson, J. (1986) Conditions favourable for the formation of warm-climate eolian and sandsheets. *Sedimentology* 33, 795-816

Loureiro, H.S.C., Bahiense, I.C., Neves, J.P., Guimarães, J.T., Teixeira, L.R.; Santos, R.A. & Melo, R.C. (2009) Geologia e recursos minerais da parte norte do corredor de deformação do Paramirim (Projeto Barra-Oliveira dos Brejinhos): Salvador, Companhia Baiana de Pesquisa Mineral – CBPM, Companhia Pesquisa de Recursos Minerais – CPRM. *Série Arquivos Abertos*, 33, 122p.

Lowe, D.R. (1988) Suspended-load fallout rate as an independent variable in the analysis of current structures. *Sedimentology* 35, 765-776.

Major, J.J. (1997) Depositional processes in large-scale debris-flow experiments. *J. Geol.*105, 345-366.

Marconato, A.; Almeida, R.P.; Turra, B.B. & Fragoso-Cesar, A.R.S. (2014) Pre-vegetation fluvial floodplains and channel-belts in the Late Neoproterozoic-Cambrian Santa Bárbara group (Southern Brazil). *Sed. Geol.* 300, 49-61.

Martins-Neto, M.A. (2009) Sequence stratigraphic framework of Proterozoic successions in eastern Brazil. *Mar. Pet. Geol*. 26, 163-176.

Martins-Neto, M.A., Pedrosa Soares, A.C. & Lima, S.A.A. (2001) Tectono-sedimentary evolution of sedimentar basins from Late Paleoproterozoic to Late Neoproterozoic in the São Francisco craton and Araçuaí fold belt, eastern Brazil. *Sed. Geol*., 141/142, 343-370.

McKie, T., Jolley, S. J. & Kristensen, M.B. (2010) Stratigraphic and structural compartmentalization of dryland fluvial reservoirs: Triassic Heron Cluster, Central North Sea. In: S.J. Jolley, Q.J. Fisher, R.B. Ainsworth, P. Vrolijk and S. Delisle (Eds.), Reservoir Compartmentalization. *Spec. Publ. Geol. Soc.*, 347, 165-198.

McCormick, D.S. & Grotzinger, J.P. (1993) Distinction of marine from alluvial facies in the Paleoproterozoic (1.9 Ga) Burnside Formation, Kilihigok Basin, N.W.T., Canada. *J. Sed. Pet.* 63, 398-419.

Miall, A.D. (1978) Lithofacies types and vertical profile models in braided rivers deposits: a summary. In: *Fluvial Sedimentology* (Ed. by A.D Miall), *Can. Soc. Pet. Geol.*5, 597-604.

Miall, A.D., 1985. Architectural-Elements Analysis: A New Method of Facies Analysis Applied to Fluvial Deposits. *Earth-Science Reviews* 22, 261-308.

Miall, A.D. (1996) The Geology of Fluvial Deposits: Sedimentary Facies, Basin Analysis, and Petroleum Geology, 582 pp. SpringerVerlag, Berlin.

Mountney, N.P. (2012) A stratigraphic model to account for complexity in Aeolian dune and interdune successions. *Sedimentology*, 59, 964-989.

Nemec, W. & Postma, G. (1993) Quaternary alluvial fans in southwestern Crete: sedimentation processes and geomorphic evolution. In: *Alluvial Sedimentation* (Ed. by M. Marzo and C. Puigdefabregas), *Spe. Publ. Intr. Ass. Sediment*. 17, 235-276.

Nemec, W. & Steel, R.J. (1984) Alluvial and coastal conglomerates: their significant features and some comments on gravelly mass flow deposits In: *Sedimentology of gravels and conglomerates* (Ed. by E.H. Koster and R.J. Steel), *Can. Soc. Pet. Geol*. 10, 1-31.

Nummendal, D. & Swift, D. J. P. (1987) Transgressive stratigraphy at sequence-bounding unconformities: some principles derived from Holocene and Cretaceous examples. In: *Sea-level fluctuation and coastal evolution* (Ed. by D. Nummendal, O. H. Pilkey and J.D. Howard), *Spec. Publ. SEPM* 41, 241-260.

Pedreira, A.J.C.L. (1994) O Supergrupo Espinhaço na Chapada Diamantina Centro-Oriental, Bahia: Sedimentação, Estratigrafia e Tectônica. *Unpublished PhD Thesis,* Universidade São Paulo*,* 126p.

Pedreira, A.J. & De Waele, B. (2008) Contemporaneous evolution of the Palaeoproterozoic-Mesoproterozoic sedimentary basins of the São Francisco-Congo Craton. In: *West Gondwana: Pre-Cenozoic Correlations Across the South Atlantic Region,* (Ed. by R.J. Pankhurst, R.A.J. Trouw, B.B. Brito Neves, B.B. & M.J. De Wit), *Geol. Soc. Spec. Publ*., 294, 33-48.

Plink-Björklund, P. (2005) Stacked fluvial and tide-dominated estuarine deposits in high-frequency (fourth-order) sequences of the Eocene Central Basin, Spitsbergen. *Sedimentology* 52, 391-428.

Pyrcz, M. J., Catuneanu, O. & Deutsch, C. V. (2005) Stochastic surface-based modeling of turbidite lobes. *AAPG Bul*. Vol 89 (2), 177-192.

Raja Gabaglia, G.P., Rodrigues, E.B., Magalhaes, A.J.C., Arregui, C.D. & Savini, R. (2006) Criteria do recognise sequence orders and tectonic imprint in cyclic siliciclastic record: a key to high-resolution stratigraphy. *IAS Intern. Meeting*, Fukuoka, Japan.

Ramaekers, P. & Catuneanu, O. (2004) Development and sequences of the Athabasca Basin, early Proterozoic, Saskatchewan and Alberta, Canada. In: *The Precambrian Earth: tempos and events*, (Ed. by P.G. Eriksson W. Altermann, D.R. Nelson, W.U. Mueller & O. Catuneanu O.), p. 705– 23.

Rebouças, V.O. (2011) Estratigrafia de sequências da Formação Açuruá nas proximidades de Guiné, Chapada Diamantina – Bahia. *Unpublished Monography*, Universidade Federal da Bahia, Salvador. 84pp.

Santana, A. (2007) Ciclicidade no registro sedimentar do intervalo superior do Grupo Paraguaçu, Mesoproterozoico, Chapada Diamantina. *Unpublished Monography*, Universidade Federal da Bahia, Salvador. 76pp

Santana, R.O. (2009) Estratigrafia de Sequências de alta resolução na base da Formação Tombador, nos arredores de Lençóis, Chapada Diamantina. *Unpublished Monography*, Universidade Federal da Bahia, Salvador. 126pp

Santos, C.M. (2009) Análise Estratigráfica das Formações Guiné – Tombador, Chapada Diamantina, Bahia. *Unpublished Monography*, Universidade Federal da Bahia, Salvador. 136pp.

Savini, R.R. & Raja Gabaglia, G.P. (1997) Curso de Campo da Chapada Diamantina – Guias de Campo. Lençóis (BA). PETROBRAS. 15p.

Scherer, C.M.S (2002) Preservation of aeolian genetic units by lava flow in the Lower Cretaceous of the Paraná Basin, southern Brazil. *Sedimentology* 49, 97-116.

Scherer, C.M.S., Lavina, E.L.C., Filho, D.C.D., Oliveira, F.M., Bongiolo, D.E. & Aguiar E.S. (2007) Stratigraphy na facies architecture of the fluvial-aeolian-lcustrine Sergi Formation (Upper Jurassic), Recôncavo Basin, Brazil. *Sed. Geol*. 194, 169-193.

Schobbenhaus, C. (1996) As tafrogêneses superpostas Espinhaço e Santo Onofre, estado da Bahia: Revisão e novas propostas. *Rev. Bras.Geocien*., 4, 265-276.

Schobbenhaus, C. & Kaul, P.F.T. (1971) Contribuição a estratigrafia da Chapada Diamantina, Bahia Central. *Mineração e Metalurgia*, 53(315), 116-120.

Schoengut, J.A. (2011) Sedimentological and ichnological characteristics of modern and ancient channel-fills, Willapa Bay, Washington. MsC thesis, University of Alberta, 216 pp.

Schum, S. (1993) River response to base level change: implication for sequence stratigraphy. *J. Geol*., 101, 279-294.

Shanley, K.W. & McCabe, P.J. (1994) Perspectives on the Sequence Stratigraphy of Continental Strata. *AAPG Bul*., 78(4), 544-568.

Silva Filho, C.V.R. (2009) Sistemas deposicionais nas Formações Tombador e Guiné nos arredores do Morro do Pai Inácio, Chapada Diamantina–BA. *Unpublished Monography*, Universidade Federal da Bahia, 120p.

Silva Born, L.R. (2011) A Formação Tombador na porção nordeste da Chapada Diamantina - BA: Estratigrafia, Faciologia e Ambientes de Sedimentação. *Unpublished MsC Thesis*, Universidade Federal do Rio Grande do Sul, Brasil.

Simpson, E.L., Dilliard, K.A., Rowell, B.F. & Higgins, D. (2002) The fluvial-to-marine transition within the post-rift Lower Cambrian Hardyston Formation, Eastern Pennsylvania, USA. *Sed. Geol.* 147, 127-142.

Sloss, L.L., Krumbein, W.C. & Dapples, E.C. (1949) Integrated facies analysis. In: Longwell, C.R. (Ed.) Sedimentary facies in geologic history. *Geol. Soc. Am. Mem*., 39, 91-124.

Sohn, Y.K., Rhee, C.W. & Kim, B.C. (1999) Debris Flow and Hyperconcentrated Flood-Flow Deposits in an Alluvial Fan, Northwestern Part of the Cretaceous Yongdong Basin, Central Korea. *J. Geol*. 107, 111-132.

Swift, D.J.P. (1975) Barrier-island genesis: evidence from the central Atlantic shelf, eastern USA. *Sed. Geol.* 14, 1-43.

Swift, D.J.P., Kofoed, J.W., Saulsbury, F.B. & Sears, P.C (1972) Holocene evolution of the shelf surface, central and southern Atlantic shelf of North America. In: *Shelf sediment transport: process and pattern* (Ed. by D.J.P. Swift, D.B. Duane, O.H. Pilkey), pp-499-574, Stroudsburg, Pennsylvania, Dowden.

Tirsgaard, H. & Øxnevad, I.E.I. (1998) Preservation of pre-vegetational mixed fluvio–aeolian deposits in a humid climatic setting: an example from the Middle Proterozoic Eriksfjord Formation, Southwest Greenland. *Sed. Geol*., 120, pp. 295-317.

Todd, S.P. (1989) Sream-driven, high-density gravelly traction carpets: possible deposits in the Trabeg Conglomerate Formation, SW Ireland and some theoretical considerations of their origin. *Sedimentology* 36, 513-530.

Tunbridge, I.P. (1981) Sandy high-energy flood sedimentation—some criteria for recognition, with an example from the Devonian of S.W. England. *Sed. Geol*. 28, 79–95.

Varajão, A.D. & Gomes, N.S. (1997) Petrological significance of illitic clays in Proterozoic sandstones of the Tombador Formation, Chapada Diamantina, Brazil. *Zbl. Geol. Paläont. Teil I*, (3-6), 767-778.

Visser, M.J. (1980) Neap-spring cycles reflected in Holocene subtidal large-scale bedforms deposits: a preliminary note. *Geology* 8, 543-546.

Wells, N.A. (1984) Sheet debris flow and sheetflood conglomerates in Cretaceous cool maritime alluvial fans, south Orkney Islands, Antarctica. In: *Sedimentology of gravels and conglomerates* (Ed. by E.H. Koster and R.J. Steel), *Can. Soc. Pet. Geol*. 10, 133-145.

Wells, S.G. & Harvey, A.M. (1987) Sedimentological and geomorphic variations in storm generated alluvial fans, Howgill fells, northwest England. *Geol. Soc. Am. Bull*. 98, 182-198.

Went, D.J. (2005) Pre-vegetation alluvial fan facies and processes: an example from the Cambro-Ordovician Rozel Conglomerate Formation, Jersey, Channel Islands. *Sedimentology* 52, 693-713.

Williams, G.E. (1971) Flood deposits of the sand-bed ephemeral streams of central Australia. *Sedimentology* 17, 1-4.

Wonham, J.P., Cyrot, M., Nguyen, T., Louhouamou, J. & Ruau, O. (2010) Integrated approach to geomodelling and dynamic simulation in a complex mixed siliciclastic–carbonate reservoir, N'Kossa field, Offshore Congo. In: *Reservoir Compartmentalization* (Ed. by S.J. Jolley, Q.J. Fisher, R.B. Ainsworth, P. Vrolijk and S. Delisle), *Spec. Publ. Geol. Soc.*, 347, 133-163.

Chapter 6 – The connection between chapters 2 through 5 and support from the petrographic analysis: conclusions and further investigations

This study demonstrated that a high-resolution stratigraphic approach can be applied to a Mesoproterozoic intracratonic sag basin, even considering the differences in tectonic and sedimentary controls when comparing Precambrian and Phanerozoic sedimentary successions, as long as facies, facies relationships, and sandbody geometry can be well defined in Mesoproterozoic successions. This study also provides a practical stratigraphic methodology that can be applied in Petroleum Geology, particularly to the definition of production zone boundaries.

In the Chapada Diamantina Basin, changes in paleogeography due to relative sea level fluctuations are recorded at all hierarchical levels, with a magnitude that increases with the hierarchical rank. These changes are supported by distinct physical attributes and facies shifting associated with sequence boundaries observed at different hierarchical orders, such as regional unconformities, changes of zircon age signature, changes of paleoflow direction and facies shifting of different magnitudes. Therefore, the hierarchy system that applies to the Precambrian Tombador Formation is based on changes of depositional trends that were observed in the rock record and includes sequences of different orders as follows:

- the sequences associated with a particular tectonic setting are designated as 'first order' and are separated by first-order sequence boundaries where changes in the tectonic setting are recorded (i.e., sequence Middle Espinhaço II);
- the second-order sequences represent the major subdivisions of the first-order sequence and reflect cycles of change in the stratal stacking pattern observed at the 10^2 m-scale (i.e., 200-300 m, sequences Middle Espinhaço II Lower and Middle Espinhaço II Upper);
- changes in the stratal stacking pattern at the 10^1 m-scale indicate third-order sequences (i.e., 40-70 m, sequences A-H);
- changes in the stratal stacking pattern at the 10^0 m-scale are assigned to fourth order hierarchy (i.e., 8-12 m).

The criteria applied to assign sequence hierarchies in this study are based on rock attributes, they are easy applied, and can be used as a baseline for the study of sequence stratigraphy in Precambrian and Phanerozoic basins placed in similar tectonic settings.

SU1 is the regional unconformity between the first-order sequences Middle Espinhaço I and Middle Espinhaço II. This unconformity is clearly defined based on the change of depositional systems and shifting of the flow pattern across SU1 (a comparison of the paleogeographic reconstructions is presented in Fig. 2.17 and Fig. 3.15). Such changes reflect the intra-cratonic regional-scale extensional stress regime that took place at the southeastern and western margins of the Congo craton at ca. 1375 Ma (i.e., the Kibaran extension). SU8 is the regional unconformity between the first-order sequences Middle Espinhaço II and Upper Espinhaço. This angular unconformity is a sequence boundary associated with a major hiatus (100 to 400 Ma) between two sag basin fill successions (Figs. 5.21 and 5.22). The basin-forming mechanism related to the sequence Upper Espinhaço is interpreted as a result from the late Kibaran or Greenvilian events during the assembly of the Rodinia Supercontinent. Thus, the SU1 and SU8 unconformities are, respectively, the lower and upper boundaries of the first-order sequence Middle Espinhaço II. This sequence, aged at ca. 1416 ± 28 Ma and entirely included in the Tombador Formation, represents a distinct sag basin fill in the polycyclic history of the Espinhaço Supergroup in the Chapada Diamantina Basin. Moreover, the Espinhaço Supergroup in the Chapada Diamantina Basin includes four first-order sequences: Lower Espinhaço, Middle Espinhaço I, Middle Espinhaço II, and Upper Espinhaço, each related to a distinct and individualized basin fill cycle (Fig. 5.2). The time span related to basin-forming mechanisms and sedimentation for each of these first-order sequences is more likely smaller than the hiatuses associated with their sequence boundaries. In the Chapada Diamantina Basin, tectonics at the intra-plate and plate margins triggered extensions that led to the formation of rift (e.g., the Statherian rift event) and sag (e.g., the Kibaran event) basins, while compressions led to uplift and erosion and hence, promoted first-order cyclicity.

The first-order sequence Middle Espinhaço II is divided into two second-order units separated by the angular unconformity SU6: sequences Lower Middle Espinhaço II and Upper Middle Espinhaço II. Convincing evidence of basin reorganization is recorded across SU6 such as: (a) the shift of facies and flow pattern (Fig. 5.4), (b) the distinct zircon age signatures (Fig. 5.20), (c) the composition of conglomerates from sequence Upper Middle Espinhaço II (Fig. 5.14), and (d) the dip of strata and change on geographic occurrence of the second-order sequences (Fig. 5.21). Within the sequence Lower Middle Espinhaço II, the third-order sequences A-E exhibit lowstand fluvial sand sheets, undifferentiated transgressive-highstand sand-rich floodplain, transgressive estuarine, and highstand offshore tidal bars deposits. In contrast, the sequence Upper Middle Espinhaço II is characterized by fining-upward continental alluvial successions (sequences F-G) that are composed of conglomerates overlain by fluvial and eolian strata. The occurrence of the sequence Lower Middle Espinhaço II is restricted to the study area, but the sequence Upper Middle Espinhaço II extends farther to the north and northwest beyond the Sincorá Range, where conglomerates overlie the unconformity (SU1) with the basement or with the Açuruá Formation.

The third-order depositional sequences A-E correspond to the Lower Tombador Formation and record the deposition of unincised fluvial and tide-dominated estuarine systems, in which the observed facies distribution is similar to that found in estuaries related to incised-valley systems. At the seismic scale photo-mosaics, these sequences exhibit sheet-like geometry, homogeneous thickness, no evidence of fluvial scouring, and cyclicity that can be traced for more than 35 km on the regional strike along the cliffs of the Northern Sincorá Range (Fig. 3.17). The paleogeographic reconstruction suggests that shallow braided- and ephemeral sheetflood fluvial systems crossed a wide, gently dipping fluvial braidplain linked to a tide-dominated coast (Fig. 3.15). The sequences F-G are typical continental sequences that mark the establishment of alluvial fan and fluvial-eolian systems, as suggested by the facies lateral variability and radial fluvial paleocurrent pattern (Figs. 5.13 and 5.14). The dominant fluvial paleoflow towards the southwest and the variations to the northwest and southeast indicates a source area located to the east/northeast. The integration of data from this study with those from Silva Born (2012) and Bállico (2012) indicates the existence of three alluvial fans that had at least a 40-km coverage radius. Although the sequences F-G do not exhibit a marine or tidal influence, it is inconclusive whether they were downstream- or upstream-controlled and hence, no systems tract nomenclature was used (Fig. 5.26). An investigation along the depositional down-dip direction would provide such evidence, but the erosion extends southwards and precludes the study of those sequences. The sequence H is bounded at its base by the SU8 and hence, it represents the lower portion of the first-order sequence Upper Espinhaço, which is composed of transgressive sandstones (from the Tombador Formation) and overlying shallow marine mudstones (from the Caboclo Formation). Previous interpretation assumed that these two formations were part of the same sedimentary succession. The upper boundary of sequence H was not investigated in this study.

Petrographic analyses indicate that the sandstones are quartz arenites ($Q_{99.77}F_{0.20}RF_{0.03}$, Folk, 1974), irrespective of the sequence and the systems tracts to which they are included. Such monotonous detrital composition more likely resulted from one of the following factors or from a combination of them: (a) a high degree of reworking in all sequences; (b) long transportation distance; (c) intensive weathering on the basement (i.e., the source area, which is composed of high-degree metamorphic rocks such as TTG (tonalite-trondhjemite-granodiorite), migmatites, granitoids, and metasedimentary rocks metamorphosed in granulite facies); and (d) post-depositional weathering. The quartz arenite sandstone composition also explains the low values of K, U and Th from spectral gamma ray log, and reinforces the interpretation of intense weathering both on sandstones as well as on their source area (low K, dissolution of feldspar grains), sandstone deposition in oxidizing condition (low U, continental and shallow marine settings), and low content of heavy minerals and terrigenous clays (low Th). Post-depositional weathering is also indicated by the strong depletion of CaO and Na_2O relative to Upper Continental Crust revealed by the major and trace elements compositions of the crystal-tuff and volcaniclastic interval from the sequence G (Fig. A1.4). Fluvial sandstones from sequences A-G are well cemented by early diagenetic quartz overgrowths and are characterized by mechanically infiltrated clay coatings and pore-filling aggregates or mud clasts that were transformed into illite, sericite, and/or muscovite. No diagnostic diagenetic event was identified in the transgressive to highstand sandstones from sequences A-E. Silex cementation is markedly strong in the sandstones from sequences F-G. The comparison between gamma ray log (GR) and vertical facies description enabled the use of the first to differentiate sandstone from mudstone. Generally, sandstone has GR values smaller than 120 counts per second (cps) whereas mudstone has GR values higher than 120 cps.

The fourth-order sequences are best recognized within the third-order transgressive systems tract, and they exhibit distinct facies associations depending on their occurrence at updip or downdip location. Downdip, the fourth-order sequences are composed of tidal channel, tidal bar and overlying shoreface heterolithic strata. At this hierarchical level, GPR results proved that it is an independent method that helped with the interpretation of the architectural elements and complemented the interpretation of the depositional systems, the stacking pattern, and the sequence stratigraphic surfaces based on other independent techniques such as vertical sections, GR logs, and photomosaics. The radar images applied to estuarine successions confirmed not only their retrogradational stacking pattern but also the mappability of stratigraphic surfaces from outcrops to subsurface (Fig. 5.28). Updip, there are two types of fourth-order sequences: a) those preserved at the sand-rich floodplain, which are composed of cyclic successions of sand-bed braided or distal ephemeral sheetflood deposits capped by eolian sand sheet or mudstone layers, and b) those preserved at the tide-influenced braided fluvial sand sheet, which consist of cyclic successions of fluvial strata bounded by tide-influenced intervals (Fig. 5.27). Fourth-order sequences were also recognized within the third-order shallow marine highstand systems tract. In this case, they are formed of offshore tidal bars and shoreface heterolithic strata (Fig. 5.28). Mappability is indeed one important criterion for assigning fourth-order stratigraphic surfaces. Fine-grained intervals from downdip and updip setttings are chrono-equivalent intervals that can be correlated for at least 17 km and more likely formed as a response of marine floodings. Because the fourth-order sequences are bounded by maximum flooding surfaces, they are more properly classified as genetic stratigraphic sequences.

The methodological application of high-resolution stratigraphy to petroleum reservoirs is directly related to reservoir stratigraphic compartmentalization (Fig. 5.29). The maximum regressive surface subdivides the sequence A into two main production zones at third-order hierarchy: one equivalent to the lowstand and other represented by the transgressive-highstand systems tract. The vertical and lateral homogeneity of the lowstand sand-bed braided fluvial facies association suggests this zone would have the best porosity, permeability, and lateral distribution. On the other hand, the presence of fine-grained facies strata promotes a series of horizontal heterogeneities within the transgressive and highstand interval. Such lower-order compartmentalization is better characterized based on fourth-order sequence boundaries. In fact, those intervals constitute the most important horizontal heterogeneities and effective barriers to vertical flow and hence, they are the preferable boundaries of higher resolution production zones. Thus, the stratigraphic compartmentalization indicates that the third-order transgressive-highstand interval is composed of four production zones (i.e., fourth-order sequences). Nevertheless, despite their overall tabular, layer-cake geometry, the dip and strike correlation of the fourth-order sequences exhibit facies variations between the fluvial and estuarine settings that may constitute less effective barriers to horizontal flow. In a real gas or oil field, such high-resolution heterogeneities more likely control gas, oil, and water flow within the reservoir and hence give important insights to optimize hydrocarbon production and to maintain the energy of the reservoirs. Therefore, this knowledge is essential to choose intervals for production and fluid injection, and to close intervals with high water-cut in the wells. Beyond the fourth-order, the highest hierarchical order identified in this study, there are no longer mappable stratigraphic surfaces at the reservoir scale; rather, only contacts between individual facies or facies associations are available for study.

However, some issues related to the Tombador Formation remain open, demanding further investigations, such as the following:

(i) an attempt to acquire data southward from the Sincorá Range to extend the stratigraphic correlation of sequences A-G. Such a reseach would enable more accurate paleoshoreline interpretation and hence, more accurate paleogeographic reconstructions.

(ii) a paleogeographic reconstruction of the Tombador Formation encompassing the Western and the Eastern Chapada Diamantina. The integration of such data would help to unravel the tectnosedimentary evolution of the basin.

(iii) a search for evidence of downstream control on sequences F-G westwards from the Sincorá Range. Downdip, theese continental sequences may be connected to coastal/shallow marine deposits that would indicate downstream control and hence, the intepretation of systems tracts.

(iv) an attempt to define fourth-order sequences in continental sequences F-G, which is totally dependent on the abovementioned control. At downstream-controlled sequences, high-resolution stratigraphy in fluvial and eolian deposits would not be a problem. However, high-resolution characterization at upstream-contolled sequences is not trivial.

(v) understanding the basin-forming mechanism related to the SU8 and the first-order sequence Upper Espinhaço, because this tectonic event has not yet been recognized in the São Francisco/Congo craton.

(vi) understanding the climate control on deposition of the Precambrian siliciclastic successions is a challenge yet to be achieved. In this study, climate influence is suggested to explain fluvial discharge variability based on the interpretation of different fluvial styles (i.e. braided versus ephemeral sheet flood). There are abundant literature on astronomical forcing signal embedded in cyclostratigraphy, mainly in carbonatic or evaporitic intervals. Would it be possible to recognize such signals to explain cyclicity of braided and ephemeral sheet flood fluvial intervals, if there are same, in the Precambrian?

(vii) understanding the quartz arenite composition of the sandstones. Such composition together with low values of K, U and Th (from spectral gamma ray logs) and depletion of CaO and Na2O relative to Upper Continental Crust point to intense weathering on sandstone or on their source area. A provenance research would help to clarify these issues.

References

Abreu, F.R. 1991. Estudo das mineralizações auríferas filoneanas da região da cidade de Diamantina/MG. Unpublisehd MSc. Thesis, UNICAMP.

Alexander, J. & Fielding, C.R. 1997. Gravel antidunes in the tropical Burdekin River, Queensland, Australia: Sedimentology 44, 327-337.

Alkmim, F.F. 2004. O que faz de um cráton um cráton? O cráton de São Francisco e as revelações Almeidianas ao delimitá-lo. In: Manteso-Neto, V.; Bartorelli, A.; Carneiro, C.D.R., Brito Neves, B.B. (Eds.), Geologia do continente Sul-Americano: evolução da obra de Fernando Flávio Marques de Almeida, pp. 17-35.

Alkmim, F.F. & Martins-Neto, M. 2011. A bacia intracratônica do São Francisco: Arcabouço estrutural e cenários evolutivos. In: Pinto, C. P. & Martins-Neto, M. A. (Eds.), Bacia do São Francisco: geologia e recursos naturais. SBG/MG, Belo Horizonte, pp. 9-30.

Alkmim, F.F. & Martins-Neto, M. 2012. Proterozoic first-order sequence sedimentary sequences of the São Francisco craton, eastern Brazil. Marine and Petroleum Geology 33, 127-139.

Allen, G. P. & Posamentier, H. W. 1993. Sequence stratigraphy and facies model of an incised valley fill: the Gironde estuary, France. Journal Sedimentary Petrology 63 (3), 378-391.

Allen, J.R.L. 1963. The classification of cross-stratified units, with notes on their origin. Sedimentology 2, 93-114.

Almeida, F.F.M. 1977. O craton de São Francisco. Revista Brasileira de Geociências 7(4), 349-364.

Annan, A.P. 2001. Ground Penetration Radar - Workshop notes. Sensors and Software Inc. Mississauga, Ontário, Canada, 192 pp.

Aragão, M.O. 2009. Ambientes Sedimentares em Torno da Discordância Entre as Formações Tombador e Guiné, Chapada Diamantina, Bahia. Unpublished monography, Universidade Federal da Bahia, 91 pp.

Araujo, A.J.S. 2012. Análise estratigráfica das Formações Açuruá e Tombador nas proximidades de Barra da Estiva, Chapada Diamantina-Ba. Unpublished monography, Universidade Federal da Bahia, 41 pp.

Ashworth, P.J.; Smith, G.H. S.; Best, J.L.; Bridges, J.S.; Lane, S.N.; Lunt, I.A.; Reesink, A.J.H.; Simpson, C.J. & Thomas, R.E. 2011. Evolution and sedimentology of a channel fill in the sandy braided South Saskatchewan River and its comparison to the deposits of an adjacent compound bar. Sedimentology, 58, 1860-1883.

Aspler, L.B., Wisotzek, I.E., Chiarenzelli, J.R., Losonczy, M.F., Cousens, B.L., McNicoll, V.J. & Davis, W.J. 2001. Paleoproterozoic intracratonic basin processes, from breakup of Kenorland to assembly of Laurentia: Hurwitz Basin, Nunavut, Canada. Sedimentary Geology 141, 287-318.

Babinski, M., Van Schmus, W.R., Chemale Jr., F., Brito Neves, B.B. & Rocha, A.J.D. 1993. Idade isocrônica Pb/Pb em rochas carbonáticas da Formação Caboclo, em Morro do Chapéu. In: Anais do 2º Simpósio do Craton do São Francisco, Salvador, pp. 160-163.

Babinski, M., Brito Neves, B.B., Machado, N., Noce, C.M., Uhlein, A. & van Schmus, W.R. 1994. Problemas da metodologia U/Pb em zircões de vulcânicas continentais: caso do Grupo Rio dos Remédios, Supergrupo Espinhaço, no Estado da Bahia. In: Anais 42º Congresso Brasileiro de Geologia, Sociedade Brasileira de Geologia, Balneário Camboriú, vol. 2, pp. 409-410.

Babinski, M., Pedreira, A.J., Brito Neves, B.B., & Van Schmus, W.R. 1999. Contribuição à geocronologia da Chapada Diamantina. 7° Simpósio Nacional de Estudos Tectônicos. Brazilian Geological Society, Lençóis, pp. 118-120.

Ballance, P.F. 1984. Sheet-flow dominated gravel fans on the non-marine middle Cenozoic Simmler Formation, central California. Sedimentary Geology 38, 337-359.

Bállico, M.B. 2012. Análise de facies e sequências deposicionais em sistemas continentais e estuarinos do topo da Formação Tombador, Mesoproterozóico, Chapada Diamantina, Brasil. Unpublished MsC Thesis, Universidade Federal do Rio Grande do Sul. Porto Alegre. 100p.

Barbosa, J.S.F. & Domingues, J.M.L. 1994. Mapa geológico do Estado da Bahia ao Milionésimo. Salvador: SICM/SGM, map scale 1:1.000.000.

Barbosa, J.S.F. & Sabaté, P. 2004. Archean and Paleoproterozoic crust of the São Francisco Craton, Bahia, Brazil: geodynamic features. Precambrian Research 133, 1-27.

Battilani, G.A.; Varajão, A.F.D.C. & Gomes, N.S. 1999. Metamorphic degree variation in proterozoic sandstones of the Tombador Formation, Bahia State, Brazil. Zbl. Geol. Paläont. Teil I, (7-8), 917-926.

Beblo, M.; Berktold, A.; Bleil, U.; Gebrande, H.; Grauert, B.; Haack, U.; Haak, V.; Kern, H.; Miller, H.; Petersen, N.; Pohl, J.; Rummel, F. & Schopper, J.R. 1982. Physical properties of rocks. In: K.H. Hellwege (Ed.), Numerical Data and Functional Relationships in Science and Technology. Springer-Verlag Berlin, Heidelberg, NewYork.

Berra, F., Felletti, F. 2011. Syndepositional tectonics recorded by soft-sediment deformation and liquefation structures (continental Lower Permian sediments, Southern Alps, Northern Italy): Stratigraphic significance. Sedimentary Geology 235, 249-263.

Best, J., Bridge, J. 1992. The morphology and dynamics of low amplitude bedwaves upon upper stage plane beds and preservation of planar laminae. Sedimentology 39, 737-752.
Bhatia, M.R., 1983. Plate tectonics and geochemical composition of sandstones. The Journal of Geology 91, 611-627.

Bhattacharya, J.P. 1991. Regional to subregional facies architecture of river-dominated deltas in the Alberta subsurface, Upper Cretaceous Dunvegan Formation. In: Miall, A.D. & Tyler, N. (Eds.), The Three-Dimensional Facies Architecture of Terrigenous Clastic Sediments, and Its Implications for Hydrocarbon Discovery and Recovery, Concepts and Models in Sedimentology and Paleontology, SEPM Special Publication 3, 289-206.

Bhattacharya, J.P. 2006. Deltas. In: Posamentier, H.W. & Walker, R.G. (Eds.), Facies Models Revisted, SEPM (Society for Sedimentaty Geology) Special Publication 84, 237-292.

Bhattacharya, J.P. 2010. Deltas. In: James, N.P. & Dalrymple, R.W. (Eds.), Facies Models 4, Geologial Association of Canada IV, Series Geotext 6, 233-264.

Bhattacharya, J.P., Walker, R.G. 1992. Deltas. In: Walker, R.G. & James, N.P. (Eds.), Facies Models: Response to Sea Level Change. Geologial Association of Canada, pp. 157-177.

Blair, T.C. 2000. Sedimentology and progressive tectonic unconformities of the sheetflood-dominated Hells Gate alluvial fan, Death Valley, California. Sedimentary Geology 132, 233-262.

Blair, T.C. & McPherson, J.G. 1994a. Alluvial fan processes and forms. In: (Ed. by Abrahams, A.D. & Parsons A. (Eds.), Geomorphology of deserts environments. pp. 354-402 Chapman & Hall, London.

Blair, T.C. & McPherson, J.G. 1994b. Alluvial fans and their natural distinction from rivers based on morphology, hydraulic processes, sedimentary processes, and facies assemblages. J. Sed. Res. 64, 451-490.

Blissenbach, E. 1954. Geology of alluvial fans in semi-arid regions. Geological Society American Bulletin 65, 139-148.

Blum, M.D. 1992. Climatic and eustatic controls on Gulf Coastal Plain sedimentation: an example from the late Quaternary of the Colorado River. In: Armentrout, J.M. & Perkins, R.F. (Eds.), Sequence stratigraphy as an exploration tool: concepts and practices in the Gulf Coast. SEPM, Gulf Coast Section, Eleventh Annual Research Conference, Houston, pp. 71-84.

Blum, M.D. & Price, D.M. 1998. Quaternary alluvial plain construction in response to glacio-eustatic and climatic controls, Texas Gulf Coast Plain. In: Shanley, K. & McCabe, P. (Eds.), Relative role of eustasy, climate, and tectonism in continental rocks. SEPM, Special Publication 59, 31-48.

Bomfim, L.F. & Pedreira, A.J. 1990. Geologia da Chapada Diamantina Oriental, Bahia (Folha Lençóis). In: Bomfim, L.F. & Pedreira, A.J., (Orgs.), Programa de Levantamentos Geológicos Básicos do Brasil. Lençóis (Folha SD.24-V-A-V) Estado da Bahia, Texto Explicativo, DNPM/CPRM, Brasília, pp. 25-73.

Bose, P.K., Eriksson, P.G., Sarkar, S., Wright, D.T., Samanta, P., Mukhopadhyay, S., Mandal, S., Banerjee, S., & Altermann, W. 2013. Sedimentation patterns during the Precambrian: a unique record? Marine and Petroleum Geology 33, 34-68.

Boyd, R.; Dalrymple, R.W.; & Zaitlin, B.A. 2006. Estuarine and incised-valley facies models. In: Posamentier, H.W.; Walker, R.G. (Eds.), Facies Models Revisited. SEPM Special Publication 84, 171-235.

Boynton, W.V. 1984. Cosmochemistry of the rare earth elements: meteorite studies. In: Henderson, P. (Ed.), Rare Earth Element Geochemistry. Elsevier, Amsterdam, pp. 63-114.

Brewster, M.L. & Annan, A.P. 1994. Ground penetrating radar monitoring of a controlled DNAPL release: 200 MHz radar. Geophysics, 59, 1211-1221.

Bridge, J.S. 2006. Fluvial facies models: recent developments. In: Posamentier, H. & Walker, R.G. (Eds.), Facies Models Revisited, SEPM Special Publication 84, 85-170.

Bristow, C.S. 1993. The interaction between channel geometry, water flow, sediment transport and deposition in braided rivers. In: Best, J.L. & Bristow, C.L. (Eds.), Braided rivers. Geological Society of London Special Publication 75, 13-72.

Bristow, C. S. & Jol, H. M. 2003. An introduction to ground penetrating radar (GPR) in sediments. In: Bristow, C. S. & Jol, H. M. (Eds.), Ground Penetrating Radar in Sediments. Geological Society, London, Special Publications, 211, 1-7.

Brito Neves, B. B. 2003. A saga dos descendentes de Rodínia na construção do Gondwana. Revista Brasileira de Geociências 33(1), 77-88.

Brito Neves, B.B., Kawashita, K., Cordani, V.G., & Delhal, J. 1979. A evolução geocronológica da Cordilheira do Espinhaço: dados novos e integração. Revista Brasileira de Geociências 9, 71-85.

Brito Neves, B.B.; Campos Neto, M.C.; & Fuck, R.A. 1999. From Rodinia to Western Gondwana: an approach to the Brasiliano-Pan African Cycle and orogenic collage. Episodes 22(3), 155-166.

Bruun, P. 1962. Sea-level rise as a cause of shore erosion. American Society of Civil Engineers Proceedings, Journal of the Waterways and Harbors Division 88, 117-130.

Burgess, P.M., Gurnis, M., & Moresi, L. 1997. Formation of sequences in the cratonic interior of North America by interaction between mantle, eustatic, and stratigraphic processes. Geological Society of America Bulletin 108, 1515-1535.

Campos Neto, M.C. 2000. Orogenic systems from Southwestern Gondwana. An approach to Brasiliano-Pan African Cycle and orogenic collage in Southeastern Brazil. In: Cordani, U.G.;

Milani, E.J.; Thomaz Filho, A.; & Campos, D.A. (Eds.), Tectonic evolution of South America. 31st Int. Geol. Congress. Rio de Janeiro, pp. 335-365.

Cant. D.J. &Walker, R.G. 1978. Fluvial processes and facies sequences in sandy braided South Saskatchewan River, Canada. Sedimentology 25, 625-648.

Carter, R.M., Fulthorpe, C.S., & Naish, T.R. 1998. Sequence concepts at seismic and outcrop scale: the distinction between physical and conceptual stratigraphic surfaces. Sedimentary Geology 122, 165-179.

Cas, R.A.F. & Wright, J.V. 1988. Volcanic Successions, modern and ancient: a geological approach to processes, products and successions. Unwin Hyman, London (528 pp.).

Castro, M.R. 2003. Estratigrafia de Sequências na Formação Tombador, Grupo Chapada Diamantina, Bahia. PhD Thesis, Universidade São Paulo. 128p.

Catuneanu, O. 2006. Principle of sequence stratigraphy. Elsevier, 375 pp.

Catuneanu, O. & Eriksson, P.G. 1999. The sequence stratigraphic concept and the Precambrian rock record: an example from the 2.7-2.1 Ga Transvaal Supergroup, Kaapvaal craton. Precambrian Research 97, 215-251.

Catuneanu, O., Galloway, W.E., Kendall, C.G.St.C., Miall, A.D., Posamentier, H.W., Strasser, A. & Tucker, M.E. 2011. Sequence Stratigraphy: Methodology and Nomenclature. Newsletter on Stratigraphy, Special Issue 44(3), 173-245.

Catunenau, O., Martins-Neto, M.A. & Eriksson, P.G. 2005. Precambrian sequence stratigraphy. Sedimentary Geology 176 (1-2), 67-95.

Chakraborty, P.P. & Paul, S. 2008. Force regressive wedges on a Neoproterozoic siliciclastic shelf: Chandarpur Group, Central India. Precambrian Research 162, 227-247.

Chakraborty, P.P., Sarkar, A., Das, K., & Das, P. 2009. Alluvial fan to storm-dominated shelf transition in the Mesoproterozoic Singhora Group, Chattisgarh Supergroup, Central India. Precambrian Research 170, 88-106.

Chemale Jr., F., Alkmim, F.F., & Endo, I. 1993. Late Proterozoic tectonismin the interior of the São Francisco craton. In: Findlay, R.H., Unrug, R., Banks, M.R., & Veevers, J.J. (Eds.), Gondwana Eight: Assembly, Evolution and Dispersal. Balkema, Rotterdam, pp. 29-41.

Chemale Jr., F., Quade, H., & Van Schmus, W.R. 1998. Petrography, geochemistry and geochronology of the Borrachudo and Santa Bárbara metagranites, Quadrilatero Ferrífero, Brazil. Zentralblatt fuer Geologie und Palaontologie Teil I 3-6, 739-750.

Chemale Jr, F., Dussin, I.A., Martins, M.S., Alkmim, F.F. & Queiroga, G. 2010. The Espinhaço Supergroup in Minas Gerais: a Stenian Basin? VII South American Symposium on Isotope Geology. Universidade de Brasília, pp. 552-555.

Chemale Jr., F., Philipp, R.P., Dussin, I.A., Formoso, M.L.L., Kawashita, K., & Bertotti, A.L. 2011. Lu–Hf and U-Pb age determinations of Capivarita Anorthosite in the Dom Feliciano Belt, Brazil. Precambrian Research 186, 117-126.

Chemale Jr., F., Dussin, I.A., Alkmim, F.F., Martins, M.S., Queiroga, G., Armstrong, R., & Santos, M.N. 2012. Unravelling a Proterozoic basin history through detrital zircon geochronology: the case of the Espinhaço Supergroup, Minas Gerais, Brazil. Gondwana Research 22, 200-206.

Coleman, J.M. 1981. Deltas process of deposition and models for exploration. 2nd Ed. Burgress Publishing Company, 194 pp.

Coleman, J.M. &, Wright, L.D. 1975. Modern river deltas: variability of processes and sand bodies. In: Broussard, M.L., (Ed.), Deltas, Models for Exploration. Houston Geological Society, pp. 99-149.

Collinson, J.D. 1996. Alluvial sediments. In: Reading, H.G. (Ed.), Sedimentary environments: processes, facies and stratigraphy, Blackwell Science, London, Third Edition, 37-82.

Collinson, J.D. & Thompson, D.B. 1989. Sedimentay structures (2nd Edition). Unwin, London, 207 pp.

Condie, K.C. 1993. Chemical composition and evolution of the upper continental crust: contrasting results from surface samples and shales. Chemical Geology 104, 1-37.

Corbeanu, R. M., Soegaard, K., Szerbiak, R.B., Thurmond, J.B., McMechan, G.A., Wang, D., Snelgrove, S., Forster, C.B. & Menitove, A. 2001. Detailed internal architecture of a fluvial channel sandstone determined from outcrop cores, and 3-D ground-penetrating radar: Examples form the Middle Cretaceous Ferron Sandstone, east-central Utah. American Association of Petroleum Geologists Bulletin 85, 1583-1608.

Corcoran, P.L., Mueller, W.U., & Chown, E.H. 1998. Climatic and tectonic influences on fan deltas and wave- to tide-controlled shoreface deposits: evidence from the Archaean Keskarrah Formation, Slave Province, Canada. Sedimentary Geology 120, 125-152.

Cordani, U.G., Fraga, L.M., Reis, N., Tassinari, C.C.G., & Brito-Neves, B.B. 2010. On the origin and tectonic significance of the intra-plate events of Grenvillian-type age in South America: a discussion. Journal of South American Earth Sciences 29, 143-159.

Costa, L.A.M.; Inda, H.A.V. 1982. O aulacógeno do Espinhaço. Revista Ciências da Terra 1, 13-18.

Costas, S. & FitzGerald, D. 2011. Sedimentary architecture of a spit-end (Salisbury Beach, Massachusetts): The imprints of sea-level rise and inlet dynamics. Marine Geology, 284, 203-216.

Cotter, E. 1978. The evolution of fluvial style, with special reference to the central Appalachian palaeozoic. In: Miall, A.D. (Ed.), Fluvial Sedimentology. Canadian Society of Petroleum Geologists, Memoir 5, 361-383.

Cowan, C.C. & James, N.P. 1992. Diastasis cracks: mechanically generated synaeresis-lyke cracks in Upper Cambrian shallow water oolite and ribbon carbonates. Sedimentology 39, 1101-1118.

Cruz, S.C.P. 2004. A interação entre o Aulacógeno do Paramirim e o Orógeno Araçuaí-Oeste Congo. Unpublished PhD thesis, Universidade Federal de Ouro Preto, 503 pp.

D'Agrella, M.S., Pacca, I.G., Renne, P.R., Onstott, T.C., & Teixeira, W. 1990. Paleomagnetismof Middle Proterozoic (1.01 to 1.08 Ga) mafic dykes in southeastern Bahia State-São Francisco Craton, Brazil. Earth and Planetary Science Letters 101, 332-348.

Dalrymple, R.W. 1992. Tidal depositional systems. In: Walker, R.G. & James, N.P. (Eds.), Facies Models: response to sea level changes. Geology Association of Canada, pp. 195-218.

Dalrymple, R.W. 1999. Tide-dominated deltas, do they exist or are they all estuaries? American Association of Petroleum Geologists Annual Convention, San Antonio, Texas, Official Program with Abstracts, p. A29.

Dalrymple, R.W. 2010. Tidal depositional systems. In: James, N.P. & Dalrymple, R.W. (Eds.), Facies Models 4. Geologial Association of Canada IV, Series GEOtext 6, 201-231.

Dalrymple, R.W. & Choi, K. 2007. Morphologic and facies trends through the fluvial-marine transition in tide-dominated depositional systems: A schematic framework for environmental and sequence-stratigraphic interpretation. Earth-Science Reviews 81 (3-4), 135-174.

Dalrymple, R.W., Narbonne, G.M., & Smith, L. 1985. Eolian action and the distribution of Cambrian shales in North America. Geology 13, 607-610.

Dalrymple, R.W.; Knight, R.J.; Zaitlin, B.A.; & Middleton, G.V. 1990. Dynamics and facies model of a macrotidal sand-bar complex. Cobequid Bay-Salmon River Estuary. Sedimentology 37, 577-612.

Danderfer, A. 1990. Análise descritiva e cinemática do Supergrupo Espinhaço na região da Chapada Diamantina, BA. Unpublished MsC Thesis, Universidade Federal de Ouro Preto, UFOP. 99 p.

Danderfer, A., & Dardenne, M.A. 2002. Tectonoestratigrafia da bacia Espinhaço na porção centro-norte do cráton do São Francisco: registro de uma evolução polihistórica descontínua. Revista Brasileira de Geociências 32 (4), 449-460.

Danderfer, A., De Waele, B., Pedreira, A.J., & Nalini, H.A. 2009. New geochronological constraints on the geological evolution of Espinhaço basin within the São Francisco Craton, Brazil. Precambrian Research 170, 116-128.

Davies, T.R.H. 1986. Large debris flows: a macro-viscous phenomenon. Acta Mech. 63, 161-178.

Davies, T.R.H. 1990. Debris-flow surges - experimental simulation. Journal of Hydrology 29, 18-46.

De Waele, B., Johnson, S.P., & Pisarevsky, S.A. 2008. Palaeoproterozoic to Neoproterozoic growth and evolution of the eastern Congo Craton: its role in the Rodinia puzzle. Precambrian Research 160, 127-141.

Delgado, I.M., Souza, J.D., Silva, L.C., Filho, N.C.S., Santos, R.A., Pedreira, A.J., Guimarães, J.T., Angelim, L.A.A., Vasconcelos, A.M., Gomes, I.P., Filho, J.V.L., Valente, C.R., Perrota, M.M., & Heineck, C.A. 2003. In: Bizzi, L.A., Schobbenhaus, C., Vidotti, R.M., & Gonçalves, J.H., (Eds.), Geotectônica do Escudo Atlântico. Geologia, Tectônica e Recursos Minerais do Brasil, CPRM, Brasília. 334 pp.

Denny, C.S. 1967, Fans and pediments. American Journal of Science 265, 81-105.

Derby, O.A. 1906. The Serra do Espinhaço, Brazil. Journal of Geology 14, 374-401.

Dominguez, J.M.L. 1992. Estratigrafia de sequências aplicada a terrenos pré-Cambrianos: exemplos para o Estado da Bahia. Revista Brasileira de Geociências 22, 422-436.

Dominguez, J.M.L. 1993. As coberturas do Craton do São Francisco: Uma abordagem do ponto de vista da análise de bacias. In: Dominguez, J.M.L. & Misi A. (Eds.), O Cráton do São Francisco, SBG/SGM/CNPQ, Salvador, pp. 137-159.

Dominguez, J. M. L., & Wanless, H. R. 1991. Facies architecture of a falling sea-level strandplain, Doce River coast, Brazil. In: Swift, D. J. P.; Oertel, G. F.; Tillman, R. W.; & Thorne, J. A. (Eds.), Shelf sand and sandstone bodies: geometry, facies and sequence stratigraphy. International Association of Sedimentologists Special Publication 14, 259-281.

Dussin, I.A. 1994. Evolution structurale de la region de l'Espinhaço meridional, bordure sud-est du craton São Francisco, Brésil. Tectoniques superposees au Protérozoïque. (Ph.D. thesis) Université D'orléans.

Dussin, I.A. & Chemale Jr., F. 2011. Geologia Estrutural e Estratigrafia do Sistema Espinhaço-Chapada Diamantina e sua aplicação nas Bacias Mesocenozóicas da Margem Passiva Brasileira. Relatório Final FUNDEP, Belo Horizonte (302 pp.).

Dussin, I.A. & Dussin, T.M. 1995. Supergrupo Espinhaço: Modelo de Evolução Geodinâmica. Geonomos 1, 19-26.

Eilertsen, R. S., Corner, G. D., Aasehim, O. & Hansen, L. 2011. Facies characteristics and architecture related to palaeodepth of Holocene fjord-delta sediments. Sedimentology 58, 1784-1809.

Ékes, C. & Friele, P. 2003. Sedimentary architecture and post-glacial evolution of Cheekye fan, soutwertern British Columbia, Canada. In: Bristow, C. S. & Jol, H. M. (Eds.), Ground Penetrating Radar in Sediments. Geological Society, London, Special Publication 211, 87-98.

Els, B.G. 1990. Determination of some palaeohydraulic parameters for a fluvial Witwatersrand succession. South African Journal of Geology 93, 531-537.

Eriksson, E.G., Condie, K.C., Tirsgaard, H., Mueller, W.U., Altermann, W., Miall, A.D., Aspler, L.B., Catuneanu, O. & Chiarenzelli, J.R. 1998. Precambrian clastic sedimentation systems. Sedimentary Geology 120, 5-53.

Eriksson, K.A. 1973. The Timeball Hill Formation - a fossil delta. Journal of Sedimentary Petrology 43(4), 1046-1053.

Eriksson, K.A. & Simpson, E.L. 2004. Precambrian Tidalites: recognition and significance. In: Eriksson, P.G.; Altermann, W., Nelson, D.R., Mueller, W.U., & Catuneanu O., (Eds.), The Precambrian Earth: Tempos and Events. Elsevier, Amsterdam., pp. 631-642. Elsevier, Amsterdam.

Eriksson, K.A., Simpson, E.L. & Mueller, W. 2006. An unusual fluvial to tidal transition in the mesoarchean Moodis Group, South Africa: A response to high tidal range and active tectonics. Sedimentary Geology 190, 13-24.

Eriksson, P.G. & Catuneanu, O. 2004. Third-order sequence stratigraphy in the Palaeoproterozoic Daspoort Formation (Pretoria Group, Transvaal Supergroup), Kaapvaal craton. In: Eriksson, P.G.; Altermann, W., Nelson, D.R., Mueller, W.U., & Catuneanu O., (Eds.), The Precambrian Earth: Tempos and Events. Elsevier, Amsterdam. pp. 724- 35.

Eriksson, P.G., Reczko, B.F.F., Boshoff, A.J., Schreiber, U.T., Neut, M.V., & Snyman, C.P. 1995. Architectural elements from Lower Proterozoic braid-delta and high-energy tidal flat deposits in the Magaliesberg Formation, Transvaal Supergroup, South Africa. Sedimentary Geology 97, 99-117.

Eriksson, P.G., Condie, K.C., Trisgaard, H., Muller, W., Altermann, W.; Catuneanu, O., & Chiarenzali, J. 1998. Precambrian clastic sedimentation systems. Sedimentary Geology 120, 5-53.

Eriksson, P.G., Bumby, A.J., & Popa, M. 2004. Sedimentation through time. In: Eriksson, P.G.; Altermann, W., Nelson, D.R., Mueller, W.U., & Catuneanu O., (Eds.), The Precambrian Earth: Tempos and Events. Elsevier, Amsterdam. pp. 593-680.

Eriksson, P. G., Catunenau, O., Sarkaf, S. & Tirsgaard, H. 2005a. Patterns of sedimentation in the Precambrian. Sedimentary Geology 176, 17-42.

Eriksson, P.G., Catuneanu, O., Nelson, D.R. & Popa, M. 2005b. Controls on Precambrian sea level change and sedimentary cyclicity. Sedimentary Geology 176, 43-65.

Eriksson, P.G., Catuneanu, O., Els, B.G., Bumpy, A.J., Van Rooy, J.L. & Popa, M. 2005c. Kaapval craton: changing first- and second-order controls on sea level from c. 3.0 Ga to 2.0 Ga. Sedimentary Geology 176, 121-148.

Ernst, R.E., Bleeker, W., Söderlund, U., & Kerr, A.C. 2013a. Large igneous provinces and supercontinents: toward completing the plate tectonic revolution. Lithos 174, 1-14.

Ernst, R.E., Pereira, E., Hamilton, M.A., Pisarevsky, S.A., Rodrigues, J., Tassinari, C.C.G., Teixeira, W., & Van-Dunem, V. 2013b. Mesoproterozoic intraplate magmatic ‘barcode’ record of the Angola portion of the Congo Craton: newly dated magmatic events at 1505 and 1110 Ma and implications for Nuna (Columbia) supercontinent reconstructions. Precambrian Research 230, 103-118.

Evans, D.A.D. 2009. The palaeomagnetically viable, long-lived and all-inclusive Rodinia supercontinent reconstruction. In: Murphy, J.B. & Hynes, A.J. (Eds.), Ancient Orogens and Modern Analogues. Geological Society Special Publication 327, pp. 371-404.

Evans, D.A.D., Heaman, L.M., Trindade, R.I.F., D'Agrella-Filho, M.S., Smirnov, A.V., & Catelani, E.L. 2010. Precise U-Pb Baddeleyite ages from Neoproterozoic mafic dykes in Bahia, Brazil, and their paleomagnetic/paleogeographic implications. Meeting of the Americas, Abstract GP31E-07. Eos Transactions AGU, 91(26).

Fanti, F. & Catuneanu, O. 2010. Fluvial sequence stratigraphy: the Waipiti Formation, West-Central Alberta, Canada. Journal of Sedimentary Research 80, 320-338.

Fernandez-Alonso, M., Cutten, H., De Waele, B., Tack, L., Tahon, A., Baudet, D., & Barrit, S.D. 2012. The Mesoproterozoic Karagwe-Ankole Belt (formerly the NE Kibara Belt): the result of prolonged extensional intracratonic basin development punctuated by two short-lived far-field compressional events. Precambrian Research 216-219, 63-86.

Folk, R.L. 1974. Petrology of sedimentary rocks. Hemphills, Austin, Texas.

Fuller, A.O. 1985. A contribution to the conceptual modelling of pre-Devonian fluvial systems. Transactions of the Geological Society of South Africa 88, 189-194.

Galloway, W.E. 1989. Genetic straigraphic sequences in basin analysis, I. Architecture and genesis of flooding-surface bounded depositional units. American Association of Petroleum Geologists Bulletin 73, 125-142.

Gilbert, J.M., Robles, J.M. 2005. Firmground ichnofacies recording high-frequency marine flooding events (Langhian transgression, Vallès-Penedès Basin, Spain). Geologica Acta 3 (3), 295-305.

Gorczyk,W., Hobbs, B., Gessner, K., Gerya, T. 2013. Intracratonic geodynamics. Gondwana Reseach 24, 838-848.

Gruber, L., Pimentel, M.M., Brito Neves, B.B., Armstrong, R. & Fuck. R.A. 2011. Proveniência U-Pb em zircão (SHRIMP) da Formação Tombador, Grupo Chapada Diamantina, BA. Anais do XIII Congr. Bras. Geoquímica, pp. 1155-1158.

Guadagnin, F., Chemale Jr., F., Magalhães, A.J.C., Santana, A., Dussin, I. & Takehara, L. 2015. Age constraints on crystal-tuff from the Espinhaço Supergroup - Insights into the Paleoproterozoic to Mesoproterozoic intracratonic basin cycles of the Congo- São Francisco Craton. Gondwana Research 27, 363-376.

Guimarães, J.T. & Pedreira, A.J. 1990. Geologia da Chapada Diamantina Oriental, Bahia. Folha Utinga. In: Guimarães J.T. & Pedreira, A.J., (Orgs.), Programa de Levantamentos Geológicos Básicos do Brasil. Utinga (Folha SD 24-V-A-II) Estado da Bahia, Texto Explicativo, DNPM/CPRM, Brasília, pp. l19-92.

Guimarães, J.T., Martins, A.A.M., Andrade Filho, E.L., Loureiro, H.S.C., Arcanjo, J.B.A., Neves, J.P., Abram, M.B., Silva, M.G., Melo, R.C., & Bento, R.V. 2005. Projeto Ibitiara-Rio de Contas Geological map. Brazilian Geological Survey and Bahia Mineral Research Company, scale 1:200.000.

Guimarães, J.T., Santos, R.A., Melo. R.C. 2008. Geologia da Chapada Diamantina Ocidental (Projeto Ibitiara-Rio de Contas). Salvador, Companhia Baiana de Pesquisa Mineral-CBPM / Companhia Pesquisa de Recursos Minerais-CPRM. Série Arquivos Abertos 31, 64p.

Haddad, D., Watts, A.B., Lindsay, J. 2001. Evolution of the intracratonic Officer Basin, central Australia: implications from subsidence analysis and gravity modeling. Basin Research 13, 217-238.

Hadlari, T., Rainbird, R.H. & Donaldson, J.A. 2006. Alluvial, eolian and lacustrine sedimentology of a Paleoproterozoic half-graben, Baker Lake Basin, Nunavut, Canada. Sed. Geol. 190, 47-70.

Hampton, B.A. & Horton, B.K. 2007. Sheetflow fluvial processes in a rapidly subsiding basin, Altiplano plateau, Bolivia. Sedimentology 54, 1121-1147.

Herron, M.M. 1988. Geochemical classification of terrigenous sands and shales from core or log data. Journal of Sedimentary Petrology 58, 820-829.

Heubeck, C. & Lowe, D.R. 1994. Depositional and tectonic setting of the Archean Moodies Group, Barbeton Greenstone Belt, South Africa. Precambrian Research 68, 257-290.

Hunter, R.E. 1977. Terminology of cross-stratified sedimentary layers and climbing-ripple structures. Journal of Sedimentary Petrology 47, 697-706.

Inda, H.A.V. & Barbosa, J.F. 1978. Texto explicativo para o mapa geológico do Estado da Bahia escala 1:1.000.000. SME/COM. Salvador, 137p.

Ingersoll, R.V. 2012. Tectonics of sedimentary basins, with revised nomenclature. In: Busby, C. & Azor, A. (Eds.), Tectonics of Sedimentary Basins: Recent Advances. Wiley-Blackwell, Oxford, pp. 3-43.

Jackson, S.E., Pearsona, N.J., Griffina, W.L., & Belousova, E.A. 2004. The application of laser ablation-inductively coupled plasma-mass spectrometry to in situ U-Pb zircon geochronology. Chemical Geology 211, 47-69.

Jardim de Sá, E.F. 1981. A Chapada Diamantina e a Faixa Santo Onofre: um exemplo de tectônica intra-placa no Proterozóico Médio do Craton do São Francisco. In: Inda, H.A.V.; Marinho, M.M.; & Duarte, F.B. (Eds.), Geologia e Recursos Minerais do Estado da Bahia. Secretaria de Minas e Energia do Estado da Bahia, Textos Básicos 4, 111-120.

Jardim de Sá, E.F., Bartels, R.L., Brito Neves, B.B., & McReath, I. 1976. Geocronologia e o modelo tectono-magmático da Chapada Diamantina e Espinhaço Setentrional, Bahia. In: XXIX Congresso Brasileiro de Geologia, Ouro Preto, Sociedade Brasileira de Geologia, Anais 4, 205-257.

Jarvis, A., Reuter, H.I., Nelson, A., & Guevara, E. 2008. Hole-filled Seamless SRTM Data V4. International Centre for Tropical Agriculture (CIAT) (available from http://srtm.csi.cgiar.org).

Jol, H.M. & Bristow, C.S. 2003. GPR in sediments: advice on data collection, basic processing and interpretation, a good practice guide. In: Bristow, C. S. & Jol, H. M. (Eds.), Ground Penetrating Radar in Sediments. Geological Society, London, Special Publication 211, 9-27.

Jol, H. M., Smith, D. G. & Meyers, R. A. 1996. Digital ground penetrating radar (GPR): An improved and very effective geophysical tool for studying modem coastal barriers (examples for the Atlantic, Gulf and Pacific coasts, U.S.A.). Journal of Coastal Research 12, 960-968.

Jorry, S. J. & Biévre G. 2011. Integration of sedimentology and ground-penetrating radar for high-resolution imaging of a carbonate platform. Sedimentology 58, 1370-1390.

Kingston, D.R., Dishroon, C.P., & Williams, P.A. 1983. Global basin classification. Bulletin of the American Association of Petroleum Geologists 67, 2175-2193.

Kocurek, G. & Havhlom, K. G. 1993. Eolian sequence stratigraphy - a conceptual framework. In: Siliciclastic Sequence Stratigraphy Recent Developments and Applications (Ed. by P.W. Weimer and H.W. Posamentier), AAPG Memoir 58, 393-409.

Kocurek, G. & Lancaster, N. 1999. Aeolian system sediment state: theory and Mojave Desert Kelso dune field example. Sedimentology, 46, 505-515

Kokureck, G. & Nielson, J. 1986. Conditions favourable for the formation of warm-climate eolian and sandsheets. Sedimentology 33, 795-816

Kocurek, G.; Townsley, E.Y.; Havholm, K.; & Sweet, M.L. 1992. Dune and dune-field development on Padre Island, Texas, with implications for interdune deposition and water-table-control on accumulation. Journal of Sedimentary Petrology 62, 622-636.

Kokonyangi, J.W., Kampunzu, A.B., Armstrong, R., Yoshida, M., Okudaira, T., Arima, M., & Ngulube, D.A. 2006. The Mesoproterozoic Kibaride belt (Katanga, SE D.R. Congo). Journal of African Earth Sciences 46, 1-35.

Kröner, A. & Cordani, U. 2003. African, southern India and South American cratons were not part of the Rodinia supercontinent: evidence from field relationships and geochronology. Tectonophysics 375, 325-352.

Lacassie, J.P., Roser, B., Del Solar, J.R., & Hervé, F. 2004. Discovering geochemical patterns using self-organizing neural networks: a new perspective for sedimentary provenance analysis. Sedimentary Geology 165, 175-191.

Langford, R. & Bracken, B. 1987. Medano Creek, Colorado, a model for upper-flow-regime fluvial deposition: Journal of Sedimentary Petrology 57, 863-870.

Le Bas, M.J., Le Maitre, R.W., Streckeisen, A., & Zanettin, B. 1986. A chemical classification of volcanic rocks on the total alkali-silica diagram. Journal of Petrology 27, 745-750.

Leite, C.M.M. 2002. A evolução geodinâmica da orogênese Paleoproterozoica nas regiões de Capim Grosso - Jacobina e Pintadas - Mundo Novo (Bahia, Brasil): metamorfismo, anatexia crustal e tectônica. Unpublished PhD thesis, Universidade Federal da Bahia, UFBA, 414 pp.

Li, Z.X., Bogdanova, S.V., Collins, A.S., Davidson, A., De Waele, B., Ernst, R.E., Fitzsimons, I.C.W., Fuck, R.A., Gladkochub, D.P., Jacobs, J., Karlstrom, K.E., Lu, S., Natapov, L.M., Pease, V., Pisarevsky, S.A., Thrane, K., & Vernikovsky, V. 2008. Assembly, configuration, and break-up history of Rodinia: a synthesis. Precambrian Research 160, 179-210.

Lindsay, J.F. 2002. Supersequences, superbasins, supercontinents - evidence from the Neoproterozoic-Early Palaeozoic basins of central Australia. Basin Research 14, 207-223.

Lindsay, J.F. & Leven, J.H. 1996. Evolution of a Neoproterozoic to Palaeozoic intracratonic setting, Officer Basin, South Australia. Basin Research 8, 403-424.

Long, D.G.F. 1978. Proterozoic stream deposits: some problems of recognition and interpretation of ancient sandy fluvial systems. In: Miall, A.D. (Ed.), Fluvial Sedimentology. Canadian Society of Petroleum Geologists Memoir V, pp. 313-342.

Long, D.G.F. 2004. Precambrian rivers. In: Eriksson, P.G.; Altermann, W.; Nelson, D.R.; Mueller, W.U.; & Catuneanu, O. (Eds.), The Precambrian Earth: Tempos and Events. Elsevier, Amsterdam, pp. 660-663.

Loureiro, H.S.C., Lima, E.S., Macedo, E.R., Silveira, F.V., Bahiense, I.C., Arcanjo, J.B.A., Moraes Filho, J.C., Neves, J.P., Guimarães, J.T., Teixeira, L.R., Abram, M.B., Santos, R.A., & Melo, R.C. 2008. Projeto Barra-Oliveira dos Brejinhos Geological map. Brazilian Geological Survey and Bahia Mineral Research Company, scale 1:200.000.

Loureiro, H.S.C.; Bahiense, I.C.; Neves, J.P., Guimarães, J.T.; Teixeira, L.R.; Santos, R.A.; & Melo, R.C. 2009. Geologia e recursos minerais da parte norte do corredor de deformação do Paramirim (Projeto Barra-Oliveira dos Brejinhos): Estado da Bahia. Salvador: CPRM (Serviço Geológico do Brasil), Programa Recursos Minerais do Brasil. Convênio CBPM-CPRM. Série Arquivos Abertos 33, 122p.

Lowe, D.R. 1988. Suspended-load fallout rate as an independent variable in the analysis of current structures. Sedimentology 35, 765-776.

Ludwig, K.R. 2003. Using Isoplot/Ex, version 3.00, A Geochronological Toolkit for Microsoft Excel. Berkeley Geochronology Center Special Publication No. 1.

MacEachern, J.A. & Bann, K.L. 2008. The role of ichnology in refining shallow marine facies models. In: Hampson, G.J., Steel, R.J., Burgess, P.M., & Dalrymple, R.M., (Eds.), Recent Advance in Models of Siliciclastic Shallow-Marine Environment, SEPM Special Publication 90, 73-116.

Machado, N., Schrank, A., Abreu, F.R., Knauer, L.G., & Almeida-Abreu, P.A. 1989. Resultados preliminares da geocronologia U/Pb na Serra do Espinhaço Meridional. Simpósio de Geologia do Núcleo Minas Gerais. Sociedade Brasileira de Geologia, 10, pp. 171-174.

Magalhães, A.J.C.; Scherer, C.M.S., Raja Gabaglia, G.P. Bállico, M.B. & Catuneanu, O. 2014. Unincised fluvial and tide-dominated estuarine systems from the Mesoproterozoic Lower Tombador Formation, Chapada Diamantina basin, Brazil. Journal of South American Earth Sciences 56, 68-90.

Magalhães, A.J.C.; Scherer, C.M.S.; Raja Gabaglia, G.P. & Catuneanu, O. 2015a. Mesoproterozoic delta systems of the Açuruá Formation, Chapada Diamantina, Brazil. Precambrian Research 257, 1-21.

Magalhães, A.J.C, Raja Gabaglia, G.P., Scherer, C.M.S., Bállico, M.B., Guadagnin, F., Bento Freire, E., Silva Born, L.R.. & Catuneanu, O. 2015b. Sequence hierarchy in a Mesoproterozoic interior sag basin: from basin fill to reservoir scale, the Tombador Formation, Chapada Diamantina Basin, Brazil. Basin Research, 1-40, doi:10.1111/bre.12117.

Major, J.J. 1997. Depositional processes in large-scale debris-flow experiments. Journal of Geology105, 345-366.

Marconato, A.; Almeida, R.P.; Turra, B.B.; & Fragoso-Cesar, A.R.S. 2014. Pre-vegetation fluvial floodplains and channel-belts in the Late Neoproterozoic-Cambrian Santa Bárbara group (Southern Brazil). Sedimentary Geology 300, 49-61.

Marshak, S. & Alkmim, F.F. 1989. Proterozoic contraction/extension tectonics of the southern São Francisco region, Minas Gerais, Brazil. Tectonics 8, 555-571.

Martins-Neto, M.A. 2000. Tectonics and sedimentation in a paleo/Mesoproterozoic rift-sag basin (Espinhaço basin, southeastern Brazil). Precambrian Reseach 103, 147-173.

Martins-Neto, M.A. 2009. Sequence stratigraphic framework of Proterozoic successions in eastern Brazil. Marine and Petroleum Geology 26, 163-176.

Martins-Neto, M.A., Pedrosa Soares, A.C. & Lima, S.A.A. 2001. Tectono-sedimentary evolution of sedimentar basins from Late Paleoproterozoic to Late Neoproterozoic in the São Francisco craton and Araçuaí fold belt, eastern Brazil. Sedimentary Geology 141/142, 343-370.

Maynard, J.R.; Feldman, H.R.; & Alway, R. 2010. From bars to valleys: the sedimentology and seismic geomorphology of fluvial to estuarine incised-valley fills of the Grand Rapids Formation (Lower Cretaceous), Iron River Field, Alberta, Canada. Journal of Sedimentary Research 80, 611-638.

McCormick, D.S. & Grotzinger, J.P. 1993. Distinction of marine from alluvial facies in the Paleoproterozoic (1.9 Ga) Burnside Formation, Kilihigok Basin, N.W.T., Canada. Journal of Sedimentary Petrology 63, 398-419.

McKie, T., Jolley, S. J. & Kristensen, M.B. 2010. Stratigraphic and structural compartmentalization of dryland fluvial reservoirs: Triassic Heron Cluster, Central North Sea. In: Jolley S.J., Fisher Q.J., Ainsworth R.B., Vrolijk P. & Delisle S. (Eds.), Reservoir Compartmentalization. Special Publication Geological Society 347, 165-198.

McLennan, S.M., Hemming, S.,McDaniel, D.K., & Hanson, G.N. 1993. Geochemical approaches to sedimentation, provenance, and tectonics. In: Johnsson, M.J. & Basu, A. (Eds.), Processes Controlling the Composition of Clastic Sediments. Geological Society of America Special Paper, 284, pp. 21-40.

Meert, J.G. 2012. What's in a name? The Columbia (Paleopangaea/Nuna) supercontinent. Gondwana Research 21, 987-993.

Meert, J.G. & Torsvik, T.H. 2003. The making and unmaking of a supercontinent: Rodinia revisited. Tectonophysics 375, 261-288.

Miall, A.D. 1978. Lithofacies types and vertical profile models in braided rivers deposits: a summary. In: Miall A.D (Ed.), Fluvial Sedimentology. Canadian Society of Petroleum Geologists 5, 597-604.

Miall, A.D. 1985. Architectural-Elements Analysis: A New Method of Facies Analysis Applied to Fluvial Deposits. Earth-Science Reviews 22, 261-308.

Miall, A.D. 1988. Architectural-element and bounding surface in fluvial deposits: anatomy of the Kayenta Formation (Lower Jurassic), southwest Colorado. Sedimentary Geology 55, 233-262.

Miall, A.D. 1996. The Geology of Fluvial Deposits: Sedimentary Facies, Basin Analysis, and Petroleum Geology. Springer-Verlag, Berlin, 582 pp.

Milani, E.J. & Ramos, V.A. 1998. Orogenias Paleozóicas no domínio sul-ocidental do Gondwana e os ciclos de subsidência da Bacia do Paraná. Revista Brasileira de Geociências 28, 473-484.

Montes, M.L. 1977. Os Conglomerados Diamantíferos da Chapada Diamantina - Bahia, Brasil. Brasília, Unpublished MsC dissertation, Universidade Federal de Brasilia, 102 pp.

Moucha, R., Forte, A.M., Mitrovica, J.X., Rowley, D.B., Quéré, S., Simmons, N.A., & Grand, S.P. 2008. Dynamic topography and long-therm sea-level variations: there is no such thing as a stable continental platform. Earth and Planetary Science Letters 271, 101-108.

Mountney, N.P. 2012. A stratigraphic model to account for complexity in Aeolian dune and interdune successions. Sedimentology, 59, 964-989.

Nemec, W. & Postma, G. 1993. Quaternary alluvial fans in southwestern Crete: sedimentation processes and geomorphic evolution. In: Marzo, M. & Puigdefabregas, C. (Eds.), Alluvial Sedimentation. Internal Association of Sedimentologists Special Publication 17, 235-276.

Nemec, W. & Steel, R.J. 1984. Alluvial and coastal conglomerates: their significant features and some comments on gravelly mass flow deposits In: Koster E.H. & Steel R.J. (Eds.), Sedimentology of gravels and conglomerates, Canadian Society of Petroleum Geologists 10, 1-31.

Nocita, B.W. & Lowe, D.R. 1990. Fan-delta sequence in the Archean Fig Tree Group, Barbeton Greenstone Belt, South Africa. Precambrian Research 48, 375-393.

Nummendal, D. & Swift, D. J. P. 1987. Transgressive stratigraphy at sequence-bounding unconformities: some principles derived from Holocene and Cretaceous examples. In: Nummendal, D.,; Pilkey, O. H.; Howard, J. D. (Eds.), Sea-level fluctuation and coastal evolution, Society of Economics Paleontologists and Mineralogists Special Publication 41, 241-260.

Orton, G.J. & Reading, H.G. 1993. Variability of deltaic processes in terms of sediment supply, with particular emphasis on grain size. Sedimentology 40, 475-512.

Pedreira, A.J. 1994. O supergrupo Espinhaço na Chapada Diamantina Centro-Oriental, Bahia: sedimentologia, estratigrafia e tectônica. Unpublished PhD thesis, Universidade de São Paulo, 125 pp.

Pedreira, A. J. 1997. Sistemas deposicionais da Chapada Diamantina Centro-oriental, Bahia. Revista Brasileira de Geociências 27, 229-240.

Pedreira, A.J. & De Waele, B. 2008. Contemporaneous evolution of the Palaeoproterozoic-Mesoproterozoic sedimentary basins of the São Francisco-Congo Craton. In: Pankhurst, R.J., Trouw, R.A.J., Brito Neves, B.B., De Wit, & M.J., (Eds.), West Gondwana: Pre-Cenozoic Correlations Across the South Atlantic Region, London, Geological Society Special Publication 294, 33-48.

Pedreira, A.J. & Margalho, R.S.F.X. 1990. Geologia da Chapada Diamantina Oriental, Bahia (Folha Mucugê). In: Pedreira, A.J., Margalho, R.S.F.X., (Orgs.), Programa de Levantamentos Geológicos Básicos do Brasil. Mucugê (Folha SD.24-V-C-II), Estado da Bahia, Texto Explicativo, DNPM/CPRM, Brasília, pp.19-68.

Pedreira, A.J., Dossin, I.A., Uhlein, A., Dossin, T.M., & Garcia, A.J.V. 1989. Kibaran (Mid-Proterozoic) evolution and mineralizations in Eastern Brazil. IGCP 255 Newsletter 2, 57-63.

Pflug, R. 1965. A Geologia da parte meridional da Serra do Espinhaço e zonas adjacentes. National Mineral Production Department Bulletin 266, 1-51.

Pinto, L.G.R., Pádua, M.B., Ussami, N., Vitorello, I., Padilha, A.L., & Braitenberg, C. 2010. Magnetotelluric deep soundings, gravity and geoid in the south São Francisco craton: geophysical indicators of cratonic lithosphere rejuvenation and crustal underplating. Earth and Planetary Science Letters 297, 423-434.

Piper, J.D.A. 2007. The Neoproterozoic supercontinent Palaeopangaea. Gondwana Research 12, 202-227.

Pisarevsky, S.A.; Wingate, M.T.D.; Powell, C.M.; Johnson, S.; & Evans, D.A.D. 2003. Models of Rodinia assembly and fragmentation. Geological Society Special Publication 206, 35-55.

Pisarevsky, S.A., Elming, S., Pesonen, L.J., & Li, Z. 2013. Mesoproterozoic paleogeography: Supercontinent and beyond. Precambrian Research. http://dx.doi.org/10.1016/j.precamres.2013.05.014.

Plink-Björklund, P. 2005. Stacked fluvial and tide-dominated estuarine deposits in high-frequency (fourth-order) sequences of the Eocene Central Basin, Spitsbergen. Sedimentology 52, 391-428.

Plink-Björklund, P. 2011. Effects of tides on deltaic deposition: Causes and responses, Sedimentary Geology 279, 107-133.

Posamentier, H.W. 2001. Lowstand alluvial bypass systems: incised vs. unincised. American Association of Petroleum Geologists Bulletin 85, 1771-1793.

Posamentier, H.W. & Allen, G.P. 1999. Siliciclastic sequence stratigraphy: concepts and applications. SEPM (Society for Sedimentaty Geology) Special Publication, Concepts in Sedimentology and Paleontology 7, 210 pp.

Pringle, J.K., Westerman, A.R., Clark, J.D., Guest, J.A., Ferguson, R.J. & Gardiner, A.R. 2003. The use of vertical radar profiling (VRP) in GPR surveys of ancient sedimentary strata. In: Bristow, C. S. & Jol, H. M. (Eds.), Ground Penetrating Radar in Sediments. Geological Society, London, Special Publication 211, 225-246.

Pulham, A.J. 1989. Controls on internal structure and architecture of sandstone bodies within Upper Carboniferous fluvial-dominated deltas, County Clare, western Ireland. In: Whately M.K.G. & Pickering, K.T., (Eds.), Deltas: Sites and Traps for Fossil Fuels, Geological Society Special Publication 41, 179-203.

Pyrcz, M. J., Catuneanu, O. & Deutsch, C. V. 2005. Stochastic surface-based modeling of turbidite lobes. AAPG Bulletim 89 (2), 177-192.

Rainbird, R.H. 1992. Anatomy of a large-scale braid-plain quartzarenite from the Neoproterozoic Shaler group, Victoria Island, Northwest Territories, Canada. Canadian Journal of Earth Sciences 29, 2537-2550.

Raja Gabaglia, G.P., Rodrigues, E.B., Magalhaes, A.J.C., Arregui, C.D. & Savini, R. 2006. Criteria do recognise sequence orders and tectonic imprint in cyclic siliciclastic record: a key to high-resolution stratigraphy. IAS International Meeting, Fukuoka, Japan.

Ramaekers, P. & Catuneanu, O. 2004. Development and sequences of the Athabasca Basin, early Proterozoic, Saskatchewan and Alberta, Canada. In: P.G. Eriksson W. Altermann, D.R. Nelson, W.U. Mueller & O. Catuneanu O. (Eds), The Precambrian Earth: tempos and events, p. 705- 23.

Rebouças, V.O. 2011. Estratigrafia de sequências da Formação Açuruá nas proximidades de Guiné, Chapada Diamantina - Bahia. Unpublished monography, Universidade Federal da Bahia, Salvador. 84pp.

Reineck, H.E. & Singh, I.B. 1973. Depositional Sedimentary Environment with reference to Terrigenous Clastics. Springer-Verlag, 439 pp.

Ribeiro, A., Teixeira, W., Dussin, I.A., Avila, C.A., & Nascimento, D. 2013. U-Pb LA-ICP-MS detrital zircon ages of the São João del Rei and Carandaí basins: new evidence of intermittent Proterozoic rifting in the São Francisco paleocontinent. Gondwana Research 24, 713-726.

Rogers, J.J.W. & Santosh, M. 2002.Mesoproterozoic supercontinent: introduction. Gondwana Research 5, 3-4.

Roser, B.P. & Korsch, R.J. 1988. Provenance signatures of sandstone-mudstone suites determined using discriminant function analysis of major-element data. Chemical Geology 67, 119-139.

Rosset, A., De Min, A., Marques, L.S., Macambira, M.J.B., Ernesto, M., Renne, P.R., & Piccirillo, E.M. 2007. Genesis and geodynamic significance of Mesoproterozoic and Early Cretaceous tholeiitic dyke swarms from the São Francisco craton (Brazil). Journal of South American Earth Sciences 24, 69-92.

Santana, A. 2007. Ciclicidade no registro sedimentar do intervalo superior do Grupo Paraguaçu, Mesoproterozoico, Chapada Diamantina. Unpublished monography, Universidade Federal da Bahia, Salvador. 76pp.

Santana, R.O. 2009. Estratigrafia de Sequências de Alta Resolução da Base da Formação Tombador, nos Arredores de Lençóis, Chapada Diamantina-Ba. Unpublished monography, Universidade Federal da Bahia, 124 p.

Santos, C.M. 2009. Análise Estratigráfica das Formações Guiné - Tombador, Chapada Diamantina, Bahia. Unpublished monography, Universidade Federal da Bahia, 136 pp.

Santos, P.R.S. 2011. Sistema deposicional da Formação Açuruá nos arredores de Guiné, Chapada Diamantina-Ba. Unpublished monography, Universidade Federal da Bahia, 90 pp.

Santos, M.N., Chemale Jr., F., Dussin, I.A., Martins, M., Assis, T.A.R., Jelinek, A.R., Guadagnin, F., & Armstrong, R. 2013. Sedimentological and paleoenvironmental constraints of the Statherian and Stenian Espinhaço rift system, Brazil. Sedimentary Geology 290, 47-59.

Savini, R.R. & Raja Gabaglia, G.P. 1997. Curso de Campo da Chapada Diamantina - Guias de Campo. Lençóis (BA). PETROBRAS. 15p.

Scherer, C.M.S. 2002. Preservation of aeolian genetic units by lava flow in the Lower Cretaceous of the Paraná Basin, southern Brazil. Sedimentology 49, 97-116.

Scherer, C.M.S., Lavina, E.L.C., Filho, D.C.D., Oliveira, F.M., Bongiolo, D.E. & Aguiar E.S. 2007. Stratigraphy and facies architecture of the fluvial-aeolian-lcustrine Sergi Formation (Upper Jurassic), Recôncavo Basin, Brazil. Sedimentary Geology 194, 169-193.

Schobbenhaus, C. 1996. As tafrogêneses superpostas Espinhaço e Santo Onofre, estado da Bahia: Revisão e novas propostas. Revista Brasileira de Geociências, 4, 265-276.

Schobbenhaus, C. & Kaul, P.F.T. 1971. Contribuição a estratigrafia da Chapada Diamantina, Bahia Central. Mineração e Metalurgia, 53(315), 116-120.

Schobbenhaus, C., Hoppe, A., Baummann, A., & Lork, A. 1994. Idade U/Pb do vulcanismo Rio dos Remédios Chapada Diamantina, Bahia. In: Scheibe, L.F. (Org.), Sociedade Brasileira de Geologia, 38° Congresso Brasileiro de Geologia, 397-398.

Schoengut, J.A. 2011. Sedimentological and ichnological characteristics of modern and ancient channel-fills, Willapa Bay, Washington. MsC thesis, University of Alberta, 216 pp.

Schumm, S.A. 1968, Speculations concerning paleohydrologic controls of terrestrial sedimentation. Geological Society of America Bulletin 79, 1573-1588.

Schumm, S.A. 1977. The Fluvial System. John Wiley, London, 377 pp.

Schum, S.A. 1993. River response to base level change: implication for sequence stratigraphy. Journal of Geology 101, 279-294.

Schumm, S.A. & Ethridge, F.G. 1994. Origin, evolution, and morphology of fluvial systems. In: Dalrymple, R.W.; Boyd, R.; & Zaitlin, B.A. (Eds.), Incised-valleys systems: origin and sedimentary sequences. SEPM, Special Publication 51, 11-27.

Schumm, S.A.; Mosley, M.P.; & Weaver, W.E. 1987. Experimental fluvial geomorphology. New York, Willey, 413 pp.

Shanley, K.W. & McCabe, P.J. 1994. Perspectives on the Sequence Stratigraphy of Continental Strata. AAPG Bulletim 78(4), 544-568.

Shanley, K.W., McCabe, P.J., & Hettinger, R.D. 1992, Tidal influences in Cretaceous fluvial strata from Utah, USA: a key to sequence stratigraphic interpretation. Sedimentology 39, 905-930.

Shaw, R., Etheridge, M., & Lambeck, K. 1991. Development of the Late Proterozoic to Mid-Paleozoic intracratonic Amadeus Basin in Central Australia: a key to understanding tectonic forces in plate interiors. Tectonics 10, 688-721.

Silva Born, L.R. 2011. A Formação Tombador na porção nordeste da Chapada Diamantina - BA: Estratigrafia, Faciologia e Ambientes de Sedimentação. Unpublished MsC Thesis, Universidade Federal do Rio Grande do Sul, Brasil.

Silva Filho, C.V.R. 2009. Sistemas deposicionais nas Formações Tombador e Guiné nos arredores do Morro do Pai Inácio, Chapada Diamantina-BA. Unpublished monography, Universidade Federal da Bahia, 120p.

Silva, A.M., Chemale, F., Kuyumjian, R.M., & Heaman, L. 1995. Mafic dyke swarms of Quadrilátero Ferrífero and Southern Espinhaço, Minas Gerais, Brazil. Revista Brasileira de Geociências 25, 124-137.

Silva, L.C., McNaughton, N.J., Melo, R.C., & Fletcher, I.R. 1997. U-Pb Shrimp ages in the Itabuna-Caraíba TTG high-grade complex: the first window beyond the Paleoproterozoic overprint of the eastern Jequié Craton, NE Brazil. In: II ISGAM - International Symposium on Granites and Associated Mineralisations, Sociedade Brasileira de Geologia, Salvador, Brazil, pp.282-283.

Silveira, E.M., Söderlund, U., Oliveira, E.P., Ernst, R.E., & Menezes Leal, A.B. 2013. First precise U-Pb baddeleyite ages of 1500 Ma mafic dykes from the São Francisco Craton, Brazil, and tectonic implications. Lithos 174, 144-156.

Simons, D.B., Richardson, E.V., & Nordin, C.F.Jr. 1965. Sedimentary structures generated by flow in alluvial channels. In: Middleton, G.V., (Ed.), Primary Sedimentary Structures and Their Hydrodynamic Interpretation. SEPM Special Publication 12, 34-52.

Simpson, E.L.; Dilliard, K.A.; Rowell, B.F.; & Higgins, D. 2002. The fluvial-to-marine transition within the post-rift Lower Cambrian Hardyston Formation, Eastern Pennsylvania, USA. Sedimentary Geology 147, 127-142.

Sloss, L.L. 1963. Sequences in the cratonic interior of North America. Geological Society of America Bulletin 74, 93-114.

Sloss, L.L., Krumbein, W.C. & Dapples, E.C. 1949. Integrated facies analysis. In: Longwell, C.R. (Ed.) Sedimentary facies in geologic history. Geological Society of America Memoir 39, 91-124.

Smith, G.A. 1986. Coarse-grained nonmarine volcaniclastic sediment: Terminology and depositional process. Geological Society of America Bulletin 97, 1-10.

Smith, N.D. 1972. Some sedimentological aspects of planar cross-stratification in a sandy braided river. Journal of Sedimentary Petrology 42, 624-634.

Sohn, Y.K., Rhee, C.W. & Kim, B.C. 1999. Debris Flow and Hyperconcentrated Flood-Flow Deposits in an Alluvial Fan, Northwestern Part of the Cretaceous Yongdong Basin, Central Korea. Journal of Geology 107, 111-132.

Sønderholm, M. & Tirsgaard, H. 1998. Proterozoic flucial styles: response to changes in accommodation space (Rivieradal sandstones, eastern North Greenland). Sedimentary Geology 120, 257-274.

Souza Junior, J.P. 2011. Sistema deposicional das Formações Tombador e Açuruá na cidade de Barra da Estiva, Bahia. Uundergraduate monography, Universidade Federal da Bahia, 104 pp.

Spalletti, L.A. & Piñol, F.C. 2005. From Alluvial Fan to Playa: An Upper Jurassic 1167 Ephemeral Fluvial System, Neuquén Basin, Argentina. Gondwana Research 8, 363-383.

Suter, J.R. 2006. Facies models revisited: clastic shelves. In: Posamentier, H.W. & Walker, R. (Eds.), Facies Models Revisited, SEPM Special Publication 84, 339-398.

Swift, D.J.P. 1975. Barrier-island genesis: evidence from the central Atlantic shelf, eastern USA. Sedimentary Geology 14, 1-43.

Swift, D.J.P.; Kofoed, J.W.; Saulsbury, F.B.; & Sears, P.C. 1972. Holocene evolution of the shelf surface, central and southern Atlantic shelf of North America. In: Swift, D.J.P.; Duane, D.B.; Pilkey, O.H. (Eds.), Shelf sediment transport: process and pattern, Stroudsburg, Pennsylvania, Dowden, pp-499-574.

Tack, L., Wingate, M.T.D., De Waele, B., Meert, J., Belousova, E., Griffin, B., Tahon, A., & Fernandez-Alonso, M. 2010. The 1375 Ma "Kibaran event" in Central Africa: prominent emplacement of bimodal magmatism under extensional regime. Precambrian Research 180, 63-84.

Tänavsuu-Milkeviciene, K. & Plink-Björklund, P. 2009. Recognizing tide-dominated versus tide-influenced deltas: Middle Devonian Strata of the Baltic Sea. Journal of Sedimentary Research 79, 887-905.

Taylor, S.R. & McLennan, S.M. 1985. The continental crust: its composition and evolution. Blackwell, Oxford.

Thopson, C., McMechan, G., Szerbiak, P. & Gaynor, N. 1995. Three-dimensional GPR imaging of compex stratigraphy within the Ferron sandstone, Castle Valley, Utah. Symposium on the Application of Geophysics to Engineering and Environmental Problems. Preceedings, 435-543.

Tirén, S.A., Wänstedt, S. & Sträng, T. 2001. Moredalen - a canyon in the Fennoscandian Shield and its implication on site selection for radioactive waste disposal in south-eastern Sweden. Engineering Geology 61, 99-118.

Tirsgaard, H. 1993. The architecture of Precambrian high energy tidal channel deposits: an example from the Lyell Land Group (Eleonore Bay Supergroup), northeast Greenland. Sedimentary Geology 88, 137-152.

Tirsgaard, H. & Øxnevad, I.E.I. 1998. Preservation of pre-vegetational mixed fluvio-aeolian deposits in a humid climatic setting: an example from the Middle Proterozoic Eriksfjord Formation, Southwest Greenland. Sedimentary Geology 120, 295-317.

Todd, S.P. 1989. Sream-driven, high-density gravelly traction carpets: possible deposits in the Trabeg Conglomerate Formation, SW Ireland and some theoretical considerations of their origin. Sedimentology 36, 513-530.

Todd, S.P. 1996. Process deduction from flucial sedimentary structures. In: Carling, P.A. & Dawson, M.R., (Eds.), Advances in fluvial dynamics and stratigraphy. John Wiley & Sons, pp 299-350.

Torsvik, T.H., Smethurst, M.A., Meert, J.G., Van der Voo, R., McKerrow, W.S., Brasier, M.D., Sturt, B.A., & Walderhaug, H.J. 1996. Continental break-up and collision in the

Neoproterozoic and Palaeozoic: A tale of Baltica and Laurentia. Earth Science Reviews 40, 229-258.

Torsvik, T.H.,Müller, R.D., Van der Voo, R., Steinberger, B., & Gaina, C. 2008. Global platemotion frames: toward a unified model. Reviews of Geophysics 46, RG3004. http://dx.doi.org/10.1029/2007RG000227.

Trompette, R., Uhlein, A., Silva, M.E., & Karmann, A.1992. The Brasiliano São Francisco craton revisited (central Brazil). Journal of South American Earth Sciences 6, 49-57.

Turnbridge, I.P. 1981. Sandy high-energy flood sedimentation - some criteria for recognition, with an example form the Devonian of southwest England. Sedimentary Geology 28, 79-95.

Turner, B.R. 1981. Possible origin of low angle cross-strata and horizontal lamination in Beaufort Group sandstones of the southern Karoo Basion. Transactions of the Geological Society of South Africa 84, 193-197.

Turpin, L., Maruejol, P., & Cuney, M. 1988. U-Pb, Rb-Sr and Sm-Nd chronology of granitic basement hydrothermal albitites and uranium mineralizations (Lagoa Real, South Bahia, Brazil). Contributions to Mineralogy and Petrology 98, 139-147.

Uhlein, A., Trompette, R.R., & Egydio-Silva, M. 1998. Proterozoic rifting and closure, SE border of the São Francisco Craton, Brazil. Journal of South American Earth Sciences 11, 191-203.

Van Balen, R.T. & Heeremans, M. 1998. Middle Proterozoic-early Palaeozoic evolution of central Baltoscandian intracratonic basins: evidence for asthenospheric diapirs. Tectonophysics 300, 131-142.

Van Wagoner, J.C. 1995. Overview of sequence stratigraphy of foreland basin deposits: terminology, summary of papers, and glossary of sequence stratigraphy. In: Van Wagoner, J.C., Bertram, G.T., (Eds.), Sequence Stratigraphy of Foreland Basin Deposits. American Association of Petroleum Geologists Memoir 64, pp.ix-xxi.

Varajão, A.D. & Gomes, N.S. 1997. Petrological significance of illitic clays in Proterozoic sandstones of the Tombador Formation, Chapada Diamantina, Brazil. Zbl. Geol. Paläont. Teil I, (3-6), 767-778.

Visser, M.J. 1980. Neap-spring cycles reflected in Holocene subtidal large-scale bedforms deposits: a preliminary note. Geology 8, 543-546.

Vries, S.T., Pryer, L.L., & Fry, N. 2008. Evolution of Neoarchean and Proterozoic basins of Australia. Precambrian Research 166, 39-53.

Weil, A.B., Van der Voo, R., Niocaill, C.M., & Meert, J.G. 1998. The Proterozoic supercontinent Rodinia: paleomagnetically derived reconstructions for 1100 to 800 Ma. Earth and Planetary Science Letters 154, 12-24.

Wellner, R.W. & Bartek, L.R. 2003. The effect of sea level, climate, and shelf physiography on the development of incised-valley complexes: A modern example from the East China Sea: Journal of Sedimentary Research 73, 926-940.

Wells, N.A. 1984. Sheet debris flow and sheetflood conglomerates in Cretaceous cool maritime alluvial fans, south Orkney Islands, Antarctica. In: Koster, E.H. & Steel, R.J., (Eds.), Sedimentology of gravels and conglomerates. Canadian Society of Petroleum Geologists 10, 133-145.

Wells, S.G. & Harvey, A.M. 1987. Sedimentological and geomorphic variations in storm generated alluvial fans, Howgill fells, northwest England. Geological Society of America Bulletin 98, 182-198.

Went, D.J. 2005. Pre-vegetation alluvial fan facies and processes: an example from the Cambro-Ordovician Rozel Conglomerate Formation, Jersey, Channel Islands. Sedimentology 52, 693-713.

Williams, G.E. 1971. Flood deposits of the sand-bed ephemeral streams of central Australia. Sedimentology 17, 1-4.

Willis, B.J., Bhattachayra, J.P., Gabel, S.L., & White, C.D. 1999. Architecture of a tide-influenced river delta in the Frontier Formation of central Wyoming, USA. Sedimentology 46, 677-688.

Winchester, J.A. & Floyd, P.A. 1977. Geochemical discrimination of different magma series and their differentiation products using immobile elements. Chemical Geology 20, 325-343.

Wonham, J.P., Cyrot, M., Nguyen, T., Louhouamou, J. & Ruau, O. 2010. Integrated approach to geomodelling and dynamic simulation in a complex mixed siliciclastic-carbonate reservoir, N'Kossa field, Offshore Congo. In: Jolley, S.J., Fisher, Q.J., Ainsworth, R.B., Vrolijk, P., & Delisle, S., (Eds.), Reservoir Compartmentalization. Special Publication Geological Society 347, 133-163.

Woolfe, K.J.; Larombe, P.; Naish, T.; & Purdon, R.G. 1998. Lowstand rivers need not incise the shelf: an example from the Great Barrier Reef, Australia, with implications for sequence stratigraphic models: Geology 26, 75-78.

Zecchin, M. & Catuneanu, O. 2013. High-resolution sequence stratigraphy of clastic shelves I: Units and bounding surfaces. Marine and Petroleum Geology 39, 1-25.

Zhao, G., Sum, M., & Wilde, S.A. 2002. Did South America and West Africa marry and divorce or was it a long-lasting relationship? Gondwana Research 5, 591-596.

Appendix 1 – " Age constraints on crystal-tuff from the Espinhaço Supergroup – Insight into the Paleoproterozoic to Mesoproterozoic intracratonic basin cycles of the Congo-São Francisco Craton", Gondwana Research vol 27 (2015), 363-376.

ABSTRACT

The U-Pb data from the volcanic and detrital zircon grains of the Tombador Formation in Chapada Diamantina, Bahia, provide the depositional age of the top of this unit and define the main sedimentary sources of the Archean, Paleoproterozoic and Mesoproterozoic Eras. The lithofacies, petrographic and geochemical data from crystal-tuff samples indicated that a volcanic source was located to the east of the Chapada Diamantina region. The available zircon data defined three first-order intracratonic basinal cycles, including the Lower (Statherian), Middle (Calymmian) and Upper (Stenian-early Tonian) Espinhaço basins. These sequences are well exposed at the Espinhaço Supergroup type-section in the Chapada Diamantina region. The zircon Hf isotope data from the 1.4 Ga crystal-tuff in the Middle Espinhaço and the 1.2 Ga tuffaceous rock in the Upper Espinhaço suggested different sources, with model ages of 2.1 to 1.9 Ga and < 1.9 Ga, respectively. The tectonic development of these Paleoproterozoic to Mesoproterozoic intracratonic basins can be explained by the far-field stress at the paleoplate margins, which has been shown in other Phanerozoic intracratonic basins. The data presented here support a tectonic scenario in which the Congo-São Francisco paleoplate interior recorded the main global events related to the geodynamic processes after the Columbia supercontinent collage and the formation and fragmentation of the Rodinia supercontinent.

Keywords: Espinhaço Supergroup; Congo-São Francisco Craton; U-Pb and Lu-Hf zircon dating; Precambrian intracratonic sequences

A1.1. Introduction

Approaches for reconstructing past continental configurations include matching similar geological features (collisional orogens, rift and passive margins, large igneous provinces and others), using paleontological data, tracking ocean floor spreading vectors and using paleomagnetism (Rogers and Santosh, 2004; Ernst et al., 2013a). It is difficult to reconstruct the position and composition of supercontinents prior to Pangea (Rodinia, Columbia/Nuna, Atlantica, Kenorland and others) due to the scarcity of preserved kinematic indicators, the limited reliable data on paleomagnetic poles and poor continental blocks preservation. Using the same geological information, several reconstructions can result in different paleoplate kinematic configurations (as seen in the reconstructions for the Mesoproterozoic and Neoproterozoic Eras; Torsvik et al., 1996, 2008; Weil et al., 1998; Meert and Torsvik, 2003; Piper, 2007; Li et al., 2008; Evans, 2009).

Supercontinent interiors typically host a series of intracratonic successor basins that consist of several first-order sequences that are bounded by major unconformities (Lindsay, 2002; Ingersoll, 2012). This structure likely resulted from the dynamic topography that was generated by subduction and/or the long-wavelength cycles of supercontinent aggregation and dispersal, which are superimposed by eustasy and sediment supply (Burgess et al., 1997; Lindsay, 2002; Moucha et al., 2008) or crustal underplating (Pinto et al., 2010). Preexisting structures (such as sutures) play an important role in supercontinent geodynamics (Gorczyk et al., 2013). The above description fits the Phanerozoic record of the intracratonic rift-sag basins, in which an entire stratigraphic succession of several million years of deposition reveals unconformities that may correspond to tens to hundreds of millions of years of erosion and/or nondeposition (Sloss, 1963; Shaw et al., 1991; Milani and Ramos, 1998; Lindsay, 2002). In addition to the fossil record, magmatic rocks can constrain the ages of the main stratigraphic sequences. Magmatic events in intracratonic basins are relatively rare and usually result from tectonism along plate margins or large plume eruptions. Precambrian intracratonic basins have similar structures relative to their Phanerozoic counterparts (Van Balen and Heeremans, 1998; Aspler et al., 2001; Vries et al., 2008; Alkmim and Martins-Neto, 2012; Chemale et al., 2012; Ribeiro et al., 2013). Thus, understanding the chronological framework of the Precambrian intracratonic sequences, regional correlations and tectonic setting that produced magmatism in these basins can help constrain supercontinental reconstructions.

The Congo-São Francisco Craton was a single continental block following the Paleoproterozoic Era (D'Agrella et al., 1990; De Waele et al., 2008; Cordani et al., 2010) and evolved through a long history of intracratonic and passive margin basin filling, magmatism, orogenic build-up and foreland basin filling (Almeida, 1977; Marshak and Alkmim, 1989; Trompette et al., 1992; Chemale et al., 1993; Zhao et al., 2002; De Waele et al., 2008; Pedreira and De Waele, 2008; Silveira et al., 2013). Recently, Ernst et al. (2013a) identified Large Igneous Provinces (LIPs) of the same age on the African and American portions of the Congo-São Francisco Craton. In addition, these authors used the LIP "barcode" method (sensu Ernst et al., 2013a) to propose an unconventional connection with Siberia during the Mesoproterozoic Era (Ernst et al., 2013a and b; Pisarevsky et al., 2013; Silveira et al., 2013). Understanding the timing and nature of the basin-forming events and the tectonic settings of the magmatic events in the Congo-São Francisco Craton can be useful in reconstructing the paleoplate configuration and determining the participation of the craton in the Paleoproterozoic and Mesoproterozoic supercontinents.

The Espinhaço Supergroup (hereafter ES) is an important stratigraphic sequence in the Paleo- and Mesoproterozoic record of South America. The ES is widely distributed over the São Francisco Craton as a rift-sag successor basin. This basin was initiated after the orogenetic collapse of the Transamazonian/Eburnean (Paleoproterozoic) orogens approximately 1.8 Ga and lasted until rifting occurred approximately 0.9 Ga (Brito Neves et al., 1979; Marshak and Alkmim, 1989; Chemale et al., 1993; Martins-Neto, 2000). Several important lacunae have been recognized within the ES (Derby, 1906; Pedreira, 1994; Schobbenhaus, 1996; Danderfer et al., 2009; and others). However, the time span of the deposition and unconformities remain contentious (Brito Neves et al., 1979; Machado et al., 1989; Silva et al., 1995; Cordani et al., 2010). Recent geochronological studies in the ES have used U-Pb dating for igneous and detrital zircon grains to understand the regional lacunae and depositional history of the sequence (Danderfer et al., 2009; Chemale et al., 2012; Ribeiro et al., 2013; Santos et al., 2013).

In the present study, crystal-rich volcaniclastic rocks (crystal-tuff) in the Tombador Fm. (Chapada Diamantina Group) were discovered, and U-Pb dating of these tuffs improved the chronological framework of the ES. By combining these new data with previously published and reliable ages (preferably U-Pb), we propose an updated chrono-stratigraphic chart for the entire ES. This chrono-stratigraphic chart includes first-order sequences, environments and the related global tectonic events. The crystal-tuff petrographic and geochemical compositions can be used to define the source and tectonic setting. In addition, the distributions of the similar volcanic age cluster in the age spectra of the detrital zircons in the Tombador Fm. sandstones can be used to define the source and vertical distribution of the volcanic material. We compare the Lu-Hf signature (model ages and εHf) of the volcanic zircon crystals from the Tombador and Sopa-Brumadinho Fms. In addition, the implications for the Congo-São Francisco Craton tectonic evolution and paleogeography during the Mesoproterozoic Era are discussed.

A1.2. Geological setting

The São Francisco cratonic basement crops out south, west and east of Chapada Diamantina (Fig. A1a; Alkmim, 2004). Four distinct terrains make up the São Francisco Craton basement west and east of Chapada Diamatina (Bahia State). These terrains are known as the Gavião, Serrinha and Jequié Blocks and the Itabuna-Salvador-Curaçá Belt (Barbosa and Sabaté, 2004). The Gavião and Serrinha Blocks are primarily composed of Paleo- to Mesoarchean tonalite-trondhjemite gneisses (TTGs) and Paleoarchean to Paleoproterozoic greenstone belt associations. The Jequié Block and the Itabuna-Salvador-Curaçá Belt consist of Archean granulite terrain (Barbosa and Sabaté, 2004). The Jequié Block is composed of Neoarchean ortho-granulites and migmatites. The Itabuna-Salvador-Curaçá Belt is composed of Meso- to Neoarchean high-grade rocks. All four terrains were partially reworked during the Transamazonian/Eburnean Cycle during the Paleoproterozoic Era (ca. 2.2 to 2.0 Ga; Barbosa and Sabaté, 2004).

Proterozoic and Phanerozoic sedimentary sequences extensively cover the cratonic basement (Fig. A1a). The Paleoproterozoic to Mesoproterozoic cover sequences formed in an intracratonic setting as part of the ES. During the Neoproterozoic Era, glacial, marine siliciclastic, marine carbonatic and continental deposits (all belonging to the São Francisco Supergroup) covered most of the craton. These deposits covered the craton as an extension of the craton passive margins or as foreland basins of the Aracuaí-West Congo, Brasília, Rio Preto, Sergipano and Rio Pardo Neoproterozoic to Eopaleozoic belts (Marshak and Alkmim, 1989; Trompette et al. 1992; Chemale et al., 1993; Fig. A1a).

A1.2.1. The Espinhaço Supergroup

The ES occurs in eastern Brazil, is oriented roughly NS and straddles over 1,000 km of the São Francisco Craton interior (Fig. A1a). At the Paramirim Aulacogen, the ES is exposed at Chapada Diamantina (a large plateau located in the northern half of the craton) and in the northern part of the Espinhaço mountain range (Setentrional Espinhaço; Pedreira and De

Waele, 2008; Danderfer et al., 2009; Alkmim and Martins-Neto, 2012; Fig. A1b). The Southern Espinhaço mountain range (Meridional Espinhaço) is part of the external sector of the Neoproterozoic fold and thrust belt in the Araçuaí belt (Pflug, 1965; Dussin and Dussin, 1995; Uhlein et al., 1998; Martins-Neto, 2000; Fig. A1a).

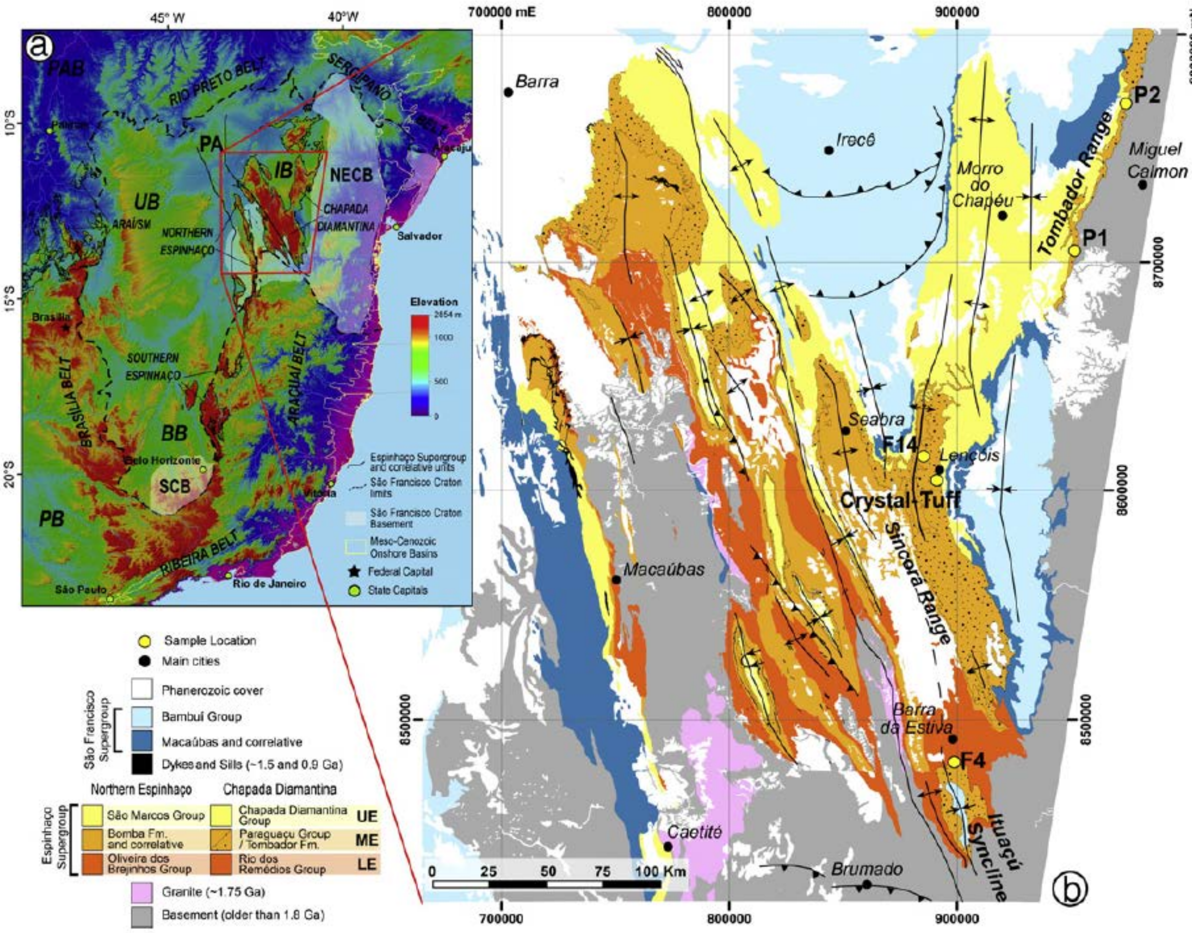

Fig. A1: Study area and sample locations, in eastern Chapada Diamantina. The digital elevation model of east Brazil is shown in 'a' with the Espinhaço Supergroup location at the São Francisco Craton border and Paramirim Aulacogen (PA). The Southern and Northeastern Craton basement (SCB and NECB) and the Neoproterozoic-Phanerozoic Intracratonic Cover are indicated (BB – Bambuí Basin; IB – Irecê Basin; PAB – Parnaíba Basin; PB – Paraná Basin; UB – Urucuia Basin). The Lower, Middle and Upper Espinhaço sequences are shown in map 'b' at Paramirim Aulacogen with indications of the Tombador Fm. extent and sampling sites (modified after Barbosa and Domingues, 1994; Guimarães et al., 2005; Loureiro et al., 2008; DEM source: SRTM/NASA obtained at http://srtm.csi.cgiar.org/ on 07/22/2011; Jarvis et al., 2008).

At Chapada Diamantina, the ES is divided into three main stratigraphic units, the Rio dos Remédios, Paraguaçú and Chapada Diamantina groups (Pedreira, 1994; Guimarães et al., 2005; Pedreira and De Waele, 2008). The Rio dos Remédios Group includes the continental siliciclastic sequences of the Serra da Gameleira, Lagoa de Dentro and Ouricuri do Ouro Fms. and the volcanic rocks of the Novo Horizonte Fm., dated at 1752 ± 4 Ma (Schobbenhaus et al., 1994) and 1748 ± 1 Ma (Babinski et al., 1999). The Paraguaçú Group includes the shallow-water marine, deltaic, fluvial and eolian deposits of the Mangabeira and Açuruá Fms. that were intruded by mafic dyke swarms dated at 1514 ± 22 Ma (Babinski et al., 1999) and 1501 ± 9.1 Ma (Silveira et al., 2013). The Chapada Diamantina Group occur at the top of the ES at Chapada Diamantina, and it consists of the continental deposits of the Tombador Fm. (ca. 1.4 Ga), the transgressive shallow marine fine-grained package of the Caboclo Fm. (deposited ca. 1.2 Ga, based on whole-rock Pb-Pb isochron; Babinski et al., 1993) and the estuarine and fluvial strata of the Morro do Chapéu Fm. The Morro do Chapéu Fm. represents a lowstand-to-transgressive fill of incised valleys (Dominguez, 1992; Pedreira, 1994).

In the Northern Espinhaço range, the ES is divided into three groups (Guimarães et al., 2005; Loureiro et al., 2008). These groups include the continental and volcanic sequences of the Oliveira dos Brejinhos Group (volcanism at 1735 ± 6 Ma and 1582 ± 8 to 1569 ± 14; Danderfer et al., 2009) followed by the continental and shallow marine deposits of the São Marcos and Santo Onofre groups. In Southern Espinhaço, the ES is composed of the alluvial-fluvial Bandeirinha Fm. and overlain by the Diamantina and Conselheiro Mata groups. The Diamantina Group consists of the siliciclastic deposits and bimodal volcanic rocks of the São João da Chapada Fm. (volcanism ca. 1.7 Ga; Brito Neves et al., 1979; Dussin, 1994; Silva et al., 1995; Chemale et al., 2012), the diamond-bearing alluvial-fluvial sequence of the Sopa-Brumadinho Fm. (depositional age ca. 1.2 Ma; Chemale et al., 2012) and the eolian to shallow marine deposits of the Galho do Miguel Fm. The coastal to shallow marine Conselheiro Mata Group occurs at the top of the ES.

The entire section of the ES is intruded by mafic dyke swarms dated at 934 ± 14 Ma (Chapada Diamantina; Loureiro et al., 2008), 906 ± 2 Ma (Southern Espinhaço; Abreu, 1991) and 890 ± 130 Ma (Northern Espinhaço; Danderfer et al., 2009).

The three main basinal cycles, the Statherian (1.8 - 1.68 Ga), Calymmian-early Ectasian (1.6 - 1.38 Ma) and Stenian-early Tonian (1.2 - 0.9 Ga; the Lower, Middle and Upper Espinhaço basins, respectively; sensu Chemale et al., 2012) are well preserved in the Chapada Diamantina and Northern Espinhaço regions. In Southern Espinhaço, only the Lower and Upper cycles are exposed (see discussion section 5.3).

The studied section of the ES, the Tombador Fm., is a regressive fluvial succession that was deposited on a broad alluvial plain by rivers that flowed westward from a mountain range in the eastern region of the Congo-São Francisco Craton. The formation thickness varied from 600 to 350 m. Ephemeral fluvial deposits, with conglomerates and minor eolian reworking, are interbedded with braided fluvial deposits. Together, these deposits compose 70% of the Tombador Fm. Estuarian packages at the base and shallow marine transgressive deposits near the top complement this unit (Magalhães, personal communication).

A1.3. Methods

Detailed sedimentologic-stratigraphic studies applying sequence stratigraphy were conducted at Chapada Diamantina. At the Ribeirão de Baixo section (UTM coordinates, datum WGS84, 24s zone: 240.731 mE, 8.607.276 mN), the authors identified crystal-rich volcaniclastic rocks in the Tombador Fm. (detailed in Figs. 2 and 3 and Supplementary Material A1). In addition, it were identified conglomerates that hosted volcanic clasts. The Tombador Fm. was sampled at various stratigraphic levels to compare their detrital and volcanic U-Pb zircon age signatures. The Tombador Fm. volcaniclastic rocks were collected from the Ribeirão de Baixo section (Upper Tombador Fm.), and the sedimentary rocks (sandstones) were collected from the Ituaçú Syncline and Pai-Inácio Anticline (Lower Tombador Fm.) and Tombador Range (Upper Tombador Fm.; Fig. A1b and supplementary kml file). The volcanic and detrital zircon grains from the Tombador and Sopa-Brumadinho (Upper Espinhaço Basin in the Southern Espinhaço range) Fms. were analyzed with the Lu-Hf method to compare their mantle source.

The major oxides were determined by ICP-AES and the rare earth and refractory elements were determined by ICP-MS. The major and trace element chemistry, detection limits and sample weights are reported in the electronic supplementary material (Geochemistry data.xls).

For the zircon geochronology, volcaniclastic and sandstone samples were milled, sorted by size and separated using density and magnetic methods. The heavy minerals were analyzed using a microscope, and zircon crystals were handpicked and mounted in epoxy resin. After abrasion and polishing, the zircon grains were imaged under backscattered electron and cathodoluminescence detectors. U-Pb and Lu-Hf analyses were obtained with a Laser Ablation system (New Wave UP 213) attached to an MC-ICPMS (Neptune) instrument in the Geochronology Laboratory at the Universidade de Brasília. The zircon grains were initially analyzed for U-Pb and then for Lu-Hf, on the same area or in the same zircon grain.

In situ U-Pb analyses were performed with mixed collectors (Faraday cups and MICs) configured for the simultaneous measurement of Th, U, Pb and Hg isotopes. The U-Pb isotope data were acquired in static mode with a spot size of 30 μm, a shot repetition rate of 10 Hz and an output energy of between 0.3 and 1.1 mJ/min. The laser-induced elemental fractional and instrumental mass discrimination were corrected with the reference zircon GJ-1 (Jackson et al., 2004). Two GJ-1 samples were analyzed for every ten zircon spot samples. The external error was calculated based on the propagation error of the GJ-1 mean and the individual zircon sample (or spot).

For the Lu-Hf method, the analyzed masses were 171, 173, 175, 176, 177, 178 and 179 in Faraday cups (with an axial Faraday cup mass of 177). Isotope data were acquired using static mode with 50 1.054 s cycles. All values were corrected for blank values. A laser output power of between 5 and 6.5 J/cm2, a shot repetition rate of 10 Hz and a laser spot size of between 40 and 55 μm were used. The coolant flow (Ar) input rate was 15 l/min, the auxiliary flow (Ar) rate was 0.8 l/min, and the carrier flow was mixed Ar and He at input rates of 0.75 and 0.45 l/min, respectively. Chemale et al. (2011) described the detailed analytical methods and data treatment for the U-Pb and Lu-Hf methods.

The data were reduced with a laboratory macro and were analyzed in spreadsheets. Isoplot 3 software (Ludwig, 2003) was used to generate concordia diagrams, histograms and relative probability plots. For the concordia age calculations, frequency histograms and probability plots, only analyses that were within 100 ± 10% of concordance were used. All calculated ages are reported at the 95% confidence level. Ellipses in the concordia diagram are reported at the 68.3% confidence level. The U-Pb and Lu-Hf analytical data are presented in spreadsheets in the electronic supplementary material (U-Pb and Lu-Hf zircon data.xls).

A1.4. Results

A1.4.1 Crystal-rich volcaniclastic rocks: field, petrographic and geochemical characteristics

Two main lithofacies associations were identified in the Tombador Fm. at the Ribeirão de Baixo section: braided fluvial and tidal bars. The complete outcrop description is provided in Supplementary Material A1. The crystal-tuff layers were preserved in fluvial plains, and some volcanic clasts were recognized in fluvial sands (Figs. A2 and A3).

The crystal-tuff beds included an assemblage of magmatic components mixed with detrital materials. The magmatic origin is supported by the presence of juvenile crystal components dominated by sharp extinction, very angular to subangular and inclusion-free volcanic quartz, and plagioclase and microcline feldspars with minor relicts of devitrified glass embedded in the originally glassy recrystallized groundmass. Subordinate plutonic and metamorphic quartz grains occur, as do rare muscovite and opaque minerals. The quartz grains frequently exhibit resorption embayments (Fig. A3d). Figure 3b illustrates two normal graded beds of crystal-rich volcaniclastic rocks (indicated by the black triangles) above a sand bar, with a large clast of chloritized pumice above. Figure 3c shows a large recrystallized volcanic glass at the base of a sandstone bed. The field and petrographic characteristics, such as the dark, fine-grained (of volcanic origin) granules and pebbles, the abundant angular volcanic quartz, the recrystallized glassy groundmass and the resorption embayments, allowed us to classify these rocks as crystal-rich volcaniclastic rocks, sensu Cas and Wright (1988).

As volcaniclastic rocks, their chemical compositions reflect a mixture of epiclastic and volcanic fragments. Several techniques and tools are available for classifying either epiclastic sandstones or volcanic rocks based on their chemical compositions (e.g., Le Bas, 1986; Herron, 1988; Roser and Korsch, 1988; McLennan et al., 1993; Lacassie et al., 2004). However, few methods are able to distinguish between volcaniclastic and normal epiclastic sandstones because it is difficult to determine the amount each source rock contributed to these rock types.

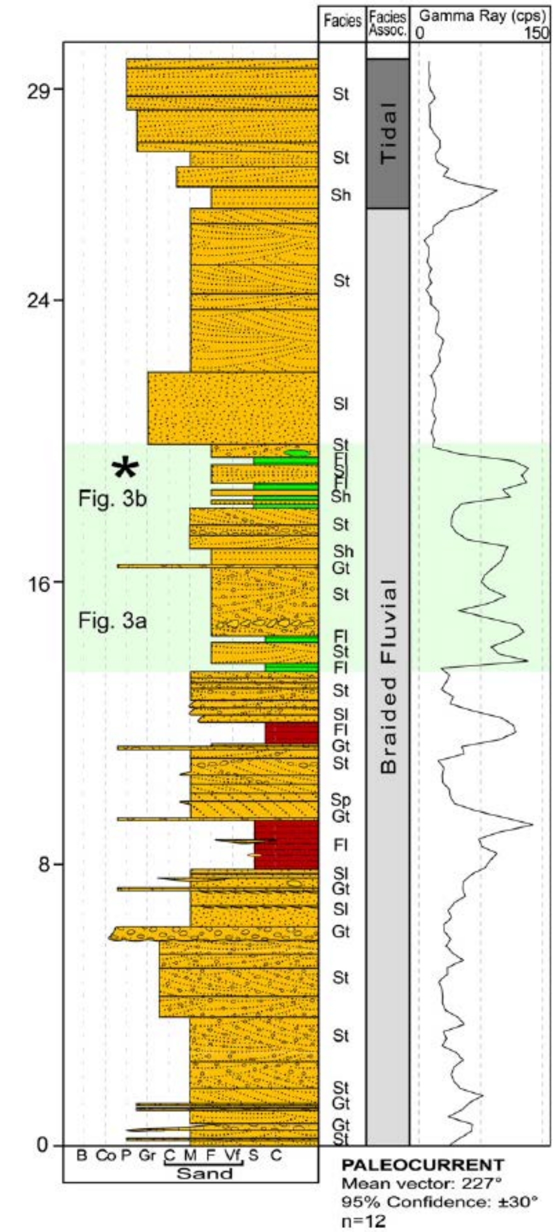

Fig. A2: Measured stratigraphic section summarizing facies succession, gamma-ray and paleocurrents of the Tombador Fm. at the Ribeirão de Baixo section. The green strip corresponds to the tuffaceous interval and the asterisk represents the collected sample (Crystal-tuff sample). The outcrop photographs are indicated. Complete outcrop description is provided in the electronic Supplementary Material A1.

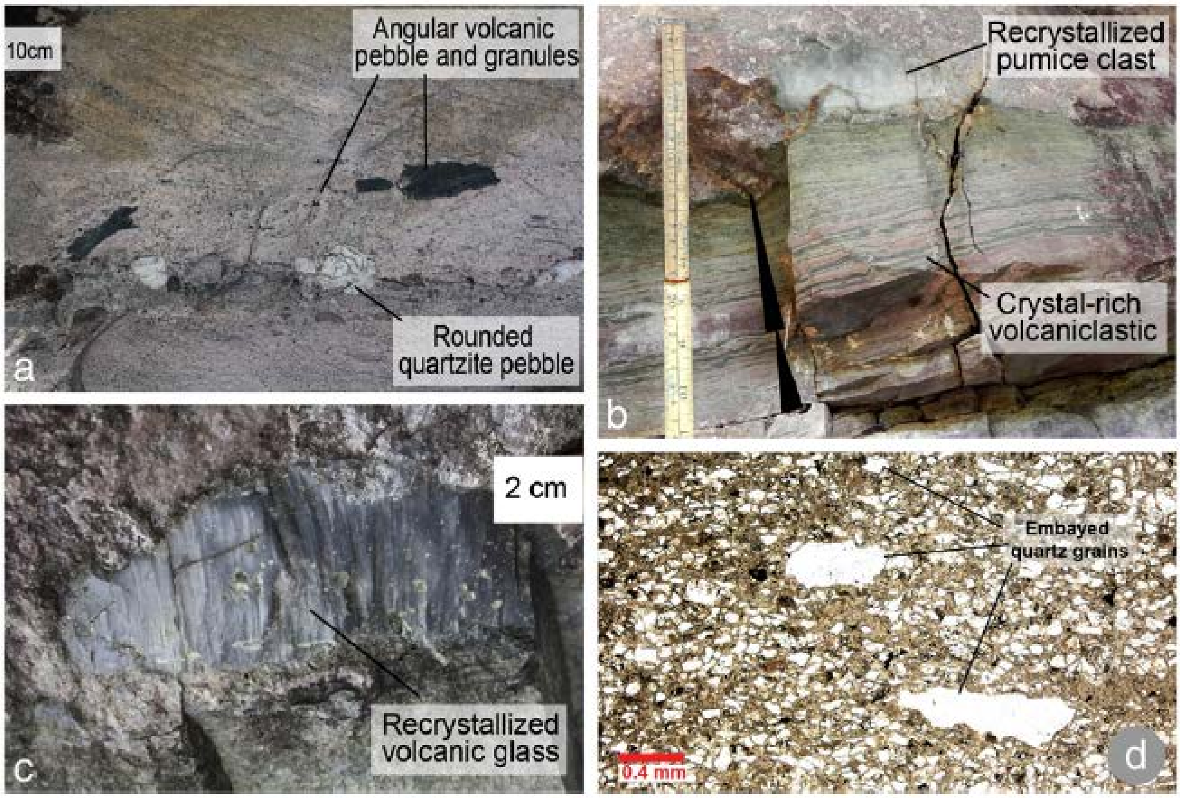

Fig. A3: Crystal-tuff lithofacies identified in the Ribeirão de Baixo section: 'a,' gravel bar with abundant pebbles and granules of angular volcanic rocks and rounded quartzite pebbles; 'b,' two normal graded beds of crystal-rich volcaniclastic rocks (crystal-tuff; black triangles) and a large recrystallized pumice clast; 'c,' clast of volcanic glass; and 'd,' crystal-tuff main petrographic characteristics as abundant, angular and inclusion-free volcanic quartz grains and three embayed quartz grains.

One possible approach to distinguish between these rock types is to compare the chemical compositions of the analyzed samples with the geochemical datasets available for igneous and sedimentary rocks of known and distinct sources. Several geochemical datasets are available, including datasets with major, trace and rare earth elements. For example, Condie (1993), who, aiming to understand the average chemical composition of the Upper Continental Crust (UCC) as a function of age, published a large geochemical dataset including major, trace and rare earth elements in plutonic and volcanic rocks of varied compositions and ages. In addition, this dataset includes cratonic sandstones (epiclastic), greywackes (volcaniclastic) and shales. To distinguish between the different tectonic settings of the sandstone suites, Bhatia (1983) published a less complete dataset that only included the major elements of sandstones deposited in Oceanic Island Arc (OIA), Continental Island Arc (CIA), Active Continental

Margin (ACM) and Passive Margin (PM) tectonic settings. Roser and Korsch (1988) and Lacassie et al. (2004) proposed the use of four distinct geochemical classes, including P1 (mafic), P2 (intermediate), P3 (felsic) and P4 (recycled), to constrain the compositions of the sandstones source rocks. Regarding the composition and differentiation of volcanic rocks, Winchester and Floyd (1977) proposed the use of immobile elements, particularly the Zr/TiO2 and Nb/Y ratios, to discriminate between different volcanic magma series and rock types.

We compared the chemical composition of our crystal-tuff with the data presented by Bhatia (1983), Condie (1993) and Lacassie et al. (2004), as well as the composition of the UCC described by Taylor and McLennan (1985), to constrain the crystal-tuff source composition and, together with the Winchester and Floyd (1977) scheme, constrain the crystal-tuff tectonic setting.

The SiO2 content in the crystal-tuff samples varied from 72 to 83 Wt%. In addition, the Al2O3 and Fe2O3t contents varied from 8 to 13 Wt% and the K2O content varied from 1.2 to 6.2 Wt%. These samples were classified as arkoses and litharenites in the Herron (1988) plot (Fig. A4 and supplementary material). The major elements in the crystal-tuff were generally concentrated near the acid and recycled sources in the multi-element correlation diagrams (Fig. A4a). In this case, the SiO2, Al2O3, Fe2O3t, MgO, K2O and TiO2 remained immobile whereas the Na2O and CaO were mobile. The most discriminating major elements were SiO2, TiO2 and MgO (Fig. A4a). Regarding the source rock composition, the samples plot in the felsic (P3) to recycled (P4) sources, and regarding the basin tectonic setting, the samples plot in the ACM to PM tectonic trend in the SiO2 versus TiO2 diagram (Fig. A4a).

The samples were slightly enriched in SiO2 and slightly depleted in Al2O3, Fe2O3t and MgO relative to the UCC. Additionally, the K2O and TiO2 concentrations were similar and the CaO and Na2O concentrations were depleted relative to the UCC (Fig. A4c). A comparison of the crystal-tuff major element composition with published datasets revealed that the compositional fields of the samples mainly overlapped with Mesoproterozoic felsic volcanic rocks (MFV), volcaniclastic greywackes, ACM through PM tectonic settings and felsic to recycled sources (P3 to P4). In addition, the crystal-tuff behaved differently than the cratonic sandstones (Fig. A4c).

The large ion lithophile element (LILE) profiles were variable in the analyzed samples when normalized to the UCC. The Ba and Rb concentrations were slightly depleted, and the Sr concentration followed a depleted pattern with less Sc, V and Co depletion (Fig. A4c). In addition, the high field strength elements (HFSE) were variable in the analyzed samples. The Nb and Ta concentrations were slightly depleted; the La, Sm, Yb, Th and U concentrations were slightly enriched; and the Zr and Hf concentrations were enriched relative to the UCC (Fig. A4c). When plotted in the Winchester and Floyd (1977) discrimination diagram, the samples were classified as rhyodacite/dacite with a calc-alkaline composition (Fig. A4d).

The rare earth element (REE) content varied between 110 and 330 ppm. The chondrite normalized REE pattern for the samples were similar to the volcaniclastic greywackes (Fig. A4e), which were enriched in LRRE (light rare earth elements) relative to the HREE (heavy rare earth elements). In addition, the samples and volcaniclastic greywackes had similar Eu negative anomalies and flat HREE patterns. The LREE/HREE ratio ranged from 6 and 16, and the negative Eu anomaly ranged from 0.52 and 0.68.

A1.4.2. Tombador Formation crystal-tuff U-Pb zircon dating

One crystal-tuff layer was sampled at the Ribeirão de Baixo section (the sample location is provided in section 3 and in the supplementary kml file). Zircon grains were predominantly well-formed gray-colored and elongated crystals. Some grains were rounded to sub-rounded, and others consisted of broken crystal fragments. A few yellow-colored zircon crystals were also observed. The zircon grains were predominantly zoned in the cathodoluminescence images, but some grains were homogeneous and a few presented core and rim structures (Fig. A5).

Of the 116 zircon crystals analyzed, 92 were within 100 ± 10% of concordance. The zircon age populations were mainly Statherian (1.8 - 1.6 Ga) and Calymmian (1.6 - 1.4 Ga), with some Paleo- (3.6 - 3.2 Ga), Meso- (3.2 - 2.8 Ga), Neoarchean (2.8 - 2.5 Ga) and Rhyacian-Orosirian (2.3 - 2.05 Ga and 2.05 - 1.8 Ga; Fig. A6) ages. The 14 youngest zircon grains in the crystal-tuff yielded a weighted mean 207Pb/206Pb age of 1436 ± 26 Ma. The 13 youngest zircon grains within 100 ± 10% of concordance lie along a chord that was forced to origin with an upper intercept age of 1437 ± 50 Ma. Two concordant zircons yielded a concordia age of 1416 ± 28 Ma (Fig. A6 and supplementary material).

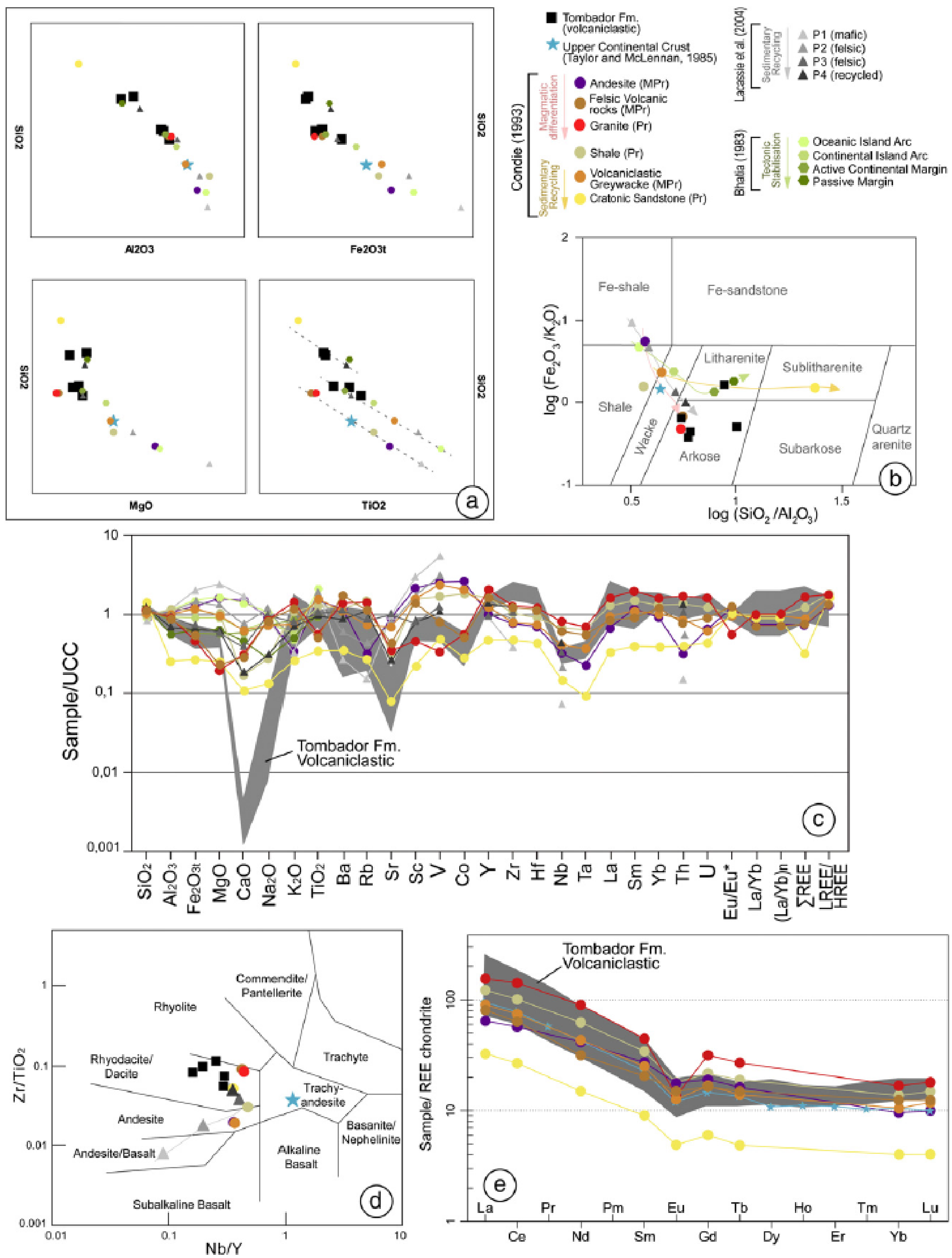

Fig. A4: Geochemical diagrams for the crystal-rich volcaniclastic rocks (plotted as black squares or as a gray band and showing the compositional field). Data used for the comparison are shown based on the graphical legend. In 'a,' multi-element correlation diagram for the main major elements; 'b,' the sandstone classification scheme of Herron (1988, where the samples are classified as arkoses or litharenites); 'c,' a multi-elements spider diagram for major, large ion lithophile and high field strength elements normalized to the upper continental crust from Taylor and McLennan (1985); 'd,' a volcanic rocks discrimination diagram (Winchester and Floyd, 1977), in which the samples are classified as rhyodacite/dacite of calc-alkaline signature; and 'e,' a spider diagram of the REE normalized to the chondrite (Boynton, 1984), which indicates the crystal-tuff compositional field overlap with the MFV and volcaniclastic greywackes (Pr - Proterozoic; MPr - Mesoproterozoic).

A1.4.3 Tombador Formation sandstone U-Pb detrital zircon dating

To identify the ca. 1.4 Ga zircon age cluster (U-Pb) in the Tombador Fm. detrital zircon age record and to constrain the vertical distribution of the volcanic and detrital material, we analyzed four sandstone samples from distinct stratigraphic levels. Two of these samples were from the lower section in the Tombador Fm. (stratigraphically below the crystal-tuff level), and two were from the same stratigraphic level as the crystal-tuff (from the upper section in the Tombador Fm.).

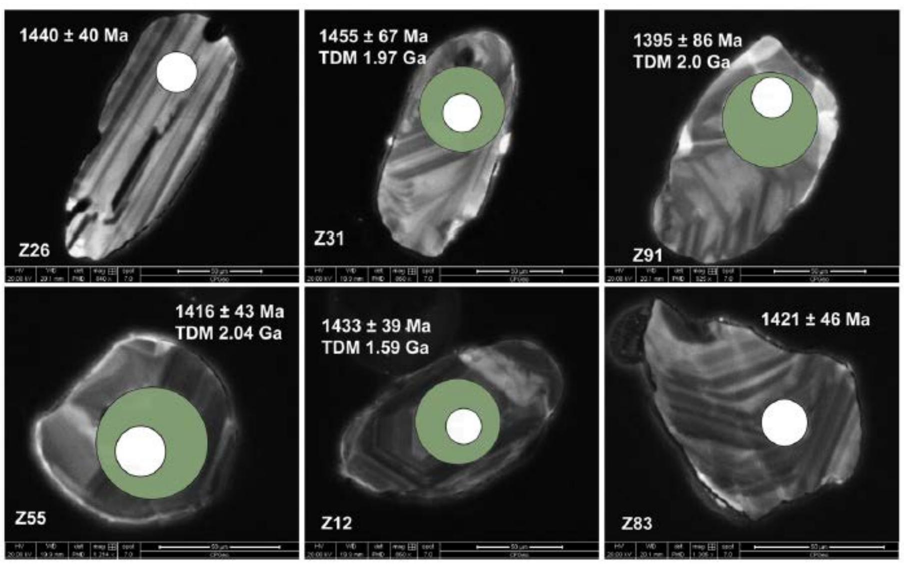

Fig. A5: Cathodoluminescence images of the youngest zircon grains from the crystal-tuff sample. These images are of zoned crystals. Crystals Z26 and Z83 are broken parts of major zircon grains, and grain Z55 is rounded. White and green circles represent the areas that were abraded by the laser probe for the U-Pb and Lu-Hf analysis, respectively.

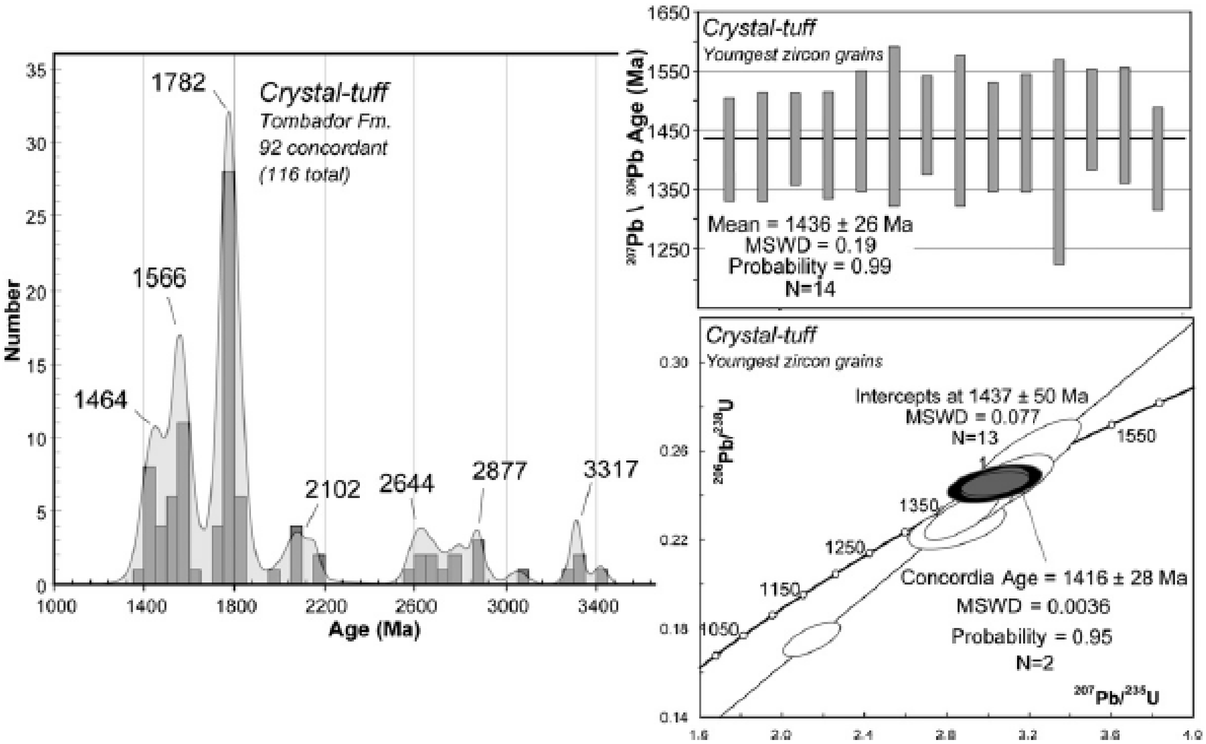

Fig. A6: Histogram and relative probability plot of the 92 concordant zircon grains from the Tombador Fm. crystal-tuff sample. The insets show the concordia diagram (below) and the weighted mean of the Pb/Pb age (above) for the crystal-tuff youngest zircon grains. In the concordia diagram, the two dark gray ellipses present a concordia age of 1416 ± 28 Ma (black ellipse). The white ellipses align through the origin and 1437 ± 50 Ma.

Samples from the lower section in the Tombador Fm. were collected at the Ituaçú Syncline (Barra da Estiva town; F4 sample, UTM coordinates 249.931 mE, 8.485.498 mN) and Pai-Inácio Anticline (Lençóis town; F14 sample, UTM coordinates 234.407 mE, 8.620.342 mN; Fig. A1b and supplementary kml file). Both samples (F4 and F14) yielded inherited zircon grains in three well-defined age clusters, including the Paleoarchean (3.6 - 3.2 Ga), Neoarchean (2.8 - 2.5 Ga) and Paleoproterozoic (2.5 - 1.6 Ga) age clusters. Sample F4 presents 60 concordant zircon grains from 93 analyzed grains, and sample F14 presents 54 concordant zircon grains from 90 analyzed grains (Fig. A7).

The sandstone samples from the upper Tombador Fm. were collected at the Tombador Range (P1 sample, UTM coordinates 317.984 mE, 8.772.976 mN; P2 sample, UTM coordinates 297.207 mE, 8.708.140 mN; Fig. A1b and supplementary kml file). Sample P1 contained 60 concordant zircon crystals from 92 analyzed crystals. The two main zircon age populations were between 3.50 and 3.10 Ga (Paleoarchean; 26 zircon grains) and 2.20 and 1.99 Ga

(Rhyacian/Orosirian; 18 zircon grains). The other populations were Mesoproterozoic (Calymmian, 1.6 - 1.4 Ga; and Ectasian, 1.4 - 1.2 Ga; six zircon grains), Neoarchean (2.8 - 2.5 Ga; five zircon grains) and Statherian (1.8 - 1.6 Ga; three zircon grains; Fig. A7). Sample P2 yielded 57 concordant zircon grains from 67 analyzed grains. The main age population occurred between 2.15 and 2.00 Ga (Rhyacian/Orosirian; 22 zircons), followed by the Neoarchean (2.8 - 2.5 Ga) and Siderian (2.5 - 2.3 Ga; 16 zircons), Mesoarchean (3.2 - 2.8 Ga; four zircons), Statherian (1.8 - 1.6 Ga; three zircons), Calymmian (1.6 - 1.4 Ga; three zircons) and Paleoarchean (3.6 - 3.2 Ga; two zircons; Fig. A7) ages. Unlike the sandstone samples from the lower Tombador Fm. (F4 and F14), which presented only inherited zircon grains, the age pattern in the upper section samples (P1 and P2) were similar to the age pattern in the crystal-tuff sample, presenting abundant Mesoproterozoic (Calymmian, 1.6 - 1.4 Ga, and Ectasian, 1.4 - 1.2 Ga) zircon grains (Figs. 6 and 7).

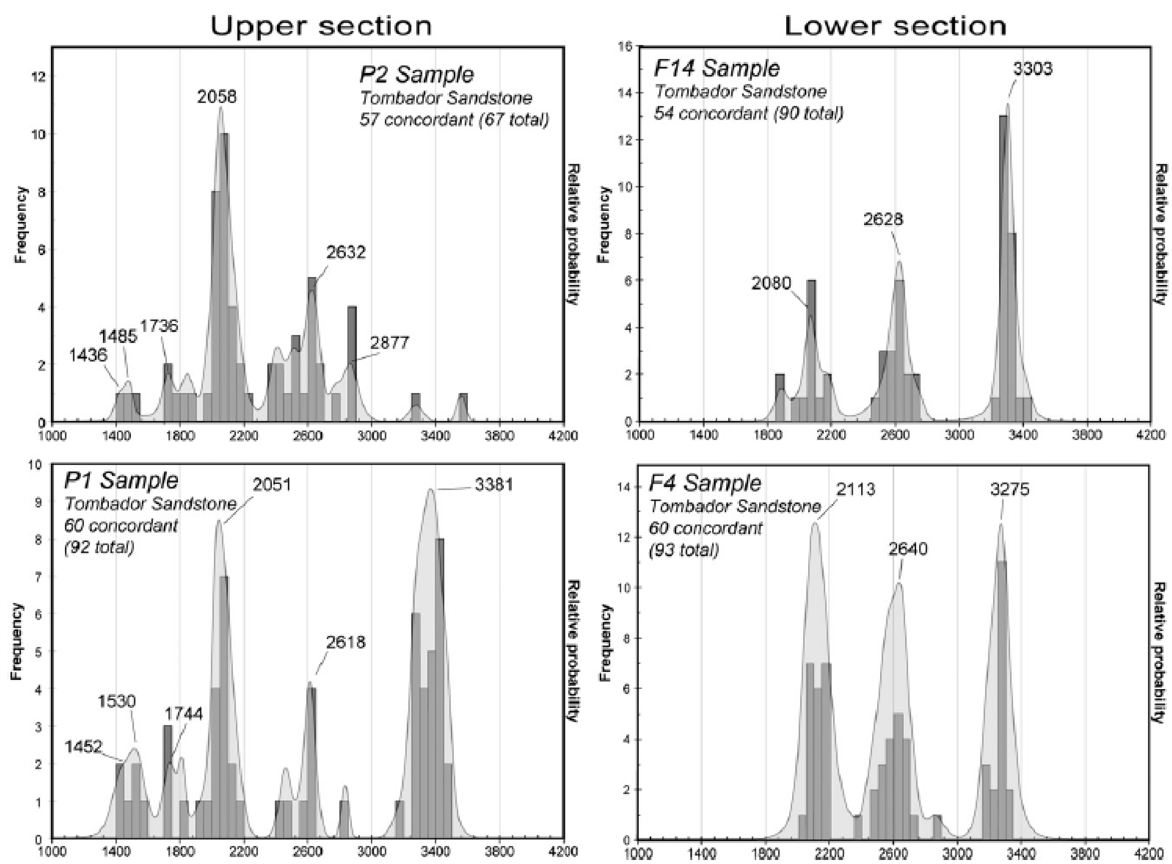

Fig. A7: Histogram and relative probability plots for the sandstone samples in the Tombador Fm. lower (F4 and F14) and upper sections (P1 and P2). The lower Tombador Fm. sandstone samples present only basement zircon grains. The upper Tombador Fm. sandstone samples present basement and Mesoproterozoic zircon grains.

A1.4.4 Tombador and Sopa-Brumadinho Formations Lu-Hf zircon data

We analyzed zircon grains from the Upper Espinhaço tuffaceous conglomerate matrix (Sopa-Brumadinho Fm.) and from the Middle Espinhaço crystal-tuff (Tombador Fm.) using the Lu-Hf method, to establish the crustal residence time of the zircons. A total of 35 zircon grains were analyzed, including grains from the Tombador Fm. crystal-tuff and the Sopa Brumadinho Fm. tuffaceous conglomerate matrix (for the U-Pb zircon ages in the SB Fm., see Chemale et al., 2012 and supplementary material U-Pb and Lu-Hf zircon data.xls).

The Lu-Hf depleted mantle model ages (TDM) of the Tombador Fm. crystal-tuff zircon grains varied between 3.6 and 1.8 Ga, and the εHf values varied from -8.5 to 8. The youngest zircon crystals (according to their U-Pb ages) had TDM of between 2.07 and 1.95 Ga and εHf values of between -5.5 and -1.5 (Fig. A8). The TDM of the Sopa-Brumadinho Fm. tuffaceous conglomerate matrix zircon grains varied between 3.4 and 1.5 Ga, and the εHf values varied between -27.2 and 4.7. The youngest zircon grains had TDM that were mainly younger than 1.9 Ga and εHf values that were less than 2 (Fig. A8). However, these grains generally had more negative εHf values.

A1.5. Discussion

Our geochronological data can be coupled with geochemical, sedimentological and stratigraphic data to determine the geologic history of the ES. In the following discussion, we present an updated chronostratigraphic chart for the ES and discuss its implications for the tectonic evolution of the Congo-São Francisco Craton.

A1.5.1 The depositional age of the Tombador Formation and the nature of the volcanic and detrital contributions

A1.5.1.1 Crystal-tuff

The crystal-tuff samples were composed of an assemblage of juvenile magmatic components mixed with varying proportions of detrital siliciclastic materials. The tuffaceous materials were well preserved on the flood-plain with little transport or reworking.

The major and trace element compositions of the crystal-tuff overlap with the MFV and volcaniclastic greywacke compositions with negative Sr, Co, Nb and Ta anomalies relative to the UCC (Fig. A4c). The strong depletion of CaO and Na2O potentially resulted from post-depositional weathering. In addition, the Zr, Hf, La and Th enrichment potentially resulted from an old, recycled component, which was identified based on the presence of recycled quartz grains and from the detrital zircon age spectra (Figs. 3, 6 and 7).

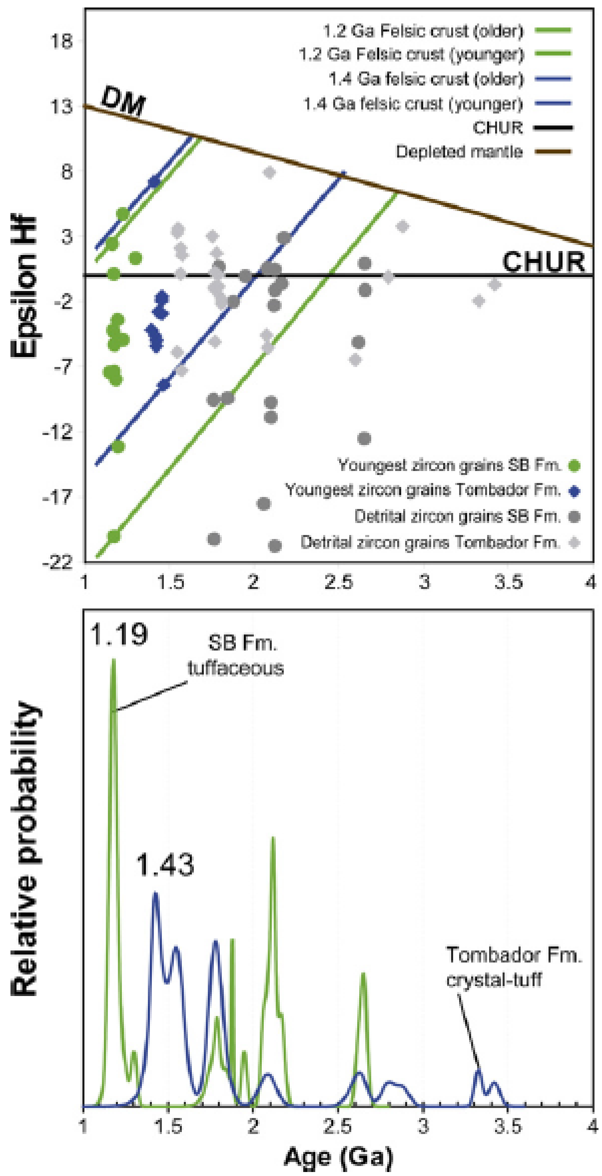

Fig. A8: Epsilon Hf versus U-Pb age for selected zircon grains from the Sopa-Brumadinho (SB; Southern Espinhaço) and Tombador Fms. (Chapada Diamantina) tuffaceous rocks. The below graphic represents the U-Pb zircon age probability plot of the two samples.

The REE indicated a felsic volcanic source composition rather than a normal cratonic sandstone composition which is depleted in REE relative to the chondrite (Fig. A4e). The

Winchester and Floyd (1977) scheme indicated that the source for the felsic volcaniclastic material may have been calc-alkaline (Fig. A4d).

The crystal-tuff zircon age distribution comprises abundant Statherian (1.8 - 1.6 Ga) and Calymmian (1.6 - 1.4 Ga) zircon grains with minor contributions of Mesoarchean (3.2 - 2.8 Ga), Neoarchean (2.8 - 2.5 Ga) and Paleoproterozoic (Rhyacian, 2.3 - 2.05 Ga) source rocks (Fig. A6). The youngest zircon grains from the crystal-rich volcaniclastic layers were zoned and elongated crystals. Some of these crystals were broken pieces of major elongated crystals (Fig. A5). These crystals yielded a weighted mean 207Pb/206Pb age of 1436 ± 26 Ma (14 zircon grains), and two concordant zircons yielded an age of 1416 ± 28 Ma (Fig. A6 and supplementary material). The best age estimate for the crystal-tuff deposition is approximately 1420 Ma. The zircon grains formed between 1.40 and 1.46 Ga had Hf model ages (TDM) from 2.38 to 1.59 Ga, and εHf values from -12.97 to 7.43. The most abundant population had a TDM of approximately 2.0 Ga and εHf values of between -4.18 and -1.62 (Fig. A8). Thus, the youngest zircon population (U-Pb ages) contains juvenile and re-melted zircon crystals, that were formed ca. 1.5 Ga, 1.7 - 1.8 Ga, 2.1 - 2.2 Ga or during the Archean Era (4.0 - 2.5 Ga).

A1.5.1.2 Sandstone detrital zircon grains

The Tombador Fm. lower section contains only inherited zircons, with ages that fall within three well-defined clusters. These clusters represent the basement rocks of the Chapada Diamantina (Barbosa and Sabaté, 2004) and include the following: Paleoarchean (3.6 - 3.2 Ga), Neoarchean (3.2 - 2.8 Ga) and Paleoproterozoic (2.5 - 1.6 Ga; Fig. A7). Based on the age ranges observed in the detrital zircons, the most likely source regions include the Gavião Block and the Itabuna-Salvador-Curaçá Belt of the São Francisco Craton basement.

In the upper section of the Tombador Fm., the pattern of inheritance changes as there is an influx of Mesoproterozoic-aged zircons. The upper Tombador Fm. detrital zircons yielded varying proportions of basement (older than 1.8 Ga) and Mesoproterozoic zircon grains (Fig. A7). This distribution pattern is very similar to the crystal-tuff zircon age distribution. The ca. 1.7 and 1.5 Ga detrital zircon grains represent recycling of the ES lower sections, the Rio dos Remédios (ca. 1.7 Ga) and the Paraguaçú groups (ca. 1.5 Ga; see discussion section 5.3). The youngest zircon grains from the upper Tombador Fm. crystal-tuff and sandstone samples (P1 and P2) were between 1.4 and 1.45 Ga (Figs. 6 and 7).

The Tombador Fm. unconformably overlies the Açuruá Fm. (i.e., the top of the Paraguaçú Group). The low-angle unconformity that separates these formations and the well-documented paleocurrent changes from eastward in the Açuruá Fm. to westward in the Tombador Fm. (Pedreira, 1994; Pedreira and DeWaele, 2008) indicate a tectonic tilt of the Congo-São Francisco Craton from anomalous topography east of Chapada Diamantina. The addition of Mesoproterozoic zircon grains in the upper Tombador Fm. detrital zircon assemblage (relative to the lower Tombador Fm.) support the source area change (Fig. A7). Based on the westward sediment transport of the Tombador Fm. (Pedreira, 1994; Pedreira and De Waele, 2008), we suggest that the volcanic source area was located east of the Chapada Diamantina, most likely in the Congo Craton.

An important regional intraplate extensional regime was established at ca. 1375 Ma in the Congo Craton. This extensional regime was associated with voluminous S- and A-type granitoids and mafic-ultramafic complexes that were found in the Karagwe-Ankolian Belt (KAB) east of the Congo Craton (Tack et al., 2010; Fernandez-Alonso et al., 2012, and references therein) and in the Kunene complexes and related granites west of the Congo Craton (Ernst et al., 2013b, and references therein). Both events may have triggered the Congo-São Francisco paleoplate tilt and volcanism.

The syn-sedimentary volcanism at ca. 1.42 Ga has not been recorded in the ES units. However, Chemale et al. (2012) determined the ca. 1.4 Ga detrital zircon ages in the Conselheiro Mata Group in the Southern Espinhaço range. This group is coeval with the Cabloco Fm., which overlies the Tombador Fm. (see discussion section 5.3 and Fig. A9).

A1.5.2 The source for the Tombador and Sopa-Brumadinho Formations zircon crystals

The Tombador and Sopa-Brumadinho Fms. tuffaceous materials had different crystallization ages (ca. 1.4 and ca. 1.2 Ga, respectively). To distinguish their source, we compared the Lu-Hf data of the volcanic and detrital zircon grains.

The Lu-Hf TDM for the zircon grains in the crystal-tuff sample (Tombador Fm.) were between 3.6 and 1.8 Ga, and the εHf values were between -8.5 and 8. However, the youngest zircon crystals (according to their U-Pb ages) had TDM that were predominantly between 2.07 and 1.95 Ga and εHf values that were between -5.5 and -1.5 (Fig. A8). The TDM of the Sopa-Brumadinho Fm. zircon grains varied between 3.4 and 1.5 Ga, and the εHf values varied between -27.2 and 4.7. The youngest zircon grains had TDM that were predominantly younger than 1.9 Ga and εHf values that were less than 2 (Fig. A8). However, these grains generally had more negative εHf values.

These data suggests that different magma sources contributed to the ca. 1.4 Ga Tombador Fm. crystal-tuff and to the ca. 1.2 Ga Sopa-Brumadinho Fm. tuffaceous conglomerate matrix. Further studies may address the volcanic material sources of the Middle and Upper Espinhaço Basin cycles.

A1.5.3. The Espinhaço Supergroup and regional correlation

The subsidence, uplift, eustasy and sedimentation rates in the Paleo- to Mesoproterozoic intracratonic basins were likely similar to the uplift, eustasy and sedimentation rates that have been observed in modern intracratonic basins. Thus, Precambrian intracratonic basins contain unconformity-bound sequences that were deposited over several million years. Lacunae present in these sequences may be associated with continental uplift due to major tectonism.

Traditionally, the Paleo- to Mesoproterozoic ES units were treated as continuous deposits from 1.7 to 0.9 Ga (e.g., Martins-Neto, 2000). Gaps in the sedimentary record of the long-lived Paleo- to Mesoproterozoic intracratonic basins have been identified, by using U-Pb geochronology (Fernandez-Alonso et al., 2012; Ribeiro et al., 2013), especially regarding the ES (Danderfer et al., 2009; Chemale et al., 2012; Silveira et al., 2013; Santos et al., 2013).

A1.5.3.1. Lower Espinhaço Basin (Statherian IF basin)

The Lower Espinhaço sequence commenced immediately after the Transamazonian/Eburnean Cycle (2.2 to 2.0 Ga) and following intraplate rifting of the Congo-São Francisco Craton (e.g., Brito Neves et al., 1979).

The sedimentary and volcanic rocks from the first basinal cycle were deposited from 1.80 Ga to 1.68 Ga and are well exposed in Southern Espinhaço, Northern Espinhaço and Chapada Diamantina as an internal fracture basin (IF, after Kingston et al., 1983). The Statherian section includes the basal portion of the Diamantina Group in Southern Espinhaço, the Oliveira dos Brejinhos Group in Northern Espinhaço and the Rio dos Remédios Group at Chapada Diamantina (Fig. A9; Martins-Neto, 2000; Pedreira and DeWaele, 2008; Danderfer et al., 2009; Chemale et al., 2012; Santos et al., 2013).

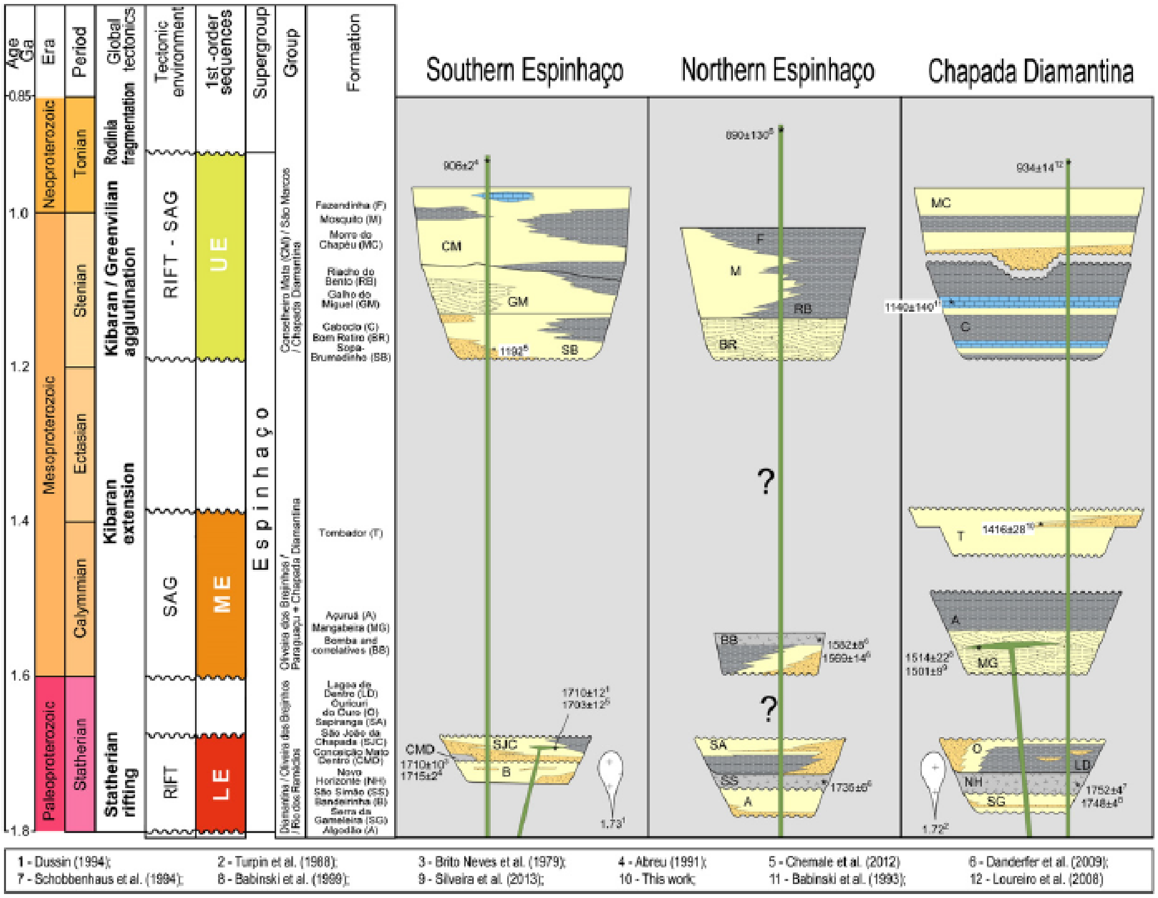

Fig. 9: Regional correlation of the Espinhaço Supergroup from the Statherian to Tonian Periods, showing basin type, depositional environments, unconformities, formal lithostratigraphic hierarchical units, first-order sequences and main global tectonic events (modified after Pflug, 1965; Pedreira, 1994; Schobbenhaus, 1996; Martins-Neto, 2000; Danderfer and Dardenne, 2002; Guimarães et al., 2005; Loureiro et al., 2008; Pedreira and De Waele, 2008; Danderfer et al. 2009; Alkmim and Martins-Neto, 2012; Santos et al., 2013).

In Southern Espinhaço, the Statherian rifting event is represented by typical rift deposits that contain alluvial fan conglomerates, braided fluvial and eolian sandstones (from the Bandeirinha and São João da Chapada Fms.; Santos et al., 2013) and bimodal magmatism from alkaline to peralkaline acid and SiO2-undersaturated potassic alkaline compositions (Chemale et al., 2012, and references therein). The acid-alkaline magmatism in Southern Espinhaço is represented by Conceição do Mato Dentro rhyolite and Borrachudo-type plutonic bodies that were crystallized between 1.75 and 1.70 Ga with an Archean crustal residence time (Nd model ages approximately 3.0 to 2.8 Ga; Brito Neves et al., 1979; Machado et al., 1989; Abreu, 1991; Dussin, 1994; Silva et al., 1995). This acid magmatism occurs as part of (or is tectonically imbricated with) the São João da Chapada Fm. (Fig. A9). This acid magmatism is thought to result from the melting of lower anhydrous crustal sources that have alkaline to peralkaline signatures (Chemale et al., 1998). The middle portion of the São João da Chapada Fm. is cut by SiO2-undersaturated and highly K-alkaline magma (hematite-phyllite) with ages between 1.72 and 1.70 Ga (Dussin, 1994; Chemale et al., 2012).

A similar section can be observed in Northern Espinhaço and at Chapada Diamantina. The basal section of the Lower Espinhaço Basin contains eolian and alluvial sediments from the Algodão and Serra da Gameleira Fms. These sediments are interlayered and are overlain by the alkaline acid lavas and tuffs of the São Simão and Novo Horizonte Fms. (Fig. A9; Guimarães et al., 2005; Alkmim and Martins-Neto, 2012). This acid magmatism was dated between 1.75 and 1.73 Ga by Schobbenhaus et al. (1994), Babinski et al. (1999) and Danderfer et al. (2009). The Lagoa Real alkaline-to-peralkaline pluton, which occurs south and southwest of Chapada Diamantina, is dated at 1724 ± 5 Ma (Turpin et al., 1988). This pluton is interpreted as cogenetic with the magmatism of the Oliveira dos Brejinhos and Rio dos Remédios groups (Fig. A9).

These units are succeeded by continental alluvial, fluvial, eolian and lacustrine sediments in the Pajeú and Sapiranga Fms. in Northern Espinhaço, and in the Lagoa de Dentro and Ouricuri do Ouro Fms. at Chapada Diamantina (Fig. A9; Guimarães et al., 2005; Alkmim and Martins-Neto, 2012).

Basinal development was associated with a regional extensional event that occurred after the orogenetic completion of the Transamazonian/Eburnean cycle collage of the Columbia Supercontinent (Rogers and Santosh, 2002; Meert, 2012; Ernst et al. 2013b). This widespread acid alkaline magmatism may be related to plume activity during the late Paleoproterozoic (Statherian).

A1.5.3.2. Middle Espinhaço Basin (Calymmian rift-sag basin)

The stratigraphic units of the Middle Espinhaço Basin were deposited between 1.60 and 1.38 Ga. These sequences are exposed only in Northern Espinhaço and at Chapada Diamantina as a rift-sag basin. Although it was identified detrital zircon ages between 1.60 and 1.38 Ga in the Upper Espinhaço Basin units in the Southern Espinhaço range (Chemale et al., 2012), the Calymmian sedimentation is not preserved in this region.

In Northern Espinhaço, the rifting episode is represented by the deposition of alluvial fans, braided fluvial, eolian, deltaic, lacustrine and volcanic packages of the Bomba Fm. and overlying sediments. The Bomba Fm. occurs at the top of the Middle Espinhaço section in the Northern Espinhaço and is composed of intermediate to acid volcanic lavas that were formed between 1582 ± 8 Ma and 1569 ± 14 Ma (Fig. A9; Danderfer et al., 2009).

At Chapada Diamantina, the Middle Espinhaço initiated with low-stand, alluvial-fluvial and eolian sedimentation of the Mangabeira Fm. and was followed by transgressive shallow-marine to high-stand deltaic sediments of the Açuruá Fm. (Guimarães et al., 2005). A tholeiitic mafic dyke swarm, which intruded the basal portion of the Mangabeira Fm., was formed at 1514 ± 22 Ma (Babinski et al., 1999) and at 1501 ± 9.1 Ma (Silveira et al., 2013). This intrusion constrains the minimum depositional age of this unit. These lithological units are interpreted as typical sag sequences (Fig. A9).

The overlying units that belong to the Tombador Fm. (where our crystal-rich volcaniclastic rocks were dated at 1436 ± 26 Ma) represent a new sag phase. The Tombador Fm. was deposited with an angular unconformable relationship with the underlying Açuruá Fm. and with a significant change of source area (Pedreira, 1994; Pedreira and De Waele, 2008). The volcanic activity, angular unconformity and sedimentary source direction change for the fluvial environment suggested that intraplate tectonic movement occurred before and/or during the deposition of the Tombador Fm. (see discussion section 5.1).

This new basin cycle (1.60 to 1.38 Ga) in the intraplate setting of the Congo-São Francisco Craton exhibited a significant increase in sedimentary input and coeval magmatism at 1.4 Ga (the top of Tombador Fm.). This basinal cycle potentially resulted from extensional tectonics at the margin of the Congo-São Francisco Craton (De Waele et al., 2008; Tack et al., 2010; Ernst et al., 2013b).

A1.5.3.3. Upper Espinhaço Basin (Stenian-Tonian rift-sag basin)

The Upper Espinhaço Basin is exposed in Southern and Northern Espinhaço and at Chapada Diamantina. This sequence was deposited between 1.19 and 0.9 Ga (Fig.A 9).

In Southern Espinhaço, the basal section of the Upper Espinhaço units consists of diamond-bearing Sopa-Brumadinho Fm. (approximately 1.19 - 1.17 Ga) that unconformably overlies the São João da Chapada Fm. (approximately 1.70 Ga) at the top of the Lower Espinhaço

Basin (Fig. A9; Chemale et al., 2012; Santos et al., 2013). Chemale et al. (2012) observed conglomerate layers with a greenish matrix in the Sopa-Brumadinho Fm. This matrix possesses an alkali acid chemical signature. The youngest zircon population of the greenish matrix is dated at 1192 Ma and is estimated to be the age of the volcanic event. This youngest zircon population established the maximum depositional age for the Upper Espinhaço sequence (Chemale et al., 2012). The zircon grains have Hf model ages of between 2.7 and 1.52 Ga and εHf values of between -27.2 and 4.7 (see section 5.2). These values demonstrate that the zircons have juvenile and recycled signatures (Fig. A8). The Sopa-Brumadinho Fm. is overlain by the Galho do Miguel Fm. eolian-marine sediments and the Conselheiro Mata Group shallow marine platform sediments (Fig. A9; Martins-Neto, 2000). The Upper Espinhaço Basin accounts for more than 70% of the total stratigraphic thickness in Southern Espinhaço.

The coeval section of the Conselheiro Mata Group is well exposed at Chapada Diamantina and is represented by shallow marine sedimentation (tidal and supratidal sediments) in the Caboclo and Morro do Chapéu Fms. (Fig. A9; Pedreira, 1994; Pedreira and De Waele, 2008). The Caboclo carbonates were dated by the Pb-Pb method at 1140 ± 140 Ma (Babinski et al., 1993). We interpreted this marine sequence as transgressive and paraconformable with underlying units of the Tombador Fm.

In the Northern Espinhaço, the basal units comprise thick packages of eolian sediments that belong to the Bom Retiro Fm. (Fig. A9; Loureiro et al., 2008). The transgressive marine sediments are represented by the dominant pelitic section of the Riacho do Bento (base) and Fazedinha Fms. (top), which are interlayered with sandstone and pelites of the Mosquito Fm. (Fig. A9; Loureiro et al., 2008; Alkmim and Martins-Neto, 2012). These units are regionally correlated with the Conselheiro Mata Group and the Cabloco and Morro do Chapéu Fms. (Southern Espinhaço and Chapada Diamantina, respectively; Fig. A9).

The rifting of the Congo-São Francisco Craton is directly linked to the fragmentation of the Rodinia Supercontinent, and started at 0.9 Ga with the emplacement of mafic tholeiitic dyke swarms and gabbroic bodies (Silva et al., 1995; Rosset et al., 2007; Evans et al., 2010; Silveira et al., 2013). These magmatic bodies intruded the entire Espinhaço sequences and constrain the minimum age for the ES deposition (Fig. A9). In Southern Espinhaço, this event was dated to 933 ± 20 Ma and 906 ± 2 Ma (Machado et al., 1989; Abreu, 1991; Dussin and Chemale, 2011; Supplementary Figure 10), and at Chapada Diamantina the dyke swarms were dated to 934 ± 14 Ma (Loureiro et al., 2008). The Northern Espinhaço project (Danderfer et al., 2009) dated the mafic dyke swarms that cut units of the Lower Espinhaço sequence. These authors used only one zircon to calculate a magmatic age of 854 ± 23 Ma (MSWD = 6.7; Danderfer et al., 2009). However, we recalculated the age using all three Neoproterozoic dated zircon crystals. These crystals were somewhat discordant, which resulted in an age of 890 ± 130 Ma (Fig. A9).

Here, the Upper Espinhaço was hypothesized to result from intraplate sedimentation with a strong influence from the late Kibaran or Grenvilian events and resulting from the compressional tectonism at the margins of the Congo Craton (as described by Kokonyangi et al., 2006; De Waele et al., 2008; and Fernandez-Alonso et al., 2012). The final basinal cycle that was observed in the ES was likely resulted from events that were associated with the assembly of Rodinia. This cycle is similar to the Neopaleozoic sedimentation cycles that were described for the Central Australian Basins during the Alice Spring Orogeny (Lindsay and Leven, 1996; Haddad et al., 2001; Lindsay, 2002) and for the Paraná Basin (South America) during the Gondwanides (Milani and Ramos, 1998), when Pangea assembled.

A1.6. Conclusions

Our U-Pb and Lu-Hf zircon data provided important constraints regarding the Paleo- and Mesoproterozoic sedimentary evolution of the Congo-São Francisco Craton as part of the Columbia-Rodinia supercontinental cycle. The U-Pb zircon age of 1436 ± 26 Ma obtained from the crystal-tuff in the upper section of the Tombador Fm. confirms the presence of the Middle Espinhaço Basin in the São Francisco Craton with underlying units of the Mangabeira and Açuruá Fms. The detrital zircon grains indicated that a shift occurred in the source area near the top of the Tombador Fm. The lower Tomador Fm. contains only inherited zircon grains. However, the upper section contains the basement (older than 1.8 Ga) and Mesoproterozoic grains. The major contributions corresponded to the main cycles of accretion and reworking in the Congo-São Francisco Craton basement rocks and occurred between 3.4 and 3.2 Ga, 2.8 and 2.5 Ga and 2.1 and 1.9 Ga. In addition, two important zircon age populations (between 1.8 and 1.7 and 1.6 and 1.5 Ga) were identified in the detrital record and were related to the reworking of the Lower Espinhaço Basin materials.

The 1.4 Ga Tombador Fm. crystal-tuff zircon Lu-Hf model ages (TDM) were primarily older than 2.0 Ga. However, the zircon grains from the 1.19 Ga Sopa-Brumadinho Fm. tuffaceous conglomerate matrix had a TDM of less than 1.9 Ga. This result suggests that different magmatic sources contributed the volcanic material.

A correlation between the ES units in the São Francisco Craton in the Southern and Northern Espinhaço ranges and at Chapada Diamantina is presented here. The Lower Espinhaço Statherian rift basin (1.80 to 1.68 Ga) is well recorded in the three regions and is represented by bimodal magmatism and by alluvial to fluvial sediments. The Middle Espinhaço was deposited during the Calymmian period (1.6 - 1.4 Ga) as a (rift-)sag basin with eolian, fluvial-deltaic and marine sediments. These deposits are only exposed at Chapada Diamantina and in Northern Espinhaço. The last basinal cycle, the Upper Espinhaço Basin, formed during the Stenian-Tonian (1.19 - 0.90 Ga) as a rift-sag basin and was exposed in three regions.

Thus, the time span from 1.80 to 0.90 Ga was recorded in the craton interior based on three first-order intracratonic basin development cycles that were limited by major unconformities and related to global tectonics. The first cycle is related to the intraplate geodynamics that occurred after the collage of the Columbia Supercontinent in the Transamazonian/Eburnean orogenies. The second basin cycle, the Middle Espinhaço, was strongly influenced by the extensional stages of the Karagwe-Ankolian Belt and the Kunene Complex at the southeastern and western margins of the Congo Craton, respectively (Tack et al., 2010; Fernandez-Alonso et al., 2012; Ernst et al., 2013b). The third basin cycle, the Upper Espinhaço, is directly connected to the Grenvillian/Late Kibaran event during the formation of the Rodinia Supercontinent (De Waele et al., 2008).

The aggregation and dispersal of supercontinents have the potential to create conditions that affect the development and preservation of long-lived intracratonic basins. This scenario was recognized during the formation of the Pangea Supercontinent, whose dispersed pieces preserved several intracratonic basins, such as the Paraná, Central Australian, Karoo and North American basins. Recognizing chronocorrelate depositional cycles in the Precambrian intracratonic basin can be useful in testing supercontinental reconstructions (i.e., Columbia/Rodinia). The detailed petrological, sedimentological-stratigraphic and isotopic studies of the Paleo- to Mesoproterozoic intraplate basins in the Congo-São Francisco Craton, the Tocantins Province and the Amazonian Craton of the South American Platform may provide important insights into the supercontinent theory.

A1.7. Acknowledgements

FG would like to thank CNPq (grant 141182/2010-5) for financial support for field work and analysis. L. S. Born, C. Born and M. B. Bálico are thanked for helping with the stratigraphic analysis and collecting samples and J. Gualberto, L. Ferreira and E. Zacchi are thanked for helping with sample preparation and analysis. We would like to acknowledge the reviewer and the editor Prof. Joseph Meert for their comments and suggestions that significantly improved the original version of the manuscript.

A1.8. Appendix A. Supplementary data (SD)

Supplementary data associated with this article can be found in the online version, at http://dx.doi.org/10.1016/j.gr.2013.10.009. These data include Google maps of the most important areas described in this article.

A.1.8.1. SDA1. Supplementary Data - Concordia diagram for the Pedro Lessa dyke swarm

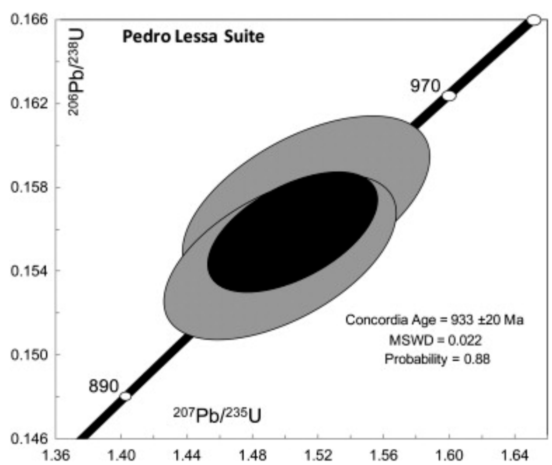

Fig. SDA1: Concordia diagram for the Pedro Lessa dyke swarm, which intrudes the Espinhaço Supergroup entire section in the Southern Espinhaço range (data from Dussin and Chemale, 2011; Supplementary material 3).

A.1.8.2. SUPPLEMENTARY MATERIAL 1 (SM1): Lithofacies analysis of the Tombador Fm. exposed in the Ribeirão de Baixo section.

SM1.1 Lithofacies analysis

The vertical description of the outcrop along the Ribeirão de Baixo river was based on the definition of small-scale lithofacies by Miall (1996), with some modifications and additions (Table SM1.1). The lithofacies were combined into larger-scale facies associations.

The outcrop is dominated by lenticular to slightly tabular beds of very coarse to medium-grained sandstones, pebbly conglomerates, massive mudstones and minor crystal-rich volcaniclastic layers (Figs. A1.2, A1.3 and SM1.1). The sandstones are well cemented and exhibit trough cross-bed to planar stratification; granular to pebble materials are dispersed in the matrix. The southward paleocurrent direction is consistent with other measures throughout the Sincorá Range (Magalhães, *personal communication*).

SM1.1.1 Lithofacies association

Two main lithofacies associations are identified in the profile: i) braided fluvial and ii) tidal bars.

SM1.1.1.1 Braided fluvial flood association

The braided fluvial flood lithofacies association occurs in five fining upward cycles composed of amalgamated, poorly channelized sandstone beds interbedded with pebbly matrix supported conglomerates and laminated mudstones.

The conglomerate beds are less than 40 cm thick, matrix-supported, composed of rounded quartzite pebbles and angular to subrounded pebbles and granules of dark volcanic rocks (facies Gt) (Figs. 2 and 3).

While highly cemented, the poorly channelized sandstones are mature, very coarse to medium-grained quartz-arenites and generally exhibit trough cross-stratification (facies St) (Fig. SM1a).

The sandstone beds less than 1 m thick have a lenticular to slightly tabular geometry and can be followed laterally for several meters. The massive aspect and planar-to-through cross-stratified sandstone is abundant throughout these sandstone bodies (facies Sm, Sp and St). Both tabular and lenticular sandstone bodies have sharp contact with the over- and underlying conglomerates or mudstones. The sandstones contain granules and pebbles oriented along the stratification or at the base of a depositional cycle; many also have volcanic origins (Fig.

SM1a). The paleocurrents measured from sandstones beds exhibit a preferential depositional direction towards the SW.

Table SM1.1: Lithofacies identified in the Tombador Formation at the Ribeirão de Baixo section (modified from Miall, 1996).

Facies code	Facies	Sedimentary structure	Intepretation (process)
Gt	Matrix-suported gravel	Trough cross-beds, normal grading	Migration of sinous crest gravel bars
St	Sand, fine to very coarse; may be granular	Trough cross-beds	Migration of sinuous crest subaqueous dune (3D)
St	Sand, fine to very coarse; may be granular	Trough cross-beds, tidal bundles, mud couple	Migration of sinuous crest subaqueous dune (3D) on tide regime
Sp	Sand, fine to coarse, may be pebbly	Planar cross-beds	Migration of straight crest subaqueous bedforms (2D)
Sl	Sand, very fine to coarse	Low angle lamination (<15^{o}) cross-bed	Plane-bed flow, filling of scour fills, atenuated dunes (transitional flow regime)
Sm	Sand, fine to granular	Massive, or faint lamination	Sediment flow deposit
Fm	Silt or mud	Massive	Deposition from suspension or from very low currents
Fl	Silt or mud	Fine lamination, very small ripples	Deposition from suspension or from very low currents

The mudstones are red to dark brown, massive to laminated and interbedded with medium to coarse-grained sandstone or thin conglomerate beds (Fig. SM1b). The thickest bed is 1.2 m thick and contains linsen and pseudonodules, caused by overload towards its base and desiccation cracks, rain drops and ripples on its top (Fig. SM1c and d). The mudstones (facies Fl) are strongly recrystallized but still exhibit primary sedimentary structures.

The green crystal tuff horizons are massive (facies Fm), are only up to 20 cm thick and laterally exhibit fairly constant thickness. They are characterized by sharp planar contacts and interbedding with fine-grained sandstone layers and mudstones (Fig. A3). The tuff layers (facies Fl) interbedded with red fine-grained sandstone can be up to 60 cm thick.

The sandstone beds exhibit evidence of high-energy unconfined fluvial bar deposits. They are interpreted as downstream accretion bars with a consistent southward paleoflow direction. The mudstones are interpreted to represent muddy floodplains. The desiccation crack and rain drop evidence suggests semiarid to arid climate conditions.

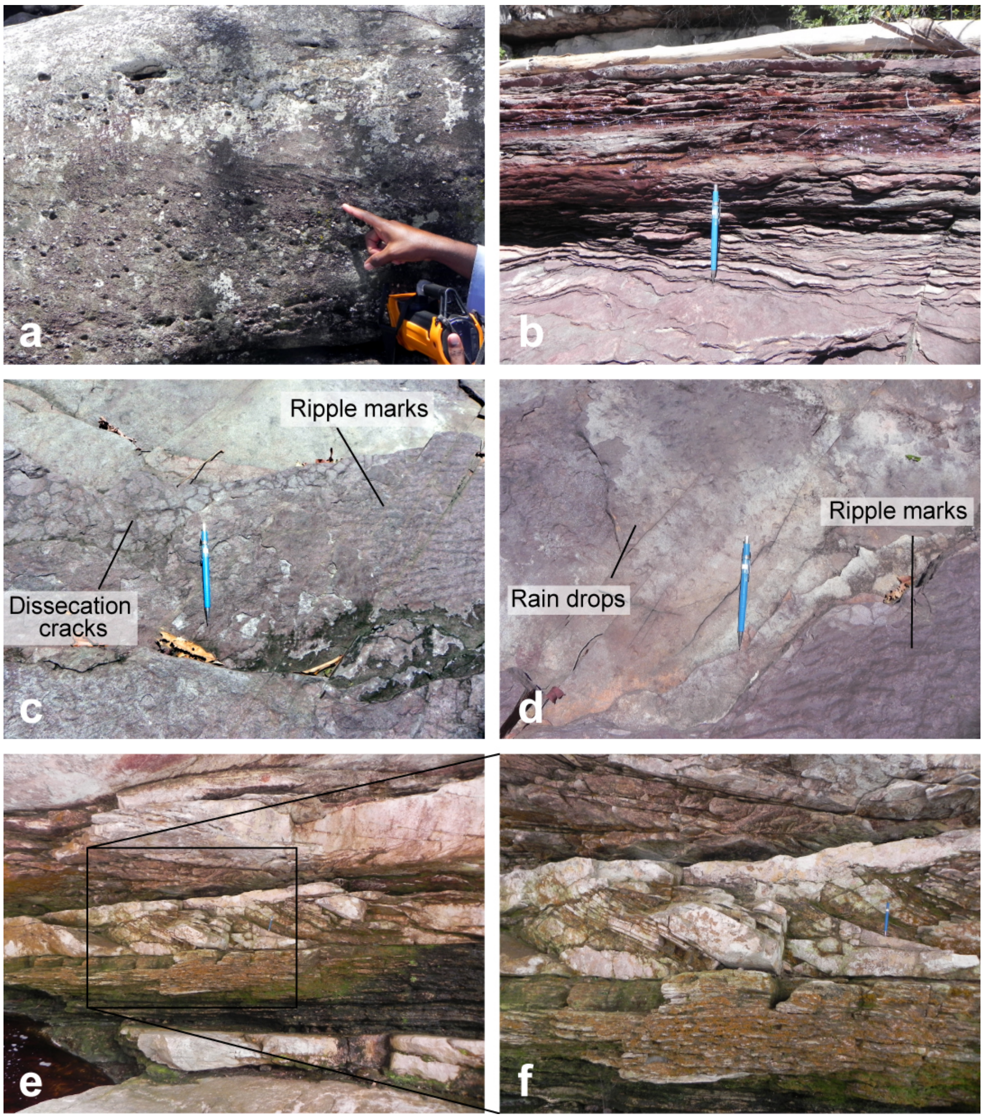

Figure SM1. Fluvial and tide influenced fluvial associations at Ribeirão de Baixo section. Planar to through cross-stratified sandstone at the gravel bar is shown in 'a'; laminated mudstone at the flood plain is shown in 'b'; sub-aerial structures, such as dissecation cracks, ripple marks and rain drops at the flood plain are shown in 'c' and 'd'; sigmoidal external geometry of sand bodies within the tide influenced fluvial deposits are shown in 'e' and 'f`.

SM1.1.1.2 Tide influenced fluvial association

This facies association occurs as coarsening upward packages. The horizontally laminated fine sandstones underlie medium to very coarse-grained sandstones with medium- to large-scale trough cross-bedding and bidirectional paleocurrents. The sigmoidal external geometry encompasses sand bodies with tidal bundles and reactivation surfaces. The sandstones have a fairly lenticular geometry and lack mudstone drapes (Fig. SM1e and f).

The evidence of tidal bundles, reactivation surface and bidirectional depositional paleoflow directions support tidal influence on fluvial deposits. The depositional environment is interpreted as a shallow, sandy braided fluvial system supplying sediments to the shoreline, where the tides rework sand deposits at the river mouths.

The shallow marine tidal bar deposits are common in the upper part of the Tombador Fm. throughout the Sincorá Range (Magalhães, *personal communication*).

SM1.8. References:

Miall, A.D., 1996. The Geology of Fluvial Deposits: Sedimentary Facies, Basin Analysis and Petroleum Geology. Springer-Verlag, Berlin, 582p.

arch 5, 591-596.

A1.8.3. Supplementary material 2 (SM2): Geochemical data discussed in this article.

	Major elements								LILE						
Sample	SiO2	Al2O3	Fe2O3t	MgO	CaO	Na2O	K2O	TiO2	Ba	Rb	Sr	Sc	V	Co	Y
FMG-21A I	74,79	12,70	2,35	0,94	0,02	0,07	6,22	0,49	682,00	125,40	53,80	8,00	33,00	2,30	37,30
FMG-21A II	72,62	13,30	3,72	1,23	0,01	0,06	5,76	0,56	491,00	127,90	44,70	10,00	56,00	2,50	31,30
FMG-21B	83,70	9,55	1,97	1,36	0,01	0,39	1,20	0,33	88,00	21,50	74,90	4,00	27,00	5,90	36,00
FMG-21CI	83,13	8,28	1,85	0,83	0,01	0,03	3,64	0,34	286,00	80,90	11,20	5,00	27,00	2,20	26,10
FMG-21CII	75,17	12,45	2,71	1,12	0,01	0,06	6,09	0,39	596,00	128,40	36,60	8,00	46,00	2,10	24,60
Graywackes (Mpr; Condie, 1993)	66,10	15,00	5,80	2,10	2,60	2,80	2,50	0,77	600,00	80,00	240,00	17,00	140,00	20,00	27,00
Shale (Pr; Condie, 1993)	63,10	17,50	5,65	2,20	0,71	1,06	3,62	0,64	642,00	165,00	108,00	17,00	100,00	18,00	35,00
Cratonic sandstone (Pr; Condie, 1993)	92,15	3,87	1,32	0,55	0,45	0,51	0,88	0,17	190,00	30,00	27,00	2,40	29,00	2,80	10,30
Andesite (MPr; Condie, 1993)	59,40	16,21	6,30	3,50	6,20	3,60	1,15	0,74	648,00	35,00	315,00	23,00	154,00	26,00	22,00
Felsic volcanic rocks (MPr; Condie, 1993)	73,30	13,20	2,70	0,50	1,20	3,20	4,00	0,25	952,00	125,00	150,00	15,00	48,00	5,00	35,00
Granite (Pr; Condie, 1993)	73,30	13,50	2,30	0,42	1,30	3,20	4,80	0,28	750,00	156,00	120,00	5,00	20,00	5,50	45,00
OIA (Bhatia, 1983)	58,83	17,11	7,47	3,65	5,83	4,10	1,60	1,06							
CIA (Bhatia, 1983)	70,69	14,04	4,48	1,97	2,68	3,12	1,89	0,64							
ACM (Bhatia, 1983)	73,86	12,89	2,88	1,23	2,48	2,77	2,90	0,46							
PM (Bhatia, 1983)	81,95	8,41	3,08	1,39	1,89	1,07	1,71	0,49							
P1 (Lacassie et al., 2004)	54,86	17,28	9,93	5,20	7,01	3,29	1,10	0,94	150,00	16,70	333,80	31,90	315,50		20,00
P2 (Lacassie et al., 2004)	63,03	16,47	7,22	2,81	3,16	4,52	1,58	0,92	322,20	45,80	263,80	18,80	182,30		26,20
P3 (Lacassie et al., 2004)	72,54	14,13	3,50	1,25	1,58	3,79	2,65	0,50	606,80	92,00	342,70	8,30	73,60		20,20
P4 (Lacassie et al., 2004)	80,44	10,24	3,15	1,31	0,74	1,16	2,34	0,47	466,60	121,80	85,80	8,60	61,60		29,20
UCC (Taylor and McLennan, 1985)	66,00	15,20	5,00	2,20	4,20	3,90	3,40	0,50	550,00	112,00	350,00	11,00	60,00	10,00	22,00

	HFSE							Rare earth elements																		
Sample	Zr	Hf	Nb	Ta	Yb	Th	U	La	Ce	Pr	Nd	Sm	Eu	Gd	Tb	Dy	Ho	Er	Tm	Yb	Lu	Eu/Eu*	La/Yb	(La/Yb)n	∑REE	LREE/HREE
FMG-21A I	484,00	12,50	7,30	0,70	4,08	13,70	3,70	42,40	82,40	9,02	31,00	5,47	1,08	4,89	0,84	6,09	1,22	3,48	0,59	3,48	0,59	0,64	10,39	7,02	193,19	7,80
FMG-21A II	313,70	8,30	9,30	1,00	2,93	15,90	3,20	79,80	150,10	16,36	53,20	8,67	1,45	5,55	0,77	5,12	0,87	2,92	0,49	2,92	0,49	0,64	27,24	18,40	328,75	16,07
FMG-21B	277,10	7,90	5,80	0,60	3,01	16,50	5,10	31,10	61,90	6,58	23,90	3,78	0,71	4,58	0,86	6,17	1,12	3,11	0,48	3,11	0,48	0,52	10,33	6,98	147,76	6,43
FMG-21CI	392,80	10,20	6,70	0,60	3,11	9,20	3,30	22,60	48,50	5,11	18,10	2,92	0,64	2,84	0,52	3,98	0,86	2,59	0,43	2,59	0,43	0,68	7,27	4,91	112,67	6,57
FMG-21CII	294,40	7,60	7,40	0,70	2,55	13,20	2,80	33,00	69,70	7,58	27,60	4,78	0,88	3,44	0,55	3,64	0,77	2,31	0,37	2,31	0,37	0,66	12,94	8,74	157,58	10,16
Graywackes (Mpr; Condie, 1993)	148,00	4,20	10,00	0,80	2,20	9,00	1,70	28,00	60,00		26,00	4,90	0,93	4,34	0,66					2,20	0,38	0,62	12,73	8,60	127,41	15,69
Shale (Pr; Condie, 1993)	196,00	5,20	16,80	1,40	2,86	14,30	3,40	38,00	81,70		37,50	6,68	1,32	5,60	0,90					2,86	0,48	0,66	13,29	8,98	175,04	16,65
Cratonic sandstone (Pr; Condie, 1993)	89,00	2,50	3,70	0,20	0,84	4,20	1,20	10,10	21,60		9,00	1,75	0,36	1,52	0,23					0,84	0,13	0,67	12,02	8,13	45,57	15,38
Andesite (MPr; Condie, 1993)	145,00	4,00	8,00	0,50	2,00	3,40	1,80	20,00	46,00		25,00	5,30	1,30	4,94	0,77					2,00	0,32	0,78	10,00	6,76	105,63	11,99
Felsic volcanic rocks (MPr; Condie, 1993)	230,00	6,50	15,00	1,20	2,60	8,20	2,50	25,00	51,20		19,00	4,00	1,10	4,26	0,71					2,60	0,40	0,81	9,62	6,50	108,27	12,45
Granite (Pr; Condie, 1993)	240,00	7,00	20,00	1,50	3,50	18,00	4,50	48,00	115,00		54,00	8,70	1,00	8,17	1,28					3,50	0,58	0,36	13,71	9,27	240,23	16,68
OIA (Bhatia, 1983)																										
CIA (Bhatia, 1983)																										
ACM (Bhatia, 1983)																										
PM (Bhatia, 1983)																										
P1 (Lacassie et al., 2004)	73,30		1,80			1,60																				
P2 (Lacassie et al., 2004)	162,70		5,20			5,70																				
P3 (Lacassie et al., 2004)	189,60		8,20			10,90																				
P4 (Lacassie et al., 2004)	229,70		10,40			13,30																				
UCC (Taylor and McLennan, 1985)	190,00	5,80	25,00	2,20	2,20	10,70	2,80	30,00	64,00	7,10	26,00	4,50	0,88	3,80	0,64	3,50	0,80	2,30	0,33	2,20	0,32	0,65	13,64	9,21	146,37	9,47

UCC NORM

FMG-21A I	1,13	0,84	0,47	0,43	0,00	0,02	1,83	0,98	1,24	1,12	0,15	0,73	0,55	0,23	1,70
FMG-21A II	1,10	0,88	0,74	0,56	0,00	0,02	1,69	1,12	0,89	1,14	0,13	0,91	0,93	0,25	1,42
FMG-21B	1,27	0,63	0,39	0,62	0,00	0,10	0,35	0,66	0,16	0,19	0,21	0,36	0,45	0,59	1,64
FMG-21CI	1,26	0,54	0,37	0,38	0,00	0,01	1,07	0,68	0,52	0,72	0,03	0,45	0,45	0,22	1,19
FMG-21CII	1,14	0,82	0,54	0,51	0,00	0,02	1,79	0,78	1,08	1,15	0,10	0,73	0,77	0,21	1,12
Graywackes (Mpr; Condie, 1993)	1,00	0,99	1,16	0,95	0,62	0,72	0,74	1,54	1,09	0,71	0,69	1,55	2,33	2,00	1,23
Shale (Pr; Condie, 1993)	0,96	1,15	1,13	1,00	0,17	0,27	1,06	1,28	1,17	1,47	0,31	1,55	1,67	1,80	1,59
Cratonic sandstone (Pr; Condie, 1993)	1,40	0,25	0,26	0,25	0,11	0,13	0,26	0,34	0,35	0,27	0,08	0,22	0,48	0,28	0,47
Andesite (MPr; Condie, 1993)	0,90	1,07	1,26	1,59	1,48	0,92	0,34	1,48	1,18	0,31	0,90	2,09	2,57	2,60	1,00
Felsic volcanic rocks (MPr; Condie, 1993)	1,11	0,87	0,54	0,23	0,29	0,82	1,18	0,50	1,73	1,12	0,43	1,36	0,80	0,50	1,59
Granite (Pr; Condie, 1993)	1,11	0,89	0,46	0,19	0,31	0,82	1,41	0,56	1,36	1,39	0,34	0,45	0,33	0,55	2,05
OIA (Bhatia, 1983)	0,89	1,13	1,49	1,66	1,39	1,05	0,47	2,12							
CIA (Bhatia, 1983)	1,07	0,92	0,90	0,90	0,64	0,80	0,56	1,28							
ACM (Bhatia, 1983)	1,12	0,85	0,58	0,56	0,59	0,71	0,85	0,92							
PM (Bhatia, 1983)	1,24	0,55	0,62	0,63	0,45	0,27	0,50	0,98							
P1 (Lacassie et al., 2004)	0,83	1,14	1,99	2,36	1,67	0,84	0,32	1,88	0,27	0,15	0,95	2,90	5,26		0,91
P2 (Lacassie et al., 2004)	0,96	1,08	1,44	1,28	0,75	1,16	0,46	1,84	0,59	0,41	0,75	1,71	3,04		1,19
P3 (Lacassie et al., 2004)	1,10	0,93	0,70	0,57	0,38	0,97	0,78	1,00	1,10	0,82	0,98	0,75	1,23		0,92
P4 (Lacassie et al., 2004)	1,22	0,67	0,63	0,60	0,18	0,30	0,69	0,94	0,85	1,09	0,25	0,78	1,03		1,33

FMG-21A I	2,55	2,16	0,29	0,32	1,85	1,28	1,32															0,98	0,76	0,76	1,32	0,82
FMG-21A II	1,65	1,43	0,37	0,45	1,33	1,49	1,14															0,98	2,00	2,00	2,25	1,70
FMG-21B	1,46	1,36	0,23	0,27	1,37	1,54	1,82															0,80	0,76	0,76	1,01	0,68
FMG-21CI	2,07	1,76	0,27	0,27	1,41	0,86	1,18															1,04	0,53	0,53	0,77	0,69
FMG-21CII	1,55	1,31	0,30	0,32	1,16	1,23	1,00															1,02	0,95	0,95	1,08	1,07
Graywackes (Mpr; Condie, 1993)	0,78	0,72	0,40	0,36	1,00	0,84	0,61															0,95	0,93	0,93	0,87	1,66
Shale (Pr; Condie, 1993)	1,03	0,90	0,67	0,64	1,30	1,34	1,21															1,01	0,97	0,97	1,20	1,76
Cratonic sandstone (Pr; Condie, 1993)	0,47	0,43	0,15	0,09	0,38	0,39	0,43															1,02	0,88	0,88	0,31	1,62
Andesite (MPr; Condie, 1993)	0,76	0,69	0,32	0,23	0,91	0,32	0,64															1,19	0,73	0,73	0,72	1,27
Felsic volcanic rocks (MPr; Condie, 1993)	1,21	1,12	0,60	0,55	1,18	0,77	0,89															1,25	0,71	0,71	0,74	1,31
Granite (Pr; Condie, 1993)	1,26	1,21	0,80	0,68	1,59	1,68	1,61															0,56	1,01	1,01	1,64	1,76
OIA (Bhatia, 1983)																										
CIA (Bhatia, 1983)																										
ACM (Bhatia, 1983)																										
PM (Bhatia, 1983)																										
P1 (Lacassie et al., 2004)	0,39		0,07			0,15																				
P2 (Lacassie et al., 2004)	0,86		0,21			0,53																				
P3 (Lacassie et al., 2004)	1,00		0,33			1,02																				
P4 (Lacassie et al., 2004)	1,21		0,42			1,24																				

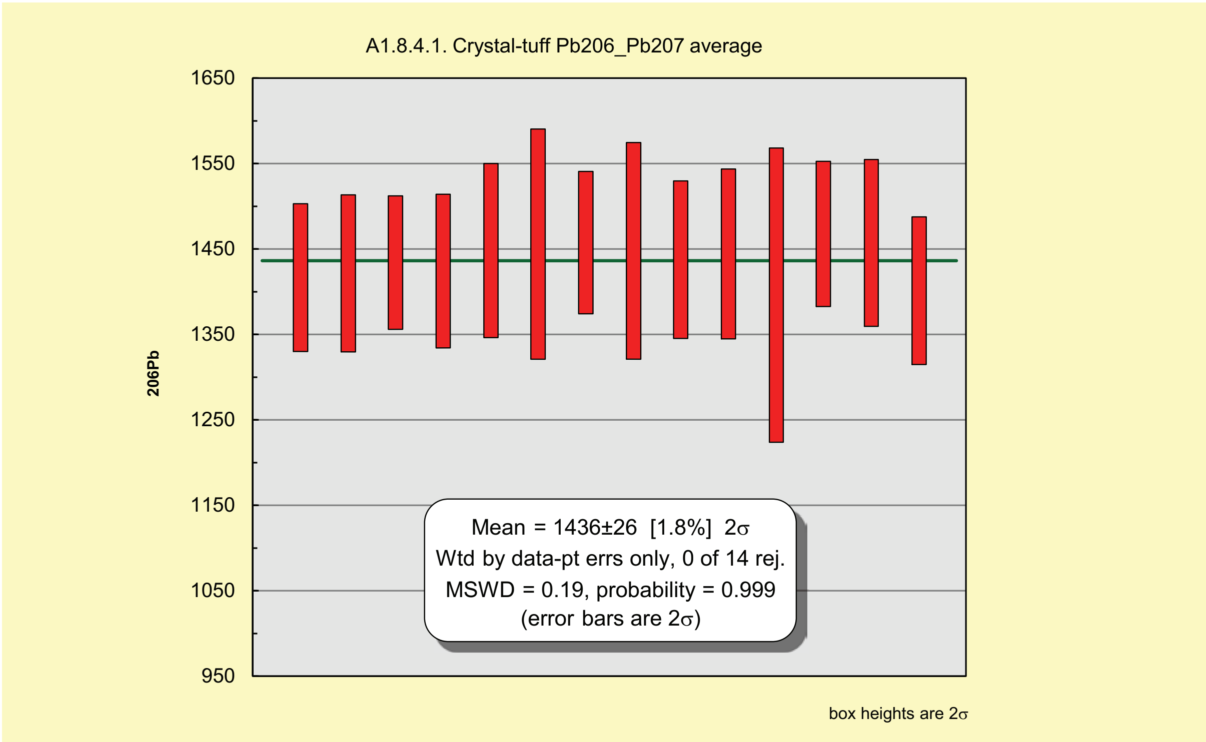

A1.8.4.1. Crystal-tuff Pb206_Pb207 average A1.8.5.

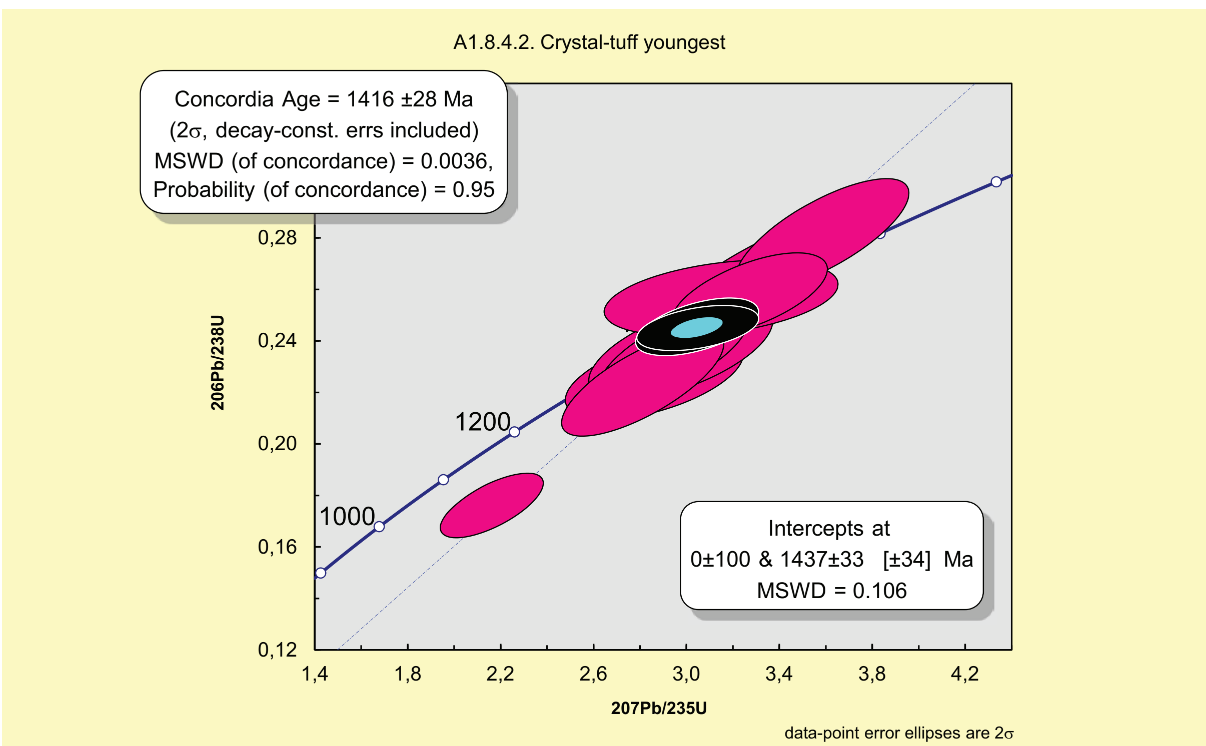

A1.8.4.2. Crystal-tuff youngest

A1.8.4.3. U-Pb zircon data of Crystal-tuff sample (Crystal-rich volcaniclastic layer, Tombador Fm.).

	Spot Number	f_{206}	Pb (ppm)	Th (ppm)	U (ppm)	$^{232}Th/^{238}U$[a]	Isotope ratios[b] $^{207}Pb/^{235}U$	1 s [%]	$^{206}Pb/^{238}U$	1 s [%]	Rho[c]	$^{207}Pb/^{206}Pb$[d]	1 s [%]	Ages (Ma) $^{206}Pb/^{238}U$	1 s abs	$^{207}Pb/^{235}U$	1 s abs	$^{207}Pb/^{206}Pb$	1 s abs	% Conc[e]	Best estimate age (Ma)	±2s
Volcanic	Z55	0,0003	31	80	116	0,70	3,035	3,60	0,246	1,90	0,53	0,090	3,05	1417	27	1416	51	1416	43	100	1416	85
	Z83	0,0005	39	99	125	0,80	3,037	3,56	0,245	1,48	0,42	0,090	3,24	1414	21	1417	50	1421	46	100	1421	90
	Z12	0,0008	13	30	58	0,52	2,872	4,10	0,230	3,09	0,75	0,090	2,70	1337	41	1375	56	1433	39	93	1433	76
	Z18	0,0007	21	81	80	1,01	3,185	5,61	0,257	4,61	0,82	0,090	3,19	1474	68	1454	82	1424	45	104	1424	88
	Z30	0,0012	9	49	42	1,18	3,089	4,87	0,246	3,37	0,69	0,091	3,52	1418	48	1430	70	1447	51	98	1447	100
	Z31	0,0006	4	13	19	0,70	2,848	5,53	0,226	3,01	0,54	0,091	4,64	1313	40	1368	76	1455	67	90	1455	132
	Z36	0,0004	20	43	78	0,55	3,041	3,64	0,241	2,26	0,62	0,091	2,86	1392	31	1418	52	1457	42	96	1457	82
	Z61	0,0012	11	33	37	0,89	2,965	5,50	0,236	3,33	0,60	0,091	4,38	1368	45	1399	77	1447	63	95	1447	124
	Z80	0,0004	17	87	63	1,40	2,936	4,46	0,235	3,09	0,69	0,091	3,21	1362	42	1391	62	1437	46	95	1437	90
	Z88	0,0017	6	19	23	0,83	2,799	5,15	0,223	3,81	0,74	0,091	3,45	1300	50	1355	70	1444	50	90	1444	98
	Z91	0,0009	15	45	63	0,72	3,142	6,61	0,257	2,37	0,36	0,089	6,17	1476	35	1443	95	1395	86	106	1395	169
	Z93	0,0004	21	69	84	0,83	3,581	4,30	0,282	3,18	0,74	0,092	2,90	1603	51	1545	66	1467	42	109	1467	83
	Z94	0,0003	40	130	172	0,76	3,263	4,24	0,259	2,60	0,61	0,091	3,36	1483	39	1472	62	1457	49	102	1457	96
	Z26	0,0005	49	182	225	0,82	2,142	4,27	0,175	2,95	0,69	0,089	3,09	1039	31	1163	50	1400	43	74		
Detrital	Z67	0,0009	18	41	58	0,72	3,599	3,36	0,276	1,67	0,50	0,095	2,91	1571	26	1549	52	1520	44	103	1520	87
	Z32	0,0009	12	17	50	0,35	3,277	5,02	0,250	2,99	0,60	0,095	4,03	1440	43	1476	74	1527	62	94	1527	121
	Z78	0,0007	20	35	61	0,58	3,704	4,63	0,282	3,58	0,77	0,095	2,93	1600	57	1572	73	1535	45	104	1535	88
	Z10	0,0003	45	37	150	0,25	3,665	3,18	0,278	2,26	0,71	0,095	2,24	1584	36	1564	50	1537	34	103	1537	68
	Z96	0,0019	6	4	24	0,14	3,637	6,66	0,275	2,82	0,42	0,096	6,04	1566	44	1558	104	1546	93	101	1546	183
	Z21	0,0008	18	22	62	0,35	3,577	3,17	0,270	2,28	0,72	0,096	2,21	1542	35	1544	49	1547	34	100	1547	67
	Z33	0,0002	38	29	149	0,19	3,570	4,35	0,269	3,88	0,89	0,096	1,96	1537	60	1543	67	1551	30	99	1551	60
	Z46	0,0002	56	100	208	0,48	3,802	2,31	0,287	1,52	0,66	0,096	1,73	1625	25	1593	37	1552	27	105	1552	53
	Z97	0,0001	67	292	506	0,58	3,360	2,71	0,253	1,98	0,73	0,096	1,85	1452	29	1495	40	1557	29	93	1557	56
	Z6	0,0005	16	44	55	0,81	3,784	5,41	0,283	5,10	0,94	0,097	1,81	1607	82	1589	86	1566	28	103	1566	55
	Z11	0,0005	27	51	88	0,58	3,866	3,34	0,289	1,23	0,37	0,097	3,10	1636	20	1607	54	1568	49	104	1568	95
	Z64	0,0004	46	41	138	0,30	3,721	2,93	0,278	2,02	0,69	0,097	2,12	1581	32	1576	46	1570	33	101	1570	65
	Z52	0,0005	17	45	64	0,70	3,598	3,86	0,268	2,98	0,77	0,097	2,45	1532	46	1549	60	1573	38	97	1573	75
	Z19	0,0007	35	54	108	0,50	3,845	3,58	0,286	2,05	0,57	0,097	2,93	1622	33	1602	57	1576	46	103	1576	91
	Z111	0,0008	15	22	48	0,46	3,885	4,92	0,288	2,30	0,47	0,098	4,35	1632	37	1611	79	1583	69	103	1583	135
	Z72	0,0003	33	72	119	0,61	3,77	2,97	0,28	2,06	0,69	0,10	2,14	1586	33	1587	47	1587	34	100	1587	67
	Z74	0,0004	29	59	97	0,61	3,73	2,85	0,28	1,66	0,58	0,10	2,31	1571	26	1579	45	1589	37	99	1589	72
	Z17	0,0005	31	43	105	0,41	3,820	3,00	0,280	2,15	0,72	0,099	2,09	1590	34	1597	48	1606	34	99	1606	66
	Z24	0,0005	62	172	212	0,82	4,047	5,96	0,280	4,96	0,83	0,105	3,30	1592	79	1644	98	1710	57	93	1710	111
	Z103	0,0020	39	105	128	0,83	4,228	8,83	0,291	5,10	0,58	0,105	7,22	1648	84	1679	148	1719	124	96	1719	243
	Z79	0,0010	17	68	52	1,31	4,585	5,13	0,314	2,05	0,40	0,106	4,70	1761	36	1747	90	1730	81	102	1730	159
	Z85	0,0012	16	49	46	1,07	4,48	5,77	0,30	2,50	0,43	0,11	5,21	1710	43	1726	100	1746	91	98	1746	178
	Z35	0,0003	45	127	150	0,86	4,456	2,06	0,301	1,01	0,49	0,107	1,80	1697	17	1723	36	1754	32	97	1754	62
	Z16	0,0004	47	100	141	0,72	5,094	2,84	0,344	2,01	0,71	0,107	2,00	1907	38	1835	52	1754	35	109	1754	69
	Z20	0,0005	48	96	135	0,72	5,090	3,58	0,344	2,60	0,73	0,107	2,47	1905	50	1834	66	1756	43	108	1756	85
	Z27	0,0004	69	166	200	0,84	5,227	3,52	0,352	3,02	0,86	0,108	1,81	1944	59	1857	65	1761	32	110	1761	62
	Z22	0,0004	50	70	135	0,52	5,069	2,07	0,341	0,55	0,27	0,108	2,00	1891	10	1831	38	1763	35	107	1763	69
	Z8	0,0003	40	54	105	0,52	5,031	1,80	0,338	1,13	0,63	0,108	1,40	1878	21	1825	33	1765	25	106	1765	48
	Z57	0,0001	24	38	81	0,47	4,589	2,68	0,308	1,78	0,66	0,108	2,00	1730	31	1747	47	1768	35	98	1768	69
	Z73	0,0006	43	146	124	1,18	4,80	3,00	0,32	2,40	0,80	0,11	1,79	1799	43	1785	53	1768	32	102	1768	62
	Z65	0,0006	32	116	88	1,33	4,411	3,16	0,296	1,62	0,51	0,108	2,71	1671	27	1714	54	1769	48	94	1769	94
	Z99	0,0006	26	61	90	0,69	4,528	3,46	0,303	1,47	0,42	0,108	3,13	1709	25	1736	60	1769	55	97	1769	109
	Z47	0,0011	47	387	188	2,08	4,557	2,83	0,305	1,90	0,67	0,108	2,09	1718	33	1741	49	1770	37	97	1770	73
	Z76	0,0002	29	80	76	1,06	4,550	2,96	0,305	2,23	0,75	0,108	1,95	1716	38	1740	52	1770	35	97	1770	68
	Z69	0,0004	40	35	118	0,30	4,66	2,98	0,31	1,74	0,58	0,11	2,42	1751	30	1761	52	1772	43	99	1772	84
	Z89	0,0005	26	44	74	0,60	4,89	4,07	0,33	2,81	0,69	0,11	2,94	1827	51	1801	73	1772	52	103	1772	102
	Z66	0,0007	19	34	47	0,72	4,930	3,10	0,330	2,40	0,77	0,108	1,96	1838	44	1807	56	1773	35	104	1773	68
	Z7	0,0004	16	34	42	0,83	4,878	2,63	0,326	1,71	0,65	0,109	2,00	1819	31	1798	47	1775	36	103	1775	70
	Z77	0,0002	55	96	152	0,63	4,769	2,34	0,319	1,08	0,46	0,109	2,08	1783	19	1779	42	1776	37	100	1776	72
	Z4	0,0003	33	66	93	0,72	4,614	4,45	0,308	4,03	0,91	0,109	1,89	1730	70	1752	78	1778	34	97	1778	66
	Z53	0,0010	11	22	36	0,60	4,451	3,29	0,296	1,96	0,60	0,109	2,64	1674	33	1722	57	1781	47	94	1781	92
	Z75	0,0005	39	73	116	0,63	4,98	2,54	0,33	1,55	0,61	0,11	2,01	1846	29	1817	46	1783	36	104	1783	70
	Z58	0,0003	36	61	118	0,52	4,789	2,16	0,318	0,98	0,45	0,109	1,93	1782	18	1783	39	1785	34	100	1785	67
	Z82	0,0002	44	110	114	0,98	4,885	2,22	0,324	1,30	0,59	0,109	1,80	1810	24	1800	40	1788	32	101	1788	63
	Z51	0,0004	36	183	121	1,53	4,988	2,87	0,331	1,23	0,43	0,109	2,59	1843	23	1817	52	1788	46	103	1788	91
	Z34	0,0009	17	71	58	1,25	4,874	4,00	0,323	2,80	0,70	0,110	2,86	1803	51	1798	72	1791	51	101	1791	100
	Z45	0,0005	42	164	146	1,14	5,184	2,36	0,343	0,89	0,38	0,110	2,19	1899	17	1850	44	1795	39	106	1795	77
	Z63	0,0003	52	107	148	0,73	4,832	3,26	0,319	2,32	0,71	0,110	2,29	1786	41	1790	58	1796	41	99	1796	81
	Z106	0,0013	12	47	44	1,09	4,585	3,67	0,302	1,65	0,45	0,110	3,28	1703	28	1746	64	1798	59	95	1798	116
	Z98	0,0007	33	177	131	1,37	4,704	3,26	0,310	1,67	0,51	0,110	2,80	1742	29	1768	58	1799	50	97	1799	99
	Z40	0,0009	16	47	57	0,83	4,848	4,43	0,319	3,64	0,82	0,110	2,53	1785	65	1793	79	1803	46	99	1803	90
	Z23	0,0009	26	95	72	1,33	5,022	3,35	0,330	1,71	0,51	0,110	2,88	1838	31	1823	61	1806	52	102	1806	102
	Z108	0,0010	11	34	40	0,86	4,391	4,68	0,288	3,34	0,71	0,110	3,29	1633	54	1711	80	1807	59	90	1807	116
	Z9	0,0005	19	58	53	1,10	4,913	3,16	0,322	2,70	0,85	0,111	1,66	1797	48	1804	57	1813	30	99	1813	59
	Z81	0,0003	32	77	89	0,87	4,434	3,02	0,290	1,93	0,64	0,111	2,32	1642	32	1719	52	1814	42	91	1814	82
	Z104	0,0013	26	88	82	1,08	4,901	4,03	0,319	1,78	0,44	0,111	3,62	1785	32	1802	73	1822	66	98	1822	129
	Z109	0,0007	12	38	36	1,06	5,574	3,49	0,330	2,35	0,67	0,122	2,59	1839	43	1912	67	1993	52	92	1993	101
	Z41	0,0006	23	41	68	0,61	6,640	3,32	0,375	2,77	0,84	0,128	1,82	2055	57	2065	68	2075	38	99	2075	74
	Z71	0,0006	30	69	74	0,93	6,54	3,53	0,37	2,43	0,69	0,13	2,56	2022	49	2051	72	2080	53	97	2080	104
	Z14	0,0006	43	136	131	1,05	6,283	2,97	0,352	2,00	0,67	0,129	2,19	1945	39	2016	60	2090	46	93	2090	90
	Z102	0,0020	7	18	19	0,99	6,737	5,18	0,376	3,95	0,76	0,130	3,36	2058	81	2077	108	2097	70	98	2097	138
	Z44	0,0002	65	80	177	0,46	7,698	2,35	0,416	2,05	0,87	0,134	1,16	2241	46	2196	52	2155	25	104	2155	49
	Z113	0,0000	1	0	1	0,07	6,847	12,80	0,365	10,43	0,82	0,136	7,41	2005	209	2092	268	2178	161	92	2178	316
	Z38	0,0005	44	48	108	0,45	11,601	3,69	0,483	3,18	0,86	0,174	1,88	2542	81	2573	95	2597	49	98	2597	95
	Z54	0,0008	94	91	180	0,51	12,651	1,99	0,526	1,47	0,74	0,174	1,34	2725	40	2654	53	2600	35	105	2600	69
	Z42	0,0005	50	53	106	0,50	12,358	2,79	0,503	2,40	0,86	0,178	1,42	2625	63	2632	73	2637	37	100	2637	73
	Z29	0,0009	20	33	42	0,78	11,792	2,46	0,474	1,76	0,72	0,180	1,72	2502	44	2588	64	2656	46	94	2656	89
	Z105	0,0012	13	25	26	0,94	13,352	5,48	0,532	4,89	0,89	0,182	2,47	2750	134	2705	148	2671	66	103	2671	129
	Z86	0,0004	43	40	77	0,52	12,80	2,42	0,50	1,98	0,82	0,19	1,38	2612	52	2665	64	2705	37	97	2705	73
	Z39	0,0011	20	72	46	1,59	14,389	2,66	0,536	2,36	0,88	0,195	1,24	2766	65	2776	74	2783	34	99	2783	68
	Z59	0,0005	44	36	72	0,50	14,998	2,66	0,556	2,32	0,87	0,196	1,31	2849	66	2815	75	2791	37	102	2791	72
	Z15	0,0007	31	57	59	0,97	15,595	5,39	0,551	5,33	0,99	0,205	0,78	2829	151	2852	154	2869	22	99	2869	44
	Z3	0,0010	21	36	38	0,95	14,610	3,57	0,516	3,17	0,89	0,205	1,63	2681	85	2790	99	2870	47	93	2870	92
	Z84	0,0005	34	64	56	1,15	16,02	2,83	0,56	2,42	0,85	0,21	1,47	2881	70	2878	82	2876	42	100	2876	83
	Z95	0,0008	69	149	149	1,01	18,082	2,08	0,571	1,43	0,69	0,230	1,51	2911	42	2994	62	3051	46	95	3051	90
	Z48	0,0008	30	61	51	1,20	23,466	1,92	0,637	1,59	0,83	0,267	1,07	3179	50	3246	62	3288	35	97	3288	69
	Z13	0,0005	49	51	71	0,72	25,107	3,40	0,675	3,35	0,98	0,270	0,60	3326	111	3312	113	3304	20	101	3304	39
	Z1	0,0005	35	34	48	0,71	24,487	3,94	0,650	3,89	0,99	0,273	0,66	3230	125	3288	130	3323	22	97	3323	43
	Z25	0,0007	32	32	40	0,83	29,053	1,23	0,727	0,76	0,62	0,290	0,96	3522	27	3455	42	3417	33	103	3417	64
	Z2	0,0005	29	90	87	1,05	5,769	3,14	0,319	2,47	0,79	0,131	1,94	1784	44	1942	61	2114	41	84		
	Z5	0,0002	28	75	120	0,62	3,590	4,52	0,247	4,05	0,90	0,106	2,00	1421	58	1547	70	1725	35	82		

Z28	0,0003	54	124	149	0,84	5,317	2,68	0,356	2,22	0,83	0,108	1,50	1961	44	1872	50	1774	27	111
Z37	0,0014	80	322	541	0,60	3,526	2,18	0,252	1,23	0,56	0,101	1,80	1450	18	1533	33	1650	30	88
Z41B	0,0008	52	123	210	0,59	4,795	3,13	0,296	1,98	0,63	0,118	2,43	1671	33	1784	56	1919	47	87
Z43	0,0006	49	140	205	0,69	5,072	3,01	0,298	2,17	0,72	0,124	2,09	1679	36	1831	55	2009	42	84
Z48	0,0023	195	1995	1884	1,07	1,375	10,69	0,121	9,65	0,90	0,082	4,59	739	71	878	94	1247	57	59
Z50	0,0009	96	261	420	0,63	4,361	2,59	0,270	1,59	0,61	0,117	2,05	1543	25	1705	44	1910	39	81
~~Z56~~	0,0293	126	105	220	0,48	12,431	3,97	0,535	3,04	0,77	0,168	2,55	2764	84	2638	105	2542	65	109
Z60	0,0014	73	161	232	0,70	3,453	5,47	0,219	4,86	0,89	0,114	2,51	1277	62	1516	83	1868	47	68
Z62	0,0006	60	420	205	2,06	6,546	15,63	0,259	15,03	0,96	0,183	4,27	1487	223	2052	321	2680	115	55
Z68	0,0007	21	122	68	1,81	4,95	3,01	0,30	1,45	0,48	0,12	2,64	1677	24	1812	55	1969	52	85
Z70	0,0009	99	212	406	0,52	5,72	3,55	0,28	2,91	0,82	0,15	2,04	1599	46	1934	69	2315	47	69
Z87	0,0011	155	1599	1366	1,18	1,35	5,90	0,10	4,21	0,71	0,10	4,13	606	26	869	51	1615	67	38
Z90	0,0003	10	46	39	1,20	2,91	3,60	0,23	2,08	0,58	0,09	2,94	1321	28	1385	50	1486	44	89
~~Z92~~	0,0009	37	14	609	0,02	0,528	8,04	0,063	1,96	0,24	0,061	7,80	395	8	431	35	629	49	63
Z100	0,0015	76	481	530	0,91	1,862	6,99	0,150	5,52	0,79	0,090	4,28	898	50	1068	75	1432	61	63
Z101	0,0023	2	19	12	1,59	3,147	10,29	0,214	6,88	0,67	0,107	7,65	1251	86	1444	149	1741	133	72
Z107	0,0007	33	95	135	0,70	3,797	3,82	0,260	2,29	0,60	0,106	3,06	1490	34	1592	61	1730	53	86
Z110	0,0023	6	30	23	1,30	3,275	6,06	0,243	2,31	0,38	0,098	5,60	1402	32	1475	89	1582	89	89
Z112	0,0004	22	61	47	1,31	11,795	2,07	0,457	1,37	0,66	0,187	1,55	2427	33	2588	54	2717	42	89
~~Z114~~	0,0010	65	9109	1195	7,67	0,455	7,53	0,058	4,98	0,66	0,057	5,64	361	18	381	29	503	28	72
~~Z115~~	0,0051	22	42	48	0,88	11,180	3,15	0,452	1,84	0,59	0,180	2,55	2403	44	2538	80	2649	68	91

a Th/U ratios are calculated relative to GJ-1 reference zircon

b Corrected for background and within-run Pb/U fractionation and normalised to reference zircon GJ-1 (ID-TIMS values/measured value); 207Pb/235U calculated using (207Pb/206Pb)/(238U/206Pb * 1/137.88)

c Rho is the error correlation defined as the quotient of the propagated errors of the 206Pb/238U and the 207/235U ratio

d Corrected for mass-bias by normalising to GJ-1 reference zircon and common Pb using the model Pb composition of Stacey and Kramers (1975)

e Degree of concordance = [(206Pb/238U age) / (207Pb/206U age)]*100

Reference

Stacey, J.S., Kramers, J.D., 1975. Approximation of terrestrial lead isotope evolution by a two-stage model. Earth and Planetary Science Letters 26, 207–221.

A1.8.4.4. Lu-Hf data of zircon grains from Crystal-tuff sample (Crystal-rich volcaniclastic layer, Tombador Fm.).

Spot Number	U/Pb Age (Ma)	±2s	Sample (Present day ratios) $^{176}Hf/^{177}Hf$	±2SE	$^{176}Lu/^{177}Hf$	±2SE	Chur $^{176}Hf/177Hf$ (t)	DM 176Hf/177Hf (t)	Sample Initial Ratios 176Hf/177Hf (t)	eHf(0)	eHf(t)	±2SE	DM Model Ages (Ga) T DM	T DM Crustal	Mafic	Felsic
Z91	1395	169	0,28180	6,15E-05	0,00055	6,75E-05	0,28190	0,28223	0,28178	-35,01	-4,18	0,77	2,00	2,39	2,80	2,22
Z55	1416	85	0,28177	9,44E-05	0,00067	5,83E-06	0,28188	0,28221	0,28175	-35,81	-4,64	0,18	2,04	2,43	2,85	2,26
Z18	1424	88	0,28175	9,36E-05	0,00050	5,05E-05	0,28188	0,28220	0,28174	-36,52	-4,99	0,67	2,05	2,46	2,89	2,28
Z12	1433	76	0,28211	7,08E-05	0,00090	2,45E-05	0,28187	0,28220	0,28208	-23,95	7,43	0,41	1,59	1,69	1,80	1,65
Z80	1437	90	0,28182	6,62E-05	0,00094	5,14E-05	0,28187	0,28219	0,28179	-34,20	-2,81	0,24	1,99	2,34	2,71	2,18
Z61	1447	124	0,28174	6,29E-05	0,00051	5,47E-06	0,28188	0,28221	0,28173	-36,91	-5,42	0,14	2,07	2,49	2,93	2,30
Z31	1455	132	0,28182	9,07E-05	0,00048	2,36E-06	0,28186	0,28218	0,28180	-34,21	-1,97	0,10	1,97	2,30	2,64	2,15
Z36	1457	82	0,28182	5,52E-05	0,00043	4,70E-06	0,28186	0,28218	0,28181	-33,97	-1,62	0,05	1,95	2,28	2,62	2,14
Z94	1457	96	0,28180	5,36E-05	0,00099	1,55E-04	0,28186	0,28218	0,28178	-34,73	-2,93	0,56	2,01	2,36	2,73	2,20
Z93	1467	83	0,28164	5,06E-05	0,00094	1,15E-04	0,28185	0,28217	0,28161	-40,46	-8,42	1,28	2,23	2,71	3,22	2,49
Z46	1522	53	0,28184	6,67E-05	0,00054	5,60E-06	0,28182	0,28213	0,28182	-33,47	0,22	0,01	1,94	2,21	2,50	2,09
Z96	1546	183	0,28190	8,24E-05	0,00030	1,57E-05	0,28180	0,28211	0,28189	-31,25	3,25	0,37	1,84	2,04	2,25	1,96
Z33	1551	60	0,28191	1,02E-04	0,00041	4,94E-05	0,28180	0,28211	0,28190	-30,93	3,57	0,50	1,84	2,03	2,22	1,94
Z06	1566	55	0,28182	8,22E-05	0,00082	4,13E-05	0,28179	0,28210	0,28179	-34,29	0,10	0,01	1,99	2,25	2,54	2,14
Z11	1568	95	0,28186	7,10E-05	0,00052	3,37E-05	0,28179	0,28210	0,28185	-32,69	2,07	0,20	1,91	2,13	2,37	2,03
Z19	1576	91	0,28184	6,88E-05	0,00043	1,32E-05	0,28178	0,28209	0,28183	-33,48	1,55	0,09	1,94	2,17	2,42	2,07
Z16	1754	69	0,28177	5,52E-05	0,00059	1,23E-05	0,28167	0,28196	0,28175	-35,87	3,00	0,12	2,03	2,22	2,41	2,14
Z22	1763	69	0,28166	5,08E-05	0,00100	4,55E-05	0,28166	0,28195	0,28163	-39,67	-1,10	0,09	2,20	2,48	2,78	2,36
Z57	1768	69	0,28168	1,09E-04	0,00051	9,94E-06	0,28166	0,28195	0,28166	-39,05	0,22	0,01	2,15	2,40	2,67	2,29
Z69	1772	84	0,28155	4,64E-05	0,00137	1,85E-04	0,28165	0,28194	0,28151	-43,61	-5,29	0,97	2,38	2,75	3,15	2,58
Z66	1773	68	0,28164	5,40E-05	0,00057	3,60E-05	0,28165	0,28194	0,28162	-40,49	-1,18	0,10	2,21	2,50	2,79	2,37
Z04	1778	66	0,28172	8,67E-05	0,00074	1,89E-05	0,28165	0,28194	0,28170	-37,54	1,69	0,08	2,11	2,32	2,54	2,23
Z75	1783	70	0,28159	8,36E-05	0,00048	9,06E-06	0,28178	0,28209	0,28158	-42,17	-7,29	0,31	2,27	2,72	3,19	2,52
Z51	1788	91	0,28170	7,61E-05	0,00149	6,32E-05	0,28164	0,28193	0,28165	-38,52	0,02	0,00	2,19	2,43	2,70	2,32
Z82	1788	63	0,28164	5,19E-05	0,00064	7,57E-05	0,28164	0,28193	0,28162	-40,42	-0,85	0,12	2,21	2,49	2,78	2,37
Z23	1806	102	0,28161	7,70E-05	0,00093	5,78E-06	0,28163	0,28192	0,28158	-41,42	-1,80	0,06	2,27	2,56	2,87	2,43
Z108	1807	116	0,28160	1,99E-04	0,00074	1,00E-04	0,28163	0,28192	0,28157	-42,02	-2,16	0,36	2,28	2,58	2,90	2,45
Z41	2075	74	0,28134	9,83E-05	0,00026	2,24E-06	0,28146	0,28172	0,28133	-51,26	-4,71	0,21	2,60	2,95	3,31	2,80
Z71	2080	104	0,28131	1,37E-04	0,00037	1,29E-05	0,28145	0,28171	0,28130	-52,06	-5,55	0,34	2,63	3,01	3,39	2,85
Z14	2090	90	0,28169	9,12E-05	0,00039	7,11E-06	0,28145	0,28171	0,28167	-38,83	7,93	0,32	2,14	2,17	2,20	2,15
Z38	2597	95	0,28097	6,98E-05	0,00067	5,78E-05	0,28112	0,28132	0,28093	-64,29	-6,48	0,68	3,11	3,46	3,82	3,32
Z59	2791	72	0,28099	7,98E-05	0,00018	4,71E-06	0,28099	0,28117	0,28098	-63,37	-0,15	0,01	3,04	3,22	3,40	3,15
Z84	2876	83	0,28108	1,12E-04	0,00070	3,16E-06	0,28093	0,28111	0,28104	-60,45	3,75	0,07	2,97	3,04	3,11	3,01
Z01	3323	43	0,28064	7,87E-05	0,00095	2,92E-05	0,28063	0,28077	0,28058	-75,85	-1,96	0,07	3,57	3,74	3,92	3,67
Z25	3417	64	0,28058	5,73E-05	0,00048	4,50E-05	0,28057	0,28069	0,28055	-77,86	-0,72	0,07	3,60	3,74	3,87	3,68

Assumed Values	
t (Ma)	4560
λ (Ga-1) [a]	0,01867
$(^{176}Hf/^{177}Hf)^0$chur [b]	0,282785
$(^{176}Hf/^{177}Hf)^i$ chur	0,279718
$(^{176}Lu/^{177}Hf)^0$ chur [b]	0,0336
$(^{176}Hf/^{177}Hf)$DM [c]	0,28325
$(^{176}Lu/^{177}Hf)$DM [c]	0,0388
$(^{176}Lu/^{177}Hf)$BSE [d]	0,015
$^{176}Lu/^{177}Hf$ [e]	0,022
$^{176}Lu/^{177}Hf$ [e]	0,010

a ^{176}Lu decay constant (Söderlund et al., 2004)
b Chondritic values (Bouvier et al., 2008)
c Present day Depleted Mantle (Griffin et al., 2000; updated by Andersen et al., 2009)
d Goodge and Vervoort, 2006. EPSL 243, 711-731
e $^{176}Lu/^{177}Hf$ ratios of mafic and felsic crust from Pietranik et al. (2008).

References

Andersen, T., Andersson, U.B., Graham, S., Aberg, G., Simonsen, S.L., 2009. Granitic magmatism by melting of juvenile continental crust: new constraints on the source of Palaeoproterozoic granitoids in Fennoscandia from Hf isotopes in zircon. Journal of the Geological Society 166, 233-247.

Bouvier A., Vervoort, J.D., Patchett, P.J., 2008. The Lu-Hf and Sm-Nd isotopic composition of CHUR: Constraints from unequilibrated chondrites and implications for the bulk composition of terrestrial planets. Earth and Planetary Science Letters 273, 48-57.

Goodge, J.W., Vervoort, J.D., 2006. Origin of Mesoproterozoic A-type granites in Laurentia: Hf isotope evidence. Earth and Planetary Science Letters 243, 711-731.

Griffin, W.L., Pearson, N.J., Belousova, E., Jackson, S.E., O'Reilly, S.Y., van Achterberg, E., Shee, S.R., 2000. The Hf isotope composition of cratonic mantle: LAM-MC-ICPMS analysis of zircon megacrysts in kimberlites. Geochimica et Cosmochimica Acta 64, 133-147.

Pietranik, A.B., Hawkesworth, C.J., Storey, C.D., Kemp, A.I.S., Sircombe, K.N., Whitehouse, M.J., Bleeker, W., 2008. Episodic, mafic crust formation from 4.5 to 2.8 Ga: New evidence from detrital zircons, Slave craton, Canada. Geology 36, 875-878.

Söderlund, U., Patchett, J.P., Vervoort, J.D., Isachsen, C., 2004. The 176Lu decay constant determined by Lu-Hf and U-Pb isotope systematics of Precambrian mafic intrusions. Earth and Planetary Science Letters 219, 311-324.

A1.8.4.5. Lu-Hf data of zircon grains from the greenish tuffaceous matrix of the Sopa-Brumadinho Fm. conglomerate, Southern Espinhaço (U-Pb ages after Chemale et al., 2012).

Spot Number	U/Pb Age (Ma)	±2s	Sample (Present day ratios) 176Hf/177Hf	±2SE	176Lu/177Hf	±2SE	Chur 176Hf/177Hf (t)	DM 176Hf/177Hf (t)	Sample Initial Ratios 176Hf/177Hf (t)	eHf(0)	eHf(t)	±2SE	DM Model Ages (Ga) T DM	T DM Crustal	Mafic	Felsic
A42	1149	14	0,28187	4,18E-05	0,00101	2,91E-05	0,28206	0,28241	0,28185	-32,42	-7,45	0,31	1,92	2,40	2,91	2,18
A24	1164	39	0,28214	4,91E-05	0,00103	1,46E-04	0,28205	0,28240	0,28211	-22,91	2,40	0,42	1,56	1,80	2,06	1,69
A41	1171	15	0,28194	3,52E-05	0,00062	8,53E-05	0,28204	0,28239	0,28192	-30,01	-4,24	0,64	1,81	2,22	2,65	2,04
A23	1174	24	0,28206	4,63E-05	0,00057	8,71E-06	0,28204	0,28239	0,28204	-25,80	0,08	0,00	1,65	1,95	2,27	1,82
A1	1176	19	0,28193	6,67E-05	0,00079	6,34E-05	0,28204	0,28239	0,28192	-30,09	-4,34	0,42	1,82	2,23	2,66	2,05
A19	1176	22	0,28149	6,06E-05	0,00053	2,79E-05	0,28204	0,28239	0,28147	-45,93	-20,03	1,42	2,41	3,20	4,01	2,85
A22	1176	15	0,28184	3,26E-05	0,00037	1,68E-05	0,28204	0,28239	0,28183	-33,44	-7,37	0,43	1,93	2,42	2,92	2,20
A27	1178	14	0,28191	4,86E-05	0,00096	1,56E-04	0,28204	0,28239	0,28189	-30,98	-5,33	0,93	1,87	2,29	2,75	2,10
A14	1187	19	0,28182	4,41E-05	0,00058	1,94E-06	0,28203	0,28238	0,28181	-34,14	-7,99	0,16	1,97	2,46	2,99	2,24
A12	1188	17	0,28128	6,78E-05	0,00076	1,98E-05	0,28203	0,28238	0,28126	-53,19	-27,22	1,10	2,70	3,64	4,63	3,22
A38	1195	19	0,28195	4,33E-05	0,00077	7,04E-05	0,28203	0,28237	0,28193	-29,62	-3,44	0,37	1,80	2,19	2,59	2,02
A10	1198	19	0,28167	6,98E-05	0,00052	5,19E-06	0,28203	0,28237	0,28165	-39,56	-13,13	0,34	2,17	2,79	3,44	2,52
A13	1227	27	0,28188	5,25E-05	0,00039	7,75E-06	0,28201	0,28235	0,28187	-32,17	-4,97	0,21	1,88	2,31	2,75	2,12
A34	1227	39	0,28218	4,53E-05	0,00159	1,26E-04	0,28201	0,28235	0,28214	-21,54	4,70	0,52	1,52	1,70	1,90	1,62
A2	1303	16	0,28201	4,33E-05	0,00050	1,20E-04	0,28196	0,28229	0,28199	-27,51	1,32	0,33	1,71	1,97	2,25	1,86
A8	1761	29	0,28142	8,42E-05	0,00071	2,47E-05	0,28166	0,28195	0,28139	-48,41	-9,57	0,49	2,52	3,01	3,52	2,79
A7	1765	57	0,28110	7,25E-05	0,00046	3,76E-06	0,28166	0,28195	0,28109	-59,42	-20,24	0,82	2,92	3,67	4,44	3,34
A43	1790	15	0,28170	7,01E-05	0,00119	8,81E-05	0,28164	0,28193	0,28166	-38,32	0,63	0,05	2,16	2,40	2,65	2,29
A6	1842	27	0,28136	6,23E-05	0,00057	5,28E-06	0,28161	0,28189	0,28134	-50,28	-9,45	0,23	2,58	3,06	3,56	2,85
A39	1877	5	0,28157	4,59E-05	0,00103	1,31E-04	0,28159	0,28187	0,28153	-43,08	-2,01	0,26	2,34	2,63	2,94	2,50
A36	1948	15	0,28157	3,55E-05	0,00086	3,88E-05	0,28154	0,28181	0,28154	-42,97	-0,09	0,00	2,32	2,56	2,82	2,46
A15	2056	15	0,28099	4,31E-05	0,00024	5,22E-06	0,28147	0,28173	0,28098	-63,61	-17,53	0,51	3,06	3,73	4,41	3,44
A26	2077	20	0,28149	4,17E-05	0,00052	8,50E-06	0,28146	0,28172	0,28147	-45,74	0,52	0,01	2,41	2,63	2,85	2,53
A35	2100	20	0,28119	3,64E-05	0,00069	4,47E-05	0,28144	0,28170	0,28117	-56,24	-9,74	0,73	2,81	3,28	3,77	3,08
A37	2100	20	0,28116	3,73E-05	0,00064	2,89E-05	0,28144	0,28170	0,28113	-57,46	-10,91	0,60	2,86	3,35	3,87	3,14
A28	2116	14	0,28138	3,14E-05	0,00041	2,18E-06	0,28143	0,28169	0,28137	-49,60	-2,32	0,03	2,54	2,83	3,13	2,71
A16	2121	13	0,28141	3,97E-05	0,00044	5,56E-06	0,28143	0,28168	0,28140	-48,51	-1,15	0,02	2,51	2,76	3,03	2,65
A20	2121	13	0,28086	3,12E-05	0,00047	5,45E-06	0,28143	0,28168	0,28084	-67,98	-20,75	0,37	3,24	3,98	4,73	3,66
A30	2121	29	0,28146	4,85E-05	0,00044	4,25E-06	0,28143	0,28168	0,28144	-46,92	0,46	0,01	2,44	2,66	2,89	2,57
A5	2161	17	0,28141	9,31E-05	0,00062	2,34E-05	0,28140	0,28165	0,28138	-48,66	-0,64	0,03	2,52	2,76	3,01	2,66
A3	2175	20	0,28151	8,42E-05	0,00078	6,85E-06	0,28139	0,28164	0,28147	-45,24	2,87	0,05	2,40	2,55	2,71	2,49
A33	2617	16	0,28101	4,56E-05	0,00096	2,59E-05	0,28110	0,28131	0,28096	-62,92	-5,17	0,17	3,09	3,40	3,72	3,26
A9	2649	18	0,28075	8,12E-05	0,00037	4,05E-06	0,28108	0,28128	0,28073	-72,02	-12,52	0,22	3,38	3,88	4,38	3,67
A40	2652	24	0,28114	3,01E-05	0,00067	4,97E-05	0,28108	0,28128	0,28110	-58,22	0,89	0,07	2,89	3,05	3,21	2,98
A32	2654	16	0,28108	4,44E-05	0,00064	3,32E-05	0,28108	0,28128	0,28105	-60,35	-1,14	0,07	2,96	3,18	3,39	3,09

Assumed Values	
t (Ma)	4560
λ (Ga-1) [a]	0,01867
$(^{176}Hf/^{177}Hf)^0$chur [b]	0,282785
$(^{176}Hf/^{177}Hf)^i$ chur	0,279718
$(^{176}Lu/^{177}Hf)^0$ chur [b]	0,0336
$(^{176}Hf/^{177}Hf)$DM [c]	0,28325
$(^{176}Lu/^{177}Hf)$DM [c]	0,0388
$(^{176}Lu/^{177}Hf)$BSE [d]	0,015
$^{176}Lu/^{177}Hf$ [e]	0,022
$^{176}Lu/^{177}Hf$ [e]	0,010

a ^{176}Lu decay constant (Söderlund et al., 2004)
b Chondritic values (Bouvier et al., 2008)
c Present day Depleted Mantle (Griffin et al., 2000; updated by Andersen et al., 2009)
d Goodge and Vervoort, 2006. EPSL 243, 711-731
e $^{176}Lu/^{177}Hf$ ratios of mafic and felsic crust from Pietranik et al. (2008).

References

Andersen, T., Andersson, U.B., Graham, S., Aberg, G., Simonsen, S.L., 2009. Granitic magmatism by melting of juvenile continental crust: new constraints on the source of Palaeoproterozoic granitoids in Fennoscandia from Hf isotopes in zircon. Journal of the Geological Society 166, 233-247.

Bouvier A., Vervoort, J.D., Patchett, P.J., 2008. The Lu-Hf and Sm-Nd isotopic composition of CHUR: Constraints from unequilibrated chondrites and implications for the bulk composition of terrestrial planets. Earth and Planetary Science Letters 273, 48-57.

Goodge, J.W., Vervoort, J.D., 2006. Origin of Mesoproterozoic A-type granites in Laurentia: Hf isotope evidence. Earth and Planetary Science Letters 243, 711-731.

Griffin, W.L., Pearson, N.J., Belousova, E., Jackson, S.E., O'Reilly, S.Y., van Achterberg, E., Shee, S.R., 2000. The Hf isotope composition of cratonic mantle: LAM-MC-ICPMS analysis of zircon megacrysts in kimberlites. Geochimica et Cosmochimica Acta 64, 133-147.

Pietranik, A.B., Hawkesworth, C.J., Storey, C.D., Kemp, A.I.S., Sircombe, K.N., Whitehouse, M.J., Bleeker, W., 2008. Episodic, mafic crust formation from 4.5 to 2.8 Ga: New evidence from detrital zircons, Slave craton, Canada. Geology 36, 875-878.

Söderlund, U., Patchett, J.P., Vervoort, J.D., Isachsen, C., 2004. The 176Lu decay constant determined by Lu-Hf and U-Pb isotope systematics of Precambrian mafic intrusions. Earth and Planetary Science Letters 219, 311-324.

A1.8.4.6. U-Pb zircon data of F4 sample (Sandstone layer, Tombador Fm.).

Spot Number	f_{206}	Pb (ppm)	Th (ppm)	U (ppm)	$^{232}Th/^{238}U$ [a]	Isotope ratios[b] $^{207}Pb/^{235}U$	1 s [%]	$^{206}Pb/^{238}U$	1 s [%]	Rho[c]	$^{207}Pb/^{206}Pb$ [d]	1 s [%]	Ages (Ma) $^{206}Pb/^{238}U$	1 s abs	$^{207}Pb/^{235}U$	1 s abs	$^{207}Pb/^{206}Pb$	1 s abs	% Conc[e]	Best estimate age (Ma)	±2s
Z37	0,0024	25	8	53	0,15	5,999	8,03	0,347	6,19	0,77	0,125	5,11	1919	119	1976	159	2035	104	6	2035	203
Z14	0,0010	97	136	204	0,67	6,586	4,82	0,377	4,24	0,88	0,127	2,30	2063	87	2057	99	2052	47	-1	2052	92
Z33N	0,0007	80	4	169	0,03	6,474	2,54	0,370	1,64	0,64	0,127	1,94	2030	33	2042	52	2055	40	1	2055	78
Z45	0,0015	40	76	81	0,95	6,342	3,20	0,362	1,61	0,50	0,127	2,76	1990	32	2024	65	2059	57	3	2059	111
Z98	0,0013	70	137	109	1,27	6,503	4,82	0,370	4,37	0,91	0,127	2,01	2031	89	2046	99	2062	42	1	2062	81
Z31	0,0016	87	160	141	1,14	6,827	3,74	0,385	3,12	0,84	0,129	2,06	2099	66	2089	78	2080	43	-1	2080	83
Z27	0,0030	85	180	137	1,32	6,666	3,20	0,375	2,52	0,79	0,129	1,98	2052	52	2068	66	2084	41	2	2084	81
Z60	0,0035	98	224	149	1,52	6,888	3,68	0,385	3,09	0,84	0,130	1,99	2099	65	2097	77	2095	42	0	2095	81
Z07	0,0043	32	64	62	1,04	7,075	10,13	0,393	8,76	0,87	0,130	5,08	2139	187	2121	215	2103	107	-2	2103	208
Z40	0,0055	136	206	253	0,82	6,593	5,90	0,362	5,27	0,89	0,132	2,65	1991	105	2058	121	2127	56	6	2127	110
Z51	0,0012	85	106	156	0,68	7,191	3,07	0,392	2,40	0,78	0,133	1,92	2134	51	2135	66	2137	41	0	2137	80
Z62	0,0020	85	115	149	0,77	6,684	3,34	0,365	2,57	0,77	0,133	2,14	2004	51	2070	69	2138	46	6	2138	89
Z16B	0,0029	27	55	61	0,91	7,040	5,84	0,381	4,64	0,79	0,134	3,55	2083	97	2116	124	2149	76	3	2149	149
Z09	0,0022	30	96	51	1,89	6,667	8,78	0,361	7,06	0,80	0,134	5,22	1988	140	2068	182	2149	112	8	2149	219
Z75	0,0017	49	110	82	1,35	7,217	4,45	0,391	3,69	0,83	0,134	2,48	2127	79	2139	95	2150	53	1	2150	104
Z44	0,0040	20	38	33	1,14	7,213	12,42	0,390	10,28	0,83	0,134	6,98	2121	218	2138	266	2155	150	2	2155	293
Z61	0,0010	104	212	158	1,35	7,533	4,29	0,406	3,88	0,91	0,135	1,81	2197	85	2177	93	2158	39	-2	2158	76
Z16N	0,0019	30	95	54	1,77	7,411	6,60	0,399	5,27	0,80	0,135	3,97	2165	114	2162	143	2159	86	0	2159	167
Z23	0,0017	63	192	117	1,65	7,671	4,77	0,412	3,86	0,81	0,135	2,79	2222	86	2193	105	2166	60	-3	2166	118
Z21	0,0015	30	42	65	0,65	7,534	6,88	0,402	5,25	0,76	0,136	4,44	2178	114	2177	150	2176	97	0	2176	188
Z57	0,0098	57	229	89	2,60	6,791	6,32	0,359	5,11	0,81	0,137	3,72	1980	101	2084	132	2190	82	10	2190	159
Z64	0,0059	8	1	13	0,05	10,153	19,69	0,481	15,78	0,80	0,153	11,77	2532	400	2449	482	2380	280	-6	2380	546
Z03	0,0023	33	24	52	0,46	9,494	5,19	0,431	4,22	0,81	0,160	3,02	2312	98	2387	124	2452	74	6	2452	145
Z26	0,0007	135	187	166	1,13	10,318	2,01	0,466	1,44	0,71	0,161	1,41	2464	35	2464	50	2463	35	0	2463	68
Z50	0,0011	84	132	133	1,00	9,589	3,42	0,421	2,88	0,84	0,165	1,85	2264	65	2396	82	2510	46	10	2510	90
Z81	0,0029	120	116	117	1,00	11,061	2,80	0,476	2,30	0,82	0,168	1,60	2512	58	2528	71	2541	41	1	2541	80
Z78	0,0021	41	68	57	1,21	11,441	5,04	0,490	4,81	0,95	0,169	1,51	2572	124	2560	129	2550	39	-1	2550	75
Z119	0,0051	176	256	254	1,02	10,680	2,59	0,451	1,86	0,72	0,172	1,80	2401	45	2496	65	2573	46	7	2573	90
Z55	0,0021	54	65	69	0,95	11,277	6,06	0,477	5,65	0,93	0,172	2,19	2512	142	2546	154	2573	56	2	2573	110
Z43	0,0017	61	87	90	0,97	11,318	3,88	0,477	2,97	0,77	0,172	2,50	2516	75	2550	99	2577	64	2	2577	125
Z29	0,0116	123	351	171	2,06	10,901	3,90	0,458	1,37	0,35	0,173	3,65	2431	33	2515	98	2583	94	6	2583	184
Z41	0,0008	86	59	119	0,50	11,915	3,69	0,493	3,15	0,85	0,175	1,92	2583	81	2598	96	2609	50	1	2609	98
Z84	0,0014	62	31	71	0,43	11,642	4,46	0,481	3,70	0,83	0,175	2,49	2533	94	2576	115	2610	65	3	2610	127
Z116	0,0015	92	110	119	0,93	12,161	4,02	0,502	3,69	0,92	0,176	1,60	2621	97	2617	105	2614	42	0	2614	82
Z19	0,0027	69	146	116	1,27	11,368	3,11	0,466	2,69	0,86	0,177	1,57	2464	66	2554	80	2626	41	6	2626	81
Z46	0,0058	39	61	64	0,95	11,622	6,44	0,469	5,16	0,80	0,180	3,85	2480	128	2574	166	2649	102	6	2649	199
Z71	0,0050	214	474	363	1,32	11,364	2,30	0,458	2,03	0,88	0,180	1,08	2431	49	2553	59	2652	29	8	2652	56
Z87	0,0042	125	196	142	1,38	12,559	2,70	0,506	1,79	0,66	0,180	2,03	2639	47	2647	72	2653	54	1	2653	105
Z18	0,0025	59	149	105	1,42	11,580	2,83	0,466	1,97	0,70	0,180	2,03	2466	49	2571	73	2655	54	7	2655	105
Z65	0,0008	137	162	164	1,00	12,568	2,76	0,503	2,40	0,87	0,181	1,36	2625	63	2648	73	2666	36	2	2666	71
Z70N	0,0020	145	123	207	0,60	14,180	3,09	0,549	2,81	0,91	0,187	1,29	2822	79	2762	85	2718	35	-4	2718	69
Z02	0,0009	65	35	77	0,46	15,466	5,40	0,550	5,04	0,93	0,204	1,96	2823	142	2844	154	2859	56	1	2859	110
Z91	0,0011	191	140	165	0,85	20,958	1,86	0,609	1,59	0,85	0,250	0,98	3064	49	3137	58	3183	31	4	3183	61
Z12	0,0020	124	128	165	0,78	22,433	2,84	0,651	2,17	0,76	0,250	1,83	3232	70	3203	91	3184	58	-1	3184	114
Z17	0,0007	94	69	120	0,58	21,354	2,42	0,617	1,78	0,73	0,251	1,65	3097	55	3155	76	3191	53	3	3191	103
Z86	0,0005	83	38	73	0,53	21,141	3,04	0,605	2,83	0,93	0,254	1,13	3048	86	3145	96	3207	36	5	3207	71
Z42	0,0004	118	86	131	0,66	22,309	3,18	0,634	2,98	0,94	0,255	1,13	3166	94	3197	102	3217	36	2	3217	71
Z94	0,0004	127	77	108	0,71	21,683	1,96	0,598	1,81	0,92	0,263	0,75	3021	55	3170	62	3265	25	7	3265	48
Z69	0,0011	186	128	189	0,68	23,710	2,62	0,650	2,30	0,88	0,265	1,25	3228	74	3257	85	3274	41	1	3274	80
Z111	0,0007	148	88	134	0,66	24,347	3,23	0,667	2,95	0,91	0,265	1,31	3293	97	3282	106	3276	43	-1	3276	84
Z104	0,0010	170	122	165	0,75	24,147	3,71	0,661	3,47	0,93	0,265	1,33	3271	113	3274	122	3276	44	0	3276	85
Z13	0,0011	73	56	86	0,65	23,909	3,34	0,650	2,64	0,79	0,267	2,04	3230	85	3265	109	3286	67	2	3286	131
Z67	0,0036	185	238	203	1,18	22,552	1,79	0,613	1,37	0,77	0,267	1,15	3084	42	3208	57	3286	38	6	3286	74
Z06	0,0026	27	16	33	0,48	25,240	8,39	0,686	6,34	0,76	0,267	5,49	3367	214	3318	278	3288	181	-2	3288	352
Z34	0,0018	38	40	39	1,03	23,068	6,83	0,624	5,88	0,86	0,268	3,46	3126	184	3230	221	3295	114	5	3295	222
Z52	0,0004	149	66	166	0,40	23,155	3,14	0,626	2,90	0,92	0,268	1,20	3134	91	3233	101	3295	39	5	3295	77
Z05B	0,0022	88	64	89	0,73	23,976	2,00	0,648	1,10	0,55	0,268	1,67	3220	35	3267	65	3296	55	2	3296	107
Z58	0,0027	123	101	107	0,95	24,801	4,67	0,669	4,18	0,90	0,269	2,08	3302	138	3300	154	3300	69	0	3300	134
Z77	0,0033	260	265	286	0,93	23,844	3,12	0,641	2,57	0,82	0,270	1,77	3194	82	3262	102	3304	58	3	3304	114
Z05N	0,0071	69	134	73	1,84	23,563	3,48	0,627	2,66	0,76	0,273	2,25	3138	83	3250	113	3321	75	6	3321	145
~~Z53~~	~~0,0168~~	~~129~~	~~329~~	~~151~~	~~2,19~~	~~24,256~~	~~5,19~~	~~0,622~~	~~4,77~~	~~0,92~~	~~0,283~~	~~2,03~~	~~3117~~	~~149~~	~~3279~~	~~170~~	~~3379~~	~~69~~	~~8~~		
Z01	0,0066	41	76	64	1,19	8,717	6,69	0,349	5,65	0,84	0,181	3,60	1928	109	2309	155	2665	96	28		
~~Z04~~	~~0,0268~~	~~68~~	~~289~~	~~151~~	~~1,93~~	~~5,748~~	~~8,15~~	~~0,272~~	~~6,98~~	~~0,86~~	~~0,153~~	~~4,20~~	~~1549~~	~~108~~	~~1939~~	~~158~~	~~2385~~	~~100~~	~~35~~		
~~Z08~~	~~0,1223~~	~~246~~	~~1933~~	~~1180~~	~~1,65~~	~~3,524~~	~~17,02~~	~~0,089~~	~~7,47~~	~~0,44~~	~~0,287~~	~~15,29~~	~~551~~	~~41~~	~~1533~~	~~261~~	~~3399~~	~~520~~	~~84~~		
~~Z11~~	~~0,0902~~	~~237~~	~~1735~~	~~943~~	~~1,85~~	~~3,658~~	~~5,18~~	~~0,116~~	~~3,43~~	~~0,66~~	~~0,229~~	~~3,87~~	~~708~~	~~24~~	~~1562~~	~~81~~	~~3043~~	~~118~~	~~77~~		
~~Z11B~~	~~0,0251~~	~~148~~	~~508~~	~~331~~	~~1,55~~	~~8,060~~	~~3,41~~	~~0,303~~	~~2,37~~	~~0,69~~	~~0,193~~	~~2,45~~	~~1705~~	~~40~~	~~2238~~	~~76~~	~~2769~~	~~68~~	~~38~~		
~~Z15~~	~~0,0211~~	~~217~~	~~726~~	~~475~~	~~1,54~~	~~13,934~~	~~2,31~~	~~0,383~~	~~2,00~~	~~0,87~~	~~0,264~~	~~1,15~~	~~2088~~	~~42~~	~~2745~~	~~63~~	~~3272~~	~~38~~	~~36~~		
~~Z20~~	~~0,1284~~	~~249~~	~~1709~~	~~775~~	~~2,22~~	~~5,704~~	~~6,23~~	~~0,210~~	~~2,91~~	~~0,47~~	~~0,197~~	~~5,51~~	~~1231~~	~~36~~	~~1932~~	~~120~~	~~2799~~	~~154~~	~~56~~		
Z22	0,0092	96	319	159	2,02	19,769	3,55	0,549	2,36	0,66	0,261	2,66	2823	67	3080	109	3252	86	13		
~~Z24~~	~~0,0320~~	~~274~~	~~954~~	~~548~~	~~1,75~~	~~8,340~~	~~2,63~~	~~0,296~~	~~2,24~~	~~0,85~~	~~0,204~~	~~1,37~~	~~1673~~	~~38~~	~~2269~~	~~60~~	~~2860~~	~~39~~	~~41~~		
~~Z25~~	~~0,0127~~	~~228~~	~~449~~	~~353~~	~~1,28~~	~~10,409~~	~~2,58~~	~~0,402~~	~~2,20~~	~~0,85~~	~~0,188~~	~~1,35~~	~~2179~~	~~48~~	~~2472~~	~~64~~	~~2723~~	~~37~~	~~20~~		
Z28	0,0095	297	435	377	1,16	16,973	1,86	0,465	1,39	0,75	0,265	1,23	2460	34	2933	55	3276	40	25		
~~Z30~~	~~0,0545~~	~~279~~	~~1298~~	~~709~~	~~1,84~~	~~5,131~~	~~6,80~~	~~0,203~~	~~6,06~~	~~0,89~~	~~0,184~~	~~3,09~~	~~1190~~	~~72~~	~~1841~~	~~125~~	~~2685~~	~~83~~	~~56~~		
~~Z32~~	~~0,0172~~	~~123~~	~~425~~	~~259~~	~~1,65~~	~~7,169~~	~~8,12~~	~~0,353~~	~~3,24~~	~~0,40~~	~~0,147~~	~~7,44~~	~~1951~~	~~63~~	~~2133~~	~~173~~	~~2313~~	~~172~~	~~16~~		
~~Z33~~	~~0,1262~~	~~297~~	~~2054~~	~~999~~	~~2,07~~	~~4,806~~	~~6,24~~	~~0,125~~	~~5,36~~	~~0,86~~	~~0,280~~	~~3,19~~	~~758~~	~~41~~	~~1786~~	~~111~~	~~3360~~	~~107~~	~~77~~		
~~Z35~~	~~0,0939~~	~~139~~	~~1791~~	~~362~~	~~4,98~~	~~6,108~~	~~4,51~~	~~0,173~~	~~3,69~~	~~0,82~~	~~0,255~~	~~2,59~~	~~1031~~	~~38~~	~~1991~~	~~90~~	~~3219~~	~~83~~	~~68~~		
~~Z36~~	~~0,0622~~	~~300~~	~~1328~~	~~951~~	~~1,41~~	~~4,200~~	~~3,69~~	~~0,165~~	~~2,93~~	~~0,80~~	~~0,184~~	~~2,23~~	~~987~~	~~29~~	~~1674~~	~~62~~	~~2690~~	~~60~~	~~63~~		
Z38	0,0027	192	289	303	0,96	10,763	1,93	0,433	1,06	0,55	0,180	1,62	2318	24	2503	48	2657	43	13		
Z39	0,0035	66	157	85	1,86	10,048	4,38	0,398	3,86	0,88	0,183	2,08	2161	83	2439	107	2680	56	19		
~~Z49~~	~~0,0246~~	~~259~~	~~1032~~	~~606~~	~~1,72~~	~~7,483~~	~~4,11~~	~~0,284~~	~~3,83~~	~~0,93~~	~~0,191~~	~~1,49~~	~~1610~~	~~62~~	~~2171~~	~~89~~	~~2753~~	~~41~~	~~42~~		
~~Z66~~	~~0,0972~~	~~463~~	~~2650~~	~~1547~~	~~1,73~~	~~4,108~~	~~4,46~~	~~0,125~~	~~4,10~~	~~0,92~~	~~0,239~~	~~1,77~~	~~758~~	~~31~~	~~1656~~	~~74~~	~~3111~~	~~55~~	~~76~~		
Z68	0,0039	158	204	264	0,78	10,000	6,41	0,406	6,25	0,98	0,179	1,41	2197	137	2435	156	2640	37	17		
~~Z70B~~	~~0,0476~~	~~325~~	~~2081~~	~~1011~~	~~2,07~~	~~4,539~~	~~7,57~~	~~0,129~~	~~7,39~~	~~0,98~~	~~0,256~~	~~1,63~~	~~780~~	~~58~~	~~1738~~	~~132~~	~~3222~~	~~52~~	~~76~~		
Z74	0,0034	143	187	262	0,72	10,538	2,41	0,432	1,85	0,77	0,177	1,55	2313	43	2483	60	2626	41	12		
~~Z80~~	~~0,0154~~	~~235~~	~~334~~	~~561~~	~~0,60~~	~~6,801~~	~~3,72~~	~~0,273~~	~~3,33~~	~~0,90~~	~~0,181~~	~~1,65~~	~~1556~~	~~52~~	~~2086~~	~~78~~	~~2659~~	~~44~~	~~41~~		
~~Z83~~	~~0,0304~~	~~121~~	~~463~~	~~250~~	~~1,86~~	~~4,701~~	~~3,18~~	~~0,201~~	~~2,83~~	~~0,89~~	~~0,170~~	~~1,44~~	~~1179~~	~~33~~	~~1767~~	~~56~~	~~2556~~	~~37~~	~~54~~		
Z93	0,0005	13	1	18	0,05	9,333	10,43	0,478	6,04	0,58	0,142	8,51	2519	152	2371	247	2247	191	-12		
~~Z95~~	~~0,0723~~	~~292~~	~~1427~~	~~740~~	~~1,94~~	~~5,213~~	~~3,37~~	~~0,147~~	~~3,04~~	~~0,90~~	~~0,257~~	~~1,45~~	~~885~~	~~27~~	~~1855~~	~~63~~	~~3228~~	~~47~~	~~73~~		
~~Z103~~	~~0,0833~~	~~194~~	~~1128~~	~~457~~	~~2,49~~	~~6,746~~	~~4,11~~	~~0,201~~	~~2,18~~	~~0,53~~	~~0,243~~	~~3,49~~	~~1181~~	~~26~~	~~2079~~	~~85~~	~~3142~~	~~110~~	~~62~~		
~~Z105~~	~~0,0267~~	~~214~~	~~806~~	~~366~~	~~2,22~~	~~7,790~~	~~3,06~~	~~0,288~~	~~2,73~~	~~0,89~~	~~0,196~~	~~1,38~~	~~1631~~	~~45~~	~~2207~~	~~68~~	~~2795~~	~~39~~	~~42~~		
~~Z109~~	~~0,0534~~	~~293~~	~~1335~~	~~803~~	~~1,68~~	~~4,250~~	~~8,12~~	~~0,110~~	~~7,83~~	~~0,97~~	~~0,281~~	~~2,13~~	~~672~~	~~53~~	~~1684~~	~~137~~	~~3367~~	~~72~~	~~80~~		
~~Z114~~	~~0,0130~~	~~118~~	~~404~~	~~188~~	~~2,17~~	~~8,975~~	~~3,75~~	~~0,342~~	~~3,20~~	~~0,85~~	~~0,190~~	~~1,95~~	~~1897~~	~~61~~	~~2335~~	~~88~~	~~2744~~	~~54~~	~~31~~		
~~Z121~~	~~0,0429~~	~~268~~	~~2082~~	~~693~~	~~3,02~~	~~7,368~~	~~3,09~~	~~0,240~~	~~2,36~~	~~0,76~~	~~0,223~~	~~2,00~~	~~1387~~	~~33~~	~~2157~~	~~67~~	~~2999~~	~~60~~	~~54~~		

a Th/U ratios are calculated relative to GJ-1 reference zircon

b Corrected for background and within-run Pb/U fractionation and normalised to reference zircon GJ-1 (ID-TIMS values/measured value); 207Pb/235U calculated using (207Pb/206Pb)/(238U/206Pb * 1/137.88)

c Rho is the error correlation defined as the quotient of the propagated errors of the 206Pb/238U and the 207/235U ratio

d Corrected for mass-bias by normalising to GJ-1 reference zircon and common Pb using the model Pb composition of Stacey and Kramers (1975)

e Degree of concordance = [(206Pb/238U age) / (207Pb/206U age)]*100

Reference

Stacey, J.S., Kramers, J.D., 1975. Approximation of terrestrial lead isotope evolution by a two-stage model. Earth and Planetary Science Letters 26, 207–221.

A1.8.4.7. U-Pb zircon data of F14 sample (Sandstone layer, Tombador Fm.).

						Isotope ratios[b]							Ages (Ma)								
Spot Number	f_{206}	Pb (ppm)	Th (ppm)	U (ppm)	$^{232}Th/^{238}U^{a}$	$^{207}Pb/^{235}U$	1 s [%]	$^{206}Pb/^{238}U$	1 s [%]	Rho[c]	$^{207}Pb/^{206}Pb^{d}$	1 s [%]	$^{206}Pb/^{238}U$	1 s abs	$^{207}Pb/^{235}U$	1 s abs	$^{207}Pb/^{206}Pb$	1 s abs	% Conc[e]	Best estimate age (Ma)	±2s
Z100	0,0083	20	22	28	0,80	4,880	4,86	0,309	4,22	0,87	0,114	2,40	1737	73	1799	87	1871	45	7	1871	87
Z60	0,0021	145	228	211	1,09	4,906	3,18	0,307	2,59	0,82	0,116	1,84	1726	45	1803	57	1894	35	9	1894	68
Z45	0,0015	97	94	133	0,71	6,494	2,75	0,387	2,14	0,78	0,122	1,72	2107	45	2045	56	1983	34	-6	1983	66
Z91N	0,0066	142	200	214	0,94	5,945	16,04	0,344	10,19	0,64	0,125	12,39	1908	194	1968	316	2032	252	6	2032	491
Z63	0,0008	272	218	446	0,49	6,710	2,15	0,385	1,40	0,65	0,127	1,63	2098	29	2074	45	2050	33	-2	2050	65
Z97	0,0022	207	182	319	0,58	6,367	2,55	0,363	1,99	0,78	0,127	1,58	1998	40	2028	52	2058	33	3	2058	64
Z93	0,0010	179	269	215	1,26	6,906	2,60	0,392	2,01	0,77	0,128	1,65	2134	43	2099	55	2066	34	-3	2066	66
Z34	0,0014	201	149	291	0,52	7,119	2,39	0,402	1,85	0,77	0,128	1,52	2180	40	2126	51	2075	32	-5	2075	61
Z87	0,0021	174	135	251	0,54	6,848	3,58	0,385	3,12	0,87	0,129	1,74	2100	66	2092	75	2083	36	-1	2083	71
Z75	0,0015	59	60	81	0,75	7,066	2,88	0,396	1,20	0,42	0,129	2,62	2152	26	2120	61	2088	55	-3	2088	107
Z19	0,0009	138	148	244	0,61	7,844	3,94	0,428	3,52	0,89	0,133	1,78	2295	81	2213	87	2138	38	-7	2138	74
Z09	0,0046	80	167	189	0,89	7,562	5,02	0,403	4,44	0,88	0,136	2,35	2181	97	2180	110	2180	51	0	2180	100
Z84	0,0016	89	50	126	0,39	8,558	2,85	0,454	2,50	0,88	0,137	1,36	2412	60	2292	65	2187	30	-10	2187	58
Z83	0,0024	13	0	14	0,03	10,906	9,91	0,494	7,87	0,79	0,160	6,03	2586	203	2515	249	2459	148	-5	2459	289
Z14	0,0085	20	1	20	0,05	10,479	22,09	0,460	21,44	0,97	0,165	5,32	2441	523	2478	547	2509	133	3	2509	260
Z17	0,0018	221	259	439	0,59	10,289	3,15	0,452	2,06	0,65	0,165	2,39	2403	50	2461	78	2509	60	4	2509	117
Z13	0,0015	172	220	234	0,95	12,039	4,59	0,522	3,94	0,86	0,167	2,36	2708	107	2607	120	2530	60	-7	2530	116
Z66B	0,0007	133	90	146	0,62	12,061	2,11	0,509	1,16	0,55	0,172	1,76	2652	31	2609	55	2576	45	-3	2576	88
Z66N	0,0008	140	103	167	0,62	12,180	2,23	0,514	1,70	0,76	0,172	1,44	2672	46	2618	58	2577	37	-4	2577	72
Z73	0,0009	204	56	239	0,24	10,853	2,79	0,453	2,09	0,75	0,174	1,84	2408	50	2511	70	2595	48	7	2595	93
Z85	0,0007	144	94	142	0,67	12,159	2,55	0,505	2,21	0,86	0,175	1,29	2634	58	2617	67	2604	33	-1	2604	65
Z30	0,0008	207	127	231	0,56	12,639	3,43	0,524	3,13	0,91	0,175	1,41	2717	85	2653	91	2605	37	-4	2605	71
Z44	0,0006	272	105	314	0,34	12,306	2,41	0,509	1,63	0,68	0,175	1,77	2653	43	2628	63	2609	46	-2	2609	90
Z46N	0,0024	106	58	118	0,49	13,388	5,21	0,548	4,99	0,96	0,177	1,48	2817	141	2707	141	2627	39	-7	2627	76
Z46	0,0014	183	86	200	0,44	13,338	1,30	0,545	0,93	0,72	0,178	0,90	2803	26	2704	35	2630	24	-7	2630	46
Z61	0,0024	356	194	517	0,38	12,887	2,36	0,525	2,03	0,86	0,178	1,21	2722	55	2671	63	2634	32	-3	2634	62
Z62-2	0,0042	274	180	393	0,46	11,235	1,99	0,453	1,47	0,74	0,180	1,34	2410	35	2543	51	2650	36	9	2650	69
Z39	0,0049	295	342	412	0,84	12,261	1,98	0,489	1,70	0,86	0,182	1,02	2567	44	2625	52	2670	27	4	2670	53
Z95	0,0010	96	100	80	1,26	14,114	3,61	0,544	3,20	0,89	0,188	1,68	2801	90	2757	100	2725	46	-3	2725	89
Z40	0,0009	135	96	117	0,83	15,346	2,49	0,589	2,06	0,83	0,189	1,39	2985	62	2837	70	2734	38	-9	2734	74
Z79	0,0000	9	1	6	0,11	22,086	15,36	0,615	11,95	0,78	0,260	9,65	3092	369	3188	490	3248	314	5	3248	611
Z15	0,0028	154	115	188	0,62	24,606	20,69	0,678	20,17	0,97	0,263	4,63	3335	673	3293	681	3267	151	-2	3267	295
Z59	0,0016	107	37	95	0,39	23,114	2,88	0,636	2,50	0,87	0,264	1,43	3174	79	3232	93	3268	47	3	3268	91
Z20	0,0065	224	180	259	0,70	27,455	2,16	0,750	1,92	0,89	0,266	0,98	3607	69	3400	73	3280	32	-10	3280	63
Z26	0,0007	157	92	120	0,77	25,464	1,79	0,694	1,24	0,69	0,266	1,30	3399	42	3326	60	3283	43	-4	3283	83
Z08	0,0028	37	21	43	0,50	23,751	5,59	0,648	4,86	0,87	0,266	2,77	3219	156	3258	182	3283	91	2	3283	177
Z27	0,0013	90	57	69	0,82	24,904	3,08	0,677	2,67	0,86	0,267	1,55	3333	89	3304	102	3287	51	-1	3287	99
Z92	0,0007	131	61	96	0,64	25,870	1,82	0,703	1,41	0,77	0,267	1,15	3433	48	3342	61	3287	38	-4	3287	74
Z22	0,0004	210	123	189	0,65	25,732	2,68	0,699	2,54	0,94	0,267	0,88	3417	87	3336	90	3288	29	-4	3288	56
Z32	0,0005	160	64	136	0,48	25,285	2,23	0,684	1,92	0,86	0,268	1,12	3361	65	3319	74	3294	37	-2	3294	72
Z76	0,0009	113	44	72	0,61	25,687	1,47	0,695	1,25	0,85	0,268	0,78	3402	43	3335	49	3294	26	-3	3294	50
Z94	0,0008	146	63	108	0,59	25,451	1,63	0,687	1,33	0,81	0,269	0,95	3372	45	3326	54	3298	31	-2	3298	61
Z25	0,0004	276	117	214	0,55	27,353	1,98	0,738	1,71	0,86	0,269	1,00	3562	61	3396	67	3300	33	-8	3300	65
Z81	0,0016	130	114	117	0,99	27,588	1,69	0,744	1,02	0,60	0,269	1,35	3585	36	3405	57	3300	44	-9	3300	87
Z77	0,0007	148	51	92	0,56	26,333	1,80	0,710	1,56	0,86	0,269	0,91	3457	54	3359	61	3301	30	-5	3301	59
Z58	0,0014	60	26	51	0,52	26,060	3,52	0,702	3,15	0,89	0,269	1,58	3429	108	3349	118	3301	52	-4	3301	102
Z03	0,0008	543	468	594	0,79	27,522	5,18	0,741	4,30	0,83	0,269	2,89	3573	154	3402	176	3303	96	-8	3303	186
Z35	0,0007	162	64	107	0,61	25,884	3,69	0,696	3,56	0,97	0,270	0,96	3405	121	3342	123	3305	32	-3	3305	62
Z98	0,0003	244	109	209	0,53	25,428	1,46	0,681	1,02	0,70	0,271	1,04	3348	34	3325	48	3311	34	-1	3311	67
Z72	0,0017	181	113	141	0,80	25,564	1,30	0,684	1,03	0,79	0,271	0,80	3359	35	3330	43	3312	26	-1	3312	52
Z31	0,0006	157	147	181	0,82	27,020	3,79	0,719	3,53	0,93	0,273	1,37	3491	123	3384	128	3322	45	-5	3322	88
Z16	0,0037	317	299	423	0,71	22,812	3,28	0,603	3,05	0,93	0,274	1,20	3042	93	3219	106	3331	40	9	3331	78
Z64	0,0008	119	37	96	0,38	28,173	2,91	0,714	2,68	0,92	0,286	1,11	3472	93	3425	100	3398	38	-2	3398	74
Z78	0,0045	88	134	80	1,69	28,378	1,87	0,713	1,16	0,62	0,289	1,48	3469	40	3432	64	3411	50	-2	3411	98
~~Z01~~	~~0,0210~~	~~379~~	~~891~~	~~1153~~	~~0,78~~	~~12,625~~	~~7,77~~	~~0,483~~	~~4,43~~	~~0,57~~	~~0,190~~	~~6,39~~	~~2539~~	~~112~~	~~2652~~	~~206~~	~~2739~~	~~175~~	~~7~~		
~~Z02~~	~~0,1144~~	~~949~~	~~5146~~	~~5055~~	~~1,03~~	~~4,638~~	~~7,01~~	~~0,094~~	~~6,81~~	~~0,97~~	~~0,360~~	~~1,65~~	~~577~~	~~39~~	~~1756~~	~~123~~	~~3748~~	~~62~~	~~85~~		
Z04	0,0012	83	145	156	0,93	8,287	2,83	0,453	2,15	0,76	0,133	1,84	2407	52	2263	64	2135	39	-13		
Z05	0,0016	243	499	372	1,35	7,152	7,92	0,305	7,79	0,98	0,170	1,45	1717	134	2131	169	2557	37	33		
~~Z6~~	~~0,0110~~	~~421~~	~~1091~~	~~1545~~	~~0,71~~	~~4,460~~	~~4,03~~	~~0,258~~	~~3,80~~	~~0,94~~	~~0,125~~	~~1,35~~	~~1481~~	~~56~~	~~1724~~	~~69~~	~~2032~~	~~27~~	~~27~~		
Z07	0,0016	129	164	201	0,82	13,502	2,28	0,570	1,10	0,48	0,172	2,00	2909	32	2715	62	2574	51	-13		
~~Z10~~	~~0,0248~~	~~67~~	~~120~~	~~117~~	~~1,04~~	~~17,884~~	~~31,15~~	~~0,468~~	~~29,29~~	~~0,94~~	~~0,277~~	~~10,60~~	~~2474~~	~~725~~	~~2984~~	~~929~~	~~3348~~	~~355~~	~~26~~		
~~Z12~~	~~0,0156~~	~~136~~	~~341~~	~~387~~	~~0,89~~	~~6,573~~	~~13,61~~	~~0,236~~	~~12,88~~	~~0,95~~	~~0,202~~	~~4,40~~	~~1365~~	~~176~~	~~2056~~	~~280~~	~~2844~~	~~125~~	~~52~~		
Z19B	0,0074	300	644	995	0,65	2,936	10,14	0,171	7,94	0,78	0,125	6,30	1016	81	1391	141	2025	128	50		
~~Z23~~	~~0,0428~~	~~17~~	~~4~~	~~17~~	~~0,26~~	~~15,610~~	~~12,61~~	~~0,551~~	~~11,80~~	~~0,94~~	~~0,205~~	~~4,45~~	~~2831~~	~~334~~	~~2853~~	~~360~~	~~2869~~	~~128~~	~~1~~		
~~Z29~~	~~0,1828~~	~~2140~~	~~10053~~	~~6709~~	~~1,51~~	~~3,999~~	~~17,59~~	~~0,059~~	~~13,39~~	~~0,76~~	~~0,493~~	~~11,40~~	~~368~~	~~49~~	~~1634~~	~~287~~	~~4221~~	~~481~~	~~91~~		
~~Z33~~	~~0,0857~~	~~45~~	~~10~~	~~33~~	~~0,32~~	~~14,422~~	~~24,22~~	~~0,411~~	~~8,34~~	~~0,34~~	~~0,254~~	~~22,74~~	~~2221~~	~~185~~	~~2778~~	~~673~~	~~3212~~	~~731~~	~~31~~		
Z37	0,0016	385	21	372	0,06	16,083	4,52	0,478	4,00	0,89	0,244	2,09	2518	101	2882	130	3147	66	20		
~~Z43~~	~~0,1482~~	~~1100~~	~~6137~~	~~4276~~	~~1,45~~	~~3,319~~	~~7,08~~	~~0,066~~	~~6,77~~	~~0,96~~	~~0,365~~	~~2,09~~	~~412~~	~~28~~	~~1485~~	~~105~~	~~3770~~	~~79~~	~~89~~		
Z48	0,0073	131	207	150	1,39	19,549	2,07	0,520	1,65	0,79	0,273	1,26	2699	44	3069	64	3322	42	19		
~~Z51~~	~~0,0472~~	~~389~~	~~1316~~	~~1226~~	~~1,08~~	~~5,231~~	~~4,63~~	~~0,181~~	~~4,33~~	~~0,94~~	~~0,210~~	~~1,64~~	~~1073~~	~~46~~	~~1858~~	~~86~~	~~2902~~	~~48~~	~~63~~		
~~Z53~~	~~0,0627~~	~~546~~	~~1805~~	~~1798~~	~~1,01~~	~~10,097~~	~~9,52~~	~~0,312~~	~~5,73~~	~~0,60~~	~~0,235~~	~~7,61~~	~~1751~~	~~100~~	~~2444~~	~~233~~	~~3084~~	~~235~~	~~43~~		
~~Z55~~	~~0,1703~~	~~783~~	~~7810~~	~~3996~~	~~1,97~~	~~2,855~~	~~11,39~~	~~0,043~~	~~11,26~~	~~0,99~~	~~0,477~~	~~1,76~~	~~274~~	~~31~~	~~1370~~	~~156~~	~~4170~~	~~73~~	~~93~~		
~~Z56~~	~~0,1201~~	~~559~~	~~3093~~	~~2595~~	~~1,20~~	~~2,717~~	~~11,86~~	~~0,072~~	~~11,21~~	~~0,95~~	~~0,275~~	~~3,85~~	~~446~~	~~50~~	~~1333~~	~~158~~	~~3333~~	~~128~~	~~87~~		
~~Z57~~	~~0,0656~~	~~359~~	~~1348~~	~~1181~~	~~1,15~~	~~5,145~~	~~7,10~~	~~0,130~~	~~7,00~~	~~0,99~~	~~0,288~~	~~1,21~~	~~786~~	~~55~~	~~1844~~	~~131~~	~~3406~~	~~41~~	~~77~~		
~~Z62~~	~~0,0118~~	~~344~~	~~368~~	~~619~~	~~0,60~~	~~8,495~~	~~1,50~~	~~0,326~~	~~1,14~~	~~0,76~~	~~0,189~~	~~0,98~~	~~1817~~	~~21~~	~~2285~~	~~34~~	~~2735~~	~~27~~	~~34~~		
~~Z65~~	~~0,1349~~	~~454~~	~~1147~~	~~1524~~	~~0,76~~	~~4,592~~	~~4,96~~	~~0,106~~	~~4,64~~	~~0,93~~	~~0,314~~	~~1,77~~	~~649~~	~~30~~	~~1748~~	~~87~~	~~3543~~	~~63~~	~~82~~		
~~Z67~~	~~0,0165~~	~~268~~	~~469~~	~~562~~	~~0,84~~	~~8,727~~	~~5,47~~	~~0,352~~	~~4,88~~	~~0,89~~	~~0,180~~	~~2,45~~	~~1946~~	~~95~~	~~2310~~	~~126~~	~~2649~~	~~65~~	~~27~~		
~~Z68~~	~~0,0270~~	~~480~~	~~776~~	~~1771~~	~~0,44~~	~~2,944~~	~~2,78~~	~~0,164~~	~~2,16~~	~~0,78~~	~~0,131~~	~~1,75~~	~~976~~	~~21~~	~~1393~~	~~39~~	~~2106~~	~~37~~	~~54~~		
~~Z69~~	~~0,0168~~	~~104~~	~~328~~	~~130~~	~~2,54~~	~~12,724~~	~~3,85~~	~~0,328~~	~~3,56~~	~~0,93~~	~~0,282~~	~~1,46~~	~~1827~~	~~65~~	~~2659~~	~~102~~	~~3372~~	~~49~~	~~46~~		
~~Z70N~~	~~0,1544~~	~~718~~	~~5802~~	~~4054~~	~~1,44~~	~~2,106~~	~~9,77~~	~~0,041~~	~~9,48~~	~~0,97~~	~~0,377~~	~~2,36~~	~~256~~	~~24~~	~~1151~~	~~112~~	~~3818~~	~~90~~	~~93~~		
~~Z70B~~	~~0,1438~~	~~1504~~	~~4240~~	~~4497~~	~~0,95~~	~~4,385~~	~~4,18~~	~~0,094~~	~~3,80~~	~~0,91~~	~~0,338~~	~~1,74~~	~~579~~	~~22~~	~~1709~~	~~71~~	~~3656~~	~~64~~	~~84~~		
~~Z71~~	~~0,0191~~	~~214~~	~~343~~	~~328~~	~~1,06~~	~~11,942~~	~~2,04~~	~~0,324~~	~~1,72~~	~~0,84~~	~~0,267~~	~~1,10~~	~~1810~~	~~31~~	~~2600~~	~~53~~	~~3290~~	~~36~~	~~45~~		
~~Z74~~	~~0,0105~~	~~102~~	~~134~~	~~108~~	~~1,25~~	~~18,272~~	~~1,59~~	~~0,440~~	~~1,24~~	~~0,78~~	~~0,301~~	~~0,99~~	~~2349~~	~~29~~	~~3004~~	~~48~~	~~3477~~	~~34~~	~~32~~		
~~Z80~~	~~0,0867~~	~~20~~	~~15~~	~~17~~	~~0,93~~	~~60,549~~	~~38,13~~	~~0,704~~	~~31,73~~	~~0,83~~	~~0,624~~	~~21,14~~	~~3435~~	~~1090~~	~~4183~~	~~1595~~	~~4565~~	~~965~~	~~25~~		
~~Z88~~	~~0,0405~~	~~15~~	~~1~~	~~11~~	~~0,06~~	~~14,273~~	~~2,47~~	~~0,489~~	~~2,28~~	~~0,93~~	~~0,212~~	~~0,94~~	~~2565~~	~~59~~	~~2768~~	~~68~~	~~2920~~	~~27~~	~~12~~		
~~Z89~~	~~0,0140~~	~~413~~	~~552~~	~~943~~	~~0,59~~	~~4,420~~	~~3,07~~	~~0,232~~	~~2,62~~	~~0,85~~	~~0,138~~	~~1,60~~	~~1345~~	~~35~~	~~1716~~	~~53~~	~~2205~~	~~35~~	~~39~~		
~~Z90~~	~~0,1387~~	~~623~~	~~2763~~	~~2735~~	~~1,02~~	~~2,945~~	~~9,66~~	~~0,066~~	~~8,80~~	~~0,91~~	~~0,325~~	~~3,99~~	~~410~~	~~36~~	~~1394~~	~~135~~	~~3594~~	~~144~~	~~89~~		
Z91B	0,0052	141	228	292	0,79	5,128	5,10	0,297	4,93	0,97	0,125	1,29	1678	83	1841	94	2030	26	17		
~~Z96~~	~~0,0136~~	~~18~~	~~9~~	~~22~~	~~0,40~~	~~7,217~~	~~9,53~~	~~0,400~~	~~7,21~~	~~0,76~~	~~0,131~~	~~6,23~~	~~2167~~	~~156~~	~~2139~~	~~204~~	~~2111~~	~~132~~	~~-3~~		
~~Z99~~	~~0,1812~~	~~416~~	~~3137~~	~~2191~~	~~1,44~~	~~2,291~~	~~25,86~~	~~0,038~~	~~25,22~~	~~0,98~~	~~0,442~~	~~5,73~~	~~238~~	~~60~~	~~1210~~	~~313~~	~~4057~~	~~232~~	~~94~~		

a Th/U ratios are calculated relative to GJ-1 reference zircon
b Corrected for background and within-run Pb/U fractionation and normalised to reference zircon GJ-1 (ID-TIMS values/measured value); 207Pb/235U calculated using (207Pb/206Pb)/(238U/206Pb * 1/137.88)
c Rho is the error correlation defined as the quotient of the propagated errors of the 206Pb/238U and the 207/235U ratio
d Corrected for mass-bias by normalising to GJ-1 reference zircon and common Pb using the model Pb composition of Stacey and Kramers (1975)
e Degree of concordance = [(206Pb/238U age) / (207Pb/206U age)]*100

Reference

Stacey, J.S., Kramers, J.D., 1975. Approximation of terrestrial lead isotope evolution by a two-stage model. Earth and Planetary Science Letters 26, 207–221.

A1.8.4.8. U-Pb zircon data of P1 sample (Sandstone layer, Tombador Fm.).

Spot Number	f_{206}	Pb (ppm)	Th (ppm)	U (ppm)	$^{232}Th/^{238}U$[a]	Isotope ratios[b] $^{207}Pb/^{235}U$	1 s [%]	$^{206}Pb/^{238}U$	1 s [%]	Rho[c]	$^{207}Pb/^{206}Pb$[d]	1 s [%]	Ages (Ma) $^{206}Pb/^{238}U$	1 s abs	$^{207}Pb/^{235}U$	1 s abs	$^{207}Pb/^{206}Pb$	1 s abs	% Conc[e]	Best estimate age (Ma)	±2s
A-III-8	0,0010	26	77	158	0,50	2,952	4,96	0,240	2,61	0,53	0,089	4,22	1386	36	1395	69	1409	59	2	1409	117
A-III-7	0,0003	32	129	197	0,66	2,938	3,62	0,236	2,05	0,57	0,090	2,99	1368	28	1392	50	1429	43	4	1429	84
A-IV-22	0,0019	8	18	36	0,51	3,375	10,65	0,263	2,22	0,21	0,093	10,42	1506	33	1499	160	1489	155	-1	1489	304
A-III-11	0,0003	47	118	261	0,46	3,271	3,66	0,253	1,28	0,35	0,094	3,43	1455	19	1474	54	1502	52	3	1502	101
A-III-10	0,0001	57	172	320	0,54	3,416	3,48	0,262	2,08	0,60	0,095	2,79	1501	31	1508	53	1518	42	1	1518	83
A-III-25	0,0003	76	132	672	0,20	3,719	3,65	0,280	2,03	0,56	0,096	3,04	1591	32	1575	58	1555	47	-2	1555	93
A-IV-24	0,0013	15	75	66	1,15	4,168	7,72	0,287	3,18	0,41	0,105	7,03	1626	52	1668	129	1720	121	5	1720	237
A-III-15	0,0004	60	185	257	0,73	4,717	2,67	0,323	1,39	0,52	0,106	2,28	1806	25	1770	47	1728	39	-5	1728	77
A-II-12	0,0004	46	115	256	0,46	4,645	2,35	0,315	0,95	0,41	0,107	2,15	1766	17	1757	41	1748	38	-1	1748	74
B-I-3	0,0000	92	325	833	0,39	5,074	1,89	0,332	1,47	0,78	0,111	1,19	1848	27	1832	35	1813	22	-2	1813	42
A-IV-03	0,0023	51	361	283	1,28	5,128	5,19	0,314	3,91	0,75	0,118	3,42	1763	69	1841	96	1930	66	9	1930	129
A-IV-10	0,0004	12	73	62	1,18	5,754	4,09	0,340	2,84	0,70	0,123	2,94	1888	54	1940	79	1995	59	5	1995	115
B-I-5	0,0002	161	747	1272	0,59	6,775	1,32	0,395	0,84	0,63	0,124	1,02	2148	18	2082	28	2019	21	-6	2019	41
A-I-14	0,0002	98	207	344	0,61	7,078	1,74	0,411	1,03	0,59	0,125	1,40	2220	23	2121	37	2027	28	-10	2027	56
B-I-7	0,0003	140	69	1056	0,07	6,853	1,43	0,395	0,73	0,51	0,126	1,23	2145	16	2093	30	2041	25	-5	2041	49
A-I-20	0,0005	42	108	156	0,70	6,676	2,63	0,383	1,56	0,59	0,126	2,12	2091	33	2069	54	2048	43	-2	2048	85
A-IV-09	0,0010	14	33	65	0,51	6,359	4,81	0,364	2,38	0,50	0,127	4,18	2000	48	2027	97	2053	86	3	2053	168
A-II-01	0,0004	39	130	145	0,90	6,528	3,25	0,372	2,51	0,77	0,127	2,06	2040	51	2050	67	2059	42	1	2059	83
A-IV-04	0,0006	37	323	180	1,80	6,215	4,52	0,353	3,79	0,84	0,128	2,46	1951	74	2007	91	2065	51	6	2065	100
A-II-6	0,0003	69	404	274	1,49	6,855	2,69	0,389	1,44	0,54	0,128	2,27	2120	31	2093	56	2066	47	-3	2066	92
B-I-2	0,0002	124	530	964	0,55	6,689	1,69	0,378	1,07	0,64	0,128	1,30	2068	22	2071	35	2074	27	0	2074	53
A-II-17	0,0011	20	106	101	1,06	6,628	3,87	0,373	2,62	0,68	0,129	2,85	2042	54	2063	80	2084	59	2	2084	116
B-I-8	0,0004	153	710	1219	0,59	7,225	2,21	0,403	1,59	0,72	0,130	1,54	2182	35	2140	47	2100	32	-4	2100	63
A-I-22	0,0006	17	45	61	0,74	6,841	4,26	0,378	3,25	0,76	0,131	2,75	2068	67	2091	89	2114	58	2	2114	114
A-III-23	0,0004	80	258	513	0,51	6,783	2,59	0,370	1,34	0,52	0,133	2,21	2030	27	2083	54	2137	47	5	2137	93
A-III-14	0,0004	61	64	205	0,31	7,657	2,76	0,413	1,85	0,67	0,134	2,05	2230	41	2192	60	2156	44	-3	2156	87
A-II-2	0,0005	62	114	236	0,49	8,906	2,49	0,405	1,60	0,64	0,159	1,91	2193	35	2328	58	2450	47	10	2450	92
A-V-5	0,0003	48	94	129	0,73	10,436	1,84	0,471	1,35	0,73	0,161	1,26	2490	33	2474	46	2462	31	-1	2462	61
A-I-8	0,0017	62	131	168	0,79	11,764	2,50	0,501	1,72	0,69	0,170	1,81	2618	45	2586	65	2561	46	-2	2561	91
A-III-12	0,0008	91	212	264	0,81	12,303	2,70	0,509	1,95	0,72	0,175	1,86	2652	52	2628	71	2609	49	-2	2609	95
B-I-1	0,0002	122	849	698	1,23	12,864	2,39	0,531	2,21	0,93	0,176	0,91	2747	61	2670	64	2612	24	-5	2612	46
A-II-19	0,0003	55	129	201	0,65	12,378	2,76	0,509	2,37	0,86	0,176	1,43	2654	63	2634	73	2618	37	-1	2618	73
A-IV-19	0,0005	42	66	106	0,62	12,383	2,69	0,507	2,29	0,85	0,177	1,41	2643	60	2634	71	2627	37	-1	2627	73
B-I-9	0,0003	199	929	1076	0,87	15,819	1,39	0,571	1,10	0,80	0,201	0,84	2913	32	2866	40	2833	24	-3	2833	47
A-III-13	0,0002	137	108	295	0,37	22,233	1,96	0,647	1,10	0,56	0,249	1,62	3216	35	3194	63	3180	52	-1	3180	101
A-II-7	0,0004	91	119	207	0,58	24,589	2,68	0,682	2,42	0,90	0,261	1,16	3353	81	3292	88	3255	38	-3	3255	74
A-I-17	0,0009	145	191	315	0,61	23,338	1,53	0,642	1,20	0,78	0,264	0,95	3196	38	3241	50	3269	31	2	3269	61
A-I-5	0,0028	48	135	136	0,99	24,504	3,22	0,674	2,78	0,86	0,264	1,62	3320	92	3289	106	3269	53	-2	3269	104
A-I-23	0,0010	44	76	91	0,83	24,751	2,84	0,676	2,60	0,92	0,265	1,13	3330	87	3298	94	3279	37	-2	3279	73
A-I-18	0,0004	80	117	164	0,72	24,306	2,42	0,662	2,14	0,89	0,266	1,12	3274	70	3281	79	3285	37	0	3285	72
A-I-24	0,0007	35	32	72	0,45	23,655	2,51	0,640	2,35	0,93	0,268	0,90	3191	75	3254	82	3294	30	3	3294	58
A-II-13	0,0023	13	25	36	0,71	24,565	4,64	0,659	4,19	0,90	0,270	2,01	3264	137	3291	153	3308	66	1	3308	130
A-III-18	0,0004	78	183	205	0,90	22,109	1,53	0,590	1,04	0,68	0,272	1,12	2989	31	3189	49	3317	37	10	3317	73
A-I-7	0,0009	95	205	274	0,76	26,390	2,70	0,696	2,46	0,91	0,275	1,11	3406	84	3361	91	3334	37	-2	3334	73
A-I-15	0,0004	74	66	150	0,44	25,622	0,93	0,673	0,45	0,48	0,276	0,81	3317	15	3332	31	3342	27	1	3342	53
A-I-25	0,0008	40	101	81	1,26	25,505	1,72	0,664	1,36	0,79	0,279	1,06	3282	45	3328	57	3355	35	2	3355	70
A-IV-16	0,0011	50	56	103	0,55	24,792	2,12	0,639	1,78	0,84	0,281	1,15	3186	57	3300	70	3370	39	5	3370	76
A-IV-14	0,0007	47	109	135	0,81	23,641	2,23	0,607	1,89	0,85	0,282	1,17	3058	58	3254	72	3376	40	9	3376	77
A-I-4	0,0010	82	384	223	1,74	28,627	3,06	0,733	2,76	0,90	0,283	1,32	3545	98	3441	105	3381	45	-5	3381	88
A-IV-20	0,0045	10	21	18	1,18	26,206	5,03	0,669	3,74	0,74	0,284	3,36	3301	123	3354	169	3386	114	3	3386	223
A-I-12	0,0015	26	47	51	0,94	27,582	2,29	0,696	1,92	0,84	0,287	1,25	3407	66	3404	78	3403	42	0	3403	83
A-II-4	0,0006	75	74	161	0,46	27,945	1,83	0,704	1,45	0,79	0,288	1,12	3438	50	3417	63	3405	38	-1	3405	75
A-I-6	0,0011	88	239	246	0,98	28,686	3,24	0,722	2,98	0,92	0,288	1,26	3504	104	3443	111	3407	43	-3	3407	84
A-V-1	0,0027	7	17	14	1,20	26,567	5,42	0,667	4,90	0,90	0,289	2,32	3296	161	3368	183	3411	79	3	3411	155
A-I-19	0,0010	29	83	58	1,44	27,322	4,37	0,685	4,22	0,97	0,289	1,11	3364	142	3395	148	3414	38	1	3414	75
A-IV-05	0,0020	19	55	50	1,12	26,801	3,17	0,669	2,79	0,88	0,291	1,49	3302	92	3376	107	3420	51	3	3420	100
A-I-16	0,0006	69	167	135	1,24	27,736	2,20	0,691	1,86	0,84	0,291	1,18	3386	63	3410	75	3424	40	1	3424	79
A-I-21	0,0022	8	25	16	1,57	27,644	3,38	0,688	1,96	0,58	0,291	2,76	3375	66	3407	115	3425	94	1	3425	185
A-V-7	0,0004	61	95	92	1,04	29,840	2,08	0,720	1,80	0,86	0,301	1,05	3494	63	3482	72	3474	37	-1	3474	72
A-I-3	0,0000	40	141	110	1,30	30,398	4,75	0,732	4,70	0,99	0,301	0,70	3541	166	3500	166	3476	24	-2	3476	48
A-III-20	0,0008	4	25	21	1,21	3,802	7,21	0,261	6,45	0,89	0,105	3,22	1497	97	1593	115	1722	56	13		
A-IV-18	0,0011	18	106	79	1,35	4,888	4,61	0,294	2,77	0,60	0,121	3,69	1662	46	1800	83	1964	72	15		
A-IV-02	0,0008	7	36	47	0,77	6,641	5,23	0,353	3,87	0,74	0,136	3,53	1950	75	2065	108	2181	77	11		
A-III-20	0,0012	72	220	316	0,70	7,334	4,01	0,352	3,39	0,85	0,151	2,14	1946	66	2153	86	2356	50	17		
A-II-11	0,0008	30	150	129	1,17	10,801	1,78	0,417	0,86	0,48	0,188	1,56	2248	19	2506	45	2722	42	17		
A-III-18	0,0016	100	244	304	0,81	17,074	9,50	0,499	9,30	0,98	0,248	1,97	2609	243	2939	279	3173	62	18		
A-III-16	0,0004	105	90	222	0,41	22,539	1,51	0,581	1,21	0,80	0,281	0,91	2953	36	3207	48	3370	31	12		
A-II-10	0,0021	65	2293	1568	1,47	1,968	7,23	0,064	6,08	0,84	0,222	3,92	402	24	1104	80	2993	117	87		
A-II-15	0,0027	92	274	689	0,40	7,086	2,08	0,239	1,84	0,89	0,215	0,95	1381	25	2122	44	2944	28	53		
A-II-16	0,0012	88	486	422	1,16	15,636	2,71	0,400	2,59	0,96	0,283	0,78	2170	56	2855	77	3382	26	36		
A-II-18	0,0025	40	685	570	1,21	2,432	5,32	0,131	4,85	0,91	0,135	2,19	792	38	1252	67	2163	47	63		
A-II-20	0,0019	9	129	86	1,51	2,545	4,53	0,195	4,10	0,90	0,095	1,93	1149	47	1285	58	1520	29	24		
A-III-3	0,0011	40	113	152	0,75	12,031	7,57	0,312	7,46	0,99	0,279	1,24	1752	131	2607	197	3359	42	48		
A-IIII-4	0,0021	79	635	1072	0,60	0,894	6,36	0,082	4,73	0,74	0,079	4,25	510	24	649	41	1168	50	56		
A-IIII-5	0,0022	112	541	889	0,61	4,081	9,17	0,148	8,81	0,96	0,200	2,53	888	78	1650	151	2830	72	69		
A-IIII-6	0,0030	43	807	1140	0,71	0,402	12,93	0,044	5,25	0,41	0,066	11,82	280	15	343	44	796	94	65		
A-III-9	0,0007	85	566	439	1,30	7,555	3,89	0,277	3,43	0,88	0,198	1,83	1575	54	2180	85	2809	51	44		
A-III-17	0,0006	40	39	1033	0,04	0,675	7,06	0,057	3,12	0,44	0,086	6,33	358	11	524	37	1333	84	73		
A-III-17	0,0034	88	848	1017	0,84	1,577	24,02	0,132	17,48	0,73	0,087	16,48	797	139	961	231	1358	224	41		
A-III-20	0,0020	77	274	394	0,70	5,627	10,19	0,299	9,63	0,94	0,137	3,35	1686	162	1920	196	2184	73	23		
A-III-21	0,0080	4	25	21	1,21	2,466	87,10	0,281	7,92	0,09	0,064	86,74	1595	126	1262	1099	732	635	-118		
A-III-21	0,0012	64	348	319	1,10	11,172	3,74	0,327	3,56	0,95	0,247	1,15	1826	65	2538	95	3169	37	42		
A-III-22	0,0016	78	400	397	1,01	9,683	13,61	0,311	13,45	0,99	0,226	2,08	1746	235	2405	327	3022	63	42		
A-III-24	0,0020	66	734	1760	0,42	1,279	7,45	0,107	2,48	0,33	0,087	7,02	653	16	836	62	1360	95	52		
A-IV-01	0,0010	32	378	279	1,36	7,210	5,76	0,178	5,39	0,94	0,293	2,02	1057	57	2138	123	3435	69	69		
A-IV-06	0,0017	28	1381	1340	1,04	0,382	8,39	0,037	6,90	0,82	0,074	4,77	236	16	329	28	1053	50	78		
A-IV-07	0,0016	49	709	557	1,28	4,298	3,05	0,166	2,35	0,77	0,187	1,95	992	23	1693	52	2720	53	64		
A-IV-12	0,0019	39	171	353	0,49	3,239	4,76	0,160	3,42	0,72	0,147	3,32	954	33	1467	70	2314	77	59		

A-IV-15	0,0012	23	93	81	1,17	16,208	3,09	0,425	2,63	0,85	0,277	1,62	2281	60	2889	89	3345	54	32	
A-V-2	0,0029	38	730	658	1,12	1,074	7,97	0,073	4,06	0,51	0,107	6,86	452	18	741	59	1753	120	74	
B-I-4	0,0040	156	8891	7329	1,22	0,613	7,31	0,067	6,06	0,83	0,066	4,07	421	26	485	35	802	33	48	
B-I-6	0,0040	114	3940	1966	2,02	3,003	5,53	0,186	5,19	0,94	0,117	1,90	1100	57	1408	78	1913	36	43	

a Th/U ratios are calculated relative to GJ-1 reference zircon
b Corrected for background and within-run Pb/U fractionation and normalised to reference zircon GJ-1 (ID-TIMS values/measured value); 207Pb/235U calculated using (207Pb/206Pb)/(238U/206Pb * 1/137.88)
c Rho is the error correlation defined as the quotient of the propagated errors of the 206Pb/238U and the 207/235U ratio
d Corrected for mass-bias by normalising to GJ-1 reference zircon and common Pb using the model Pb composition of Stacey and Kramers (1975)
e Degree of concordance = [(206Pb/238U age) / (207Pb/206U age)]*100

Reference

Stacey, J.S., Kramers, J.D., 1975. Approximation of terrestrial lead isotope evolution by a two-stage model. Earth and Planetary Science Letters 26, 207–221.

A1.8.4.9. U-Pb zircon data of P2 sample (Sandstone layer, Tombador Fm.).

Spot Number	f_{206}	Pb (ppm)	Th (ppm)	U (ppm)	$^{232}Th/^{238}U$ [a]	Isotope ratios[b] $^{207}Pb/^{235}U$	1 s [%]	$^{206}Pb/^{238}U$	1 s [%]	Rho[c]	$^{207}Pb/^{206}Pb$ [d]	1 s [%]	Ages (Ma) $^{206}Pb/^{238}U$	1 s abs	$^{207}Pb/^{235}U$	1 s abs	$^{207}Pb/^{206}Pb$	1 s abs	% Conc[e]	Best estimate age (Ma)	±2s
B-II-09	0,0002	70	1455	1719	0,85	3,284	2,77	0,265	1,70	0,61	0,090	2,19	1515	26	1477	41	1423	31	-6	1423	61
B-III-20	0,0002	135	89	554	0,16	3,681	2,21	0,288	1,45	0,65	0,093	1,67	1632	24	1567	35	1481	25	-10	1481	48
B-IV-15	0,0016	13	117	88	1,34	3,225	8,42	0,246	2,18	0,26	0,095	8,13	1418	31	1463	123	1529	124	7	1529	244
B-II-18	0,0003	167	2135	1901	1,13	4,551	4,24	0,313	3,85	0,91	0,106	1,76	1754	68	1740	74	1724	30	-2	1724	59
B-IV-09	0,0006	34	78	110	0,72	4,694	3,49	0,321	1,93	0,55	0,106	2,91	1793	35	1766	62	1735	50	-3	1735	99
B-V-13	0,0015	14	92	88	1,05	4,784	5,87	0,319	2,98	0,51	0,109	5,05	1786	53	1782	105	1778	90	0	1778	176
B-I-3	0,0003	92	162	427	0,38	5,205	2,37	0,335	1,30	0,55	0,113	1,98	1864	24	1853	44	1841	36	-1	1841	72
B-IV-5	0,0005	49	133	149	0,90	5,440	2,64	0,347	1,58	0,60	0,114	2,11	1922	30	1891	50	1857	39	-3	1857	77
B-III-21	0,0005	36	114	103	1,12	6,368	2,20	0,381	1,49	0,68	0,121	1,62	2080	31	2028	45	1975	32	-5	1975	63
B-II-03	0,0006	115	-1604	-976	1,66	5,898	4,58	0,342	3,83	0,84	0,125	2,52	1898	73	1961	90	2028	51	6	2028	100
B-IV-01	0,0003	138	369	364	1,02	6,992	2,01	0,405	1,37	0,68	0,125	1,46	2190	30	2110	42	2034	30	-8	2034	58
B-V-07	0,0009	19	44	105	0,42	6,597	4,29	0,381	2,98	0,70	0,125	3,08	2083	62	2059	88	2035	63	-2	2035	123
B-I-20	0,0008	76	-4706	-5145	0,92	6,841	4,06	0,395	2,45	0,60	0,126	3,24	2144	53	2091	85	2039	66	-5	2039	129
B-II-07	0,0002	91	1313	1444	0,92	7,109	2,06	0,410	1,49	0,72	0,126	1,42	2215	33	2125	44	2040	29	-9	2040	57
B-I-5	0,0002	164	374	661	0,57	7,089	2,67	0,409	1,95	0,73	0,126	1,82	2209	43	2123	57	2040	37	-8	2040	73
B-II-16	0,0003	106	517	847	0,61	7,285	2,29	0,419	1,81	0,79	0,126	1,41	2256	41	2147	49	2044	29	-10	2044	56
B-II-14	0,0002	133	1266	1993	0,64	7,325	1,81	0,420	1,05	0,58	0,126	1,47	2262	24	2152	39	2049	30	-10	2049	59
B-IV-22	0,0012	18	101	69	1,48	6,274	4,72	0,359	2,42	0,51	0,127	4,06	1980	48	2015	95	2051	83	3	2051	163
B-V-11	0,0013	17	135	95	1,43	6,612	3,63	0,378	2,03	0,56	0,127	3,00	2067	42	2061	75	2055	62	-1	2055	121
B-I-11	0,0002	156	-136823	-257825	0,53	7,135	2,31	0,407	1,37	0,59	0,127	1,87	2203	30	2128	49	2057	38	-7	2057	75
B-IV-03	0,0006	46	235	130	1,83	6,767	4,52	0,386	3,72	0,82	0,127	2,58	2105	78	2081	94	2058	53	-2	2058	104
B-II-01	0,0009	155	-736	-1249	0,59	6,292	4,31	0,357	3,68	0,85	0,128	2,25	1966	72	2017	87	2070	47	5	2070	91
B-II-20	0,0015	27	187	214	0,88	7,477	3,43	0,424	2,94	0,86	0,128	1,77	2278	67	2170	75	2070	37	-10	2070	72
B-IV-24	0,0016	9	79	35	2,25	6,596	4,41	0,373	2,73	0,62	0,128	3,47	2044	56	2059	91	2073	72	1	2073	141
B-I-7	0,0003	226	-252	-4362	0,06	7,432	3,16	0,420	2,43	0,77	0,128	2,03	2262	55	2165	68	2074	42	-9	2074	82
B-IV-02	0,0005	98	407	314	1,30	6,093	5,67	0,342	5,38	0,95	0,129	1,79	1898	102	1989	113	2085	37	9	2085	73
B-IV-25	0,0011	18	49	66	0,75	6,852	4,51	0,382	2,67	0,59	0,130	3,63	2087	56	2093	94	2098	76	1	2098	149
B-I-2	0,0002	126	266	501	0,53	7,384	3,76	0,411	3,34	0,89	0,130	1,72	2218	74	2159	81	2104	36	-5	2104	71
B-I-8	0,0004	256	-2749	-5254	0,53	7,582	2,68	0,416	1,45	0,54	0,132	2,25	2243	33	2183	59	2126	48	-5	2126	94
B-I-16	0,0008	59	-34378	-98057	0,35	7,378	3,45	0,405	2,72	0,79	0,132	2,13	2192	60	2158	75	2127	45	-3	2127	89
B-IV-23	0,0009	16	44	59	0,74	7,092	4,39	0,389	2,83	0,64	0,132	3,36	2116	60	2123	93	2130	71	1	2130	140
B-II-15	0,0004	63	1039	970	1,08	7,845	2,09	0,422	1,39	0,66	0,135	1,56	2271	32	2213	46	2161	34	-5	2161	66
B-V-09	0,0006	18	81	100	0,81	6,843	4,51	0,368	3,33	0,74	0,135	3,04	2020	67	2091	94	2163	66	7	2163	129
B-IV-13	0,0012	15	35	57	0,61	7,620	5,20	0,399	2,92	0,56	0,138	4,31	2165	63	2187	114	2208	95	2	2208	186
B-III-10	0,0009	47	162	119	1,38	9,965	2,88	0,473	1,94	0,67	0,153	2,13	2499	49	2432	70	2376	51	-5	2376	99
B-V-06	0,0006	41	103	183	0,57	9,914	2,25	0,467	1,67	0,74	0,154	1,51	2472	41	2427	55	2389	36	-3	2389	71
B-V-16	0,0005	31	130	146	0,90	9,551	2,55	0,444	1,95	0,76	0,156	1,65	2370	46	2392	61	2411	40	2	2411	78
B-I-12	0,0005	113	-53149	-155353	0,34	10,327	2,44	0,477	1,95	0,80	0,157	1,46	2513	49	2465	60	2425	35	-4	2425	70
B-II-13	0,0002	175	1255	2185	0,58	11,715	2,22	0,518	1,80	0,81	0,164	1,30	2693	48	2582	57	2496	33	-8	2496	64
B-II-21	0,0003	89	510	620	0,83	11,012	2,84	0,485	2,19	0,77	0,165	1,81	2550	56	2524	72	2504	45	-2	2504	89
B-V-18	0,0017	3	33	14	2,34	10,144	8,66	0,442	8,23	0,95	0,167	2,68	2358	194	2448	212	2524	68	7	2524	132
B-I-19	0,0006	131	-6318	-6521	0,98	12,313	2,17	0,531	1,44	0,66	0,168	1,62	2745	39	2629	57	2540	41	-8	2540	81
B-II-05	0,0004	158	-1348	-914	1,49	11,589	3,05	0,488	2,27	0,74	0,172	2,04	2563	58	2572	78	2579	53	1	2579	103
B-III-03	0,0004	189	768	416	1,86	12,882	2,21	0,533	1,97	0,89	0,175	1,00	2756	54	2671	59	2607	26	-6	2607	51
B-III-07	0,0010	108	476	268	1,79	11,732	2,59	0,482	2,11	0,81	0,176	1,50	2537	54	2583	67	2620	39	3	2620	77
B-IV-11	0,0010	34	67	65	1,04	12,843	2,14	0,527	1,00	0,47	0,177	1,89	2727	27	2668	57	2624	50	-4	2624	97
B-I-1	0,0002	124	425	363	1,18	13,578	2,24	0,553	1,83	0,82	0,178	1,29	2836	52	2721	61	2636	34	-8	2636	67
B-IV-08	0,0008	33	76	67	1,15	12,789	2,40	0,520	2,04	0,85	0,178	1,26	2700	55	2664	64	2637	33	-2	2637	65
B-II-25	0,0005	87	391	518	0,76	13,920	2,04	0,556	1,74	0,85	0,182	1,06	2850	50	2744	56	2668	28	-7	2668	55
B-IV-12	0,0015	19	79	61	1,31	12,755	3,62	0,505	2,46	0,68	0,183	2,66	2636	65	2662	96	2681	71	2	2681	140
B-I-15	0,0005	159	-197515	-183923	1,08	15,107	3,21	0,568	2,96	0,92	0,193	1,24	2898	86	2822	91	2768	34	-5	2768	67
B-I-17	0,0012	78	-1141	-3617	0,32	15,932	3,33	0,568	2,82	0,85	0,204	1,77	2898	82	2873	96	2855	51	-1	2855	99
B-I-9	0,0003	320	-3398	-4444	0,77	16,753	1,69	0,593	1,11	0,65	0,205	1,28	3001	33	2921	49	2866	37	-5	2866	72
B-V-05	0,0016	11	66	42	1,57	15,470	4,37	0,545	3,85	0,88	0,206	2,06	2806	108	2845	124	2872	59	2	2872	116
B-IV-04	0,0018	22	34	43	0,79	15,635	4,83	0,549	4,03	0,84	0,207	2,66	2820	114	2855	138	2879	76	2	2879	150
B-I-21	0,0012	77	-1038	-2792	0,37	25,903	3,16	0,709	2,84	0,90	0,265	1,39	3454	98	3343	106	3277	46	-5	3277	89
B-IV-06	0,0006	84	257	155	1,67	32,766	1,79	0,747	1,59	0,89	0,318	0,82	3597	57	3574	64	3560	29	-1	3560	57
B-I-22	0,0003	117	-1064	-945	1,13	5,290	2,95	0,356	1,60	0,54	0,108	2,48	1962	31	1867	55	1763	44	-11		
B-V-04	0,0014	33	117	165	0,72	4,710	3,62	0,281	2,45	0,68	0,122	2,66	1596	39	1769	64	1979	53	19		
B-I-14	0,0002	232	-299428	-374323	0,81	7,096	2,50	0,416	1,71	0,69	0,124	1,81	2240	38	2124	53	2012	37	-11		
B-I-18	0,0003	202	-18528	-12698	1,47	7,211	2,75	0,420	1,77	0,64	0,125	2,10	2258	40	2138	59	2024	43	-12		
B-I-23	0,0009	46	-141	-277	0,51	9,016	3,51	0,470	2,71	0,77	0,139	2,23	2484	67	2340	82	2216	50	-12		
B-V-08	0,0011	13	151	78	1,96	6,940	4,71	0,359	2,56	0,54	0,140	3,95	1977	51	2104	99	2230	88	11		
~~B-I-4~~	~~0,0039~~	~~164~~	~~4606~~	~~3925~~	~~1,18~~	~~0,641~~	~~7,68~~	~~0,069~~	~~5,97~~	~~0,78~~	~~0,068~~	~~4,83~~	~~428~~	~~26~~	~~503~~	~~39~~	~~858~~	~~44~~	~~50~~		
B-I-6	0,0040	186	-14984	-8378	1,80	3,099	6,77	0,188	6,29	0,93	0,119	2,50	1113	70	1433	97	1946	49	43		
B-IV-14	0,0013	12	134	73	1,86	7,911	24,86	0,291	24,44	0,98	0,197	4,56	1648	403	2221	552	2801	128	41		
B-IV-18	0,0029	32	583	212	2,76	3,680	5,44	0,191	3,95	0,73	0,140	3,74	1127	45	1567	85	2224	83	49		

a Th/U ratios are calculated relative to GJ-1 reference zircon

b Corrected for background and within-run Pb/U fractionation and normalised to reference zircon GJ-1 (ID-TIMS values/measured value); 207Pb/235U calculated using (207Pb/206Pb)/(238U/206Pb * 1/137.88)

c Rho is the error correlation defined as the quotient of the propagated errors of the 206Pb/238U and the 207/235U ratio

d Corrected for mass-bias by normalising to GJ-1 reference zircon and common Pb using the model Pb composition of Stacey and Kramers (1975)

e Degree of concordance = [(206Pb/238U age) / (207Pb/206U age)]*100

Reference

Stacey, J.S., Kramers, J.D., 1975. Approximation of terrestrial lead isotope evolution by a two-stage model. Earth and Planetary Science Letters 26, 207–221.

A1.8.4.10. U-Pb zircon data from zircons of the Pedra Lessa Suite (tholeiitic dyke)

							Isotope ratios[b]							Ages (Ma)						
	Spot **N**umber	f_{206}	Pb (ppm)	Th (ppm)	U (ppm)	$^{232}Th/^{238}U$[a]	$^{207}Pb/^{235}U$	1 s [%]	$^{206}Pb/^{238}U$	1 s [%]	Rho[c]	$^{207}Pb/^{206}Pb$[d]	1 s [%]	$^{206}Pb/^{238}U$	1 s abs	$^{207}Pb/^{235}U$	1 s abs	$^{207}Pb/^{206}Pb$	1 s abs	% Conc[e]
Igneous zircons	Zr-257-G2	0,0002	208	1735	980	1,78	1,513	3,30	0,157	1,77	0,54	0,070	2,78	941	17	935	31	922	26	-2
	Zr-257-G3	0,0003	146	818	724	1,14	1,497	3,13	0,155	1,68	0,54	0,070	2,64	927	16	929	29	933	25	1
Inherited zircons	Zr-257-G4	0,0032	53	64	127	0,50	1,748	3,07	0,090	2,78	0,91	0,141	1,29	554	15	1026	31	2241	29	75
	Zr-257-G1	0,0001	257	408	542	0,76	7,339	2,78	0,395	1,51	0,54	0,135	2,34	2145	32	2154	60	2162	50	1
	Zr-257-F-1-1	0,0016	95	10	262	0,04	6,633	2,55	0,376	1,70	0,66	0,128	1,91	2059	35	2064	53	2069	39	0
	Zr-257-F-2	0,0007	48	48	110	0,44	6,995	3,37	0,382	2,44	0,73	0,133	2,32	2087	51	2111	71	2134	50	2

A1.8.5. Supplementary material 4 KML file containing the Google map Of Tombador Fm. outcrop area and sample location, in eastern Chapada Diamantina (file available online).

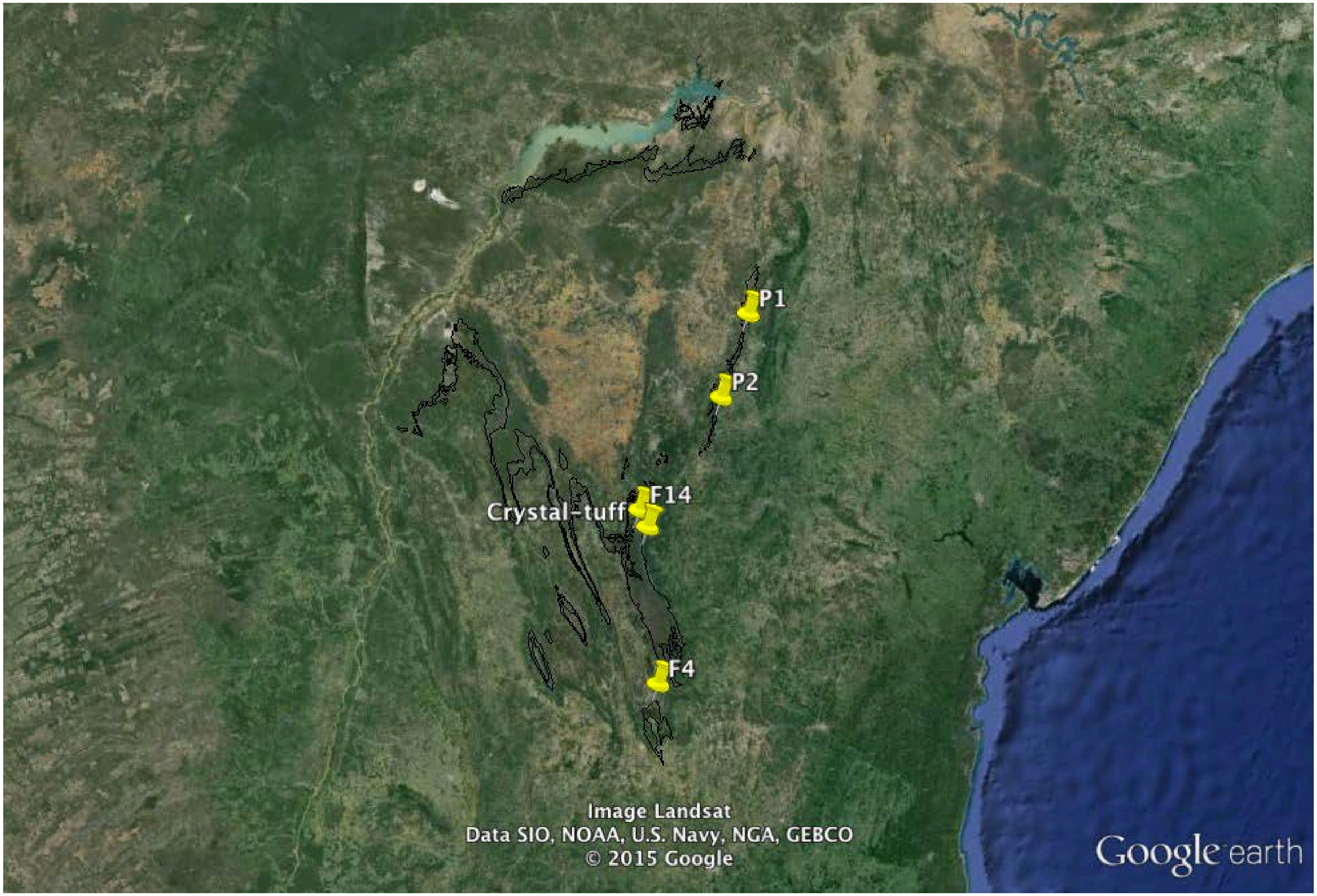

A1.9. References

Abreu, F.R., 1991. Estudo das mineralizações auríferas filoneanas da região da cidade de Diamantina/MG. MS. thesis, UNICAMP.

Alkmim, F.F., 2004. O que faz de um craton um craton? O craton do São Francisco e as revelações Almeidianas ao delimitá-lo. In: Manteso-Neto, V., Bartorelli, A., Carneiro, C.D.R., Brito Neves, B.B. (Eds.), Geologia do continente Sul Americano: evolução da obra de Fernando Flávio Marques de Almeida. Beca, São Paulo, 17-35

Alkmim, F.F., Martins-Neto, M.A., 2012. Proterozoic first-order sedimentary sequences of the São Francisco craton, eastern Brazil. Marine and Petroleum Geology 33, 127-139.

Almeida, F.F.M., 1977. O craton de São Francisco. Brazilian Journal of Geology 7, 349-364.

Aspler, L.B., Wisotzek, I.E., Chiarenzelli, J.R., Losonczy, M.F., Cousens, B.L., McNicoll, V.J., Davis, W.J., 2001. Paleoproterozoic intracratonic basin processes, from breakup of Kenorland to assembly of Laurentia: Hurwitz Basin, Nunavut, Canada. Sedimentary Geology 141, 287-318.

Babinski, M., Van Schmus, W.R., Chemale Jr., F., Brito Neves, B.B., Rocha, A.J.D., 1993. Idade isocrônica Pb/Pb em rochas carbonáticas da Formação Caboclo, em Morro do Chapéu. 2º Simpósio do Craton do São Francisco. Brazilian Geological Society, Salvador, 160-163.

Babinski, M., Pedreira, A.J., Brito Neves, B.B., Van Schmus, W.R., 1999. Contribuição à geocronologia da Chapada Diamantina. 7° Simpósio Nacional de Estudos Tectônicos. Brazilian Geological Society, Lençóis, 118-120.

Bhatia, M.R., 1983. Plate tectonics and geochemical composition of sandstones. The Journal of Geology 91, 611-627.

Barbosa, J.S.F., Domingues, J.M.L., 1994. Mapa geológico do Estado da Bahia ao Milionésimo. Salvador: SICM/SGM, map scale 1:1.000.000.

Barbosa, J.S.F., Sabaté, P., 2004. Archean and Paleoproterozoic crust of the São Francisco Craton, Bahia, Brazil: geodynamic features. Precambrian Research 133, 1-27.

Boynton,W.V., 1984. Cosmochemistry of the rare earth elements: meteorite studies. In: Henderson, P. (Ed.), Rare Earth Element Geochemistry. Elsevier, Amsterdam, 63-114.

Brito Neves, B.B., Kawashita, K., Cordani, V.G., Delhal, J., 1979. A evolução geocronológica da Cordilheira do Espinhaço: dados novos e integração. Brazilian Journal of Geology 9, 71-85.

Burgess, P.M., Gurnis, M., Moresi, L., 1997. Formation of sequences in the cratonic interior of North America by interaction between mantle, eustatic, and stratigraphic processes. Geological Society of America Bulletin 108, 1515-1535.

Cas, R.A.F., Wright, J.V., 1988. Volcanic Successions, modern and ancient: A geological approach to processes, products and successions. Unwin Hyman, London, 528 pp.

Chemale Jr., F., Alkmim, F.F., Endo, I., 1993. Late Proterozoic tectonism in the interior of the São Francisco craton. In: Findlay, R.H., Unrug, R., Banks, M.R., Veevers, J.J. (Eds.), Gondwana eight: assembly, evolution and dispersal. Balkema, Rotterdam, 29-41.

Chemale Jr., F., Quade, H., Van Schmus, W.R., 1998. Petrography, geochemistry and geochronology of the Borrachudo and Santa Bárbara metagranites, Quadrilatero Ferrífero, Brazil. Zentralblatt fuer Geologie und Palaontologie Teil I 3-6, 739-750.

Chemale Jr., F., Philipp, R.P., Dussin, I.A., Formoso, M.L.L., Kawashita, K., Bertotti, A.L., 2011. Lu-Hf and U-Pb age determinations of Capivarita Anorthosite in the Dom Feliciano Belt, Brazil. Precambrian Research 186, 117-126.

Chemale Jr., F., Dussin, I.A., Alkmim, F.F., Martins, M.S., Queiroga, G., Armstrong, R., Santos, M.N., 2012. Unravelling a Proterozoic basin history through detrital zircon geochronology: The case of the Espinhaço Supergroup, Minas Gerais, Brazil. Gondwana Research 22, 200-206.

Condie, K.C., 1993. Chemical composition and evolution of the upper continental crust: Contrasting results from surface samples and shales. Chemical Geology 104, 1-37.

Cordani, U.G., Fraga, L.M., Reis, N., Tassinari, C.C.G., Brito-Neves, B.B., 2010. On the origin and tectonic significance of the intra-plate events of Grenvillian-type age in South America: A discussion. Journal of South American Earth Sciences 29, 143-159.

D'Agrella, M.S., Pacca, I.G., Renne, P.R., Onstott, T.C., Teixeira, W., 1990. Paleomagnetism of Middle Proterozoic (1.01 to 1.08 Ga) mafic dykes in southeastern Bahia State - São Francisco Craton, Brazil. Earth and Planetary Science Letters 101, 332-348.

Danderfer, A., Dardenne, M.A., 2002. Tectonoestratigrafia da bacia Espinhaço na porção centro-norte do craton do São Francisco: registro de uma evolução polistórica descontínua. Brazilian Journal of Geology 32, 449-460.

Danderfer, A., De Waele, B., Pedreira, A.J, Nalini, H.A., 2009. New geochronological constraints on the geological evolution of Espinhaço basin within the São Francisco Craton-Brazil. Precambrian Research 170, 116-128.

Derby, 1906. The Serra do Espinhaço, Brazil. Journal of Geology 14, 374-401.

De Waele, B., Johnson, S.P., Pisarevsky, S.A., 2008. Palaeoproterozoic to Neoproterozoic growth and evolution of the eastern Congo Craton: Its role in the Rodinia puzzle. Precambrian Research 160, 127-141.

Dominguez, J.M.L., 1992. Estratigrafia de sequências aplicada a terrenos pré-Cambrianos: exemplos para o Estado da Bahia. Brazilian Journal of Geology 22, 422-436.

Dussin, I.A., 1994. Evolution structurale de la region de l´Espinhaço meridional, bordure sud-est du craton São Francisco, Brésil. Tectoniques superposees au Protérozoïque. Ph.D. thesis, Université D'orléans.

Dussin, I.A., Dussin, T.M., 1995. Supergrupo Espinhaço: Modelo de Evolução Geodinâmica. Geonomos 1, 19-26.

Dussin, I.A., Chemale Jr., F., 2011. Geologia Estrutural e Estratigrafia do Sistema Espinhaço-Chapada Diamantina e sua aplicação nas Bacias Mesocenozóicas da Margem Passiva Brasileira. Final Report, FUNDEP, Belo Horizonte, 302 pp.

Ernst, R.E., Bleeker, W., Söderlund, U., Kerr, A.C., 2013a. Large Igneous Provinces and supercontinents: Toward completing the plate tectonic revolution. Lithos 174, 1-14.

Ernst, R.E., Pereira, E., Hamilton, M.A., Pisarevsky, S.A., Rodrigues, J., Tassinari, C.C.G., Teixeira, W., Van-Dunem, V., 2013b. Mesoproterozoic intraplate magmatic 'barcode' record of the Angola portion of the Congo Craton: Newly dated magmatic events at 1505 and 1110 Ma and implications for Nuna (Columbia) supercontinent reconstructions. Precambrian Research 230, 103-118.

Evans, D.A.D., 2009. The palaeomagnetically viable, long-lived and all-inclusive Rodinia supercontinent reconstruction. In: Murphy, J.B., Hynes, A.J. (Eds.), Ancient Orogens and Modern Analogues. Geological Society Special Publication 327, 371-404.

Evans, D.A.D., Heaman, L.M., Trindade, R.I.F., D'Agrella-Filho, M.S., Smirnov, A.V., Catelani, E.L., 2010. Precise U–Pb Baddeleyite ages from Neoproterozoic mafic dykes in Bahia, Brazil, and their paleomagnetic/paleogeographic implications. Eos Transactions AGU 91(26), Meeting of the Americas, Abstract GP31E-07.

Fernandez-Alonso, M., Cutten, H., De Waele, B., Tack, L., Tahon, A., Baudet, D., Barrit, S.D., 2012. The Mesoproterozoic Karagwe-Ankole Belt (formerly the NE Kibara Belt): The result of prolonged extensional intracratonic basin development punctuated by two short-lived far-field compressional events. Precambrian Research 216-219, 63-86.

Gorczyk, W., Hobbs, B., Gessner, K., Gerya, T., 2013. Intracratonic geodynamics. Gondwana Reseach 24, 838-848.

Guimarães, J.T., Martins, A.A.M., Andrade Filho, E.L., Loureiro, H.S.C., Arcanjo, J.B.A., Neves, J.P., Abram, M.B., Silva, M.G., Melo, R.C., Bento, R.V., 2005. Projeto Ibitiara–Rio de Contas Geological map. Brazilian Geological Survey and Bahia Mineral Research Company, scale 1:200.000.

Haddad, D., Watts, A.B., Lindsay, J., 2001. Evolution of the intracratonic Officer Basin, central Australia: implications from subsidence analysis and gravity modeling. Basin research 13, 217-238.

Herron, M.M., 1988. Geochemical classification of terrigenous sands and shales from core or log data. Journal of Sedimentary Petrology 58, 820-829.

Ingersoll, R.V., 2012. Tectonics of sedimentary basins, with revised nomenclature. In: Busby, C., Azor, A. (Eds.), Tectonics of sedimentary basins: Recent advances. Wiley-Blackwell, Oxford, 3-43.

Jackson, S.E., Pearsona, N.J., Griffina, W.L., Belousova, E.A., 2004. The application of laser ablation-inductively coupled plasma-mass spectrometry to in situ U–Pb zircon geochronology. Chemical Geology 211, 47-69.

Jarvis, A., Reuter, H.I., Nelson, A., Guevara, E., 2008. Hole-filled seamless SRTM data V4. International Centre for Tropical Agriculture (CIAT), available from http://srtm.csi.cgiar.org.

Kingston, D.R., Dishroon, C.P., Williams, P.A., 1983. Global basin classification. Bulletin of the American Association of Petroleum Geologists 67, 2175-2193

Kokonyangi, J.W., Kampunzu, A.B., Armstrong, R., Yoshida, M., Okudaira, T., Arima, M., Ngulube, D.A., 2006. The Mesoproterozoic Kibaride belt (Katanga, SE D.R. Congo). Journal of African Earth Sciences 46, 1-35.

Lacassie, J.P., Roser, B., Del Solar, J.R., Hervé, F., 2004. Discovering geochemical patterns using self-organizing neural networks: a new perspective for sedimentary provenance analysis. Sedimentary Geology 165, 175-191.

Le Bas, M.J., Le Maitre, R.W., Streckeisen, A., Zanettin, B., 1986. A chemical classification of volcanic rocks on the total alkali-silica diagram. Journal of Petrology 27, 745-750.

Li, Z.X., Bogdanova, S.V., Collins, A.S., Davidson, A., De Waele, B., Ernst, R.E., Fitzsimons, I.C.W., Fuck, R.A., Gladkochub, D.P., Jacobs, J., Karlstrom, K.E., Lu, S., Natapov, L.M., Pease, V., Pisarevsky, S.A., Thrane , K., Vernikovsky , V., 2008. Assembly, configuration, and break-up history of Rodinia: A synthesis. Precambrian Research 160, 179–210.

Lindsay, J.F., 2002. Supersequences, superbasins, supercontinents – evidence from the Neoproterozoic-Early Palaeozoic basins of central Australia. Basin Research 14, 207-223.

Lindsay, J.F, Leven, J.H., 1996. Evolution of a Neoproterozoic to Palaeozoic intracratonic setting, Officer Basin, South Australia. Basin Research 8, 403-424.

Loureiro, H.S.C., Lima, E.S., Macedo, E.R., Silveira, F.V., Bahiense, I.C., Arcanjo, J.B.A., Moraes Filho, J.C., Neves, J.P., Guimarães, J.T., Teixeira, L.R., Abram, M.B., Santos, R.A., Melo, R.C., 2008. Projeto Barra–Oliveira dos Brejinhos Geological map. Brazilian Geological Survey and Bahia Mineral Research Company, scale 1:200.000.

Ludwig, K.R., 2003. Using Isoplot/Ex, version 3.00, a geochronological toolkit for Microsoft Excel. Berkeley Geochronology Center Special Publication No. 1.

Machado, N., Schrank, A., Abreu, F.R., Knauer, L.G., Almeida-Abreu, P.A., 1989. Resultados preliminares da geocronologia U/Pb na Serra do Espinhaço Meridional. Simpósio de Geologia do Núcleo Minas Gerais, Brazilian Geological Society 10, 171-174.

Marshak, S., Alkmim, F.F., 1989. Proterozoic contraction/extension tectonics of the southern São Francisco region, Minas Gerais, Brazil. Tectonics 8, 555-571.

Martins-Neto M.A., 2000. Tectonics and sedimentation in a paleo/mesoproterozoic rift-sag basin (Espinhaço basin, southeastern Brazil). Precambrian Reseach 103, 147-173.

McLennan, S.M., Hemming, S., McDaniel, D.K., Hanson, G.N., 1993. Geochemical approaches to sedimentation, provenance, and tectonics. In: Johnsson. M.J., Basu, A. (Eds.), Processes Controlling the Composition of Clastic Sediments. Geological Society of America Special Paper 284, 21-40.

Meert, J.G., Torsvik, T.H., 2003. The making and unmaking of a supercontinent: Rodinia revisited. Tectonophysics 375, 261-288.

Meert, J.G., 2012. What's in a name? The Columbia (Paleopangaea/Nuna) supercontinent. Gondwana Research 21, 987-993.

Milani, E.J., Ramos, V.A., 1998. Orogenias Paleozóicas no domínio sul-ocidental do Gondwana e os ciclos de subsidência da Bacia do Paraná. Brazilian Journal of Geology 28, 473-484.

Moucha, R., Forte, A.M., Mitrovica, J.X., Rowley, D.B., Quéré, S., Simmons, N.A., Grand, S.P., 2008. Dynamic topography and long-therm sea-level variations: There is no such thing as a stable continental platform. Earth and Planetary Science Letters 271, 101-108.

Pedreira, A.J.C.L., 1994. O Supergrupo Espinhaço na Chapada Diamantina Centro-Oriental, Bahia: Sedimentação, Estratigrafia e Tectônica. Ph.D thesis, Universidade São Paulo.

Pedreira, A.J., De Waele, B., 2008. Contemporaneous evolution of the Palaeoproterozoic-Mesoproterozoic sedimentary basins of the São Francisco-Congo Craton. In: Pankhurst, R.J., Trouw, R.A.J., Brito Neves, B.B., De Wit, M.J. (Eds.), West Gondwana: Pre-Cenozoic Correlations across the South Atlantic Region. Geological Society Special Publications 294, 33-48.

Pinto, L.G.R., Pádua, M.B., Ussami, N., Vitorello, I., Padilha, A.L., Braitenberg, C., 2010. Magnetotelluric deep soundings, gravity and geoid in the south São Francisco craton: Geophysical indicators of cratonic lithosphere rejuvenation and crustal underplating. Earth and Planetary Science Letters 297, 423-434.

Piper, J.D.A., 2007. The Neoproterozoic supercontinent Palaeopangaea. Gondwana Research 12, 202-227.

Pisarevsky, S.A., Elming, S., Pesonen, L.J., Li, Z.. Mesoproterozoic paleogeography: Supercontinent and beyond. Precambrian Research (2013), http://dx.doi.org/10.1016/j.precamres.2013.05.014

Pflug, R., 1965. A Geologia da parte meridional da Serra do Espinhaço e zonas adjacentes. National Mineral Production Department Bulletin 266, 1-51.

Ribeiro, A., Teixeira, W., Dussin, I.A., Avila, C.A., Nascimento, D., 2013. U-Pb LA-ICP-MS detrital zircon ages of the São João del Rei and Carandaí basins: New evidence of intermittent Proterozoic rifting in the São Francisco paleocontinent, Gondwana Research 24, 713-726.

Rogers, J.J.W., Santosh, M., 2002. Mesoproterozoic Supercontinent: Introduction. Gondwana Research 5, 3-4.

Rogers, J.J.W., Santosh, M., 2004. Continents and Supercontinents. Oxford University Press, New York.

Roser, B.P., Korsch, R.J., 1988. Provenance signatures of sandstone-mudstone suites determined using Discriminant Function Analysis of major-element data. Chemical Geology 67, 119-139.

Rosset, A., De Min, A., Marques, L.S., Macambira, M.J.B., Ernesto, M., Renne, P.R., Piccirillo, E.M., 2007. Genesis and geodynamic significance of Mesoproterozoic and Early Cretaceous tholeiitic dyke swarms from the São Francisco craton (Brazil). Journal of South American Earth Sciences 24, 69-92.

Santos, M.N., Chemale Jr., F., Dussin, I.A., Martins, M., Assis, T.A.R., Jelinek, A.R., Guadagnin, F., Armstrong, R., 2013. Sedimentological and paleoenvironmental constraints of the Statherian and Stenian Espinhaço rift system, Brazil. Sedimentary Geology 290, 47-59.

Schobbenhaus, C., Hoppe, A., Baummann, A., Lork, A., 1994. Idade U/Pb do vulcanismo Rio dos Remédios Chapada Diamantina, Bahia. In: Scheibe, L.F. (Org.), 38° Congresso Brasileiro de Geologia. Brazilian Geological Society, 397-398.

Schobbenhaus, C., 1996. As tafrogêneses superpostas Espinhaço e Santo Onofre, estado da Bahia: Revisão e novas propostas. Brazilian Journal of Geology 26, 265-276.

Shaw, R., Etheridge, M., Lambeck, K., 1991. Development of the Late Proterozoic to Mid-Paleozoic intracratonic Amadeus Basin in Central Australia: a key to understanding tectonic forces in plate interiors. Tectonics 10, 688-721.

Silva, A.M., Chemale, F., Kuyumjian, R.M., Heaman, L., 1995. Mafic dyke swarms of Quadrilátero Ferrífero and Southern Espinhaço, Minas Gerais, Brazil. Brazilian Journal of Geology 25, 124-137.

Silveira, E.M., Söderlund, U., Oliveira, E.P., Ernst, R.E., Menezes Leal, A.B., 2013. First precise U-Pb baddeleyite ages of 1500 Ma mafic dykes from the São Francisco Craton, Brazil, and tectonic implications. Lithos 174, 144-156.

Sloss, L.L., 1963. Sequences in the Cratonic Interior of North America. Geological Society of America Bulletin 74, 93-114.

Tack, L., Wingate, M.T.D., De Waele, B., Meert, J., Belousova, E., Griffin, B., Tahon, A., Fernandez-Alonso, M., 2010. The 1375 Ma "Kibaran event" in Central Africa: Prominent emplacement of bimodal magmatism under extensional regime. Precambrian Research 180, 63-84.

Taylor, S.R., McLennan, S.M., 1985. The Continental Crust: its composition and evolution. Blackwell, Oxford.

Torsvik, T.H., Smethurst, M.A., Meert, J.G., Van der Voo, R., McKerrow, W.S., Brasier, M.D., Sturt, B.A., Walderhaug, H.J., 1996. Continental break-up and collision in the Neoproterozoic and Palaeozoic: A tale of Baltica and Laurentia. Earth Science Reviews 40, 229-258.

Torsvik, T.H., Müller, R.D., Van der Voo, R., Steinberger, B., Gaina, C., 2008. Global plate motion frames: toward a unified model. Reviews of Geophysics 46, RG3004, doi: 10.1029/2007RG000227

Trompette, R., Uhlein, A., Silva, M.E., Karmann, 1992. The Brasiliano São Francisco craton revisited (central Brazil). Journal of South American Earth Sciences 6, 49-57.

Turpin, L., Maruejol, P., Cuney, M., 1988. U-Pb, Rb-Sr and Sm-Nd chronology of granitic basement hydrothermal albitites and uranium mineralizations (Lagoa Real, South Bahia, Brazil). Contributions to Mineralogy and Petrology 98, 139-147.

Uhlein, A., Trompette, R.R., Egydio-Silva, M., 1998. Proterozoic rifting and closure, SE border of the São Francisco Craton, Brazil. Journal of South American Earth Sciences 11, 191-203.

Van Balen, R.T., Heeremans, M., 1998. Middle Proterozoic-early Palaeozoic evolution of central Baltoscandian intracratonic basins: evidence for asthenospheric diapirs. Tectonophysics 300, 131-142.

Vries, S.T., Pryer, L.L., Fry, N., 2008. Evolution of Neoarchean and Proterozoic basins of Australia. Precambrian Research 166, 39-53.

Weil, A.B., Van der Voo, R., Niocaill, C.M., Meert, J.G., 1998. The Proterozoic supercontinent Rodinia: paleomagnetically derived reconstructions for 1100 to 800 Ma. Earth and Planetary Science Letters 154, 12-24.

Winchester, J.A., Floyd, P.A., 1977. Geochemical discrimination of different magma series and their differentiation products using immobile elements. Chemical Geology 20, 325-343.

Zhao, G., Sum, M., Wilde, S.A., 2002. Did South America and West Africa marry and divorce or was it a long-lasting relationship? Gondwana Research 5, 591-596.

Appendix 2 – Vertical sections

(Download the vertical sections from the thesis pdf file for better visualization)

A2.1. Vertical Section 1 – Barra da Estiva

A2.2. Vertical Section 2 – Ronei

A2.3. Vertical Section 3 – Pati-Andaraí

A2.4. Vertical Section 4 – Guiné

A2.5. Vertical Section 7 – Fumaça

A2.6. Vertical Section 10 – Morrão

A2.7. Vertical Section 11 – BR242

A2.8. Vertical Section 14 – Impossíveis

A2.9. Vertical Section B – Pai Inácio hill

A2.10. Vertical Section (not presented in this thesis)– Ponte Rio Santo Antonio

VERTICAL SECTION #01
BARRA DA ESTIVA -B

Projeto CHAPADA UFRGS/PETROBRAS

Interpreter: Jorge Magalhães
Date: 25/01/2011

Scale: 1:100
Datum: SAD69 - 24 S
Coordinates UTM: 0249896 mE 8485548 mN

Location map

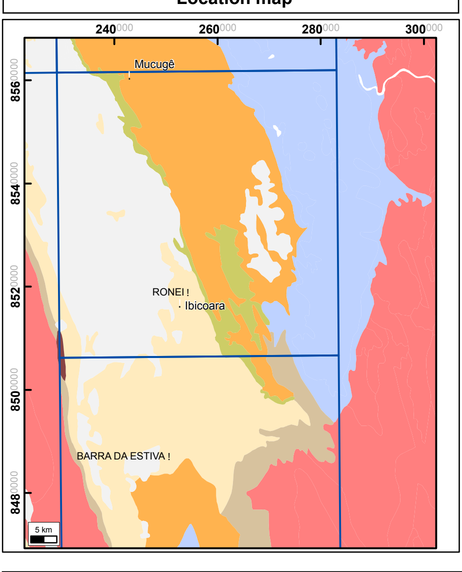

Project area

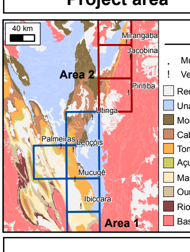

Legend
- . Municipality
- ! Vertical Section
- Recent
- Una Gr.
- Morro do Chapéu Fm.
- Caboclo Fm.
- Tombador Fm.
- Açuruá Fm.
- Mangabeira Fm.
- Ouricuri do Ouro Fm.
- Rio dos Remédios Gr.
- Basement

Stratigraphy

ERA	SUPER-GROUP	GROUP	FORMATION	DEPOSITIONAL SYSTEM
MESO-PROTEROZOIC	ESPINHAÇO	CHAPADA DIAMANTINA	Morro do Chapéu	Estuarine/ Fluvial
			Caboclo	Shallow marine
			Tombador	Alluvial fan/ Fluvial/Eolian/ Estuarine
PALEO-PROTEROZOIC		PARAGUAÇU	Açuruá	Shallow marine/ Coastal
			Mangabeira	Eolian

Sedimentary Facies

Gravel = G   Sand = S   Fine = F

Gcm	Clast-supported Massive	Sw	Wavy cross lamination
Gci	Clast-supported Reverse grading	St(t)	Tidal bundle
Gh	Horizontal stratification	Ss(t)	Sigmoidal cross stratification (tidal)
Gt	Tangential cross stratification	Ht	Laminated heterolith
Sh	Horizontal lamination	Fl	Horizontal lamination
Sl	Low angle lamination	Fm	Massive
St	Trough cross stratification	Sh(e)	Eolian horizontal lamination
Sp	Planar cross stratification	Sl(e)	Eolian low angle lamination
Sm	Massive	St(e)	Eolian trough cross stratification
Sr	Ripple cross lamination	Sa(e)	Eolian adhesion structure
Sf	Convolution		

Meter	Sand: M Bl Sx Gr G M F Mf S Ag	Facies (Code)	Facies Assoc.	Paleocurrent	Photo Mosaic	Description	Stratigraphy: Litho	Crono

Shallow marine

So: N104/5SW

Siltstone, purple.

Soil.

Sandstone medium- to coarse-grained, subhorizontal lamination.

Sandstone fine-grained pink, interbedded with purple siltstone.

Sandstone very fine-grained, lenticular bedding..

Sandstone fine-grained, interbedded with siltstone, laminated.

Siltstone, purple, laminated.

Coordinates: 250343/8478086 h=884m

Coordintes:250420/8?78452 h=876m

Sandstone laminated.

Sandstone fine-grained, bands of siltstone.

So: N100/6SW

Ripple marks.

Sandstone very fine-grined, laminated siltstone.

Sandstone fine-grained, laminated.

So: Horizontal

Sandstone medium-grained, band of very coarse-grained sandstone.

Tidal channel

Coordinates: 250411/8478506 h=876m

Sandstone massive, cut and filling features, low angle lamination at the base, filling channel,

Trough cross stratification

Sandstone medium-grained, limitaded by cut and filling low angle lamination at the base.

Coordinates 250408/8478598 h=879m

22m gap.

Tidal channel

Coordinates: 250390/8478888 h=857m

Tidal bundle over ripples.

Tidal bundle.

Sandstone medium-to coarse-grained, massive, cm-scale trough cross stratification, ripples on top.

Sandstone fine- to medium-grained, trough cross stratification.

Siltstone.

Sandstone fine-grained, laminated.

Sandstone fine- to medium-grained , subhorizontal lamination on top.

Sandstone medium to coarse-grained scattered granules.

Filmes de silte.

Ripple on top.

Sandstone fine- to medium-grained subhorizontal lamination.

M/dm-scale trough cross stratification.

n=22

Channel.

Sandstone medium-grained, trough cross stratification.

Sandstone very fine-grained, laminated.

Fold with vergence N345.

Sandstone fine- to medium-grained with ripples.

Sandstone medium-grained, subhorizontal lamination, trough cross stratification at the base.

Cm-scale trough and planar cross stratification.

Sandstone medium-grained, massive.

Planar cross stratification.

Ripple on top.

Sandstone medium-grained, m-scale trough cross stratification.

Sandstone with trough cross stratification.

Sandstone medium-grained, cut and filling features.

Coordinates:250323/8479062 h=845m

BR-142

Sand-bed braided fluvial

Morro da Torre

Coordinates: 250238/8485960 h=1462m

Heterolith, sandstone medium- to coarse-grained and siltstone, laminated.

Sandstone medium- to coarse-grained with trough cross stratification.

Heterolith, fine-grained sandstone and siltstone.

Subhorizontal lamination.

Sandstone medium-grained, trough cross stratification, cut and fill features.

Subhorizontal lamination on top and massive on the base.

Sandstone medium-grained cut and fill features.

Trough cross stratification.

Sandstone with planar cross stratification.

Dm-scale trough cross stratification.

Planar cross stratification on top.

Trough cross stratification.

Planar cross stratification.

Sandstone medium-grained trough cross stratification..

Sandstone medium-grained massive.

Coordinates: 250198/8485888 h=1445m

12m gap.

Tidal bar

Coordinates: 250183/8485850 h=1433m

Fracture.

Sandstone medium-grinedmud drapes on top.

Sandstone medium-grained, massive.

Sandstone fine-grained subhorizontal lamination.

Sandstone coarse-grained massive.

Sandstone fine-grained, laminated.

Sandstone medium-grained.

Sandstone medium-grained , mud drapes.

Coordinates: 250150/8485878 h=1415m

17m gap.

Fractured zone.

Tidal bar

Coordinates: 250073/8485864 h=1398m

Sandstone medium-grained, tidal bundle.

So: N140/85W

Sandstone medium- to fine-grained, bands of granules on the base , tidal bundle.

Sandstone coarse- to medium-grained bands of granules and peebles on the base.

Sandstone medium to coarse-grained with granules.

Siltstone laminated, grey/green.

Sandstone medium-grained with mud drapes.

Coordinates: 250073/8485864 h=1391m

Gap.

Tidal channel

Coordinates: 250077/8485802 h=1389m.

Sandstone, trough cross stratification.

Sandstone, laminated, normal grading.

Low angle lamination.

Sandstone medium-grained, with coarse-grained to granules at the base, normal grading.

n=5

Sandstone very fine-grained, laminated interbedded with siltstone.

Sandstone medium-grained with interbeds of very fine-grained sandstone.

Sandstone medium-grained with cm-scale trough cross stratification. Erosive base, very coarse-grained to granular sandstone.

Sandstone medium-grained interbeded with mudstone layers.

Subvertical fractures.

Tidal bar

Sandstone with laminação sub-horizontal, erosive bottom surface.

Sandstone, dm-scale trough cross stratification.

Sandstone medium- to coarse-grained, laminated, mud drapes.

Sandstone medium-grained, trough cross stratification at the base.

Sandstone medium- to coarse-grained massive.

n=3

Sandstone medium-grained massive.

Sandstone medium- to coarse-grained, massive.

So: N85/6SE

Sandstone medium- to coarse-grained, cm-scale planar cross stratification, sitstone layer on top.

Sandstone medium- to coarse-grained, cm-scale planar cross stratification.

Sandstone medium- to coarse-grained, subhorizontal lamination, fine-grained sandstone on top.

Sandstone very fine-grained, subhorizontal lamination.

Sandstone medium- to coarse-grainde, massive, interbeds of mudstone.

Sandstone medium-grined planar cross stratification.

Sandstone medium-grained with trough cross stratification.

Coordinates: 250307/8485808 h=1367m

9m gap.

Tidal channel

Sandstone medium- to coarse-grained,bands of granules, cm-scale trough cross stratification.

Sandstone coarse-grained, cm-scale planar cross stratification, interbeds of siltstone.

n=3

Sandstone medium- to coarse-grained, massive, fraturado.

So: N65/8SE

Coordenada: 250104/8485680 h=1354m

Siltstone, laminated.

Quartz vein.

Sandstone medium- to coarse-grained horizontal lamination.

Coordinates: 250080/8485698 h=1345m

Gap

Coordinates: 250040/8485696 h=1343m

Tidal bar

Sandstone medium- to coarse-grained, bands of granules, vertical fractures.

Sandstone with vertical fractures.

Sandstone with tidal bundle and vertical fractures.

Coordinates: 250003/8485688 h=1346m

16m gap.

Fault zone.

So: N30/8°SE

Sandstone with interbeds of siltstone laminated with tidal bundle.

Coordinates 250027/8485612 h=1328m

18m gap.

Fault zone.

Meter	Sand: M Bl Sx Gr G M F Mf S Ag	Facies (Code)	Facies Assoc.	Paleocurrent	Photo Mosaic	Description	Stratigraphy: Litho	Crono

UFRGS

VERTICAL SECTION #01
BARRA DA ESTIVA -A

Projeto CHAPADA UFRGS/PETROBRAS

Interpreter: Jorge Magalhães
Date: 25/01/2011

Scale: 1:100
Datum: SAD69 - 24 S

Coordinates UTM: 0249896 mE 8485548 mN

Location map

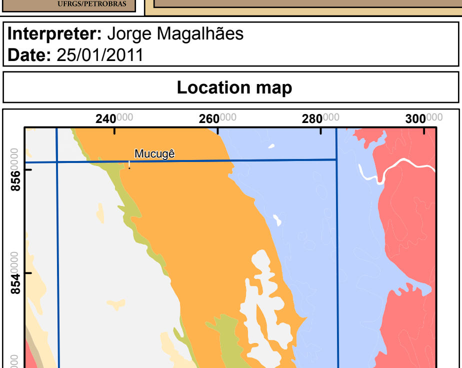

Project area

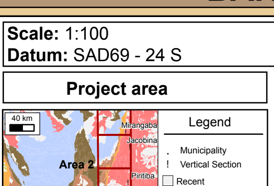

Stratigraphy

ERA	SUPER-GROUP	GROUP	FORMATION	DEPOSITIONAL SYSTEM
MESO-PROTEROZOIC	ESPINHAÇO	CHAPADA DIAMANTINA	Morro do Chapéu	Estuarine/ Fluvial
			Caboclo	Shallow marine
			Tombador	Alluvial fan/ Fluvial/Eolian/ Estuarine
PALEO-PROTEROZOIC		PARAGUAÇU	Açuruá	Shallow marine/ Coastal
			Mangabeira	Eolian

Sedimentary Facies

Gravel = G Sand = S Fine = F

Gcm	Clast-supported Massive	Sw	Wavy cross lamination
Gci	Clast-supported Reverse grading	St(t)	Tidal bundle
Gh	Horizontal stratification	Ss(t)	Sigmoidal cross stratification (tidal)
Gt	Tangential cross stratification	Ht	Laminated heterolith
Sh	Horizontal lamination	Fl	Horizontal lamination
Sl	Low angle lamination	Fm	Massive
St	Trough cross stratification	Sh(e)	Eolian horizontal lamination
Sp	Planar cross stratification	Sl(e)	Eolian low angle lamination
Sm	Massive	St(e)	Eolian trough cross stratification
Sr	Ripple cross lamination	Sa(e)	Eolian adhesion structure
Sf	Convolution		

Meter	Sand: M Bl Sx Gr G M F Mf S Ag	Facies (Code)	Facies Assoc.	Paleocurrent	Photo Mosaic	Description	Stratigraphy: Litho	Crono

Paleocurrent:

So: N170/14SW

n=9

So: N10/4SE

So: N60/6SE

So: N50/6SE

So: N29/19SE

So: N30/16SE

So: N0°/11°

n=9

So: N60/5SE

So: N70/8SE

n=7

So: N8/12SE

So: N30/11SE

So: N45/8SE

So: N45/11SE

So: N25/6SE

So: N100/10SW

So: N60/1SE

So: N65/10SE

So: 75/9SE

So: 40/7SE

So: N70/3SE

So: N75/3SE

So: N75/4SE

So: N90/16S

So: N85/10SE

So: N90/3S

So: N80/8SE

So: N80/7SE

So: N90/8S

n=7

So: N75/11SE

So: N65/11SE

Description:

Coordinates 249993/8485564 h=1310m

Sandstone fine- to medium-grained trough cross stratification e bands of granules with a siltstone layer on top.
Sandstone medium- to coarse-grained, truncating siltstone and laterally covered by siltstone, laminated.

Sandstoe medium-grained with tidal bundle, subvertical fracture and siltstone laminated on top.

Sandstone and mustone, horizontal lamination.
Sandstone coarse- to medium-grained with tidal bundle.

IMPD written on the outcrop.
Sandstone coarse-grained with tidal bundles.

Sandstone medium-grained, siltstone laminated on top.
Sandstone medium-grained, tidal band with siltstone on top.

Sandstone very fine-grained, internal mud drapes.

Siltstone horizontal lamination.
Sandstone very fine-grained with internal mud drapes, tangential cross stratification.

Sandstone very fine-grained laminated, with siltstone and very coarse-grained sandstone level on top.

Coordinates 249953/8485548 h=1298m

6m gap.

Coordinates 249907/8485568 h=1289m

Sandstone fine- to medium-grained horizontal lamination.

Sandstone coarse-grained, massive.

Sandstone coarse-graineddm-scale planar cross stratification.
Coordinates 249896/8485576 h=1285m

9m gap.

Coordinates 249497/8484784 h=1197m
Sandstone medium- to coarse-grained, massive , subvertical fractures.

Sandstone medium-grained with trough cross stratification.
Sandstone medium-grained, horizontal lamination.
Sandstone very coarse-grained to granular with trough cross stratification.

Sandstone very coarse- to granular, massive.

Sandstone coarse- to very coarse-grained with bands of granules. Ripple marks on top.
Sandstone very coarse-grained, low angle lamination with bands of siltstone.
Sandstone coarse- to very coarse-grained interbedded with mudstone drapes.

Sandstone medium- to coarse-grained with cm-scale planar cross stratification.
Sandstone medium- to coarse-grained massive.

Sandstone coarse-grained , trough cross stratification.

Sandstone fine-grained horizontal lamination, cm-scale planar cross stratification on top.

Sandstone medium-grained, horizontal lamination.

Sandstone medium- to coarse-grained massive.

Sandstone fine- to medium-grained, horizontal lamination.

Sandstone fine- to medium-grained, cm-scale planar cross stratification. Horizontal lamination.

Siltstone interbedded with fine- to very fine-grained sandstone, horizontal lamination.
Sandstone fine- to medium-grained, tidal bundle.
Sandstone fine- to medium-grained, planar cross stratification.
Sandstone very fine- to mediu-grained, horizontal lamination.

Sandstone fine- to medium-grained horizontal lamination, tidal bundle and mud drapes.
Siltstone interbedded with sandstone medium--grained.
Sandstone medium-grained with ripples marks on top.
Sandstone fine- to medium-grained, ripple marks.
Sandstone medium- to coarse-grained, horizontal lamination, planar cross stratification on top.

Sandstone medium-grained, horizontal lamination.

Sandstone medium-grained, horizontal lamination and siltstone layer on top.
Coordinates: 0248416/8484934 h=1177m
Sandstone coarse- to very coarse-grained on the channel.

Siltstone laminated.

Sandstone medium- to coarse-grained, normal grading to fine-grained, tidal bundles.

Sandstone fine- to coarse-grainded laminated.
Siltstone to sandstone very fine-grained, laminated.
Mudstone to siltstone, laminated.

Siltstone, laminated.

Mudstone, horizontal laminated.
Sandstone with normal grading.
Quartz vein parallel to bedding plane(182/183).
Sets up to 10cm thick, normal grading from granules to mud. Erosive bottom surface.

Sandstone coarse- to very coarse-grained ,with peebles on the stratification surface and erosive bottom surface.

Sandstone very coarse-grained with granules. Cut and fill features.
Coordinates 49405/8485000 h=1173m
Sandstone, normal grading, erosive base.
Bands of granules, with erosive base, pirite.

Sandstone very coarse-grained massive, with scattered granules.

Quartz vein.
Sandstone very fine-grained, with bands of granules

Siltstone laminated.
Sandstone, trough cross stratification, granules on the erosive base. Bands of siltstone with erosive top and straight bottom surface.
Siltstone horizontal lamination.
Sandstone very coarse-grained scattered granules.
Sandstone, normal grading.
Sandstone with bands of granules.
Coordinates 249405/8485040 h=1175

Sandstone, normal grading, low angle lamination.

Siltstone laminated.
Coordinates 249408/8485046 h=1170m

Sandstone medium- to coarse-grained, ripple-marks on top.

Sanstone, planar cross stratification, ripple on top.

Sandstone, horizontal lamination on top and tangential on the bottom surface.
Mudstone, laminated.
Sandtone, massive.
Coordinates 249412/8485084 h=1169m

13m gap.

Coordinates 249434/8485400 h=1156m

Sandstone fine- to medium-grained, horizontal lamination, cm-scale trough cross stratification on the bottom surface.

Sandstone fine-grained horizontal lamination on top, cross stratification.

Sandstone very fine-grined, with climbing ripples.

Coordinates 249434/8485464 h=1166m

Access to Morro da Torre.

9m gap.

Coordinates 250484/8486820 h=1175m
BR 142 - Barra da Estiva/Ituaçu

Heterolith composed of interbeds of laminated to massive fine-grained sandstone and siltstone.
Subhorizontal fractures.

Normal grading.

Subvertical fractures.

7,5m gap.

Gap.

Sandstone very fine-gained, climbing ripple.

Fracture, breccia.

Cracks (synaeresis?).

Coordinates 250523/8487072 h=1151m

Climbing ripple.

Coordinates 250537/848709 h=1148m

Heterolith, very fine-grained sandstone and siltstone, laminated, lenticular bedding.

Load mark (foto 235).

Subvertical fractures.

Heterolith, siltstone and very fine grained sandstone laminated, lenticular bedding and sand dikes.
Coordinates 250580/8487150 h=1135m

BR 142 - Barra da Estiva -Ituaçu
Towards Morro da Torre.

Meter	Sand	Facies (Code)	Facies Assoc.	Paleocurrent	Photo Mosaic	Description	Litho	Crono
							Stratigraphy	

UFRGS

VERTICAL SECTION #02 RONEI

Interpreter: Magalhães
Date: 27/01/2011

Scale: 1:100
Datum: SAD69 - 24 S
Coordinates UTM: 0254290 mE 8518988 mN

Location map

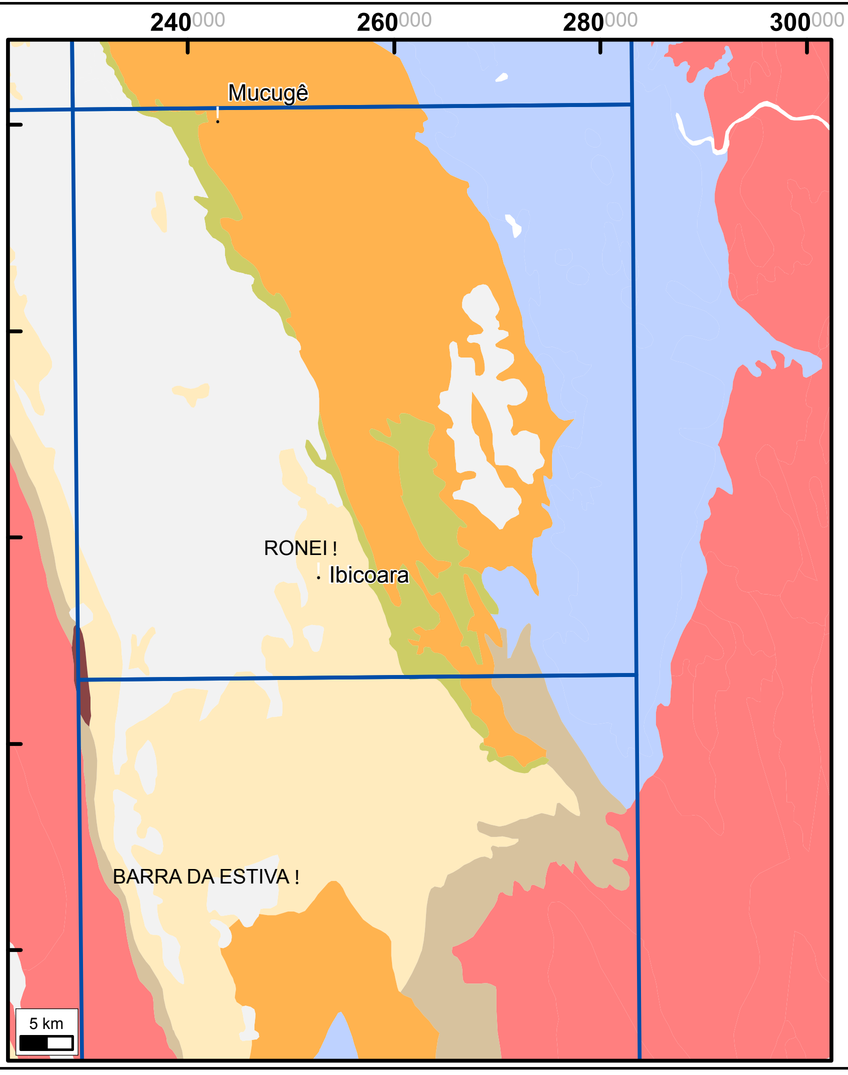

Project area

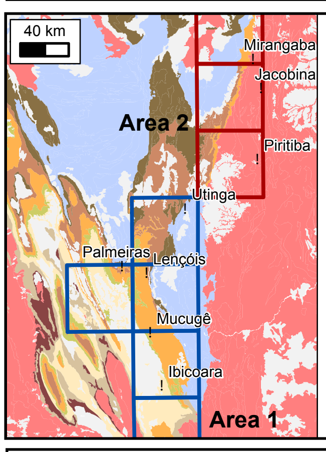

Stratigraphy

ERA	SUPER-GROUP	GROUP	FORMATION	DEPOSICIONAL SYSTEM
MESO-PROTEROZOIC	ESPINHAÇO	CHAPADA DIAMANTINA	Morro do Chapéu	Estuarine/ Fluvial
			Caboclo	Shallow marine
			Tombador	Alluvial fan/ Fluvial/Eolian/ Estuarine
PALEO-PROTEROZOIC		PARAGUAÇU	Açuruá	Shallow marine/ Coastal
			Mangabeira	Eolian

Sedimentary facies

Gravel = G **Sand** = S **Fine** = F

Gcm	Clast-supported Massive	Sw	Wavy cross lamination
Gci	Clast-supported Reverse grading	St(t)	Tidal bundle
Gh	Horizontal stratification	Ss(t)	Sigmoidal cross stratification (tidal)
Gt	Tangential cross stratification	Ht	Laminated heterolith
Sh	Horizontal lamination	Fl	Horizontal lamination
Sl	Low angle lamination	Fm	Massive
St	Trough cross stratification	Sh(e)	Eolian horizontal lamination
Sp	Planar cross stratification	Sl(e)	Eolian low angle lamination
Sm	Massive	St(e)	Eolian trough cross stratification
Sr	Ripple cross lamination	Sa(e)	Eolian adhesion structure
Sf	Convolution		

Meter	Facies (Code)	Facies Assoc.	Paleocurrent	Photo Mosaic	Description	Stratigraphy Litho	Crono

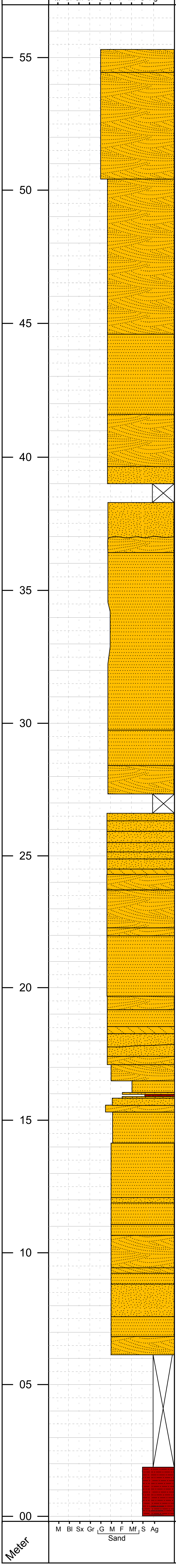

Facies (Code), top to base: St, St, St, Sh, St, Sm, Sm, St, Sh, Sh, St, Sm, Sp, St, St, St, Sh, St, Sh, Sp, Sm, St, Sh, Sm, St, Sh, Sh, Sm, Sh, St, Sh, Sm, Sh, St, LS

Facies Assoc.: Proximal / Intermediate sheetflood; Floodplain; Proximal / Intermediate sheetflood; Prodelta

Paleocurrent:

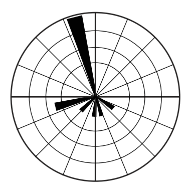

n=10

Description:

Sandstone coarse-grained with trough cross bedding and lens of fine- to medium-grained sandstone.

Sandstone medium- to coarse-grained with trough cross bedding and scattered granules

Sandstone medium- to coarse-grained with horizontal lamination and scattered granules

Sandstone medium- to coarse-grained with trough cross bedding and scattered granules

Ripple cross lamination on top of same beds.

Sandstone medium- to coarse-grained with trough cross bedding and ripple cross lamination.

Sandstone medium- to coarse-grained with horizontal lamination.

Sandstone medium- to coarse grained with trough cross bedding.

Sandstone medium-grained

Sandstone massive.

Sandstone medium- to coarse-grained with trough cross bedding.

Sandstone medium- to coarse-grained with trough cross bedding.

Sandstone gray, medium- to coarse-grained with planar cross stratification on top.

Sandstone medium-grained massive with trough cross stratification on the base.

Sandstone very fine-grained laminated.

Sandstone medium-grained

Sandstone medium-grained with horizontal lamination.

Sandstone medium-grained with trough cross bedding.

Sandstone medium-grained with lamination sub-parallel

Sandstone medium-grained

Coordinate: 0254290 mE
8518988 mN
Elevation: 1078 m

Aprox. 4.2 m covered

Meter	Facies (Code)	Facies Assoc.	Paleocurrent	Photos	Description	Stratigraphy Litho	Crono

VERTICAL SECTION #03
PATI_ANDARAI -D

Projeto CHAPADA UFRGS/PETROBRAS

Interpreter: Magalhães
Date: 16/01/2011

Scale: 1:100
Datum: SAD69 - 24 S

Coordinates UTM: 0239297 mE 8583042 mN

Location map

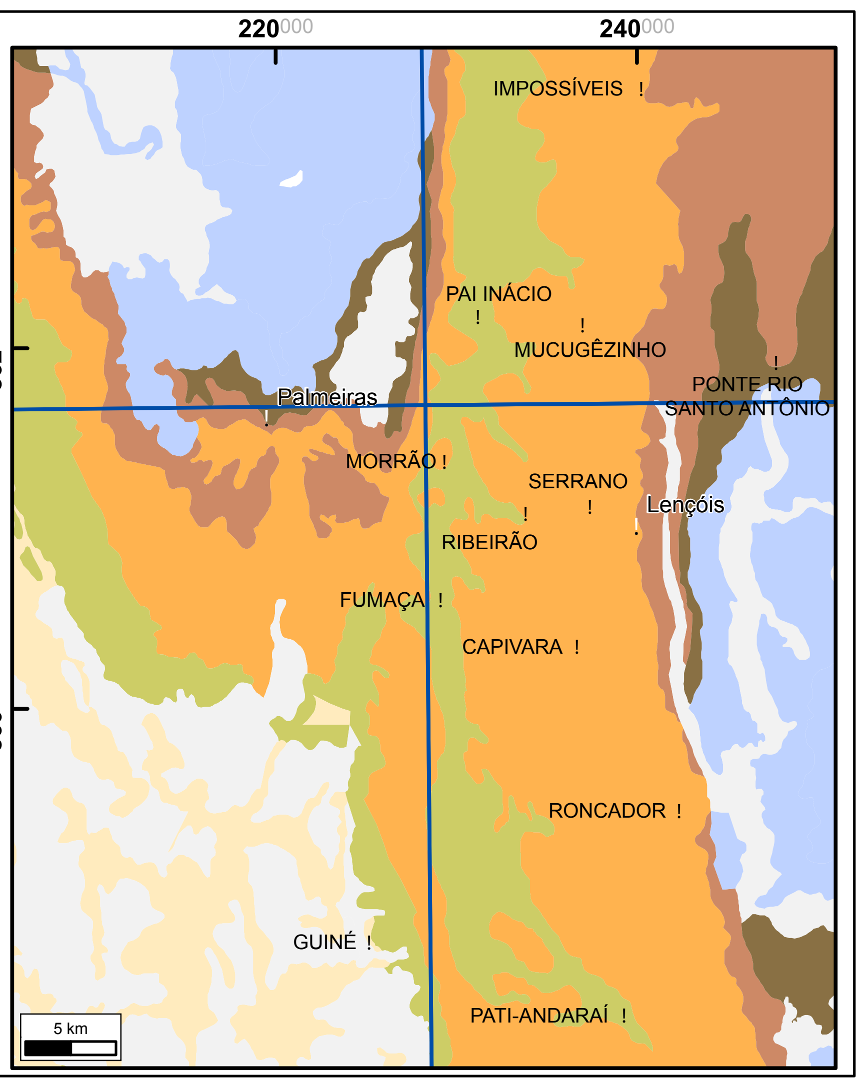

Project area

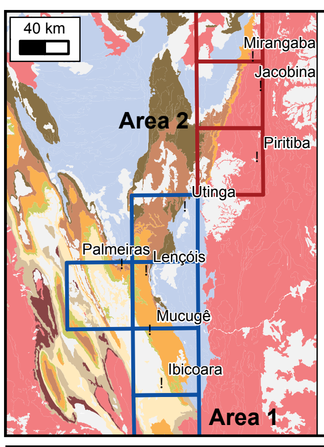

Stratigraphy

ERA	SUPER-GROUP	GROUP	FORMATION	DEPOSITIONAL SYSTEM
MESO-PROTEROZOIC	ESPINHAÇO	CHAPADA DIAMANTINA	Morro do Chapéu	Estuarine/ Fluvial
			Caboclo	Shallow marine
			Tomba-dor	Alluvial fan/ Fluvial/Eolian/ Estuarine
PALEO-PROTERO-ZOIC		PARA-GUAÇU	Açuruá	Shallow marine/ Coastal
			Manga-beira	Eólico

Sedimentary Facies

Gravel = G		Sand = S	Fine = F
Gcm	Clast-supported Massive	Sw	Wavy cross lamination
Gci	Clast-supported Reverse grading	St(t)	Tidal bundle
Gh	Horizontal stratification	Ss(t)	Sigmoidal cross stratification (tidal)
Gt	Tangential cross stratification	Ht	Laminate heterolith
Sh	Horizontal lamination	Fl	Horizontal jamination
Sl	Low angle lamination	Fm	Massive
St	Trough cross stratification	Sh(e)	Eolian horizontal lamination
Sp	Planar cross stratification	Sl(e)	Eolian low angle lamination
Sm	Massive	St(e)	Eolian trough cross stratification
Sr	Ripple cross lamination	Sa(e)	Eolian adhesion structure
Sf	Convolution		

Meter	M Bl Sx Gr G M F Mf S Ag (Sand)	Facies (Code)	Facies Assoc.	Paleocurrent	Photo Mosaic	Description	Stratigraphy: Litho	Crono

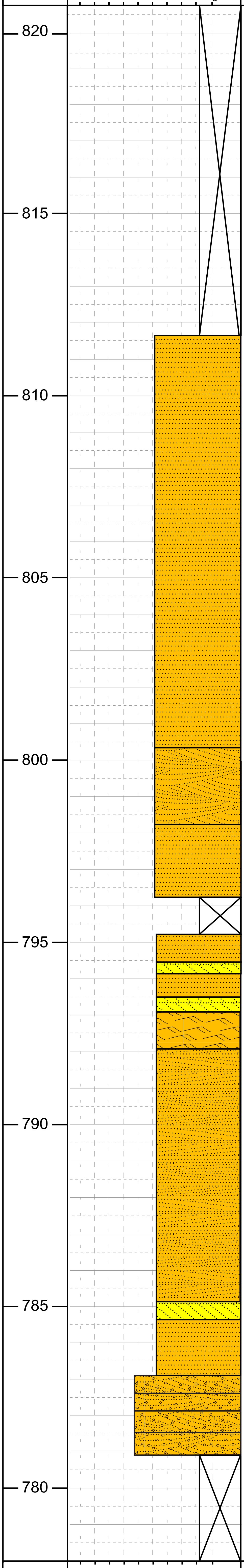

Meter	Facies (Code)	Facies Assoc.	Paleocurrent	Description	Litho
~810–797	Sh	Intermediate / distal sheetflood		Sandstone, pink, medium-grained, horizontal lamination, localized ripples, cemented.	RIO DAS FLORES
~800	St			Sandstone, pink, medium-grained, dm-scale trough cross stratification, cemented.	
~798	Sh			Coordinates: 246663/8583182 h:406m	
~795–793	Sh, Sp(e), Sh, Sp(e), Sr	Eolian dune and sandsheet		Sandstone medium-grained, cm-scale trough cross stratification , horizontal lamination and ripple marks. Sandstone medium-grained, ripples cross lamination	ANDARAÍ
~790–788	Sl			Sandstone medium-grained, ripples, well sorted, low angle lamination.	
~785	Sp(e)	Intermediate / distal sheetflood	So: N10/15SE	Sandstone pink, medium-grained, low-angle lamination, ripples.	
~784	Sh		So: N10/15SE	Coordinates: 245.686/8.583.406 h: 535m	
~782	St			Sandstone fractured	
~781				Coordinates: 245.711/8.583.416 h:530m	

M Bl Sx Gr G M F Mf S Ag
Sand

Meter | Facies (Code) | Facies Assoc. | Paleocurrent | Photo Mosaic | Description | Litho | Crono | Stratigraphy

UFRGS UNIVERSIDADE FEDERAL DO RIO GRANDE DO SUL

BR

VERTICAL SECTION #03
PATI_ANDARAI -C

Projeto CHAPADA UFRGS/PETROBRAS

Interpreter: Magalhães
Date: 16/01/2011

Scale: 1:100
Datum: SAD69 - 24 S

Coordinates UTM: 0239297 mE 8583042 mN

Location map

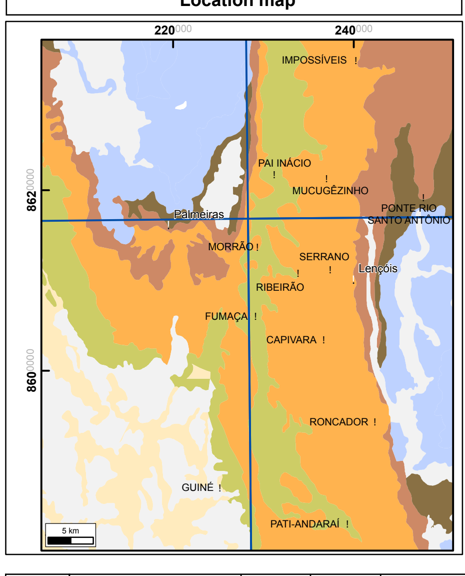

Project area

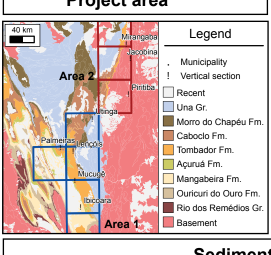

Stratigraphy

ERA	SUPER-GROUP	GROUP	FORMATION	DEPOSITIONAL SYSTEM
MESO-PROTEROZOIC	ESPINHAÇO	CHAPADA DIAMANTINA	Morro do Chapéu	Estuarine/ Fluvial
			Caboclo	Shallow marine
			Tombador	Alluvial fan/ Fluvial/Eolian/ Estuarine
PALEO-PROTEROZOIC		PARAGUAÇU	Açuruá	Shallow marine/ Coastal
			Mangabeira	Eolian

Sedimentary Facies

Gravel = G Sand = S Fine = F

Gcm	Clast-supported Massive	Sw	Wavy cross lamination
Gci	Clast-supoorted Reverse grading	St(t)	Tidal bundle
Gh	Horizontal stratification	Ss(t)	Sigmoidal cross stratification (tidal)
Gt	Tangencial cross stratification	Ht	Laminated Heterolith
Sh	Horizontal lamination	Fl	Horizontal lamination
Sl	Low angle lamination	Fm	Massive
St	Trough cross stratification	Sh(e)	Eolian horizontal lamination
Sp	Planar cross stratification	Sl(e)	Eolian low angle lamination
Sm	Massive	St(e)	Eolian trough cross stratification
Sr	Ripple cross lamination	Sa(e)	Eolian adhesion structure
Sf	Convolution		

Meter	Sand (M Bl Sx Gr G M F Mf S Ag)	Facies (Code)	Facies Assoc.	Paleocurrent	Photo Mosaic	Description	Stratigraphy: Litho	Stratigraphy: Crono

Coordinates: 246217/8593152 Elevation: 438m
Sandstone pink, medium-grained with horizontal lamination, granular bands and scattered pebbles. Conglomerate matrix supported, pebbles of white, green and pink quartzite.

Sandstone coarse-grained, greenish, with bands of granules.

Coordinates: 245675/8583396 Elevation: 542m

Sandstone coarse-grained with trough cross stratification, granules and pebbles.

Sandstone with brighting black grains.

Sandstone pink with bands of granules.
Siltstone red, laminated.
Sandstone greenish, very fine-grained with scattered pebbles.
Coordinates: 245530/8583570 Elevation: 556m

Conglomerate clast supported with white and green quartzite, sandy matrix and scarce pebbles of meta-sandstone.
Trail smooth, sub-horizontal.

Coordinates: 245624/8583438 Elevation: 546m

Sandstone coarse- to very coarse-grained with scattered pebbles.
Conglomerate clast supported, green and white quartzite, and scarce pebbles of meta-sandstone.

Sandstone coarse-grained, cut and fill features and scattered pebbles.

Conglomerate matrix supported, cut and fill features, clasts up to 7cm, greenish sandy matrix.

Coordinates: 245034/8584148 Elevation: 598m

Coordinates: 243607/8583918 Elevation: 816m

Coordinates: 243862/8584030 Elevation: 788m

Sandstone very coarse-grained, with granules and pebbles, trough cross stratification.

Coordinate: 243891/8584069

Sandstone granular to very coarse-grained, with scattered pebbles.

Sandstone coarse-grained with granules, trough cross stratification, blocky macssive.

Sandstone medium- to coarse-grained, with scattered granules, bands of granules, trough cross stratification.

Sandstone coarse- to very coarse-grained, scattered granules and peebles, massive, trough cross stratification, normal grading.
Sandstone very coarse-grained to granular, with scattered peebles.
Sandstone granular, with trough cross stratification.

Sandstone very coarse-grained, trough cross stratification and granules.

Sandstone very coarse-grained, trough cross stratification, scattered peebles.
Sandstone medium- to coarse-grained, horizontal lamination, ripple marks.
Coordinates: 243946/8584094 h:765m

Arenito muito grosso/granuloso com seixos dispersos e acanaladas.

Sandstone, massive, scattered granules, horizontal lamination.

Sandstone medium- to coarse-grained, low angle lamination, well sorted with scattered granules.

Sandstone medium- to coarse-grained, horizontal lamination.

Coordinates: 244015/8584056 h:739m

Fractures oriented to N-S.

Sandstone pink, medium- to coarse-grained, horizontal lamination and scattered granules.

Sandstone coarse-grained, horizontal lamination and granules.

Sandstone coarse- to very coarse-grained with bands of granules.

Vertical fractures oriented N-S and N345.

Sandstone medium- to coarse-grained with granules.

Sandstone coarse- to very coarse-grainde, massive, trough cross stratification, granules.

Coordinates: 244136/8584074 h:718m

m- to dm-scale trough cross stratification.

Sandstone medium- to coarse-grained, granules on bedding plain.

Sandstone medium- to coarse-grained, scattered granules, horizontal lamination.

Sandstone coarse- to very coarse-grained, trough cross stratification.

Sandstone medium- to coarse-grained, laminated.

Siltstone laminated.
Sandstone medium- to coarse-grained, cm-scale trough cross stratification.

Sandstone medium- to coarse-grained, horizontal lamination.

Sandstone medium-grained, cm-scale trough and planar cross stratification.

Sandstone medium- to coarse-grained, massive, horizontal lamination, interbedded with siltstone layers. quartz vein oriented to N340.

Sandstone coarse- to very coarse-grained, horizontal lamination, bands of granules.

Vertical fractures oriented to N340.

Riacho do Mirante.
Coordinates: 244335/8583976
Sandstone coarse- to very coarse-grained scattered granules and peebles.
Viewpoint to Rio Paraguaçu.
Fracture oriented to N180.
Coordinates: 244048/8584052 h:736m

Viewpoint to Andaraí - conglomerate fractured to N345.
Coordinates: 243744/8584020 h:890m

Sandstone coarse-grained toconglomerate, fracture zone, yellow siltstone.

Sandstone very coarse-grained to conglomerate, scattered granules and peebles.

Sandstone coarse- to very coarse-grained with granules.

Sandstone coarse-grained, horizontal lamination, ripple marks, vertical fractures.
Sandstone coarse- to medium-grained, laminated.
Sandstone medium- to coarse-grained, m-scale trough cross stratification, grain flow.
Sadstone medium- to coarse-grained, horizontal lamination.
Coordinates: 243.137/8.583.970 h:894m

Sandstone coarse-grained, scattered granules and peebles, trough cross stratification.

Sandstone to conglomerate, scattered peebles.
Coordinates: 243048/8583934 h:815m

22m gap.

Fe concretions on the trail.

Sandstone, granular, peebles of white quartzite.

Coordinates: 242616/8583754 h:864m
Conglomerate, granular to peeble of white and pink quartzite, and meta-sandstone, sandy matrixareno.

Meter	Sand	Facies (Code)	Facies Assoc.	Paleocurrent	Photo Mosaic	Description	Stratigraphy: Litho	Stratigraphy: Crono

VERTICAL SECTION #03
PATI_ANDARAI -B

Projeto CHAPADA UFRGS/PETROBRAS

Interpreter: Magalhães
Date: 16/01/2011

Scale: 1:100
Datum: SAD69 - 24 S

Coordinates UTM: 0239297 mE 8583042 mN

Location map

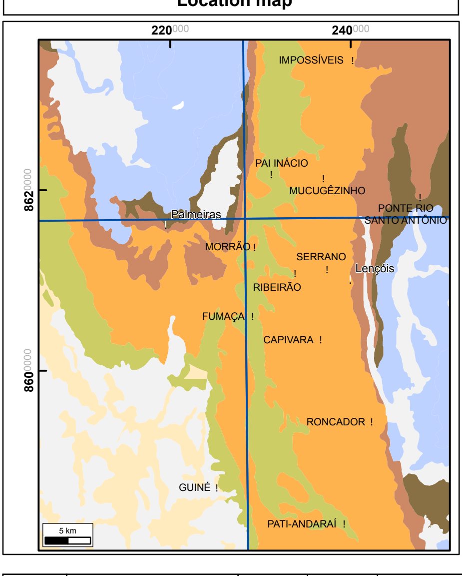

Project area

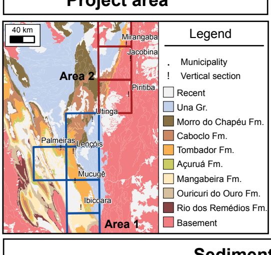

Stratigraphy

ERA	SUPER-GROUP	GROUP	FORMATION	DEPOSITIONAL SYSTEM
MESO-PROTEROZOIC	ESPINHAÇO	CHAPADA DIAMANTINA	Morro do Chapéu	Estuarine/ Fluvial
			Caboclo	Shallow marine
			Tombador	Alluvial fan/ Fluvial/Eolian/ Estuarine
PALEO-PROTEROZOIC		PARAGUAÇU	Açuruá	Shallow marine/ Coastal
			Mangabeira	Eólico

Sedimentary Facies

Gravel = G		Sand = S	Fine = F
Gcm	Clast-supportedo Massive	Sw	Wavy cross lamination
Gci	Clast-supported Reverse grading	St(t)	Tidal bundle
Gh	Horizontal statification	Ss(t)	Sigmoidal cross stratification (tidal)
Gt	Tangencial cross stratification	Ht	Laminated Heterolith
Sh	Horizontal lamination	Fl	Horizontal lamination
Sl	Low angle lamination	Fm	Massive
St	Trough cross stratification	Sh(e)	Eolian horizontal lamination
Sp	Planar cross stratification	Sl(e)	Eolian low angle lamination
Sm	Massive	St(e)	Eolian trough cross stratification
Sr	Ripple cross lamination	Sa(e)	Eolian adhesion structure
Sf	Convolution		

Description

GAP 1,3m covered

Sandstoen coarse-grained with granules.
Sandstone coarse-grained, masive, with scattered granules.

Cut and fill features.

Sandstone coarse-grained to granular with trough cross stratification.

10m covered.

Shear zone
+
vegetation cover on top

Coordinates: 240135/8582773 Elevation: 962m

Sandstone medium-grained, massive.
Coordinates: 240014/8582982 Elevation: 964m

Sandstone medium-grained with trough cross stratificataion.

Sandstone very coarse-grained with trough cross stratification.

Sandstone coarse-grained, tangential lamination at the base and scattered granules.
Sandstone coarse-grained weakly laminated.

Sandstone coarse-grained, horizontal lamination.

Sandstone medium-grained with trough cross stratification.
Sandstone medium-grained, with low angle to horizontal lamination.
Sanstone medium-grained, with trough planar stratification and weakly laminated.

Sandstone fine-grained, pink, laminated.
Coordinates: 240103/8582808 Elevation: 958m

Sandstone coarse-grained, scattered granules and trough cross stratification.
Shear bands.
Sandstone coarse-grained with granules

Coordinates: 248003/8582974 Elevation: 937m

Sandstone medium- to coarse-grained, massive.

Covered 2,5m.

Sandstone coarse-grained, trough cross stratification.

Sandstone coarse-grained and trough cross stratification.

Sandstone medium-grained, massive.

Sandstone coarse-grained, with trough cross stratification.

Sandstone coarse-grained, massive to laminated.

Sandstone medium- to coarse-grained, convoluted.

Sandstone coarse- to very coarse-grained, with trough cross stratification.

Coordinates: 239833/8583202 Elevation: 917m

Sandstone coarse-grained massive.

Sandstone medium-grained, horizontal lamination and massive on top.

Sandstone medium-grained with trough cross stratification.

Sandstone medium-grained massive.

Sandstone medium- to coarse- grained, massive.

Sandstone coarse-grained with granular bands at the base.

Sandstoen medium- to coarse-grained, with scattered granules.

Sandstone medium- to coarse-grained, massive.

Sandstone medium-grained, massive.
Sandstone medium- to coarse-grained with trough cross stratification.
Sandstone medium-grained with trough cross stratification.

Sandstone medium- to coarse-grained, massive, ripple marks on the top.

Sandstone medium- to coarse-grained, erosive bottom surface.
Sandstone medium-grained, massive.

Sandstone medium- to coarse-grained,with horizontal lamination.
Sandstone medium- to coarse-grained with trough cross stratification.

Sandstone coarse-grained, with granules and trough cross stratification.
Sandstone coarse-grained with trough cross stratification and normal grading.

Sandstone medium- to coarse-grained with ripple marks on the top.

Sandstone medium-grained massive.
Sandstone medium-grained with lens of coarse-grained sandstone.

Sandstone coarse-grained massive.

Sandstone coarse-grained laminated.

Sandstone medium- to coarse-grained with granules and trough cross stratification.

Sandstone coarse-grained with trough cross stratification.

Sandstone coarse-garined massive.

Sandstone medium-grained, with ripple marks on the top.
Sandstone coarse-grained with trough cross stratification.

Sandstone medium-grained, with ripple cross lamination.

Sandstone medium-grained, with trough cross stratification and ripple marks on top.

Sandstone medium-grained, massive.

Sandstone coarse-grained with horizontal lamination.

sandstone medium- to coarse-grained, with trough cross stratification.

Coordinates: 239796/8583160 Elevation: 877m

Sandstone coarse-grained, with trough cross stratification.

Coordinates: 239764/8513166 Elevation: 865m

Photo Mosaic	Description	Lithostratigraphy

VERTICAL SECTION #03
PATI_ANDARAI -A

Interpreter: Magalhães
Date: 16/01/2011

Scale: 1:100
Datum: SAD69 - 24 S
Coordinadtes UTM: 0239297 mE 8583042 mN

Location map

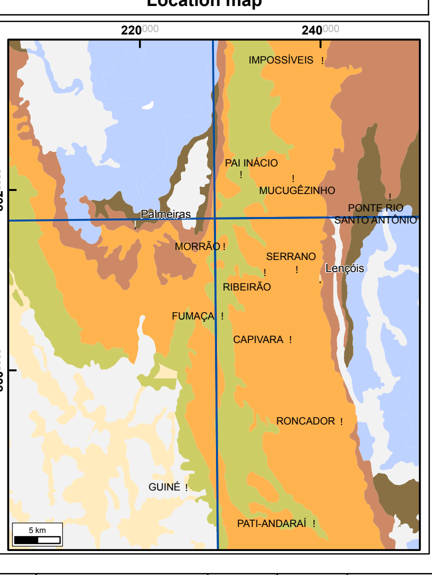

Project area

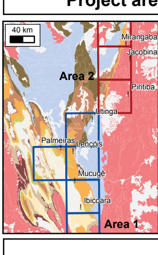

Legend
- . Municipality
- ! Vertical section
- Recent
- Una Gr.
- Morro do Chapéu Fm.
- Caboclo Fm.
- Tombador Fm.
- Açuruá Fm.
- Mangabeira Fm.
- Ouricuri do Ouro Fm.
- Rio dos Remédios Gr.
- Basement

Stratigraphy

ERA	SUPER-GROUP	GROUP	FORMATION	DEPOSITIONAL SYSTEM
MESO-PROTEROZOIC	ESPINHAÇO	CHAPADA DIAMANTINA	Morro do Chapéu	Estuarine/ Fluvial
			Caboclo	Shallow marine
			Tombador	Alluvial fan/ Fluvial/Eolian/ Estuarine
PALEO-PROTEROZOIC		PARAGUAÇU	Açuruá	Shallow marine/ Coastal
			Mangabeira	Eoliano

Sedimentary Facies

Gravel = G Sand = S Fine = F

Gcm	Clast-supported Massive	Sw	Wavy cross lamination
Gci	Clast-supported Reverse grading	St(t)	Tidal bundle
Gh	Horizontal stratification	Ss(t)	Sigmoidal cross stratification (tidal)
Gt	Tangential cross stratification	Ht	Laminate Heterolith
Sh	Horizontal lamination	Fl	Horizontal lamination
Sl	Low angle lamination	Fm	Massive
St	Trough cross stratification	Sh(e)	Eolian horizontal lamination
Sp	Planar cross stratification	Sl(e)	Eolian low angle lamination
Sm	Massive	St(e)	Eolian trough cross stratification
Sr	Ripple cross lamination	Sa(e)	Eolian adhesion structure
Sf	Convolution		

Meter	Facies (Code)	Facies Assoc.	Paleocurrent	Photo Mosaico	Description	Stratigraphy (Litho / Crono)
255–248					14m covered.	
247	Sp					
245	St				Sandstone coarse-grained with trough cross stratification.	
235					Coordinates: 239687/8583182 831m	
234	Sh				Sandstone medium-grained, massive to weakly laminated.	
229					9,2 m covered	
224	Sp				Coordinates: 239.681/8.583.184 h: 828m	
223	Fl				Siltstone yellow laminated	
222					Sandston medium- to coarse-grained.	
220	Sr	River-dominated delta-front	So: N270/15		Ripple marks on top.	
218			n=14		Sandstone medium-grained, trough cross stratification.	
216					Sandstone fine-grained massive.	
215	St		So: N 335/15NE		External geometry shallow and large channel.	
211					Sandstone fine- to medium-grained,with trough cross stratification. Coordinates: 239.559/8.583.276 Elevation: 805m	
207	St				Sandstone medium-grained with cm-scale trough cross stratification.	
206	St				Sandstone medium-grained with cm-scale trough cross stratification.	
204	St, Sr				Inter-strata lineament 172/05.	
202	Sm, Sm		So: 320/15 NE		Sandstone medium-grained, massive, amalgamated, ripple marks on top. Fracture N 265/77 SE and slicken line N 275/20.	
200	Sr, Sm		So: N 350/10 NE Fractur N 35/80 SE Fracture N 135/70 SE controls the valley fisiography		Sandstone medium-grained, massive, lenticular geometry, ripple marks on top. Coordinates: 239.517/8.583.304 Elevation: 800m	
6		Prodelta to distal delta-front			Siltstone laminated. Coordinates 239297/8583042 Elevation = 607 m	
4	Fl					
2					Sandstone very fine-grained, lenticular bedding.	
0	Fl				Siltstone laminated.	

Meter: 255, 250, 245, 240, 235, 230, 225, 220, 215, 210, 205, 200, 195, 190, 185, 180, 175, 170, 165, 160, 155, 150, 145, 140, 135, 130, 125, 120, 115, 110, 105, 100, 95, 90, 85, 80, 75, 70, 65, 60, 55, 50, 45, 40, 35, 30, 25, 20, 15, 10, 5, 0

Grain size: M Bl Sx Gr G M F Mf S Ag (Sand)

VERTICAL SECTION #04
GUINÉ -B

Projeto CHAPADA UFRGS/PETROBRAS

Interpreter: Jorge Magalhães
Data: 05/02/2011

Scale: 1:100
Datum: SAD69 - 24 S
Coordinates UTM: 0227801 mE 8588440 mN

Location map

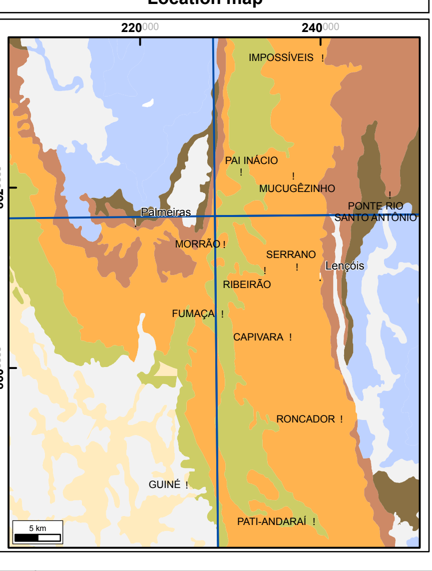

Project area

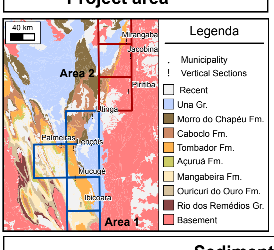

Stratigrapgy

ERA	SUPER-GROUP	GROUP	FORMATION	DEPOSITIONAL SYSTEM
MESO-PROTEROZOIC	ESPINHAÇO	CHAPADA DIAMANTINA	Morro do Chapéu	Estuarine/ Fluvial
			Caboclo	Shallow marine
			Tombador	Alluvial fan/ Fluvial/Eolian/ Estuarine
PALEO-PROTEROZOIC		PARAGUAÇU	Açuruá	Shallow marine/ Coastal
			Mangabeira	Eolian

Sedimentary Facies

Gravel = G Sand = S Fine = F

Gcm	Clast-supported Massive	Sw	Wavy cross lamination
Gci	Clast-supported Reverse grading	St(t)	Tidal bundle
Gh	Horizontal stratification	Ss(t)	Sigmoidal cross stratification (tidal)
Gt	Tangential cross stratification	Ht	Laminated heterolith
Sh	Horizontal lamination	Fl	Horizontal lamination
Sl	Low angle lamination	Fm	Massive
St	Trough cross stratification	Sh(e)	Eolian horizontal lamination
Sp	Planar cross stratification	Sl(e)	Eolian low angle lamination
Sm	Massive	St(e)	Eolian trough cross stratification
Sr	Ripple cross lamination	Sa(e)	Eolian adhesion structure
Sf	Convolution		

Meter	Sand (M Bl Sx Gr G M F Mf S Ag)	Facies (Code)	Facies Assoc.	Paleocurrent	Photo Mosaic	Description	Stratigraphy: Litho	Crono

Intermediate / distal sheetflood

St — Top of the trail. Sandstone coarse-grained ad normal grading.

St, St(e) — Dm-scale trough cross stratification.

Eolian dune and sandsheet

Sh(e) — Sandstone médio/médio grosso, bimodal milimétrica, ripple granular e gradação inversa. (So: N20/14SE)

Intermediate / distal sheetflood

Sh — Coordinates 227804/8588782 h=1364m

Sp — Planar cross stratification with granules.

Sh — Sandstone very coarse-grained with paralel lamination and alighned granules.

Sandstone very coarse-grained, laminated.

St — Sandstone, coarse- to very coarse-grained.

St, St, St — Sandstone coarse-grained with trough cross stratification and normal grading.

St, St, St, St, St — Sandstone coarse-grained with cm-scale trough cross stratification, normal grading.

Sh — Mafic sill. (So: N40/14SE)

Sandstone medium-grained, laminated.

St — Sandstone medium-grained with cm-scale trough cross stratification.

Sm — Sandstone coarse grained, massive.

St — Sandstone coarse-grained with normal grading cycles.trough cross stratification with normal grading. (n=9)

Sm — Massive.

St — Sandstone medium- to coarce-grained with trough cross stratification.

Sh — Normal grading.

Sm — Sandstone medium- to coarse-grained,massive.

Sh, St — Local cm-scale trough cross stratification. (So: N30/10SE)

Sh — Sandstone medium-grained, paralel lamination, well sorted. (So: N60/14SE)

Sh, St, Sh, St, Sh — Sandstone medium-grained, paralel lamination and cm-scale trough cross stratification on top.

Sh, St, Sh — Sandstone fine- to medium-grained laminated and trough cross stratification on top.

St — (So: N0º/11E)

St, Sh — Sandstone fine- to coarse-grained on top, with trough cross stratification.

Sh — Sandstone fine-grained, laminated.

Sh — Sandstone mediu- to coarse-grained.

Sh — Subvertical fracture.

Turmaline-rich dike

Dike turmaline-rich

40 m Gap

River-dominated delta-front

Sm, Sh — Sandstone fine- to medium-grained.

Gap.

Sh — Sandstone very fine-grained to fine-grained on top, weakly laminated. (So: N40/20SE)

Sh, Sh

6m gap.

Coordinates: 227399/8588610 h=1243m

Sh — Sandstone very fine-grained.

Sh, Sh — Sandstone fine-graided, with ripples and paralel lamination. (So: N15/10SE)

Fl

Gap.

Sh, Fl, Sh

Fl — Siltstone grey/green, laminated, sandstone fine-grained on top.

Sm — Sandstone very fine-grained, massive. (So: N0º/8E)

Coordinates 227376/8588582 h=1231m

35m gap.

Sh, St, Sm — Coordinates: 227290/8588486 h=1196m

Sh

Fl — Siltstone red/grey/green, laminated on top.

Sm — Sandstone very fine-grained, massive, laminated on top. (So: N10/17SE)

Prodelta

Coordinates 227260/8588440 h=1180m

Fl — Claystone, red, laminated.

Coordinates: 227251/8588410 h=1173m

Gap

Coordinates: 227202/8588278 h=1149m

Claystone red/yellow.

Fl — Claystone red/yellow.

Claystone red, laminated with yellow levels.

Siltstone grey/yellow.

Meter	Sand	Facies (Code)	Facies Assoc.	Paleocurrent	Photo Mosaic	Description	Litho	Crono

Stratigraphy

UFRGS

BR

Projeto CHAPADA UFRGS/PETROBRAS

VERTICAL SECTION #04 GUINÉ -A

Interpreter: Jorge Magalhães
Data: 05/02/2011

Scale: 1:100
Datum: SAD69 - 24 S
Coordinates UTM: 0227801 mE 8588440 mN

Location map

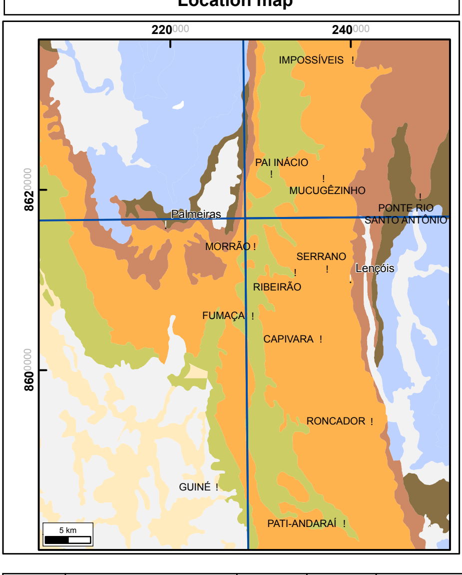

Project area

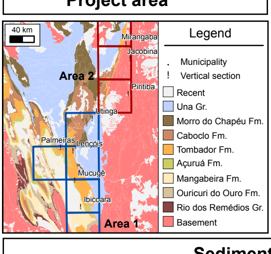

Stratigraphy

ERA	SUPER-GROUP	GROUP	FORMATION	DEPOSITIONAL SYSTEM
MESO-PROTEROZOIC	ESPINHAÇO	CHAPADA DIAMANTINA	Morro do Chapéu	Estuarine/ Fluvial
			Caboclo	Shallow marine
			Tombador	Alluvial fan/ Fluvial/Eolian/ Estuarine
PALEO-PROTEROZOIC		PARAGUAÇU	Açuruá	Shallow marine/ Coastal
			Mangabeira	Eolian

Sedimentary Facies

Gravel = G Sand = S Fine = F

Gcm	Clast-supported Massive	Sw	Wavy cross lamination
Gci	Clast-supported Reverse grading	St(t)	Tidal bundle
Gh	Horizontal stratification	Ss(t)	Sigmoidal cross stratification (tidal)
Gt	Tangential cross stratification	Ht	Laminated heterolith
Sh	Horizontal lamination	Fl	Horizontal lamination
Sl	Low angle lamination	Fm	Massive
St	Trough cross stratification	Sh(e)	Eolian horizontal Lamination
Sp	Planar cross stratification	Sl(e)	Eolian low angle lamination
Sm	Massive	St(e)	Eolian trough cross stratification
Sr	Ripple cross lamination	Sa(e)	Eolian adhesion structure
Sf	Convolution		

VERTICAL SECTION #07 FUMAÇA -B

Interpreter: Jorge Magalhães
Date: 11/02/2011

Scale: 1:100
Datum: SAD69 - 24 S
Coordinates UTM: 0233302 mE 8605862 mN

Location map

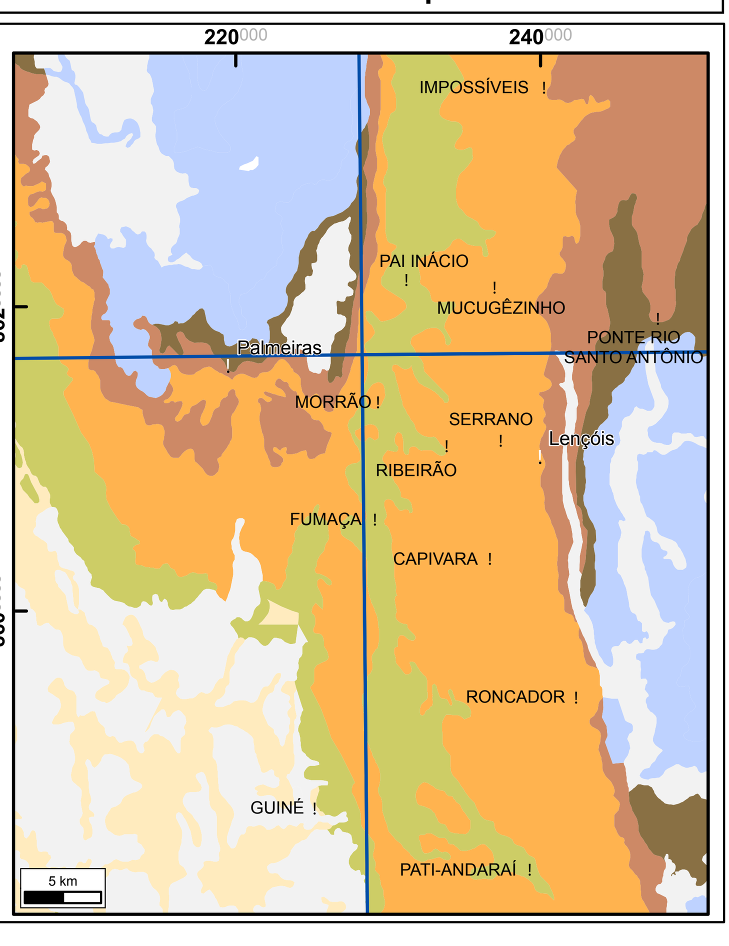

Project area

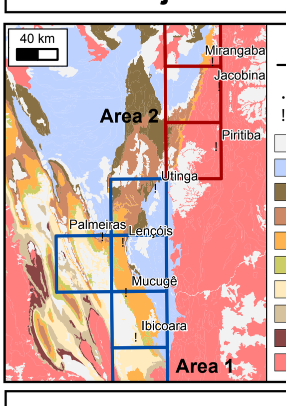

Stratigraphy

ERA	SUPER-GROUP	GROUP	FORMA-TION	DEPOSITIONAL SYSTEM
MESO-PROTEROZÓICO	ESPINHAÇO	CHAPADA DIAMANTINA	Morro do Chapéu	Estuarine/ Fluvial
			Caboclo	Shallow Marine
			Tomba-dor	Alluvial Fan/ Fluvial/Eolian/ Estuarine
PALEO-PROTERO-ZÓICO		PARA-GUAÇU	Açuruá	Shallow Marine/ Coastal
			Manga-beira	Eolian

Sedimentary Facies

Gravel = G Sand = S Fine = F

Gcm	Clast-supported massive	Sw	Wavy cross lamination
Gci	Clast supported Reverse grading	St(t)	Tidal bundle
Gh	Horizontal stratification	Ss(t)	Sigmoidal cross stratification
Gt	Tangentioal cross stratification	Ht	Laminated heterolith
Sh	Horizontal lamination	Fl	Horizontal lamination
Sl	Low angle lamination	Fm	Massive
St	Trough cross stratification	Sh(e)	Eolian horizontal lamination
Sp	Planar cross stratification	Sl(e)	Eolian low angle lamination
Sm	Massive	St(e)	Eolian trough cross stratification
Sr	Ripple cross lamination	Sa(e)	Eolian adhesion structure
Sf	Convolution		

Meter	Sand: M Bl Sx Gr G M F Mf S Ag	Facies (Code)	Facies Assoc.	Paleocurrent	Photo Mosaic	Description	Stratigraphy: Litho	Crono

Facies (Code): St, St, Sp, Sp, St, Sr, St, St, Sh, St, Sh, Sh, St

Facies Assoc.: Proximal / intermediate sheetflood

Paleocurrent: So: N70/4°SE; So: N330

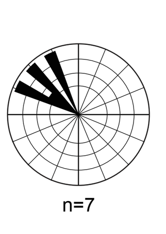

Coord. Fumaça Waterfall
233302/ 8605862
h=1276 m

End of the trail/top of the hill.

Sandstone granular to coarse-grained, cm-scale trough cross stratification with normal grading.

Ripple marks.
Sandstone medium-grained, cm-scale trough cross stratification with mud clasts up to 3 cm.
tidal bundle
Sandstone medium- to coarse-grained, with cm-scale trough cross stratification.

Trough cross stratification with granules alighned on the stratification surface.

Dm-scale trough cross stratification.

Cm-scale trough cross stratification.

Dm- to m-scale trough cross stratification
Cm-scale trough cross stratification.
Sandstone medium-grainde, trough cross stratification with scattered coarse granules, fining up.

Coord.233239/8605812, h=1268 (final do gap).

No Rio da Fumaça: Coord.233217/8605786, h=1268

100 m gap.

Facies (Code): Sh, St, Sr, Sh, St, Sh, Sh, Sh, Sl, Sh, Sp, Sh, Sm, St, Sl, Sr, Sp, Sl, Sp, Sh, Sl, St, Sp, Sh, St, St, St, Sm, Fm, Sp, St, Sm, St, St, Sp, St, Sp, St, Sp, St, Sh, Sr

Facies Assoc.: Proximal / intermediate sheetflood

Paleocurrent: So: N350/8°NE; So: N0°/5°E

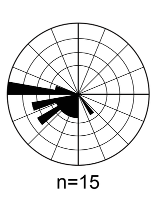

So: N340/5°NE

Coord.230183/8605360, h=1360 (begining of gap)

Trough cross stratification.
Cm-scale planar cross stratification.
Ripple marks.

Trough cross stratification with erosive bottom surface.

Gap.

Gap.

Sandstone medium-grained with subhorizontal lamination.

Gap.

Planar cross stratification.

Fe concretion.

Cm-scale trough cross stratification

Low angle lamination.
Ripple marks.
Cm-scale planar cross stratification.
Fining up.

Low angle lamination.

Ripple marks.

Ripple marks.

Levels with sandstone, medium- to coarse grained, trough cross stratification.
Planar cross stratification.
Sandstone, red, medium-to fine-grained.

Gap.
Coord. 230064/8605426, h=1293 m (Mirante do capão).
Trough cross stratification with granules.

Sandstone medium- to coarse-grained with trough cross stratification and erosive bottom surface.
Sandstone fine- to medium-grained, planar cross stratification, granules on the stratification surface..
Sandstone medium-grained trough cross stratification.

Gap.

Sandstone medium- to coarse-grained, with trough cross stratification, scattered granules.

Sandstone fine- to medium-grained, laminated.

Coord. 230001/8605504, h=1286 m

Trough cross stratification.

Trough cross stratification with ganules, erosive botom surface.
Fining up.
Ripple marks.

Meter	Sand: M Bl Sx Gr G M F Mf S Ag	Facies (Code)	Facies Assoc.	Paleocurrent	Photo Mosaico	Description	Litho	Crono

Stratigraphy

VERTICAL SECTION #07
FUMAÇA -A

Projeto CHAPADA UFRGS/PETROBRAS

Interpreter: Magalhães
Date: 11/02/2011

Scale: 1:100
Datum: SAD69 - 24 S

Coordinates UTM: 0233302 mE 8605862 mN

Location map

Project area

Stratigraphy

ERA	SUPER-GROUP	GROUP	FORMATION	DEPOSITIONAL SYSTEM
MESO-PROTEROZOIC	ESPINHAÇO	CHAPADA DIAMANTINA	Morro do Chapéu	Estuarine/ Fluvial
			Caboclo	Shallow Marine
			Tombador	Alluvial fan/ Fluvial/Eolian/ Estuarine
PALEO-PROTEROZOIC		PARAGUAÇU	Açuruá	Shallow marine/ Coastal
			Mangabeira	Eolian

Sedimentary Facies

Gravel = G Sand = S Fine = F

Gcm	Clast-supported Massive	Sw	Wavy cross lamination
Gci	Clast-supported Reverse grading	St(t)	Tidal bundle
Gh	Horizontal stratification	Ss(t)	Sigmoidal cross stratification (tidal)
Gt	Tangential cross stratification	Ht	Laminated heterolith
Sh	Horizontal lamination	Fl	Horizontal lamination
Sl	Low angle lamination	Fm	Massive
St	Trough cross stratification	Sh(e)	Eolian horizontal lamination
Sp	Planar cross stratification	Sl(e)	Eolian low angle lamination
Sm	Massive	St(e)	Eolian trough cross stratification
Sr	Ripple cross lamination	Sa(e)	Eolian adhesion structure
Sf	Convolution		

Meter | Sand | Facies (Code) | Facies Assoc. | Paleocurrent | Photo Mosaic | Description | Stratigraphy (Litho, Crono)

Description

Sandstone fine- to medium-grained, low angle lamination.

Horizontal lamination with siltstone veneers.

Sandstone fine- to medium-grained, horizontal lamination, fining up.

Siltstone with ripple marks on top.

Sandstone medium-grained grains with interbeds of sandstone fine grains, horizontal lamination

Trough cross stratification with grains on the base.

Sandstone medium- to fine-grained, fining up.

Erosive base.

Sandstone medium- to fine-grained.

Sandstone coarse-grained with granules at the base.

cm-scale Trough cross stratification

Planar cross stratification.

Sandstone medium-grained, low angle lamination.

Sandstone medium- to coarse-grained with granules, massive.

Low angle lamination.

Granular ripple , adhesion ripple , curled flake.

Siltstone laminated.

Sandstone coarse-grained, trough cross stratification.

Massive with disperse granules.

Sandstone medium- to fine-grained with granules, trough cross stratification.

Fining up.

Sandstone coarse-grained, trough cross stratification.

Planar cross stratification.

Sandstone very fine-grained laminated.

Sandstone medium- to coarse-grained, trough cross stratification.

Normal grading.

cm-scale Trough cross stratification.

Coord 229885/8605636 h=1248

Sandstone medium-grained, trough cross stratification with scattered granules.

Sand medium- to fine-grained, horizontal lamination, with scattered granules.

Mud clasts up to 4cm.

Sandstone medium- to coarse-grained, trough cross stratification with scattered granules.

Sandstone medium- to coarse-grained, trough cross stratification, with scattered granules.

Sandstone medium- to fine-grained with interbeds of siltstone layers and granular ripples.

Sandstone medium- to coarse-grained, trough cross stratification with scattered granules.

Sandstone fine- to medium-grained horizonta lamination and reverse grading.

cm-scale Sandstone mediu- to coarse-grained, trough cross stratification with scattered granules.

Sandstone medium- to very fine-grained with interbeds of granular ripple.

Sandstone medium- to coarse-grained, trough cross stratification.

Sandstone medium-grained laminated.

Sandstone medium-grained, cm-scale trough cross stratification.

Sandstone medium- to coarse-grained, cm-scale trough cross stratification, with scattered granules.

Sandstone medium- to fine-grained, laminated with reverse grading, siltsone veneers.

Low angle lamination with cm-scale trough cross stratification and scattered granules.

Sandstone medium-grained, cm-scale trough cross stratification with scattered granules.

Trough cross stratification with few scattered granules.

cm-scale Planar cross stratification with scattered granules.

cm-scale trough cross stratification with granules

Sandstone medium-grained with cm-scale trough cross stratification.

Sandstone very fine-grained level, wit interbeds of siltstone.

Sandstone very coarse- to coarse-grained with reverse grading.

Sandstone medium-grained with cm-scale trough cross stratification.

Sandstone very fine- to fine-grained with reverse grading.

Sandstone medium-grained, cm-scale trough cross stratification, with coarse- to very coarse-grained sandstone.

Arenito médio/grosso com laminação subhorizontal e acanalada de pequeno porte.

Sandstone medium- to coarse-grained, scattered granules, horizontal lamination

Sandstone medium- to coarse-grained with m-scale trough cross stratification.

Sandstone fine- to medium-grained with cm-scale trough cross stratification, coarse- to very coarse levels at the base.

Sandstone fine- to medium-grained with normal grading, horizontal lamination with band of granules.

Convolute.

Sandstone medium- to coarse-grained, grey, with trough cross stratification, normal grading with granules at the base.

Sandstone medium-grained trough cross stratification and normal grading.

cm-scale trough cross stratification.

Planar cross stratification.

Sandstone medium-grained light gray, well sorted.

Unconformity.

Coord 229880/8605804 h=1198

Sandstone fine-grained red/gray, weakly laminated.

Sandstone fine-grained with Fe concretions, massive.

Sandstone grey/red with ripple cross lamination.

Sandstone massive.

Sandstone very fine-grained laminated.

Sandstone fine-grained with ripple.

Sandstone very fine-grained with climbing ripple.

Sandstone medium-grained grey/pink rosado massive.

Ripple.

Sandstone very fine-grained/siltstone, weakly laminated.

Sandstone medium-grained blocky, massive.

Fractured.

Interbeds of siltstone, cemented.

Laminated, green to red, climbing ripples.

Sandstone medium-grained, massive.

Gap.

Sandstone very fine-grained, weakly laminated, pink.

Sandstone fine-grained, weakly laminated.

Sandstone very fine-grained, weakly laminated.

Sandstone very fine-grained laminated cemented, hardground ?

Trough cross stratification.

Sandstone cream, fine-grained, massive.

Gap.

Sandstone medium-grain planar cross stratification and mud clasts.

Sandstone cream, fine-grained, massive.

Massive.

Sandstone very fine-grained, red,weakly laminated, cemented.

Band of peebles with mud clasts up to 2 cm.

Sandstone cream, fine-grained, massive.

Sandstone coarse-grained with granules on the trough cross stratification.

Sandstone fine-grained with mud clasts up to 1 cm, weakly laminated.

Sandstone very fine-grained, massive, with fining up pattern.

Sandstone, cream, very fine- to fine-grained, massive.

Siltstone green.

2nd plateau on the trail, gap

Sandstone cream very fine-grained, cl laminação planar.

Sandstone, red, very fine-grained.

Hardground ?

Siltstone laminated, red, intercalated with sandstone medium-grained with mud clasts up to 3 cm.

Sandstone, cream medium- to coarse-grained, trough cross stratification with mud clasts up to 3 cm on top.

Sandstone coarse- to very coarse-grained with fining up pattern.

Subvertical fracture.

Sandstone, cream, trough cross stratification. Fining up pattern, Sandstone coarse- to fine-grained.

Siltstone, cream, massive.

Sandstone, grey,red, very fine-grained, cemented.

Hardground ?

Sandstone, cream, very fine-grained, weakly laminated.

Siltstone, cream, with cemented levels.

Sandstone, weakly laminated, fractured.

Sandstone, cream, very fine-grained, weakly laminated, fractured.

Siltstone, grey/green, subhorizontal lamination.

Siltstone, green, massive.

Sandstone, red, fine-grained, laminated, cemented.

(hardground)

Sandstone, fine-grained, cream, up to 20 to 40 cm on top and massive at the base.

Sandstone, red, very fine-grained, laminated, cemented (hardground).

Sandstone, cream, very fine-grained, massive.

Cemented.

Sandstone, very fine-grained, weakly laminated.

Climbing ripple.

Meter | Sand | Facies (Code) | Facies Assoc. | Paleocurrent | Photo Mosaic | Description | Stratigraphy

VERTICAL SECTION #10
MORRAO -B

Projeto CHAPADA UFRGS/PETROBRAS

Interpreter: Jorge Magalhães
Date: 13/04/2011

Scale: 1:100
Datum: SAD69 - 24 S

Coordinates UTM: 0229343 mE 8613762 mN

Location map

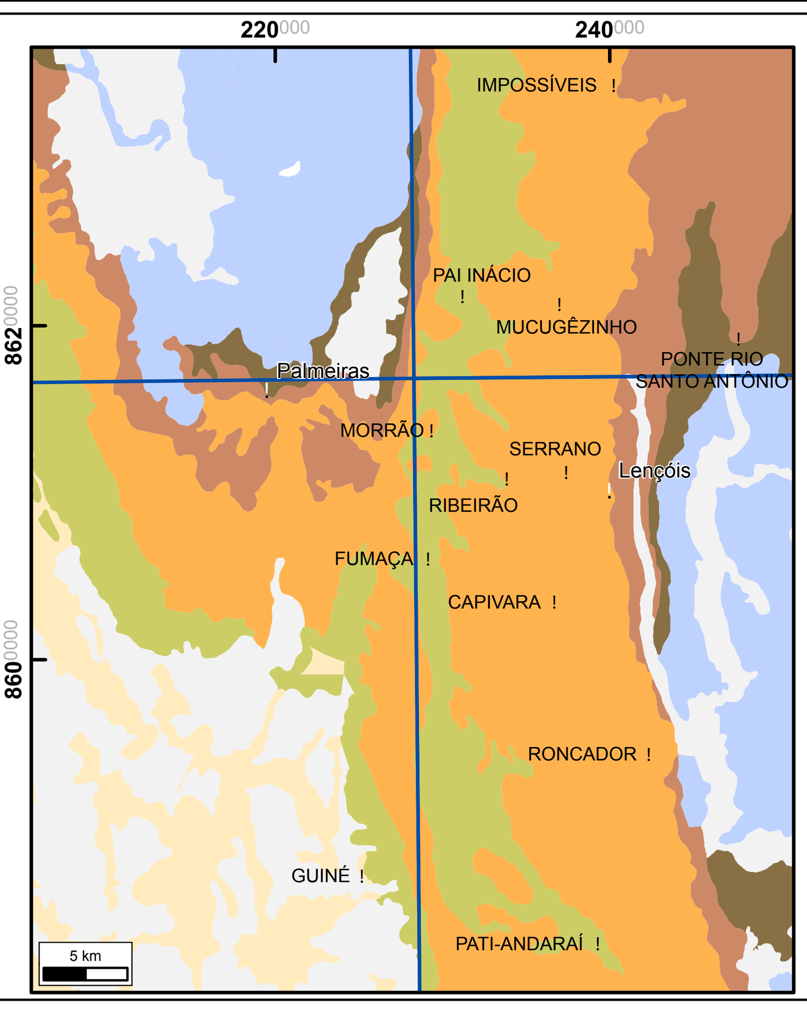

Project area

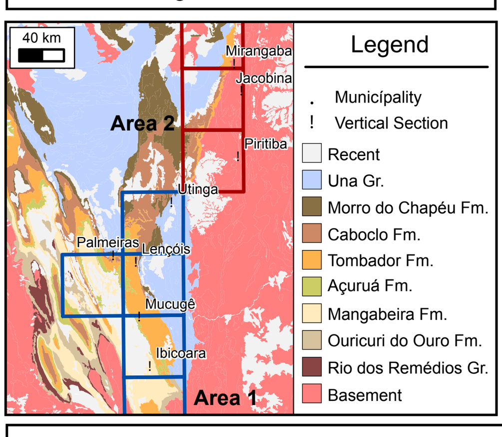

Stratigraphy

ERA	SUPER-GROUP	GROUP	FORMATION	DEPOSITIONAL SYSTEM
MESO-PROTEROZOIC	ESPINHAÇO	CHAPADA DIAMANTINA	Morro do Chapéu	Estuarine/ Fluvial
			Caboclo	Shallow marine
			Tombador	Alluvial fan/ Fluvial/Eolian/ Estuarine
PALEO-PROTEROZOIC		PARAGUAÇU	Açuruá	Shallow marine/ Coastal
			Mangabeira	Eolian

Sedimentary Facies

Gravel = G Sand = S Fine = F

Code	Facies	Code	Facies
Gcm	Clast-supported Massive	Sw	Wavy cross lamination
Gci	Clast-supported Reverse grading	St(t)	Tidal bundle
Gh	Horizontal stratification	Ss(t)	Sigmoidal cross lamination (tidal)
Gt	Tangential cross stratification	Ht	Laminated heterolith
Sh	Horizontal lamination	Fl	Horizontal lamination
Sl	Low angle lamination	Fm	Massive
St	Trough cross stratification	Sh(e)	Eolian horizontal lamination
Sp	Planar cross stratification	Sl(e)	Eolian low angle lamination
Sm	Massive	St(e)	Eolian trough cross stratification
Sr	Ripple cross lamination	Sa(e)	Eolian adhesion structure
Sf	Convolution		

Meter	Sand	Facies (Code)	Facies Assoc.	Paleocurrent	Photo Mosaic	Description	Stratigraphy: Litho	Stratigraphy: Crono

Facies (Code): Sp, Fl, Sh, Sp, Sp, Sp, Sp, Sp, Sh, Sp, Sp, Sp, Sp, Sp, Sp, Sp, Sp, St, St, St, Sl, St, St, St, St, St, Sh, St, St, St, Sh, Sh, St, Sh, St, St, St, St, Sl, Sp, St, Sl, Sl, Sf, St, St, St

Facies Assoc.: Tidal bar; Tidal bar; Distributary fluvial channel; Distributary fluvial channel

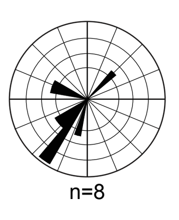

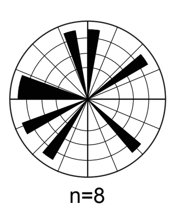

So: N240/6SE

Description:

Coordinates 229560/8614036 / h= 1383

Sandstone medium-grained, planar cross stratificationl on the bottom surface.

Siltstone yellow, with climbing ripples.

Sandstone medium-grained with tidal bundle.

Sandstone medium- to coarse-grained with granule levels.

Coordinates 229573/8614032 / h=1385

Coordinates 229474/8613894 / h=1382

Sandstone medium- to coarse-grained with granules on the stratification surface.

Sandstone medium-grained with cm-scale planar cross stratification.

Siltstone, red.

Sandstone medium-grained with cm-scale planar cross stratification.

Sandstone fine-grained, laminated with ferrous bands.

Sandstone medium-grained with mudclasts.

Convolution.

Sandstone medium-grained, with m-scale planar cross stratification.

Band of granules.

Sandstone medium-grained, convolution.

Siltstone laminated, red.

Sandstone medium-grained, cm-scale planar cross stratification, unidirectional, with scattered granules on the stratification surface.

Cut and fill features with planar cross stratification.

Granules on the stratification surface.

Sandstone medium-grained with cm-scale planar cross stratification.

Arenito médio com grânulos dispersos acompanhando a estratificação.

Sandstone, granular with trough cross stratification in different directions.

Morrão`s north face.

Coordinates 229466/613838 / h=1346

19m gap.

Coordinates 229449/8613736 / h=1527

Sandstone, granular with cm-scale trough cross stratification.

No Gama Ray reading

No Gama Ray reading
Elevation 1327m

Sandstone, granular with cm-scale trough cross stratification.

Sandstone coarse-grained with trough cross stratification.

Sandstone coarse-grained with trough cross stratification, erosive bottom surface and granular bands.

Sandstone very fine-grained, laminated.

Trough cross stratification in 3 directions.

Sandstone medium-grained, trough cross stratification.

Siltstone, red, crops out laterally on the trail.

Sandstone medium- to coarse-grained with granular bands.

Sandstone very fine-grained, laminated.

Sandstone coarse-grained with cm -cale trough cross stratification.

Sandstone medium- to coarse-grained with lamination and cm-scale trough cross stratification.

Siltstone, red.

Sandstone medium- to coarse-grained with cm-scale trough cross stratification.

Siltstone, red.

Sandstone medium-grained, laminated.

Sandstone medium-grained with planar cross stratification.

Sandstone very fine-grained, laminated.

Sandtone medium- to coarse-grained with convolution on top.

Sandstone medium- to coarse-grained, planar and trough cross stratification.

Sandstone medium- to coarse-grained with mud clasts.

Sandstone medium- to coarse-grained with cm-scale trough cross stratification.

Sandstone medium- to coarse-grained, convolution.

Coordinates 229388/8613756 / h=1286

Meter	Sand	Facies (Code)	Facies Assoc.	Paleocurrent	Photo Mosaic	Description	Litho	Crono
							Stratigraphy	

UFRGS UNIVERSIDADE FEDERAL DO RIO GRANDE DO SUL

BR

VERTICAL SECTION #10
MORRAO -A

Projeto CHAPADA UFRGS/PETROBRAS

Intepreter: Jorge Magalhães
Date: 13/04/2011

Scale: 1:100
Datum: SAD69 - 24 S
Coordinates UTM: 0229343 mE 8613762 mN

Location map

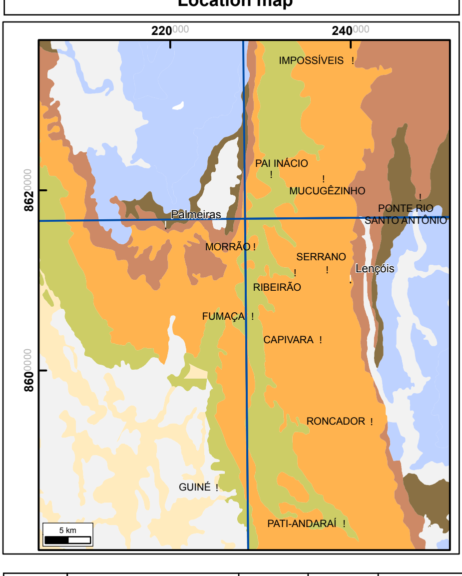

Project area

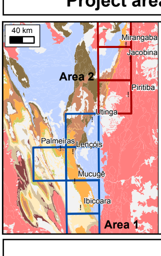

Stratigraphy

ERA	SUPER-GROUP	GROUP	FORMATION	DEPOSITIONAL SYSTEM
MESO-PROTEROZOIC	ESPINHAÇO	CHAPADA DIAMANTINA	Morro do Chapéu	Estuarine/ Fluvial
			Caboclo	Shallow Marine
			Tombador	Alluvial fan/ Fluvial/Eolian/ Estuarine
PALEO-PROTEROZOIC		PARAGUAÇU	Açuruá	Shallow Marine/ Coastal
			Mangabeira	Eolian

Sedimentary Facies

Gravel = Conglomerado **Sand** = Arenito **Fine** = Pelito

Gcm	Clast-supported Massive	Sw	Wavy cross lamination
Gci	Clast-supported Reverse grading	St(t)	Tidal bundle
Gh	Horizontal stratification	Ss(t)	Sigmoidal cross stratification (tidal)
Gt	Tangential cross stratification	Ht	Laminated heterolith
Sh	Horizontal lamination	Fl	Horizontal lamination
Sl	Low angle lamination	Fm	Massive
St	Trough cross stratification	Sh(e)	Eolian horizontal lamination
Sp	Planar cross stratification	Sl(e)	Eolian low angle lamination
Sm	Massive	St(e)	Eolian trough cross stratification
Sr	Ripple cross lamination	Sa(e)	Eolian adhesion structure
Sf	Convolution		

Meter	Sand (M Bl Sx Gr G M F Mf S Ag)	Facies (Code)	Facies Assoc.	Paleocurrent	Photo Mosaic	Description	Stratigraphy: Litho	Stratigraphy: Crono

Facies Assoc.: Distributary fluvial channels; Distributary fluvial channels; River-dominated delta-front; River-dominated delta-front; Prodelta to distal delta-front

Paleocurrent: S0 N315/3NE (n=3); So: N250/5 (n=3)

Description

24m gap.

Sandstone coarse- to medium-grained with trough cross stratification.
No Gama Ray reading.
Coordinates 229343/8613762 / H=1261
Sandstone coarse- to very coarse-grained with trough cross stratification.
Sandstone very coarse- to medium-grained, with trough cross stratification and convolution.

Sandstone very coarse- to coarse-grained with trough cross stratification.

Mocó hills towards the NE.

Planar cross stratification.
Trough cross stratification.

Sandstone fine-grained, grey/red. laminated.

Siltstone, green.

Cross stratification emphasized by ferrous material.

Sandstone medium-grained, with trough cross stratification.
Coordinates 229323/8613788 / h=1245

Sandstone, massive.

Sandstone coarse- to medium-grained, fining up, with trough cross stratification.

Mudstone, green, crops out laterally .

Sandstone medium-grained, with trough cross stratification.
Mudstone, green.
Sandstone medium-grained, massive, rich in ferrous material, with vertical fracture.
Mudstone, green.

Sandstone medium-grained, wityh fracture filled with ferrous material.
Sandstone, light grey, massive, fractured.
Sandstone medium-grained, laminated..

Sandstone medium- to coarse-grained with trough cross stratification , with granules.

Sandstone medium-to coarse-grained.

Sandstone medium-grained, light grey, with ripples on top.
Trough cross startification.

Siltstone red, laminated.

Sandstone medium- to coarse-grained.

Sandstone fine-grained, interbedded with siltstone.

Sandstone medium-grained, laminated.

Sandstone medium- to coarse-grained with convolution on top and massive on the bottom surface.

Siltstone red.
Sandstone medium- to coarse-grained massive.
Siltstone red.
Sandstone medium- to coarse-grained interbedded with fine-grained sandstone and ripple cross lamination.

Sandstone medium- to coarse-grained with trough cross stratification.

Sandstone medium- to coarse-grained and trough cross stratification with granules.
Sandstone coarse-grained with trough cross stratification.
Sandstone medium- to coarse-grained massive cemented.
Sandstone medium-grained laminated.
Elevation 1188m.

42m gap.

Sandstone medium-grained with trough cross stratification
Sandstone medium- to coarse-grained, massive.
Elevation 1142m.

26.5m gap.

Siltstone, green.
Sandstone medium-grained, massive, cemented.
Sandstone coarse-grained with trough cross stratification.

Sandstone coarse-grained, horizontal lamination.

Sandstone medium-grained, massive.
Sandstone laminated, cemented, grey/red.
Sandstone medium-grained planar cross stratification.

Sandstone very coarse- to coarse-grained, fining up, trough cross stratification and granules.

Sadstone massive, well cemented.

Sandstone coarse-grained, trough cross stratification, massive, with granules, composing sand bodies up to 60 cm thick.

Sandstone medium-grained with horizontal lamination.
Coordinates 229131/86133716 / h=1084m.

43m gap.

Sandstone very fine-grained, laminated, tofine-grained sandstone, massive.

Siltstone

Siltstone cream, weathered, massive.
Coordinates 228768 / 8613456 / h=990m

BR

VERTICAL SECTION #11 BR242

Projeto CHAPADA UFRGS/PETROBRAS

Interpreter: Jorge Magalhães
Date: 27/03/2011

Scale: 1:100
Datum: SAD69 - 24 S
Coordinadtes UTM: 0234262 mE 8620310 mN

Location map

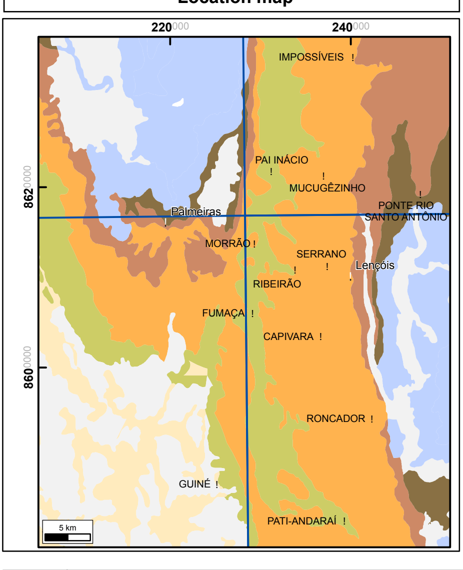

Project area

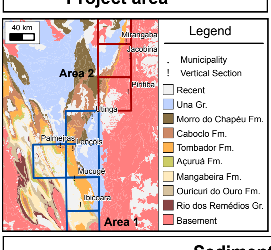

Stratigraphy

ERA	SUPER-GROUP	GROUP	FORMA-TION	DEPOSITIONAL SYSTEM
MESO-PROTEROZOIC	ESPINHAÇO	CHAPADA DIAMANTINA	Morro do Chapéu	Estuarine/ Fluvial
			Caboclo	Shallow Marine
			Tomba-dor	Alluvial fan/ Fluvial/Eolian/ Estuarine
PALEO-PROTERO-ZOIC		PARA-GUAÇU	Açuruá	Shallow Marine/ Coastal
			Manga-beira	Eolian

Sedimentary Facies

Gravel = G Sand = S Fine = F

Gcm	Clast-supported Massive	Sw	Wavy cross lamination
Gci	Clast-supported Reverse grading	St(t)	Tidal bundle
Gh	Horizontal stratification	Ss(t)	Sigmoidal cross stratification (tidal)
Gt	Tangential cross stratification	Ht	Laminated heterolith
Sh	Horizontal lamination	Fl	Horizontal lamination
Sl	Low angle lamination	Fm	Massive
St	Trough cross stratification	Sh(e)	Eolian horizontal lamination
Sp	Planar cross stratification	Sl(e)	Eolian low angle lamination
Sm	Massive	St(e)	Eolian trough cross stratification
Sr	Ripple cross lamination	Sa(e)	Eolian adhesion structure
Sf	Convolution		

Meter	M Bl Sx Gr G M F Mf S Ag (Sand)	Facies (Code)	Facies Assoc.	Paleocurrent	Photo Mosaic	Description	Stratigraphy: Litho	Stratigraphy: Crono

Coordinates: 8620986 N h: 759m 237196 E
Written on the outcrop: Visite Tapiramutá.
Trough cross stratification.

Sandstone coarse-grained, trough and planar cross stratification, with peebles.

Sandstone medium-grained, trough cross stratification, wave reworking on top.

Louro restaurant sign.

Sandstone medium-grained, low angle lamination, ripples marks on top.
Coordinates: 8621010 N h: 762m 237107 E

16,2 m gap.

Coordenadas: 8621096 N h: 768m 236982 E

Sandstone medium-grained, horizontal stratification.

Trough cross stratification.
Sandstone medium-grained, trough cross stratification.

Mud clasts.

Coordinates: 236519 mE 8621140 mN h:795m

Sandstone medium-grained, cm-scale trough cross stratification, ripple marks on top, stylolites.

Sandstone coarse-grained, with trough cross stratification ands granules.

Dm-scale trough cross stratification.

Sandstone medium-grained, laminated.

Trough cross stratification and low angle lamination.

Heterolith, sandstone very coarse- to coarse-grained, horizontal lamination, interbeds of very thin layers of mudstone.
Fracture oriented to N 230.
Transgressive lag at the heterolith bottom.

Sandstone medium-grained, laminated.

Sandstone medium-grained, laminated.

Coordinates UTM: 8620988 N h:792m 236155 E

11 m gap.

Sandstone coarse-grained, trough cross stratification and granules.
Coordinates: 236062 mE 8620946 mN h:798m
Km 343

21 m gap.

Sandstone fine-grained, interbeds of siltstone.

Sandstone filling channel with mudstone layer at the base.

Sandstone medium-grained massive, wave reworking on top.

17,2 m gap.

Sandstone medium-grained, trough cross stratification, tidal bundle.

Flat topography.

Dm-scale trough cross stratification.

Sandstone coarse-grained, massive, cm-scale trough cross stratification, scattered granules.
Subaerial unconformity: fluvial overlying estuarine.

Sandstone coarse-grained, stylolite on top.
Stylolite " egg box".

Sandstone medium-grained, with stylolites.

Amalgamated sand bodies bounded by mud drapes.

Amalgamated sand bodies.

Tidal bundle.
Mudstone dark brown.

Heterolith, siltstone and mudstone, massive.
Coarse-grained lag deposit.

Normal fault, outside profile A
N330

Sandstone coarse- to very-coarse-grained, sets up to 5cm thick, planar cross stratification.

Granules on the stratification surface.
Sandstone coarse-grained, convolution.
Sand bodies with external sigmoidal geometry.

Trough cross stratification.

Sandstone fine-grained, ripple cross lamination.

Heterolith, sandstone fine-grained with siltstone.

21,6 m gap.

Sandstone fine- to medium-grained, massive, mud clasts up to 1-2cm.
Planar cross stratification on the bottom surface, sandstone fine-grained interbed of siltstone.
Sandstone medium-grained, massive interbeds of siltstone.

Sandstone medium-grained, trough cross stratification.

Discordância Fm. Açuruá/ Fm. Tombador
Coord. 234262 / 8620310
h: 843m
Sandstone medium-grained, sigmoidal external geometry, sigmoidal to trough cross stratification.

Sandstone medium-grained massive, ripple cross lamination.

Meter	Facies (Code)	Facies Assoc.	Paleocurrent	Photos	Description	Litho	Crono
						Stratigraphy	

UFRGS

BR

VERTICAL SECTION #14
IMPOSSIVEIS

Projeto CHAPADA UFRGS/PETROBRAS

Interpreter: Magalhães
Date: 02/02/2011

Scala: 1:100
Datum: SAD69 - 24 S
Coordinates UTM: 0233197 mE 8638092 mN

Location

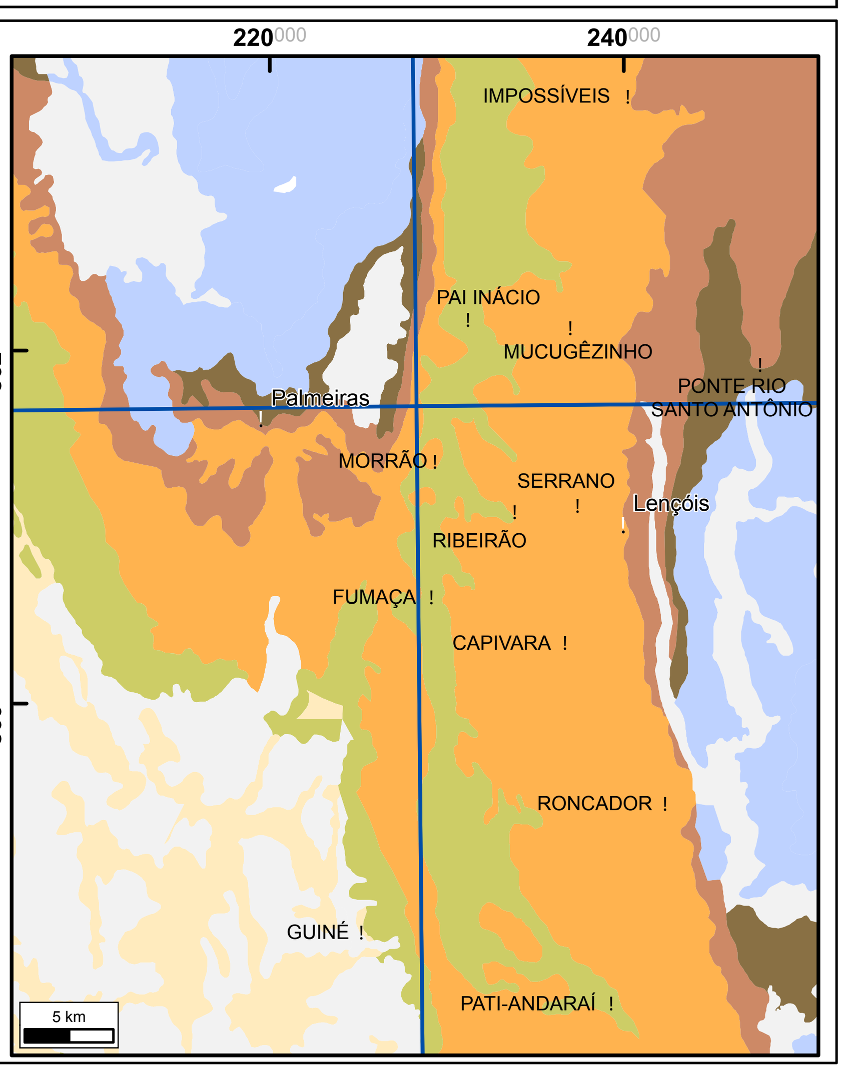

Project area

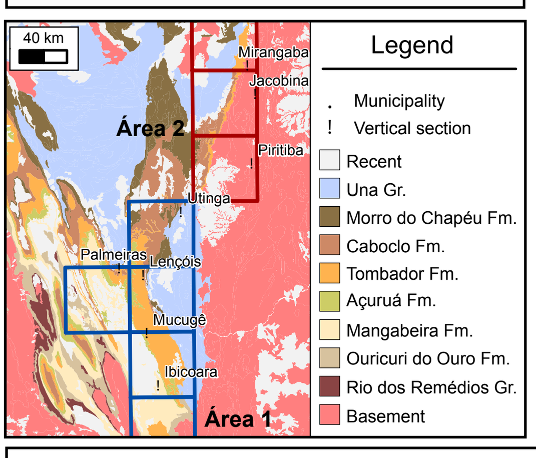

Stratigraphy

ERA	SUPER-GROUP	GROUP	FORMATION	DEPOSITIONAL SYSTEM
MESO-PROTEROZOIC	ESPINHAÇO	CHAPADA DIAMANTINA	Morro do Chapéu	Estuarine/ Fluvial
			Caboclo	Shallow marine
			Tomba-dor	Alluvial fan/ Fluvial/Eolian/ Estuarine
PALEO-PROTERO-ZOIC		PARA-GUAÇU	Açuruá	Shallow marine/ Coastal
			Manga-beira	Eolian

Sedimentary Facies

Gravel = G **Sand** = S **Fine** = F

Code	Facies	Code	Facies
Gcm	Clast-supported Massive	Sw	Wavy cross lamination
Gci	Clast-supported Reverse grading	St(t)	Tidal bundle
Gh	Horizontal stratification	Ss(t)	Sigmoidal cross stratification (tidal)
Gt	Tangencial cross stratification	Ht	Laminated heterolith
Sh	Horizontal lamination	Fl	Horizontal lamination
Sl	Low angle lamination	Fm	Massive
St	Trough cross stratification	Sh(e)	Eolian horizontal lamination
Sp	Planar cross stratification	Sl(e)	Eolian low angle lamination
Sm	Massive	St(e)	Eolian trough cross stratification
Sr	Ripple cross lamination	Sa(e)	Eolian adhesion structure
Sf	Convolution		

Meter	M Bl Sx Gr G M F Mf S Ag (Sand)	Facies (Code)	Facies Assoc.	Paleocurrent	Description	Stratigraphy: Litho	Stratigraphy: Crono

- 40 m gap to the contact with the Caboclo Fm.
- Sandstone fine-grained, clay rich, ferroan (soil)
- Fe- concretions on top of sandstone beds
- Sandstone mediu- to coarse-grainde with horizontal lamination and normal grading.
- Siltstone layer.
- Level with granules.
- Sandstone very fine-grained to siltstone with ripples.
- Sandstone medium- to coarse-grained with normal grading, horizontal lamination.
- Siltstone layer.
- Level with granules.
- Sandstone medium- to coarse-grained, with normal grading and trough cross stratification.
- Sandstone fine- to medium-grained, with normal grading, granules/mudclasts and meter-scale trough cross stratification and low angle lamination.
- Sandstone body with convex geometry.
- Siltstone layer, green, massive
- Sandstone medium- to coarse-grained, normal grading and horizontal lamination.
- Coordinates: 241968 e 8633086, h = 600 m.
- GAP - 5 meters
- Sandstone coarse- to very coarse-grained, with scattered pebbles, planar and trough cross stratification.
- Sandstone coarse- to very coarse-grained, with trough cross stratification.
- Conglomerate with normal grading, cobbles up to 40 cm.
- Conglomerate with pebbles and cobbles (25cm), composed of white quartzite, green quartzite, meta-sandstone, biotite grains
- Sandstone with low angle lamination. Cemented???
- Erosive basal surface.
- Sandstone medium- to coarse-grained, massive.
- Sandstone medium-grained, horizontal lamination.
- Sandstone medium- to coarse-grained with trough cross stratification to massive.
- Sandstone medium-grained and horizontal lamination.
- Sandstone medium-grained with trough cross stratification.
- Sandstone coarse-grained with trough cross stratification.
- Sandstone coarse-grained to granule and trough cross stratification.
- Sandstone coarse-grained to granules wth low angle lamination.
- Covered - 2 meters.
- Sandstone coarse-grained with trough cross stratification.
- Sandstone very coarse- to coarse-grained, with pepples on stratification surfaces, with trough cross bedding and tangential cross stratification at the base. Erosive bottom surfaces.
- Coordinates: 237596 e 8640942, Elevation = 960 m.
- Sandstone medium-grained, with lens of medium- to coarse-grained sandstone, weakly laminated, well sorted, with ripples.
- Sandstone medium- to coarse-grained, with trough cross stratification.
- Sandstone very coarse- to coarse-grained, with pebbles, erosive bottom surface, with trough cross stratification.
- At the top conglomere with pebbles of white and green quartzite and metasandstone.
- Sandstone medium- to coarse-grained with trough cross stratification and horizontal lamination at the base.
- First fluvial sheetflod overlying eolian sandstone.
- Sandstone medium-grained with ripples oriented to several directions.
- Sandstone medium-grained with ripples, granular ripples and inverse grading.
- Sandstone medium- to coarse-grained, bimodal, with meter-scale trough cross bedding.
- Level with granules.
- Coordinates: 234112 e 8637916, elevation = 982 m.
- Trough cross stratification and granules at the top.
- Sandstone fine- to medium-grained, with scattered granules, normal grading, fractured.
- Sandstone medium- to coarse-grained, with trough cross stratification, granules and mudclasts.
- Coordinates: 233228 e 8638110, Elevation = 984 m.
- Amalgamated sand bodies.
- Sandstone medium- to coarse-grained, trough cross stratification, external geometry lenticular, erosive bottom surface.
- Sandstone medium- to coarse-grained with trough cross stratification.
- Amalgamated sand bodies.
- Sandstone, medium-grained with trough and planar cross stratification.
- Siltstone red, with climbing ripples and sub-horizontal lamination.
- Sandstone medium-grained, lenticular, planar cross stratification.
- 4,2 m covered.
- Sandstone fine- to medium-grained, with horizontal lamination and tangential cross stratification.
- Sandstone medium-grained, laminated.
- Sandstone coarse-grained, with level of granules and trough cross stratification. Erosive bottom surface.
- Sandstone medium- to coarse-grained, with horizontal to low angle lamination.
- Sandstone coarse-grained to granular, planar cross stratification.
- Sandstone medium- to coarse-grained, with granules on the trough cross stratification surface.
- Sandstone coarse-grained to granular, with pebbles and mud clasts.
- Coordinates: 233197 e 8638092, Elevation = 966 m.
- 7 m covered
- Unconformity
- Siltstone red, laminated.

Fazenda Impossíveis | Estiva

Meter	M Bl Sx Gr G M F Mf S Ag (Sand)	Facies (Code)	Facies Assoc.	Paleocurrent	Description	Stratigraphy: Litho	Stratigraphy: Crono

UFRGS UNIVERSIDADE FEDERAL DO RIO GRANDE DO SUL

BR

VERTICAL SECTION #B
PAI INÁCIO

Interpreter: Magalhães
Date: 14/02/2011

Scala: 1:100
Datum: SAD69 - 24 S

Coordinates UTM: 0231206 mE
8621774 mN

Location map

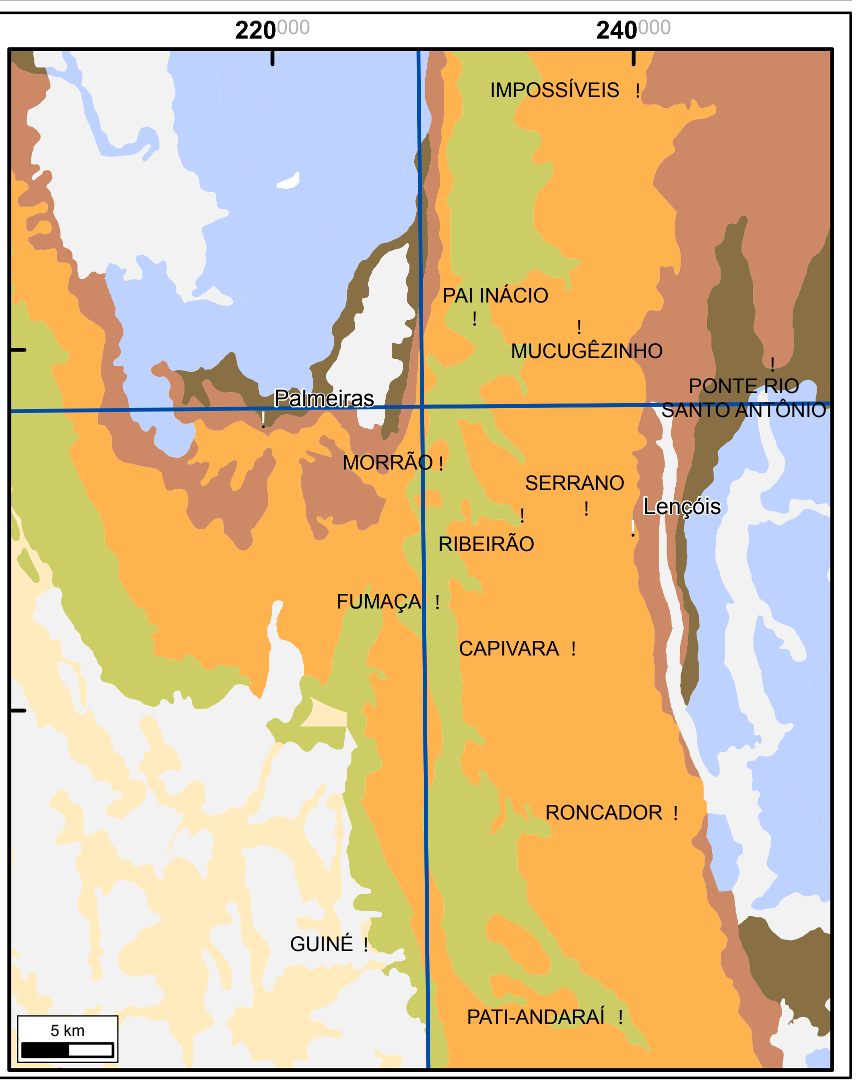

Project area

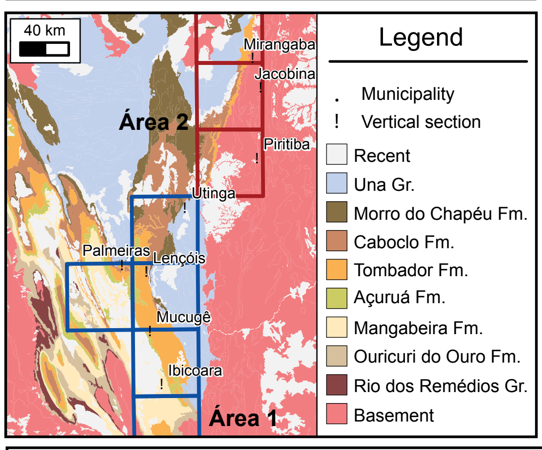

Stratigraphy

ERA	SUPER-GROUP	GROUP	FORMATION	DEPOSITIONAL SYSTEM
MESO-PROTEROZOIC	ESPINHAÇO	CHAPADA DIAMANTINA	Morro do Chapéu	Estuarine/ Fluvial
			Caboclo	Shallow marine
			Tombador	Alluvial fan/ Fluvial/Eolian/ Estuarine
PALEO-PROTEROZOIC		PARAGUAÇU	Açuruá	Shallow marine/ Coastal
			Mangabeira	Eolian

Sedimentary Facies

Gravel = G Sand = S Fine = F

Gcm	Clast-supported Massive	Sw	Wavy cross lamination
Gci	Clast-supported Reverse grading	St(t)	Tidal bundle
Gh	Horizontal stratification	Ss(t)	Sigmoidal cross stratification (tidal)
Gt	Tangencial cross stratification	Ht	Laminated heterolith
Sh	Horizontal lamination	Fl	Horizontal lamination
Sl	Low angle lamination	Fm	Massive
St	Trough cross stratification	Sh(e)	Eolian horizontal lamination
Sp	Planar cross stratification	Sl(e)	Eolian low angle lamination
Sm	Massive	St(e)	Eolian trough cross stratification
Sr	Ripple cross lamination	Sa(e)	Eolian adhesion structure
Sf	Convolution		

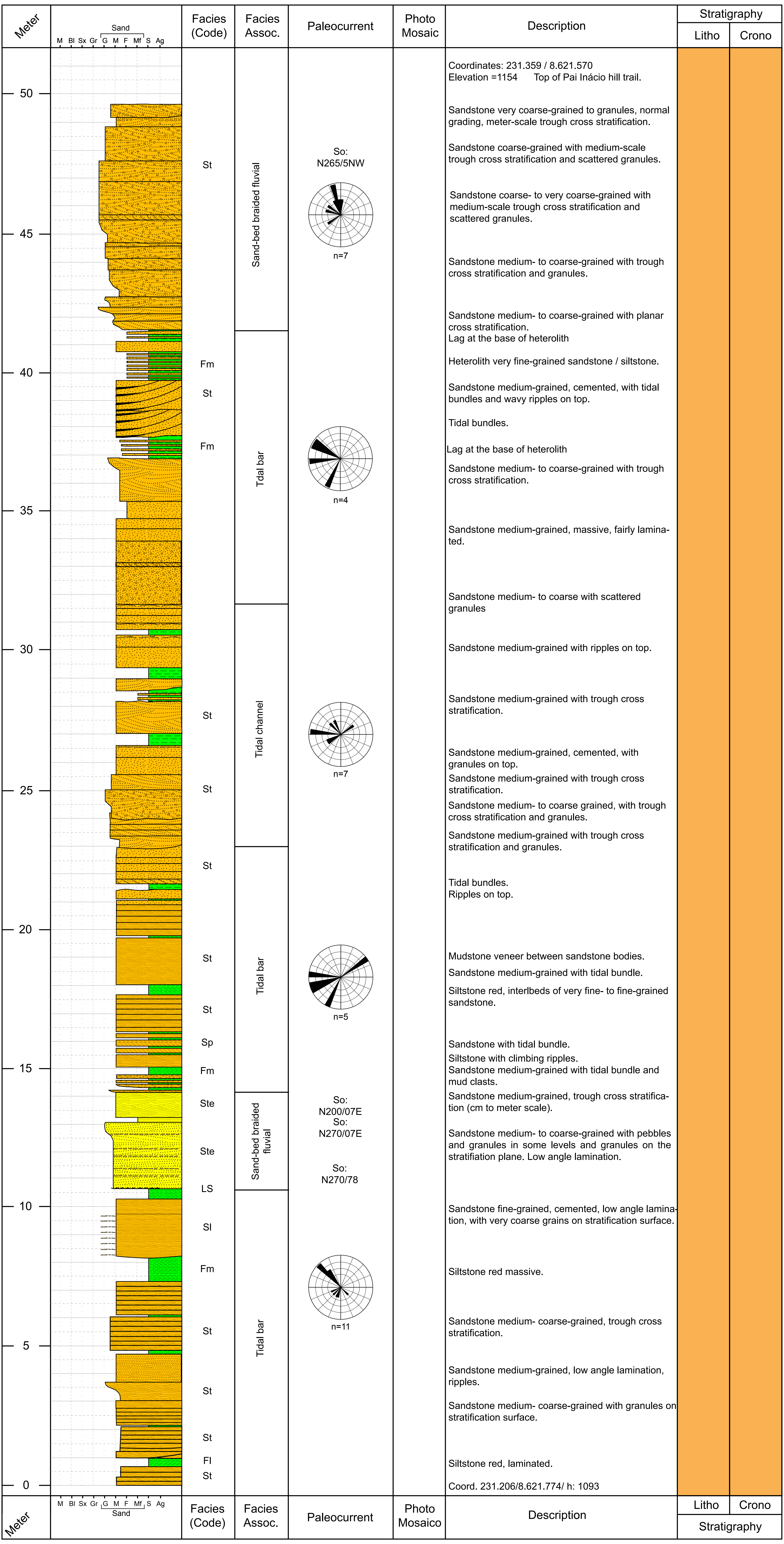

UFRGS UNIVERSIDADE FEDERAL DO RIO GRANDE DO SUL

VERTICAL SECTION
PONTE RIO SANTO ANTONIO

Projeto CHAPADA UFRGS/PETROBRAS

Interpreter: Jorge Magalhães
Date: 16/02/2011

Scale: 1:100
Datum: SAD69 - 24 S

Coordinates UTM: 0247026 mE 8617580 mN

Location map

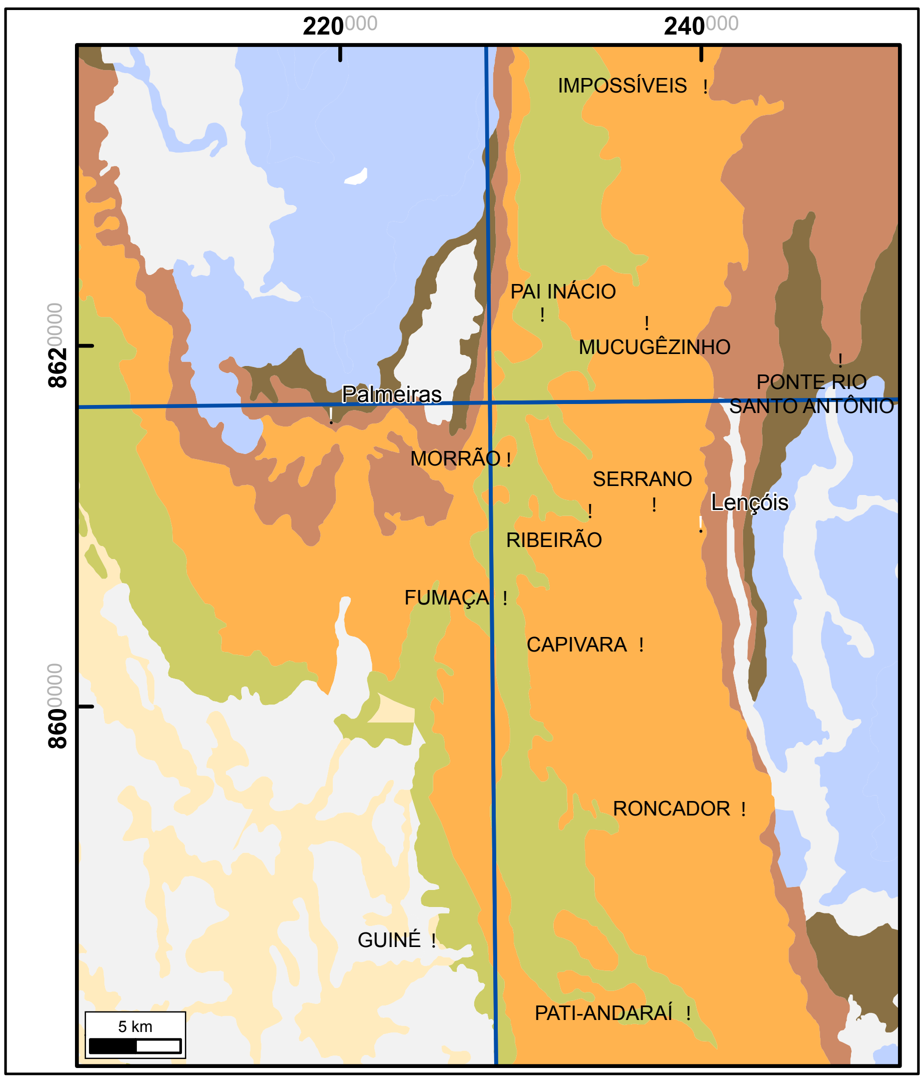

Project area

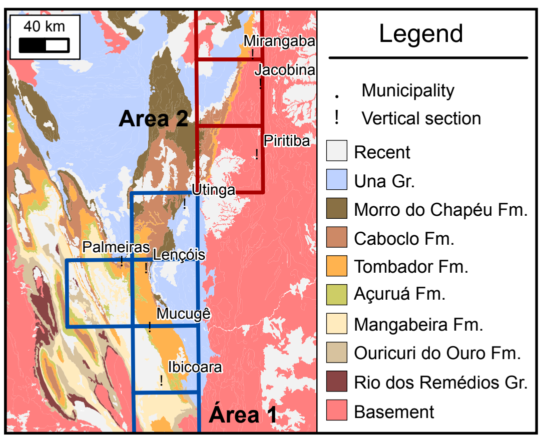

Stratigraphy

ERA	SUPER-GROUP	GROUP	FORMATION	DEPOSITIONAL SYSTEM
MESO-PROTEROZOIC	ESPINHAÇO	CHAPADA DIAMANTINA	Morro do Chapéu	Estuarine/ Fluvial
			Caboclo	Shallow Marine
			Tomba-dor	Alluvial fan/ Fluvial/Eolian/ Estuarine
PALEO-PROTERO-ZÓIC		PARA-GUAÇU	Açuruá	Shallow Marine/ Coastal
			Manga-beira	Eolian

Sedimentary Facies

Gravel = G Sand = S Fine = F

Code	Facies	Code	Facies
Gcm	Clast-supported Massive	Sw	Wavy cross lamination
Gci	Clast-supported Reverse grading	St(t)	Tidal bundle
Gh	Horizontal stratification	Ss(t)	Sigmoidal cross stratification (tidal)
Gt	Tangential cross stratification	Ht	Laminated heterolith
Sh	Horizontal lamination	Fl	Horizontal lamination
Sl	Low angle lamination	Fm	Massive
St	Trough cross stratification	Sh(e)	Eolian horizontal lamination
Sp	Planar cross stratification	Sl(e)	Eolian low angle lamination
Sm	Massive	St(e)	Eolian trough cross stratification
Sr	Ripple cross lamination	Sa(e)	Eolian adhesion structure
Sf	Convolution		

Vertical section

Meter	Lithology (M Bl Sx Gr G M F Mf S Ag — Sand)	Facies (Code)	Facies Assoc.	Paleocurrent	Photo Mosaic	Description	Stratigraphy Litho	Stratigraphy Crono
~20–16	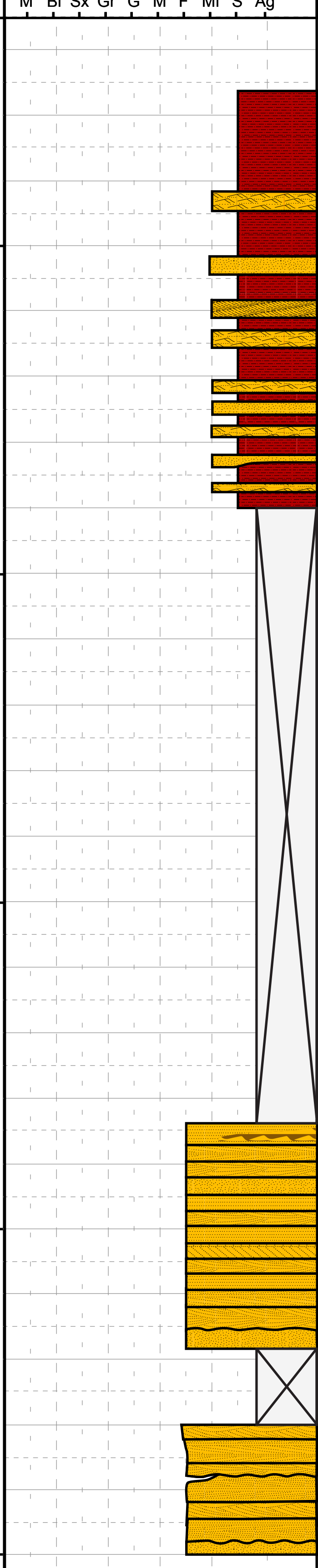	Fl, Ht, Fl, Sm, Fl, Sr, Ht, Fl, Ht, Sm, Ht, Sm, Ht	Shoreface	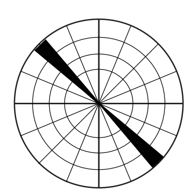 n=3		Coord. 241807 / 8611750 h=416m. Mudstone cream-red, laminated. Lenticular and wavy bedding. Climbing ripples. Mudstone cream-red laminated with interbeds or very fine-grained sandstone. Interbeds of siltstone and very fine-grained sandstone.		
15–10						Aprox. 9,7 m covered.		
05–00		Sh, Sl, St, Sm, Sh, St, Sh, Sp, St, Sh, Sl, St, Sm; St, Sl, St, Sl, St, Sl, Sm	Tidal bar	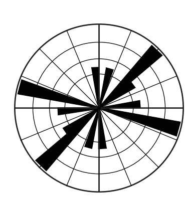 n=8; 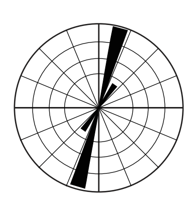 n=4		Coord. 246865 / 8617228 h=369m. Sub-horizontal lamination. Laterally, flaser. Sandstone medium-grained, horizontal lamination, siltstone layers and mudclast molds. Planar cross stratification, mudclasts molds. Bimodal cross trough bedding. Sandstone fine-grained with sub-horizontal lamination and small cross trough bedding, siltstone layers. Sandstone fine-grained with estratificação cruzada acanalada e ripples. Coord. 247026 / 8617580 h=350m		

Meter | M Bl Sx Gr G M F Mf S Ag Sand | Facies (Code) | Facies Assoc. | Paleocurrent | Photos | Description | Litho | Crono | Stratigraphy

UFRGS UNIVERSIDADE FEDERAL DO RIO GRANDE DO SUL

BR

Appendix 3 – Tables

A3.1. Table with the thicknesses measured in vertical sections

A3.2. Table with bedding plane and paleocurrent readings

A3.1. VERTICAL SECTIONS - MEASURED THICKNESSES

Vertical section number	Vertical Section name	Tombador Fm rock thickness (m)	Caboclo Fm rock thickness (m)	Açuruá Fm rock thickness (m)
1	Barra da Estiva	133.2	14.4	
2	Ronei	47.8		1.8
3	Pati Andarai	315.3		36.1
4	Guiné	29.6		217.6
7	Fumaca	131.2		153.4
8	Ribeirao	30.8		
10	Morrao	49.1		169.4
11	BR242 road	115.1		7.8
14	Impossiveis	47.6		2.5
B	Pai Inacio hill	49.8		
not presented	Ponte Sto Antonio		130.1	
not presented	Buracao	11		
not presented	Mucugê	82,4		
not presented	Igatu	93,8		
	SUBTOTAL	**1136.7**	**144.5**	**588.6**
	TOTAL		**1869.8**	

A3.2. BEDDING PLANE AND PALEOCURRENT READINGS

Vertical section number	Vertical section name	Facies Association	Formation	SO Strike	SO Dip	SO Quad	Paleocurrent (Azimuth)	Metres
1	Barra da Estiva	offshore tidal bar	Caboclo	104	5	SW	0	1238.9
1	Barra da Estiva	offshore tidal bar	Tombador				355	1249,5
1	Barra da Estiva	offshore tidal bar	Tombador				185	1249.7
1	Barra da Estiva	offshore tidal bar	Tombador				220	1249.7
1	Barra da Estiva	offshore tidal bar	Tombador	100	6	SW	0	1251.6
1	Barra da Estiva	offshore tidal bar	Tombador				0	1252.5
1	Barra da Estiva	offshore tidal bar	Tombador				185	1254.3
1	Barra da Estiva	offshore tidal bar	Tombador				0	1255
1	Barra da Estiva	tidal channel	Tombador				340	1256.3
1	Barra da Estiva	tidal channel	Tombador				0	1260.2
1	Barra da Estiva	tidal channel	Tombador				330	1283.4
1	Barra da Estiva	tidal channel	Tombador				355	1285.3
1	Barra da Estiva	tidal channel	Tombador				350	1286.7
1	Barra da Estiva	tidal channel	Tombador				355	1287.5
1	Barra da Estiva	tidal channel	Tombador				355	1287.8
1	Barra da Estiva	tidal channel	Tombador				320	1289.8
1	Barra da Estiva	tidal channel	Tombador				315	1291.8
1	Barra da Estiva	tidal channel	Tombador				240	1292.7
1	Barra da Estiva	tidal channel	Tombador				300	1293.3
1	Barra da Estiva	tidal channel	Tombador				230	1294.8
1	Barra da Estiva	tidal channel	Tombador				225	1295.7
1	Barra da Estiva	tidal channel	Tombador				270	1298.2
1	Barra da Estiva	tidal channel	Tombador				250	1299.4
1	Barra da Estiva	tidal channel	Tombador				330	1301
1	Barra da Estiva	tidal channel	Tombador				255	1301.1
1	Barra da Estiva	tidal channel	Tombador				160	1302.6
1	Barra da Estiva	tidal channel	Tombador				280	1303.4
1	Barra da Estiva	tidal channel	Tombador				275	1304.1
1	Barra da Estiva	tidal channel	Tombador				170	1304.4
1	Barra da Estiva	tidal channel	Tombador				75	1306.4
1	Barra da Estiva	tidal channel	Tombador				25	1306.4
1	Barra da Estiva	tidal channel	Tombador				300	1306.4
1	Barra da Estiva	tidal channel	Tombador				295	1311.1
1	Barra da Estiva	tidal channel	Tombador				310	1311.9
1	Barra da Estiva	sand bed braided	Tombador				185	1315.2
1	Barra da Estiva	sand bed braided	Tombador				280	1316.1
1	Barra da Estiva	sand bed braided	Tombador				190	1317
1	Barra da Estiva	sand bed braided	Tombador				260	1318
1	Barra da Estiva	sand bed braided	Tombador				255	1319
1	Barra da Estiva	sand bed braided	Tombador				300	1319.8
1	Barra da Estiva	sand bed braided	Tombador				325	1320.4
1	Barra da Estiva	sand bed braided	Tombador				275	1322
1	Barra da Estiva	sand bed braided	Tombador				290	1322.8
1	Barra da Estiva	sand bed braided	Tombador				200	1323.2
1	Barra da Estiva	sand bed braided	Tombador				250	1325.2
1	Barra da Estiva	sand bed braided	Tombador				265	1325.8
1	Barra da Estiva	sand bed braided	Tombador				240	1326.4
1	Barra da Estiva	sand bed braided	Tombador				235	1326.8
1	Barra da Estiva	tidal bar	Tombador				310	1350.4
1	Barra da Estiva	tidal bar	Tombador	315	5	SW	0	1370.7
1	Barra da Estiva	tidal bar	Tombador	140	8	SW	0	1372
1	Barra da Estiva	tidal bar	Tombador				350	1372.5
1	Barra da Estiva	tidal channel	Tombador				315	1379
1	Barra da Estiva	tidal channel	Tombador				135	1381.6
1	Barra da Estiva	tidal channel	Tombador				90	1383.6
1	Barra da Estiva	tidal channel	Tombador				70	1388.4
1	Barra da Estiva	tidal channel	Tombador				260	1389.2
1	Barra da Estiva	tidal bar	Tombador				235	1392
1	Barra da Estiva	tidal bar	Tombador				240	1395
1	Barra da Estiva	tidal bar	Tombador				240	1396.5

1	Barra da Estiva	tidal bar	Tombador	85	6	SE	0	1397.8
1	Barra da Estiva	tidal bar	Tombador				230	1399.7
1	Barra da Estiva	tidal channel	Tombador				270	1412.6
1	Barra da Estiva	tidal channel	Tombador				320	1413.7
1	Barra da Estiva	tidal channel	Tombador				260	1415.6
1	Barra da Estiva	tidal channel	Tombador	65	8	SE	0	1416.1
1	Barra da Estiva	tidal bar	Tombador				300	1425.8
1	Barra da Estiva	tidal bar	Tombador				290	1443.6
1	Barra da Estiva	tidal bar	Tombador	30	8	SE	0	1443.8
1	Barra da Estiva	tidal bar	Tombador				210	1464.6
1	Barra da Estiva	tidal bar	Tombador	170	14	SW	0	1465
1	Barra da Estiva	tidal bar	Tombador				235	1468.2
1	Barra da Estiva	tidal bar	Tombador				240	1471
1	Barra da Estiva	tidal bar	Tombador				285	1471.8
1	Barra da Estiva	tidal bar	Tombador				285	1472.8
1	Barra da Estiva	tidal bar	Tombador	2	6	SE	0	1473
1	Barra da Estiva	tidal bar	Tombador				300	1474.3
1	Barra da Estiva	tidal bar	Tombador	10	4	SE	0	1475.6
1	Barra da Estiva	tidal bar	Tombador				280	1476.6
1	Barra da Estiva	tidal bar	Tombador	60	6	SE	0	1483.2
1	Barra da Estiva	tidal bar	Tombador				290	1485.4
1	Barra da Estiva	tidal bar	Tombador	50	6	SE	0	1485.8
1	Barra da Estiva	tide dominated delta front	Açuruá	29	14	SE	0	1583
1	Barra da Estiva	tide dominated delta front	Açuruá	0	11	E		1584.2
1	Barra da Estiva	tide dominated delta front	Açuruá				10	1584.2
1	Barra da Estiva	tide dominated delta front	Açuruá	30	16	SE	0	1584.4
1	Barra da Estiva	tide dominated delta front	Açuruá				355	1588.2
1	Barra da Estiva	tide dominated delta front	Açuruá				355	1590.7
1	Barra da Estiva	tide dominated delta front	Açuruá				120	1594.1
1	Barra da Estiva	tide dominated delta front	Açuruá				6	1599.4
1	Barra da Estiva	tide dominated delta front	Açuruá	60	5	SE	0	1600.1
1	Barra da Estiva	tide dominated delta front	Açuruá				0	1600.6
1	Barra da Estiva	tide dominated delta front	Açuruá				0	1602.7
1	Barra da Estiva	tide dominated delta front	Açuruá				0	1603.5
1	Barra da Estiva	tide dominated delta front	Açuruá				155	1605.9
1	Barra da Estiva	tide dominated delta front	Açuruá				350	1608
1	Barra da Estiva	tide dominated delta front	Açuruá	70	8	SE	0	1608.9
1	Barra da Estiva	tidal channel	Açuruá				290	1612.6
1	Barra da Estiva	tidal channel	Açuruá				5	1613.2
1	Barra da Estiva	tidal channel	Açuruá				183	1615.4
1	Barra da Estiva	tidal channel	Açuruá				187	1615.7
1	Barra da Estiva	tidal channel	Açuruá	8	12	SE	0	1619.8
1	Barra da Estiva	tidal channel	Açuruá				165	1620.5
1	Barra da Estiva	tidal channel	Açuruá				272	1621.6
1	Barra da Estiva	tidal channel	Açuruá	30	11	SE	0	1623.6
1	Barra da Estiva	tidal channel	Açuruá				355	1626.7
1	Barra da Estiva	tidal channel	Açuruá	45	8	SE	0	1626.7
1	Barra da Estiva	tidal channel	Açuruá				185	1628
1	Barra da Estiva	tidal channel	Açuruá				185	1628
1	Barra da Estiva	tidal channel	Açuruá				190	1628
1	Barra da Estiva	tidal channel	Açuruá				30	1628
1	Barra da Estiva	tidal channel	Açuruá	45	10	SE	0	1628.8
1	Barra da Estiva	tidal channel	Açuruá	45	14	SE	0	1628.9
1	Barra da Estiva	tidal channel	Açuruá				275	1629.2
1	Barra da Estiva	tidal channel	Açuruá				6	1630
1	Barra da Estiva	tide dominated delta front	Açuruá				187	1631.2
1	Barra da Estiva	tide dominated delta front	Açuruá				2	1631.4
1	Barra da Estiva	tide dominated delta front	Açuruá				17	1632.8
1	Barra da Estiva	tide dominated delta front	Açuruá				196	1633
1	Barra da Estiva	tide dominated delta front	Açuruá	25	6	SE	0	1634.7
1	Barra da Estiva	tide dominated delta front	Açuruá				24	1635.4
1	Barra da Estiva	tide dominated delta front	Açuruá				15	1636
1	Barra da Estiva	tide dominated delta front	Açuruá				20	1636.8
1	Barra da Estiva	tide dominated delta front	Açuruá				10	1638.3
1	Barra da Estiva	tide dominated delta front	Açuruá	100	10	SW	0	1638.6

1	Barra da Estiva	tide dominated delta front	Açuruá				180	1639.1
1	Barra da Estiva	tide dominated delta front	Açuruá				350	1639.8
1	Barra da Estiva	tide dominated delta front	Açuruá	60	4	SE	0	1639.8
1	Barra da Estiva	tide dominated delta front	Açuruá				195	1655.8
1	Barra da Estiva	tide dominated delta front	Açuruá				150	1655.8
1	Barra da Estiva	tide dominated delta front	Açuruá				180	1656.4
1	Barra da Estiva	tide dominated delta front	Açuruá				190	1656.4
1	Barra da Estiva	prodelta	Açuruá	65	10	SE	0	1671
1	Barra da Estiva	prodelta	Açuruá	75	9	SE	0	1675.7
1	Barra da Estiva	prodelta	Açuruá	40	7	SE	0	1678.2
1	Barra da Estiva	prodelta	Açuruá	70	3	SE	0	1692
1	Barra da Estiva	prodelta	Açuruá	80	10	SE	0	1691.9
1	Barra da Estiva	prodelta	Açuruá	75	3	SE	0	1697.1
1	Barra da Estiva	prodelta	Açuruá	75	4	SE	0	1697.6
1	Barra da Estiva	prodelta	Açuruá				205	1701.8
1	Barra da Estiva	prodelta	Açuruá	90	16	S	0	1702
1	Barra da Estiva	prodelta	Açuruá				35	1703
1	Barra da Estiva	prodelta	Açuruá				25	1706
1	Barra da Estiva	prodelta	Açuruá	85	10	SE	0	1706.7
1	Barra da Estiva	prodelta	Açuruá	90	3	S	0	1711.2
1	Barra da Estiva	prodelta	Açuruá				247	1716.1
1	Barra da Estiva	prodelta	Açuruá				210	1716.1
1	Barra da Estiva	prodelta	Açuruá				7	1717.6
1	Barra da Estiva	prodelta	Açuruá				28	1717.6
1	Barra da Estiva	prodelta	Açuruá				35	1718.2
1	Barra da Estiva	prodelta	Açuruá	80	8	SE	0	1718.2
1	Barra da Estiva	prodelta	Açuruá	80	7	SE	0	1722
1	Barra da Estiva	prodelta	Açuruá	90	8	S	0	1727
1	Barra da Estiva	prodelta	Açuruá	75	11	SE	0	1731.2
1	Barra da Estiva	prodelta	Açuruá				30	1731.4
1	Barra da Estiva	prodelta	Açuruá	65	11	SE	0	1731.7
2	Ronei	sand bed braided	Tombador				345	1449.8
2	Ronei	sand bed braided	Tombador				250	1457.4
2	Ronei	sand bed braided	Tombador				220	1458.1
2	Ronei	sand bed braided	Tombador	330	5	NE	0	1474
2	Ronei	sand bed braided	Tombador				340	1479.3
2	Ronei	sand bed braided	Tombador				250	1481
2	Ronei	sand bed braided	Tombador				340	1485.4
2	Ronei	sand bed braided	Tombador				160	1487
2	Ronei	sand bed braided	Tombador				125	1488.2
2	Ronei	sand bed braided	Tombador				180	1493.8
2	Ronei	sand bed braided	Tombador	330	35	NE	0	1494.7
2	Ronei	floodplain	Açuruá	340	50	NE	0	1503.2
2	Ronei	floodplain	Açuruá				340	1503.2
3	Pati Andarai	Eolian sand sheet	Tombador				10	958
3	Pati Andarai	intermediate flash flood	Tombador				260	958.1
3	Pati Andarai	Eolian sand sheet	Tombador				10	961
3	Pati Andarai	Eolian sand sheet	Tombador				150	962
3	Pati Andarai	Eolian sand sheet	Tombador	10	15	0	0	969.9
3	Pati Andarai	Eolian sand sheet	Tombador				0	970.3
3	Pati Andarai	Eolian sand sheet	Tombador				60	970.3
3	Pati Andarai	Eolian sand sheet	Tombador	10	15	0	0	971.7
3	Pati Andarai	gravel bed braided	Tombador				230	1075
3	Pati Andarai	gravel bed braided	Tombador				230	1075
3	Pati Andarai	gravel bed braided	Tombador				250	1075
3	Pati Andarai	gravel bed braided	Tombador				210	1076.2
3	Pati Andarai	gravel bed braided	Tombador				280	1079.2
3	Pati Andarai	gravel bed braided	Tombador				300	1089.2
3	Pati Andarai	gravel bed braided	Tombador				330	1089.2
3	Pati Andarai	gravel bed braided	Tombador				180	1091.2
3	Pati Andarai	gravel bed braided	Tombador	350	10	0	0	1091.6
3	Pati Andarai	gravel bed braided	Tombador				330	1092.3
3	Pati Andarai	gravel bed braided	Tombador				340	1115.8
3	Pati Andarai	gravel bed braided	Tombador	340	12	0	0	1121.8
3	Pati Andarai	intermediate flash flood	Tombador	355	16	0	0	1133.1

3	Pati Andarai	intermediate flash flood	Tombador	320	13	0	0	1140.2
3	Pati Andarai	intermediate flash flood	Tombador				230	1155.8
3	Pati Andarai	intermediate flash flood	Tombador				230	1163.2
3	Pati Andarai	intermediate flash flood	Tombador				220	1164.7
3	Pati Andarai	intermediate flash flood	Tombador				210	1166
3	Pati Andarai	intermediate flash flood	Tombador	185	15	0	0	1173.4
3	Pati Andarai	Eolian sand sheet	Tombador				140	1175.2
3	Pati Andarai	intermediate flash flood	Tombador	345	20	0	0	1182
3	Pati Andarai	intermediate flash flood	Tombador				210	1193.6
3	Pati Andarai	intermediate flash flood	Tombador	330	15	0	0	1198
3	Pati Andarai	intermediate flash flood	Tombador	340	15	0	0	1198
3	Pati Andarai	Eolian sand sheet	Tombador	20	15	0	0	1198.4
3	Pati Andarai	Eolian sand sheet	Tombador	350	9	0	0	1198.4
3	Pati Andarai	intermediate flash flood	Tombador				300	1199.5
3	Pati Andarai	intermediate flash flood	Tombador				330	1199.8
3	Pati Andarai	intermediate flash flood	Tombador	330	13	0	0	1200.1
3	Pati Andarai	intermediate flash flood	Tombador				320	1200.8
3	Pati Andarai	intermediate flash flood	Tombador				355	1201.8
3	Pati Andarai	gravel bed braided	Tombador				0	1234.5
3	Pati Andarai	gravel bed braided	Tombador	25	10	0	0	1234.5
3	Pati Andarai	gravel bed braided	Tombador	325	11	0	0	1234.5
3	Pati Andarai	gravel bed braided	Tombador				100	1235.2
3	Pati Andarai	gravel bed braided	Tombador				155	1235.3
3	Pati Andarai	gravel bed braided	Tombador				210	1235.4
3	Pati Andarai	gravel bed braided	Tombador				125	1235.5
3	Pati Andarai	gravel bed braided	Tombador				165	1235.6
3	Pati Andarai	gravel bed braided	Tombador				175	1235.7
3	Pati Andarai	gravel bed braided	Tombador				190	1235.8
3	Pati Andarai	Eolian sand sheet	Tombador	345	11	0	0	1239
3	Pati Andarai	Eolian sand sheet	Tombador	335	13	0	0	1239
3	Pati Andarai	Eolian sand sheet	Tombador				170	1239.6
3	Pati Andarai	sand bed braided	Tombador				315	1240.4
3	Pati Andarai	sand bed braided	Tombador	90	42	0	0	1241
3	Pati Andarai	sand bed braided	Tombador				315	1264
3	Pati Andarai	sand bed braided	Tombador	165	5	0	0	1266.8
3	Pati Andarai	sand bed braided	Tombador				210	1267.4
3	Pati Andarai	sand bed braided	Tombador	345	24	0	0	1273.1
3	Pati Andarai	sand bed braided	Tombador				200	1273.4
3	Pati Andarai	sand bed braided	Tombador				225	1273.4
3	Pati Andarai	sand bed braided	Tombador				350	1275
3	Pati Andarai	sand bed braided	Tombador				355	1275
3	Pati Andarai	sand bed braided	Tombador	5	11	0	0	1276
3	Pati Andarai	sand bed braided	Tombador	60	13	0	0	1276.8
3	Pati Andarai	sand bed braided	Tombador				200	1276.9
3	Pati Andarai	sand bed braided	Tombador				240	1276.9
3	Pati Andarai	sand bed braided	Tombador				250	1276.9
3	Pati Andarai	sand bed braided	Tombador				350	1349.2
3	Pati Andarai	sand bed braided	Tombador				280	1353.9
3	Pati Andarai	sand bed braided	Tombador				290	1353.9
3	Pati Andarai	sand bed braided	Tombador	350	15	0	0	1354.3
3	Pati Andarai	sand bed braided	Tombador	340	15	0	0	1354.9
3	Pati Andarai	sand bed braided	Tombador				350	1355.4
3	Pati Andarai	sand bed braided	Tombador				320	1361.4
3	Pati Andarai	sand bed braided	Tombador	340	31	0	0	1361.8
3	Pati Andarai	sand bed braided	Tombador				180	1362
3	Pati Andarai	sand bed braided	Tombador		10	E		1378.2
3	Pati Andarai	sand bed braided	Tombador				270	1378.4
3	Pati Andarai	sand bed braided	Tombador				240	1378.7
3	Pati Andarai	sand bed braided	Tombador				260	1379.4
3	Pati Andarai	sand bed braided	Tombador	340	35	0	0	1380.6
3	Pati Andarai	sand bed braided	Tombador				190	1380.8
3	Pati Andarai	sand bed braided	Tombador	30	13	0	0	1382.4
3	Pati Andarai	sand bed braided	Tombador	10	31	0	0	1384.2
3	Pati Andarai	sand bed braided	Tombador				310	1384.4
3	Pati Andarai	sand bed braided	Tombador	355	17	0	0	1385.4

3	Pati Andarai	sand bed braided	Tombador	345	19	0	0	1387.5
3	Pati Andarai	sand bed braided	Tombador				350	1402.6
3	Pati Andarai	sand bed braided	Tombador				335	1403.2
3	Pati Andarai	sand bed braided	Tombador				240	1403.6
3	Pati Andarai	sand bed braided	Tombador				180	1403.6
3	Pati Andarai	sand bed braided	Tombador	20	30	0	0	1404.4
3	Pati Andarai	sand bed braided	Tombador				260	1404.6
3	Pati Andarai	sand bed braided	Tombador				315	1404.6
3	Pati Andarai	sand bed braided	Tombador				220	1425
3	Pati Andarai	sand bed braided	Tombador				210	1425.2
3	Pati Andarai	sand bed braided	Tombador				300	1425.4
3	Pati Andarai	sand bed braided	Tombador				250	1424.6
3	Pati Andarai	sand bed braided	Tombador				335	1437.4
3	Pati Andarai	sand bed braided	Tombador	325	35	0	0	1437.6
3	Pati Andarai	sand bed braided	Tombador				277	1442.4
3	Pati Andarai	sand bed braided	Tombador	170	10	0	0	1451.4
3	Pati Andarai	sand bed braided	Tombador				240	1451.7
3	Pati Andarai	sand bed braided	Tombador	343	10	0	0	1474.6
3	Pati Andarai	sand bed braided	Tombador				170	1475
3	Pati Andarai	sand bed braided	Tombador				355	1475
3	Pati Andarai	sand bed braided	Tombador				195	1483.2
3	Pati Andarai	sand bed braided	Tombador	335	15	0	0	1483.4
3	Pati Andarai	sand bed braided	Tombador	45	20	0	0	1485.6
3	Pati Andarai	sand bed braided	Tombador	335	15	0	0	1486.2
3	Pati Andarai	sand bed braided	Tombador				280	1492.1
3	Pati Andarai	river dominated delta front	Açuruá				140	1508.1
3	Pati Andarai	river dominated delta front	Açuruá				70	1510
3	Pati Andarai	river dominated delta front	Açuruá				65	1520
3	Pati Andarai	river dominated delta front	Açuruá				135	1520.6
3	Pati Andarai	river dominated delta front	Açuruá	270	15	0	0	1534.8
3	Pati Andarai	river dominated delta front	Açuruá				200	1536.8
3	Pati Andarai	river dominated delta front	Açuruá				145	1539.4
3	Pati Andarai	river dominated delta front	Açuruá				265	1540
3	Pati Andarai	river dominated delta front	Açuruá	335	15	0	0	1541.2
3	Pati Andarai	river dominated delta front	Açuruá				250	1541.6
3	Pati Andarai	river dominated delta front	Açuruá				310	1542
3	Pati Andarai	river dominated delta front	Açuruá				80	1542.4
3	Pati Andarai	river dominated delta front	Açuruá				50	1544
3	Pati Andarai	river dominated delta front	Açuruá				110	1553.6
3	Pati Andarai	river dominated delta front	Açuruá				145	1554.2
3	Pati Andarai	river dominated delta front	Açuruá				165	1554.2
3	Pati Andarai	river dominated delta front	Açuruá	350	10	0	0	1555.2
3	Pati Andarai	Prodelta	Açuruá	10	20	0	0	1755.6
4	Guiné	Eolian sand sheet	Tombador				30	1293.6
4	Guiné	Eolian sand sheet	Tombador	20	14	0	0	1297.8
4	Guiné	intermediate flash flood	Tombador				195	1299.6
4	Guiné	intermediate flash flood	Tombador				210	1303.8
4	Guiné	intermediate flash flood	Tombador				270	1306
4	Guiné	intermediate flash flood	Tombador				200	1307
4	Guiné	intermediate flash flood	Tombador	40	14	0	0	1307.4
4	Guiné	intermediate flash flood	Tombador				200	1308.6
4	Guiné	intermediate flash flood	Tombador				350	1312.1
4	Guiné	intermediate flash flood	Tombador	30	10	0	0	1314.6
4	Guiné	intermediate flash flood	Tombador	60	14	0	0	1315.6
4	Guiné	intermediate flash flood	Tombador				340	1316.5
4	Guiné	intermediate flash flood	Tombador				220	1317.2
4	Guiné	intermediate flash flood	Tombador		11	E		1318.7
4	Guiné	intermediate flash flood	Tombador				310	1319.8
4	Guiné	river dominated delta front	Açuruá	40	20	0	0	1415.4
4	Guiné	river dominated delta front	Açuruá	15	10	0	0	1428
4	Guiné	river dominated delta front	Açuruá				90	1428.2
4	Guiné	river dominated delta front	Açuruá		8	E		1435.1
4	Guiné	river dominated delta front	Açuruá				150	1471.1
4	Guiné	river dominated delta front	Açuruá	10	17	0	0	1475.7
4	Guiné	floodplain	Açuruá	340	17	0	0	1516

4	Guiné	floodplain	Açuruá				175	1518.1
4	Guiné	floodplain	Açuruá				155	1523.1
4	Guiné	floodplain	Açuruá				160	1528
4	Guiné	floodplain	Açuruá				170	1533.7
4	Guiné	floodplain	Açuruá	355	21	0	0	1552
4	Guiné	floodplain	Açuruá	345	19	0	0	1561
4	Guiné	floodplain	Açuruá	340	25	0	0	1572
4	Guiné	floodplain	Açuruá	355	12	0	0	1586.9
4	Guiné	floodplain	Açuruá	345	19	0	0	1624.8
4	Guiné	floodplain	Açuruá				130	1647.4
4	Guiné	floodplain	Açuruá	335	24	0	0	1651.6
4	Guiné	floodplain	Açuruá				160	1661.2
4	Guiné	floodplain	Açuruá				175	1662.5
4	Guiné	floodplain	Açuruá				175	1666.1
4	Guiné	floodplain	Açuruá				165	1668.8
4	Guiné	floodplain	Açuruá	340	25	0	0	1672.6
4	Guiné	floodplain	Açuruá				145	1672.8
4	Guiné	floodplain	Açuruá				150	1673.4
4	Guiné	floodplain	Açuruá				150	1674.8
4	Guiné	floodplain	Açuruá	335	20	0	0	1676.8
4	Guiné	floodplain	Açuruá				160	1677.5
4	Guiné	floodplain	Açuruá	345	26	0	0	1679.3
4	Guiné	floodplain	Açuruá				0	1679.4
4	Guiné	floodplain	Açuruá				355	1679.5
4	Guiné	floodplain	Açuruá	342	29	0	0	1680.4
4	Guiné	floodplain	Açuruá				130	1682.6
4	Guiné	floodplain	Açuruá				130	1745.4
4	Guiné	floodplain	Açuruá				130	1750.8
4	Guiné	floodplain	Açuruá	330	17	0	0	1753.8
4	Guiné	floodplain	Açuruá	340	16	0	0	1760.1
4	Guiné	floodplain	Açuruá	340	20	0	0	1766.6
4	Guiné	floodplain	Açuruá	340	19	0	0	1770.8
4	Guiné	floodplain	Açuruá				150	1771
7	Fumaça	tidal bar	Tombador				315	1269
7	Fumaça	tidal bar	Tombador	70	4	SE	0	1269.7
7	Fumaça	tidal bar	Tombador				335	1270
7	Fumaça	tidal bar	Tombador				290	1271.4
7	Fumaça	tidal bar	Tombador				330	1275.8
7	Fumaça	tidal bar	Tombador				310	1277
7	Fumaça	tidal bar	Tombador				305	1280.1
7	Fumaça	intermediate flash flood	Tombador	350	8	NE	0	1381.3
7	Fumaça	intermediate flash flood	Tombador				10	1384.2
7	Fumaça	intermediate flash flood	Tombador				150	1384.5
7	Fumaça	intermediate flash flood	Tombador				315	1386.2
7	Fumaça	intermediate flash flood	Tombador	0	5	E		1390.3
7	Fumaça	intermediate flash flood	Tombador				170	1395.4
7	Fumaça	intermediate flash flood	Tombador				315	1397.5
7	Fumaça	intermediate flash flood	Tombador				315	1398.8
7	Fumaça	intermediate flash flood	Tombador				335	1399.2
7	Fumaça	intermediate flash flood	Tombador				320	1400
7	Fumaça	intermediate flash flood	Tombador				350	1401.5
7	Fumaça	intermediate flash flood	Tombador				310	1402.2
7	Fumaça	intermediate flash flood	Tombador	340	5	NE	0	1403.1
7	Fumaça	intermediate flash flood	Tombador				270	1405.2
7	Fumaça	intermediate flash flood	Tombador				300	1407.8
7	Fumaça	intermediate flash flood	Tombador				340	1410
7	Fumaça	intermediate flash flood	Tombador				240	1415
7	Fumaça	intermediate flash flood	Tombador				290	1417.4
7	Fumaça	intermediate flash flood	Tombador				235	1419.5
7	Fumaça	intermediate flash flood	Tombador				190	1419.9
7	Fumaça	intermediate flash flood	Tombador				140	1425.5
7	Fumaça	intermediate flash flood	Tombador	350	9	NE	0	1425.8
7	Fumaça	intermediate flash flood	Tombador				270	1437.8
7	Fumaça	intermediate flash flood	Tombador				220	1441.2
7	Fumaça	intermediate flash flood	Tombador				270	1444.6

7	Fumaça	intermediate flash flood	Tombador				205	1445.6
7	Fumaça	intermediate flash flood	Tombador				187	1447.1
7	Fumaça	intermediate flash flood	Tombador	190	5	SE	0	1447.8
7	Fumaça	intermediate flash flood	Tombador				270	1448
7	Fumaça	intermediate flash flood	Tombador				235	1448.8
7	Fumaça	intermediate flash flood	Tombador				250	1448.9
7	Fumaça	intermediate flash flood	Tombador				280	1452.1
7	Fumaça	intermediate flash flood	Tombador				210	1457.1
7	Fumaça	intermediate flash flood	Tombador				240	1459.1
7	Fumaça	Eolian sand sheet	Tombador				0	1462.2
7	Fumaça	intermediate flash flood	Tombador				250	1462.5
7	Fumaça	intermediate flash flood	Tombador				280	1467.3
7	Fumaça	Eolian sand sheet	Tombador	280	5	NE	0	1467.9
7	Fumaça	intermediate flash flood	Tombador				270	1471.5
7	Fumaça	intermediate flash flood	Tombador				265	1471.6
7	Fumaça	intermediate flash flood	Tombador				310	1475
7	Fumaça	intermediate flash flood	Tombador				290	1478
7	Fumaça	Eolian sand sheet	Tombador				15	1478.5
7	Fumaça	Eolian sand sheet	Tombador	330	9	NE	0	1483
7	Fumaça	intermediate flash flood	Tombador				250	1486.2
7	Fumaça	intermediate flash flood	Tombador				210	1493.8
7	Fumaça	intermediate flash flood	Tombador				340	1494.2
7	Fumaça	intermediate flash flood	Tombador				5	1497.6
7	Fumaça	intermediate flash flood	Tombador				0	1498.1
7	Fumaça	river dominated delta front	Açuruá				255	1500.9
7	Fumaça	river dominated delta front	Açuruá	310	6	NE	0	1502.5
7	Fumaça	river dominated delta front	Açuruá				250	1503.4
7	Fumaça	river dominated delta front	Açuruá				280	1508.4
7	Fumaça	river dominated delta front	Açuruá				230	1509.7
7	Fumaça	river dominated delta front	Açuruá				195	1510
7	Fumaça	river dominated delta front	Açuruá	10	10	NE	0	1512.6
7	Fumaça	river dominated delta front	Açuruá	10	8	SE	0	1514
7	Fumaça	river dominated delta front	Açuruá				170	1514.3
7	Fumaça	river dominated delta front	Açuruá				230	1517.2
7	Fumaça	river dominated delta front	Açuruá				190	1521.2
7	Fumaça	river dominated delta front	Açuruá	5	5	SE	0	1521.2
7	Fumaça	river dominated delta front	Açuruá				280	1524.2
7	Fumaça	distributary fluvial channel	Açuruá				205	1529.3
7	Fumaça	distributary fluvial channel	Açuruá				170	1531.1
7	Fumaça	distributary fluvial channel	Açuruá				170	1531.7
7	Fumaça	distributary fluvial channel	Açuruá				220	1535.8
7	Fumaça	distributary fluvial channel	Açuruá				190	1536
7	Fumaça	distributary fluvial channel	Açuruá				120	1537
7	Fumaça	river dominated delta front	Açuruá				160	1577.1
7	Fumaça	river dominated delta front	Açuruá				290	1586.1
7	Fumaça	river dominated delta front	Açuruá	260	10	SE	0	1588.6
7	Fumaça	river dominated delta front	Açuruá	210	5	NW	0	1626.4
7	Fumaça	river dominated delta front	Açuruá				235	1646.9
7	Fumaça	river dominated delta front	Açuruá				220	1654.4
7	Fumaça	river dominated delta front	Açuruá				170	1655.1
7	Fumaça	river dominated delta front	Açuruá				175	1658.5
7	Fumaça	river dominated delta front	Açuruá				5	1659.4
7	Fumaça	river dominated delta front	Açuruá				355	1663.5
7	Fumaça	Prodelta	Açuruá	340	3	NE	0	1684.7
8	Ribeirão	offshore tidal bar	Tombador				240	368.8
8	Ribeirão	offshore tidal bar	Tombador				85	369.2
8	Ribeirão	offshore tidal bar	Tombador				275	362.2
8	Ribeirão	gravel bed braided	Tombador				210	372.2
8	Ribeirão	gravel bed braided	Tombador				200	383.4
8	Ribeirão	gravel bed braided	Tombador				205	385.6
8	Ribeirão	gravel bed braided	Tombador				210	386.4
8	Ribeirão	floodplain	Tombador					387.8
8	Ribeirão	gravel bed braided	Tombador	355	16		220	389.2
8	Ribeirão	gravel bed braided	Tombador				205	391.4
8	Ribeirão	gravel bed braided	Tombador				285	394.6

8	Ribeirão	gravel bed braided	Tombador					394.8
8	Ribeirão	gravel bed braided	Tombador	345	9		300	395.6
8	Ribeirão	gravel bed braided	Tombador				210	396
10	Morrão	tidal bar	Tombador				280	1437.8
10	Morrão	tidal bar	Tombador				220	1450
10	Morrão	tidal bar	Tombador				220	1454
10	Morrão	tidal bar	Tombador				220	1454.8
10	Morrão	tidal bar	Tombador				190	1457.2
10	Morrão	tidal bar	Tombador				210	1461.8
10	Morrão	tidal bar	Tombador				210	1473.8
10	Morrão	tidal bar	Tombador				230	1482.8
10	Morrão	tidal bar	Tombador				40	1487.8
10	Morrão	tidal bar	Tombador				290	1488.4
10	Morrão	distributary fluvial channel	Açuruá				210	1519.8
10	Morrão	distributary fluvial channel	Açuruá				50	1529.4
10	Morrão	distributary fluvial channel	Açuruá				340	1530
10	Morrão	distributary fluvial channel	Açuruá				240	1530.2
10	Morrão	distributary fluvial channel	Açuruá				270	1531.8
10	Morrão	distributary fluvial channel	Açuruá				130	1538.8
10	Morrão	floodplain	Açuruá	240	6	SE	0	1540.4
10	Morrão	floodplain	Açuruá				0	1550
10	Morrão	floodplain	Açuruá				90	1553.4
10	Morrão	distributary fluvial channel	Açuruá				280	1586.8
10	Morrão	distributary fluvial channel	Açuruá				300	1595.8
10	Morrão	distributary fluvial channel	Açuruá				280	1636.8
10	Morrão	floodplain	Açuruá				80	1638.8
10	Morrão	distributary fluvial channel	Açuruá				290	1643.2
10	Morrão	floodplain	Açuruá	315	3	NE	0	1648
10	Morrão	distributary fluvial channel	Açuruá				75	1659
10	Morrão	distributary fluvial channel	Açuruá				200	1742.6
10	Morrão	river dominated delta front	Açuruá	250	5	SE	0	1746.6
10	Morrão	river dominated delta front	Açuruá				120	1749.6
10	Morrão	distributary fluvial channel	Açuruá				315	1754.6
10	Morrão	distributary fluvial channel	Açuruá				335	1765.4
10	Morrão	river dominated delta front	Açuruá				0	1765.6
10	Morrão	river dominated delta front	Açuruá				0	1812
11	BR242	proximal intermediate sheetflood	Tombador				240	1269
11	BR242	proximal intermediate sheetflood	Tombador				265	1273.2
11	BR242	Eolian dunes	Tombador				70	1278
11	BR242	intermediate distal sheetflood	Tombador	40	12	SE	0	1297
11	BR242	sand bed braided	Tombador				300	1299.4
11	BR242	sand bed braided	Tombador				290	1299.4
11	BR242	sand bed braided	Tombador				300	1299.4
11	BR242	sand bed braided	Tombador				285	1299.4
11	BR242	sand bed braided	Tombador				350	1300
11	BR242	sand bed braided	Tombador				120	1300
11	BR242	sand bed braided	Tombador	95	14	SW	0	1300.6
11	BR242	tidal flat	Tombador				295	1316.8
11	BR242	tidal flat	Tombador				285	1316.8
11	BR242	tidal flat	Tombador				195	1318.4
11	BR242	tidal flat	Tombador				230	1318.8
11	BR242	tidal flat	Tombador	0	9	E		1319
11	BR242	tidal flat	Tombador				90	1319.8
11	BR242	tidal flat	Tombador				180	1319.8
11	BR242	tidal flat	Tombador				275	1320.8
11	BR242	tidal flat	Tombador				210	1320.8
11	BR242	sand bed braided	Tombador				315	1326
11	BR242	tidal flat	Tombador				260	1334.3
11	BR242	tidal flat	Tombador				240	1334.3
11	BR242	tidal flat	Tombador				175	1337.8
11	BR242	tidal flat	Tombador				245	1337.8
11	BR242	tidal flat	Tombador				20	1340.6
11	BR242	tidal flat	Tombador				310	1340.6
11	BR242	tidal flat	Tombador				175	1341
11	BR242	tidal flat	Tombador				240	1347

11	BR242	sand bed braided	Tombador				300	1366
11	BR242	tidal bar	Tombador				300	1393
11	BR242	tidal bar	Tombador				210	1398.4
11	BR242	tidal bar	Tombador				200	1398.4
11	BR242	tidal bar	Tombador				160	1398.4
11	BR242	Eolian dunes	Tombador				245	1421
11	BR242	Eolian dunes	Tombador				325	1422.5
11	BR242	sand bed braided	Tombador				320	1422.8
11	BR242	Eolian dunes	Tombador				40	1423.7
11	BR242	sand bed braided	Tombador				240	1423.8
11	BR242	sand bed braided	Tombador				250	1426.7
11	BR242	sand bed braided	Tombador				315	1428
11	BR242	sand bed braided	Tombador				255	1428.2
11	BR242	sand bed braided	Tombador				220	1431.7
11	BR242	sand bed braided	Tombador				270	1431.7
11	BR242	sand bed braided	Tombador				250	1431.7
11	BR242	sand bed braided	Tombador				160	1432.9
11	BR242	sand bed braided	Tombador				255	1433.6
11	BR242	sand bed braided	Tombador				340	1433.8
11	BR242	sand bed braided	Tombador				260	1435.2
11	BR242	sand bed braided	Tombador				215	1434.8
11	BR242	sand bed braided	Tombador				270	1435.4
11	BR242	sand bed braided	Tombador				310	1435.6
11	BR242	sand bed braided	Tombador				315	1435.6
11	BR242	sand bed braided	Tombador				250	1436.4
11	BR242	sand bed braided	Tombador				280	1439
11	BR242	sand bed braided	Tombador				190	1439.2
11	BR242	sand bed braided	Tombador				300	1440
11	BR242	tidal bar	Tombador				315	1440.3
11	BR242	tidal bar	Tombador				230	1441
11	BR242	tidal bar	Tombador				70	1441
11	BR242	tidal bar	Tombador				40	1442.6
11	BR242	tidal bar	Tombador				60	1442.8
11	BR242	tidal bar	Tombador				200	1442.8
11	BR242	tidal bar	Tombador				300	1443.2
11	BR242	tidal bar	Tombador				260	1443.2
11	BR242	tidal bar	Tombador				60	1448.2
11	BR242	tidal bar	Tombador				250	1448.2
11	BR242	tidal channel	Tombador				205	1449.2
11	BR242	tidal channel	Tombador				245	1461.8
11	BR242	tidal channel	Tombador				245	1462.6
11	BR242	tidal channel	Tombador				220	1462.6
11	BR242	tidal channel	Tombador				300	1462.6
11	BR242	tidal channel	Tombador				265	1462.6
11	BR242	tidal channel	Tombador				180	1464
11	BR242	tidal channel	Tombador				310	1465
11	BR242	tidal bar	Tombador				170	1465.7
11	BR242	tidal bar	Tombador				185	1466.3
11	BR242	tidal bar	Tombador				225	1467.5
11	BR242	tidal bar	Tombador				255	1496.6
11	BR242	tidal bar	Tombador	340	15	NE	0	1497.4
11	BR242	tidal bar	Tombador				240	1498
11	BR242	unconformity		340	10	NE	0	1498.2
11	BR242	distributary fluvial channel	Açuruá				60	1500.4
14	Impossíveis	intermediate distal sheetflood	Tombador				310	966.5
14	Impossíveis	intermediate distal sheetflood	Tombador				0	967.3
14	Impossíveis	intermediate distal sheetflood	Tombador	40	8	SE	0	971.2
14	Impossíveis	gravel bed braided	Tombador	330	9	NE	0	977.4
14	Impossíveis	gravel bed braided	Tombador				310	979.6
14	Impossíveis	gravel bed braided	Tombador				280	980.2
14	Impossíveis	intermediate flash flood	Tombador	320	7	NE	0	990.9
14	Impossíveis	proximal intermediate sheetflood	Tombador				290	1004.7
14	Impossíveis	proximal intermediate sheetflood	Tombador				260	1013
14	Impossíveis	proximal intermediate sheetflood	Tombador				145	1013.7
14	Impossíveis	Eolian sand sheet	Tombador				20	1017.4

14	Impossíveis	Eolian sand sheet	Tombador				300	1017.5
14	Impossíveis	Eolian sand sheet	Tombador				340	1017.6
14	Impossíveis	Eolian sand sheet	Tombador	330	2	NE	0	1018
14	Impossíveis	proximal intermediate sheetflood	Tombador				170	1018.2
14	Impossíveis	proximal intermediate sheetflood	Tombador				235	1018.3
14	Impossíveis	proximal intermediate sheetflood	Tombador				340	1018.4
14	Impossíveis	proximal intermediate sheetflood	Tombador				270	1019.7
14	Impossíveis	proximal intermediate sheetflood	Tombador				260	1019.9
14	Impossíveis	proximal intermediate sheetflood	Tombador	335	4	NE	0	1020.5
14	Impossíveis	proximal intermediate sheetflood	Tombador	345	5	NE	0	1020.6
14	Impossíveis	Eolian sand sheet	Tombador				90	1021.5
14	Impossíveis	Eolian sand sheet	Tombador				10	1021.5
14	Impossíveis	Eolian sand sheet	Tombador				65	1021.5
14	Impossíveis	Eolian sand sheet	Tombador				30	1021.5
14	Impossíveis	Eolian sand sheet	Tombador				105	1022.4
14	Impossíveis	Eolian sand sheet	Tombador	0	4	E		1022.4
14	Impossíveis	Eolian sand sheet	Tombador	320	5	NE	0	1022.4
14	Impossíveis	Eolian dunes	Tombador				40	1024
14	Impossíveis	sand bed braided	Tombador				270	1025.1
14	Impossíveis	sand bed braided	Tombador				230	1025.5
14	Impossíveis	sand bed braided	Tombador				305	1026.3
14	Impossíveis	sand bed braided	Tombador				315	1027.2
14	Impossíveis	sand bed braided	Tombador				280	1031.8
14	Impossíveis	floodplain	Tombador	270	5	0	0	1032.8
14	Impossíveis	floodplain	Tombador				280	1033
14	Impossíveis	sand bed braided	Tombador				290	1033.6
14	Impossíveis	sand bed braided	Tombador				300	1034.4
14	Impossíveis	sand bed braided	Tombador				250	1039.2
14	Impossíveis	sand bed braided	Tombador				130	1041.1
14	Impossíveis	sand bed braided	Tombador				300	1041.1
14	Impossíveis	sand bed braided	Tombador				260	1041.1
14	Impossíveis	sand bed braided	Tombador				290	1042.8
14	Impossíveis	sand bed braided	Tombador				310	1045.8
14	Impossíveis	sand bed braided	Tombador				200	1047.4
B	Pai Inácio hill	tidal bar	Tombador			0	340	1031.6
B	Pai Inácio hill	tidal bar	Tombador				350	1031.8
B	Pai Inácio hill	tidal bar	Tombador	265	5	NW	0	1034.7
B	Pai Inácio hill	tidal bar	Tombador				340	1034.8
B	Pai Inácio hill	tidal bar	Tombador				305	1035
B	Pai Inácio hill	tidal bar	Tombador				335	1035.3
B	Pai Inácio hill	tidal bar	Tombador				5	1036.6
B	Pai Inácio hill	tidal bar	Tombador				280	1037
B	Pai Inácio hill	tidal bar	Tombador				305	1038.6
B	Pai Inácio hill	tidal bar	Tombador				230	1038.8
B	Pai Inácio hill	tidal bar	Tombador				300	1039.7
B	Pai Inácio hill	tidal bar	Tombador				260	1042
B	Pai Inácio hill	tidal bar	Tombador				200	1043.8
B	Pai Inácio hill	tidal bar	Tombador				295	1044.6
B	Pai Inácio hill	tidal bar	Tombador				244	1049
B	Pai Inácio hill	tidal bar	Tombador				50	1050.1
B	Pai Inácio hill	tidal bar	Tombador				235	1050.4
B	Pai Inácio hill	tidal bar	Tombador				270	1051.8
B	Pai Inácio hill	tidal bar	Tombador				274	1052.7
B	Pai Inácio hill	tidal channel	Tombador				310	1055.8
B	Pai Inácio hill	tidal channel	Tombador				330	1057.2
B	Pai Inácio hill	tidal bar	Tombador				55	1059
B	Pai Inácio hill	tidal bar	Tombador				240	1061
B	Pai Inácio hill	tidal bar	Tombador				270	1062.4
B	Pai Inácio hill	tidal bar	Tombador				255	1065.4
B	Pai Inácio hill	Eolian dunes	Tombador				50	1066.8
B	Pai Inácio hill	Eolian dunes	Tombador	200	7	SE	0	1067.2
B	Pai Inácio hill	Eolian sand sheet	Tombador	270	7	SE	0	1067.8
B	Pai Inácio hill	Eolian sand sheet	Tombador				185	1068
B	Pai Inácio hill	Eolian sand sheet	Tombador				340	1068.6
B	Pai Inácio hill	Eolian sand sheet	Tombador				134	1068.7

B	Pai Inácio hill	Eolian sand sheet	Tombador				275	1069.2
B	Pai Inácio hill	Eolian sand sheet	Tombador				244	1070
B	Pai Inácio hill	tidal bar	Tombador				15	1072.1
B	Pai Inácio hill	tidal bar	Tombador				301	1074.1
B	Pai Inácio hill	tidal channel	Tombador				130	1074.6
B	Pai Inácio hill	tidal bar	Tombador				325	1075.9
B	Pai Inácio hill	tidal bar	Tombador				225	1076.5
B	Pai Inácio hill	tidal bar	Tombador				200	1076.7
B	Pai Inácio hill	tidal bar	Tombador				318	1078.5
B	Pai Inácio hill	tidal bar	Tombador				190	1078.6
B	Pai Inácio hill	tidal channel	Tombador				332	1079.7
B	Pai Inácio hill	tidal bar	Tombador				310	1080.2
B	Pai Inácio hill	tidal bar	Tombador				320	1080.6
not presented	Buracao	sand bed braided	Tombador				260	568.4
not presented	Buracao	sand bed braided	Tombador				210	569.6
not presented	Buracao	sand bed braided	Tombador	275	5	0	0	570.1
not presented	Buracao	sand bed braided	Tombador				355	573.6
not presented	Buracao	sand bed braided	Tombador				315	578
not presented	Igatu	gravel bed braided	Tombador	300	3	0	0	1009.3
not presented	Igatu	gravel bed braided	Tombador				190	1018.9
not presented	Igatu	gravel bed braided	Tombador	320	14	0	0	1018.9
not presented	Igatu	gravel bed braided	Tombador	285	10	0	0	1071.8
not presented	Igatu	gravel bed braided	Tombador				230	1071.8
not presented	Igatu	Eolian dunes	Tombador	325	10	0	0	1022.6
not presented	Igatu	Eolian sand sheet	Tombador	300	10	0	0	1263.2
not presented	Igatu	intermediate distal sheetflood	Tombador				310	1265.2
not presented	Igatu	intermediate distal sheetflood	Tombador				340	1267.5
not presented	Igatu	Eolian sand sheet	Tombador	290	13	0	0	1268.6
not presented	Igatu	Eolian dunes	Tombador	230	19	0	0	1270.8
not presented	Ponte Sto Antonio	offshore tidal bar	Caboclo				130	412.8
not presented	Ponte Sto Antonio	offshore tidal bar	Caboclo				135	413.3
not presented	Ponte Sto Antonio	offshore tidal bar	Caboclo				135	414.9
not presented	Ponte Sto Antonio	offshore tidal bar	Caboclo	10	6	SE	0	415.5
not presented	Ponte Sto Antonio	offshore tidal bar	Caboclo				45	426.2
not presented	Ponte Sto Antonio	offshore tidal bar	Caboclo				100	426.3
not presented	Ponte Sto Antonio	offshore tidal bar	Caboclo				190	426.5
not presented	Ponte Sto Antonio	offshore tidal bar	Caboclo				45	427.3
not presented	Ponte Sto Antonio	offshore tidal bar	Caboclo				350	427.5
not presented	Ponte Sto Antonio	offshore tidal bar	Caboclo				265	428.1
not presented	Ponte Sto Antonio	offshore tidal bar	Caboclo				100	428.3
not presented	Ponte Sto Antonio	offshore tidal bar	Caboclo				50	428.6
not presented	Ponte Sto Antonio	offshore tidal bar	Caboclo				10	430.1
not presented	Ponte Sto Antonio	offshore tidal bar	Caboclo				195	430.8
not presented	Ponte Sto Antonio	offshore tidal bar	Caboclo				30	431.4
not presented	Ponte Sto Antonio	offshore tidal bar	Caboclo				15	431.4
not presented	Ponte Sto Antonio	offshore tidal bar	Caboclo	255	4	NW	0	431.8
not presented	Mucugê	intermediate flash flood	Tombador	320	5	NE	0	896.1
not presented	Mucugê	intermediate flash flood	Tombador	335	6	NE	0	900.8
not presented	Mucugê	sand bed braided	Tombador				230	902.1
not presented	Mucugê	sand bed braided	Tombador				210	903.7
not presented	Mucugê	sand bed braided	Tombador				195	906.4
not presented	Mucugê	sand bed braided	Tombador	290	10	0	0	907.9
not presented	Mucugê	sand bed braided	Tombador				240	908.2
not presented	Mucugê	sand bed braided	Tombador				230	908.3
not presented	Mucugê	gravel bed braided	Tombador				200	1138.6
not presented	Mucugê	gravel bed braided	Tombador				245	1148.6
not presented	Mucugê	gravel bed braided	Tombador				260	1239.5
not presented	Mucugê	gravel bed braided	Tombador				190	1246.9
not presented	Mucugê	gravel bed braided	Tombador				220	1247.4
not presented	Mucugê	gravel bed braided	Tombador				200	1249
not presented	Mucugê	intermediate flash flood	Tombador	330	5	NE	0	1251.4

Appendix 4 – Gamma ray logs

A4.1. GR Vertical section 1 – Barra da Estiva

A4.2. GR Vertical Section 2 – Ronei

A4.3. GR Vertical Section 3 – Pati-Andaraí

A4.4. GR Vertical Section 4 – Guiné

A4.5. GR Vertical Section 7 – Fumaça

A4.6. GR Vertical Section 10 – Morrão

A4.7. GR Vertical Section 11 – BR242 (PONTE

A4.8. GR Vertical Section 14 – Impossíveis.

A4.9. GR Vertical Section B – Pai Inácio hill

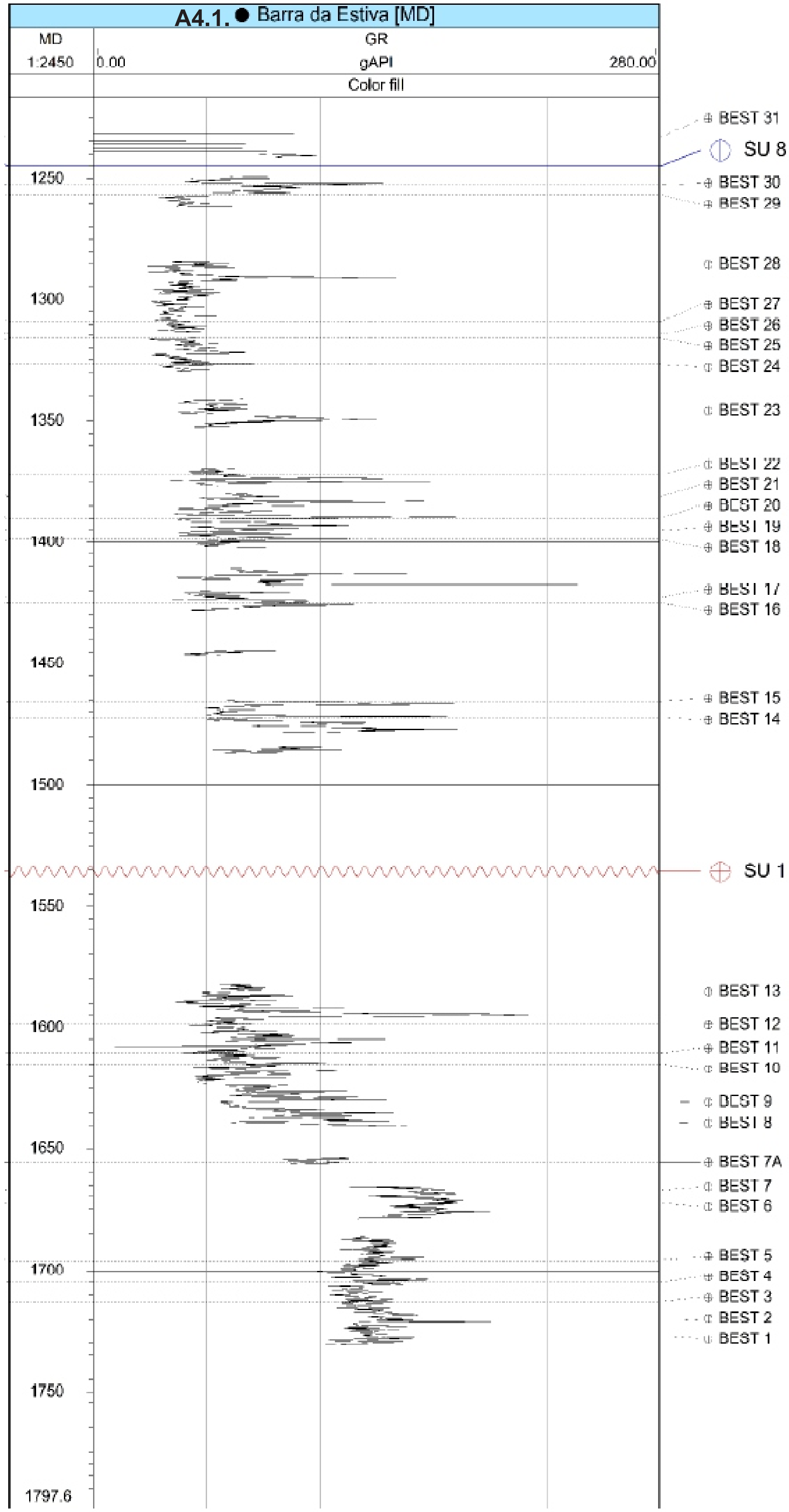
A4.1. ● Barra da Estiva [MD]
MD
1:2450
GR
0.00
gAPI
280.00
Color fill
1250
1300
1350
1400
1450
1500
1550
1600
1650
1700
1750
1797.6
BEST 31
SU 8
BEST 30
BEST 29
BEST 28
BEST 27
BEST 26
BEST 25
BEST 24
BEST 23
BEST 22
BEST 21
BEST 20
BEST 19
BEST 18
BEST 17
BEST 16
BEST 15
BEST 14
SU 1
BEST 13
BEST 12
BEST 11
BEST 10
BEST 9
BEST 8
BEST 7A
BEST 7
BEST 6
BEST 5
BEST 4
BEST 3
BEST 2
BEST 1

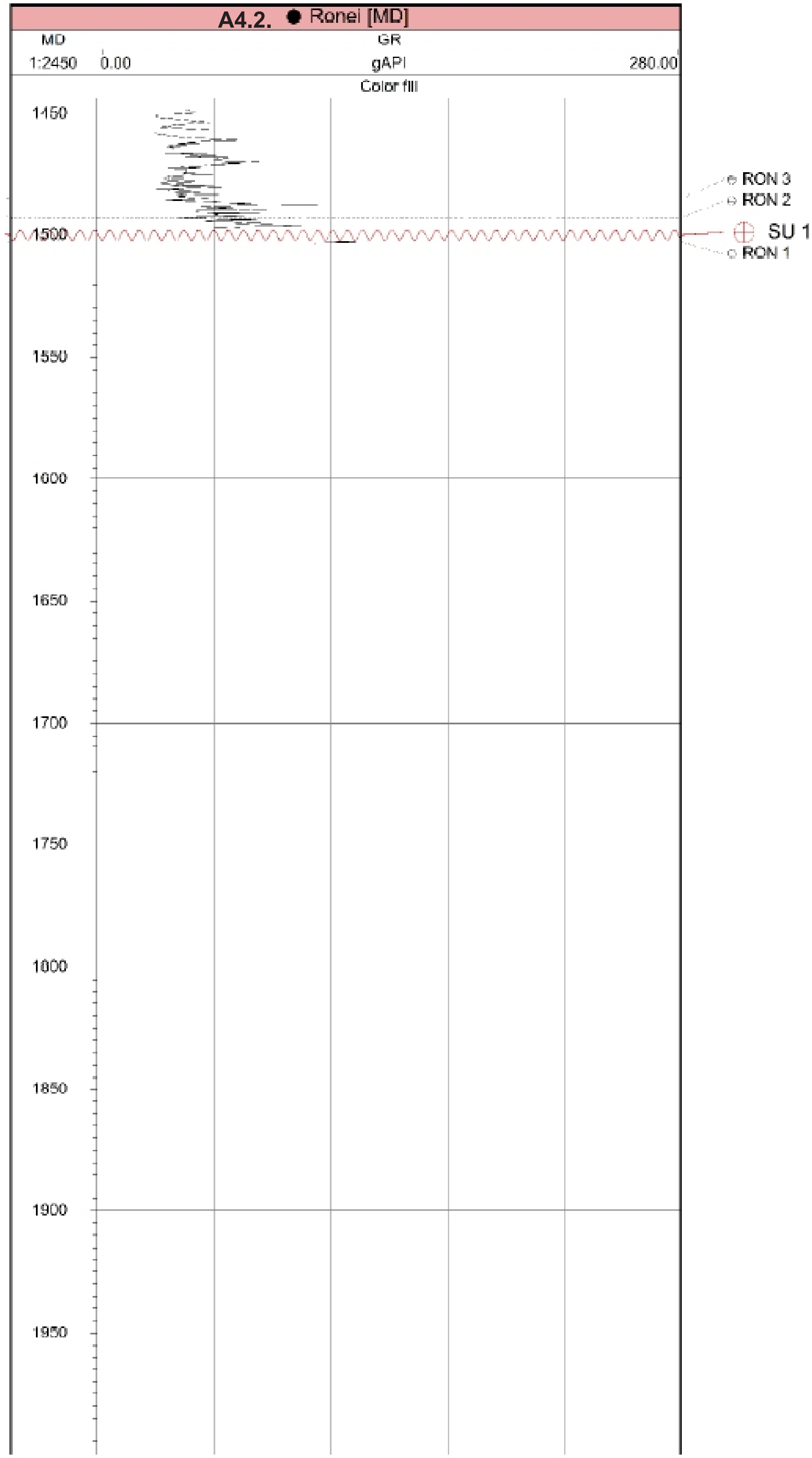
A4.2. Ronei [MD]
MD
1:2450
GR
0.00
gAPI
280.00
Color fill
1450
1500
1550
1600
1650
1700
1750
1800
1850
1900
1950
RON 3
RON 2
SU 1
RON 1

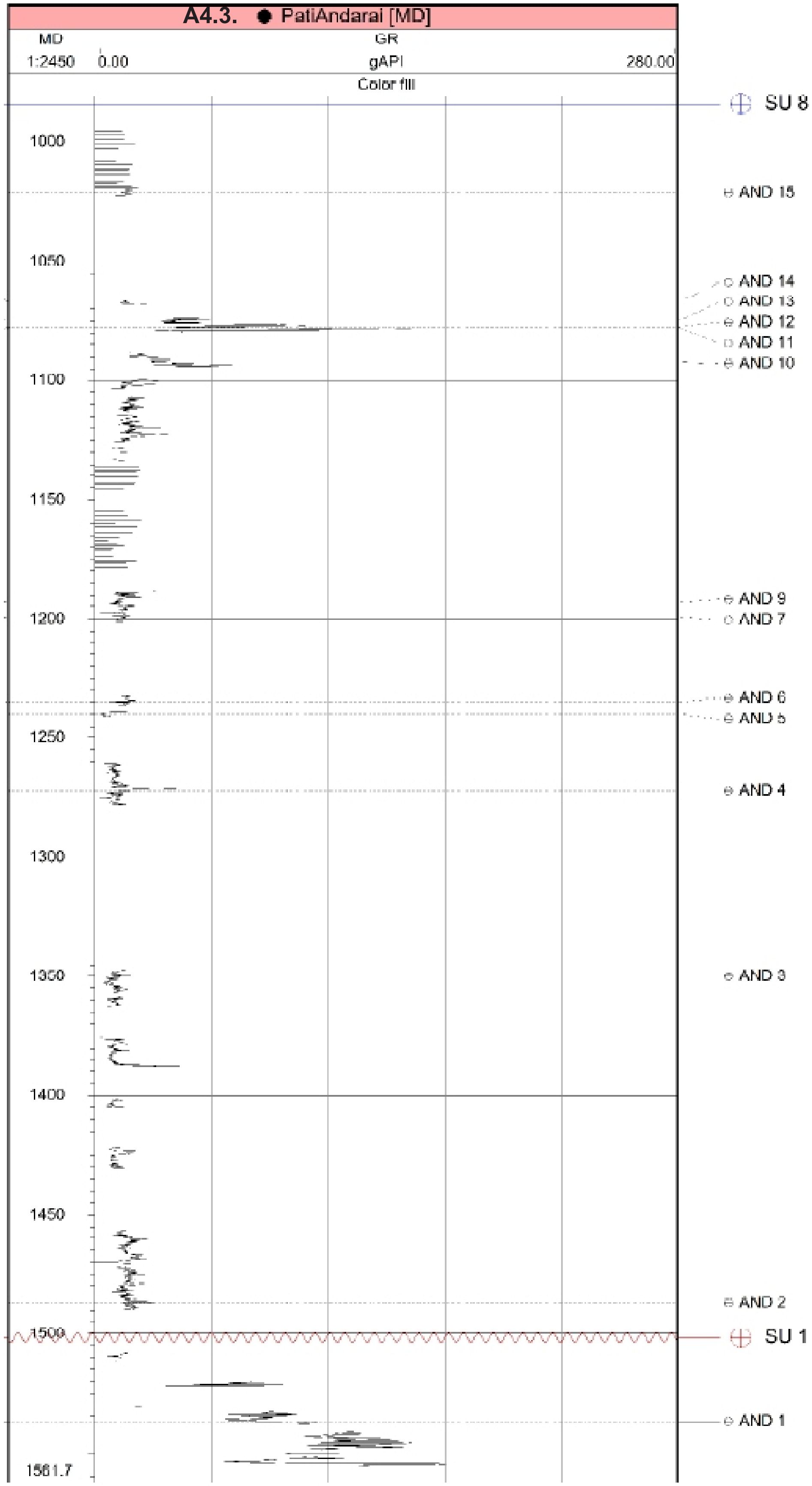

A4.3.
PatiAndarai [MD]
MD
1:2450
GR
0.00
gAPI
280.00
Color fill
SU 8
1000
AND 15
1050
AND 14
AND 13
AND 12
AND 11
AND 10
1100
1150
AND 9
AND 7
1200
AND 6
AND 5
1250
AND 4
1300
1350
AND 3
1400
1450
AND 2
1500
SU 1
AND 1
1561.7

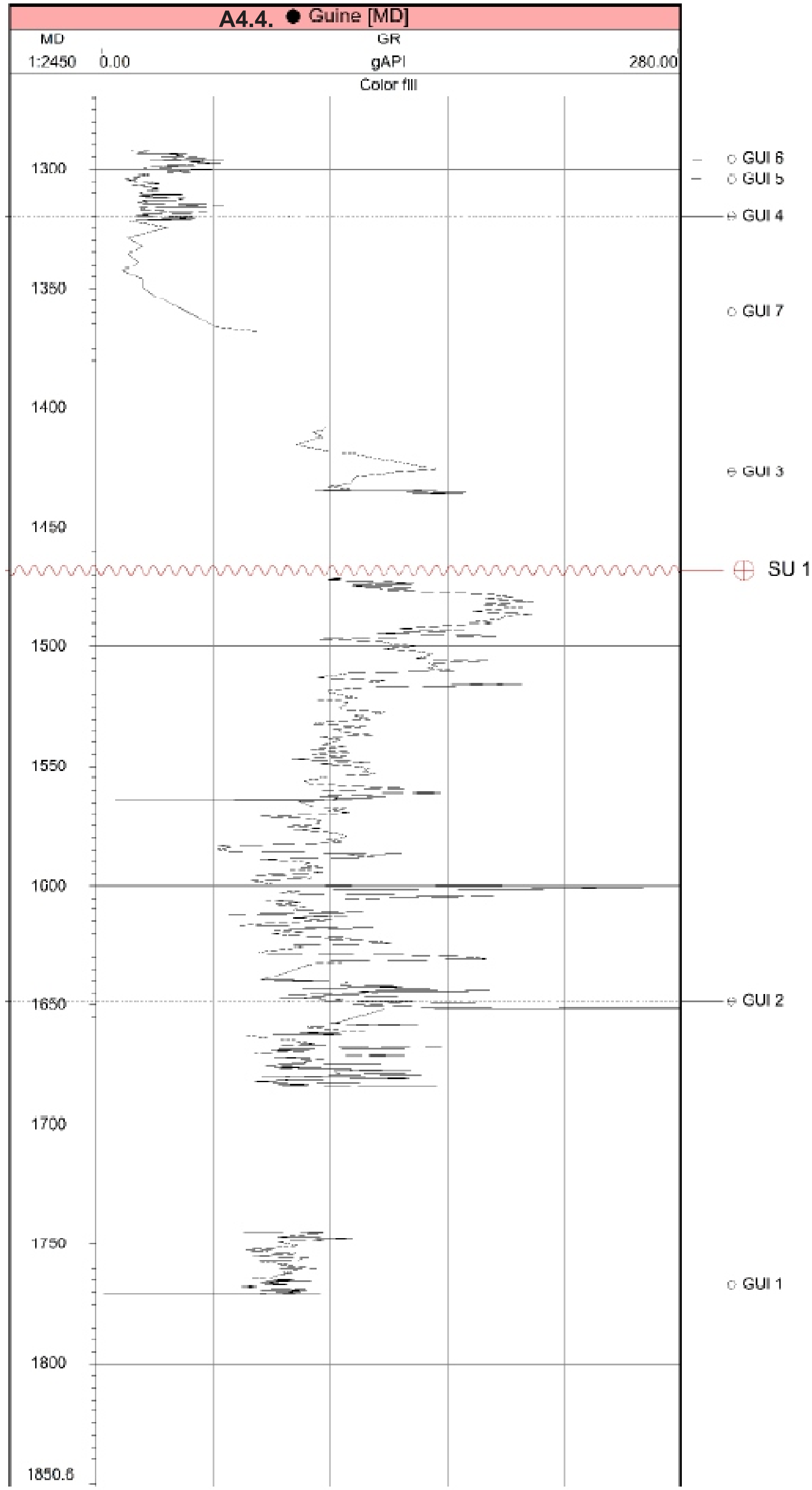
A4.4. Guine [MD]
MD
1:2450
GR
0.00
gAPI
280.00
Color fill
1300
1350
1400
1450
1500
1550
1600
1650
1700
1750
1800
1850.6
GUI 6
GUI 5
GUI 4
GUI 7
GUI 3
SU 1
GUI 2
GUI 1

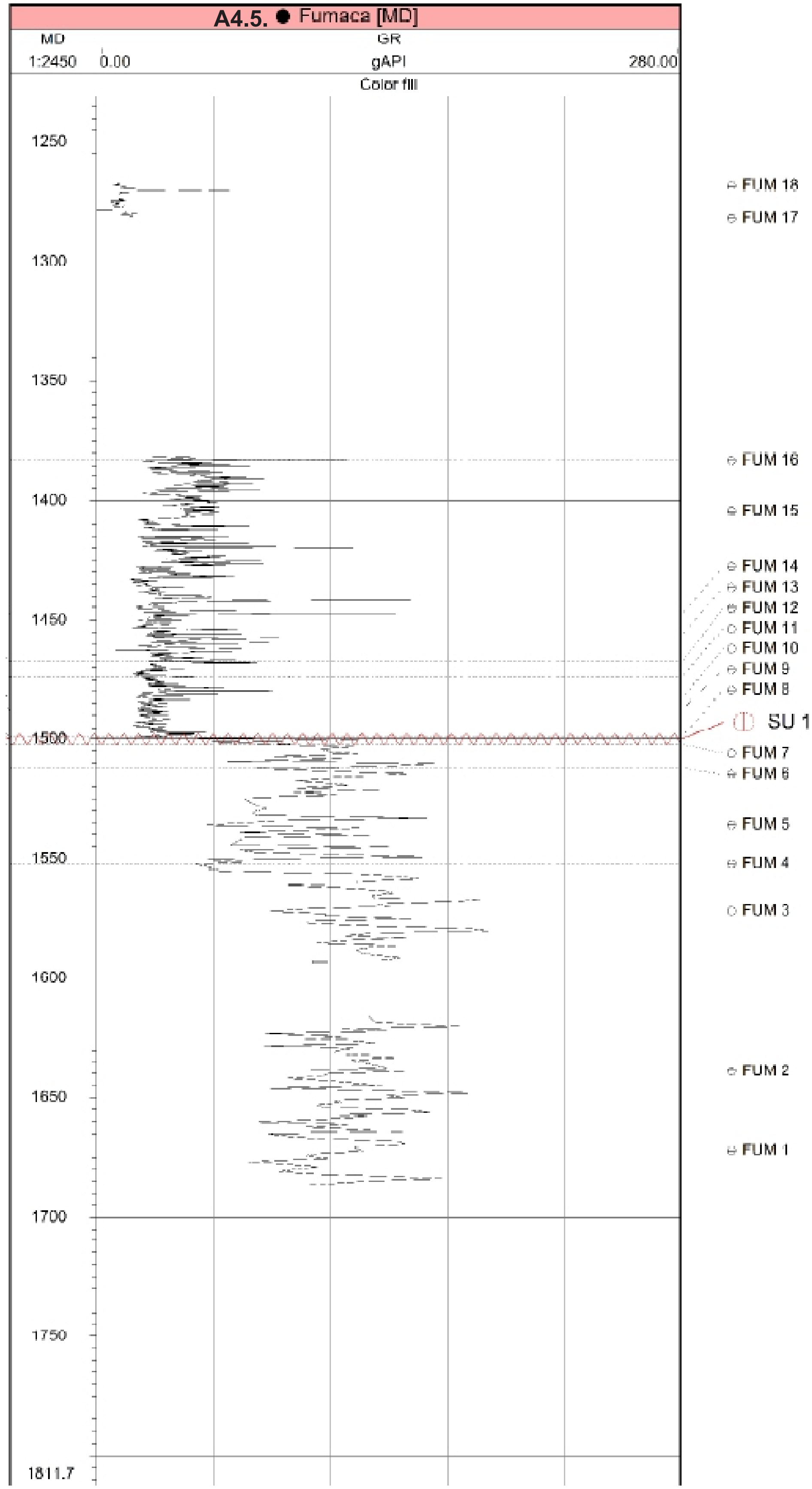
A4.5. ● Fumaca [MD]
MD
1:2450
GR
0.00
gAPI
280.00
Color fill
1250
1300
1350
1400
1450
1500
1550
1600
1650
1700
1750
1811.7
FUM 18
FUM 17
FUM 16
FUM 15
FUM 14
FUM 13
FUM 12
FUM 11
FUM 10
FUM 9
FUM 8
SU 1
FUM 7
FUM 6
FUM 5
FUM 4
FUM 3
FUM 2
FUM 1

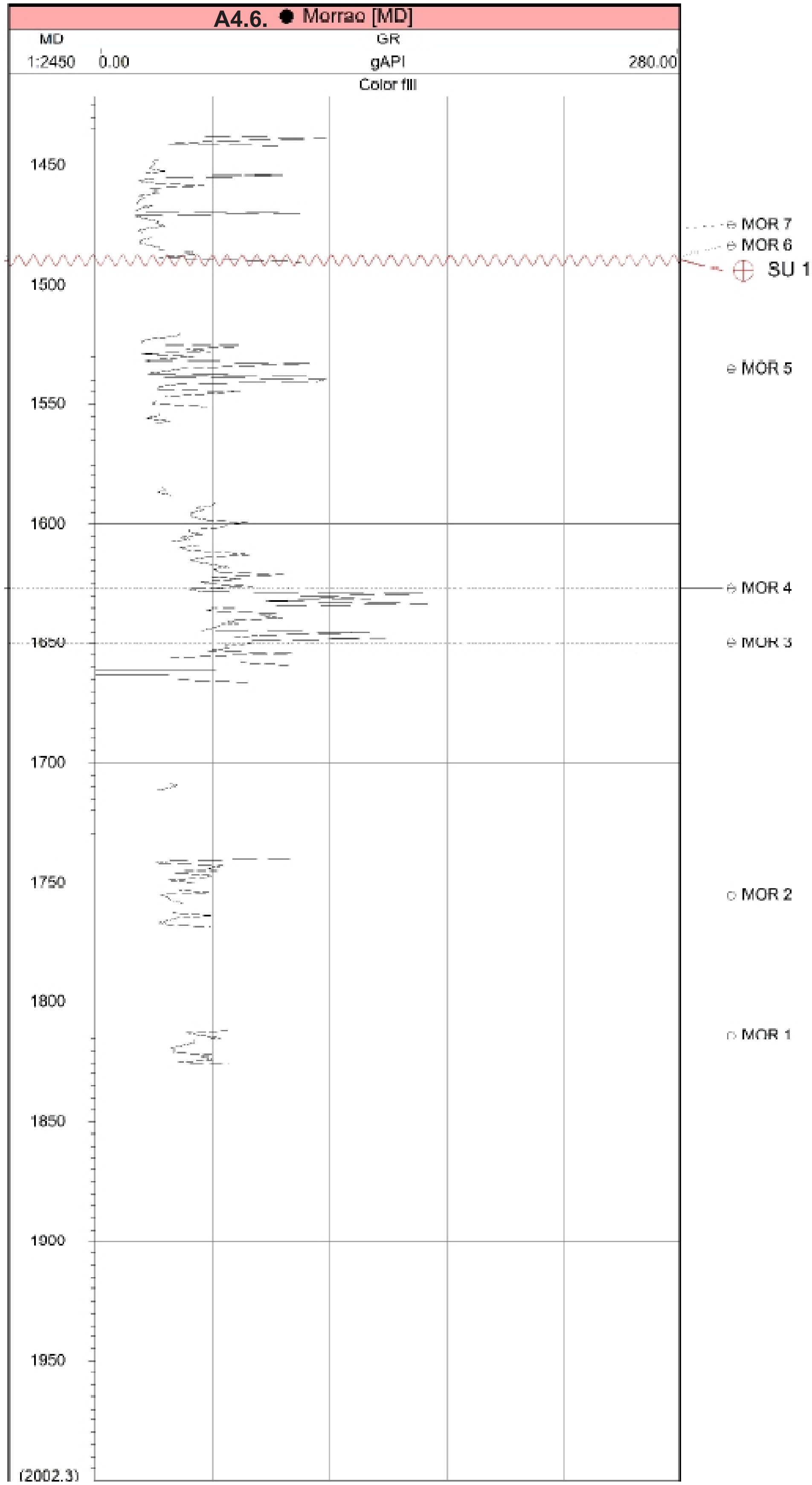
A4.6.
Morrao [MD]
MD
1:2450
GR
0.00
gAPI
280.00
Color fill
1450
1500
1550
1600
1650
1700
1750
1800
1850
1900
1950
(2002.3)
MOR 7
MOR 6
SU 1
MOR 5
MOR 4
MOR 3
MOR 2
MOR 1

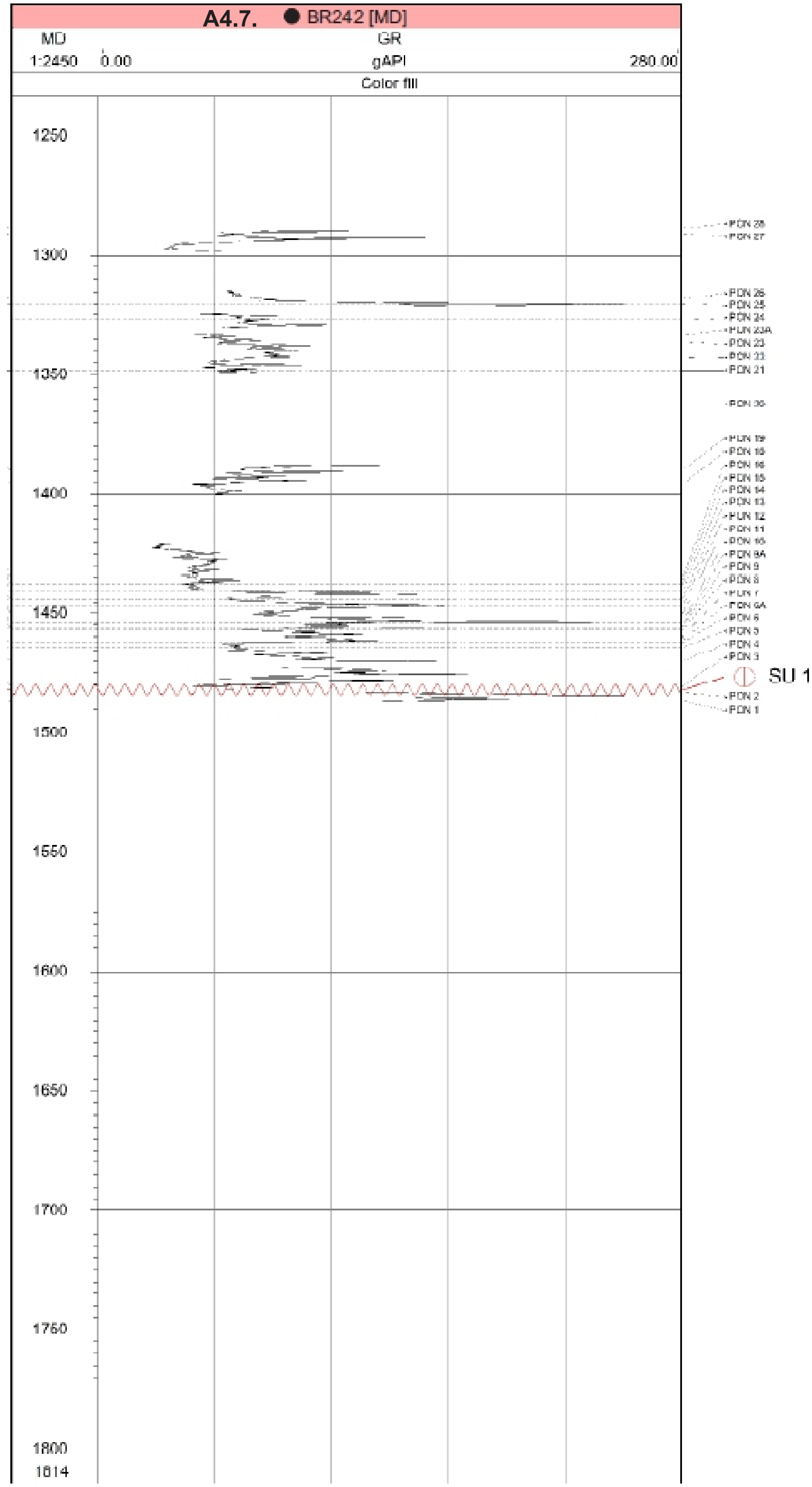
A4.7.
BR242 [MD]
MD
1:2450
GR
0.00
gAPI
280.00
Color fill
1250
1300
1350
1400
1450
1500
1550
1600
1650
1700
1750
1800
1814
SU 1

A4.8. ● Impossíveis [MD]

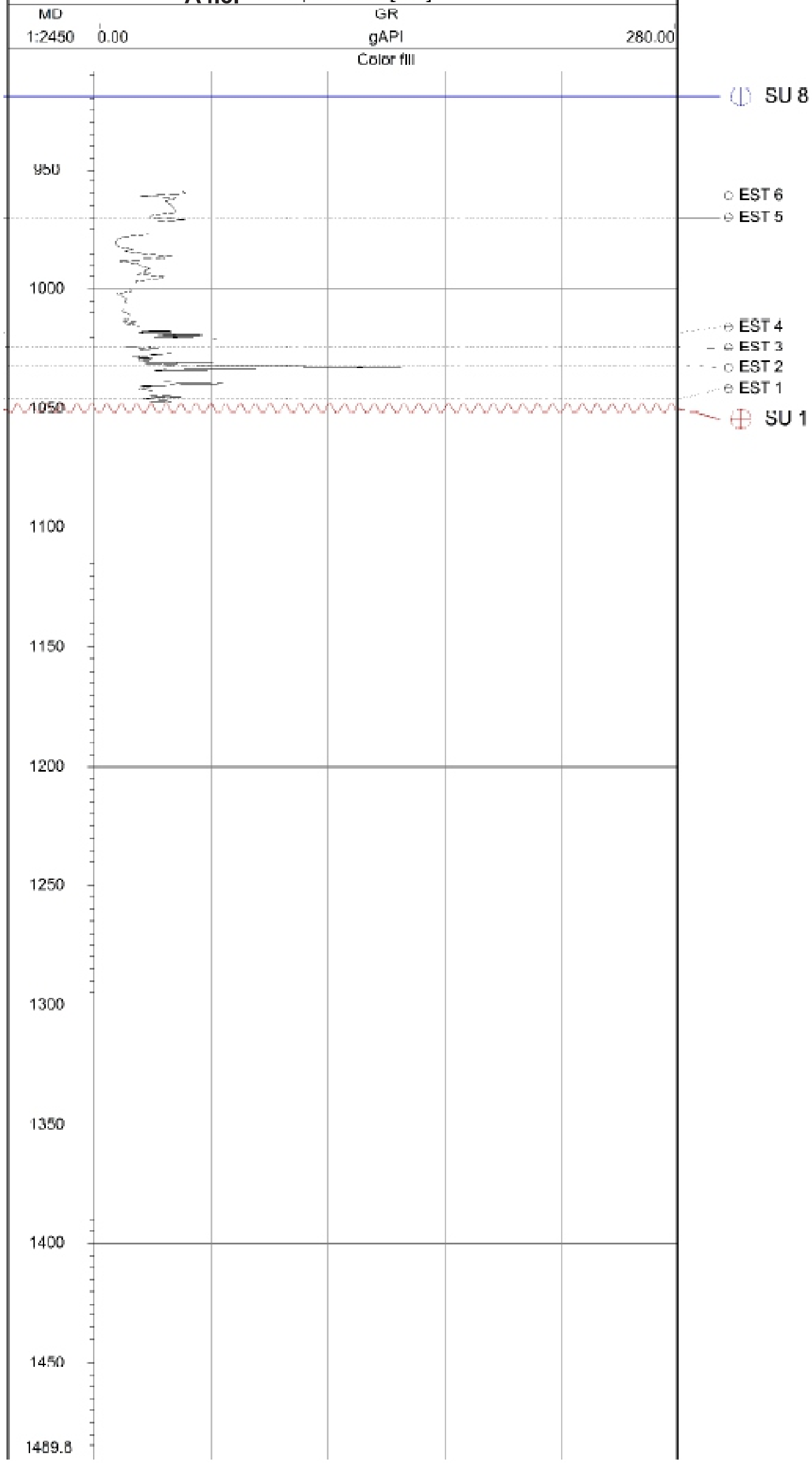

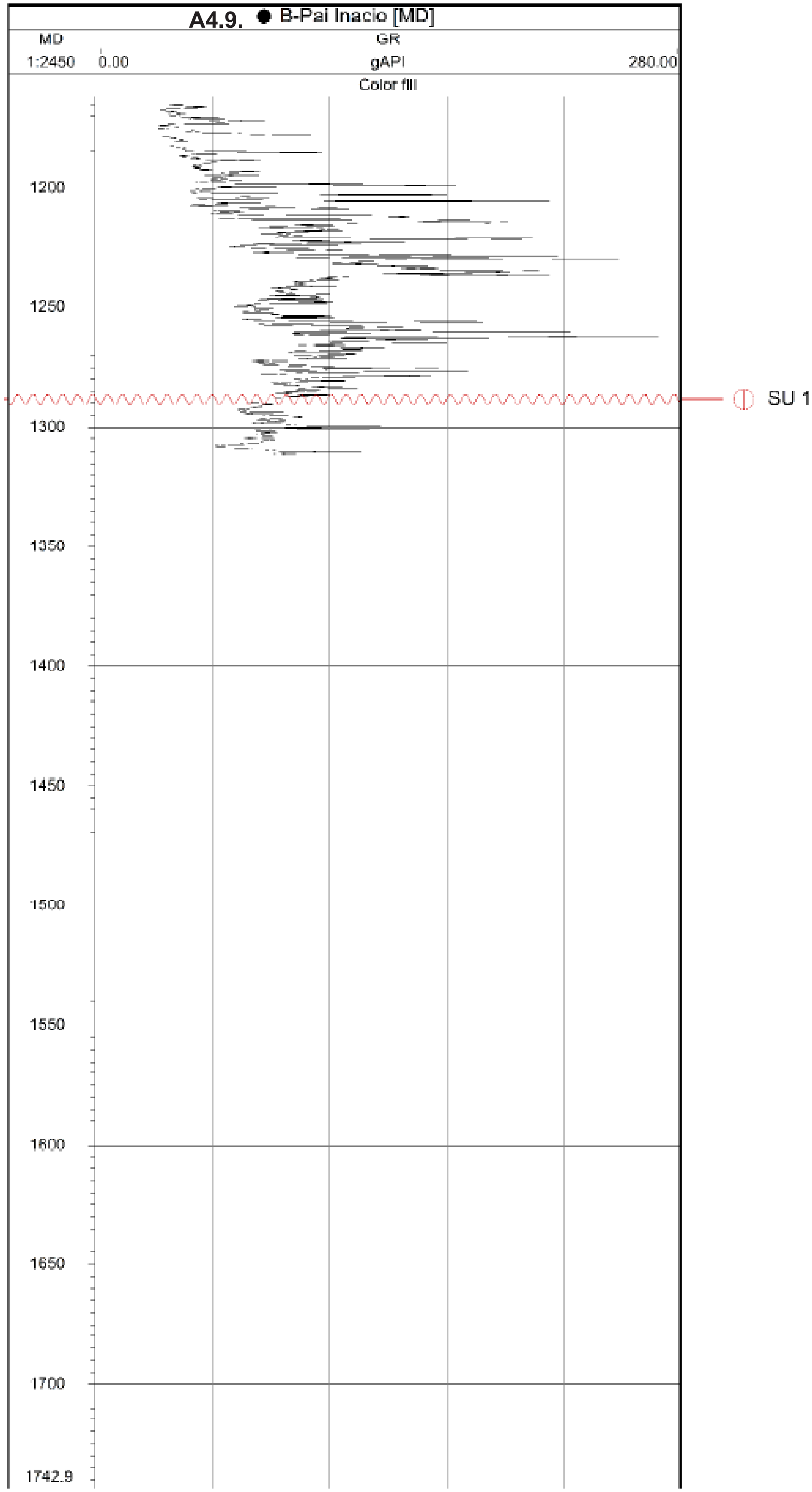
A4.9. B-Pai Inacio [MD]
MD
1:2450
GR
0.00
gAPI
280.00
Color fill
1200
1250
1300
1350
1400
1450
1500
1550
1600
1650
1700
1742.9
SU 1

Appendix 5 – Photomosaics

A5.1. Photomosaic location map

A5.2. Sobrada photomosaic

A5.3. Cravada photomosaic

A5.4. Camelo photomosaic

A5.5. Brejão photomosaic

A5.6. Pai Inácio hill – Photomosaic B

A5.7. Morro Branco – Photomosaic C

A5.1 Topographic map of North Sincora Range with photomosaics

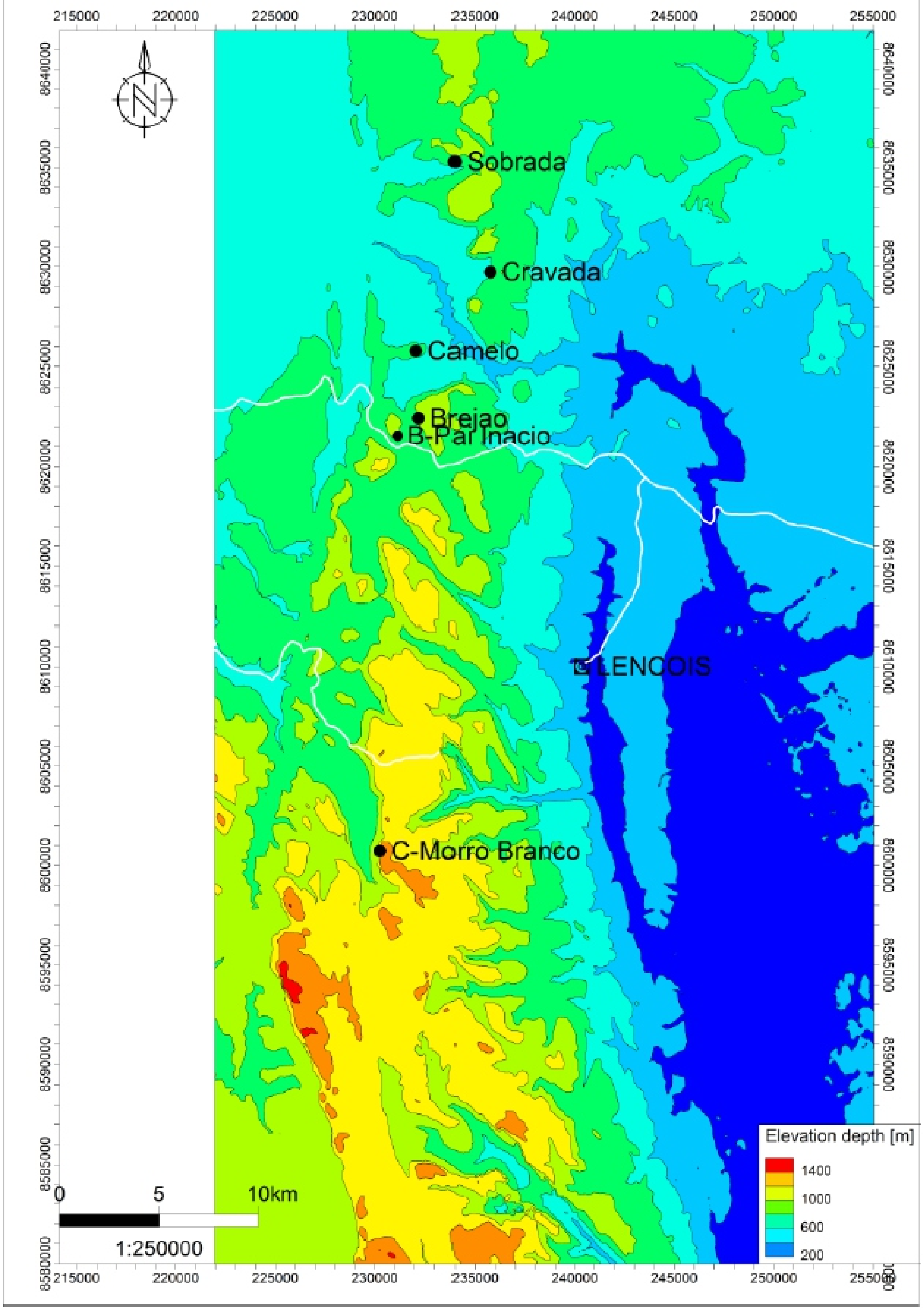

A5.2. Sobrada photomosaic

A5.3. Cravada photomosaic

A5.4. Camelo photomosaic

A5.5. Brejão photomosaic

A5.6. Pai Inacio hill photomosaic

A5.7. Morro Branco photomosaic

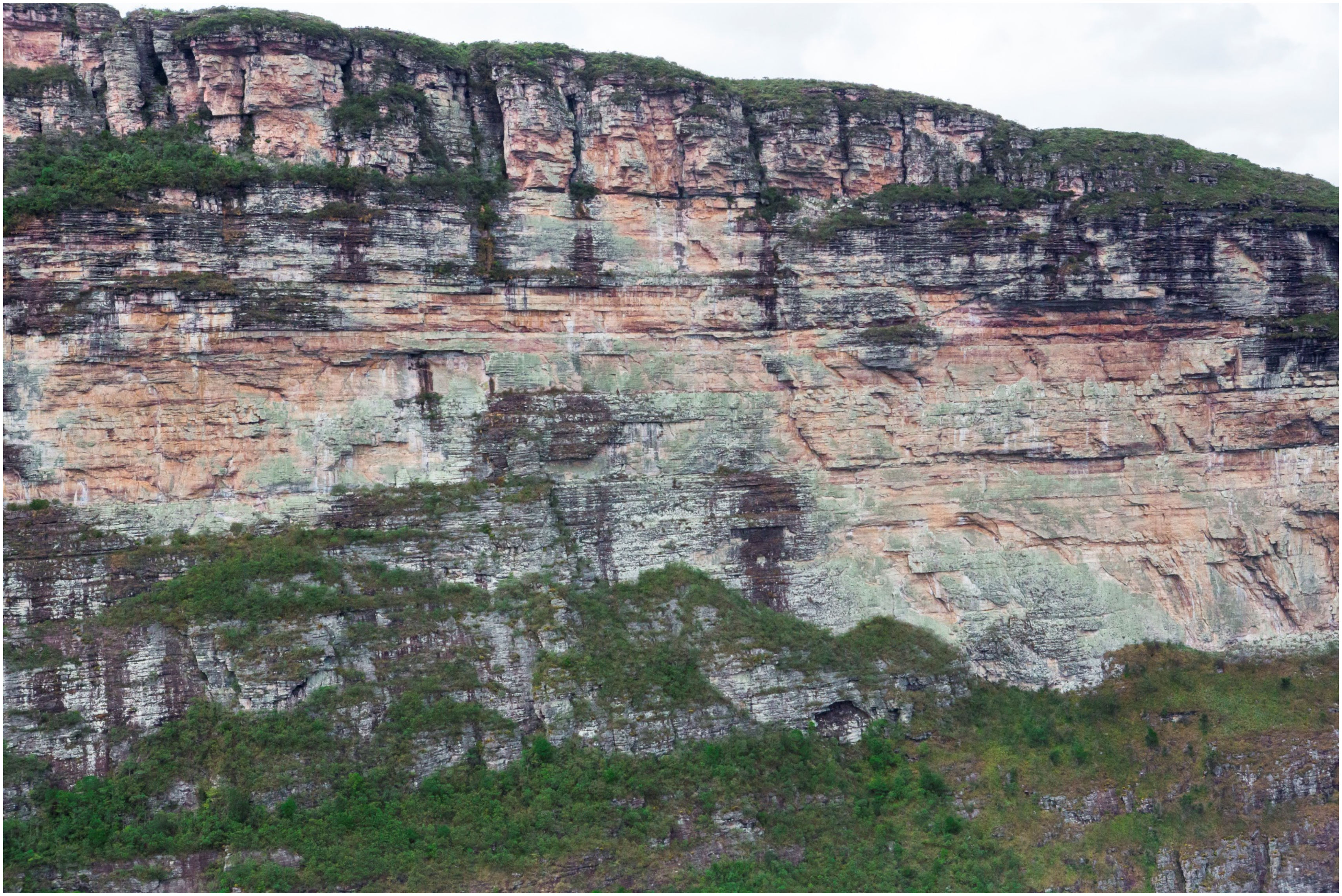

Appendix 6 – Petrographic analysis

A6.1. Stratigrahic cross-section with thin sections location

A6.2. Table with petrographic analysis results

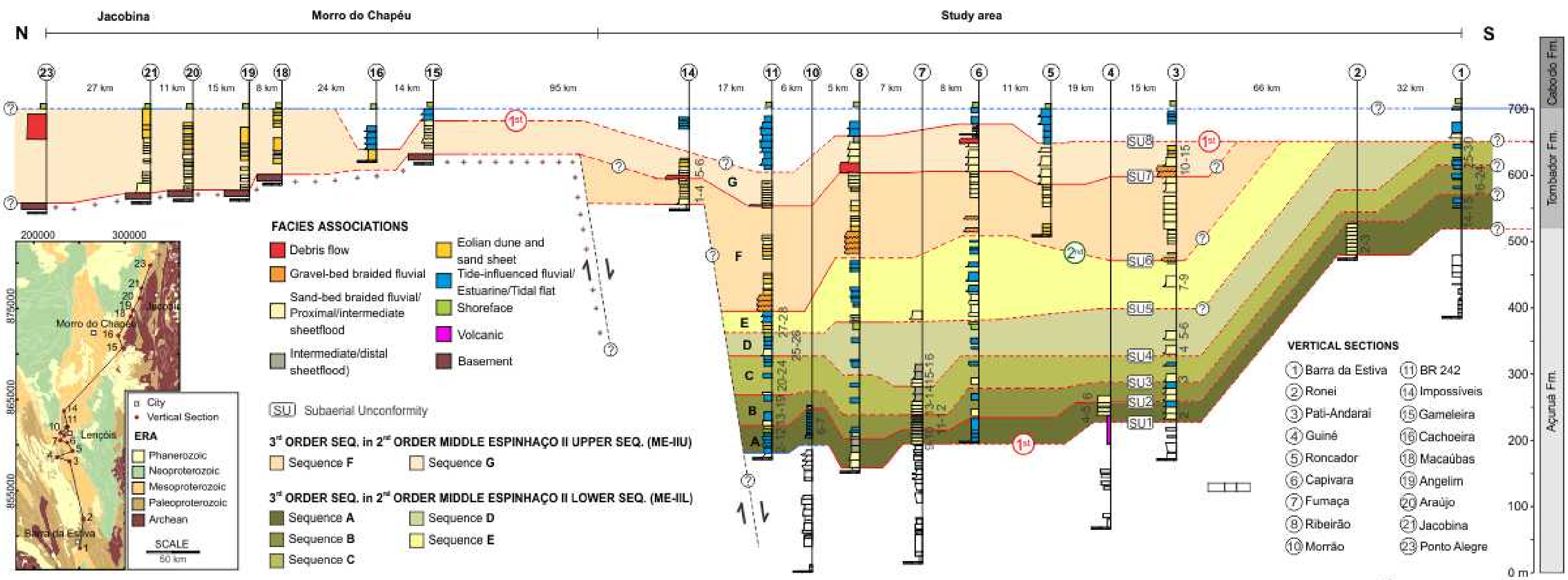

A6.1. Stratigraphic cross-section with thin sections location

A6.2. PETROGRAPHIC ANALYSIS - TOMBADOR FM - Part 1

Vertical section	Thin section	QM	QP	FELDS	CHERT DET	FR-quartzite	GR	ALT	TURM	BIOT	MUSC	INFCLAY	OWQ	ARGILM	PSEUDM	FERRUG	SILICA
1	653-BEST14	46	7										TR	14			
1	654-BEST15	68	4									4	TR	TR			
1	655-BEST16	33	11									TR	TR	7			
1	656-BEST17	41	11				TR						7	TR			
1	657-BEST18	40	8	8			4						16	12			
1	658-BEST19	34	34	3								3	TR	3			
1	659-BEST20	53	17	TR			5						5	5			
1	660-BEST21	42	17	4								4	4	TR			
1	756-BEST22	41	4				4						4	4			
1	661-BEST23	53	16				TR						5	16			
1	662-BEST24	60	16									TR	8	8			
1	663-BEST25	70	9										9	4			
1	664-BEST26	62	13									4	13	4			
1	665-BEST27	60	12				TR							4			4
1	666-BEST28	53	8											8			
1	667-BEST29	55	14				4						7	TR			
2	672-RON2	30	25									TR		30			
2	673-RON3	59	7										15	7			
3	614-AND2	70	6										10	14			
3	615-AND3	72	4										4	TR			
3	616-AND4	69	4										4				
3	617-AND5	56	11										21	1			
3	618-AND6	65	15			1							8	5			1
3	619-AND7	58	15										5	22			
3	825-AND9	55	15										9	11			
3	620-AND10	41	31						TR								
3	622-AND12	39	17										10	6			4
3	623-AND13	48	18										11	21			TR
3	624-AND14	68	16		TR							3	12				TR
3	625-AND15	69	TR										9				
4	633-GUI4	73	7										4	5			
4	634-GUI5	69	5						TR				5	9			
4	635-GUI6	46	4						42				TR				
7	809-FUM8	70	5									TR	1	11			
7	810-FUM9	62	3									2	TR	5			
7	811-FUM11	45	4									4	1	20			
7	812-FUM11	59	5									TR	6	12			
7	813-FUM13	52	6								TR	9		13			
7	814-FUM13	58	6						TR		TR	TR	TR	24			
7	815-FUM14	40	2								TR	4	TR	41			
7	816-FUM15	66	10									1	5	18			
7	817-FUM16	57	11										2	17			
7	818-FUM17	58	4								TR		12	19			
7	819-FUM18	68	6										10	16			
10	800-MOR6	63	2				1				TR		2	20			
10	801-MOR7	63	5										21	10			

11	781-PON3	72	8	TR						4		12			
11	782-PON4	53	19				TR				16	12			
11	783-PON5	60	7								9	TR			
11	784-PON6	66	16		5				TR	3	TR	5			
11	829-PON6A	60	12	TR			TR				15	12			
11	785-PON7	54	14				TR		TR		7	14			
11	786-PON8	61	10		5						10	14			
11	787-PON9	60	21		4					TR		4	TR		
11	830-PON9A	66	18	TR	2						2	4			
11	788-PON10	46	TR						7			4			
11	789-PON11	62	14	TR	TR					3	14	7			
11	791-PON13	66	7								3	7			
11	792-PON14	56	8		TR						19	14			
11	793-PON15	70	4	TR	TR						7	19			
11	794-PON16	70	7								11	TR			
11	832-PON19	57	21	TR			TR				11	11			
11	833-PON20	63	4								18	11			4
11	834-PON21	84	4		TR						TR	12			
11	835-PON22	70	4								TR	4			
11	836-PON23	66	10							3	14	4			
11	837-PON23A	55	11	TR							19	3			2
11	838-PON24	59	14								14	4			
11	839-PON25	40	17								3	40			
11	840-PON26	75	TR	TR							4	21			
11	841-PON27	60	10		5						10	15	TR		
11	842-PON28	62	24								TR	14			
11	tomb3/4_1	59	7		6					3		23			
11	tomb3/4_2	46	9,8		7,2	1,1			TR		1,8	8,9	1,2	24	
11	tomb3/4_3	61	12		4						8	15			
11	tomb_2_1/3	67	4		4						16	8		1	
11	tomb3/4_4	2					6	TR	8					30	
11	tomb2.1b	64	7,6								6,6				1,1
14	773-EST1	79	3		4					1	7	1			
14	774-EST2	65	16								13	3			
14	775-EST3	74	7								4	8			
14	776-EST4	54	16		1						3	15			
14	777-EST5	58	7		1		1				1	6			
14	778-EST6	49	28		TR		TR		TR		1	9			
B	757-PAI1	78	5						TR			12			
B	758-PAI2	69	8		5				TR	2	2	3			
B	760-PAI3	74	11						TR	TR	4	11			
B	761-PAI4	62	17								2	3			
B	762-PAI5	66	17							2	8	3			
B	763-PAI6	56	2				2				16	TR			
B	764-PAI7	66	10				TR				9				
B	765-PAI7A	65	8								8	11			
B	766-PAI8	53	8								8				
B	767-PAI9	60	15	TR			TR				3	18			
B	768-PAI10	67	9	2							TR	3	5		

B	769-PAI11	47	5					5	5	33	
B	770-PAI12	68	10				TR		4	16	
B	771-PAI13	75	5						10	10	
B	772-PAI13A	70	11						4	TR	TR
not pres	612-SV3A	53	17						7	3	10
not pres	611-SV3	67	TR						30	TR	
not pres	610-SV2	55	3						14	TR	
not pres	609-SV1	67	13						9	TR	
not pres	608-MUC2	32	21						14	25	
not pres	607-MUC1	60	16						16		8
not pres	824-MUC1A	68	16						TR		
	TOTAL	6228	1098,4	15	2	1					

Folk´s classification (1974)		
Q	**F**	**RF**
99,77%	**0,20%**	**0,03%**

A6.2. PETROGRAPHIC ANALYSIS - TOMBADOR FM - Part 2

Vertical section	Thin section	POROFR	POROMO	PORO INTER	PORO INTRA	PORO ENC	OPACOS	MATRIX	GRMUSC	MARRAM	muscdiag	ARG+ SIL	CLOR	Ti	Opdiag	CHERT AUT	HEMAT	TURMA DETR	ARG+ SILT	EPID	BIOT DETR	CAUL	FRANJ	TOTAL
1	653-BEST14	4		14	TR	4																11		100
1	654-BEST15	TR		8	TR	TR				4			TR									4	8	100
1	655-BEST16	4		19	4	4				11												7	TR	100
1	656-BEST17	7		5	5	1				16												TR	7	100
1	657-BEST18	4		TR	TR										4								4	100
1	658-BEST19	8		4	4					4													3	100
1	659-BEST20	TR	TR	5	5										5									100
1	660-BEST21			13	8					8														100
1	756-BEST22	1		19	4					8													11	100
1	661-BEST23	TR	TR	5	TR																	TR	5	100
1	662-BEST24				5					3														100
1	663-BEST25				4										4								TR	100
1	664-BEST26			4									TR		TR								TR	100
1	665-BEST27			4	4					TR			TR		4								8	100
1	666-BEST28			8													8						15	100
1	667-BEST29	3	TR	7	7																		3	100
2	672-RON2				5										10									100
2	673-RON3			12											TR									100
3	614-AND2												TR	TR										100
3	615-AND3			12	1	1							6	TR	TR									100
3	616-AND4	TR		11	1								11	TR										100
3	617-AND5			10	1								TR											100
3	618-AND6				3								TR		TR	1	1							100
3	619-AND7			TR																				100
3	825-AND9			10										TR	TR									100
3	620-AND10			5										TR	23									100
3	622-AND12	TR	TR	11	TR					9						4								100
3	623-AND13			1	1										TR	TR								100
3	624-AND14			1																				100
3	625-AND15	1		17	4									TR				TR						100
4	633-GUI4			8	3									TR										100
4	634-GUI5			9	3									TR						TR				100
4	635-GUI6			8																				100
7	809-FUM8			9	4	TR											TR							100
7	810-FUM9	3	TR	19	6																			100
7	811-FUM11		TR	20	4									TR					2					100
7	812-FUM11		TR	12	3										3									100
7	813-FUM13		TR	20	TR																			100
7	814-FUM13			11										TR	1									100
7	815-FUM14			6						5					2									100
7	816-FUM15		TR		TR										TR					TR				100
7	817-FUM16			7	1					5								TR						100
7	818-FUM17		TR	5	TR					1					1		TR	TR						100
7	819-FUM18			TR										TR	TR									100
10	800-MOR6	1		9	2																			100
10	801-MOR7			1						TR			TR					TR			TR			100
11	781-PON3									4								TR		TR	TR			100
11	782-PON4													TR	TR									100
11	783-PON5			5	4	2							11		2									100
11	784-PON6														3		2		TR					100
11	829-PON6A									1								TR						100
11	785-PON7														11									100
11	786-PON8																							100
11	787-PON9														TR		11							100
11	830-PON9A					TR							2		6									100
11	788-PON10														39		TR				4			100
11	789-PON11																							100
11	791-PON13		TR	10	TR					7														100
11	792-PON14			3																				100
11	793-PON15			TR																				100
11	794-PON16		TR	TR	4								8											100
11	832-PON19													TR	TR			TR						100
11	833-PON20			TR																				100

11	834-PON21												TR								100
11	835-PON22				4						TR		18		TR						100
11	836-PON23		TR									TR	TR	3							100
11	837-PON23A			6	4							TR			TR						100
11	838-PON24			TR							TR	TR	9				TR				100
11	839-PON25			TR								TR									100
11	840-PON26											TR	TR								100
11	841-PON27												TR								100
11	842-PON28												TR								100
11	tomb3/4_1							2													100
11	tomb3/4_2																				100
11	tomb3/4_3																				100
11	tomb_2_1/3																				100
11	tomb3/4_4						54														100
11	tomb2.1b								3,3	17,4											100
14	773-EST1			4	1																100
14	774-EST2					3		TR				TR									100
14	775-EST3			7																	100
14	776-EST4			11								TR						TR			100
14	777-EST5	3		15	3			4												1	100
14	778-EST6	TR		8	TR			4												1	100
B	757-PAI1							5				TR				TR		TR			100
B	758-PAI2							8					TR		3						100
B	760-PAI3							TR											TR		100
B	761-PAI4			9	5	2															100
B	762-PAI5			3									1								100
B	763-PAI6	1	TR	13	TR						10	TR									100
B	764-PAI7			9	4							TR	2						TR		100
B	765-PAI7A			6	TR	TR							2								100
B	766-PAI8			29	2																100
B	767-PAI9												3		1			TR			100
B	768-PAI10												6		8						100
B	769-PAI11														5						100
B	770-PAI12							TR					2								100
B	771-PAI13												TR		TR						100
B	772-PAI13A			11	4						TR		TR								100
not pres	612-SV3A			3							7										100
not pres	611-SV3							3													100
not pres	610-SV2		TR	28	TR	TR							TR								100
not pres	609-SV1		7	4																	100
not pres	608-MUC2				4								4								100
not pres	607-MUC1											TR									100
not pres	824-MUC1A													16							100

LEGEND

QM	quartz monocristallne
QP	quartz policristaline
FELDS	feldspars
CHERT DET	detrital cher
FR-quartz	quartzite
GR	grain replaced by clay minerals and mica. The grain shape is preserved
ALT	weathered
TURM	turmaline
BIOT	biotite
MUSC	muscovite
INFCLAY	mechanically infiltrated clay
OWQ	quartz owergrowth
ARGILM	clay mineral and mica without evidence of grain shape
PSEUDM	pseudomatrix
FERRUG	ferroan cement
SILICA	siilca
POROFR	porosity from fracture
POROMO	moldic porosity
POROINTER	intergranular porosity
POROINTRA	intragranular porosity
POROENC	shrinkage porosity

LEGEND

OPACOS	opaque
MATRIX	matrix
GRMUSC	grain replaced by muscovita. The grain shape is preserved
MARRAM	brown material
muscdiag	diagenetic muscovite
ARG+SIL	clay mineral and silica
CLOR	clorite
Ti	titanium mineral
Opdiag	opaque cement
CHERTAUT	diagenetic chert
HEMAT	hematite coating
TURMADET	detrital turmaline
ARG+SILT	mud and silt
EPID	epidote
BIOTDETR	detrital biotite
CAUL	caolinite
FRANJ	clay coating